

**A REVIEW OF RESEARCH
ON
AERONAUTICAL FATIGUE IN THE UNITED STATES**

2013-2015



Compiled by
Dr. Ravinder Chona
Air Force Research Laboratory
Wright-Patterson Air Force Base, Ohio, USA

**FOR PRESENTATION AT THE MEETING
OF THE
INTERNATIONAL COMMITTEE ON AERONAUTICAL FATIGUE**

1 JUNE 2015 – 5 JUNE 2015

HELSINKI, FINLAND

Approved for Public Release; Distribution is Unlimited

TABLE OF CONTENTS

<u>Section</u>	<u>Page</u>
9.1. INTRODUCTION.....	9/9
9.2. NON-DESTRUCTIVE INSPECTION/EVALUATION	9/13
9.2.1. Choosing the Correct Detection Limit ($a_{90/95}$) for Ensuring Crack Tolerance Subsequent to a Required Damage Tolerance Inspection	9/13
9.2.2. Improving ASIP Analysis Using Structural Data Visualization Organization and Archival Techniques	9/15
9.2.3. Evaluating Low Frequency Eddy Current Based Technologies for Detecting Fatigue Cracks in Multi-Layer Metallic Structures	9/18
9.2.4. Quality Assurance and Nondestructive Inspection in Support of Engineered Residual Stresses.....	9/21
9.2.5. Evaluation of NDE Methods as Applied to Metallic Honeycomb Structures.....	9/25
9.2.6. Hidden Fatigue Crack Detection in Multi-Layer Aircraft Structures Using High Frequency Guided Ultrasonic Waves.....	9/29
9.3. STRUCTURAL HEALTH MONITORING	9/31
9.3.1. The State of Nondestructive Evaluation and Structural Health Monitoring	9/31
9.3.2. SHM System Readiness for Damage Detection on Aging Aircraft	9/32
9.3.3. The Environmental Severity Index and Its Applications	9/36
9.3.4. Embedded Structural Health Monitoring System Development and Testing for Fatigue Crack Detection of Rotorcraft Structures	9/40
9.3.5. Quantification of Structural Health Monitoring for Damage Detection	9/43
9.3.6. Concept of Operations for Corrosion Environment Sensors (aka Corrosion Sensors)	9/46
9.4. STRUCTURAL TEARDOWN ASSESSMENTS	9/49
9.4.1. T-38 Fuselage Teardown: One Man’s Trash is Another Man’s Treasure.....	9/49
9.4.2. Structural Teardown Analysis.....	9/53
9.5. LOADS & ENVIRONMENT CHARACTERIZATION.....	9/57
9.5.1. F-16 ASIP Data Capture: The Missing Link in IAT Evolution	9/57
9.5.2. An Innovative Low Maintenance Data Acquisition Solution for Load Factor Capture.....	9/60
9.5.3. Loads Environment Spectra Survey (L/ESS) USCG HC-144A.....	9/61
9.5.4. Determination of Flight Loads for the HH-60G Pave Hawk Helicopter.....	9/63
9.5.5. Gust and Maneuver Loads for a Fleet of USFS Lead Airplanes.....	9/67
9.5.6. Flight Data Collection and Analysis	9/69

TABLE OF CONTENTS (*Cont'd*)

<u>Section</u>	<u>Page</u>
9.6. CHARACTERIZATION, MODELING & TESTING	9/73
9.6.1. Bird Strike and Coupon Testing of B-2 Polycarbonate Windshields Exhibiting Usage Induced Cracking	9/73
9.6.2. AC-130W Stinger II Gun Port Seal Loading and Structural Design.....	9/75
9.6.3. F-16 Block 50 Full-Scale-Durability Test Correlation and Test Findings	9/78
9.6.4. Fatigue Crack Growth Tests and Analyses on 7249-T76511 Aluminum Alloy Specimens Under Constant Amplitude and Simulated Aircraft Wing Loading	9/81
9.6.5. Analysis of the Interaction of Two Parallel Surface Cracks	9/84
9.6.6. Ti-6Al-4V Small Crack Growth Effect on Damage Tolerance Analysis.....	9/85
9.6.7. Using Virtual Strain Gauges to Correlate with Bending and Torsion Measured on a Helicopter Tail Cone Using Strain Gauges	9/88
9.6.8. Models for Corner and Through Cracks in Support of Beta Curve Development for the P-8A Poseidon Full-Scale-Fatigue-Testing	9/89
9.6.9. Titanium 6Al-4V Durability Method Development and Test Verification on Small Crack.....	9/92
9.6.10. Predicting Fatigue Crack Growth in Forgings with Bulk Residual Stress	9/95
9.6.11. A Discrete-Crack-Network-Based Fatigue Damage Assessment for Bonded and Bolted Composite Structure.....	9/99
9.6.12. Continued Development of the NASGRO Software for Fracture Mechanics and Fatigue Crack Growth Analysis	9/101
9.6.13. Long-Term Thermal Exposure Effect on Crack Growth Rate in Aluminum Alloys.....	9/103
9.6.14. Notched Fatigue Behavior of Aluminum Under Constant and Variable Amplitude Multiaxial Loads	9/106
9.6.15. Peridynamics for Progressive Damage Prediction in Composites	9/108
9.6.16. Predictive Modeling and Simulation of Crack Branching, Curvilinear Crack Paths and Life for Fatigue Crack Growth Under Cyclic Out-of-Phase Loading Conditions.....	9/112
9.6.17. 3D Measurements of Microstructurally Small Fatigue-Crack Evolution in an Aluminum Alloy	9/114
9.6.18. Innovative Capability to Quantify Fatigue Damage and Assessment of Endurance Limit in Spectrum Load Histories.....	9/115
9.6.19. Integrated Structural Modeling and Simulation	9/117
9.6.20. The Evolution of BAMF	9/119

TABLE OF CONTENTS (*Cont'd*)

<u>Section</u>	<u>Page</u>
9.6.21. Materials Characterization of High Strength Aluminum Alloys and Mixed Mode Fatigue Crack Growth Test Development	9/121
9.6.22. Material Degradation Research Projects for OSD-CPO Corrosion Program.....	9/124
9.6.23. Development of a Fatigue Testing Method for Analysis of the Corrosion Pit to Small Crack Transition.....	9/127
9.6.24. Development of Equipment and Methods for Stress Spectra Structural Testing Combined with Environmental Spectrum.....	9/130
9.6.25. Stress Intensity Factors for Finite Width Plates	9/132
9.6.26. Test Methods to Partition Residual Stress From Fatigue Crack Growth Rate Data.....	9/135
9.6.27. Dwell Fatigue Crack Growth in Alpha Titanium Alloy.....	9/139
9.6.28. Effect of Stress Ratio on Small Crack Growth in a Titanium Alloy and Application in Probabilistic Life Prediction	9/140
9.6.29. Effect of Aging Treatment on Fatigue Behavior of an Al-Cu-Mg-Ag Alloy.....	9/142
9.6.30. Thin Film Galvanic Modeling for Aircraft Structures	9/144
9.7. PROGNOSTICS & RISK ANALYSIS.....	9/149
9.7.1. Time-to-Failure Probability Distribution Estimate Using Monte Carlo Simulation	9/149
9.7.2. Modeling Repairs in Structural Risk and Reliability Assessments.....	9/152
9.7.3. Application of Structural Risk Analysis to Force Management and Force Structure Planning.....	9/154
9.7.4. Weibull Analysis of Fatigue Data From Aircraft Paint Removal Techniques – Lessons Learned	9/157
9.7.5. Instantaneous Monte Carlo Calculation of Single Flight Probability of Failure.....	9/159
9.7.6. The F-16 Canopy Sill Longeron: Using Risk Analysis to Ensure Continued Structural Safety	9/161
9.7.7. F-35A MLG Drag Brace Risk Analysis.....	9/163
9.7.8. Continued Development of the DARWIN Software for Probabilistic Damage Tolerance Analysis and Risk Assessment	9/166
9.7.9. <u>PR</u> obability <u>Of</u> <u>Failure</u> (PROF) Risk Analysis Program	9/169
9.7.10. Risk Based Fleet Management Lessons Learned	9/172
9.7.11. Reducing Uncertainty in Fatigue Life Limits of Turbine Engine Alloys.....	9/173

TABLE OF CONTENTS (*Cont'd*)

<u>Section</u>	<u>Page</u>
9.8. LIFE ENHANCEMENT CONCEPTS.....	9/177
9.8.1. Durability and Damage Evaluation of Tolerance Rivetless Nut Plates Installed in Short Edge Margin Conditions.....	9/177
9.8.2. Modeling Fatigue Failure From Cold-Worked Fastener Holes.....	9/179
9.8.3. Computation of Stress Intensity Factors for Cracks in Cold-Worked Holes	9/182
9.8.4. Residual Stresses From Cold-Working of Aircraft Fastener Holes	9/184
9.8.5. Hole Cold Expansion in the Presence of Existing Cracks.....	9/188
9.8.6. Cold-Expansion Effects on Cracked Fastener Holes Under Constant Amplitude and Spectrum Loading in the 2024-T351 Aluminum Alloy	9/190
9.8.7. Laser Peening for Improved Fatigue Strength and Lifetime for a Wing Attachment Shear Tie.....	9/193
9.8.8. Verification of Analytical Methodology to Minimize Inspection Burdens and to Utilize Full Benefits of Residual Stress Life Enhancement Technique.....	9/196
9.8.9. Simulation of Crack Growth at Cold-Worked Holes	9/198
9.8.10. Integrating Residual Stress Analysis of Critical Fastener Holes into USAF Depot Maintenance	9/202
9.8.11. Shot Peen Residual Stress Distribution During Mechanical Loading.....	9/205
9.8.12. Modeling 3D Fatigue Crack Growth in Residual Stress Fields	9/206
9.9. REPAIR CONCEPTS	9/211
9.9.1. Quality Assurance and Bondline Strain Measurement of Patch Repairs Using Fiber Optic Strain Sensors and Digital Image Correlation	9/211
9.9.2. Friction Plug Welding of 2024-T3 Aluminum.....	9/213
9.9.3. Fighter Jet Wing Repair and Refurbishment.....	9/217
9.10. REPLACEMENT CONCEPTS	9/223
9.10.1 Material Product Form and Process Substitution Guidelines for Metallic Components	9/223
9.10.2 Aluminum Alloy Substitution for Modernizing the Aging Fleet	9/226
9.11. OVERVIEWS	9/229
9.11.1. When “What We Always Do” Won’t Solve the Problem.....	9/229
9.11.2. B-1 Full-Scale-Fatigue Test	9/232
9.11.3. Equivalent Flight Hours Development for USAF HH-60G.....	9/234
9.11.4. E-6B SLEP Fatigue Analysis and Test Program.....	9/237
9.11.5. P-8A Poseidon Full-Scale-Fatigue Test	9/239

TABLE OF CONTENTS (*Cont'd*)

<u>Section</u>	<u>Page</u>
9.11.6. Full-Scale-Fatigue Test of FA-18 A/D Composite Structure for Aging Evaluation	9/241
9.11.7. Enabling High-Quality and Efficient Engineering Decisions with 3-D Visualization of Maintenance Data.....	9/243
9.11.8. Strategies for and the Importance of DaDT Analysis Validation at the System Level.....	9/245
9.11.9. Integrated Technology Development Toward ASIP Corrosion Tools	9/248
9.11.10. The F-16 Canopy Sill Longeron: Getting Control of a Multi-National Safety-of-Flight Issue.....	9/250
9.11.11. Overview of the Full-Scale-Durability Tests on F-35 Lightning II Program.....	9/254
9.11.12. Importance of Corrosion Prevention Control Plans and Corrosion Prevention Advisory Boards	9/259
9.11.13. KC-135 Damage Tolerance Toolset Modernization Overview.....	9/260
9.11.14. Durability Assessment for Non-Legacy Manufacturing Methods	9/263
9.11.15. Structural Component Corrosion Simulation – Test Program Update.....	9/267
9.11.16. Investigation of C-5 Honeycomb Floor Panel Dent Limits	9/269
9.11.17. Integrity of F/A-18 A-D Wing Root Stepped-Lap Joint	9/272
9.11.18. NDI and Maintenance Data Collection in a Digital Environment	9/277
9.11.19. Full-Scale-Fatigue Test Truncation Spectrum Verification	9/279
9.11.20. General Aircraft Structural Integrity Program (ASIP) Support	9/287
9.11.21. Detecting Crack Nucleation/Damage Mechanisms in Sea-Based Aviation Environments	9/291

9.1. INTRODUCTION

Leading government laboratories, universities and aerospace manufacturers were invited to contribute summaries of their recent aeronautical fatigue research activities. This report contains several of those contributions. Inquiries regarding a particular article should be addressed to the person whose name accompanies that article. The generous contributions of each participating organization is hereby gratefully acknowledged.

Government

- NASA – Johnson Space Center
- USA – Aviation Development Directorate
- USAF A-10 ASIP
- USAF B-1 SPO
- USAF C-5 ASIP
- USAF F-16 SPO
- USAF F-22 SPO
- USAF F-35 JPO
- USAF HH-60G ASIP
- USAF Life Cycle Management Center
- USAF ManTech
- USAF OC-ALC
- USAF OO-ALC
- USAF Research Laboratory – Aerospace Systems Directorate
- USAF Research Laboratory – Materials and Manufacturing Directorate
- USAF T-38 ASIP
- USAF WR-ALC
- USCG ALC
- United States Forest Service (USFS)
- USN – NAVAIR
- USN – Office of Naval Research

Academia

- Mississippi State University
- Purdue University
- Stanford University
- University College – London, UK
- University of Arizona
- University of South Carolina
- University of Dayton Research Institute
- University of Toledo
- University of Utah
- USAF Academy – Apogee Engineering
- USAF Academy – CAStLE
- Wichita State University – NIAR

Industry

- Acellent Technologies, Inc.
- Alcoa Defense
- Alcoa Technical Center
- APES, Inc.
- Battelle Memorial Labs
- Computational Mechanics International, Inc.
- Computational Tools, Inc.
- Correlated Solutions, Inc.
- Curtiss-Wright Controls, Avionics & Electronics
- Elder Research
- ESRD, Inc.
- Etegent Technologies, LTD.
- Fatigue Technology, Inc.
- Global Engineering and Materials, Inc.
- HBM – nCode
- Hill Engineering, LLC
- Independent Consultant
- Jacobs Technology, Inc.
- Leidas
- Lockheed Martin Corporation
- Mercer Engineering Research Center (MERC)
- Merex Aircraft Company, Inc.
- Metal Improvement Company
- Northrop Grumman Corporation
- SAFE, Inc.
- Sikorsky Aircraft Company
- Southwest Research Institute
- Spirit AeroSystems, Inc.
- TDA, Inc.
- Technical Data Analysis, Inc.
- The Boeing Company – Defense, Space & Security
- The Boeing Company – Research & Technology
- The Boeing Company – Test & Evaluation
- Tom Brussat Engineering, LLC
- TRI/Austin, Inc.

References, if any, are listed at the end of each article. Figures and tables are integrated into the text of each article.

The assistance of Jim Rudd and Pam Kearney, Universal Technology Corporation, in the preparation of this report is greatly appreciated.

One of the goals of the United States Air Force is to reduce the maintenance burden of existing and future weapon systems by eliminating programmed repair cycles. In order to achieve this goal, superior technology, infrastructure and tools are required to only bring down systems when they must be repaired or upgraded in order to preserve safety and effectiveness. This requires a condition-based-maintenance capability utilizing structural integrity concepts (CBM+SI). Knowledge is required for four Emphasis Areas: 1) Damage State Awareness, 2) Usage, 3) Structural Analysis and 4) Structural Modifications

(Figure 9.1-1). The following nine Technology Focus Areas are identified to provide this knowledge: 1) Non-Destructive Inspection/Evaluation, 2) Structural Health Monitoring, 3) Structural Teardown Assessments, 4) Loads and Environment Characterization, 5) Characterization, Modeling and Testing, 6) Prognostics and Risk Analysis, 7) Life Enhancement Concepts, 8) Repair Concepts, and 9) Replacement Concepts. The aeronautical fatigue research activities of this report have been categorized into these nine Technology Focus Areas, plus a tenth category titled “Overviews” that cuts across two or more of the nine Technology Focus Areas.

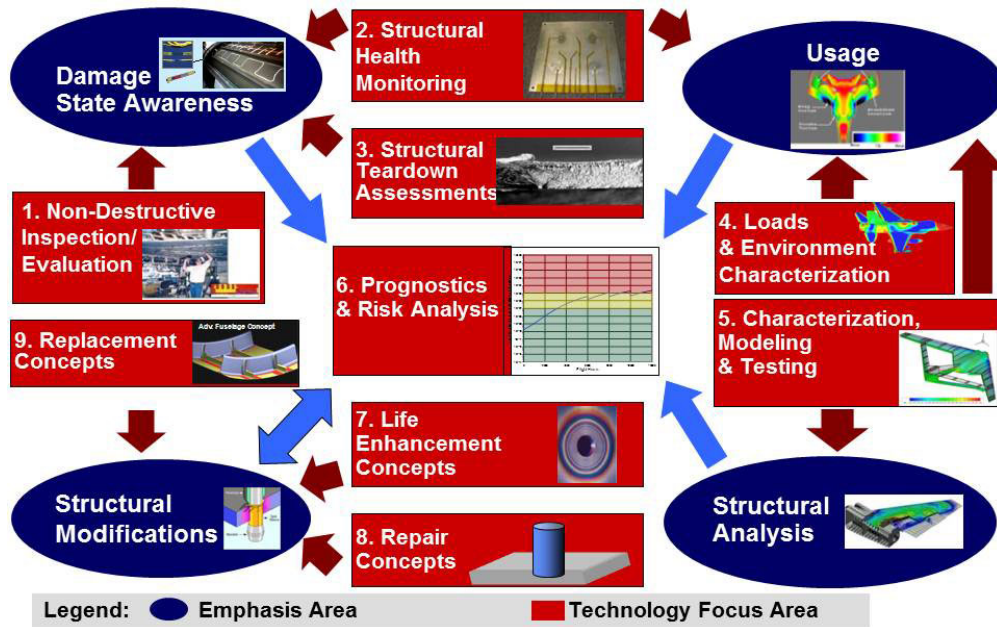


Figure 9.1-1. Condition Based Maintenance + Structural Integrity (CBM+SI)

9.2. NON-DESTRUCTIVE INSPECTION/EVALUATION

9.2.1. Choosing the Correct Detection Limit ($a_{90/95}$) for Ensuring Crack Tolerance Subsequent to a Required Damage Tolerance Inspection

Joseph Gallagher, Consultant

MIL-STD 1530C requires that the restart crack size after a damage tolerance inspection be set as a safe crack size limit associated with the nondestructive inspection (NDE) system capability. This required NDE crack size limit (a_{NDE}) is the crack size which will be detected 90% of the time with 95% confidence ($a_{90/95}$). This study focuses on the relationship between the probability of detection curve and the $a_{90/95}$ limit and on the crack growth life curve associated with crack behavior subsequent to the safety inspection. The crack growth life curve establishes the repeat inspection interval and the significant crack size (a_{cr_miss}), i.e., the crack size which, if missed during an inspection, could result in a failure prior to the next inspection (Figure 9.2-1). The study evaluates the probability of missing defined crack sizes $a_{90/95}$ and a_{cr_miss} for two NDE eddy current inspection systems, one that is manual and one that is automated (Figures 9.2-2 and 9.2-3). Choices of these two NDE systems result in significant inspection interval differences. The automated inspection could be used to replace multiple manual inspections, thus possibly allowing for conducting automated inspections within a depot, and eliminating manual field inspections. Implications associated with the relationships between the POD curve, $a_{90/95}$ crack size and the a_{cr_miss} crack size, as well as the risk of structural failure, is discussed and summarized (Figure 9.2-4).

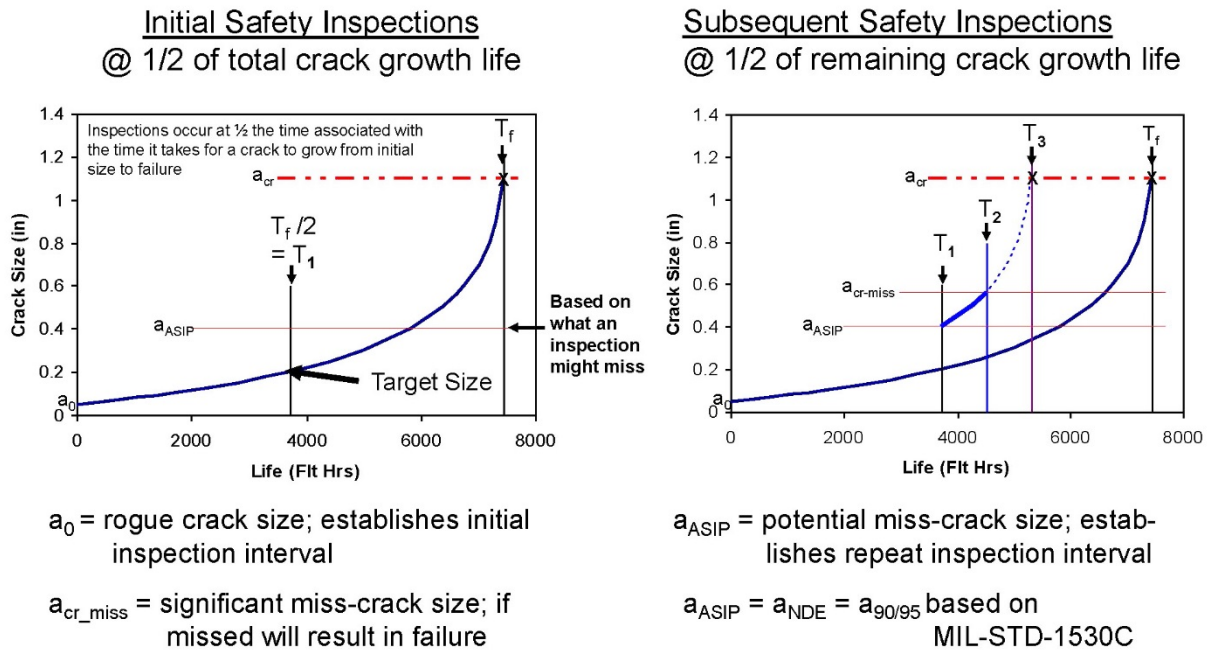


Figure 9.2-1. Characterizing Inspection Capability

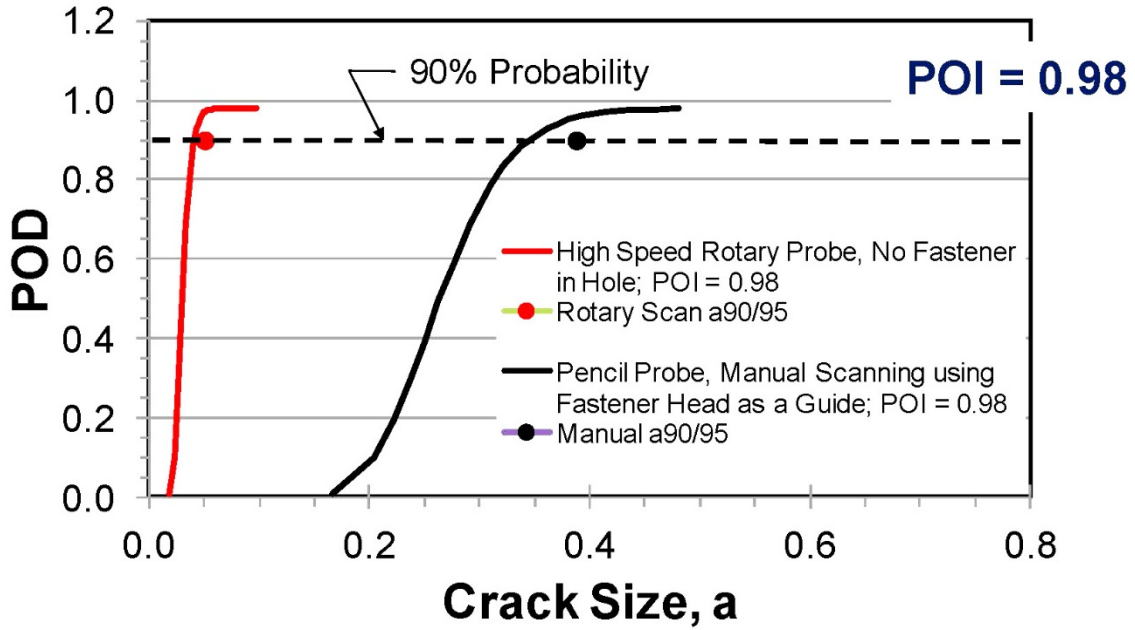


Figure 9.2-2. Comparison of Manual and Rotary Scan Eddy Current Inspection Systems

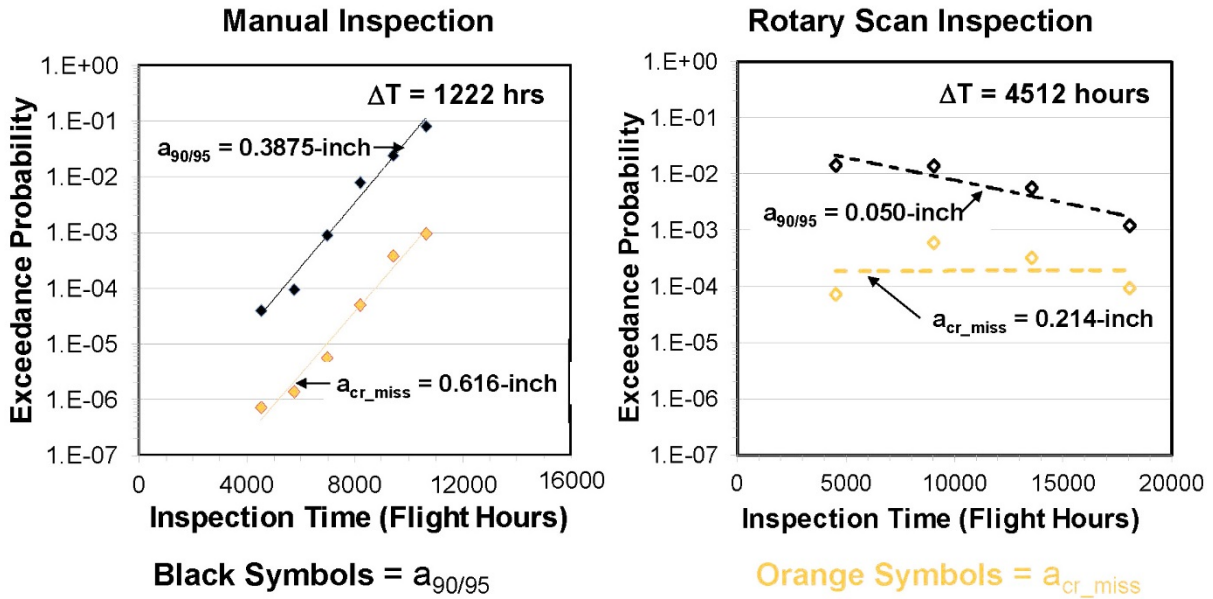


Figure 9.2-3. Comparison of Probability of Miss for Manual and Rotary Scan Systems

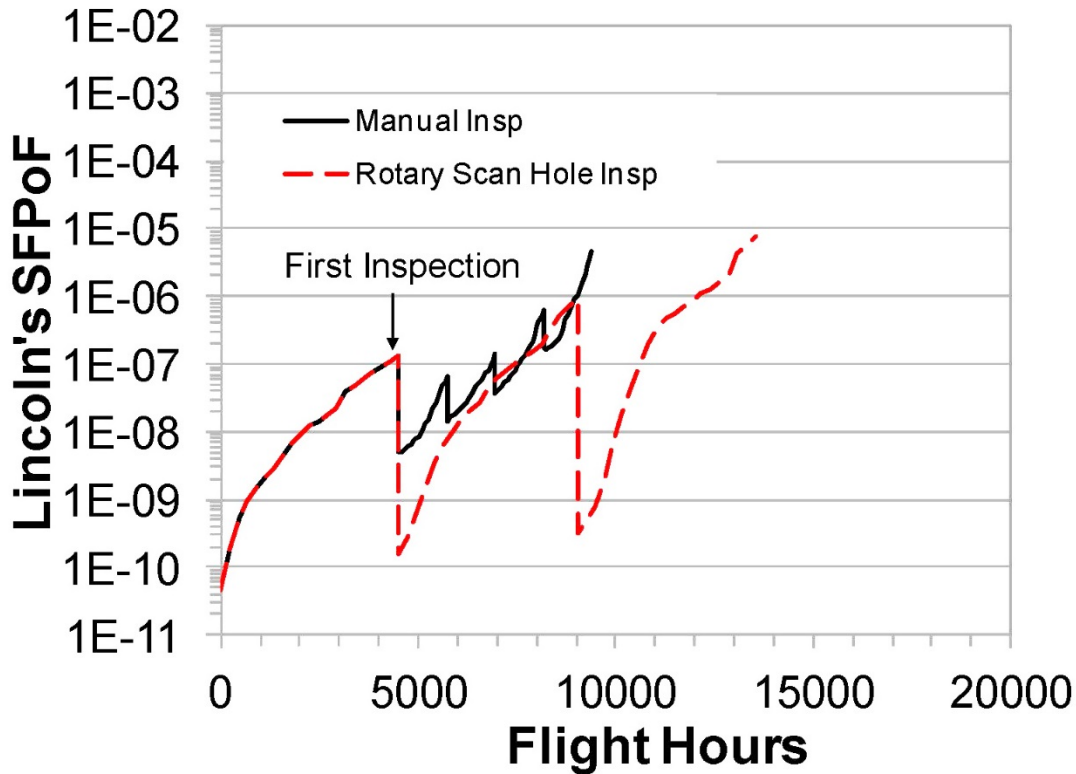


Figure 9.2-4. Comparison of Manual and Rotary Scan SFPOF (Risks)

9.2.2. Improving ASIP Analysis Using Structural Data Visualization Organization and Archival Techniques

Gary Steffes, USAF Research Laboratory – Materials and Manufacturing Directorate; Gregory Ferrell, USAF – Life Cycle Management Center; Steven Turek, USAF ManTech; Joshua Hodges, USAF; Shane Paredes, USN-NAVAIR; Gary Coyan and Thomas Sharp, Etegent Technologies; and Robert Pilarczyk, USAF – A-10 ASIP

Aircraft structural engineers are continuously searching for new processes and technologies to improve analysis in order to expedite engineering dispositions and manage the integrity of the airframe. To that end, technologies have been developed that can automatically map data to 2D and 3D structural models, and these systems have the capability to rapidly import, organize and archive high volumes of data in different formats. This enables engineers to quickly visualize data from multiple data sources (i.e., fleet NDI data, test/teardown data, nonconformance data, etc.) in locations of interests on specific structures. Visualizing the data in this manner makes it much easier to detect patterns in the data (e.g., which locations are prone to more issues) as well as quickly understand data for the fleet or for a particular airframe/serialized component. Performing this visualization is a critical part of the ASIP analysis and is used to speed dispositions and manage the integrity of the fleet that ultimately extends aircraft useful life. Additional engineering analysis algorithms have also been developed to enable/disable any mapped data and features coupled with CAD or FEA models. Data organization and archival functions allow users to query specific features within the data, in addition to tracking both specific serialized components within a structure, and associated damage to baseline and/or repaired structures. Several types of graphing and other analysis tools have also been developed to further ASIP

analysis. This technical activity follows up a previous discussion regarding a software system called NLign, which was developed to collect and map NDI and damage data to CAD models (Figures 9.2-5 through 9.2-8). The focus of this technical activity is on the engineering and analysis tools developed, and currently in use, that leverage the existing data mapping techniques. Several application examples are discussed along with the benefits of these powerful analysis tools.

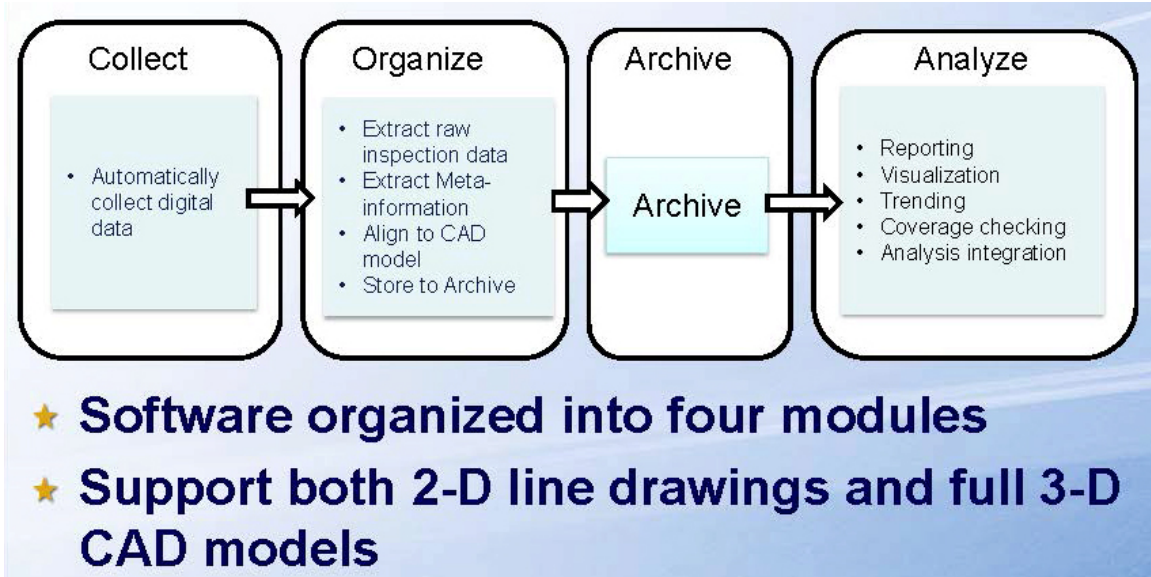


Figure 9.2-5. NLign Software Overview

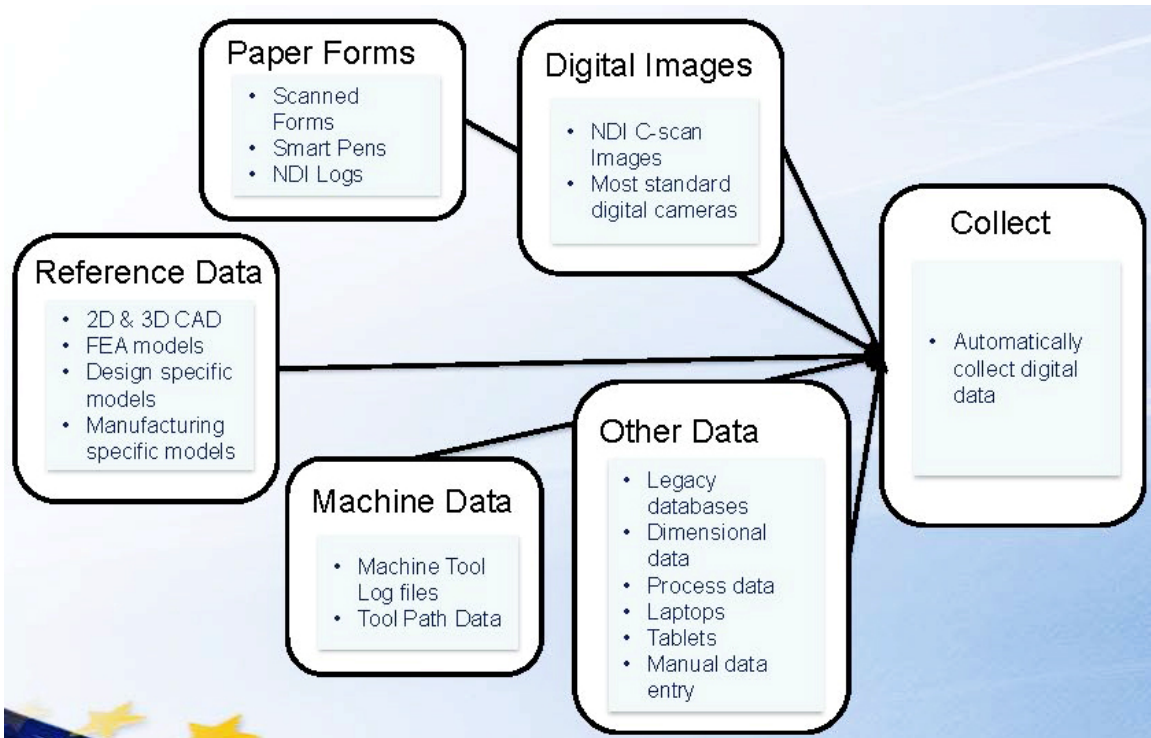


Figure 9.2-6. Collect Module of NLign Software

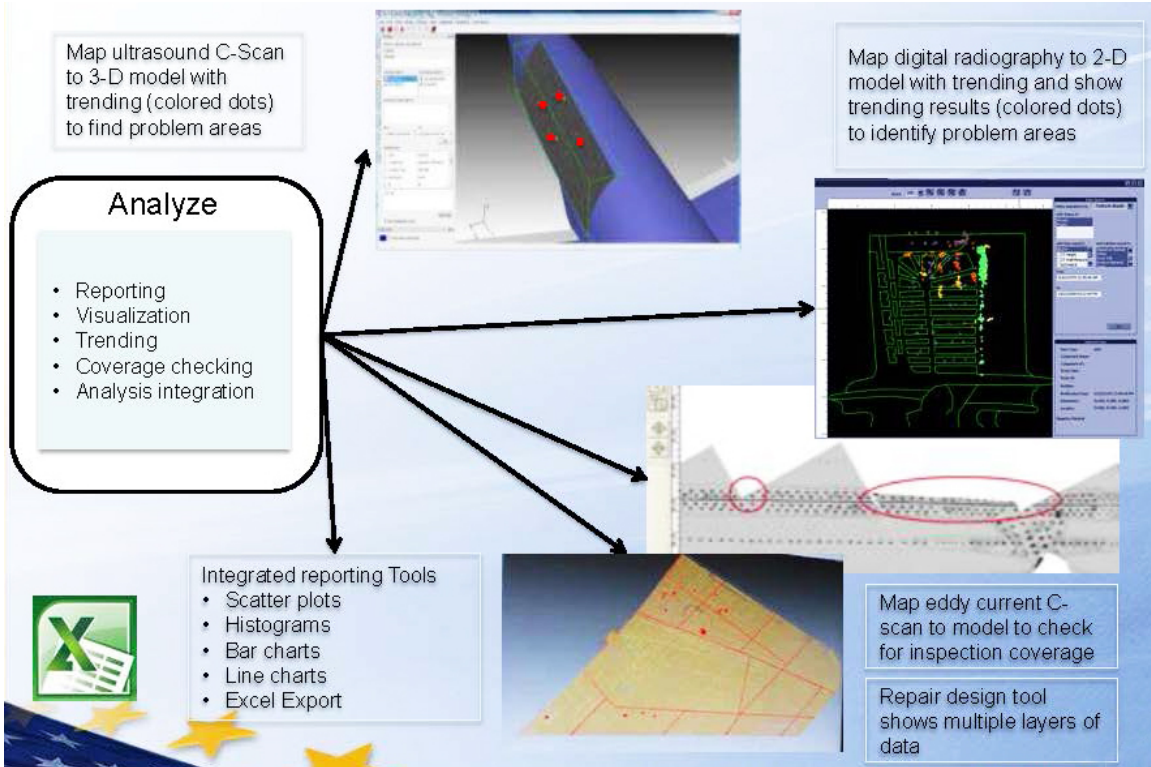
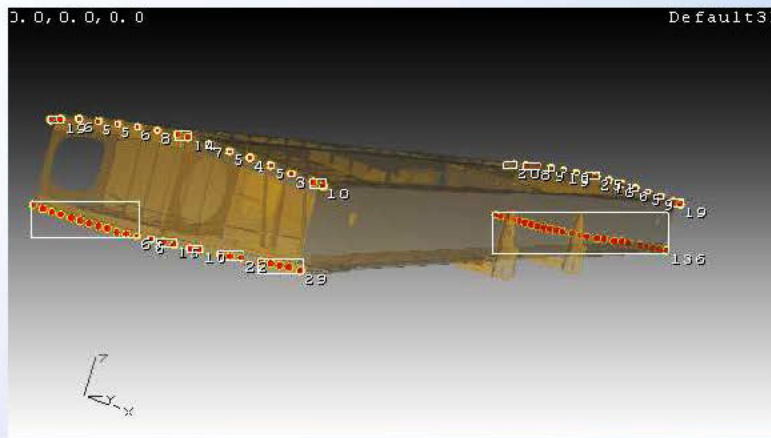


Figure 9.2-7. Analyze Module of NLog Software



- ★ 3D window shows location of trendable indications
- ★ Dots show location
- ★ Numerals show total number of features per area
- ★ Selecting dot highlights row(s) in table

Figure 9.2-8. 3-D View Window

9.2.3. Evaluating Low Frequency Eddy Current Based Technologies for Detecting Fatigue Cracks in Multi-Layer Metallic Structures

Gary Steffes and Charles Buynak, USAF Research Laboratory – Materials and Manufacturing Directorate; David Campbell, USAF-OC-ALC; Doyle Motes, David Forsyth, Mark Keiser, and Michael Mazurek, TRI/Austin, Inc.; John Aldrin, Computational Tools, Inc.

The successful development of next-generation Nondestructive Inspection (NDI) sensors that enable detection of smaller cracks without removing panels or coatings in thick, complex metallic aircraft structures generates high interest to those managing aircraft structural integrity. The detection of smaller cracks and other damage could allow increased inspection intervals and result in more economical repair actions when anomalies are detected. Previously, most NDI technique validation research has been relegated to small-scale experimental setups, such as EDM-notched specimens, to examine sensor capabilities. This leads to extrapolations in the candidate sensor's ability to identify fatigue cracks in stacked metallic layers. In this work, a large set of specimens of varying thicknesses containing fastener holes with natural fatigue cracks was fabricated and used to validate candidate sensor capabilities (Figure 9.2-9). This large set enabled flexibility in the arrangement of specimens to build up complex samples with varying configurations (Figures 9.2-10 and 9.2-11). The samples were then inspected with automated NDI methods using a giant magnetoresistance (GMR) array, a conventional low frequency eddy current spot, and a remote field eddy current ring probe (Figure 9.2-12). These were compared to manual scans with a standard low frequency ring probe and the same remote field eddy current probe. Results of the study, including eddy current signal responses, effect of different top layer thicknesses, probability of detection (POD) curves, and specific challenges faced by each sensor type are presented here (Tables 9.2-1 and 9.2-2).

- Simulate second layer cracking
- Four 7075-T6 Al specimen sets
 - Thicknesses (0.500", 0.375", 0.250", 0.100")
 - 4 - 1/4" holes per specimen
- Sixty (60) specimens tested for each thickness
 - 240 holes per set
 - 60 cracks per set

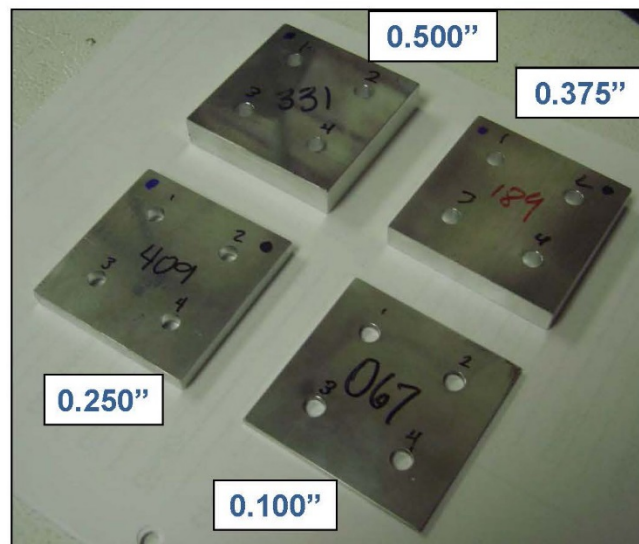
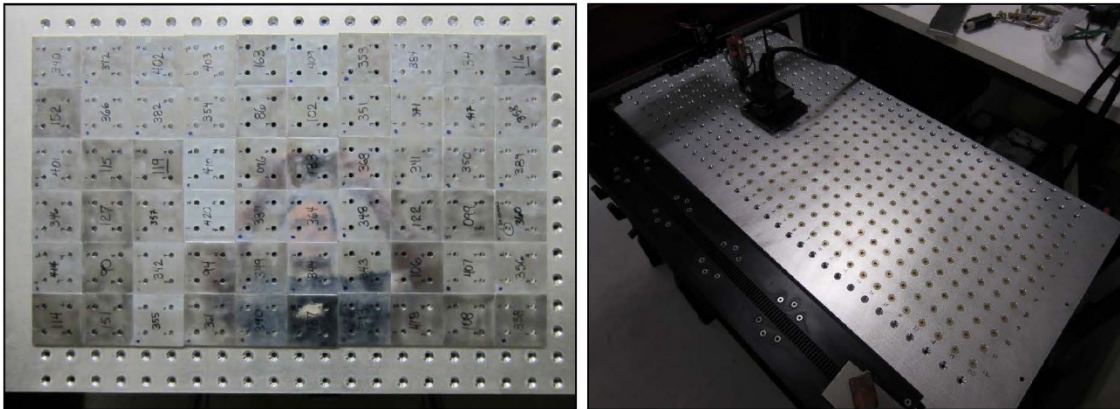
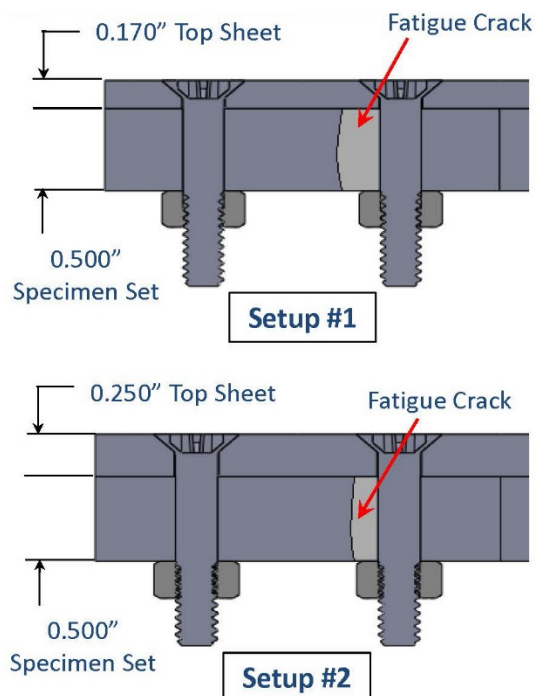


Figure 9.2-9. Fatigue Crack Specimen Sets



- Specimen Setups Included:
 - Boeing (Cd plated) steel fasteners (BACB30LU) and Al nuts
 - 1st layer consisted of 0.170" and 0.250" 7075-T6 Al top sheet
 - 2nd layer contained 60 individual 7075-T6 Al specimens at specimen set thicknesses

Figure 9.2-10. Fully Assembled Inspection Targets



- Crack content information
 - Cracks only in holes
 - Crack types
 - Toward adjacent fastener holes
 - Toward edges
 - Cracks orientations occur at 12 and 6 o'clock only
- DO NOT CONTAIN
 - Double cracked holes
 - Complete hole-to-edge or hole-to-hole cracks

Figure 9.2-11. Other Sample Set Information

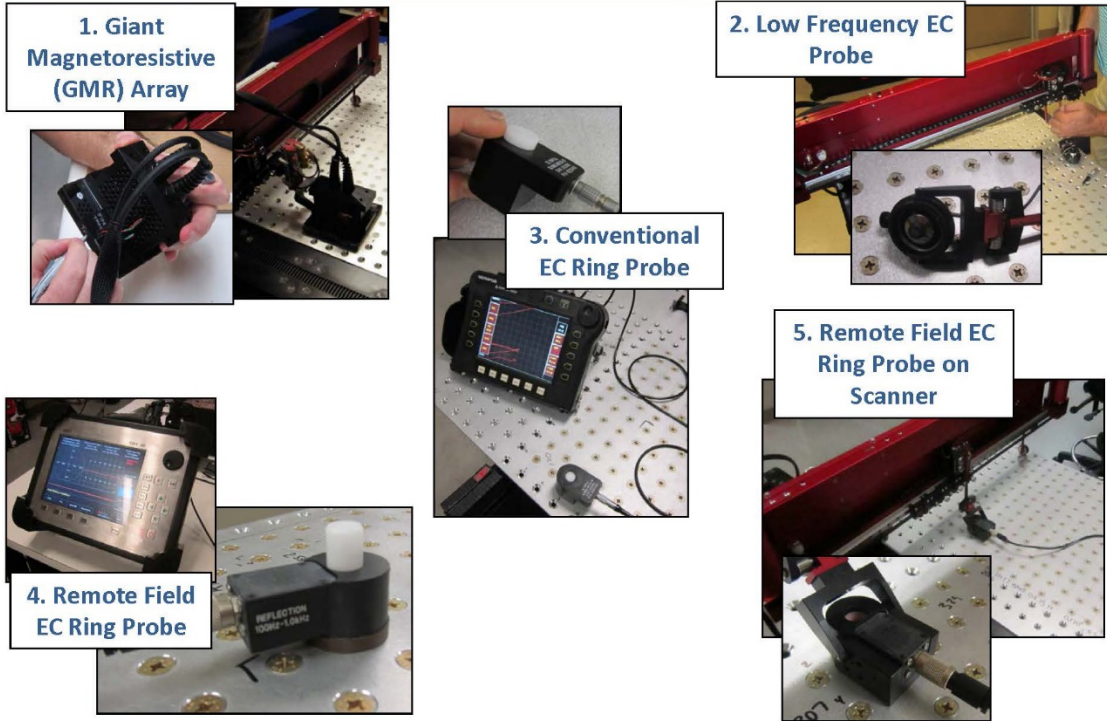


Figure 9.2-12. Sensor Systems Examined

Table 9.2-1. Results Table (0.250" Top x 0.500" Bottom)

Inspection Method	Correct (%)	False Call (%)	a90 (in)	a90/95 (in)
1a. GMR ImagIn	13%	5%	> 1.000	> 1.500
1a. GMR ImagIn Adj	20%	3%	> 1.000	> 1.500
1b. GMR ADA	80%	17%	0.370	0.471
1b. GMR ADA	62%	12%	0.480	0.584
2. LFEC	52%	6%	NA	NA
→ 3. Conventional EC ring	75%	0%	0.310	0.336
→ 4. RFEC Ring Probe	90%	0%	0.212	0.220
→ 5. RFEC Ring Probe MAUS	93%	1%	0.206	0.217
Best Results	RFEC MAUS	Tie	RFEC MAUS	RFEC MAUS

Table 9.2-2. Summary of Results

Best a90 Results	0.170" Top Sheet	0.250" Top Sheet
0.100" Specimen Set	<i>RFEC Ring Probe</i>	<i>RFEC Ring Probe</i>
0.250" Specimen Set	<i>RFEC Ring Probe MAUS</i>	<i>RFEC Ring Probe</i>
0.375" Specimen Set	<i>Conventional EC Ring Probe / RFEC Ring Probe</i>	<i>RFEC Ring Probe MAUS</i>
0.500" Specimen Set	<i>RFEC Ring Probe MAUS</i>	<i>RFEC Ring Probe MAUS</i>

- Sensitivities drop off with increasing depth for all sensor systems.
- EC ring probe results are better than the GMR Array MAUS and the LFEC MAUS for all inspections described in this work.
- RFEC averaged a better correct call rate than EC ring probe by 17%

9.2.4. Quality Assurance and Nondestructive Inspection in Support of Engineered Residual Stresses

Carl Magnuson and David Forsyth, TRI/Austin, Inc.; Tom Mills, APES, Inc.

It is well known that the use of residual stresses from peening, cold expansion, and other methods can have significant benefits to fatigue life. These benefits have been difficult to quantify analytically, and this has resulted in much conservatism in the use of these technologies. Since 2012, the A-10 ASIP office has been managing a Rapid Innovation Fund program built on three technology pillars that make it possible to relieve inspection burden at cold-worked holes. These three pillars include (1) analytical methods and software for assessing crack growth through residual stress fields (Figures 9.2-13 and 9.2-14), (2) quality assurance tools, and (3) the evaluation of in-service non-destructive inspection (NDI) methods for cracks at cold-worked holes. This technical activity focuses on the latter two elements of the program. We have developed a tool to provide initial quality assurance on a cold-worked-hole process. This tool provides a quantitative assessment of the degree of cold-work in the hole and can store the data for traceability and for detailed structural integrity assessment / risk management (Figures 9.2-15 and 9.2-16). Experience has also shown that the ability to manage cold-worked holes using the ASIP process may require different NDI than non-cold-worked holes (Figure 9.2-17). The residual stresses have two significant effects: they change the response of a crack to certain NDI methods, and they also change the location, shape, and orientation of cracks. We have evaluated standard USAF inspection techniques on cold-worked holes, and show results and comparisons to the probability of detection (Figure 9.2-18) of fatigue cracks from non-cold-worked holes.

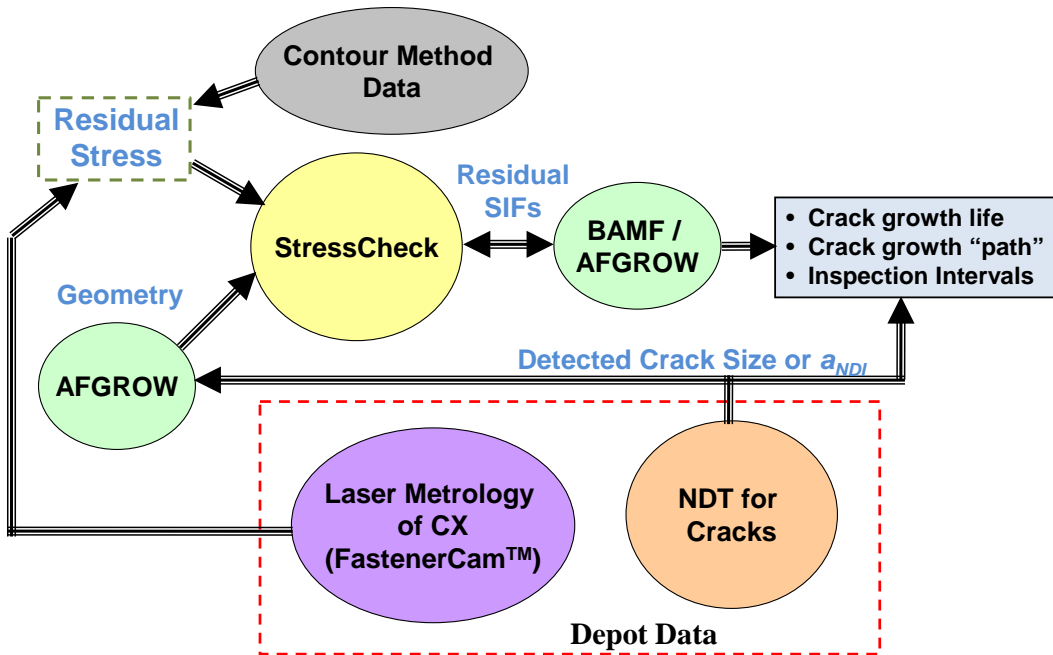


Figure 9.2-13. Integrated Modeling Package

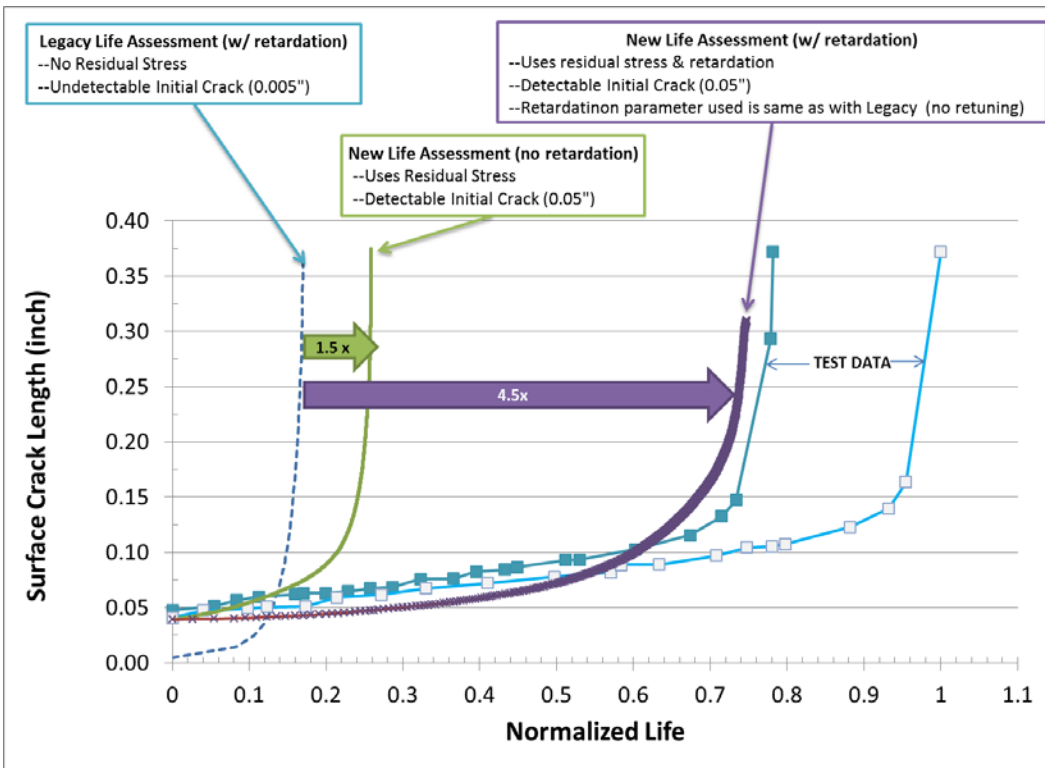


Figure 9.2-14. Life Assessments

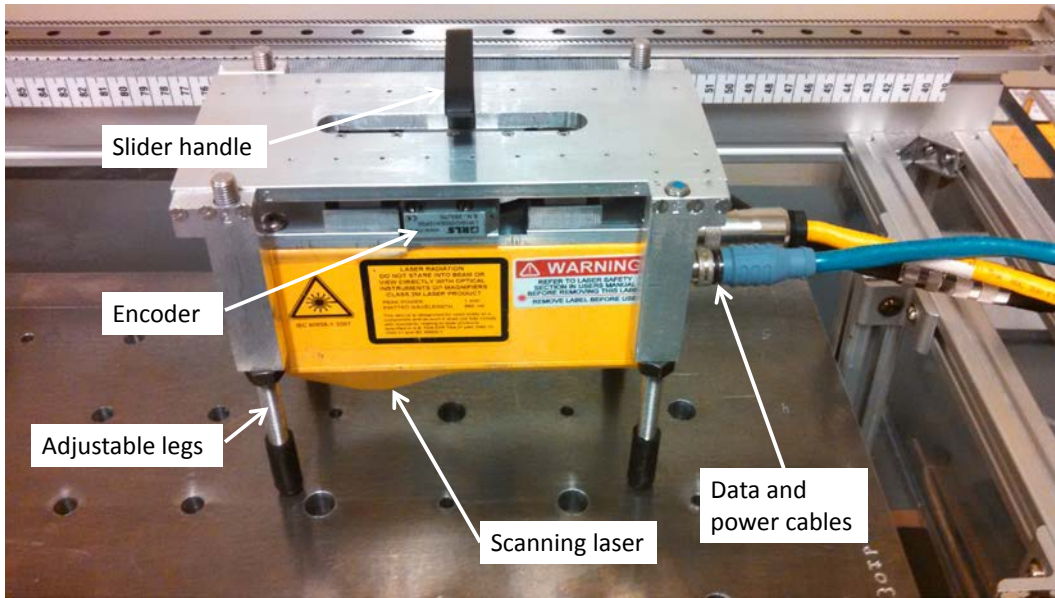


Figure 9.2-15. Phototype FastenerCam™

0.494" Diameter Straight Shank Holes

1.24% CX

4.00% CX

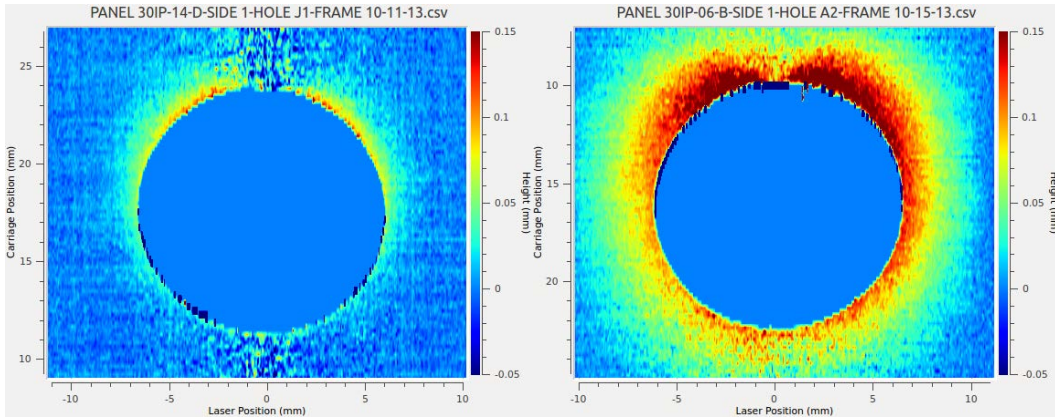


Figure 9.2-16. Raw Data

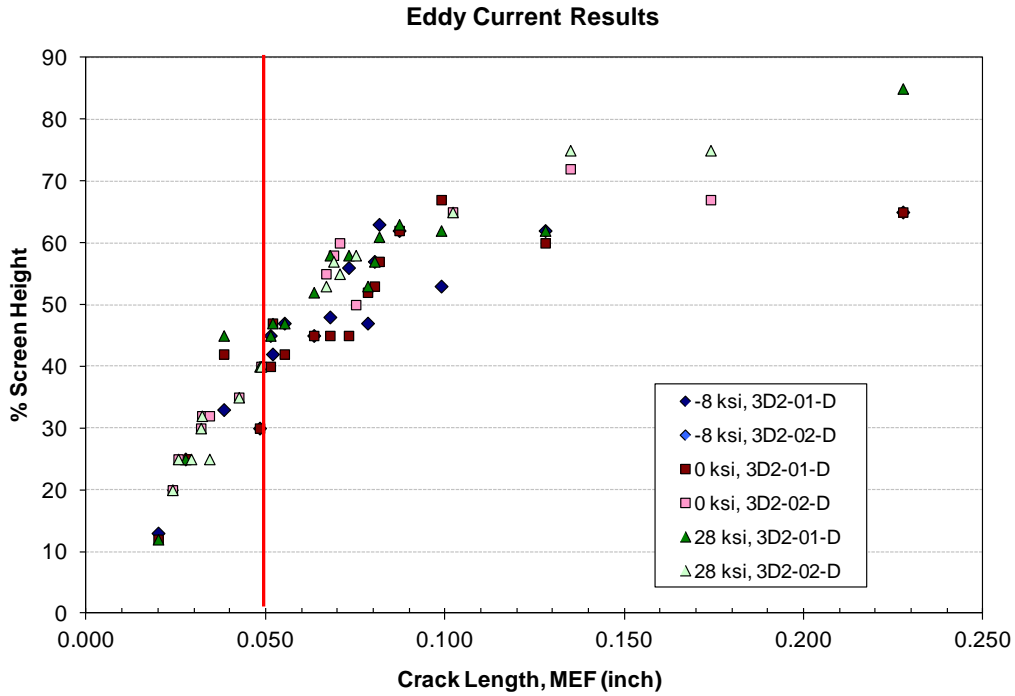


Figure 9.2-17. Bolt Hole ET Results: CX Then Fatigue

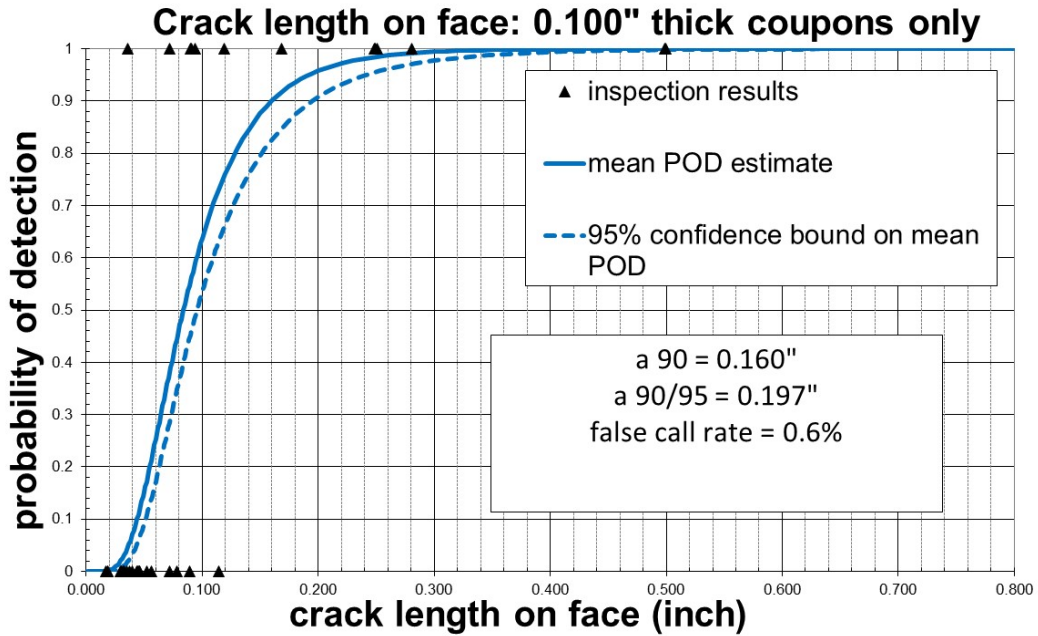


Figure 9.2-18. PoD for UT Shear Wave

9.2.5. Evaluation of NDE Methods as Applied to Metallic Honeycomb Structures

Nathan Smith, Sabyasachi Basu, and Donald Palmer, Jr., The Boeing Company – Research & Technology

Structures Bulletin EN-SB-08-012, “Nondestructive Inspection Capability Guidelines for United States Air Force Aircraft Structures,” defines the detectable flaw sizes for common aircraft materials and geometries when using surface inspection methods such as eddy current, fluorescent penetrant inspection, and magneto optical imaging (MOI). It provides flaw sizes that should be assumed when computing the re-inspection intervals for structures managed by the Air Force Aircraft Structural Integrity Program (ASIP) when no other supporting data is available. Due to the great variety of construction materials, flaw types, and inspection methods involved in honeycomb inspection (Figure 9.2-19), general probability of detection (POD) data has not been developed. Boeing and the U.S. Air Force are currently developing a quantitative NDE capability analysis and a POD study for detection of disbonds in aluminum skin/aluminum honeycomb core structures. This effort will identify the inspection methods currently used to examine honeycomb structures (Figures 9.2-20 through 9.2-25), assess the capability of different inspection methods, identify the best-practice design/manufacturing processes for honeycomb reference standards, and execute a POD study for down-selected inspection solutions as applied to metallic honeycomb structures. This effort will review the progress to date, focusing on establishment of variables, sensitivity analysis associated with a number of applicable NDE methods, and a discussion of the POD design of experiments approach.

- Fatigue cracks (or tears) form relatively quickly in the crumpled portion of the core directly below the adhesive
- Tears connect together to essentially form a “disbond” (but with the adhesive and a little bit of core still attached to the skin)
- Damage self arrests at the edge of the crushed area

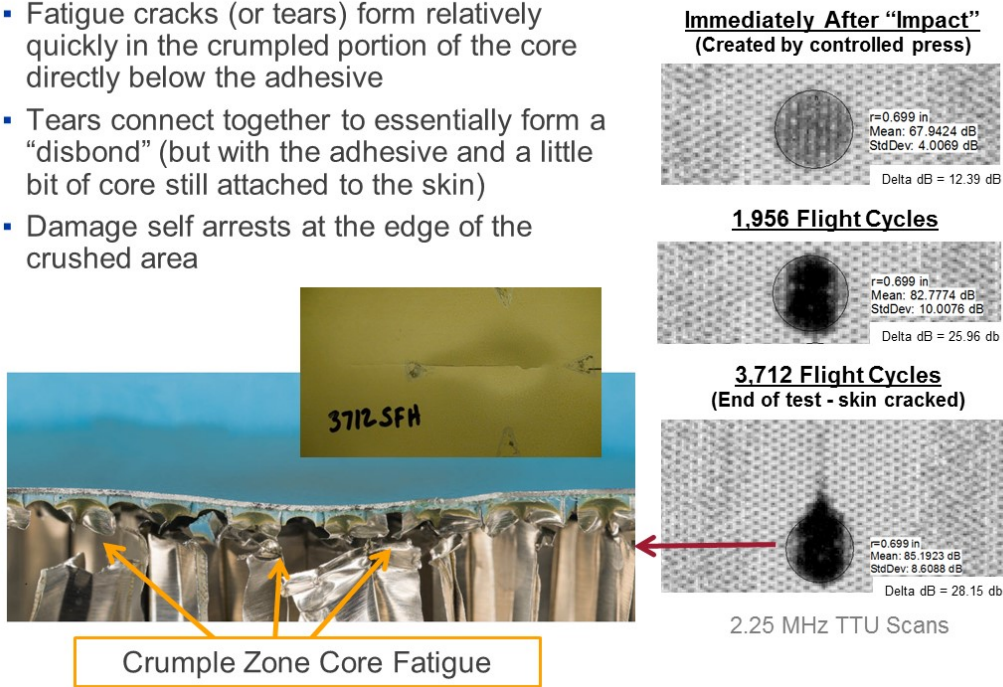
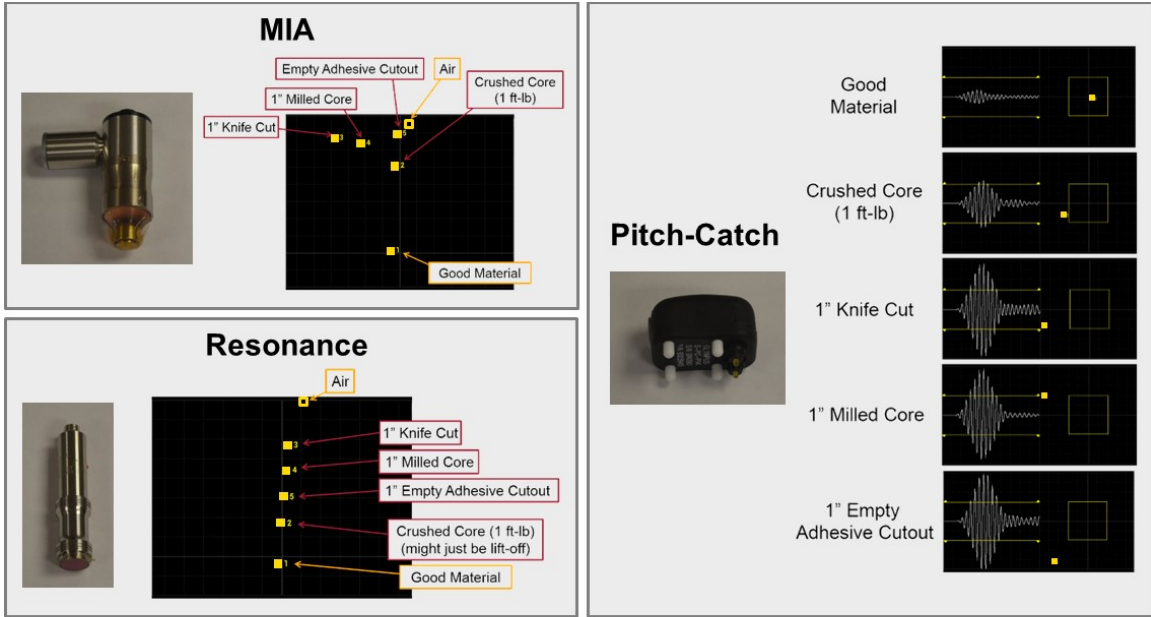
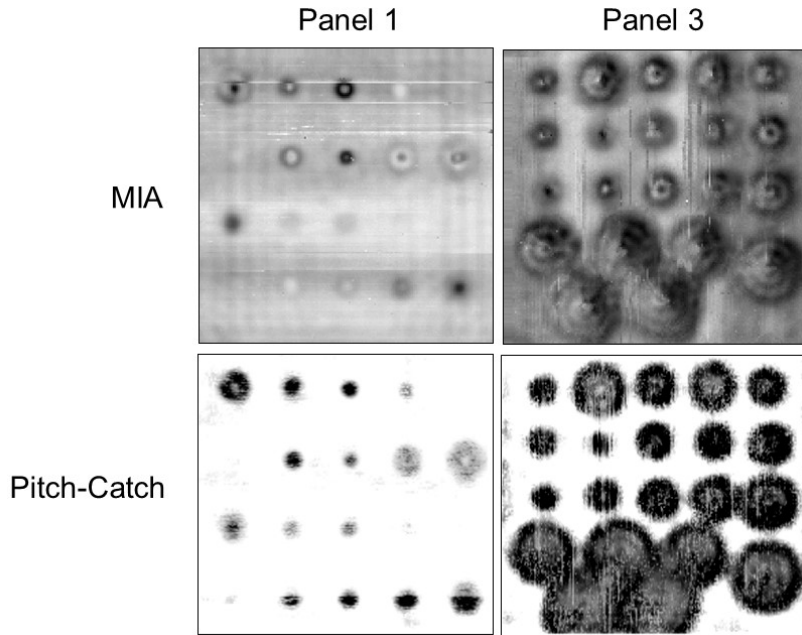


Figure 9.2-19. Crumple Zone Core Fatigue



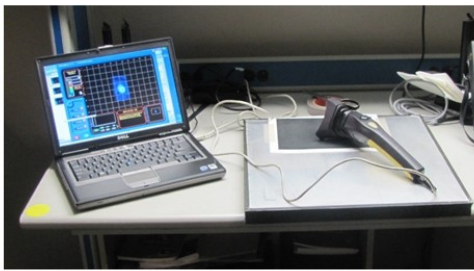
- None of the flaws were detected in the 0.080” panels
- All three modes are capable of detecting the flaws in the .025” panel

Figure 9.2-20. Handheld Bond Testers



- Collecting C-scan data improves detection
- Example scans collected with Boeing MAUS, but Olympus OmniScan or NDT Systems BondHub are other options

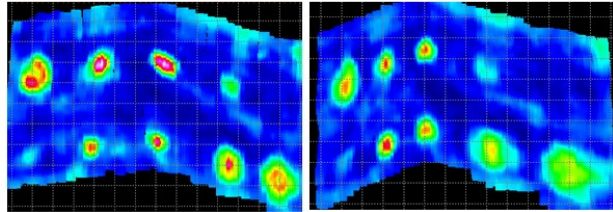
Figure 9.2-21. C-Scan Bond Testers



0.080" Skin Panel

Near Side Flaws

Far Side Flaws



- Developed by CSIRO in Australia in collaboration with Boeing
- Gates on frequency domain of signal rather than time domain
- Excellent detection of most flaws from near side and far side in both the .025" panels and the .080" panels
- Not commercially available
- Optical encoder is not very accurate

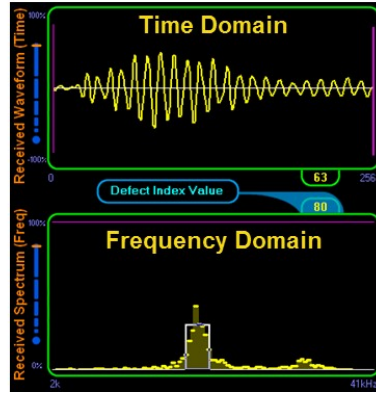
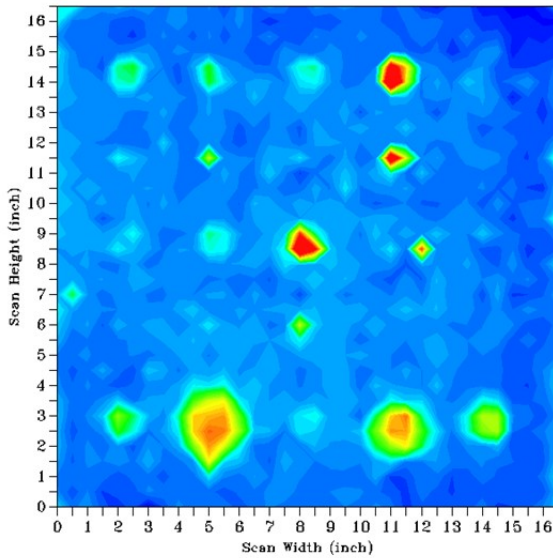


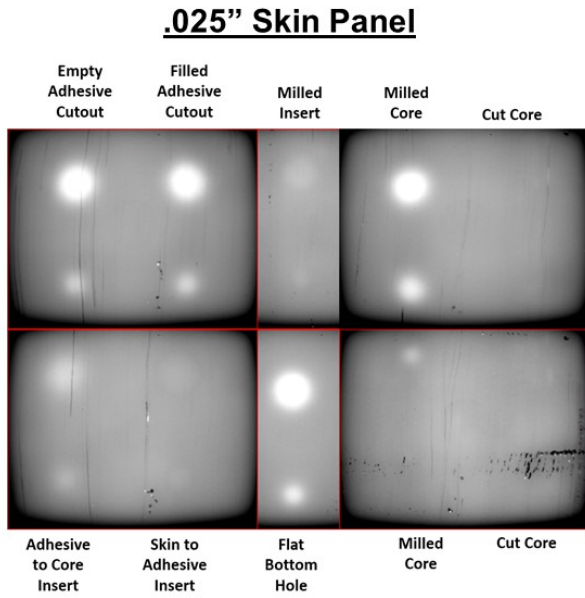
Figure 9.2-22. Bandicoot Pitch-Catch Bond Tester

.025" Skin Panel



- Measures contact time of each tap, which is dependent on the stiffness of the material
- Detected larger impact damage and milled core flaws in .080" panel

Figure 9.2-23. Computer Aided Tap Tester

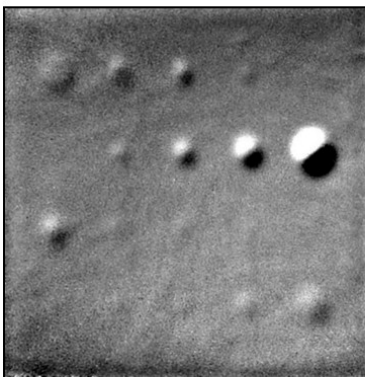


- Images collected with black water washable paint on panel to eliminate reflection
- Did not detect damage where some honeycomb stayed bonded to skin (impact damage and knife cuts)

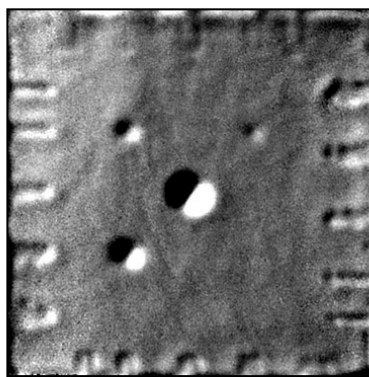
Figure 9.2-24. Flash Thermography



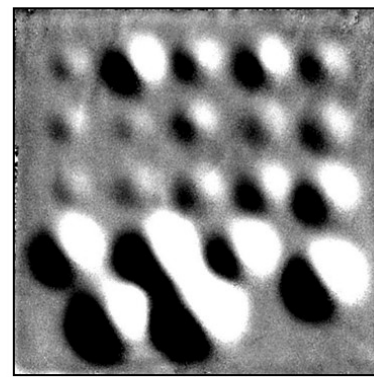
- Shearing image interferometer captures first derivative of out-of-plane deformation due to vacuum stressing
- Data collected at LTI in Norristown, PA
- Detected most of the flaw types in the .080" panels
- No surface preparation
- Requires removal of the part from the aircraft



Engineered Defect Panel #1



Engineered Defect Panel #2



Engineered Defect Panel #3
(Impact Damage)

Figure 9.2-25. Shearography (Vacuum Chamber)

9.2.6. Hidden Fatigue Crack Detection in Multi-Layer Aircraft Structures Using High Frequency Guided Ultrasonic Waves

Paul Fromme, University College-London, UK

Widespread fatigue damage, developing especially at fasteners due to the stress concentration, represents an important problem for ageing aircraft. As for aerospace structures where the areas of high stress are known, high frequency guided ultrasonic waves offer a trade-off between monitoring range and improved sensitivity for small defects. For multi-layered aircraft structures, high frequency guided ultrasonic wave modes have been shown to be sensitive for the detection of corrosion, hidden notches, and fatigue cracks.

The considered uniform multi-layer component consists of two 3 mm thick aluminum alloy plates (2014-T6) with a 0.25 mm thick sealant layer (Hysol EA 9394). Fatigue crack growth in one of the aluminum layers at a fastener hole (1/4 inch, 6.35 mm) was induced using tensile cyclic loading in a servo-hydraulic testing machine and the resulting crack area was measured optically. Typical photographs of the observed fatigue crack growth are shown in Figure 9.2-26. During fatigue testing, the crack grew quarter-elliptically from the starter notch position. No cracking of the other aluminum plate was observed. For all ultrasonic measurements, the excitation transducer was a half inch piezoelectric transducer with 1 MHz centre frequency, mounted on a 90° angle beam Perspex wedge. The wedge was clamped to the specimen on the top surface at a distance of 225 mm from the fastener hole, so that the main wave propagation line crosses the center of the hole (Figure 9.2-26).

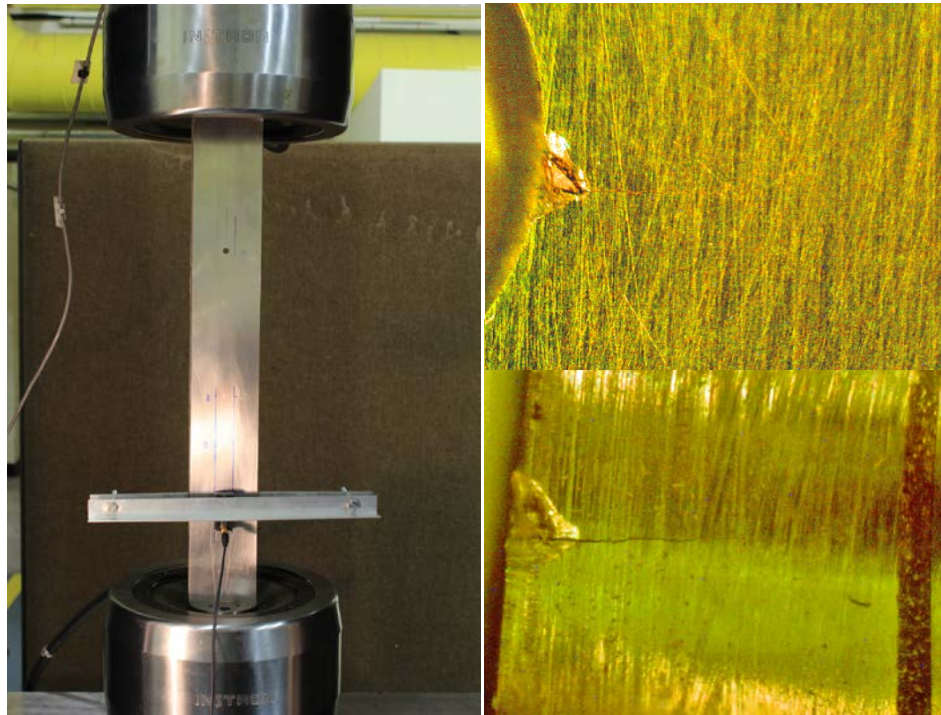


Figure 9.2-26. Specimen with Wedge Transducer in Clamps of Hydraulic Testing Machine (Left); Microscopy Photographs of Part-Thickness Fatigue Crack: Specimen Surface (Right, Top), Hole Interior (Right, Bottom)

Fatigue crack growth was monitored for 5 specimens during cyclic loading using noncontact laser measurements. The laser spot was placed on the damaged specimen surface approximately 1 mm behind the expected crack location and 1 mm from the fastener hole. In order to quantify the changes in the

guided wave pulse due to the developing fatigue crack, the energy of the time-gated first pulse was calculated. The changes in energy ratio with crack area were plotted against each other, showing an initial variation, increase in energy for a quarter-elliptical crack and subsequent drop with increasing crack area (Figure 9.2-27). Taking a safe criterion to reliably call a fatigue crack, a minimum drop in amplitude of 25% was specified (twice the observed variation). For all specimens, a larger drop than 25% was observed for a maximum crack area of 2.33 mm^2 , corresponding to a quarter-elliptical crack with 1.74 mm length and 1.34 mm depth. In principle, a shorter fatigue crack with an area of less than 0.6 mm^2 could be called for the observed initial amplitude increase.

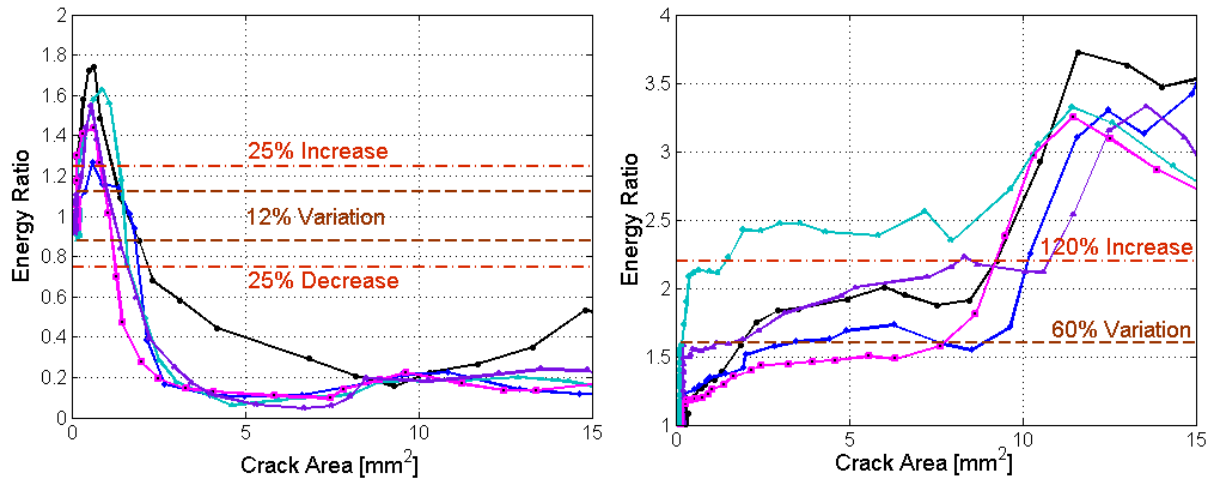


Figure 9.2-27. Left: Energy Ratio of Laser Measurement Close to Fastener Hole and Fatigue Crack for 5 Specimens Plotted Against Optically Measured Crack Area; 12% Variation Before Crack Visible and 25% Increase/Decrease in Energy Ratio Marked. Right: Energy Ratio of P/E Pulse Reflected at Fastener Hole and Fatigue Crack for 5 Specimens Plotted Against Optically Measured Crack Area; 60% Variation Before Crack Visible and 120% Increase in Energy Ratio Marked

The potential and sensitivity for the detection and monitoring of hidden fatigue cracks without local access to the fastener hole was studied to investigate the potential for SHM applications. The wedge transducer placed at a stand-off distance of 225 mm on the top specimen surface (opposite layer to fatigue crack) was driven using a standard ultrasonic pulser-receiver and the P/E signal recorded and evaluated. This was done for five tensile specimens, a sharp increase to an energy ratio of at least 3 was observed for all specimens when the crack through the bottom aluminum layer had grown to a length of at least 3.5 mm. The energy ratio versus crack area is shown in Figure 9.2-27 with an initial energy variation of up to 60%. Taking similar criteria for crack detection as for the laser measurements, a threshold of a 120% change in energy ratio was set. The largest crack area of 11.5 mm^2 for this corresponds to a crack length of 3.83 mm through the bottom aluminum layer and coincides with the observed sharp increase in energy ratio for all specimens.

The possibility of detection for hidden (2nd layer) fatigue cracks from a stand-off distance without access to the damaged specimen side was verified using standard ultrasonic pulse-echo equipment. Fatigue cracks that had grown through the thickness of the bottom aluminum layer could be reliably detected from a stand-off distance as an additional scattered guided ultrasonic wave pulse lead to a significant increase in reflected wave energy well above the experimental variations.

Chan, H., Masserey B. and Fromme, P., "High frequency guided ultrasonic waves for hidden fatigue crack growth monitoring in multi-layer model aerospace structures," *Smart Mater. Struct.* 24, 025037 (2015)

9.3. STRUCTURAL HEALTH MONITORING

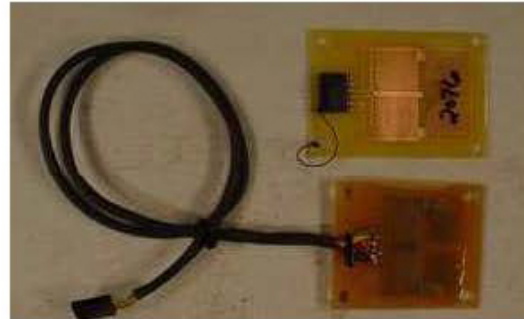
9.3.1. The State of Nondestructive Evaluation and Structural Health Monitoring

Eric Lindgren, John Brausch, Charles Buynak, and Matthew Leonard, USAF Research Laboratory – Materials and Manufacturing Directorate; and Pamela Kobryn, USAF Research Laboratory – Aerospace Systems Directorate

The capability to detect damage, such as fatigue cracks and corrosion, using nondestructive techniques is one of many required inputs to the United States Air Force (USAF) Aircraft Structural Integrity Program (ASIP) to ensure structural safety. Development and maturation of new methods to detect damage continues at a steady pace and recent focus has been on new techniques to perform nondestructive inspections (NDI) and structural health monitoring (SHM) where sensors are permanently attached to an aircraft (Figure 9.3-1). In addition, there have been renewed research and development efforts in sensors that monitor environmental conditions, such as relative humidity and coating degradation that are also generally referred to as corrosion sensors. Increased attention to this technical area has occurred due to significant investment in the development and refinement of new SHM capabilities over the past few years. This technical effort reviews the current state-of-the-art in the technical areas of damage detection (Figure 9.3-2) and in-situ corrosion monitoring (Figure 9.3-3) with a focus on ASIP applications. New capabilities, existing technical gaps, and current / planned projects within the Air Force Research Laboratory to address the evolution of these capabilities will be reviewed. The primary objective of this technical effort is to provide information and awareness of the potential opportunities to implement new and maturing damage detection capabilities within the next five years. Therefore, the information is intended to function as reference to all entities exploring the potential to use new NDI/SHM technologies to decrease the time and cost for ASIP driven inspections.



a) Active Damage Detection Sensor



b) Environmental Sensing Sensor

Figure 9.3-1. On-Board Sensing



a) Representative Sensor



b) Hot-Spots-Sensor Test

Figure 9.3-2. Damage Detection Sensors



a) Representative Environmental Sensor



b) Representative Linear Polarization Resistance (LPR) Sensor

Figure 9.3-3. Environmental Sensors

9.3.2. SHM System Readiness for Damage Detection on Aging Aircraft

Amrita Kumar, Roy Ikegami, Irene Li, David C. Zhang, Sang Jun Lee, Howard Chung, Franklin Li, and Cas Cheung – Acellent Technologies, Inc.

Safety, reliability, and sustainment costs are of great concern for aging aircraft. With many aircraft within the Air Force becoming older there is a need to inspect for fatigue cracks and corrosion in metallic aircraft structures. A major drawback of conventional NDI methods of inspection is that access to at least one side of the structure is required. This can require that the aircraft be removed from service and the structure disassembled for inspection, which can lead to a host of additional problems. Recent advances in structural health monitoring (SHM) have enabled new developments to enhance current NDI methods to facilitate the inspection of structural components that are difficult to access. Acellent Technologies has developed reliable SHM systems utilizing permanently installed sensor layers, off-board data acquisition hardware, and software for data analysis and 3D display of diagnostic results (Figure 9.3-4). This technical activity discusses the SMART Patch system (Figure 9.3-5) including sensor installation on aircraft, durability for airworthiness and probability of detection (POD) (Figure 9.3-

6) of damage such as fatigue cracks (Figure 9.3-7) and corrosion (Figure 9.3-8) especially in areas that are difficult to access without disassembling aircraft structure. The results from two Phase II SBIR projects performed by Acellent for the US Air Force to develop SHM systems to detect pitting corrosion damage in a multilayer joint in the wing cord structure for the F-15 aircraft and stress corrosion cracking in the rear flap structure of the KC-135 aircraft will be presented. Additionally, results from a BAA project performed for the Army to detect fatigue cracking in riveted joints on a military rotorcraft tailboom structure (Figure 9.3-9) will be presented to demonstrate the performance and reliability of Acellent’s SHM systems under extreme environmental and operational conditions. The mature SHM systems ready for implementation and use in the field will be discussed along with technology readiness information. This technical activity will also discuss the challenges involved in the transition of this technology to the field including issues concerned with installation of the sensors and design and testing of a new portable handheld device for data acquisition and analysis. Results of the validation testing conducted with the system on simple and complex components will be discussed along with practical issues concerning the implementation and use of the system on aircraft structures.

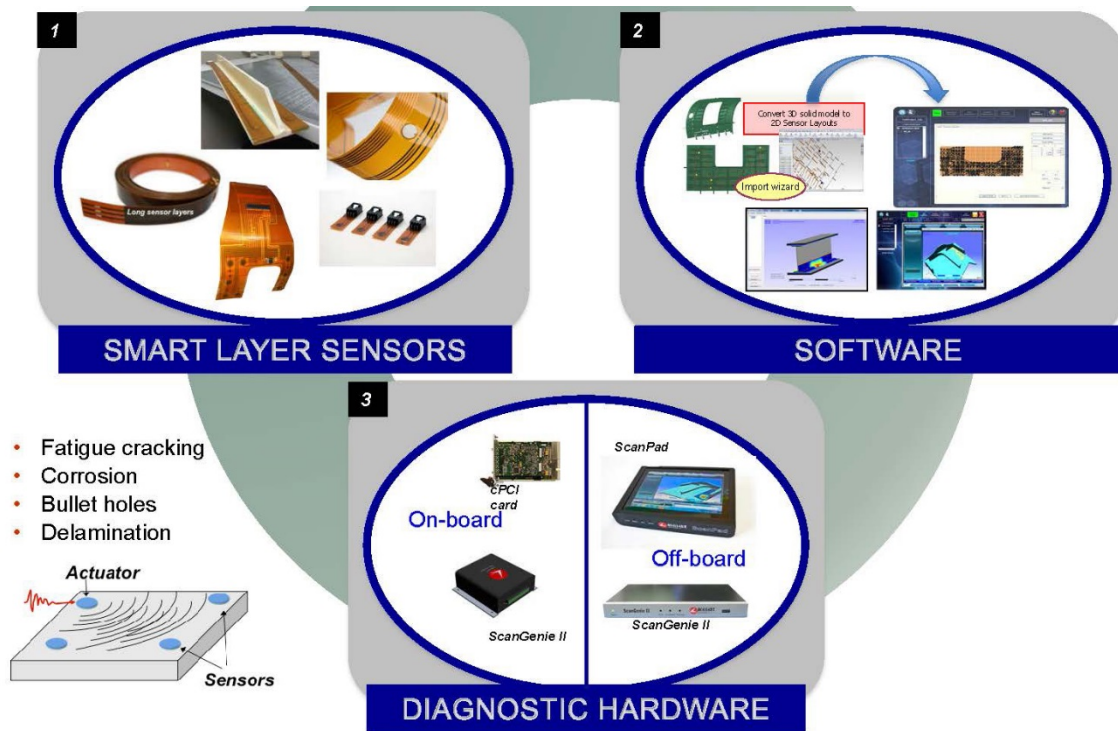


Figure 9.3-4. SHM System Solution for Active Damage Detection



Figure 9.3-5. SMART Patch System

- SHM POD generation for the **known** damage location & the **known** damage growth direction

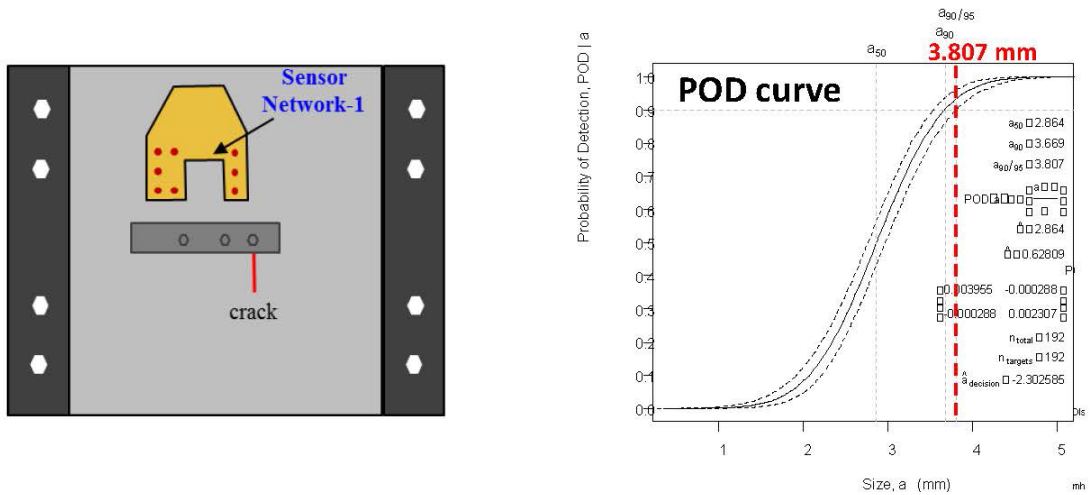


Figure 9.3-6. SHM POD Result

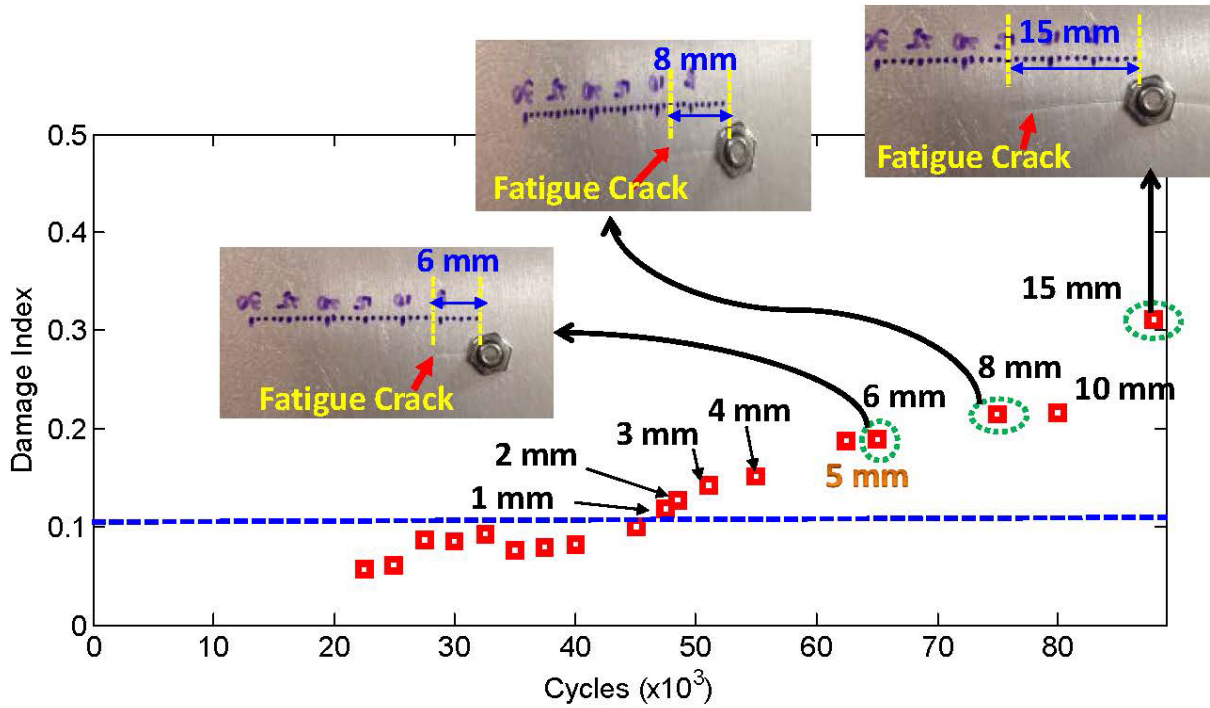


Figure 9.3-7. Fatigue Crack Detection

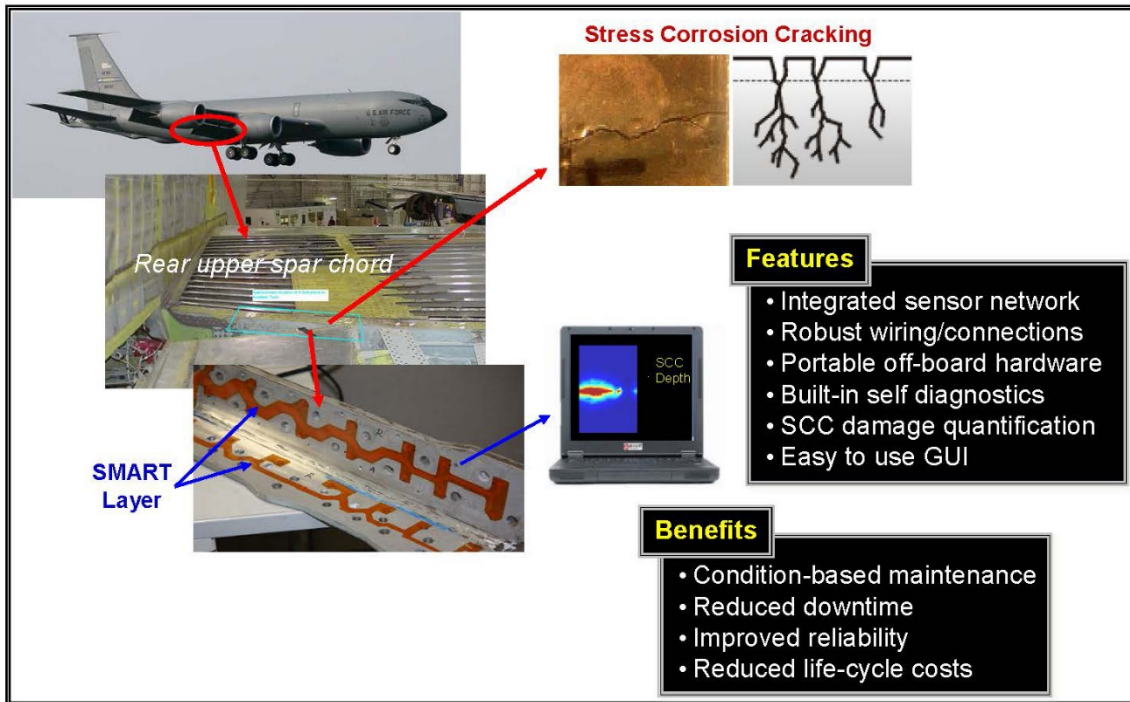


Figure 9.3-8. Stress Corrosion Cracking Detection

Targeted Application:

Aft most rivet securing the tail rotor driveshaft cover left hand support

**Current inspection criteria:**

10 hr inspection - Visual inspection with 10x power magnifying glass
or
20 hr inspection - NDI (eddy current or dye penetrant)

Approx. time taken per inspection: 1 hr

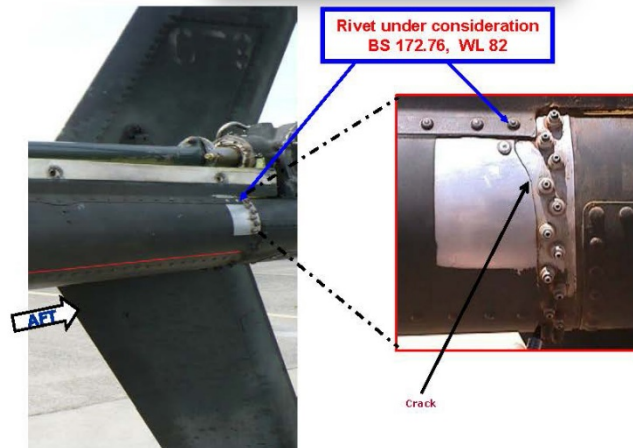


Figure 9.3-9. OH-58D Tailboom

9.3.3. The Environmental Severity Index and Its Applications

William Abbott, Battelle Memorial Labs

The term Environmental Severity Index (ESI) is at least 10 years old. It is in reality nothing more than a measure of how corrosive a local environment is. This could be measured either in terms of absolute corrosion rates or in relative terms such as one base against another. Historically the main and practical use of ESI has been for the establishment of wash intervals for assets such as aircraft and Ground Support Equipment (GSE). These requirements are set forth in T.O. 1-1-691 and divide basing environments into categories of Mild, Moderate, and Severe. Over the last decade or more an increasing amount of work has been done in the field to directly measure corrosion rates using rather simple, portable, coupon monitoring techniques (Figures 9.3-10 and 9.3-11). The general approach has been to assemble monitoring packages in the lab, mail to a local POC, and replace samples at about 3 month intervals over the course of at least 1 year. This work has proven to be very successful with sample loss rates of less than 1%. As a result, data have now been obtained at hundreds of military sites worldwide. Databases are available for the corrosion rates of low carbon steel, copper, and 3 aluminum alloys (2024, 7075, and 6061) plus values for atmospheric chlorides as determined from a unique sensing method involving silver coupons. These data are freely available to the public in two forms via the DOD Corrosion Exchange website. One is in tables contained in a book written by this author. The second is in the same data embedded within the software for corrosion algorithms developed from the same data (Figure 9.3-12). The latter is of particular significance since the same software allows for predictions of corrosion rates for locations for which corrosion rate measurements have not been made but for which weather data should be available. Fortunately, this includes most operational airfields. The question arises whether the ESI concept can be used more broadly than its traditional use. A related question is whether ESI can be measured in different ways and in particular on operational assets such as aircraft for decision-making purposes (Figure 9.3-13). The answer to both of these questions is Yes. Early studies have shown that there is a good correlation between basing ESI values for aircraft (Figure 9.3-14) and

corrosion-related maintenance (Figure 9.3-15). Then the measurement of ESI has been taken to more relevant and precise levels through the use of simple corrosion sensors which have been flight tested on a wide range of operational aircraft. This technique appears to offer a potential basis for more precise tracking of individual aircraft for CBM purposes as well as early warning of adverse conditions in known “hot spots”. Examples of results from flight tests will be shown along with other examples of the use of ESI in the evaluation of new, non-chrome paint systems.

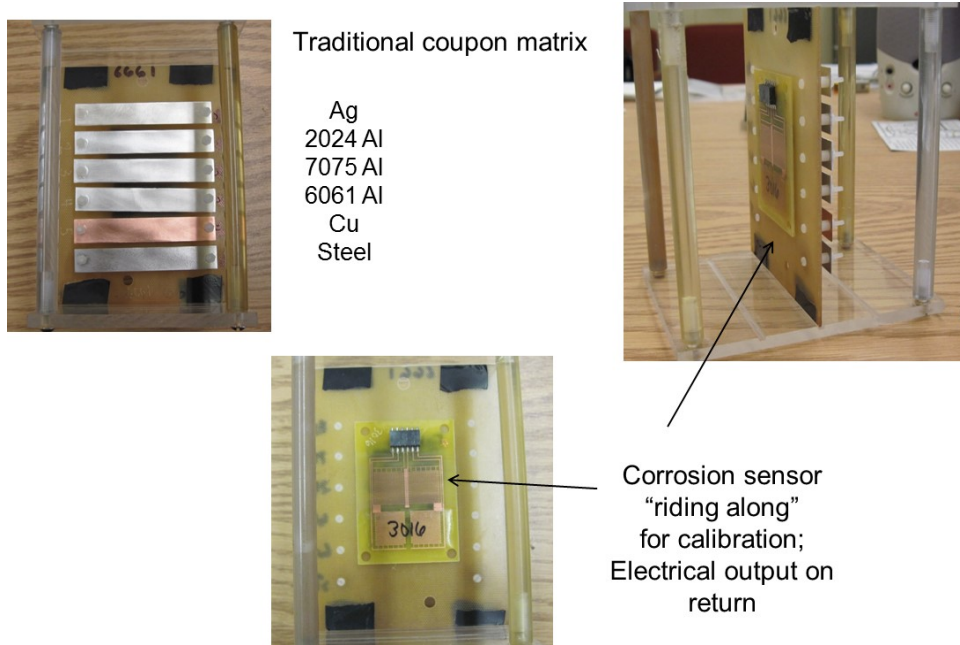


Figure 9.3-10. Coupons and Sensors for Field Deployment

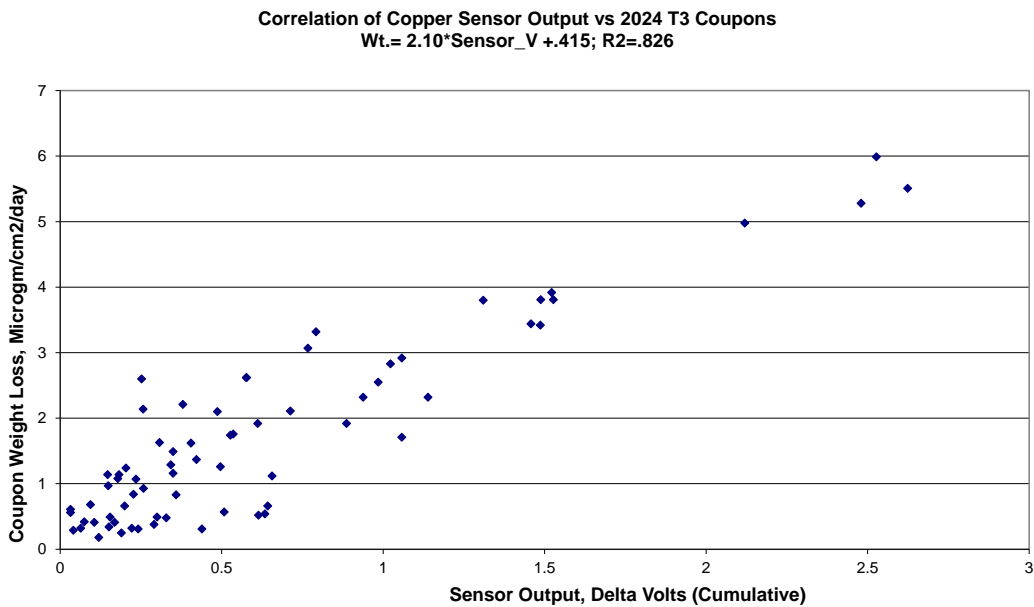
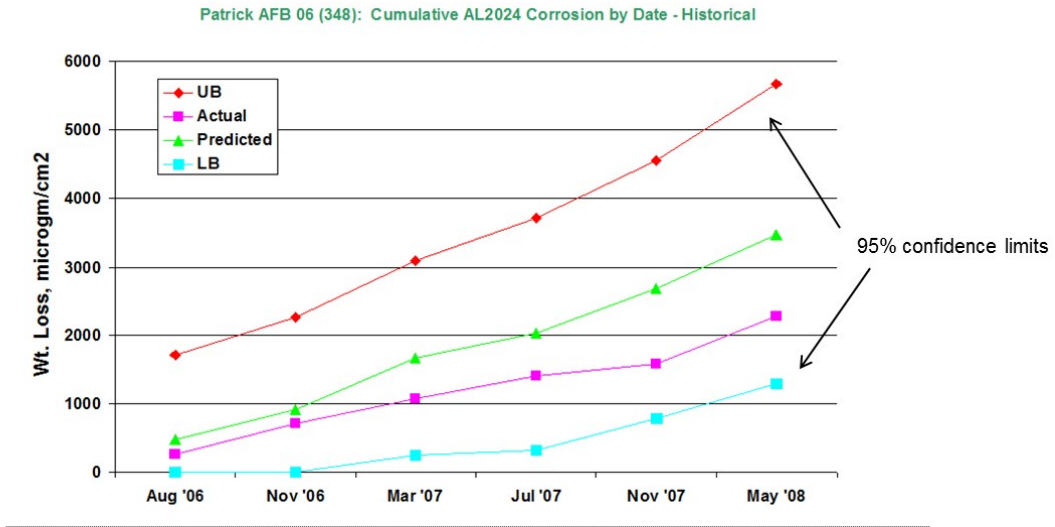


Figure 9.3-11. Sensor Output Calibration Statistics: 2024 Al vs. Copper

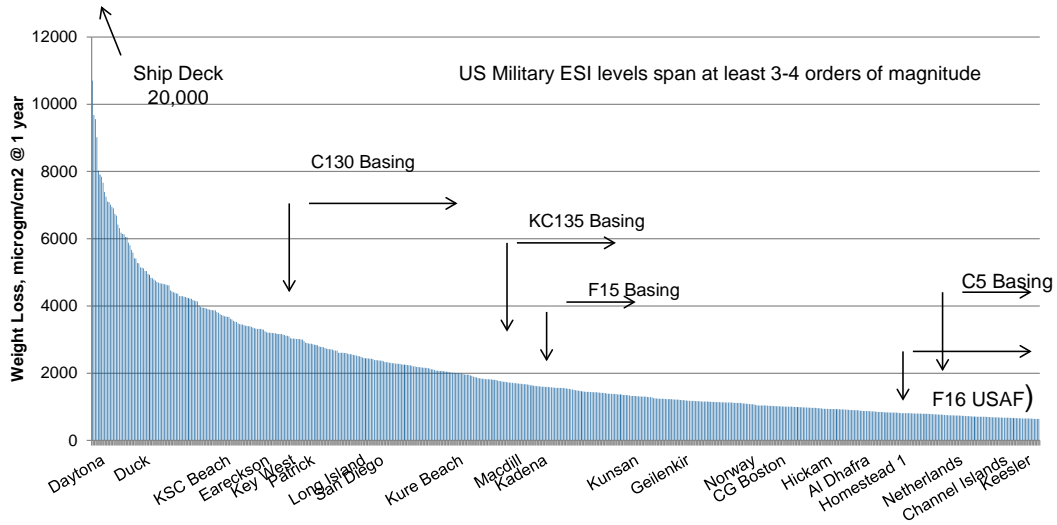


Similar Graphical Displays for All locations for Which Monitoring Done
Also Predictions are possible for non-monitored locations if weather data available

Figure 9.3-12. Example of Output from Corrosion Algorithm for 2024-T3 Al at Patrick AFB

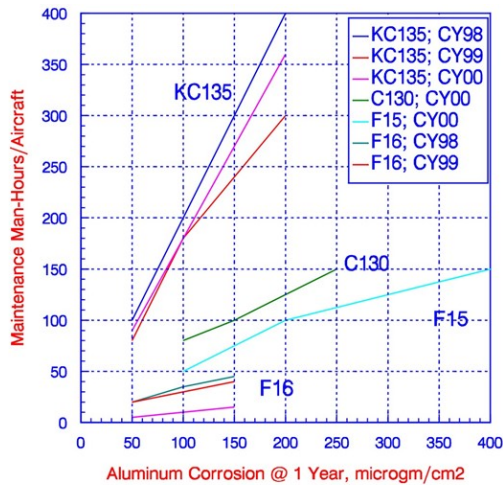


Figure 9.3-13. Examples for Flight Installations of Sensors



Severity Distributions Are Unique to Each MDS Aircraft
 Some Fleets are Based In Mild Environments
 Knowledge of ESI Distributions Important For Decisions
 Exposures of Materials In Harsh Environments May Represent Accelerated Test

Figure 9.3-14. ESI Data Distribution Among Worldwide Military Bases and Test Sites



Base level corrosion labor -- REMIS
 Corrosion rate data from Battelle

Magnitude and slopes may reflect effects of both surface area and corrosion susceptibility of specific weapons system

Conclusion
 Cumulative severity may control corrosion maintenance

Generally good correlation between basing ESI and base level maintenance with some exceptions

Figure 9.3-15. Relation of Basing Severity (ESI) to Corrosion-Related Maintenance by MDS

9.3.4. Embedded Structural Health Monitoring System Development and Testing for Fatigue Crack Detection of Rotorcraft Structures

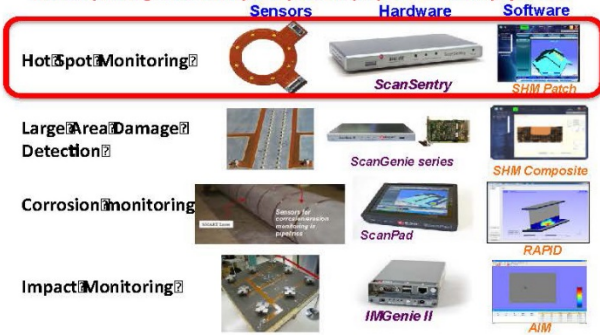
Sang Jun Lee, Amrita Kumar and David Zhang, Acellent Technologies, Inc.; Andrew Brookhart, Sikorsky Aircraft Company; Nathaniel Bordick, USA – Aviation Development Directorate

Sikorsky Aircraft Corporation (SAC) and the United States Army Aviation Development Directorate- Aviation Applied Technology Directorate (ADD-AATD) have jointly funded the Capability-Based Operations and Sustainment Technology – Aviation (COST-A) Program to develop and demonstrate an integrated set of diagnostic, prognostics, and system health assessment technologies for rotorcraft, including structural health monitoring (SHM), to reduce maintenance burden while maintaining safety. Current airframe maintenance processes rely heavily on manual inspection practices, leading to an expensive and time-consuming process to inspect enclosed compartments and structural fatigue hotspots. As part of the COST-A airframe system focus, SAC and Acellent Technologies, Inc. have teamed to develop an embedded fatigue damage detection capability. When considering an embedded SHM solution, the potential benefit may be inhibited by the potentially wide range of environmental and loading conditions to which the aircraft may be exposed. Additionally, the weight and size constraints for an embedded application pose challenges to conventional NDI and SHM approaches. The COST-A team developed a system (Figure 9.3-16), comprised of physical transducers (Figure 9.3-17), diagnostic hardware (Figure 9.3-18) and damage detection software, to address these challenges and constraints. The system was developed with a focus on providing important maintenance information at the appropriate time, and thus both on-board and off-board software components support the integrated system sensors and diagnostic hardware. The technical activity will present the approach and key challenges faced in the system development effort and results from both risk reduction (Figure 9.3-19) and system validation testing (Figure 9.3-20). Under the COST-A effort, a diagnostic hardware redesign effort was conducted, with specific attention paid to weight/size, power and communications architecture for an embedded diagnostic system. Additional system development activity was focused on developing methods for collecting high-value data in a varying environment, specifically using a combination of signal processing and collection procedures to minimize the effect of varying temperature and loads on the sensor response. Results of risk-reduction (Figure 9.3-21) and full-scale testing performed to validate the system setup and performance will also be presented. Risk-reduction testing was performed using representative stiffened-skin-test panels, tested in fatigue with varied ambient temperature and load states. Finally, full-scale airframe subassembly testing was conducted using a UH-60A cabin upper deck test article to validate the developed system. Data from that test were analyzed in a blind fashion and will be presented with test inspection and reference measurements. The technical activity will focus on hardware and software development of the embedded fatigue-damage-detection system, presenting results from risk-reduction and full-scale testing on a rotorcraft cabin section. Overall, the system was shown to accurately detect and track fatigue damage in representative and actual rotorcraft structural components, even with changing environmental conditions.

Accellent Technologies Inc.

- ✓ Global leader providing customized Structural Health Management solutions to a wide variety of industries.
- ✓ Damage/crack detection,
- ✓ Corrosion monitoring,
- ✓ Impact detection/monitoring,
- ✓ Structural state sensing & Prognostics
- ✓ Certified in AS9100:2004 Aerospace Standards and ISO9001:2008

Active (damage detection) and passive (impact detection) systems



Core components of SHM system

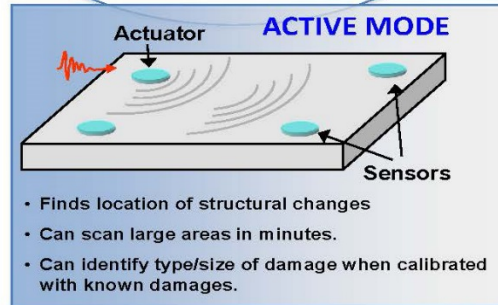


Figure 9.3-16. Accellent’s SHM System

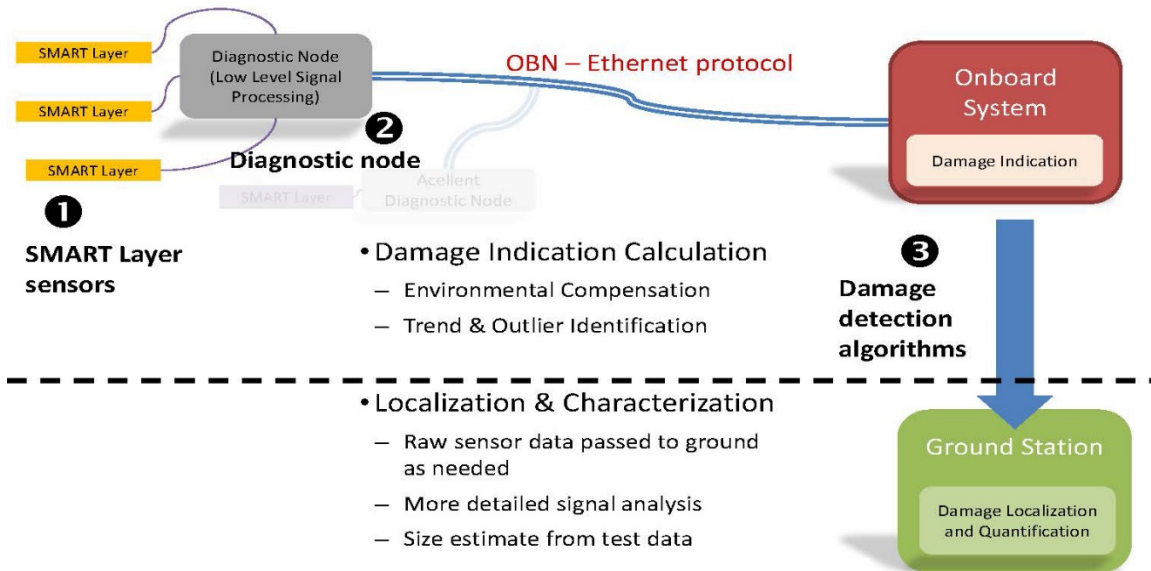


Figure 9.3-17. Fatigue Crack Monitoring Configuration for COST-A

- Trade study was performed on the system architecture, communication interface, number of channels, hardware weight and size and power consumption.
- Trade study testing results determined required hardware design parameters
- Focus on maintaining detection capability for rotorcraft structural component class
- Designed for aircraft physical conditions / problems and optimized for embedded application
- Distributed H/W
- Centralized S/W

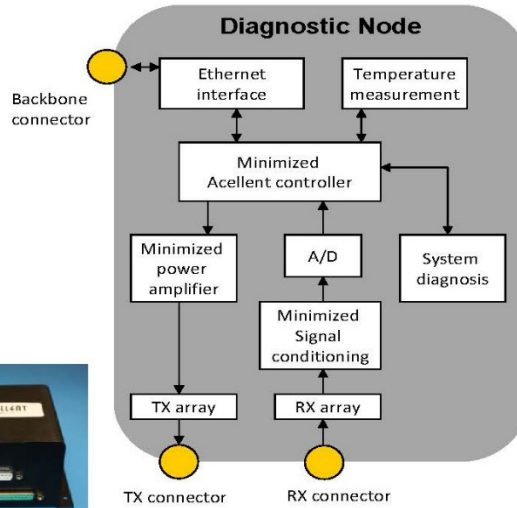
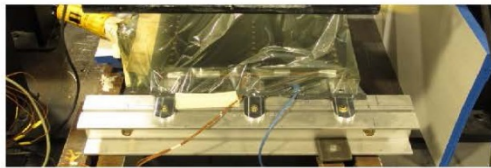
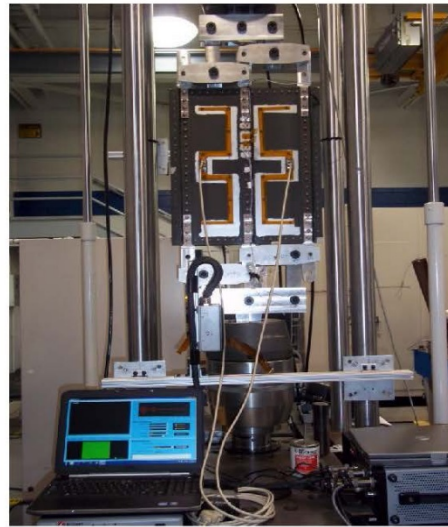


Figure 9.3-18. Diagnostic Hardware

- **Representative stiffened panel test article fabricated**
- **Fatigue Loading (load controlled):**
 - Initiation: Constant Amplitude
 - Growth: Constant Amplitude
- **Temperature Application Method**
 - Heat guns utilized with insulating enclosure
- **Applied Temperature**
 - Range: 70-130 deg F



Temperature Testing Setup



Fatigue Test Setup

Figure 9.3-19. Risk-Reduction Testing: Test Configuration

- Sensor layout for Subassembly tests:
 - 31 Acellent sensors installed in aft main gearbox mount zone
 - 22 Acellent sensors were focused near fatigue critical region in the aft main gearbox

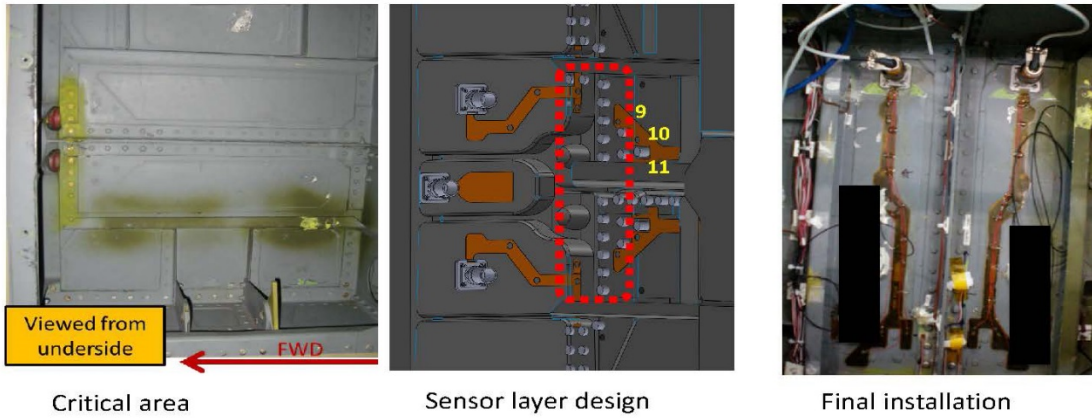


Figure 9.3-20. System Validation Tests: Sensor Layout

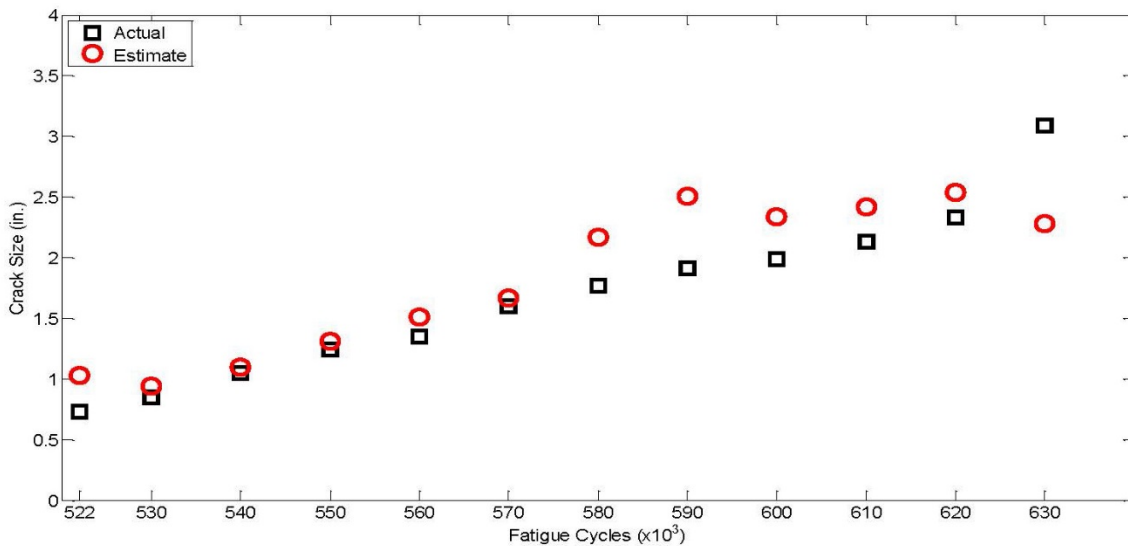


Figure 9.3-21. Risk Reduction Subcomponent Testing: Damage Quantification

9.3.5. Quantification of Structural Health Monitoring for Damage Detection

Fotis Kopsaftopoulos and Fu-Kuo Chang, Stanford University; Vishnu Janapati, Sang Jun Lee, and Frank Li, Acellent Technologies, Inc.

Structural health monitoring (SHM) technology offers a new approach to interrogate the integrity of structures in real-time or on demand without physically disassembling the structures, unlike traditional inspection techniques such as Non-destructive Inspection (NDI) which require structural disassembly as well as a human to perform the inspection. SHM uses permanently mounted sensors to gather data from structures (Figure 9.3-22) while typical NDI methods utilize removable probes to gather data. Both SHM and NDI may share the same physics for structural integrity detection during operation, however, there

clearly exist fundamentally different engineering disciplines in these two approaches. In order to transition SHM from R&D to field implementation, the reliability of the technique must be demonstrated and quantified using acceptable established procedures used by the industry. Probability of detection (POD) is a well-accepted measurement method to quantify NDI results (Figures 9.3-23 and 9.3-24). This technical activity will examine the similarities and differences between traditional ultrasound methods and Lamb-wave based SHM techniques, and will identify key areas where reliability assessment of SHM may be different from traditional NDI. Extensive studies on various cases with numerical simulations, test data, and analytical results were performed to evaluate the quantification results from structural health monitoring techniques. Appropriate procedures for evaluating the detection capability of SHM are proposed. It is anticipated that more studies will be needed to generate data to validate the procedures.

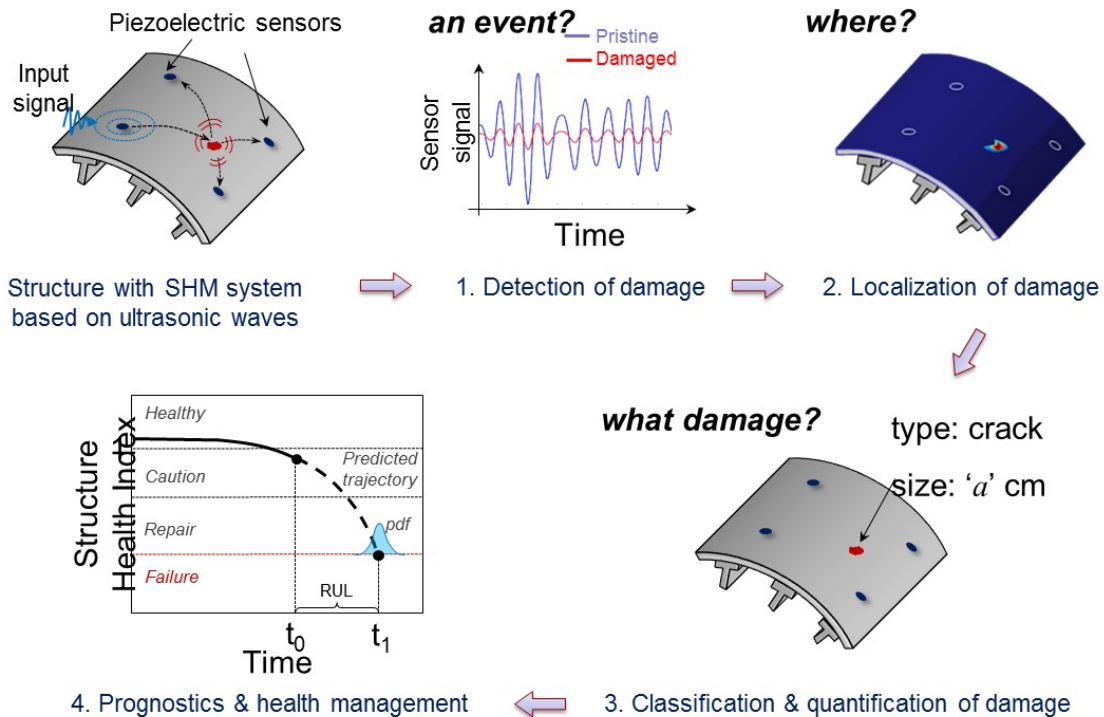


Figure 9.3-22. How an SHM System Works

- POD for NDE techniques
 - *Established method (MIL-HDBK-1823A)*
 - *Controlled experiments under fixed environments*
 - *A number of test specimens and operators are needed*

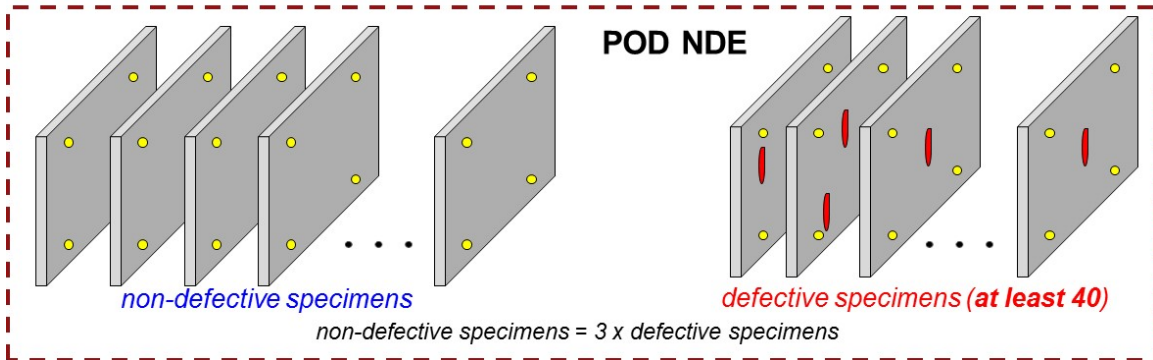


Figure 9.3-23. Probability of Detection for NDE

Main theoretical assumptions for NDE POD:

- *Uniform variance in the DIs for all the damage sizes*
- *Uncorrelated (independent) observations*
- *Linearity of the parameters*
- *Normally distributed errors*

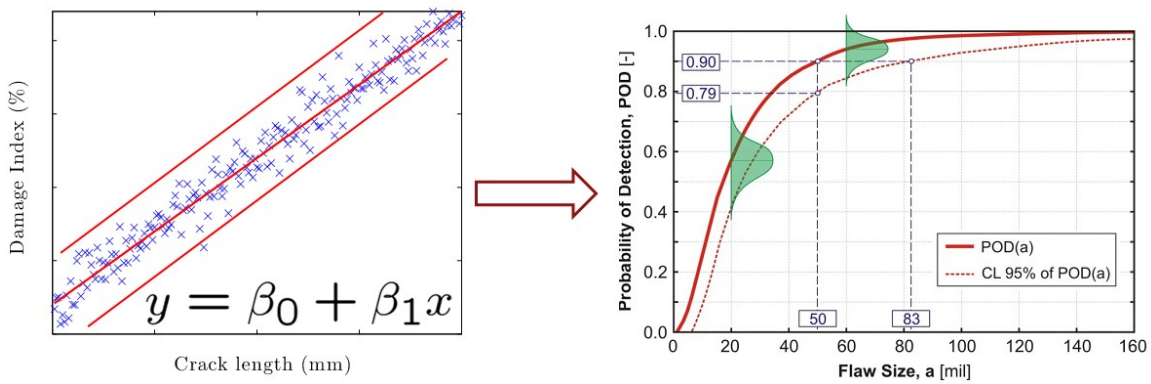


Figure 9.3-24. POD Assumptions

9.3.6. Concept of Operations for Corrosion Environment Sensors (aka Corrosion Sensors)

Eric Lindgren, John Brausch and Charles Buynak, USAF Research Laboratory – Materials and Manufacturing Directorate; David Forsyth, TRI/Austin, Inc.; Thomas Mills, APES, Inc.

Current USAF corrosion management processes focus on time-based inspections and remediating any corrosion when it is found. While this approach has contributed to the exceptional safety record of USAF aircraft, it is recognized to have a significant associated cost (Figure 9.3-25). Corrosion environment sensors have been proposed as an option to assist in the management of corrosion of structural elements of aircraft. These sensors typically measure parameters that can influence the occurrence and rate of corrosion, including humidity, relative wetness, corrosivity potential, and, for witness coupons, mass loss (Figure 9.3-26). However, how the information from these sensor systems can be converted into actionable information for either USAF structural integrity and/or maintenance communities has not been established. In addition, performance metrics and qualification processes for these types of sensors have not been fully defined. Therefore, a project by the Air Force Research Laboratory (AFRL) establishes the Concept of Operations (ConOps) for corrosion environment sensors. The primary focus of this work is to determine how the information provided by these sensors can be used for fleet management for both structural integrity management and sustainment management. The magnitude of any change in these processes will depend on the quality and relevance of the information derived from the data acquired by the sensor systems. In addition, this includes identifying meaningful metrics to calibrate and quantify the performance of the sensors relative to the measured parameters and the relationship of this measurement to damage prediction or potential. Another item explored was defining possible processes for sensor system capability validation and qualification. The technical effort describes the outcome of this project and establishes possible methods to specify requirements for the acquisition and implementation of these sensors. The information should assist in developing business case analyses to justify investment in sensor systems and, thus, a solid foundation for possible use of these systems. Another outcome of this effort identifies possible technology gaps that need to be addressed before corrosion environment sensor systems are fully integrated into fleet management processes.

- **Annual Estimates on Corrosion Impact**
 - **DoD: \$20.9B (2010)**
 - **USAF: \$6.3B (\$4.5B for Aircraft & Missiles) (2009)**
- **Upward USAF Cost Trend, 2006-2009**

	Corrosion Cost (in millions)	Total Maint. (in millions)	As a percent of maintenance
FY2006	\$3,105	\$14,659	21.2%
FY2007	\$3,537	\$15,925	22.2%
FY2008	\$3,908	\$16,403	23.8%
FY2009	\$4,485	\$18,657	24.0%

Figure 9.3-25. Cost of Corrosion

- **Classes of Sensors:**

- **Witness coupons (sacrificial):** direct, galvanic
- **Environment parameters:** humidity, temperature, chemistry, time of wetness
- **Corrosivity potential:** electrical impedance spectroscopy (EIS), linear polarization resistance (LPR), magnetometer



Representative
Environment Sensor

- **Truncated history**

- **Significant resources expended on development, demonstration, proof-of-principle, and flight tests**
 - Efforts date back to 1973, ramp up starts in 1992 (V.S. Agarwala)
 - ~1500 Battelle sensor flown on military aircraft as of 2010***
- **Capability not validated, therefore TRL<5**
- **Definition of how sensing systems provide actionable information has not been established to date**



Representative
LPR Sensor

Figure 9.3-26. Environment Sensing: Classes and History

9.4. STRUCTURAL TEARDOWN ASSESSMENTS

9.4.1. T-38 Fuselage Teardown: One Man's Trash is Another Man's Treasure

Isaac Grothe and Paul Clark, Southwest Research Institute; Michael Blinn, USAF T-38 ASIP

The sustainment of aging aircraft brings many disciplines together. Analysis through mathematical calculations and computer simulations provide the sustainment team with targeted inspection times and locations. Full-scale-fatigue testing is another way to prove out the design and fine tune the sustainer's knowledge of the airframe and its usage. Another dataset to empower engineering is the collection of field data; this comes in the form of usage data, base-station times, inspections results, repairs, modifications, and the list continues. Each of these analytical and sustainment tools have pros and cons. Analysis and fatigue testing do not capture the time-related component of aging; field data can only capture degradation for those areas accessible to the field or where previous modifications were employed. A full teardown shows reality. It captures fatigue cracking, wear, corrosion and all of their synergies that frequently result in some form of mixed-mode failures. The T-38 has been the primary fighter trainer for the Air Force since the early 1960s and has had numerous modifications and configuration changes to address problems or improve some aspect of the airframe. Like many fleets, the T-38 has been flown by different organizations over the years, each of which has their own requirements. Some of the effects to the airframe are more severe than others; however, only total flight hours are tracked for the airframe leaving questions about the true condition of the structure. In 2002, Southwest Research Institute (SwRI) started the first full scale-fuselage-fatigue test of the T-38 in its current configuration. The teardown article (Figures 9.4-1 through 9.4-3) was a retired T-38C aircraft, flown between 1965 and 2011, spanning 45 years of service and 15,000 hours of flying time, the airframe was exposed to various environments and usages. The airframe structure was damaged in some areas due to a special cause event; this was accounted for during the teardown planning. The structure was subsequently disassembled and then evaluated for suitability for teardown. The overarching goals of this destructive teardown of a retired T-38C airframe are three-fold: 1) Investigate and quantify any potential effects of engine overheating to the adjacent structure in the aft half of the airframe, as a result of a propulsion upgrade, 2) Improve the technical characterization and understanding of those components key to the Pacer Classic III (PCIII) modification program, in terms of structural integrity and remaining economic life, and 3) Provide a more holistic and proactive approach towards improved determination of structural life impact and criticality for existing and new structural critical safety items (SCSIs). The teardown article was first sent to Southwest Research Institute for pre-teardown documentation and initial nondestructive inspection (NDI) on the article for later evaluation against teardown indications (Figure 9.4-4). The procedures for aircraft structure teardown analysis, as established by the Center for Aircraft Structural Life Extension (CAStLE), were the foundation for all teardown activities as required by the contract. This effort resulted in significant payoffs for the T-38 ASIP Office; these payoffs included: 1) Using a Class A mishap in a positive and productive evaluation activity to improve understanding of the state of the fleet, 2) Discover unknowns and characterize the health of the structure, that is normally hidden due to limited or cost prohibitive access, and 3) Compare results from the teardown for known locations against analysis for adequacy and efficacy. These events align to provide a tremendous return on investment for the T-38 ASIP manager. This report captures the processes used to teardown, inspect, categorize, document, evaluate and perform failure analysis on the teardown aircraft, including relevant and impactful results (Figures 9.4-5 and 9.4-6).

T-38C

- 15,000 hours
- Variety of usages
- Airframe mods
 - Dorsal Longeron
 - Cockpit Enclosure
 - Bulkhead replacement
 - PMP
- Airframe opted for early retirement



Figure 9.4-1. Teardown Article

Teardown Assemblies

- Forward Fuselage
- Center Fuselage
- Aft Fuselage
- Vertical Stabilizer

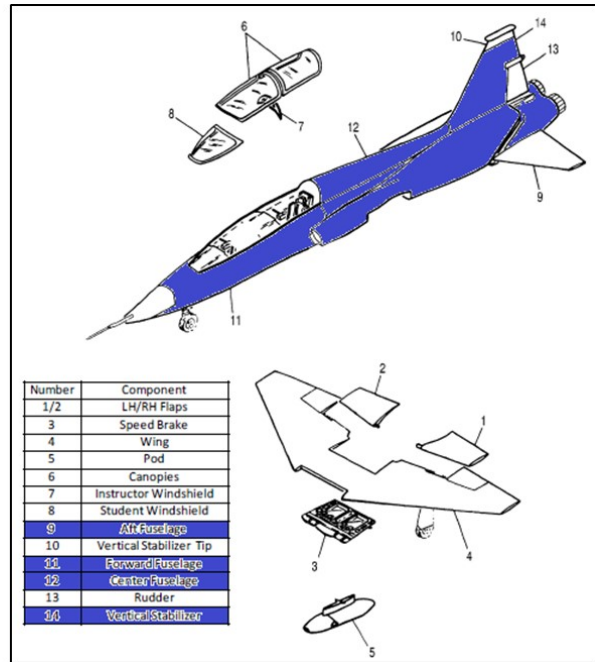


Figure 9.4-2. Major Assemblies of the T-38C

Assemblies broken into 12 teardown sections

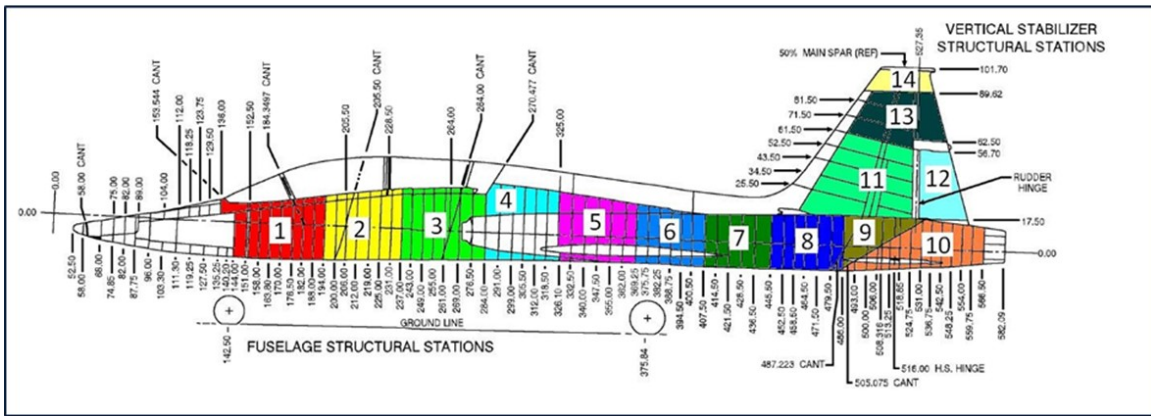


Figure 9.4-3. Airframe Teardown Sections Definition

- **Close Visual Inspection (CVI)**
- **Fluorescent Penetrant Inspection (FPI)**
- **Eddy Current**
 - Bolt Hole Eddy Current (BHEC)
 - Surface Scan Eddy Current (SSEC)
- **Magnetic Particle Inspection (MPI)**



Figure 9.4-4. NDI Types for Teardown

- 394 Parts removed and examined
- 6677 indications
 - CVI: 5222
 - Mechanical Damage: 4330
 - Cracking: 384
 - Corrosion: 497
 - Other: 11
 - FPI: 1060
 - Mechanical Damage: 19
 - Cracking: 762
 - Corrosion: 278
 - Other: 1
 - Eddy Current: 395
 - Mechanical Damage: 292
 - Cracking: 84
 - Uninspectable: 19
 - MPI: No indications

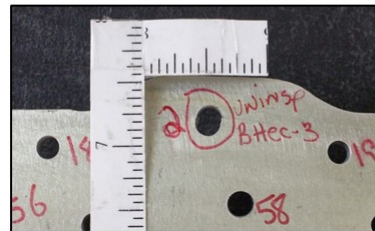


Figure 9.4-5. Summary of Teardown Inspections

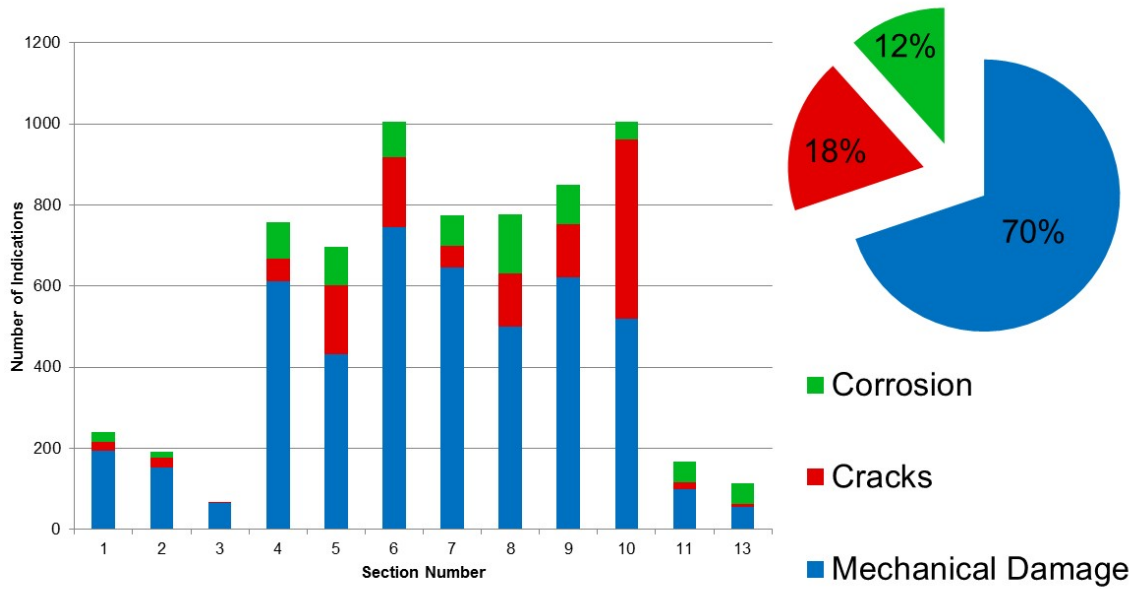


Figure 9.4-6. T-38C Fuselage Indications Summary

9.4.2. Structural Teardown Analysis

Gregory A. Shoales, USAF Academy - CASTLE

CASTLE continues to assist fleet management decisions and the United States Air Force (USAF) Aircraft Structural Integrity Program (ASIP) through multiple programs whose focus is assessing aging structures. Teardown analysis programs are required by MIL-STD-1530C at various points in the life cycle of all USAF aircraft. CASTLE has been part of teardown analysis programs since 2002 and wrote the USAF best practices guide for teardown in 2008 [1]. This publication and the results of various teardown analyses have been previously reported in ICAF and other forums. Since ICAF 2013 CASTLE has conducted teardown analysis of multiple aircraft of three different aircraft types. Aircraft types included small trainer/fighter category as well as large transport category.

The large scope of a previously reported program [2] required CASTLE to document the detailed steps of CASTLE's teardown process in a set of protocols. These eight teardown protocols were originally published in 2009 and 2010 and capture best practice processes and lessons learned from teardown programs conducted by CASTLE and others over the previous several years. The eight protocols included; five protocols to document the typical processes executed during any structural teardown (referred to by CASTLE as execution protocols), two protocols to capture critical administrative processes (referred to by CASTLE as administrative protocols), and one protocol to document specialized analysis of typical fuselage structural joints. The five execution protocols include; extraction of the structural area of interest (Protocol 3), disassembly of this structural area of interest into individual parts (Protocol 4), removal of coatings from the parts (Protocol 5), nondestructive inspection of the cleaned parts (Protocol 7), and extended analysis of prioritized nondestructive inspection indications by root-cause analysis techniques (Protocol 8). The administrative protocols include; a robust database system to capture all data produced and track program process status (Protocol 1), and an identification and tracking system for all program analysis subjects (Protocol 2). Protocol 6 details the specialized analysis of lap-joint structural elements which are typically found in large transport fuselage structure. In particular the processes specified in Protocol 6 seek to assess structural health of fuselage lap joints and the performance of applied corrosion preventive compounds (CPCs). The progression of the execution protocols from Protocol 3 through Protocol 4 is depicted in Figure 9.4-7 which has been repeated from the previous publication [2]. The continued progression of the same part from Protocol 4 through the analysis phase processes captured in Protocols 7 and 8 is depicted in Figure 9.4-8 which has been adapted from the previous publication [2]. Protocols 4 and 7 were written with significant contribution from Dr. Melinda Laubach of the National Institute for Aviation Research at Wichita State University. The nondestructive inspection steps and inspector certification requirements captured in Protocol 7 were extensively reviewed by Mr. John Brausch of the Air Force Research Laboratory at Wright-Patterson AFB, Ohio.

Since 2010 CAStLE, with the assistance of their support contractor Sabreliner Aviation, has conducted teardown analysis of structure from more than a dozen aircraft of six different aircraft types. CAStLE has also assisted others conducting their own teardown analysis programs. This continued experience led to the need to republish all eight protocols in October 2014 in order to capture further lessons learned leading to process improvements and add newly developed processes to address other structural categories. The new protocols are referenced and recommended by the USAF in a recently published ASIP structures bulletin [3].

A critical element to all CAStLE teardown analysis program processes is to prevent further damage to the subject structure once received by the program. CAStLE continues to advise those considering teardown analysis, whether conducted by CAStLE or not, on important considerations before beginning such a program. These considerations include; a clear definition of program goals, a well-documented subject history to ensure the subject is the best possible candidate for the program requirements, and selection of analysis parameters which will most efficiently obtain data to satisfy the program goals. These considerations and others are documented in the previously mentioned teardown analysis program handbook [1].

References

- [1] Shoales, G.A., "Procedures for Aircraft Structural Teardown Analysis," USAF Academy TR-2008-02, USAF Academy, CO, May 2008.
- [2] Shoales, G.A., G. Gann, and J. Wilterdink, "C/KC-135 Teardown Analysis Program: Program Update and Aircraft 1 Report," 2012 Aircraft Airworthiness and Sustainment Conference, Baltimore, MD, 2-5 April, 2012.
- [3] EZ-SB-15-001, "Aircraft Structure Teardown Inspection and Evaluation Program Protocols," USAF ASIP Structures, Wright-Patterson AFB, OH, 30 January 2015.

9.5. LOADS & ENVIRONMENT CHARACTERIZATION

9.5.1. F-16 ASIP Data Capture: The Missing Link in IAT Evolution

Kimberli Jones and Bryce Harris, USAF – Life Cycle Management Center; William Legge, Leidos

Since the first USAF F-16 (Figure 9.5-1) entered service over 30 years ago, less than 50% of the Individual Aircraft Tracking (IAT) data have been captured by flight data recorders (Figure 9.5-2). The historical focus to improve this issue has been on the fiscally-burdened idea of hardware upgrade. In 2010, with no imminent new flight data recorder on the horizon, the F-16 ASIP office concentrated exclusively on human-focused data capture improvement efforts; within three years, what was once a potential engineering liability of only 45% captured data has today become an unmatched asset with 90% valid data from over 1000 recorders (Figure 9.5-3). This high density of valid aircraft data establishes the foundation to track individual aircraft flight severity and subsequently project aircraft life for USAF's successful F-16 Aircraft Structural Integrity Program (ASIP) engineering. Human-centric data capture success rests upon three synergetic pillars: Software, processes, and people. Software: Improve their tools. A complete overhaul of the existing collection and data processing center came online in the summer of 2010. This new software, called Processing, Evaluating, Reporting, FORce Management Data Software (PERFORMS), improved processing reliability, mated easily with a webpage interface, and enabled near-real time visibility to fleet data at the engineering level. Flight data recorder download equipment software also was updated to enable a "rollover" capture of data, providing the capability to return to the jet to recapture prior data if the submitted files were invalid or corrupted. Processes: Simplify their tasks. The ASIP lines of responsibility and rules-of-engagement at the field level were not clearly defined nor enforced by local supervision. A successful campaign with senior USAF leadership resulted in clearly defined accountability lanes and structured enforcement of the ASIP capture standard at all levels of supervision. New data processing center procedures were introduced, reducing task time by 50% and enabling more time towards customer service feedback. Also, tech data procedures used to download the data (Figure 9.5-4) from the jet were rewritten to eliminate confusing options and data-loss loopholes. People: Empower their minds. In order to obtain buy-in on the importance of data capture from the field, F-16 ASIP executed a concerted effort in bridge building through in-person visits and new and improved ways of communicating with tech-savvy field users. One result of these efforts was immediate ASIP website improvements requested by the field users. Feedback from the field has increased tenfold in recent years; today, ASIP support centers are flooded daily with inputs from ASIP-invested field users who know the team by name and trust their swift responses. The inherent synergy between the three data capture pillars enables continuous improvement by one area stimulating progress in another. Today, the USAF F-16 ASIP is surpassing the DoD-standard 90% valid IAT data capture rate which previously was not thought possible with the existing recorder system. Consequently, ASIP's improved abilities in accurately tracking flight severity and maintaining airframe structural integrity proves even more critical as the aircraft continue to age while some undergo life extension modification. Human-focused data capture rate improvement was the missing link in F-16 ASIP's IAT evolution to compliance with ASIP-mandated levels.



Figure 9.5-1. F-16 Aircraft

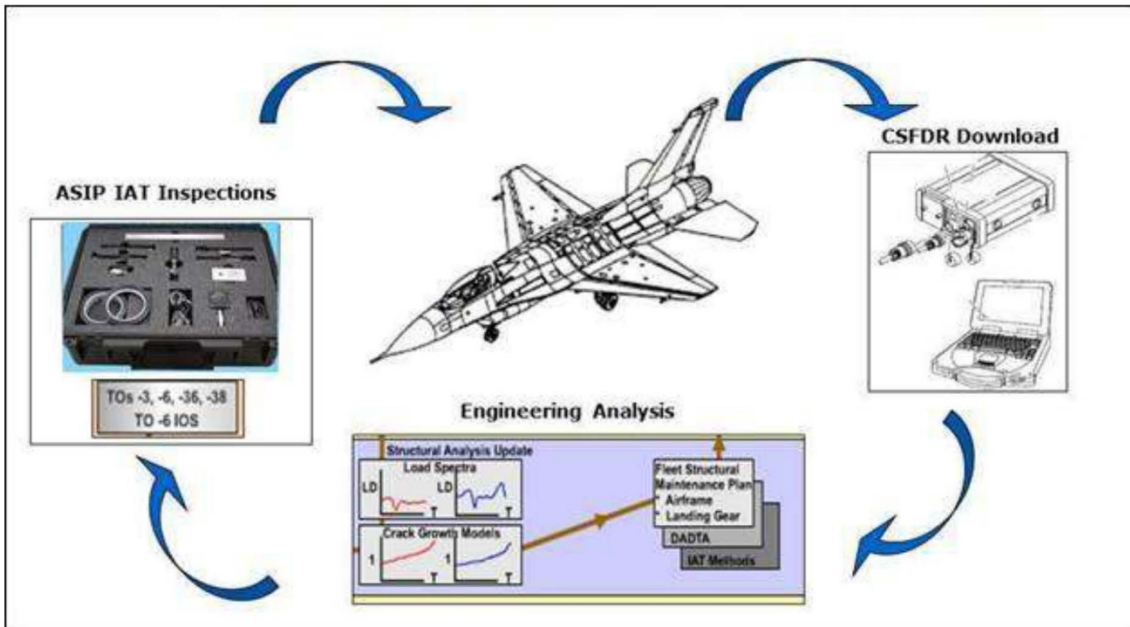


Figure 9.5-2. F-16 Data Download System View

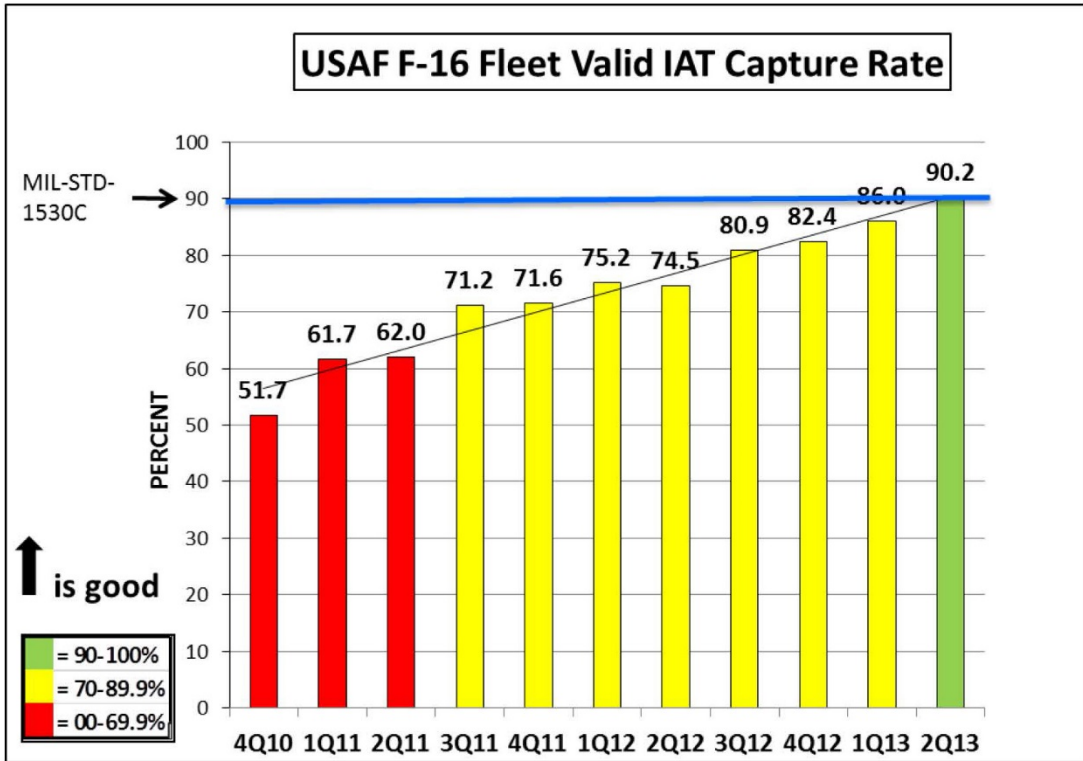


Figure 9.5-3. F-16 Valid IAT Capture Rate

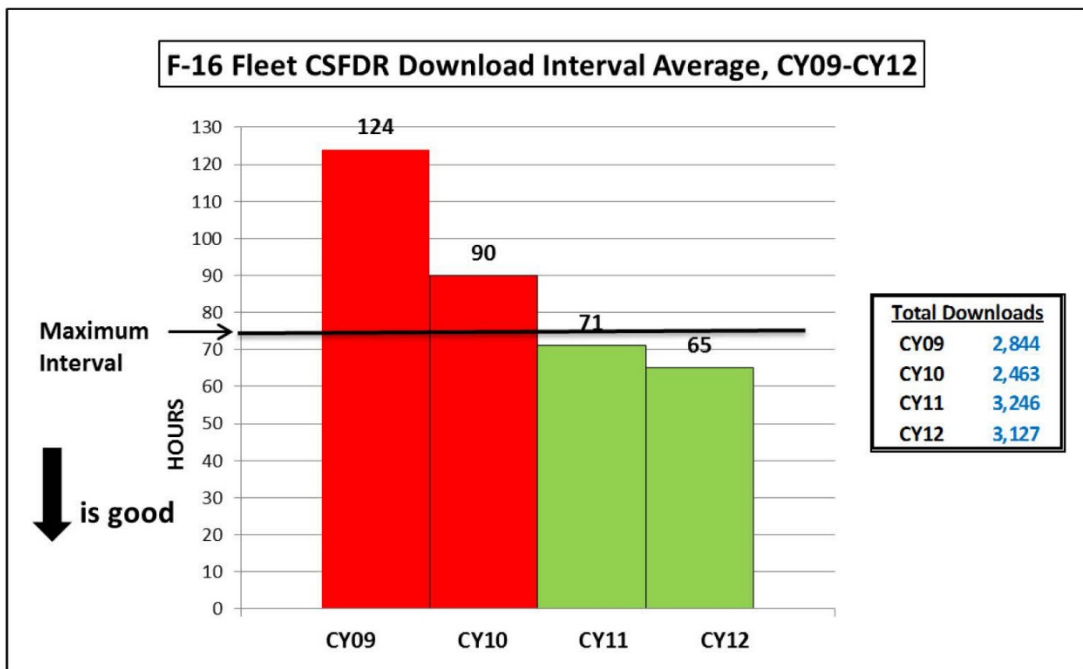


Figure 9.5-4. F-16 Average Download Rate

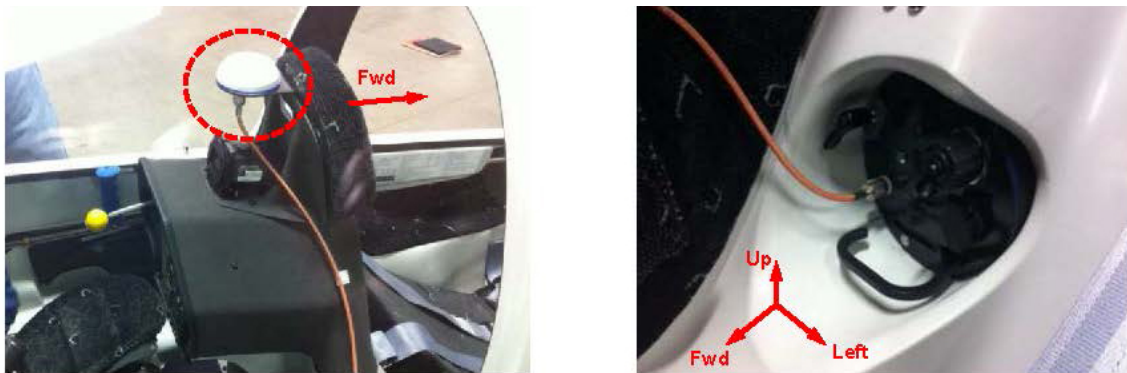
9.5.2. An Innovative Low Maintenance Data Acquisition Solution for Load Factor Capture

Jason Niebuhr, USAFA – Apogee Engineering; James Greer, Jr., USAF Academy – CASTLE; Diarmuid Corry and Elisabeth O’Brien, Curtiss-Wright Controls Avionics & Electronics

This technical activity describes an innovative approach to implementing and packaging a versatile data acquisition system for capturing load factor counts in the United States Air Force Academy (USAFA) glider training environment (Figure 9.5-5). The solution was developed by the Center for Aircraft Structural Life Extension (CASTLE) using commercial off-the-shelf flight test data acquisition equipment from the Curtiss-Wright Controls Avionics and Electronics division (CWC-AE). The system captures vertical load factor counts on aircraft for both acrobatic and basic mission types with two goals: to determine if the aircraft can safely fly missions interchangeably, and to compare with OEM load spectrum to assess the severity of usage in the USAFA glider training environment. The system has been designed so it could be installed or removed from the aircraft within minutes to maximize flexibility (Figure 9.5-6). In order to minimize the maintenance burden of installation or removal, attachment to the glider does not require tools, aircraft modifications, or mechanical fasteners. The integration of a COTS system into existing space in the aircraft is described in this technical activity. To date, four production units have been built, installed, and are currently successfully recording data in USAFA gliders.



Figure 9.5-5. USAF TG-16A



- Unable to maintain lock when integrated with recorder system
- Positioned behind front seat headrest
- Hook and loop tape for easy transfer between aircraft

Figure 9.5-6. System – GPS Location

9.5.3. Loads Environment Spectra Survey (L/ESS) USCG HC-144A

Patrick Dwyer, Technical Data Analysis, Inc.; Mark Potoschnik, USCG ALC; Craig Brooks, APES, Inc.

The United States Coast Guard's (USCG) Medium Range Surveillance (MRS) Product Line at the Aviation Logistics Center (ALC) identified a need to better understand the impact on the structural integrity that their unique usage and operations in maritime environments will have on their fixed wing asset, the HC-144A (Figure 9.5-7). The HC-144A designated the "Ocean Sentry" is the military designation for the CN-235 aircraft procured to replace the aging HU-25A fleet. MRS engineering recognized a significant difference between the service life mission definitions from the Original Equipment Manufacturers (OEMs) design assumptions relative to the USCG actual usage. This coupled with the HC-144s already experiencing corrosion in the initial depot cycles of the fleet raised a concern for the service life capability of the assets. The USCG HC-144A selected a proactive approach with the goal of "developing an USCG tailored Aircraft Structural Integrity Program to establish the living fleet condition/health with an optimized fleet management approach". To accomplish this goal, the USCG leveraged a USAF Phase III SBIR program on "Corrosion Modeling and Life Prediction Supporting Structural Prognostic Health Management". The primary tasks consist of: — Configure, procure, and install aircraft structural response monitoring hardware — Perform flight test and in-service programs to characterize USCG mission types — Conduct holistic corrosion & damage tolerance assessment (CDTA) — Define non-destructive inspection capabilities, CDTA defect criteria & damage limit states — Implement mitigation schemes to reduce corrosion & field maintenance issues — Assist in integrating USCG ASIP infrastructure for fleet maintenance. Aircraft CG2304 has been specially equipped with an instrumentation suite to conduct a Loads/Environment Spectra Survey (L/ESS) to enable the collection of data and information to begin understanding of the structural aircraft response while operating in USCG roles. The aircraft is instrumented with over eighty strategically placed strain gauges and accelerometers, and connected into existing aircraft parameter and data buses. This aircraft has collected and is continuing to collect unique L/ESS and general flight information since November 2012 while performing its duties at the assigned operational commands; Mobile, Miami, and Cape Cod with provisions to continue the collection in Corpus Christi. The focus thus far has been on establishing the infrastructure for the flow and processing of structural health monitoring data being collected and then processing that information into service life assessment capability tools. The USCG HC-144A platform usage and mission roles as anticipated are different and more severe than those assumed by the (OEM) (Figure 9.5-8): thus efforts have begun to re-establish the service life limits, adjust interval inspections, and revise fleet management. To date, this program has collected over eighteen months of valuable data, and has generated preliminary indications of the service capability impact for the fleet under current USCG operations. The technical activity provides an over view of the program and the findings to date.



Figure 9.5-7. USCG HC-144A

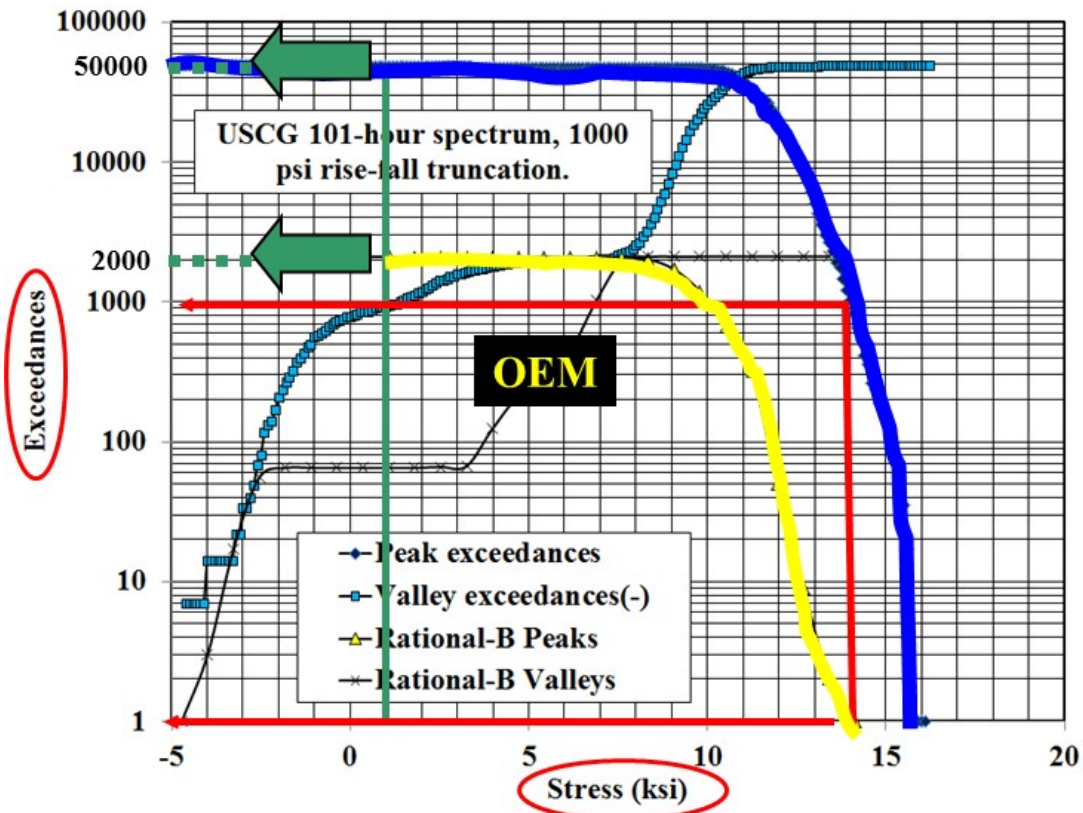


Figure 9.5-8. Significant Differences in Exceedances Between Design and Actual Usage

9.5.4. Determination of Flight Loads for the HH-60G Pave Hawk Helicopter

Robert McGinty, Gregory Wood and Jeff Brenna, Mercer Engineering Research Center (MERC); Steven Lamb, USAF-WR-ALC

The United States Air Force (USAF) is working to quantify and extend the service life of the HH-60G Pave Hawk helicopter fleet due to challenges encountered in the procurement of a replacement platform. This effort is complicated by the extensive, mission-specific modifications performed on the weapons system over its 20+ years of service. Current mission usage also deviates significantly from the original Black Hawk design specifications. The modifications to the aircraft structure and mission usage are expected to result in changes to the platform's operational flight loads. Mercer Engineering Research Center (MERC) was able to leverage several Aircraft Structural Integrity Program (ASIP) initiatives to develop a new set of comprehensive loads specific to the HH-60G airframe. Development of these loads (Figure 9.5-9) allows the HH-60G program office to better assess structural damage and repairs, assign flight severities, and perform risk analyses. ASIP initiatives that were required for loads derivation included a detailed global finite element model (Figure 9.5-10), usage data from the Loads / Environment Spectra Survey (L/ESS), and strain gage data (Figure 9.5-11) from a flight strain survey. These tools and data sets were combined to develop a sensitivity matrix relating aircraft forces and moments to strains at locations where gages were placed in the flight strain survey. The sensitivity matrix was then inverted and used with the experimental strain data to compute forces on the aircraft for any point in the sky (PITS) and corresponding flight regime. In addition, statistical tests were incorporated in the analyses to identify statistically significant forces, exclude those that were not, and to eliminate occasional bad experimental data. Results of the calculations to date are extremely promising. The computed loads have been used with the FE model to predict strains to within 200 microstrain of measured values (Figure 9.5-12), and the average correlation coefficient between the predicted and measured values is $R^2 = 0.935$ (Figure 9.5-13). Computed main rotor lift forces have been found to vary as expected with flight regime. For example, forces are higher for Hi-G pull-ups than for straight-level flight, which are in turn higher than for dives and push-overs (Figure 9.5-14). The lift forces have also been found to correlate very well with $(N_z * W)$, the product of G-load (N_z) and aircraft weight (W). The correlation made it possible, in fact, to identify a discrepancy in mission parameters during a portion of the flight strain survey because the annotated gross weights violated the established relationship. The new computed forces will make it possible to better support service life extension efforts for the helicopters in their new configurations and flight usage regimes as opposed to the original design specs from the 1970s. The new load sets also permit the HH-60G program office to better assess structural damage and repairs and perform risk analyses on the fleet.

- Use data from instrumented flight tests to compute flight loads for HH-60G aircraft to support structural analyses

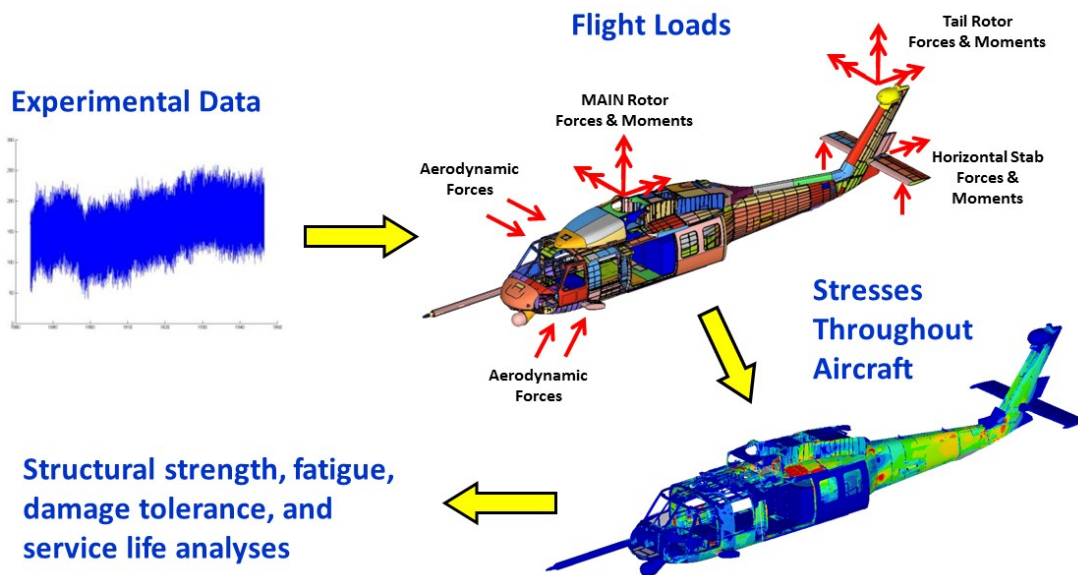


Figure 9.5-9. Loads Calculation Overview

- HH-60G Finite Element Model
 - 1,430,000 nodes
 - 1,050,000 elements
 - Primarily shell elements
 - Nominal 1" x 1" element size

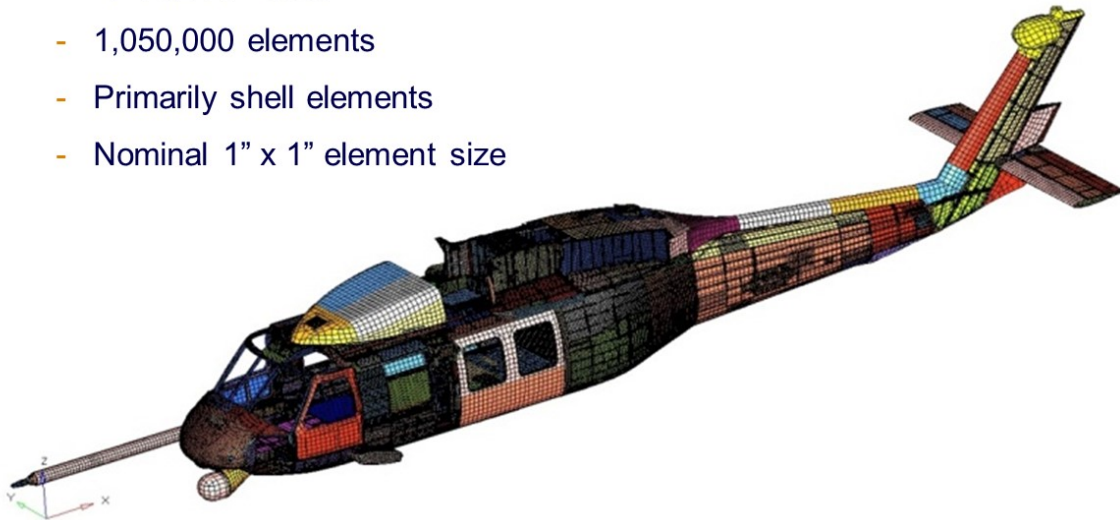


Figure 9.5-10. Finite Element Model

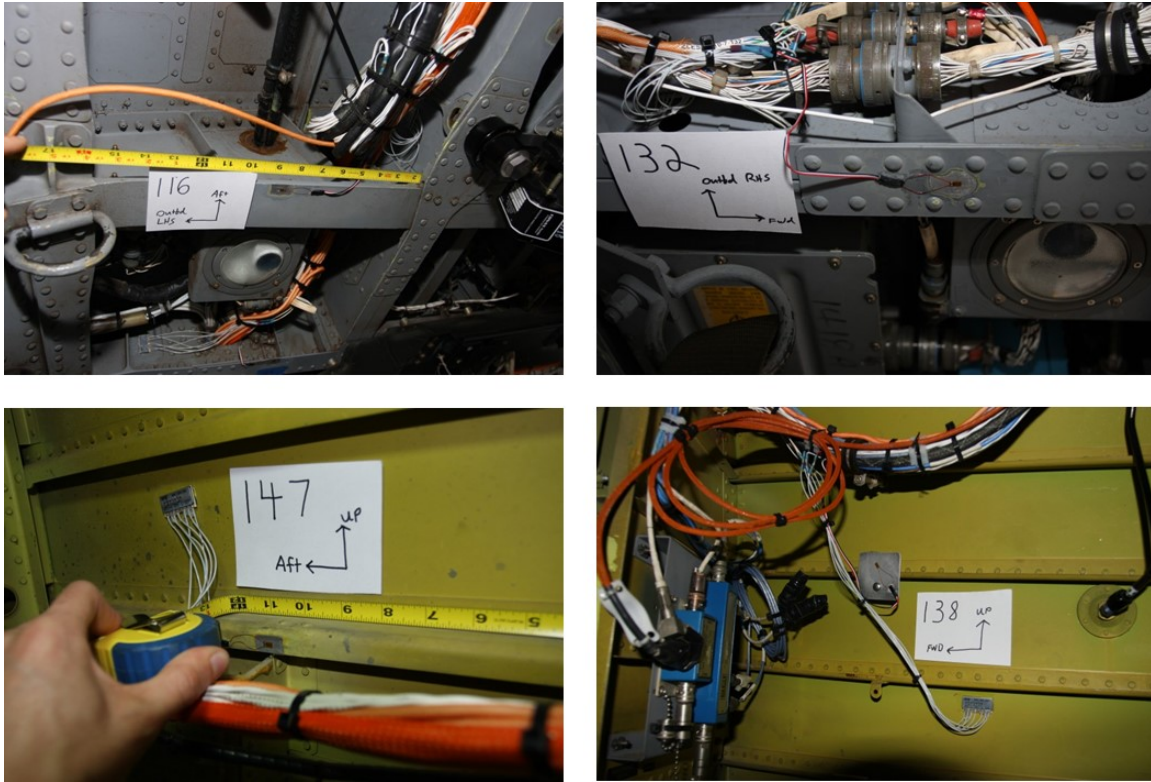


Figure 9.5-11. Strain Gage Photos

- Accuracy of computed loads is assessed by how well they lead to predicted strains matching measured data
- Chart for Sym Pull Up shows typical level of correlation ($R^2 = 0.94$)

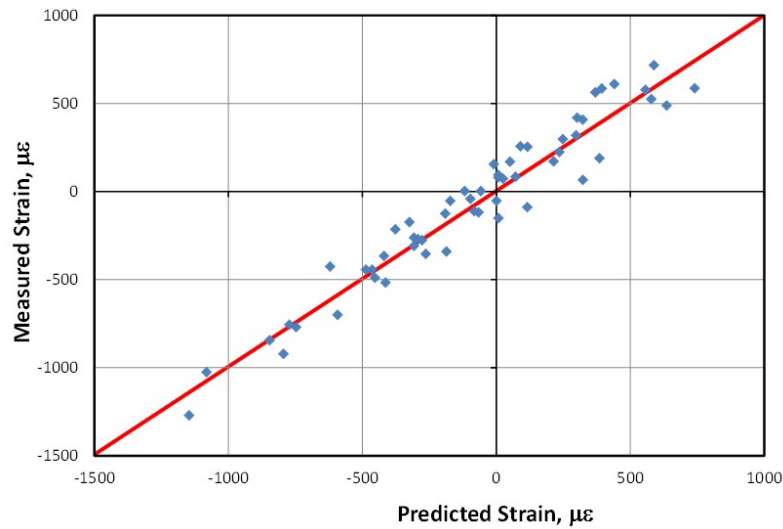


Figure 9.5-12. Strain Correlations

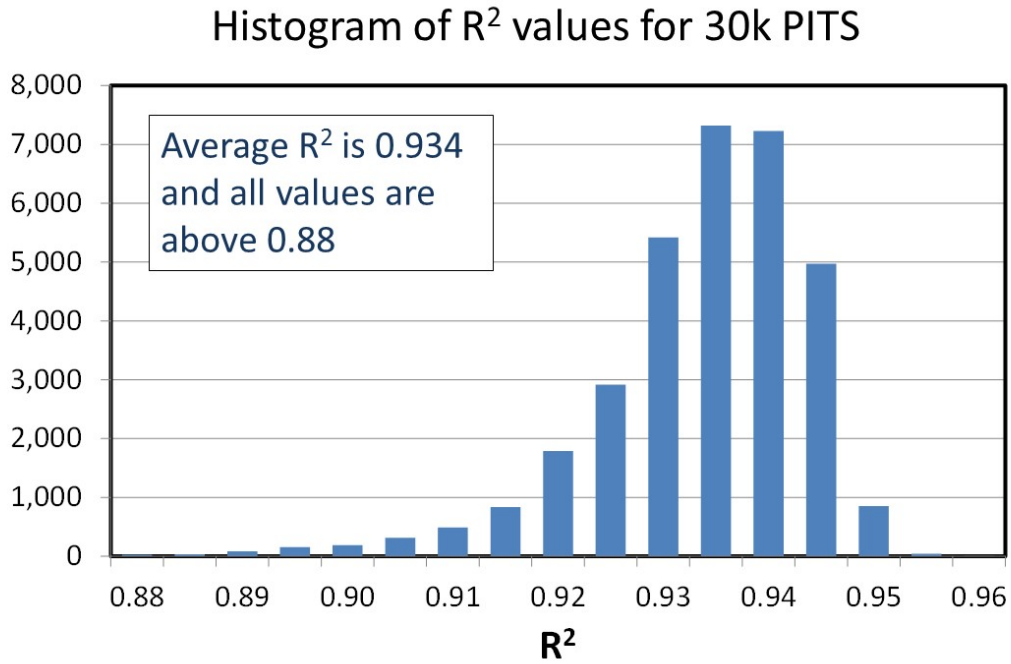


Figure 9.5-13. Correlation Coefficients

- Higher forces for pull-ups than push-overs

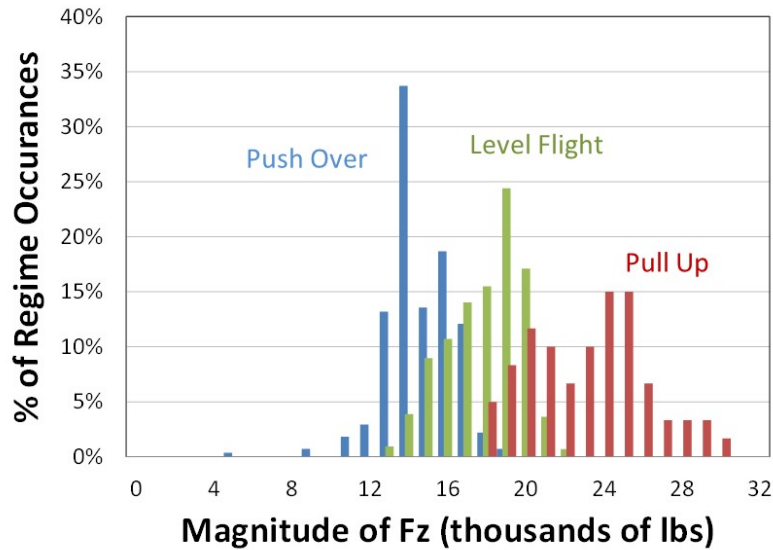


Figure 9.5-14. Computed Main Rotor List Forces

9.5.5. Gust and Maneuver Loads for a Fleet of USFS Lead Airplanes

Linda K. Kliment and Kamran Rokhsaz, Wichita State University; John Nelson and Brett Tarning, United States Forest Service (USFS)

As part of the operational loads monitoring program supported by the United States Forest Service (USFS), many aircraft flying in firefighting missions have been instrumented and flight data are recorded. The USFS has instrumented the heavy air tankers and some of the data have been analyzed in a previous study. Currently, the focus is on the lead aircraft.

USFS uses the lead airplanes as support for the heavy air tankers. The lead aircraft survey the fire area, determine flight paths into and out of the region, and lead the heavy air tankers into the fire zone. Three models of the King Air 90, used as lead aircraft, were instrumented: the C90A, the C90GT, and the E90. Flight data were collected for years 2009-2013. The results shown in this technical activity were based on 3094 flights, which contained 5773 hours and 1,056,296 nm.

Loads were found using the peak-between-means method. In addition, the normal loads were separated into those due to gusts and those from maneuvering the aircraft using the two-second rule. The flights were also separated into categories based on the type and environment. Ferry Flights were those in which the aircraft was simply flown from one airport to another, without performing any maneuvers associated with firefighting. One would expect that the Ferry Flights would most resemble the type of flights for which the airplane was designed. Normal Attitude flights were those in which firefighting operations were performed. However, in the Normal Attitude flights, the absolute pitch angles never exceeded 30 degrees and the absolute roll angles remained below 80 degrees. Extreme Attitude flights contained absolute pitch and roll angles exceeding 30 degrees and 80 degrees, respectively.

The cumulative occurrence of incremental vertical gust loads are shown in Figure 9.5-15. The data from the three types of flights are plotted individually and compared to the AC 23-13A Gust Spectra. Ferry Flights are shown to have fewer occurrences than those of the Normal and Extreme Attitude flights. This can be explained by the fact that Ferry Flights occur at higher altitudes while the Normal and Extreme Attitude flights occur closer to the ground, even during cruise. Therefore, it was expected that Ferry Flights would take place in a less turbulent atmosphere. At higher incremental values, loads from USFS flights were shown to occur less frequently than the AC 23-13A Gust Spectra. At lower loads, the occurrences from the Normal and Extreme Attitude flights exceeded those of the advisory circular.

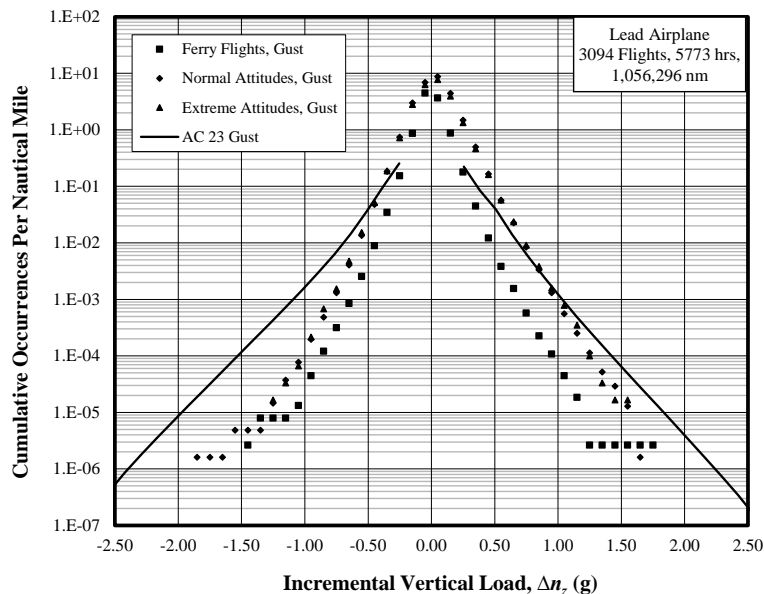


Figure 9.5-15. Cumulative Occurrence of Incremental Vertical Gust Loads

The cumulative occurrence of incremental vertical maneuver loads are shown in Figure 9.5-16. Again, the data from the three types of USFS flights are plotted, as well as the AC 23-13A Maneuver Spectra. Ferry Flights were shown to have maneuver loads that compared favorably with the AC 23-13A Maneuver Spectra. However, the maneuvering required during firefighting operations is apparent in the Normal and Extreme Attitude flight data shown in Figure 9.5-16, since maneuver loads were shown to occur at a much higher frequency than for Ferry Flights. In addition, the Normal and Extreme Attitude flights were shown to have higher loads, exceeding an incremental vertical load of 2.0 g's.

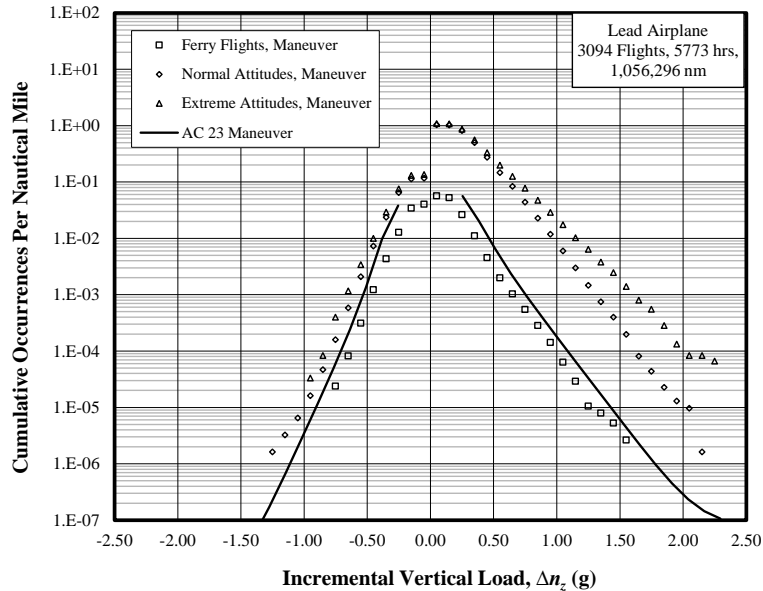


Figure 9.5-16. Cumulative Occurrence of Incremental Vertical Maneuver Loads

The gust and maneuver loads were combined together to show a cumulative occurrence of incremental vertical loads in Figure 9.5-17. The loads from the three types of USFS flights are compared to Beechcraft data, indicating the Original Analytical Spectra and the Typical Commercial Usage. As expected, Ferry Flights had loads occurring at nearly the same frequency as Typical Commercial Usage. The loads from the Extreme Attitude USFS flights exceeded the Original Analytical Spectra at higher incremental values.

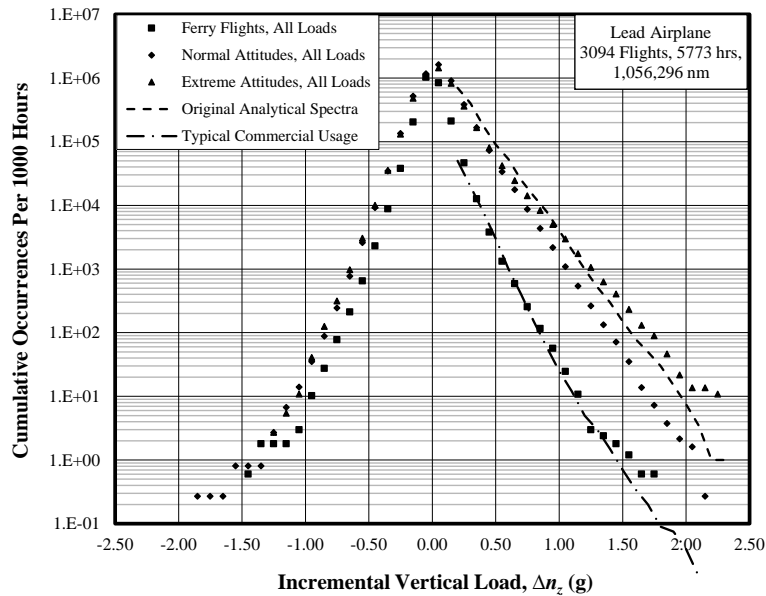


Figure 9.5-17. Cumulative Occurrence of Incremental Vertical Loads

In conclusion, the data shown indicates that lead airplanes fly in a harsher environment and are required to maneuver more during USFS firefighting roles. These data will be particularly useful when determining inspection schedules for aircraft operating in firefighting roles.

9.5.6. Flight Data Collection and Analysis

James M. Greer, Jr., USAF Academy - CAStLE

CAStLE has previously performed data collection and analysis efforts on the TG-10 sailplane and the HC-130H (USCG). The sailplane program helped identify causes of tailwheel collapse experienced by some aircraft, as well as characterize a new runway surface: AvTurf™. The HC-130H project helped the Coast Guard quantify mission severity at multiple basing locations, adding hours to the fleet of 26 aircraft. Since ICAF 2013, CAStLE has continued flight data projects in support of the TG-16 fleet and assisted in a project in support of the C-130 fleet.

TG-16 Sailplane

CAStLE continued the project, reported in ICAF 2013, to measure g -loading on the new TG-16A gliders (Figure 9.5-18) flying two missions: standard and acrobatic. The purpose of the project was to determine if these two missions are similar enough (in terms of g exceedances) to allow them to be managed as one fleet, from an ASIP perspective. Another goal of the project was to compare United States Air Force Academy (USAF) usage to the “baseline” manufacturer’s usage. For the current project, CAStLE developed a fleet of modular units (Figure 9.5-19) to instrument four aircraft. These units fit in the oxygen bottle mounting tube (not currently used for oxygen), which is located near the fore-aft center of gravity of the aircraft. The units each have a triaxial accelerometer sampling at a high sample rate ($f_s = 512$ Hz) filtered at $f_s/4 = 128$ Hz. This high sample rate is being used as previous work with the glider fleet showed some higher frequency content during ground operations (mainly when the glider is towed behind the “gator” ATV on rough terrain). The ACRA KAM-500 Data Acquisition Unit (DAU) includes cards for accelerometer data, GPS, strain gages, and CompactFlash™ card recording.

Besides having an external GPS antenna and strain gages mounted on the wing spar, all other elements of the DAU were contained on the sled in Figure 9.5-19.



Figure 9.5-18. The TG-16A Sailplane

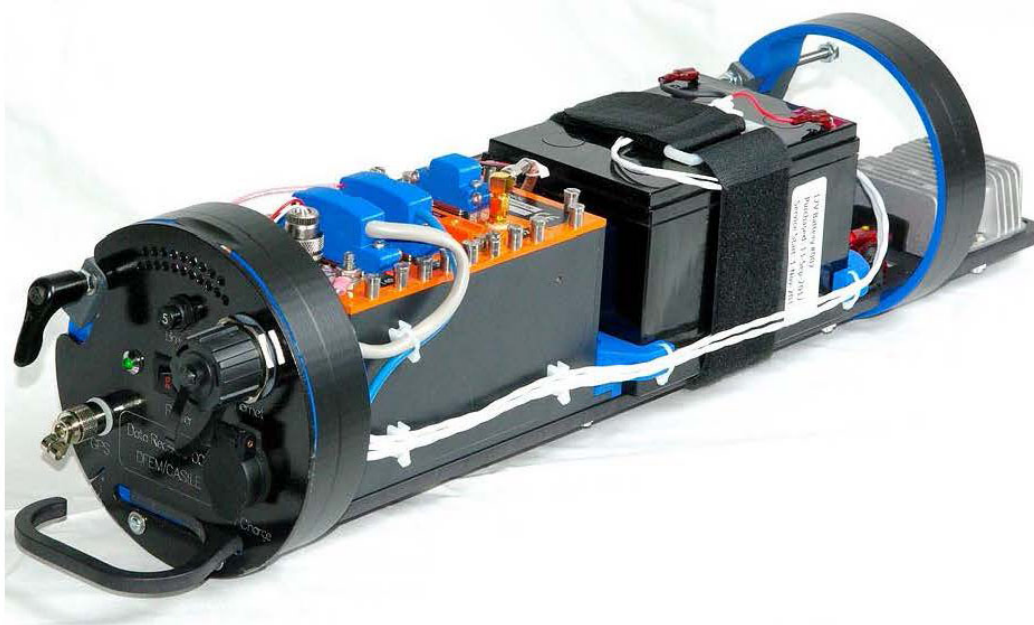


Figure 9.5-19. CASTLE Data Acquisition Module Including Battery, DC-DC Voltage Converter, and the ACRA KAM-500 DAU

Data were successfully collected from the aircraft over a 19 month period of time. In all, 333 flight hours of data were successfully captured. The data collected consisted of GPS data, three axes of accelerometer data (x, y and z) and wing bending strain data. Strain gages were not installed on the test

aircraft until September of 2013, so fewer hours (about 126) of strain data were captured. Not surprisingly, the data show the aerobatic mission to be generally more severe than the basic mission. However, making a structural assessment is complicated by the fact (1) that most of the gliders' structure is composite and (2) there is no test-based life (i.e., full-scale fatigue test data) for this aircraft. The OEM was engaged to review the data and to determine what, if any, impact the current USAFA usage of the aircraft may have on fleet management, airframe life and/or inspection intervals/methods.

C-130 Hercules

Since ICAF 2013 the USAF C-130 fleet has deployed their Loads/Environment Spectra Survey (L/ESS) system in order to better understand the fleet's varied operational usage and satisfy USAF Aircraft Structural Integrity Program (ASIP) requirements. The fleet's ASIP Manager requested CASTLE's help in writing/reviewing the system test plan and in evaluation of initial data collected during testing/operations. CASTLE also developed analysis software for the system to process the collected data. The data includes strains, accelerations, control surface positions, flight parameters and MIL-1553 bus data.

9.6. CHARACTERIZATION, MODELING & TESTING

9.6.1. Bird Strike and Coupon Testing of B-2 Polycarbonate Windshields Exhibiting Usage Induced Crazing Cracks

Jeffrey Simmons, Northrop Grumman Corporation; Michael Gran, USAF Research Laboratory – Aerospace Systems Directorate

Legacy windshields on the B-2 bomber have undergone manufacturing improvements to the current Spiral 0.5 design due to widespread polycarbonate cracking around bolt holes. At the time of discovery, extensive coupon and full-scale bird strike testing was conducted on legacy windshields to reduce the risk of a catastrophic failure from a bird strike (Figure 9.6-1). These windshields have been periodically inspected for damage and structural analysis was used to justify the replacement of a degraded legacy windshield. The current Spiral 0.5 configuration no longer exhibits thru-thickness cracks like the legacy windshields (Figure 9.6-2), instead exhibiting shallow crazing cracks (Figure 9.6-3). A second study was initiated to characterize the bird strike capability of Spiral 0.5 windshields exhibiting actual crazing crack patterns. This study used coupons cut from scrapped windshields to quantify temperature effects as well as full-scale component testing of scrapped windshields. Bird strike testing (Figure 9.6-4) was accomplished by the University of Dayton Research Institute (UDRI) Impact Physics Laboratory and culminated in a passing test 20% faster than original qualification testing. These results were used to correlate with the explicit finite element solver, x3D, resulting in simulated edge loads throughout the impact and wave propagation. Analysis using these loads has led to new guidelines for windshield replacement effectively extending their usable structural life. Additionally, the efforts of this study have provided justification for extending the time interval between periodic inspections.

- No part of bird shall enter cockpit in the event of a bird strike
 - 4 pound bird strike occurs at the critical location
 - Worst point in the flight envelope below 10,000 feet
- Legacy windshields qualified by test in 1989
 - Forward Center Section component test article

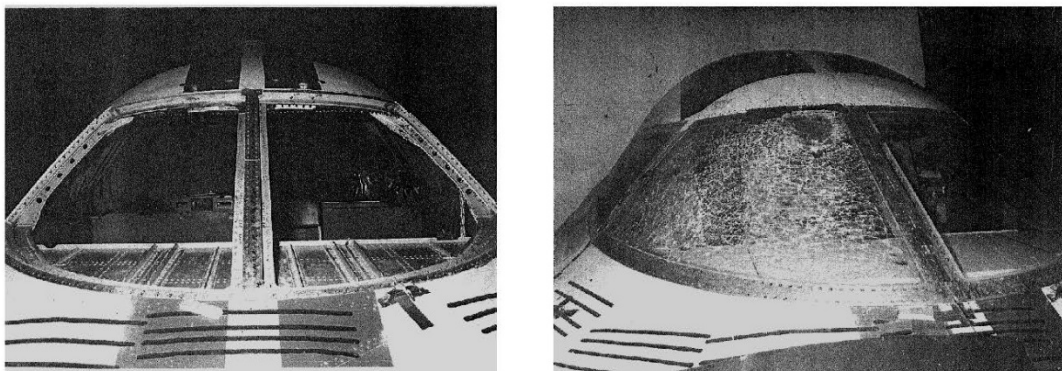


Figure 9.6-1. Bird Strike Requirement

- Thru-thickness cracks

- Exhibited extensive thru-thickness cracks after normal use
- Underwent bird strike and coupon testing
- Periodic prism analysis supported by testing

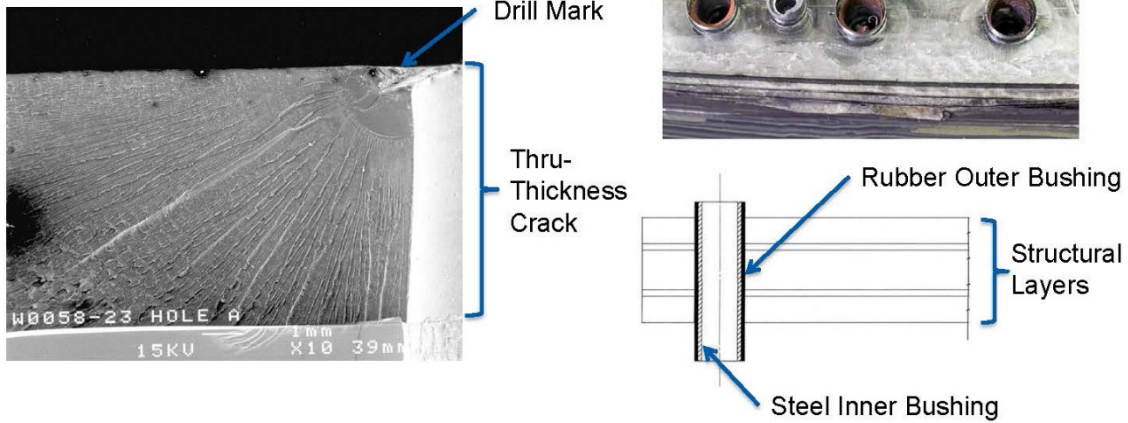


Figure 9.6-2. Legacy Windshields

- Improvements

- New drilling technique
- Changed bushing
- Removed retainer & hoist holes

- Crazing Cracks

- Partial thickness of 1 ply
- Same analysis as legacy windshields

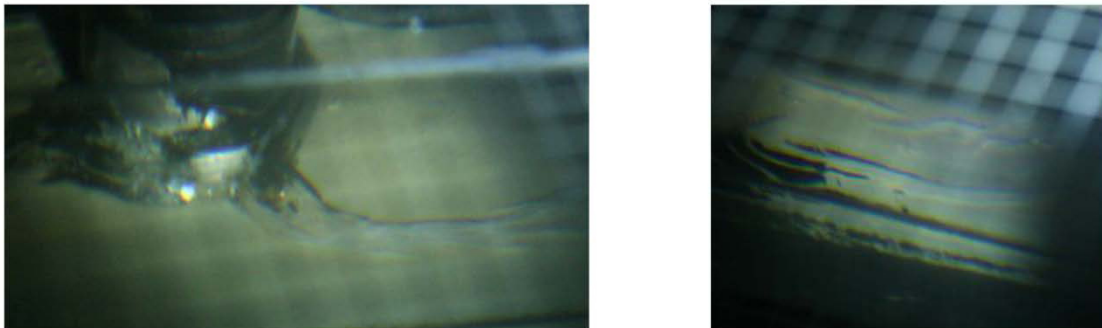
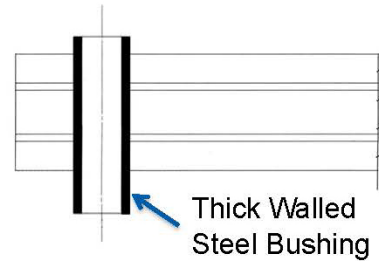


Figure 9.6-3. Spiral .5 Windshields

- Test Plan

- Test with damaged Spiral .5 windshields removed from fleet
 - Coupon testing for gross tensile strength and knockdowns
 - Bird strike testing above qualification requirements
 - Simulation for edge loads
- Update analysis with test findings



Figure 9.6-4. Spiral .5 Testing

9.6.2. AC-130W Stinger II Gun Port Seal Loading and Structural Design

Robert McGinty, Mercer Engineering Research Center (MERC); Jessie Martin, USAF-WR-ALC

This technical effort presents efforts undertaken by Mercer Engineering Research Center (MERC) to research, design, develop, and proof-test a replacement gun port seal plug assembly following the failure of an earlier design on an AC-130W Stinger II aircraft. The AC-130W fleet has been modified to include a removable 30mm Bushmaster II Trainable Gun Mount (TGM) forward of the wings, similar to the AC-130U's 25mm TGM (Figures 9.6-5 and 9.6-6). This gun is removable in order to regain cargo space when mission priorities allow. But when removed, the gun port opening must be sealed to permit fuselage pressurization. The seal plug assembly must withstand substantial loading due to fuselage pressure acting on the 43" diameter gun port. The research portion of the task consisted of identifying causes of the structural failure. This work revealed that loads on the structure are significantly higher than first thought due to loading mechanisms present in the gun boot, the flexible rubber membrane sealing the aircraft air-tight, while permitting the gun to move. The loading can be quite nonintuitive because of the radial membrane mechanics involved. MERC developed a program to calculate these loads using Radial Equilibrium Curve (REQ) theory. With new loads computed, MERC designed and developed a new seal plug assembly (Figure 9.6-7) that is both stiffer and stronger than the original, while also being lighter. A key step in the process was the minimization of collateral bending loads on the assembly by optimizing its position and orientation within the gun port using the REQ program. Extensive finite element (FE) analysis was also performed to optimize the assembly for weight, stiffness and strength. Once fabricated, the prototype assembly was mounted on an MC-130W and pressurized to qualify the new design and measure the loads exerted on it by the gun boot. A 6-axis load cell was used to measure all six components of loading that the gun boot exerts on the structure. This constituted a direct experimental verification of the radial membrane theory used to determine the loads on the assembly. It was found that the loads predicted by the theory were very accurate (Table 9.6-1). They were then used to formulate a laboratory structural test, which confirmed that the assembly could

withstand the required number of pressurization cycles without developing cracks or failures. The new seal plug assembly has now been deployed to all AC-130W aircraft.



Figure 9.6-5. C-130 Gun Ports and Boots

- AC-130W fleet has been modified to include a removable 30mm trainable gun mount (TGM)
- When TGM is removed, the gun port opening is sealed with a seal plug assembly to permit pressurization

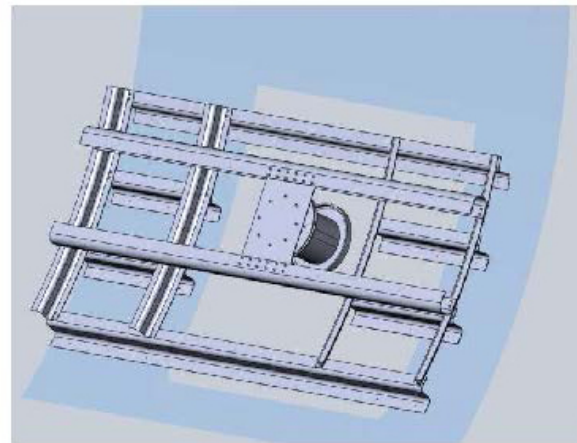


Figure 9.6-6. Removable Trainable Gun Mount and Seal Plug Assembly

- Bearing-load design approach
- Waffle plate onto I-beams onto bearing blocks onto aircraft structure
- Bearing blocks accommodate variations in aircraft structure (all I-beam/Waffle plate assemblies common throughout fleet)

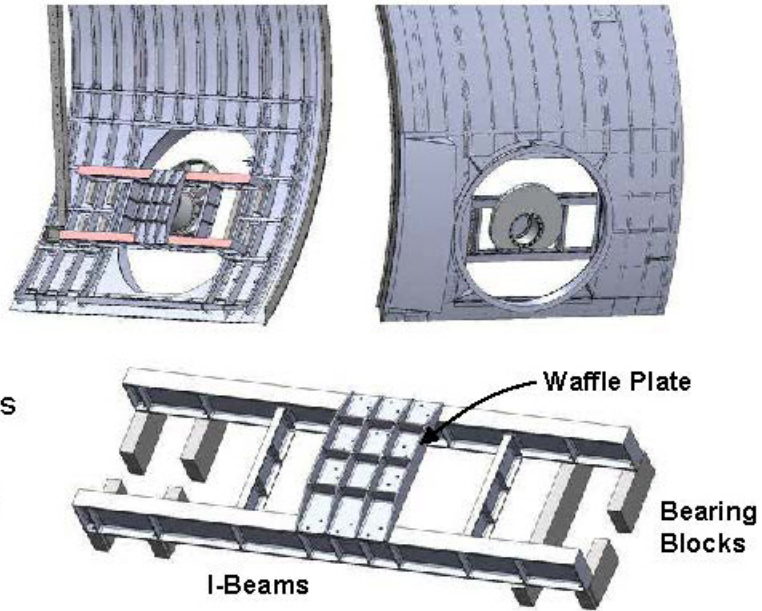


Figure 9.6-7. New Seal Plug Assembly Design

Table 9.6-1. Comparison to REQ Theory

- Tested to 4 psi fuselage pressure and results scaled to 8 psi

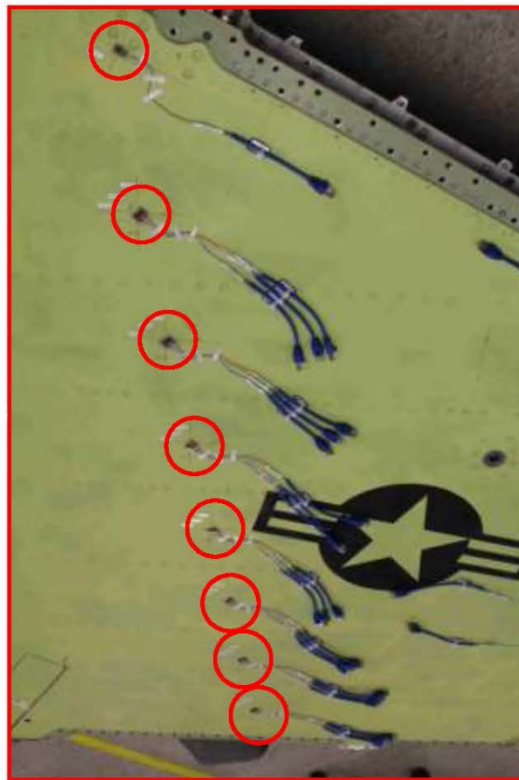
8 psi	F _x (lb)	F _{y'} (lb)	F _{z'} (lb)	M _x (in-lb)	M _{y'} (in-lb)	M _{z'} (in-lb)
Measured	90	-6,050	-430	17,000	-1,440	1,320
Predicted	0	-5,990	-840	14,770	0	0
% Diff		1%	49%	15%		

- Excellent agreement on outboard force, F_{y'}, and good agreement on moment, M_x
- Nonzero measured F_x, M_{y'}, M_{z'} values reflect manufacturing and measurement variations

9.6.3. F-16 Block 50 Full-Scale-Durability Test Correlation and Test Findings

Keith Sundstrom, Selen Minarecioglu, and Carlos Cordova, Lockheed Martin Corporation

The F-16 Program is currently conducting its third Full-Scale-Durability Test (FSDT). The current test is in support of a potential extension of the Certified Service Life of the Block 40 and Block 50 configurations. The Block 50 FSDT airframe has been more thoroughly instrumented (Figure 9.6-8) than any other test article to date. Over 1,100 strain gages (Table 9.6-2) have been installed to provide a comprehensive overview of the internal load distribution through the airframe. This technical effort will discuss the correlation of the pre-test strain surveys to the coarse grid air vehicle finite element model using the guidance and requirements of the USAF Structures Bulletin EN-SB-11-001 (Figures 9.6-9 through 9.6-11). A discussion of the structural findings from testing to date will also be included.



 - *Indicates Strain Gages*

Figure 9.6-8. Lower Wing Skin Gage Installation

Table 9.6-2. Strain Gage Distribution

Summary	Axial Gages	Vesette Gages	Rosette Gages	Total Channels
Forward Fuselage	105	7	0	112
<i>Center Fuselage*</i>	<i>357</i>	<i>43</i>	<i>50</i>	<i>550</i>
Aft Fuselage	176	120	10	326
<i>Wing*</i>	<i>192</i>	<i>0</i>	<i>80</i>	<i>432</i>
Total	830	170	140	1420

** Critical Structure Shown as an Example*

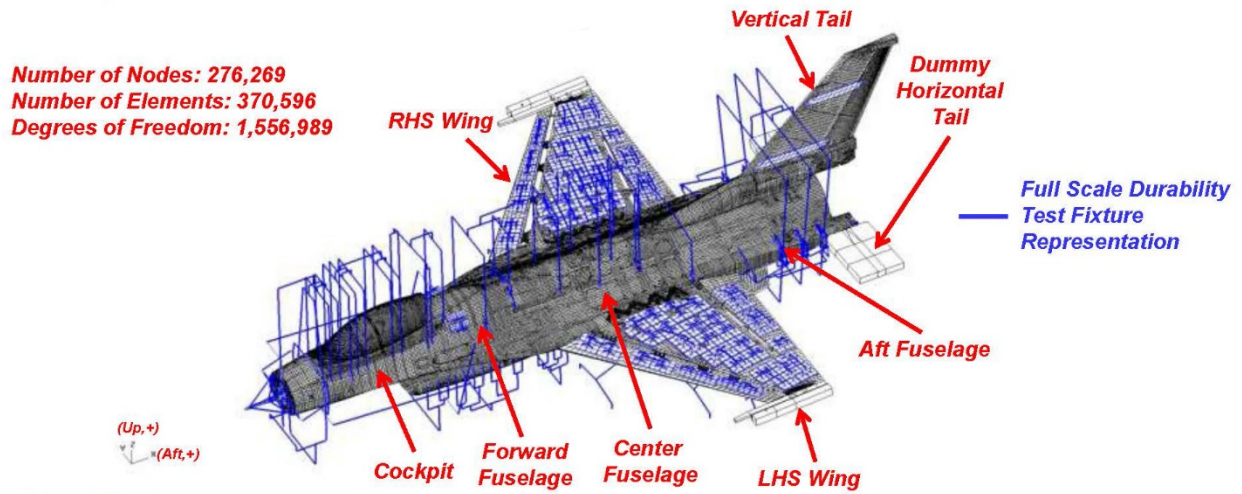


Figure 9.6-9. Coarse Grid Finite Element Model

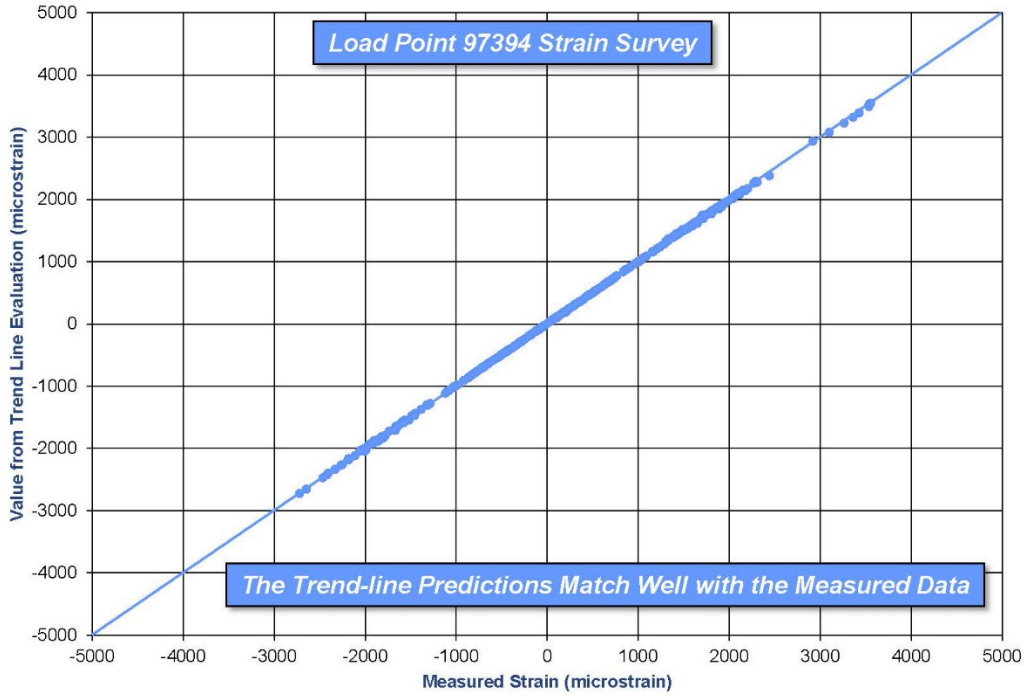


Figure 9.6-10. Wing Trend-Line Comparison

Load Point 97394 Strain Survey

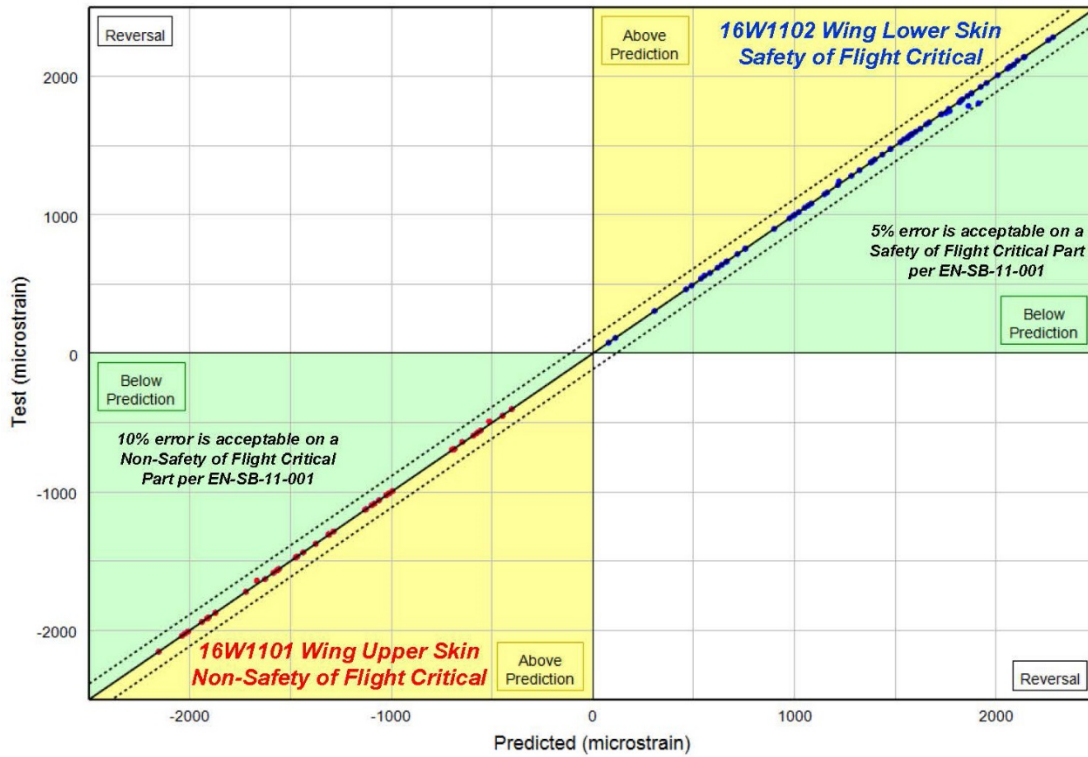


Figure 9.6-11. Wing Skin Correlation Results

9.6.4. Fatigue Crack Growth Tests and Analyses on 7249-T76511 Aluminum Alloy Specimens Under Constant Amplitude and Simulated Aircraft Wing Loading

James Newman, Jr., Mississippi State University; Kevin Walker, DSTO-Australia; Min Liao, National Research Council Canada

The wings on the Naval aircraft, P-3C, are made of 7075-T651 aluminum alloy. The aircraft is currently involved in an extensive life-extension program being conducted by a number of organizations in the United States, Canada, Australia, and Europe. In some fleets, the wings are being replaced with 7249-T76511 aluminum alloy for better fatigue and corrosive performance. A comprehensive coupon testing program, analytical model development, and a validation program were undertaken. The aim was to develop an accurate and reliable model for the 7249-T76511 material. Test methods that have been demonstrated to have significant advantages for other materials, including 7075-T651, were applied. Those methods include compression pre-cracking and variations on standard load-reduction techniques. The FASTRAN advanced non-linear life-prediction code (Figure 9.6-12) was enhanced with double the number of elements in the plastic zone ahead of the crack tip and a cycle-by-cycle approach was adopted. The current research effort at Mississippi State University was supported by the U. S. Navy. The technical effort presents the results of large-crack-growth-rate tests conducted on compact, C(T), specimens made of the 7249 alloy over a wide range of constant-amplitude loading ($R = P_{min}/P_{max} = 0.1$ to 0.9) to establish the baseline crack-growth-rate curve for fatigue-crack-growth analyses (Figure 9.6-13). The compression pre-cracking method was used to initiate cracks at sharp crack-starter notches. Low-rate data were then obtained using both the ASTM load-reduction method and a method proposed by Wu, Wallace and Koul using a constant crack-mouth-opening-displacement procedure. In addition, compression pre-cracking constant-amplitude (CPCA) tests were also conducted to generate data from near threshold to fracture. A crack-closure analysis was used to collapse the rate data from C(T) specimens into a fairly narrow band over many orders of magnitude in rates using a plane-strain constraint factor for low rates and modeled a constraint-loss regime to plane-stress conditions at high rates. Constraint factors and the constraint-loss regime were established from single-spike overload and constant-amplitude tests. Fatigue-crack-growth tests under simulated aircraft wing loading were conducted on middle-crack-tension, M(T), specimens at both high and low applied stress levels using an advanced testing system to apply spectrum load histories. The testing system recorded both the target and actual applied load sequences. The wing spectrum was obtained from Lockheed-Martin and was a full-scale fatigue test (FSFT) spectrum. The spectrum was condensed by removing stress amplitudes less than 15% of the maximum stress amplitude; and the resulting spectrum still had about 300,000 cycles (15,000 flights) in one sequence. Testing under the simulated wing spectrum loading lasted from less than one to about 3 sequences. Fatigue-crack-growth predictions were made with the FASTRAN Version 5.37 life-prediction code. Results from the spectrum tests and analyses generally agreed to within about 20% (Figures 9.6-14 and 9.6-15).

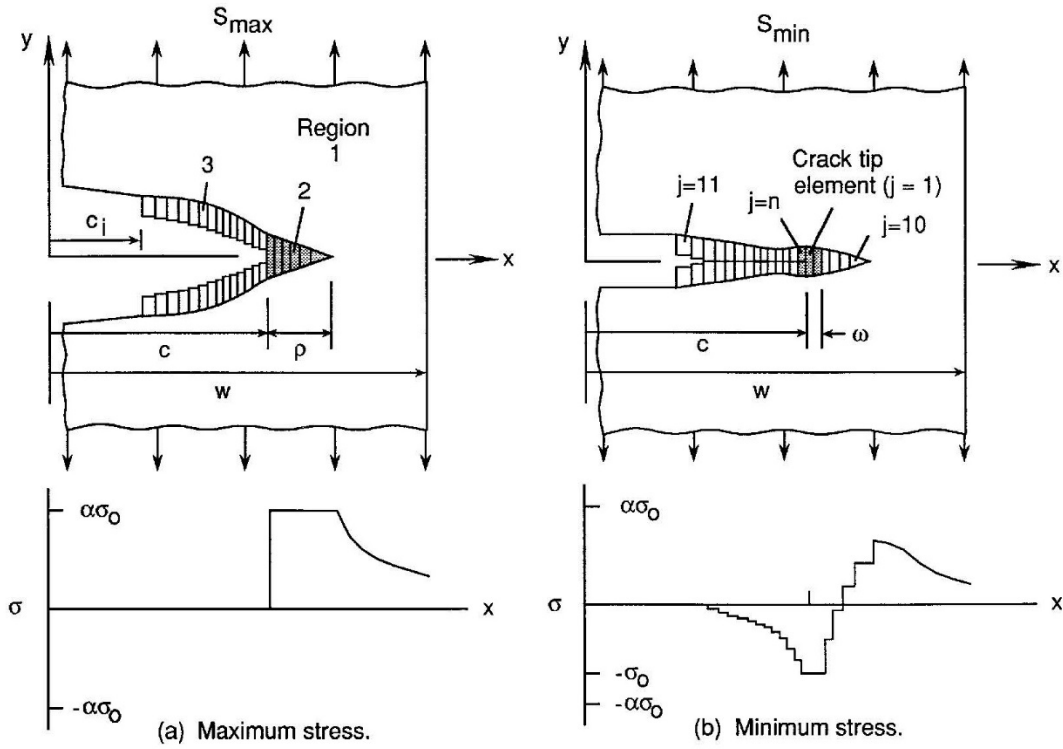


Figure 9.6-12. FASTRAN – Crack Growth and Closure Model

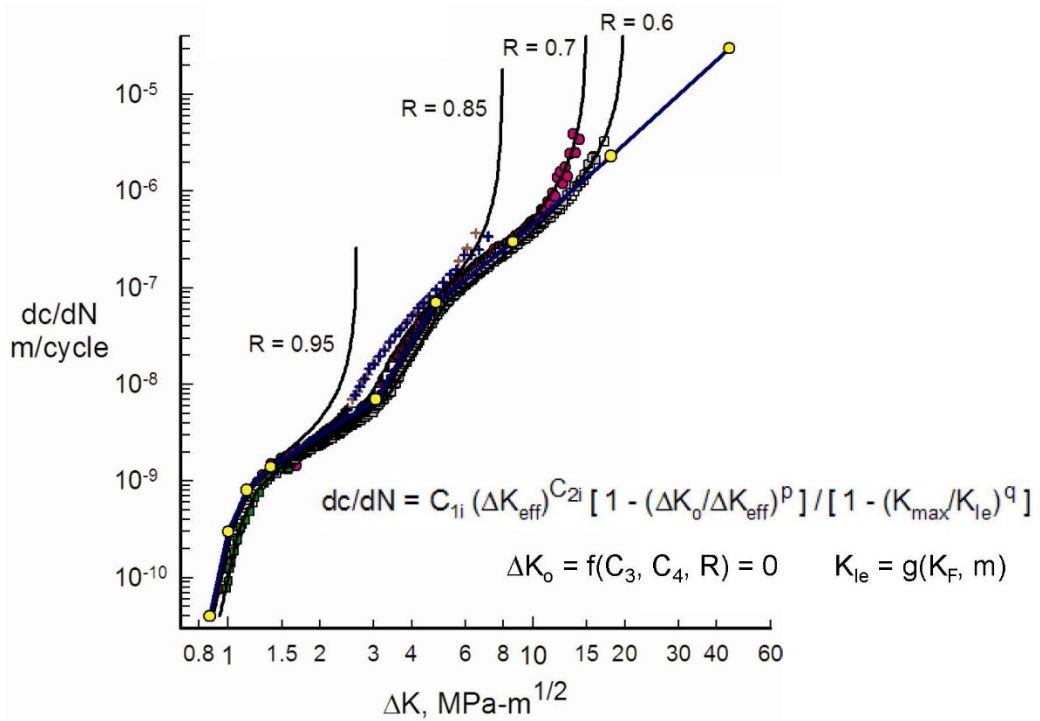


Figure 9.6-13. Comparison of Crack-Growth Equation and Data for High-R Test Data

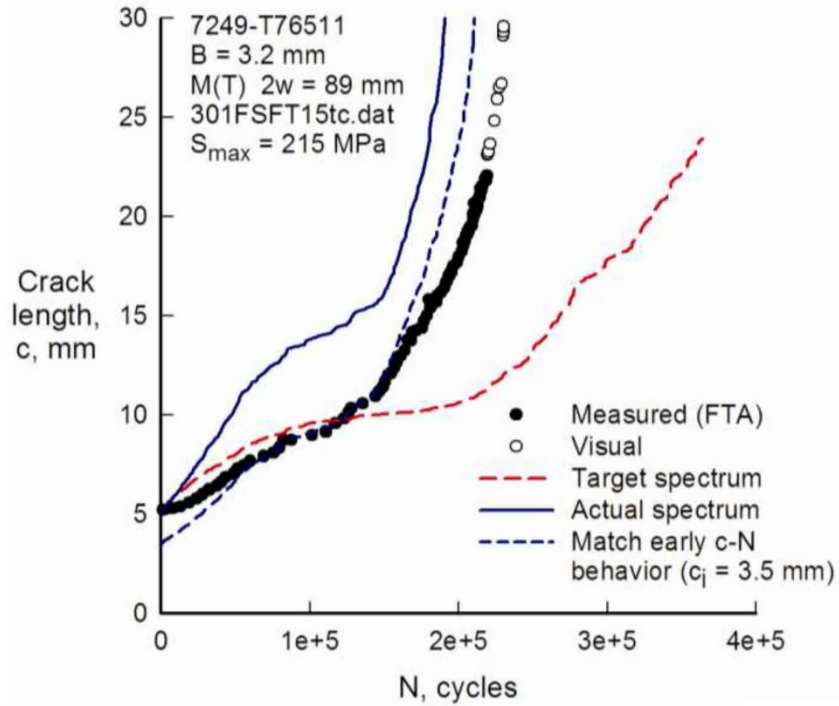


Figure 9.6-14. Measured and Calculated Crack-Length-Against-Cycles for Modified FSFT Spectrum Loading

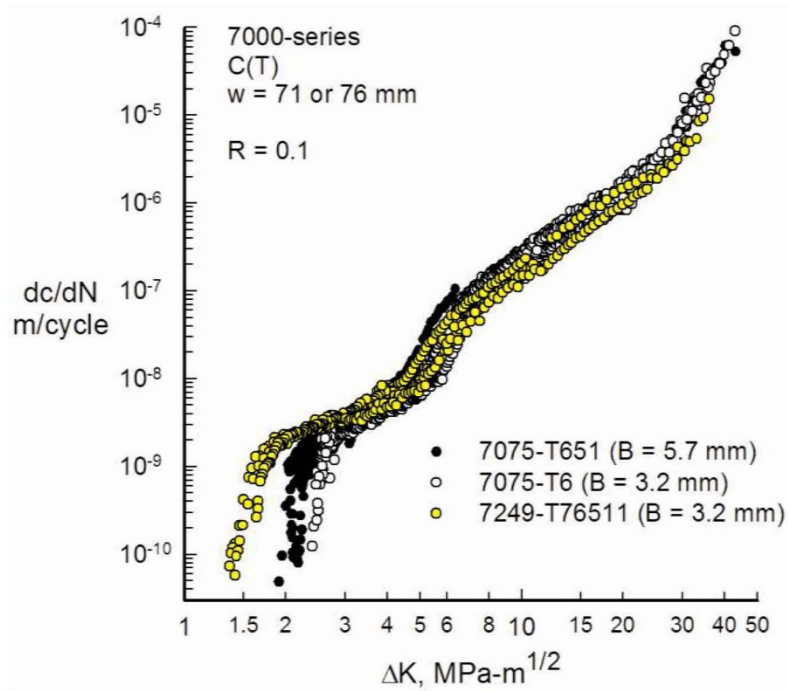


Figure 9.6-15. Comparison of 7249 and 7075 Fatigue-Crack-Growth-Rate Data at Low Stress Ratio

9.6.5. Analysis of the Interaction of Two Parallel Surface Cracks

Jeeyeon Hahn and Alten Grant, Jr., Purdue University

This technical effort deals with the interaction of non-symmetric surface cracks that occur in non-parallel planes. Multiple cracks may form in aging aircraft at stress concentrations such as fastener holes and notched components by stress corrosion and fatigue cracking. Interaction and coalescence of these cracks may significantly affect the lifetime of the structures. Depending on relative positions and orientations of neighboring cracks, local stress fields and crack driving forces can be affected by the presence of adjacent cracks. Even small subcritical cracks may rapidly grow to a size that will cause failure in service due to interaction and coalescence with other cracks (Figure 9.6-16). The interaction behavior and crack propagation direction of two parallel surface cracks is studied using three-dimensional finite element analysis (FEA) (Figure 9.6-17). FEA models with wide range of crack configurations in a finite plate under tension are evaluated to investigate the correlation between the crack shapes and the separation distance between two cracks. The relative distance (vertical and horizontal) between two cracks and size and shape of these cracks are varied to create different stress interaction fields. Stress intensity factors (SIF) along the crack fronts are obtained from FEA, and then, cracking behaviors of the cracks are predicted by taking into account the influence of the interaction on the SIF and the coalescence of two cracks. The results obtained are then compared with existing experimental and analytical data for validation.

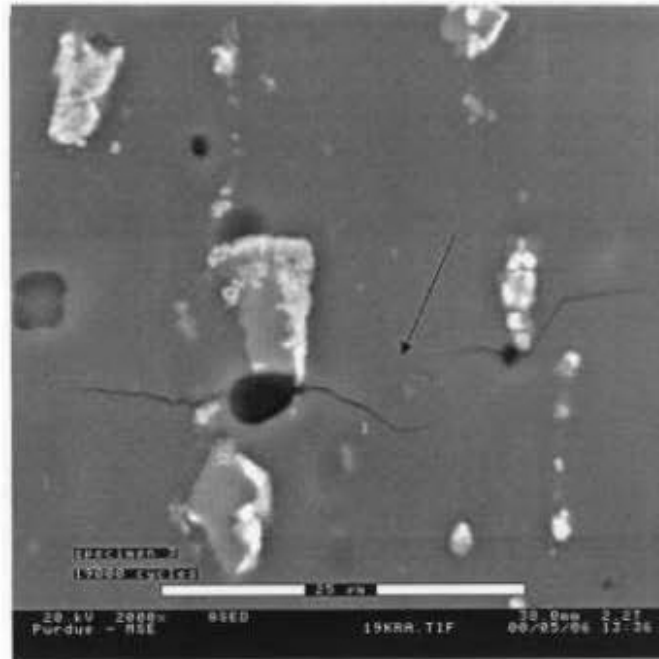


Figure 9.6-16. Multiple Fatigue Cracks Formed at Material Inhomogeneities

- Single semi-elliptical surface crack subjected to tension is modeled with $\frac{1}{2}$ symmetry
- FEM results for various crack shapes compared favorably with Newman and Raju's [4] solutions

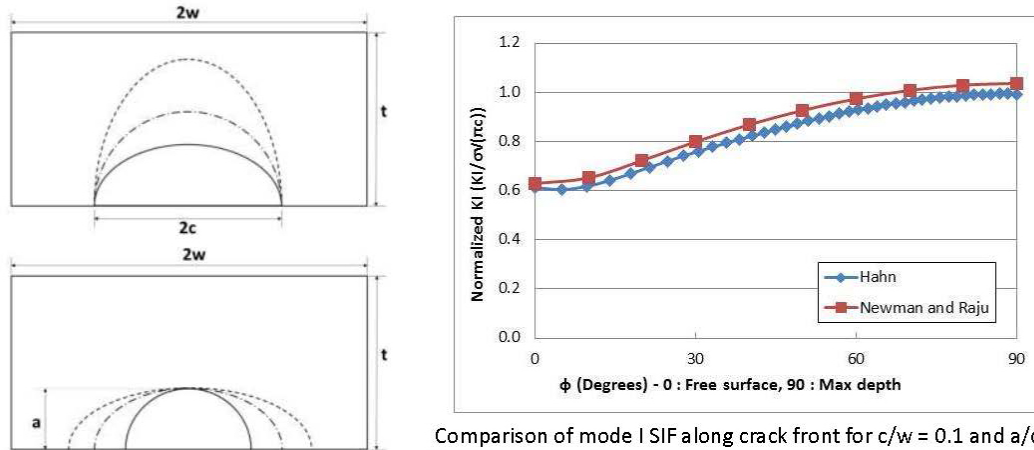


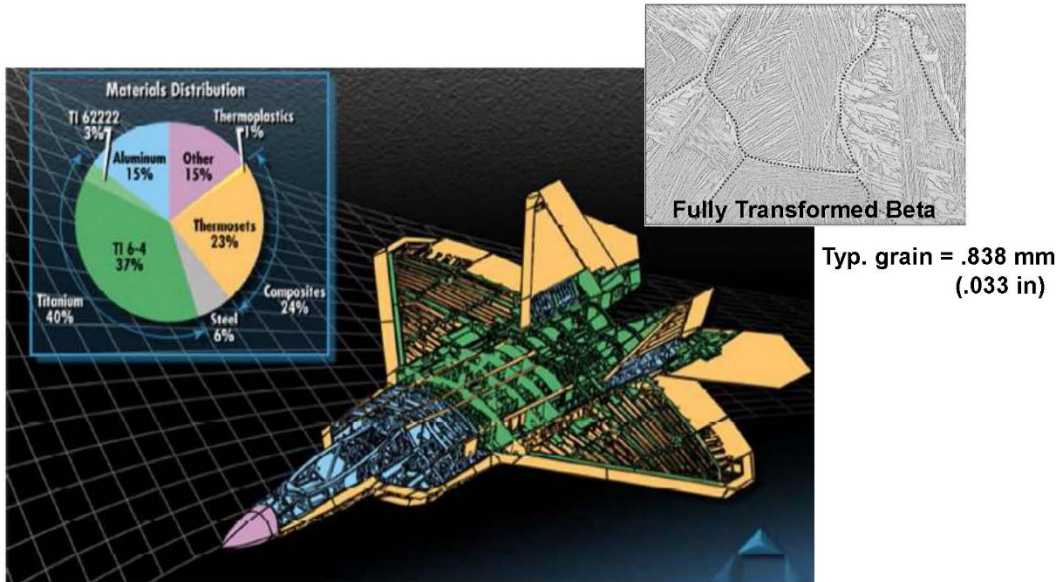
Figure 9.6-17. Comparison of 3D Single Surface Crack SIF Profile

9.6.6. Ti-6Al-4V Small Crack Growth Effect on Damage Tolerance Analysis

Peter Caruso, Ji Park, and Timothy Blasé, Lockheed Martin Corporation; Wirt Garcia and Richard Tayek, USAF F-22 SPO

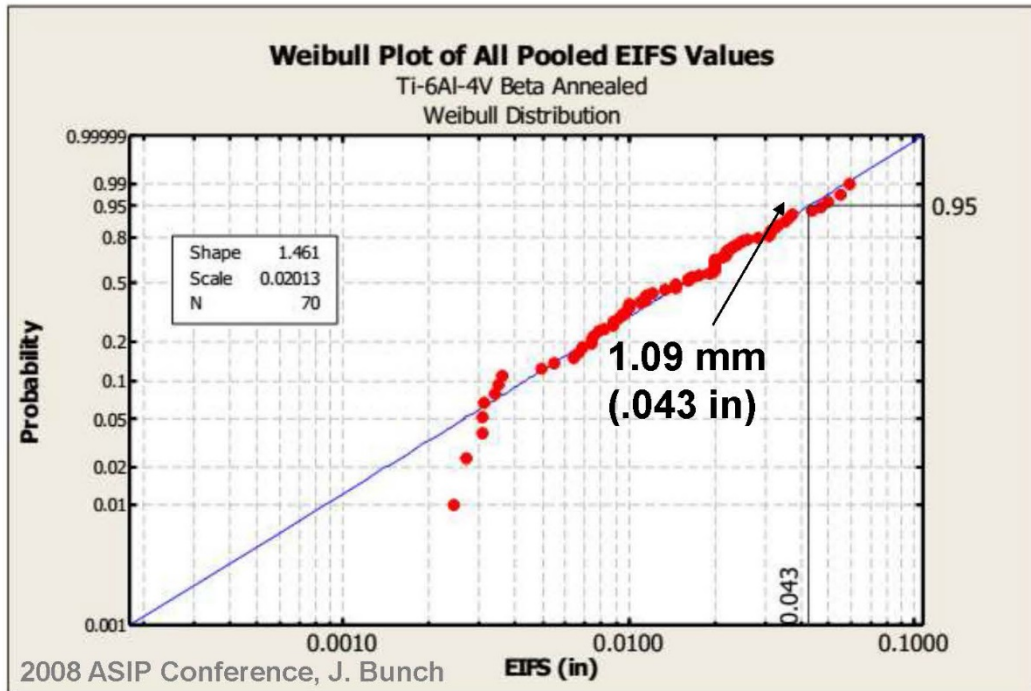
Ti-6Al-4V Beta annealed (BA) material was selected for use in F-22 and F-35 structural applications because of its excellent damage tolerance properties. Damage tolerance analysis using linear elastic fracture mechanics (LEFM) is considered valid if the crack size is large compared to the dimensions of material micro-structural features such as grain size. The typical grain size for the Ti-6Al-4V Beta annealed process is 0.50 mm to 1.27 mm (Figure 9.6-18), which approaches the damage tolerance initial flaw size of 1.27 mm (0.05 in) (Figure 9.6-19). In other materials, roughness induced crack closure (RICC) effects have been observed to accelerate the crack growth rate in the small crack region. This technical effort details the results of an investigation to validate the Ti-6Al-4V BA damage tolerance properties for corner cracks in the range of 0.76 mm and longer. Coupon testing consisting of open hole corner crack and middle tension, M(T), specimens was performed. Cyclic loading included constant amplitude, variable amplitude tension, tension-compression, and highly compressive typical design spectra. Middle tension, M(T), spectra testing was conducted to verify the crack growth retardation load interaction parameters. Both typical design and low stress (or small K level) stress levels were applied to exercise the analysis methodology. Crack growth predictions accurately predicted damage tolerance results at design stress levels (Figure 9.6-20). Analytical predictions were unconservative at very low reference stress or highly compressive spectra, where significant cycling occurred at near threshold crack growth rates. Test requirements were defined to develop improved threshold crack growth rate data using compression pre-cracking and constant amplitude (CPCA) and standard ASTM E647 methodology. Lessons learned and recommendations for damage tolerance verification testing and development of CPCA test requirements are discussed. The authors conclude that Ti-6Al-4V BA LEFM methodology was verified for damage tolerance initial flaw sizes (Figure 9.6-21),

and carefully developed threshold crack growth rate data will improve durability analysis, test correlation factors, and EIFS values.



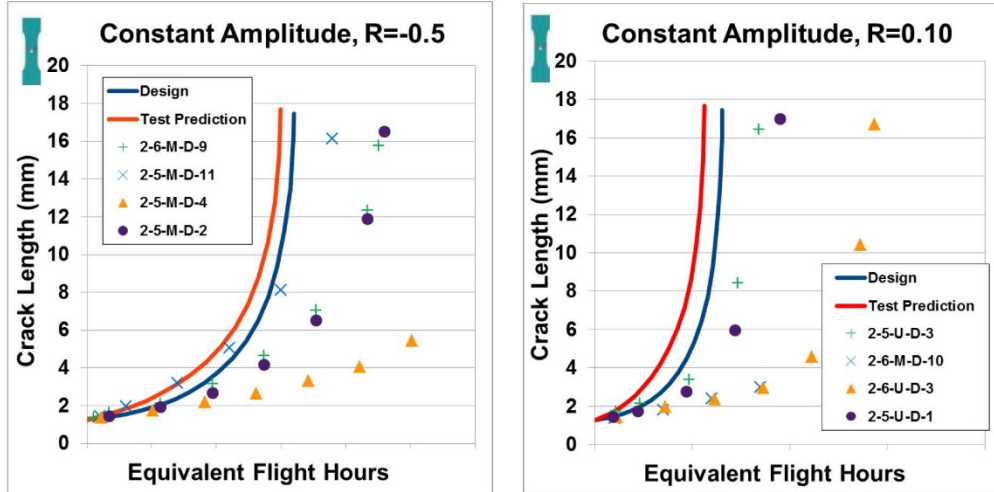
Ti-6Al-4V BA Supports Critical Structures

Figure 9.6-18. F-22 Ti-6Al-4V Applications



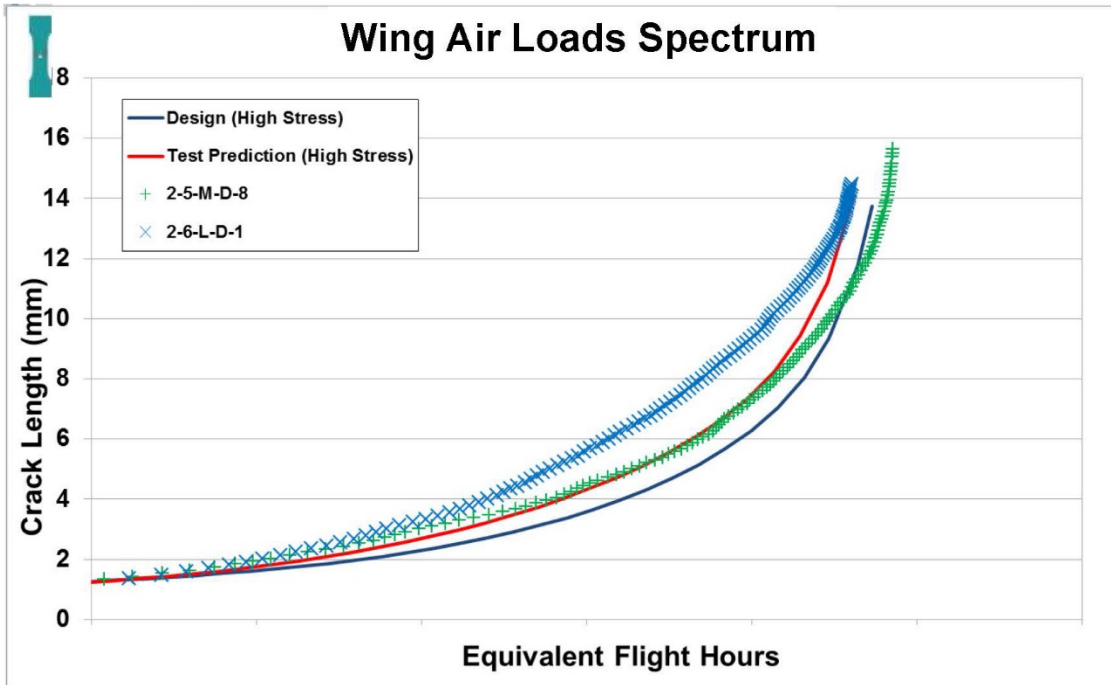
Large EIFS Creates Damage Tol. Risk

Figure 9.6-19. Full-Scale-Test EIFS Distribution



Test Prediction Meets/Exceeds Results

Figure 9.6-20. Constant-Amplitude Analytical/Experimental Correlations



Damage Tolerance Method Verified

Figure 9.6-21. Verification of Damage Tolerance Method

9.6.7. Using Virtual Strain Gauges to Correlate with Bending and Torsion Measured on a Helicopter Tail Cone Using Strain Gauges

Rob Plaskih, HBM-nCode

This technical activity describes the use of virtual strain gauges in order to correlate a full-scale structural test of a helicopter with a finite element model. It focuses on the correlation of bending and torsion moments in the tail cone. These arise from lateral loads applied at the tail. Strain gauges have been used successfully for many years to measure direct strains in a local area. By combining several carefully located gauges in a Wheatstone Bridge, this analysis can be extended to measure the macroscopic loading applied to the structure in terms of bending and torsion moments. This technical activity describes how groups of virtual strain gauges are used in the context of a FE model to derive bending and torsion moments in the tail cone of a helicopter. Rather than correlating individual local strains, which are significantly affected by local stress concentrations and non-linear effects, this approach allows the correlation of the applied loads and moments. These measurements are often much cleaner and more intuitively recognizable by the engineer. The virtual Wheatstone Bridge is modeled mathematically in the process and produces analysis output in terms of applied bending and torsion moments. Virtual strain gauges have been available in commercial software packages since the 1990s. FE post-processor packages such as nCode DesignLife (Figure 9.6-22) have used this concept to recover strains at specified locations and compute fatigue lives in an approach analogous to traditional test-based fatigue analysis.

- The type of strain gauge can be:
 - Single, Tee, Rosette, and Delta
- The orientation can be controlled by:
 - XYZ Vector
 - 2 Nodes
 - Angle Offset

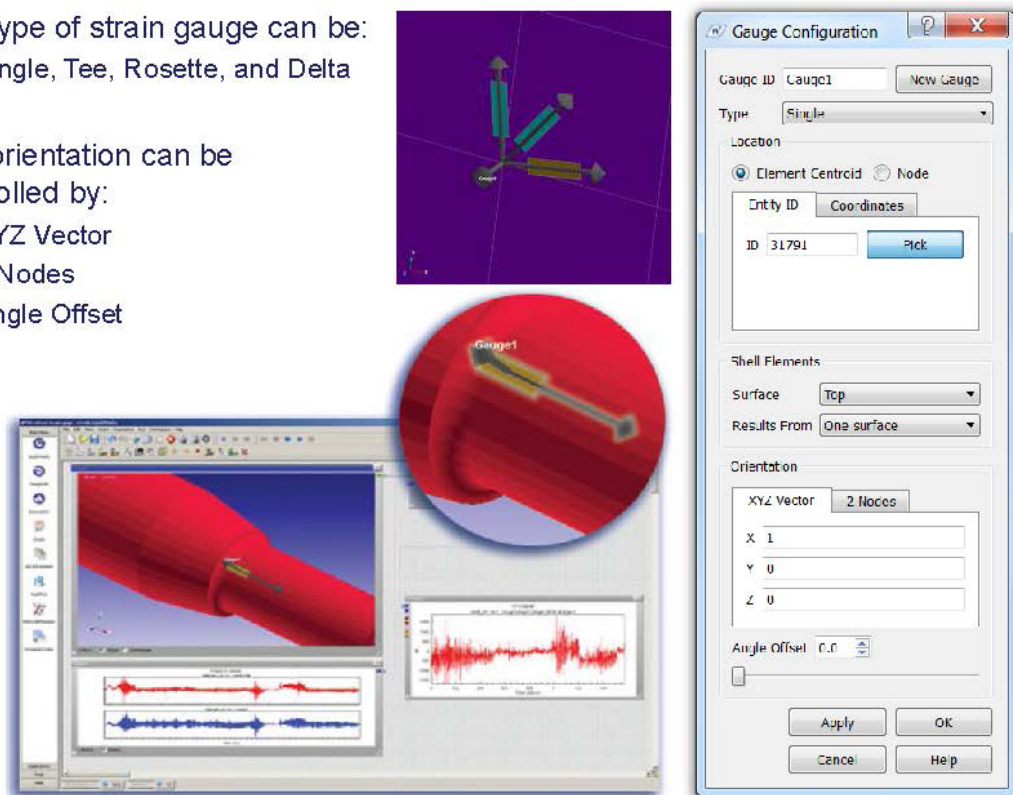


Figure 9.6-22. nCode DesignLife Virtual Strain Gauges

9.6.8. Models for Corner and Through Cracks in Support of Beta Curve Development for the P-8A Poseidon Full-Scale-Fatigue-Testing

Jason Hawks, Engineering Software Research & Development, Inc.; Pratic Bhandari and James Candela, USN – NAVAIR; NagaRaja Iyyer, Technical Data Analysis, Inc.

Beta factors for corner and thru cracks in complex geometric details are often obtained as the superposition of Stress Intensity Factors (SIFs) of several simpler cases, and beta curves are then compiled as a function of crack length to perform crack growth studies. Since closed-form solutions for this type of problems are generally not available, the alternative to the superposition approach is the development of properly formulated breakout models solved by the finite element (FE) method. When the use of FE analysis of cracks is combined with automation scripts which allow changes to parametric geometry, the approach has significant advantages over historic beta curves. This technical activity will address the modeling strategy used to compute the beta curves across various stages of crack growth at various critical locations in the structure of the P-8A Poseidon aircraft (Figure 9.6-23) using the commercial FE analysis software StressCheck. For the various phases of crack growth, a series of finite element meshes are created for a range of crack lengths (Figure 9.6-24). The meshes and the corresponding aircraft component geometry are made parametric to interface with an automation script which is simple to use, so that the analyst can account for variability in manufacturing and repairs, or to perform what-if scenarios in support of uncertainty quantification. All analyzed locations had significant geometry features in close proximity to the crack including countersunk-fastener holes, fillets, local pad-ups, and stiffeners leading to the requirement for both thru and corner crack configurations during the crack progression (Figure 9.6-25). In certain cases, load shedding to adjacent structure was included by modeling fastened sub-assemblies to update the loads applied to the breakout model as a function of crack length (Figure 9.6-26). Corner and thru cracks were analyzed in 3D due to the complexity of the geometry, and to satisfy the requirements of solution verification: To control the error of approximation in the computation of the SIFs, a sequence of finite element solutions with an increasing number of degrees of freedom were obtained for each computed beta factor. This modeling approach has several advantages over traditional beta factor development: The models are more reliable because the effects of simplifying assumptions can be evaluated and no superposition is required. In addition, effects such as traction-loaded vs. pin-loaded holes can be easily addressed. This work was performed in support of the P-8A Full Scale Fatigue Test (FSFT) for the Naval Air System Command (NAVAIR) Aircraft Structures Division.

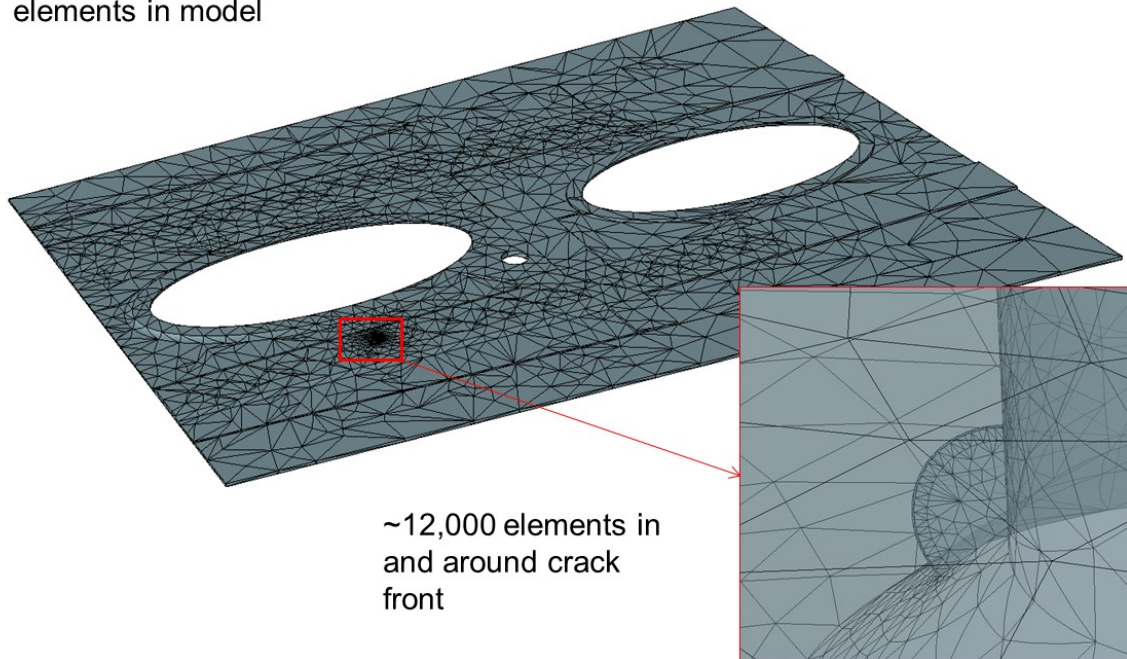
- Derivative of the Boeing 737-800ERX
- Anti-submarine and surface warfare platform



Photo Credit: The Boeing Company

Figure 9.6-23. P-8A Poseidon Aircraft

~23,000 **solid**
elements in model



~12,000 elements in
and around crack
front

Figure 9.6-24. Typical Mesh for Stress Intensity Factor Extraction

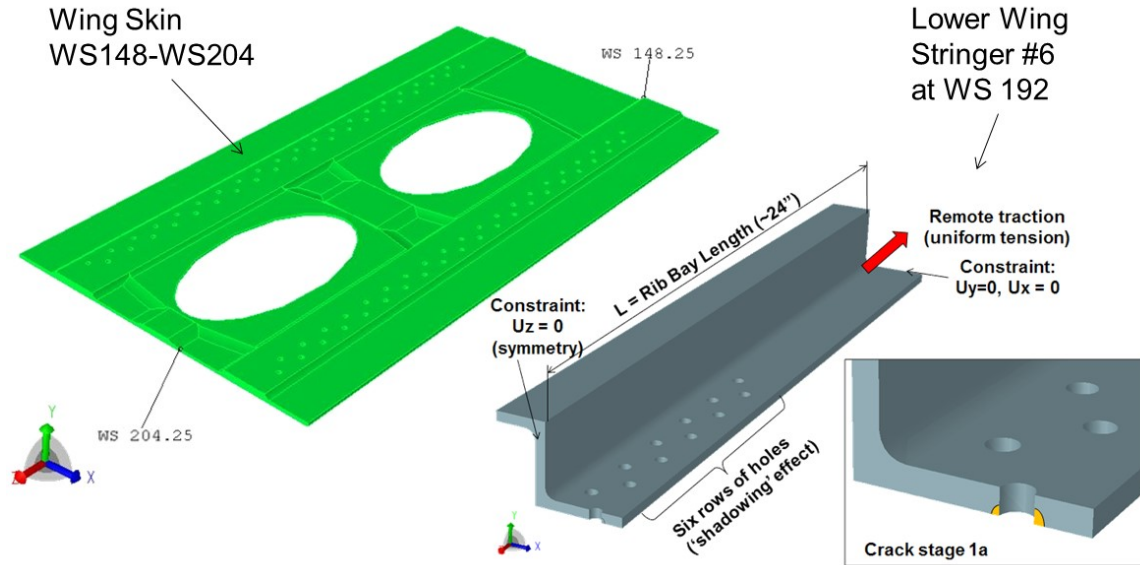


Figure 9.6-25. Typical Solid Models

- In some locations, load shedding due to crack growth played a significant role
 - Required creation of secondary models to determine reduced loading in structure

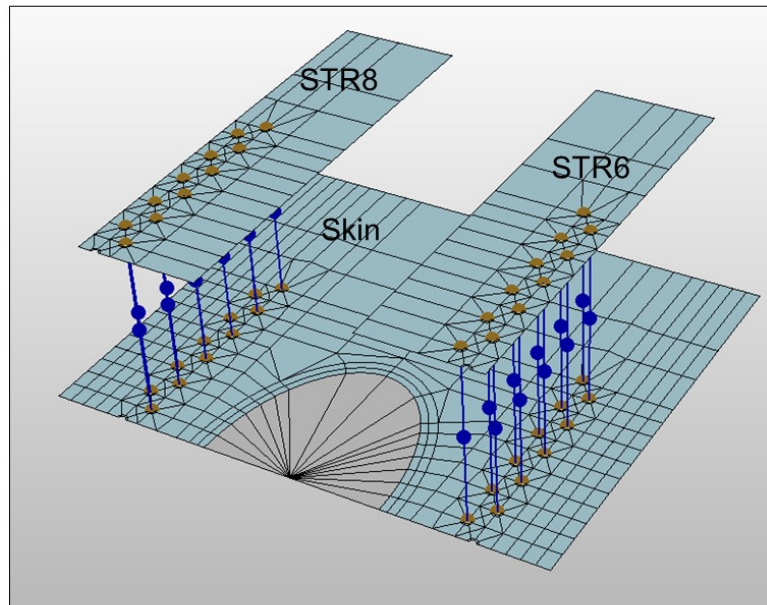


Figure 9.6-26. Modeling for Load Transfer

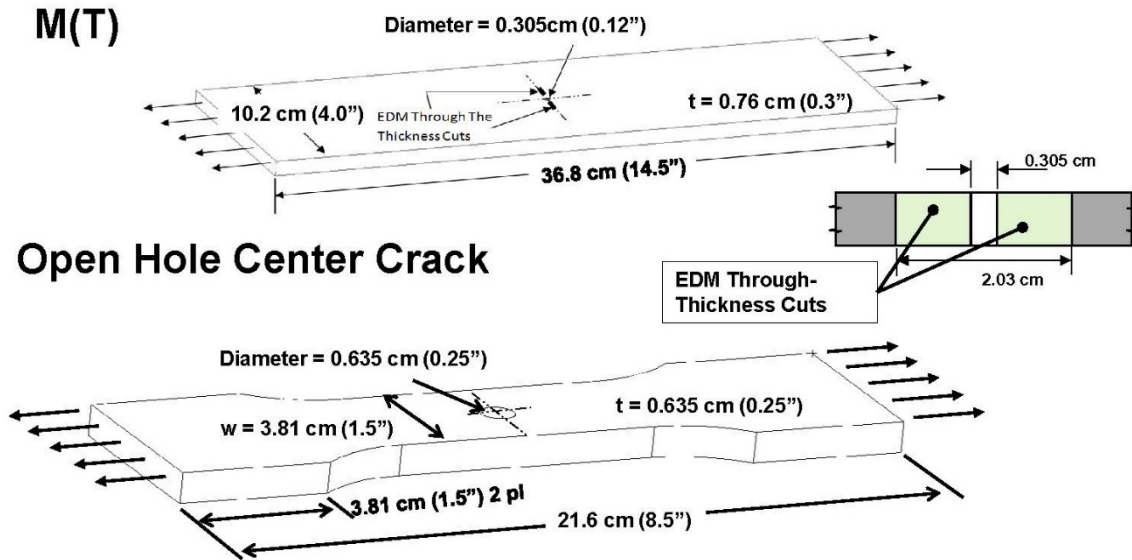
9.6.9. Titanium 6Al-4V Durability Method Development and Test Verification on Small Crack

Ji Park, Timothy Blase and Peter Caruso, Lockheed Martin Corporation; Jacob Warner, USAF F-22 SPO

Titanium 6Al-4V small-crack-growth effects on damage tolerance analysis were presented at the 2013 Aircraft Structural Integrity Program (ASIP) Conference. In this test phase, the Ti 6Al-4V crack-growth tests are performed to update and verify the durability analysis methods. It is known that fatigue analysis based on linear elastic fracture mechanics (LEFM) is not valid in the small crack region. Previous crack growth tests developed faster crack growth rates than F-22 (Figure 9.6-27) design predictions and calculated half the EIFS of F-22 test correlation analysis. Test correlation analysis had calculated a larger Equivalent Initial Flaw Size (EIFS) than the durability crack growth assumption (0.01 in). This technical activity discusses the development and verification of Ti 6Al-4V crack-growth-rate data in the threshold region. Middle tension (M(T)) (Figure 9.6-28) tests are conducted using ASTM LR, compression pre-cracking constant amplitude (CPCA) (Figure 9.6-29), and constant-Kmax methods for various constant amplitudes ($R = -0.95, -0.5, 0.05, 0.4, 0.7$ and 0.9). In the ASTM LR test, the adjusted compliance ratio (ACR) is used to remove the crack-closure effect. The compression pre-cracking generates tensile-residual stress ahead of the crack tip unlike the load-shedding method that creates compressive-residual stress and induces load-history effects. CPCA also experiences load-history effects through residual stresses; however, once the crack grows beyond two times the compressive-plastic-zone size, it's no longer affected by tensile-residual stress from the compression pre-cracking and the results are considered valid. Another method without remote closure or load-history effects is the constant-Kmax test. The results of these three test methods are compared. Kmax test results match well with ASTM LR tests for all constant-amplitude cases (Figure 9.6-30), and CPCA predicts lower threshold data than Kmax and ASTM LR for $R=0.9$. Also, open-hole durability tests were performed at constant amplitude $R=0.05$ (Figure 9.6-31) and using a variety of spectra. The applied spectra included FALSTAFF (Figure 9.6-32), wing air load, fuselage bending, and vertical tail. The durability test conditions were subjected to high and low reference load levels to challenge the analysis methodology. For the durability verification tests, the electric potential drop method is used to measure the crack size as well as an optical measurement device. Updated Ti-6Al-4V properties for durability analysis are developed.



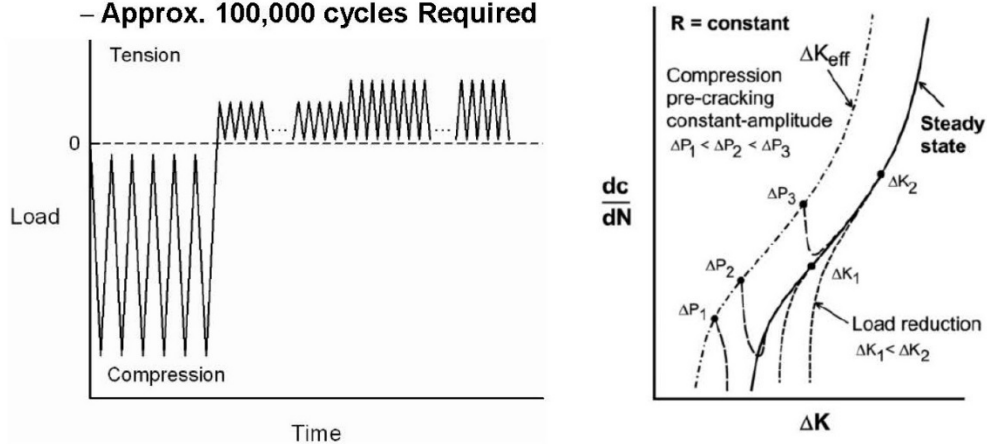
Figure 9.6-27. F-22 Aircraft



M(T): Physically Large Cracks Used for CG Rates
OH: Small Cracks Used in Method Verification

Figure 9.6-28. M(T) Test Specimen

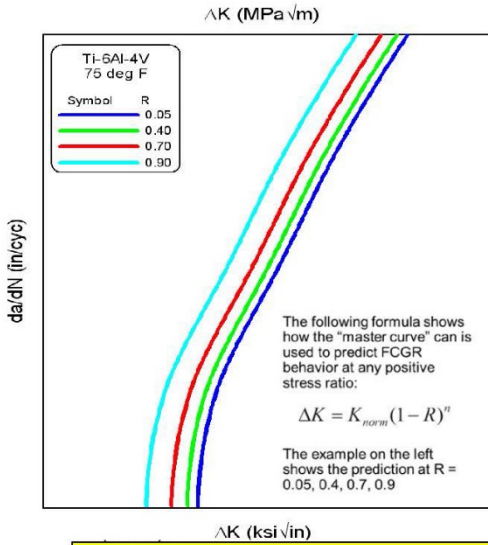
- **Near Threshold da/dN Tests (R = .90, .70, .40, .05, -.50, -.95)**
 - Comparison with ASTM Standard Load Reduction (LR)
 - Compression Precracking Constant Amplitude (CPCA)
 - Precrack* $|K_{cp}| / E = 0.00015$ to $0.0003 \text{ m}^{1/2}$ (0.001 to $0.002 \text{ in}^{1/2}$)
 - Approx. 100,000 cycles Required



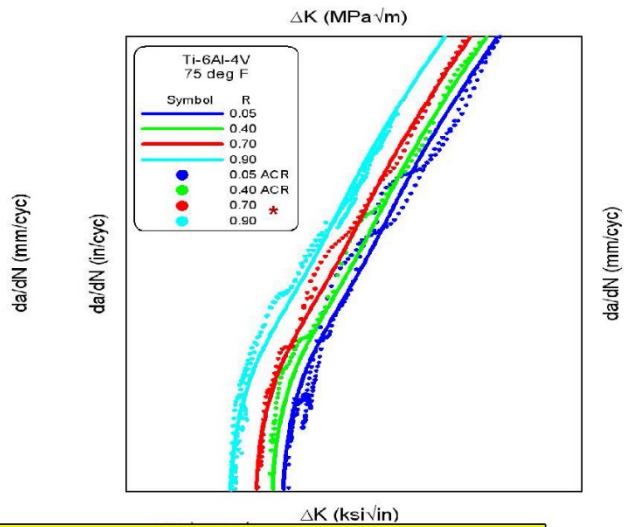
Develop da/dN Curves in Near Threshold Region

Figure 9.6-29. CPCA Test Description

Using Knorm (Master Curve), da/dN Prediction for any R value

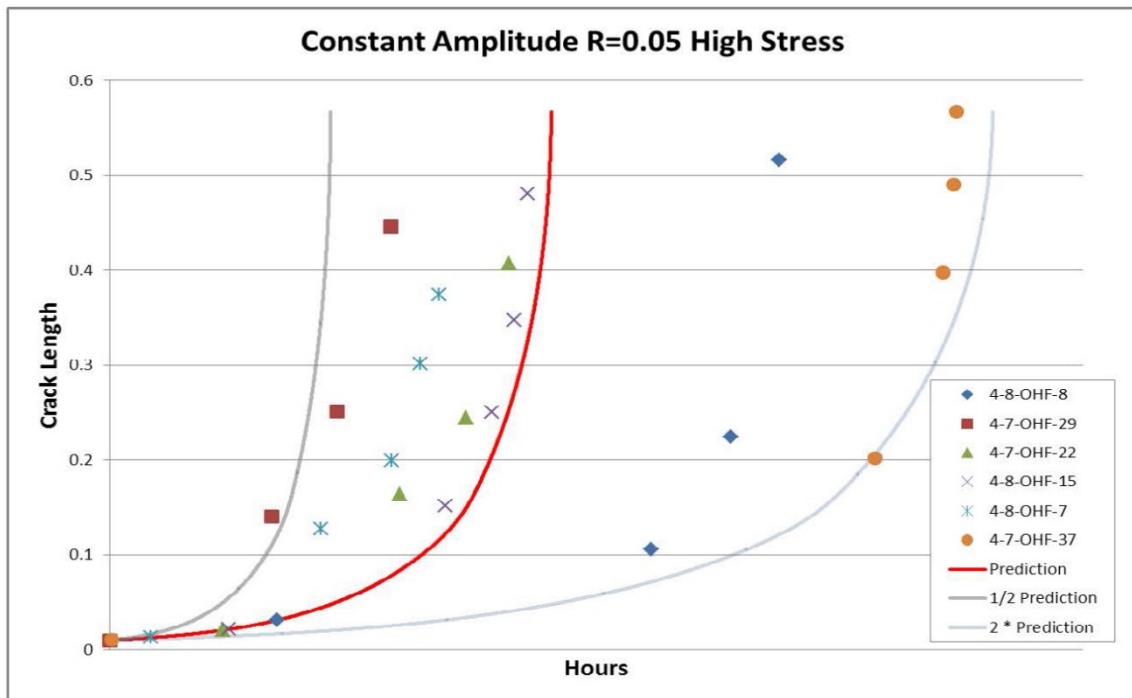


Comparison with Constant-Kmax Master Curve with ASTM LR test data



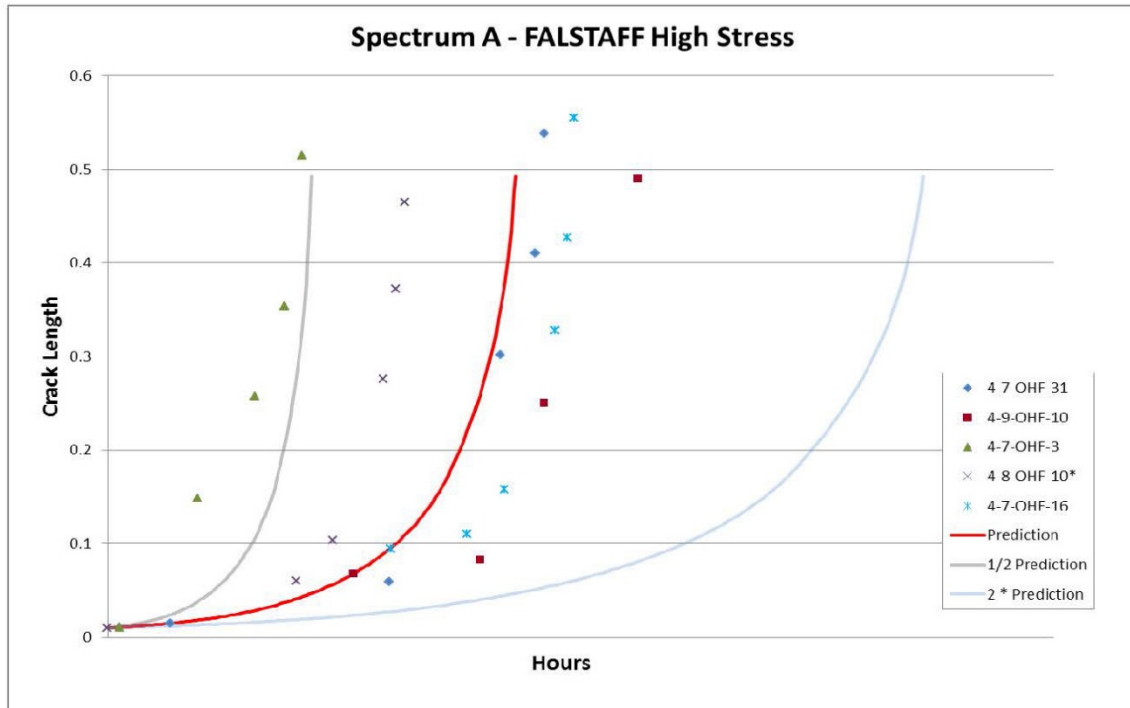
Kmax and ASTM LR Tests Have Good Correlation

Figure 9.6-30. ASTM LR vs. Constant-Kmax Results Comparison



Meets the Test Success Criteria

Figure 9.6-31. Open Hole Results (CA R = 0.05 High Stress)



Meets the Test Success Criteria

Figure 9.6-32. Open Hole Results (FALSTAFF, High Stress)

9.6.10. Predicting Fatigue Crack Growth in Forgings with Bulk Residual Stress

Robert McClung, Carl Popelar, John McFarland, and Vikram Bhamidipati, Southwest Research Institute; Mark James and John Watton, Alcoa Technical Center; Michael Hill and Adrian DeWald, Hill Engineering, LLC; Dale Ball, Lockheed Martin Corporation

Large aluminum forgings offer some manufacturing advantages for aerospace structures, but can also contain complex residual stress (RS). The effects of this RS on component lifetime are also complex, and this complexity has hindered the effective utilization of forgings. However, significant maturation of analytical and experimental tools has now made it possible to characterize and address RS effects accurately in the design cycle. This effort demonstrated and evaluated the current state of the art of these tools. Fifty-six fatigue crack growth (FCG) tests were performed on five different “design feature” (DF) coupon geometries with constant amplitude or spectrum loading. The coupons had all been machined from “logs” of Al 7085 plate that had been heat-treated in a manner to deliberately induce significant levels of bulk residual stress (Figure 9.6-33). Finite element analyses of the DF coupons were performed to calculate how bulk RS in the original specimen blanks would be redistributed as a result of the geometry changes to create the DF coupons. Probabilistic models of the variability in the RS were generated using Principal Components Analysis (PCA) based on twenty-three replicate slitting measurements of the original specimen blank geometry (Figure 9.6-34). Each of these replicate measurements was used to calculate a corresponding RS field in each of the five DF coupon geometries at each of four different locations in the original logs. Independent PCA models were then constructed for each DF coupon type and log level. Comparisons of the resulting PCA models with a limited number of independent measurements of RS in DF coupons using the contour method indicated good agreement

(Figure 9.6-35). Fatigue crack growth life analyses were performed with the NASGRO® software for each of the FCG tests conducted in this study. The analyses of the constant amplitude tests employed a simple non-interaction crack growth model with a tabular representation of the da/dN versus ΔK relationship at several discrete R-ratios. The analyses of the spectrum tests employed the NASGRO STRIPY strip-yield (crack closure) load interaction model. FCG analyses were performed for each test using the mean RS gradient and the 2-sigma (95%) RS gradients, and another analysis was performed neglecting RS. Weight function stress intensity factor solutions were used to address the combined effects of applied and residual stresses. Comparisons of the FCG analyses with the experimental crack growth and life data indicated good agreement overall (Figures 9.6-36 and 9.6-37). Nearly all total FCG test lifetimes were predicted within 2x using the mean RS gradient, and most predictions were conservative. Predictions where the fatigue crack was growing primarily in tensile RS fields tended to be relatively insensitive to variability in the RS gradient, while predictions where the fatigue crack was growing primarily in compressive RS fields tended to be very sensitive to variability in the RS gradient. Predictions neglecting RS were nearly always inaccurate, sometimes extremely so.

- 7085-T74 billet cut into many 'logs' that were quenched and aged individually to intentionally leave significant residual stress
- Coupon blanks extracted from three longitudinal positions and six transverse positions (total of eighteen unique positions) within each log

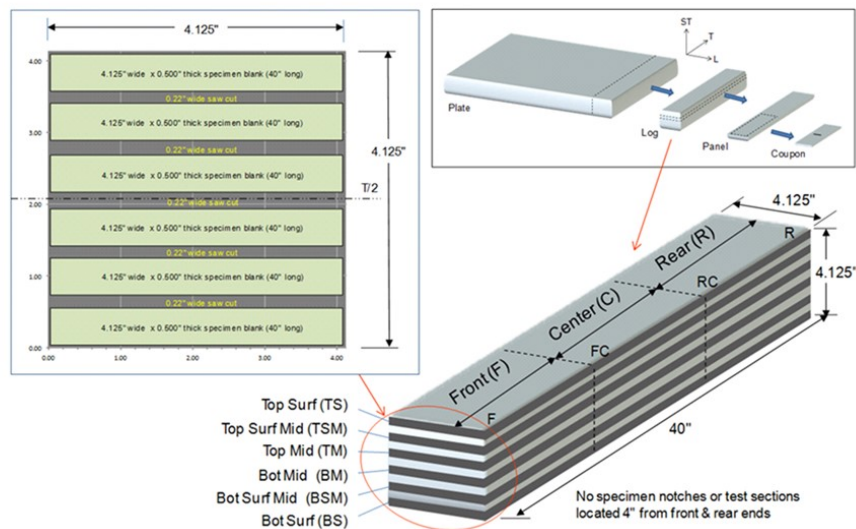


Figure 9.6-33. Billets, Logs, Coupons

- FE analysis used to translate 23 replicate measurements of RS in coupon blanks into 23 distributions of RS in the test coupons for each of the five DF types

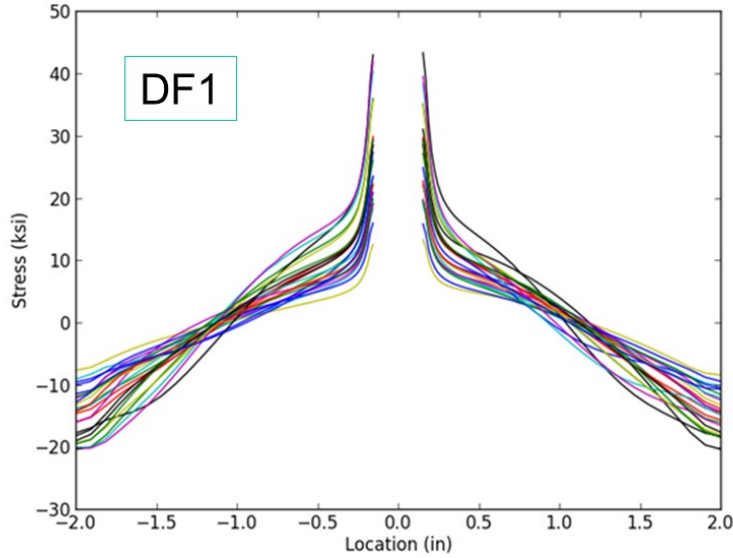


Figure 9.6-34. Probabilistic Analysis of Residual Stress in Coupons

- Resulting probabilistic model compared with individual contour measurements of RS in test coupons by Hill Engineering

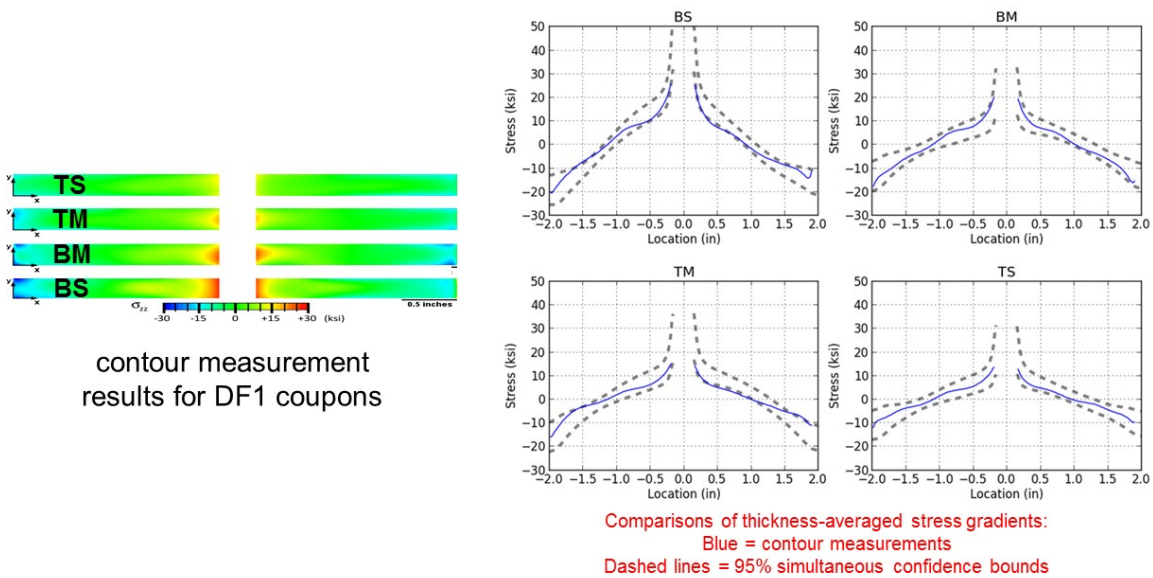


Figure 9.6-35. Comparison of Probabilistic Models with Contour Measurements

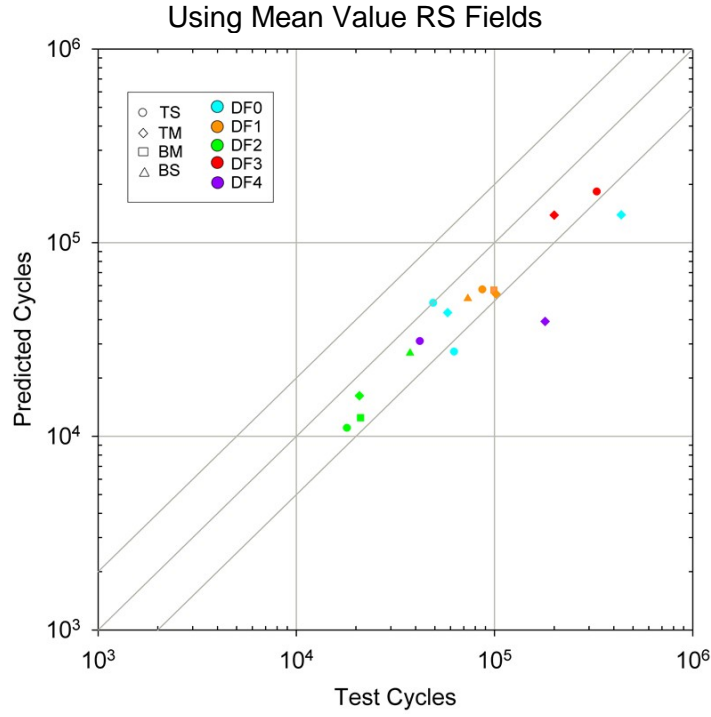


Figure 9.6-36. Summary of Constant Amplitude Predictions

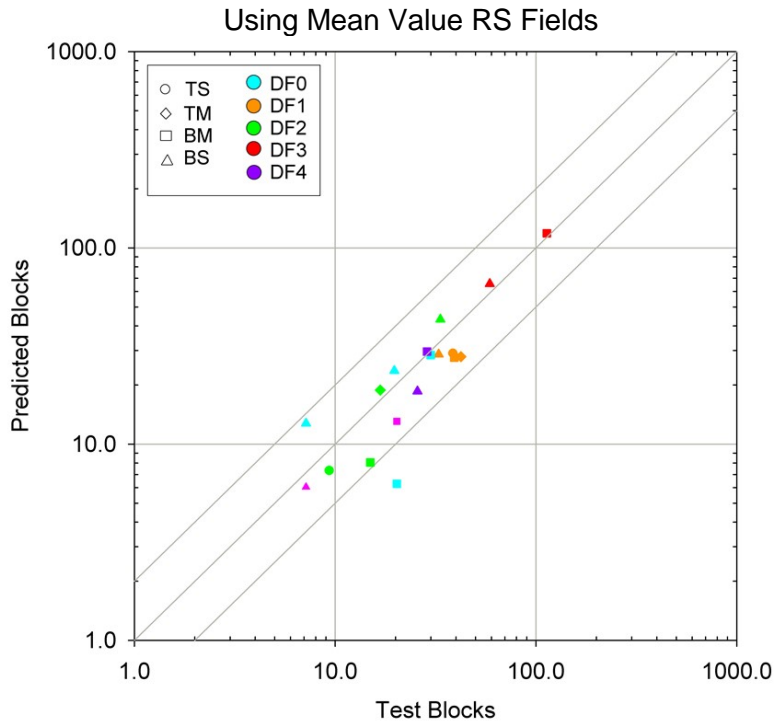


Figure 9.6-37. Summary of Spectrum Predictions

9.6.11. A Discrete-Crack-Network-Based Fatigue Damage Assessment for Bonded and Bolted Composite Structures

Jim Lua, Global Engineering and Materials, Inc.

Both bonded and bolted joints have been used extensively in the integration and repair of composite structures. The load transfer provided by either a bonded or a bolted joint often drives the design under monotonic and fatigue loading. The use of materials with higher strain capability and increased fatigue spectrums has changed the current no-growth philosophy to fatigue-life-limited design and certification concept for composite joint structures. The presence of voids and inclusions within the thin bondline in a bonded joint, and contact and nonlinear deformation in a bolted joint make life prediction a challenging task. The lack of high fidelity and damage-mechanism-driven-analysis toolkits leads to inefficient designs, higher certification costs, and sustainment issues.

The presence of discrete matrix cracking, delamination, and fiber breakage will make a conventional continuum damage mechanics (CDM) approach mesh dependent and result in a faulty prediction of the observed failure modes. Introduction of a fiber-aligned mesh for each ply and incorporation of a characteristic length scale in a CDM-based toolkit can alleviate the mesh dependency but it is still difficult to capture the interaction between matrix cracking and delamination and the intensified stress distribution resulting from the discrete damage in composite structures. In order to accurately capture the damage evolution without remeshing and their associated energy dissipation, an extended finite element method for discrete matrix crack characterization is developed under the sponsorship of NAVAIR and AFRL and implemented in Abaqus via its user-defined element [1], [2]. An overview of the CB²ATA toolkit (Composite Bonded and Bolted Analysis Toolkit for Abaqus) is shown in Figure 9.6-38.

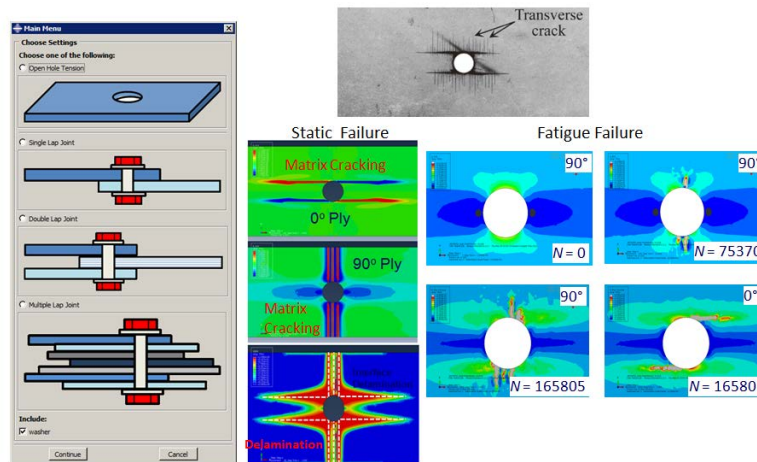


Figure 9.6-38. Capability Illustration of CB²ATA via an Open-Hole-Tension Specimen Under Static and Fatigue Loading

As can be seen from Figure 9.6-38, four (4) candidate model creation modules have been developed to facilitate the user in automatic generation of a bolted joint. Similar modules are also available to create bonded joints or a combination of bolted and bonded joints. A matrix crack will automatically be inserted along the fiber direction when a failure criterion is satisfied. In order to capture the energy dissipation during the opening and growth of a matrix crack, a mixed-mode cohesive interface is inserted. The precipitation of a matrix crack at the ply interface will intensify interface stress and promote delamination initiation and propagation that is characterized by a cohesive element approach. This energy driven failure process is used for the static failure prediction. For the fatigue damage

prediction, a cycle-dependent strength degradation model is used in conjunction with discrete-damage insertion within a ply and a continuum-damage-based evolution between the plies.

The developed toolkit has been exercised under the Tech Scout 1 using the US Air Force benchmark problems of notched and un-notched specimens under tension and compression. A residual strength prediction of an open-hole-tension specimen (OHT) of layup $[30/60/90/-60/-30]_{2s}$ after its experience of 200,000 cycles is shown in Figure 9.6-39. Both the methodology and blind and recalibrated predictions for the static tests have been presented at the Composite Materials and Computational Tools Workshop in Dayton OH organized by US Air Force on Nov. 4, 2014 and at the 56th AIAA/ASCE/AHS/ASC Structural Dynamics, and Materials Conference in Kissimmee, Florida [1].

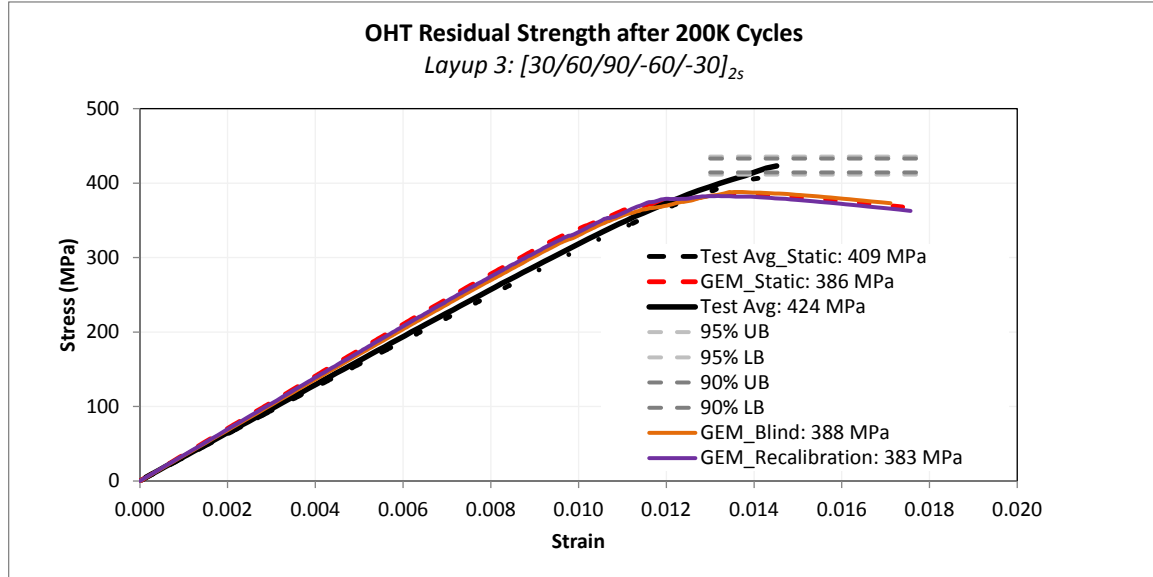


Figure 9.6-39. Residual Strength Prediction of an Open-Hole-Tension Specimen After Experiencing 200k Cycles

References

- [1] Fang, E., X. Cui, and J. Lua (2015). A phantom paired element based discrete crack network (DCN) toolkit for residual strength prediction of laminated composites, AIAA 2015-1579, 56th AIAA/ASCE/AHS/ASC Structures, Structural Dynamics, and Materials Conference.
- [2] Cui, X., X. Fang, P. Liu, and J. Lua (2015). Co-simulation of fatigue crack growth and delamination evolution in cracked aluminum plates repaired with a composite patch, AIAA 2015-1579, 56th AIAA/ASCE/AHS/ASC Structures, Structural Dynamics, and Materials Conference.

9.6.12. Continued Development of the NASGRO Software for Fracture Mechanics and Fatigue Crack Growth Analysis

Craig McClung, Joseph Cardinal, Yi-Der Lee, James Sobotka, and Vikram Bhamidipati, Southwest Research Institute®; Joachim Beek, NASA Johnson Space Center; Venkataraman Shivakumar, Randall Christian, Yajun Guo, and Michael Baldauf, Jacobs Technology, Inc.

The NASGRO® software for fracture mechanics and fatigue crack growth (FCG) analysis continued to be actively developed and widely used during 2013 and 2014. NASGRO is the standard fracture control software for all NASA Centers and is also used extensively by NASA contractors, the European Space Agency (ESA) and ESA contractors, and FAA Designated Engineering Representatives certified for damage tolerance analysis, as well as many aerospace companies worldwide. NASGRO has been jointly developed by NASA and Southwest Research Institute since 2001, with substantial financial support from NASA, the NASGRO Consortium, and the Federal Aviation Administration (FAA). The NASGRO Consortium concluded its fourth three-year cycle (2010-2013) and began its fifth cycle (2013-2016). The international participants currently include AgustaWestland, Airbus, Alcoa, Boeing, Bombardier Aerospace, Embraer, GKN Aerospace Engine Systems, Honda Aircraft Engines, Honeywell Aerospace, IHI Corporation, Israel Aerospace Industries, Lockheed Martin, Mitsubishi Aircraft Corporation, Mitsubishi Heavy Industries, Siemens Energy, Sierra Nevada Corporation, Sikorsky, SpaceX, United Launch Alliance, and UTC Aerospace Systems. In addition to Consortium members, 106 single-seat and 8 site NASGRO licenses were issued in 2013-2014 to users in 22 countries.

A new production version of NASGRO was released in 2014. Version 7.1, released in July 2014, included new stress intensity factor (SIF) solutions for a single corner crack (CC16) and two unequal corner cracks (CC17) at an offset hole in a plate under tension, bending, or pin-loading (Figure 9.6-40). These two solutions cover a very wide range of crack geometries and include new finite-width correction factors. The CC17 solution transitions to a new hybrid crack solution (HC01) for a through crack and a corner crack on opposite sides of a hole. HC01 further transitions to solution TC23 for two unequal through cracks or CC15 for a corner crack at a hole with a broken ligament, as appropriate. Other new SIF solutions included improved univariant and bivariant weight function solutions for a surface crack in a plate (SC30/SC31), and a through crack in a plate under displacement control (TC24).

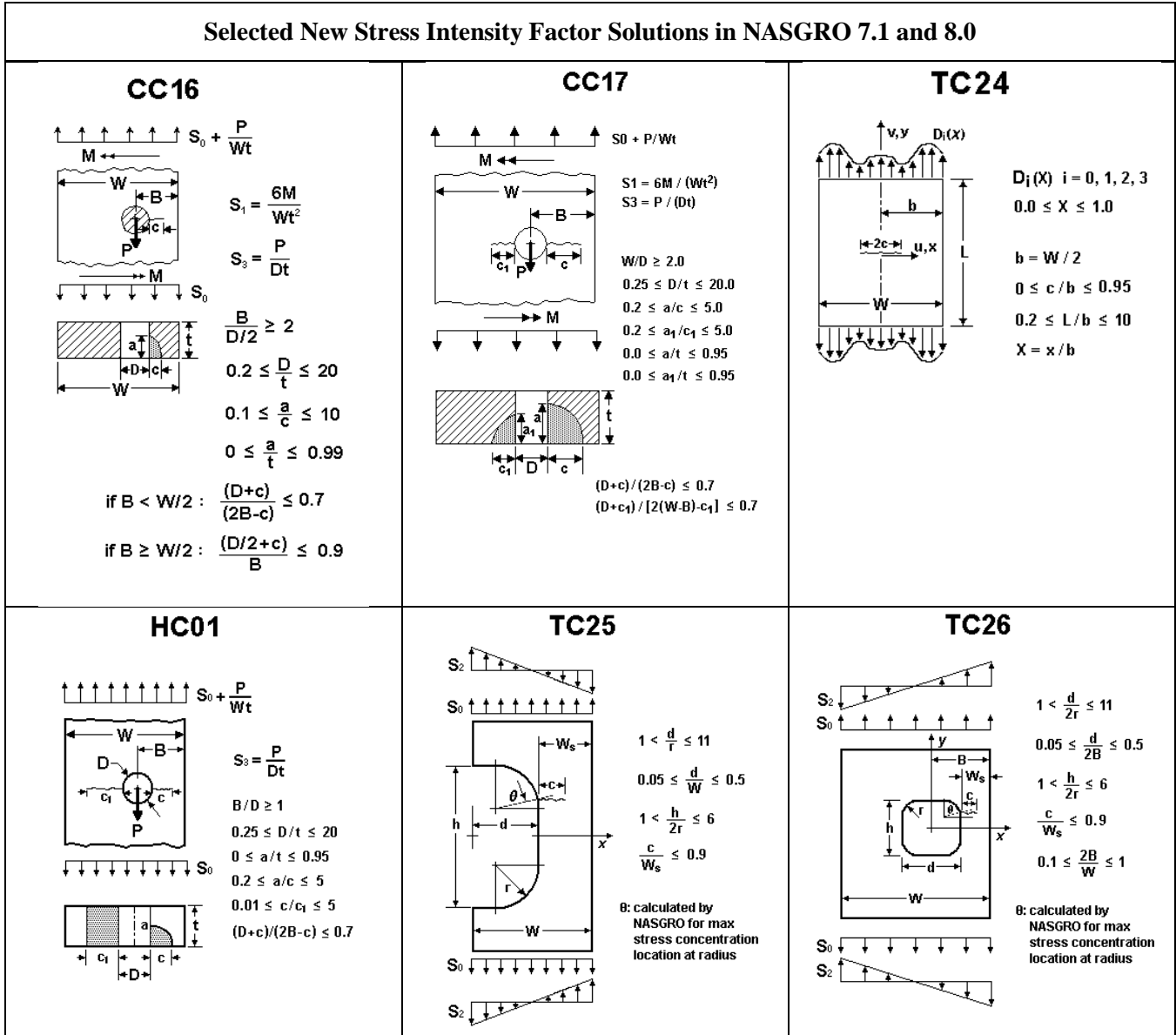


Figure 9.6-40. Selected New Stress Intensity Factor Solutions in NASGRO Versions 7.1 and 8.0

Also in v7.1, material property databases for the crack growth program NASFLA were converted to new XML formats and now support enhanced search capabilities and improved multiple-temperature capabilities. A new (optional) alternative threshold formulation was implemented in the NASGRO crack growth equation for improved accuracy in the near-threshold regime. User-specified toughness values can now be supplied by tip class or tip location, or as a constant value everywhere. Data for several materials were added to the NASA materials database. Many other smaller enhancements were also implemented.

Significant progress was achieved on NASGRO 8.0, which was in Alpha release at the end of 2014, with Beta release anticipated for early 2015 and Production release in mid-year. New SIF solutions in 8.0 include a through crack at an edge (TC25) or internal (TC26) rectangular cutout with rounded corners, along with direct access to the HC01 solution first implemented in 7.1. A new option was added to the existing through crack (TC02) model to restrain in-plane bending at the remote end. A new pin loading option was added to the weight function SIF solution for a through crack at a hole (TC13). User-

supplied SIF solutions can now be input directly as tables of K versus crack size. Other v8.0 enhancements include a new “HCF threshold check” failure criterion, GUI plotting of the Failure Assessment Diagram (FAD) failure criterion, additional XML materials database capabilities, and many other smaller features.

Southwest Research Institute has been conducting NASGRO training courses since 2006. During 2013 and 2014, SwRI trained 153 students in 8 courses, including 4 courses in San Antonio, Texas, and 4 courses at remote sites including a major rotorcraft company, a major space access company, NASA Langley Research Center, and the ESA Technical Center in the Netherlands.

Further information about NASGRO is available at www.nasgro.swri.org. POC: Craig McClung, Southwest Research Institute, craig.mcclung@swri.org, 1-210-522-2422.

9.6.13. Long-Term Thermal Exposure Effect on Crack Growth Rate in Aluminum Alloys

Lee Ann Johnson, Spirit AeroSystems, Inc.

With the increasing trend in aircraft engine efficiency, the operating temperature of engines has also increased. Consequently, the operating temperature of the structure attaching the engine to the aircraft has increased as well. While the static mechanical properties of materials exposed to elevated temperatures are fairly well documented, the effects on materials’ damage tolerance properties are not as thoroughly studied. Understanding the impact of elevated temperatures and long-term exposure on materials’ fracture toughness and crack growth rates is needed to ensure adequate inspection programs are in place for the affected structure during the entire service life of an aircraft.

While the effect on fracture toughness was also examined, the most recent technical activity evaluated the effect of long-term exposure to elevated temperatures on the crack growth rates of two different aluminum alloys commonly used in aircraft structure. Compact tension specimens were manufactured and exposed to a temperature of 350°F for 500 hours, 1000 hours, or 5000 hours. Baseline specimens with no long term exposure to high temperature were also manufactured. All pre-cracking was performed at room temperature under the same maximum load, stress ratio, and frequency for all specimens. The specimens were then tested at either room temperature or at an elevated temperature of 300°F. All specimens were tested under the same maximum load, stress ratio, and frequency.

The first aluminum alloy tested was 2024-T851 plate. This material demonstrated a slight increase in crack growth rate when tested at an elevated temperature compared to being tested at room temperature. However, the effect of long-term thermal exposure appeared to be beneficial to crack growth rate, resulting in a slight decrease in crack growth rate. The net effect of long-term thermal exposure (up to 5,000 hours) plus testing at elevated temperature had a negligible effect on crack growth rate. These crack growth rate comparisons for 2024-T851 plate are shown in Figure 9.6-41.

The second aluminum alloy tested was 2219-T852 forging. This material behaved much differently than the 2024-T851 plate material. The testing at an elevated temperature had a greater adverse effect on the crack growth rate when compared to testing at room temperature, with the crack growth life reduced by a factor of approximately two. In addition, the long-term exposure to elevated temperature had a detrimental effect on crack growth rate, with crack growth life again roughly cut in half. The length of exposure seemed to have negligible effect in the range that was tested, from 500 hours to 5,000 hours. The net effect of long-term thermal exposure (greater than 500 hours) plus testing at elevated temperature had a combined effect of reducing the crack growth life for this aluminum alloy by a factor of almost four. These crack growth rate comparisons for 2219-T852 forging are shown in Figure 9.6-42.

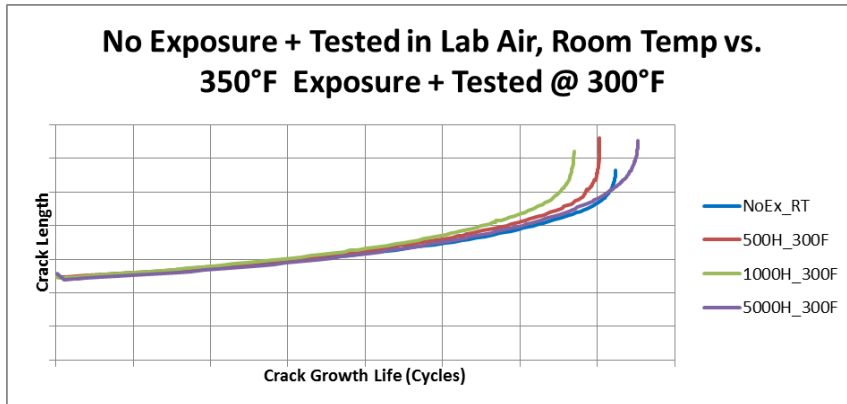
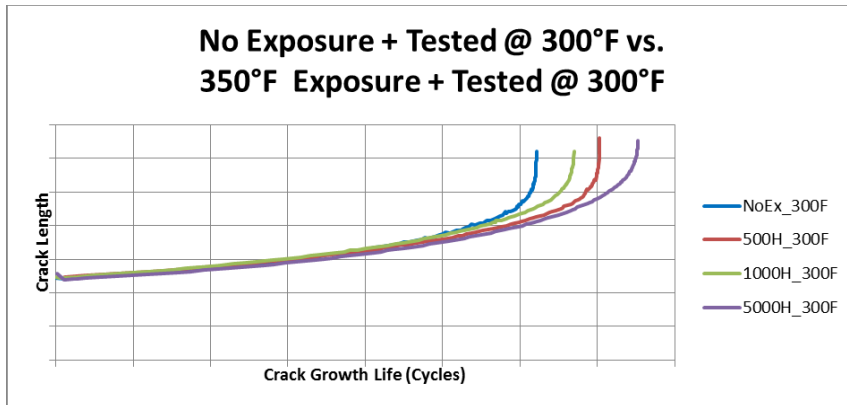
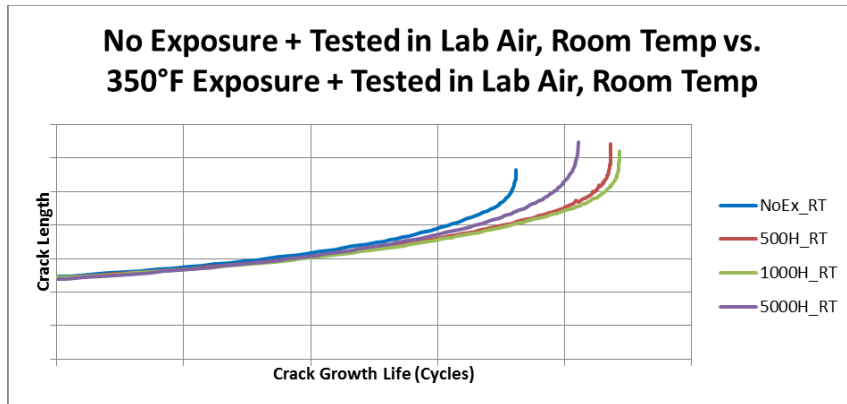
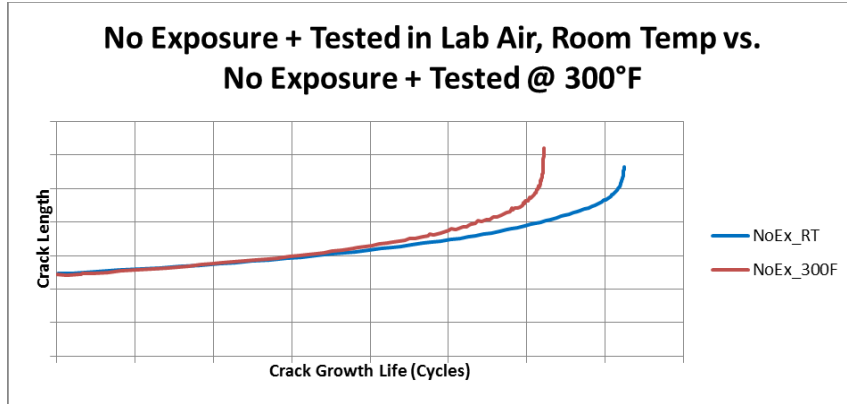


Figure 9.6-41. 2024-T851 Plate – Crack Growth Comparisons

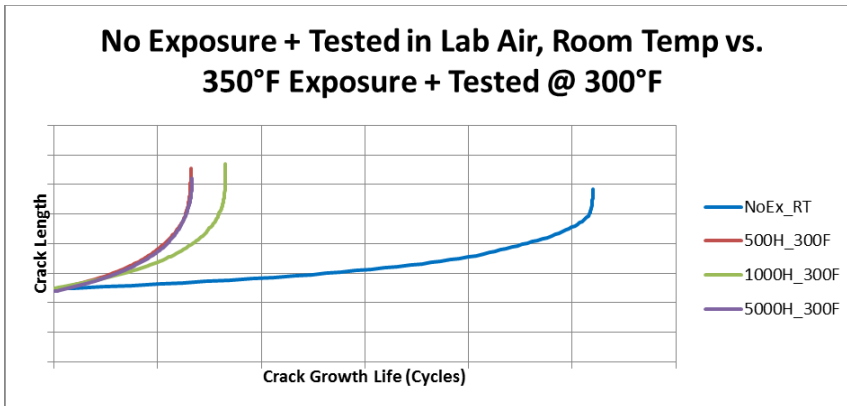
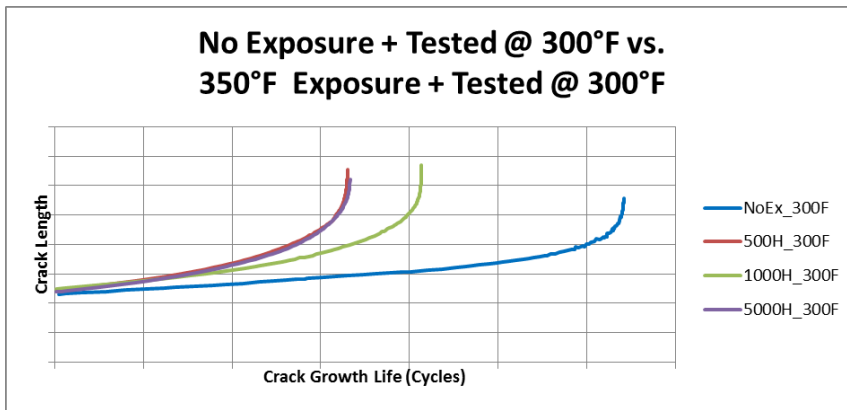
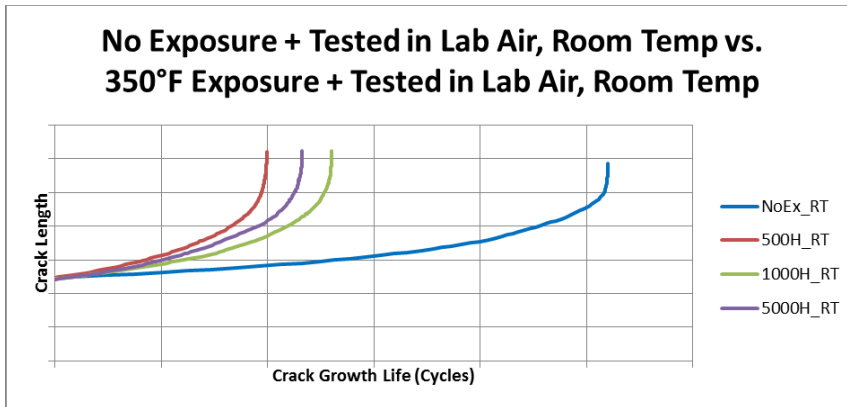
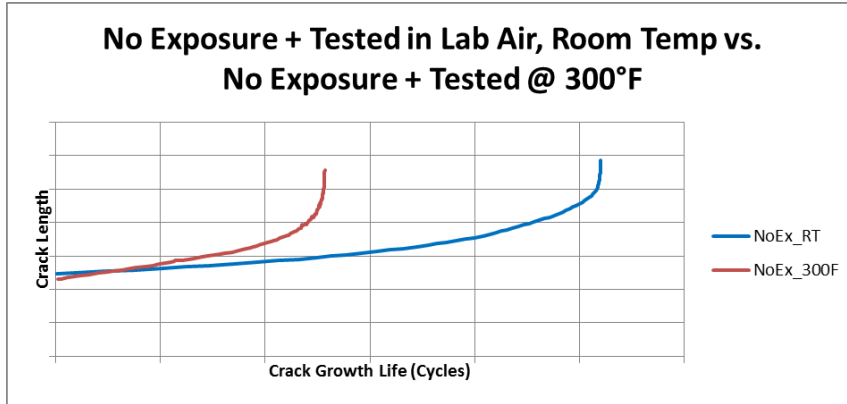


Figure 9.6-42. 2219-T852 Forging – Crack Growth Comparisons

9.6.14. Notched Fatigue Behavior of Aluminum Under Constant and Variable Amplitude Multiaxial Loads

A. Fatemi and N. Gates, University of Toledo

The need to be able to produce safe and efficient aerospace structures is greater than ever. A key element in producing such designs is the ability to confidently and accurately predict the various stages of a component's fatigue life, as fatigue is by far the largest contributor to structural failures. This not only applies to new designs being developed, but also to existing structures where damage tolerant design philosophies have been employed. Increased confidence in design translates not only into increased safety and reliability, but also reduced maintenance costs by allowing structural inspections at longer intervals.

The central objective of this research project was to use experimental data and observations from a variety of fatigue tests, along with advanced computational simulation techniques, to gain insight into the damage mechanisms at work within a material for a given loading. By doing this, it enabled various life prediction techniques to be evaluated and/or proposed based on the actual physics of material failure rather than purely empirical results. The research was focused on both crack initiation and crack growth stages of fatigue life.

A large number of fatigue tests were performed using thin-walled tubular specimens (Figure 9.6-43) of aluminum alloy 2024-T3. Tests performed included cyclic deformation tests, constant amplitude fatigue tests, and variable amplitude fatigue tests using a simulated flight spectrum. The flight spectrum used represents the loading in the lower wing skin region of a military patrol aircraft (Figure 9.6-44). Constant and variable amplitude fatigue tests were performed for both un-notched and notched specimens under axial, torsion, and combined axial-torsion loadings with and without phase differences. Notched specimens featured an open circular hole in the center of the specimen gage section. Such a wide variety of tests allowed for evaluation of each aspect of the fatigue analysis process including: cyclic plasticity modeling, notch root stress-strain estimation including gradient effects, fatigue damage calculation, cycle counting methods, cumulative damage rules, and crack growth laws including mixed-mode growth.

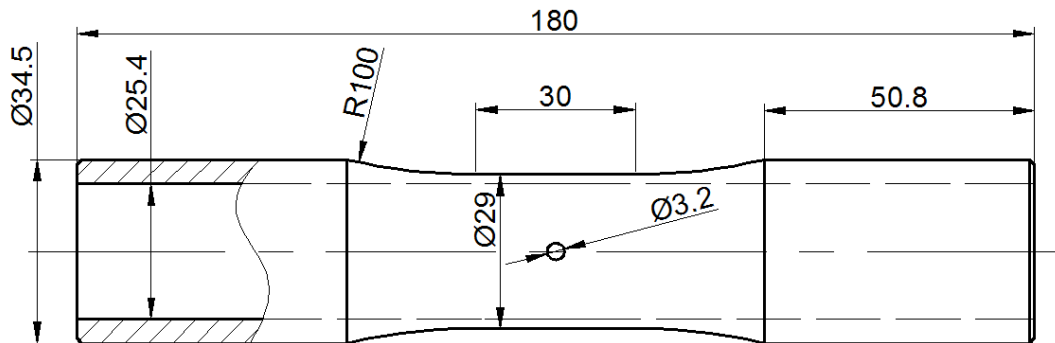


Figure 9.6-43. Thin-Wall Tubular Specimen Geometry

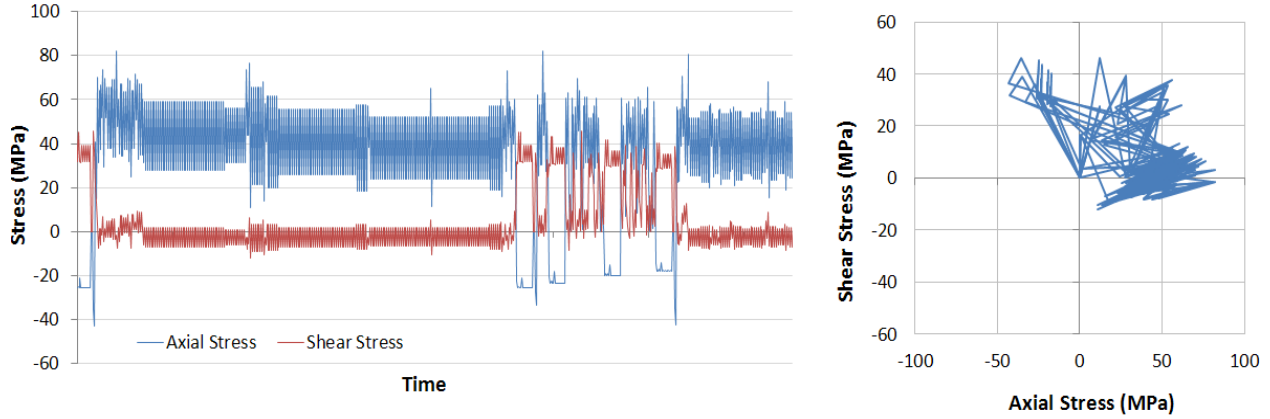


Figure 9.6-44. Sample Taken From Simulated Flight Spectrum (1000 of 914100 Data Points) Showing Load vs. Time History and Axial Stress vs. Shear Stress Plot

From the results of the constant amplitude fatigue tests, it was found that for the 2024-T3 material, cracks always initiated on planes of maximum shear regardless of the applied loading or specimen type (notched or un-notched). Therefore, experimental lives for the different loading conditions were able to be correlated within a satisfactory margin of error using a shear-based critical plane fatigue damage parameter (Fatemi-Socie in Figure 9.6-45). This correlation is far better than that obtained by using the traditional von Mises equivalent stress approach. Work is still ongoing on applying the knowledge learned from the constant amplitude tests to the more complex variable amplitude fatigue analyses, but initial results are promising with respect to achieving accurate predictions. Crack growth analyses are still in progress as well.

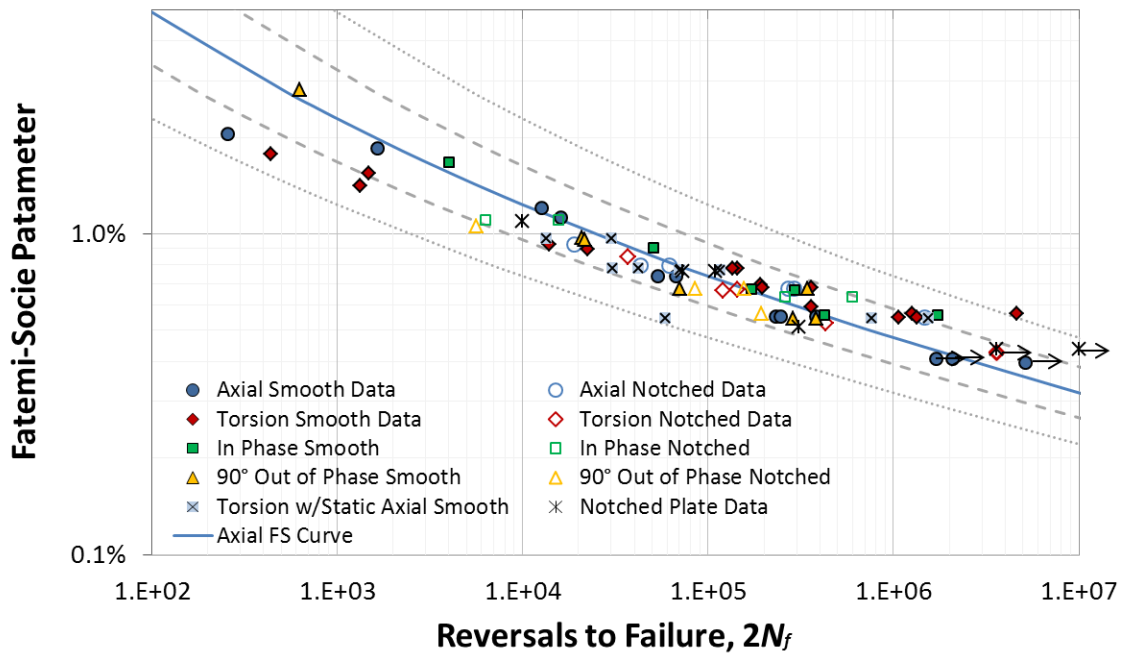


Figure 9.6- 45. Correlation of Constant Amplitude Fatigue Data for Un-Notched and Notched Specimens Under Various Loading Conditions. Scatter Bands Shown are Factors of ± 3 and ± 10

Publications From Research:

- N. R. Gates, A. Fatemi. Notched fatigue behavior and stress analysis under multiaxial states of stress. *International Journal of Fatigue* 2014; Vol. 67: pp. 2-14.
- Fatemi, N. R. Gates, D.F. Socie, N. Phan. Fatigue crack growth behavior of tubular aluminum specimens with a transverse hole under axial and torsion loadings. *Engineering Fracture Mechanics* 2014; Vol. 123: pp. 137-147.
- N. R. Gates, A. Fatemi, D.F. Socie, N. Phan. Notched Fatigue Behavior under Multiaxial Stress States. *Advanced Materials Research* 2014; Vols. 891-892: pp. 185-198.

9.6.15. Peridynamics for Progressive Damage Prediction in Composites**E. Madenci, University of Arizona**

Quantification of damage in composites is usually a daunting task. Experimental evaluation of damage that is not visible involves expensive specialized equipment, and may not be fully satisfactory in visualization of internal damage. Component level structural testing and analysis of advanced composites is prohibitively expensive and time consuming. Instead, using robust and accurate computational tools complemented by experiments at key stages is a viable and cost-effective option.

However, complex nonlinear material behavior of advanced composites cannot be described by simple constitutive models. In addition, the presence of dynamic and cyclic loading conditions further complicates their failure analysis for strength prediction. There is no existing analysis capability that can predict all possible failure modes (matrix cracking, fiber breakage and delamination) in composites because damage initiation and its progressive growth is very complex under multi-axial loading conditions and multiple-load paths. Furthermore, the microscopic damage can progress throughout the composite leading to macro scale damage such as delamination or even catastrophic failure of the composite material. This is mainly due to the load redistribution from damaged to adjacent undamaged materials as the stiffness degradation occurs. Therefore, understanding the microscopic damage mechanisms prior to the failure of the composites becomes crucial.

Existing computational methods for damage modeling in a continuous body are based on the partial differential equations (PDEs) of classical continuum mechanics. These methods suffer from an inherent limitation: the spatial derivatives appearing in PDEs require a certain degree of smoothness within the solution domain. Therefore, the basic mathematical structure of the formulation breaks down whenever a defect (e.g. crack) appears in the body. This mathematical formulation was sufficient for the analysis of monolithic materials, as the design engineer could conclude eminent structural failure when the mathematical governing equations failed. However, composite material systems display “graceful” failure; they have the ability to maintain a load even as the material is in the process of failing.

Silling [1], [2] introduced a nonlocal theory that does not require spatial derivatives – the Peridynamic (PD) theory. This feature allows damage initiation and propagation at multiple sites, with arbitrary paths inside the material, without resorting to special criteria for direction of crack growth. In the PD theory, internal forces are expressed through nonlocal interactions between the material points. This theory was later extended by Madenci and Oterkus [3], in particular for composite failure analysis. Different interactions are responsible for different bond forces (e.g., fiber, matrix, interface, etc.). By assigning different damage models to different interactions, a more realistic simulation of damage mechanisms can be obtained for heterogeneous materials under complex loading conditions. Other available methods suffer from the need to supply a kinetic relation for crack growth, while PD theory provides this relation in a natural and physical way. The inherent capability of PD theory for handling discontinuities makes it a very useful tool for numerical modeling of defect evolution in different scales. Every defect in a material is a deviation in the geometrical arrangement of its constituents at some scale.

The physics-based peridynamics (PD) methodology overcomes the weaknesses of the existing methods, and it is capable of identifying all of the failure modes without simplifying assumptions. The PD methodology effectively predicts complex failure modes in composites under general dynamic and

static loading conditions. The capability of peridynamics for progressive failure prediction is demonstrated by considering the residual strength of laminates with a hole [4] and interlaminar delamination growth in Double Cantilever Beam (DCB) and Transverse Crack Tension (TNT) specimens, [5].

Residual Strength of a Laminate with a Hole

The carbon/epoxy quasi-isotropic specimens with varying hole diameters were tested to failure under both tensile and compressive loading [6]. The damage pattern for each of the composite specimens subjected to a tensile load for four different diameter hole sizes is shown in Figure 9.6-46. The resulting fracture patterns transition from a slant to a flat failure mode as the hole size increases. These damage predictions agree well the experimental observations [7]. The damage patterns for each of the composite specimens subjected to a compressive load is shown in Figure 9.6-47. The fracture pattern is consistent for all of the different hole sizes. This failure pattern is identical to that of Suemasu et. al. [8] in their testing of an identical laminate with a 6.35 mm diameter central hole as shown by the comparison in Figure 9.6-48.

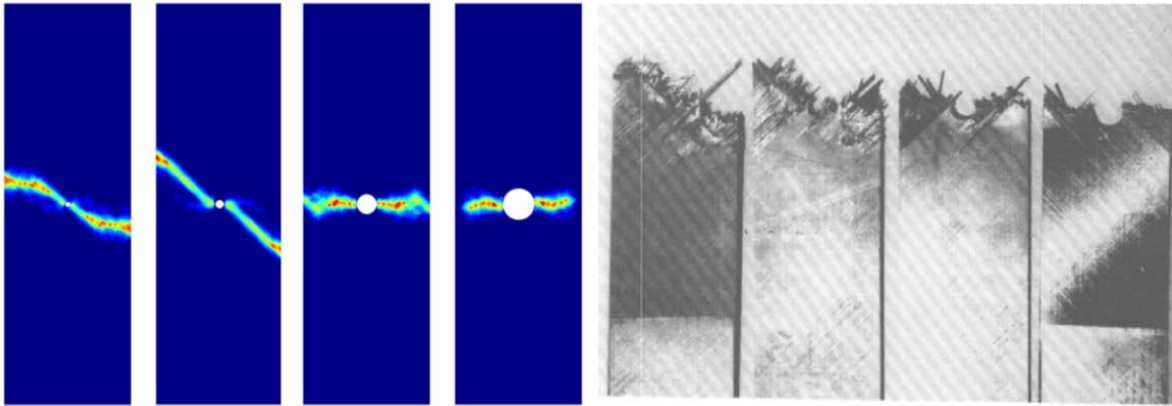


Figure 9.6-46. Under Tensile Loading: Peridynamic Damage Predictions (Left) and Experimental Damage Patterns (Right) as Hole Diameter Increases

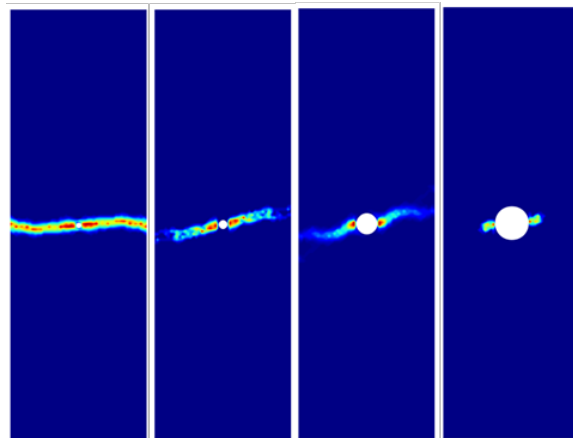


Figure 9.6-47. Under Compression Peridynamic Damage Predictions as Hole Diameter Increases

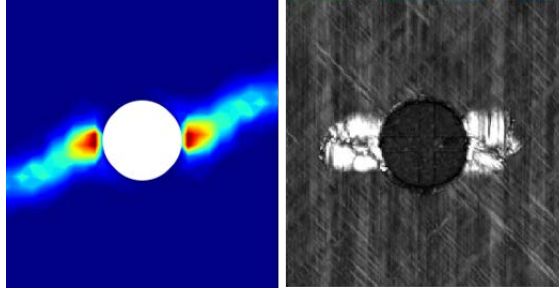


Figure 9.6-48. Under Compression: Peridynamic Damage Prediction (Left) and Experimental Damage Pattern for Hole Diameter of 6.35 mm

Interlaminar Delamination

The DCB and TCT tests are commonly used to determine Mode I and Mode II interlaminar fracture toughness of composites, G_{Ic} and G_{IIc} , respectively. As the applied opening displacement increases in DCB specimens, the delamination front shape remains as a convex curve and continues to grow, shown in Figure 9.6-49. Peridynamics successfully captures these delamination growth characteristics observed experimentally [9]. Contrary to what is typically observed in the DCB specimens, the crack front shape in the TCT specimen shows a concave curve with respect to the propagation direction. Figure 9.6-50 shows the delamination growth on the interface of continuous and discontinuous plies at different applied displacement loadings. Delamination starts at the edges, and extends to the center. Upon increasing the applied loading, the delamination fronts propagate symmetrically in the longitudinal direction while maintaining a concave front. The peridynamic simulations capture the crack front shape obtained experimentally [10].

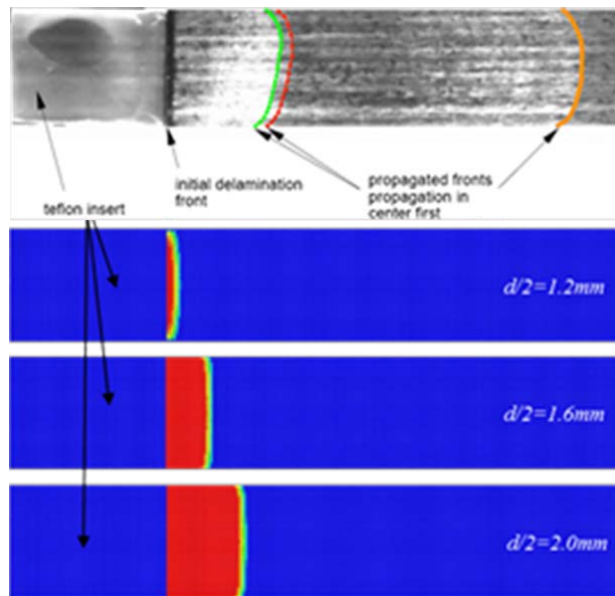


Figure 9.6-49. Delamination Growth in DCB Specimens: Simulation (Bottom) and Experimental Observations (Top)

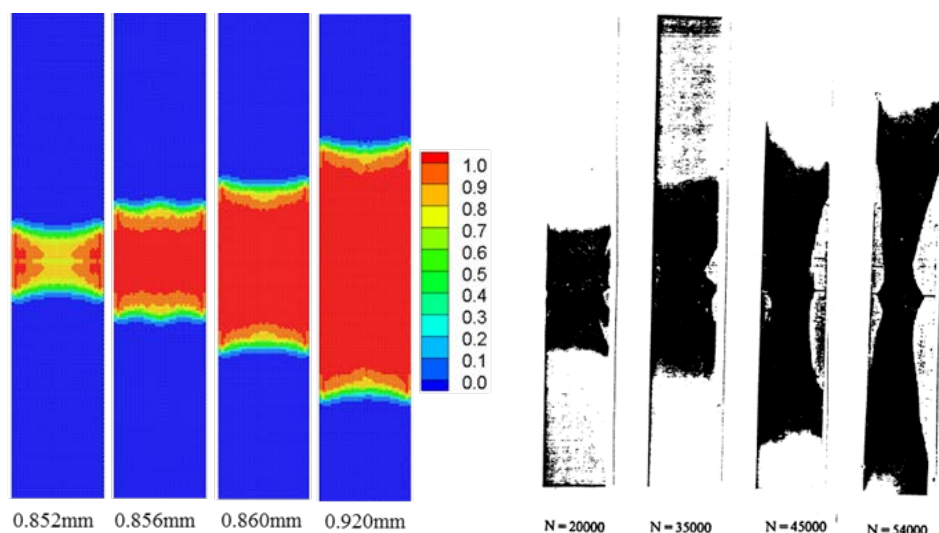


Figure 9.6-50. Delamination Propagation in TCT Specimens: Peridynamic Simulation (Left), Experimental Observations (Right)

References

- [1] Silling, S.A., 2000, "Reformulation of elasticity theory for discontinuities and long-range forces," *J. Mech. Phys. Solids*, Vol. 48, pp. 175-209.
- [2] Silling, S.A., Epton, M., Weckner, O., Xu, J. and Askari, A. 2007, "Peridynamics States and Constitutive Modeling," *J. Elast.*, Vol. 88, pp. 151-184.
- [3] Madenci, E. and Oterkus. E., 2014, Peridynamic Theory and Its Applications, *Springer*, Boston, MA.
- [4] Colavito, K, Barut, A., Madenci, E. and Phan, N., 2013, "Residual Strength of Composite Laminates with a Hole by Using Peridynamic Theory," *54th AIAA/ASME/ASCE/AHS/ASC Structures, Structural Dynamics and Materials Conference*, Boston, Massachusetts, Paper No. AIAA-2013-1761
- [5] Hu, Y., Madenci, E. and Phan, N., 2015, "Peridynamic Modeling of Defects in Composites," *56th AIAA/ASME/ASCE/AHS/ASC Structures, Structural Dynamics, and Materials Conference*, Kissimmee, Florida.
- [6] Wang, J., Callus, P. J., and Bannister, M. K., 2004, "Experimental and Numerical Investigation of the Tension and Compression Strength of Un-Notched and Notched Quasi-Isotropic Laminates," *Composite Structures*, Vol. 64, pp. 297-306.
- [7] Poon, C. 1991, Tensile Fracture of Notched Composite Laminates, No. IAR-AN-71. *National Research Council of Canada Ottawa (Ontario) Institute for Aerospace Research*.
- [8] Suemasu, H., Takahashi, H., and Ishikawa, T., 2006, On Failure Mechanisms of Composite Laminates with an Open Hole Subjected to Compressive Load, *Composites Science and Technology*, Vol. 66, pp. 634-641.
- [9] Krueger R., 2008, An approach to assess delamination propagation simulation capabilities in commercial finite element codes. NASA/TM-2008-215123.
- [10] Ye, L, Prinz, R, Klose, R., 1990, Characterization of interlaminar shear fracture toughness and delamination fatigue growth of composite materials using TCT specimen. In: Report (1990), IB 131-90/15, DLR, *Institute for Structural Mechanics*, Hamburg, Germany, 1990.

9.6.16. Predictive Modeling and Simulation of Crack Branching, Curvilinear Crack Paths and Life for Fatigue Crack Growth Under Cyclic Out-of-Phase Loading Conditions

Xiaomin Deng and Michael A. Sutton, University of South Carolina; Hubert W. Schreier, Correlated Solutions, Inc.

Summary

A theory for predictions of crack branching, curvilinear crack paths and life for fatigue crack growth events under linear elastic and cyclic out-of-phase (as well as in-phase) loading conditions have been developed and implemented in a custom finite element code CRACK3D [1], [2]. Simulations of curvilinear fatigue crack growth events were made possible by an earlier development in CRACK3D of the capability for automatic, efficient, and accurate determination of 3D mixed-mode stress intensity factors (SIFs) for fatigue crack growth with crack paths and crack fronts that may be curved [3], [4]. This earlier development was based on a 3D virtual crack closure technique (3D VCCT) and a locally structured re-meshing approach in which the local region immediately surrounding a moving crack front is automatically re-meshed with a structured mesh pattern to facilitate the 3D VCCT and maintain its accuracy. Fatigue crack growth events under out-of-phase loading conditions in cruciform aluminum specimens with a central hole and an edge crack at the hole are simulated (Figure 9.6-51). Simulation predictions of crack branching angles, crack paths and fatigue life of the branched cracks agree well with experimental measurements.

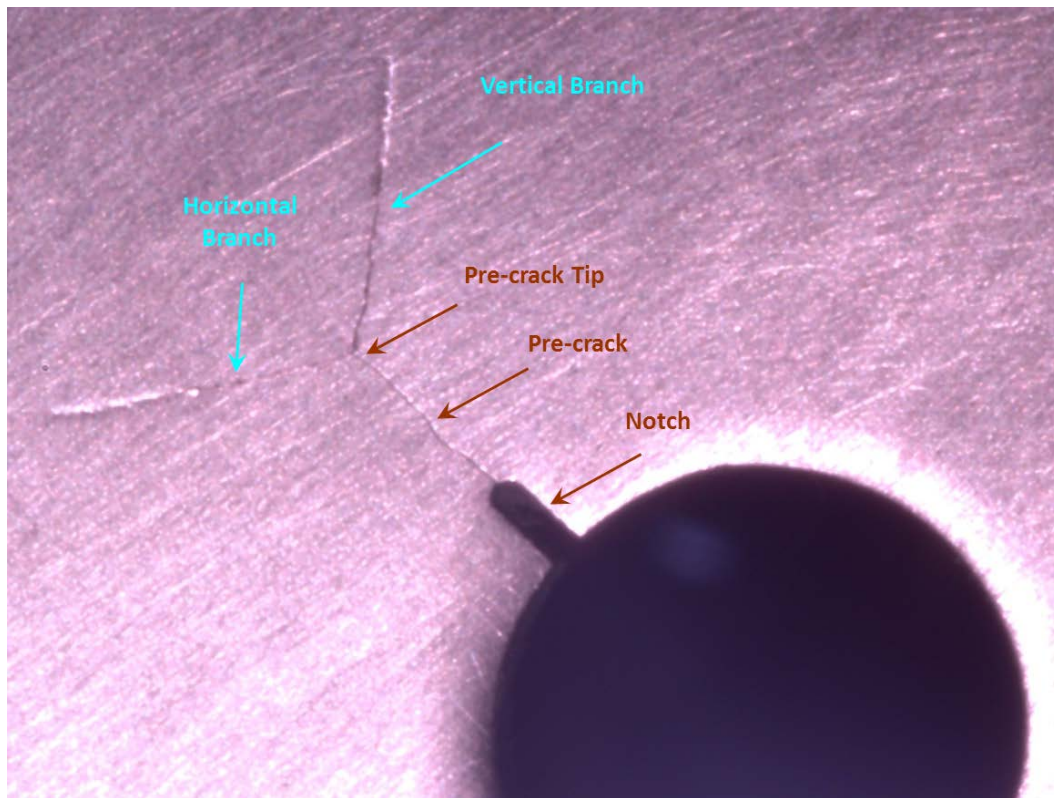


Figure 9.6-51. A Partial Image of a Cruciform Aluminum Specimen with a Central Hole and an Edge Crack at the Hole. The Specimen Contains an Initial Notch and a Fatigue Pre-Crack. Under Cyclic 1800 Out-of-Phase Biaxial Loading Conditions, Two Branch Cracks were Created at the Pre-Crack Tip and Grew as Functions of the Number of Loading Cycles

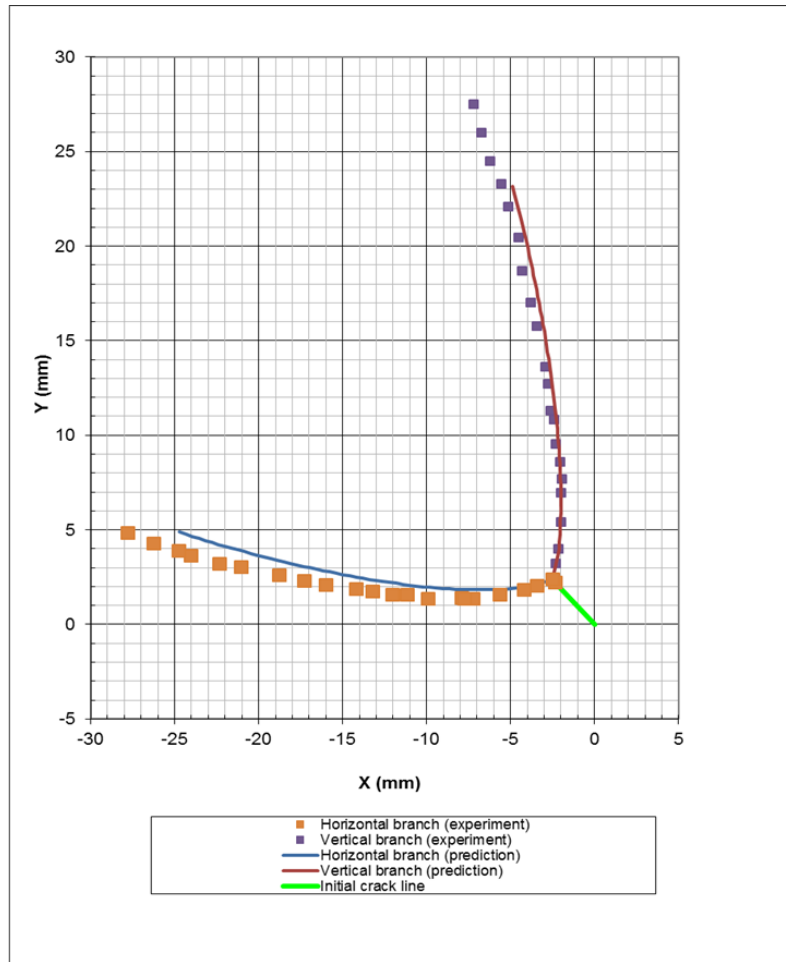


Figure 9.6-52. A Comparison of Predicted and Measured Curvilinear Crack Paths for Two Branch Cracks that were Created at an Initial Fatigue Pre-Crack Tip (see Figure 9.6-51)

Acknowledgment

This work was supported by an AFRL SBIR project (Contract#: FA8650-10-C-3001).

References

- [1] X. Deng, H.W. Schreier, "High performance computer tool for predictions of fatigue crack growth and stable crack extension in aircraft structures." Final Report for AFRL SBIR Project FA8650-10-C-3001, December 2013.
- [2] X. Deng, X. Ke, M.A. Sutton, H.S. Watts, H.W. Schreier, "Curvilinear fatigue crack growth under out-of-phase loading conditions," Conference Proceedings of the Society for Experimental Mechanics Series, v 66, n VOLUME 5, p 27-34, 2015, Fracture, Fatigue, Failure, and Damage Evolution - Proceedings of the 2014 Annual Conference on Experimental and Applied Mechanics.
- [3] X. Deng, X. Ke, M.A. Sutton, E.E. Miller, H.W. Schreier, "3D VCCT with locally structured re-meshing for evaluating mixed-mode stress intensity factors in crack growth simulations along curved crack paths," presentation at the Society of Engineering Science 49th Annual Technical Meeting, Georgia Tech, GA, USA, Oct. 10-12, 2012.
- [4] X. Deng, X. Ke, M.A. Sutton, E.E. Miller, H.W. Schreier, "FEM for 3D SIF determination for fatigue crack growth simulations with curved crack fronts and paths," presentation at the ASME

2013 International Mechanical Engineering Congress & Exposition, San Diego, CA, USA, Nov. 15-21, 2013.

9.6.17. 3D Measurements of Microstructurally Small Fatigue-Crack Evolution in an Aluminum Alloy

Ashley Spear, University of Utah

Advancing the state of structural prognosis for the United States Air Force requires an improved understanding of the early stages of fatigue-crack evolution, which have been shown to account for a significant portion of fatigue life among aerospace structures. This technical activity provides new insights into early fatigue-crack propagation (i.e., from first-observable crack shape to a nominal crack size spanning multiple grains) in aerospace-grade aluminum alloy 6061-T6 by leveraging emergent techniques in three-dimensional characterization. The experimental effort combines an existing marker banding technique with X-ray computed tomography (CT) and high-energy X-ray diffraction microscopy (HEDM). The marker banding technique enables a post-mortem mapping of the fatigue-crack shape throughout a specimen's loading history using fractographic measurements. The X-ray CT and HEDM measurements provide, respectively, a highly resolved description of the three-dimensional crack surfaces and a three-dimensional map of the grain morphologies and crystal orientations adjacent to the crack surfaces. Post-processing algorithms are developed to combine all three data sets and extract micrometer-scale information pertaining to local crack-propagation rates and crack-surface crystallography (Figure 9.6-53).

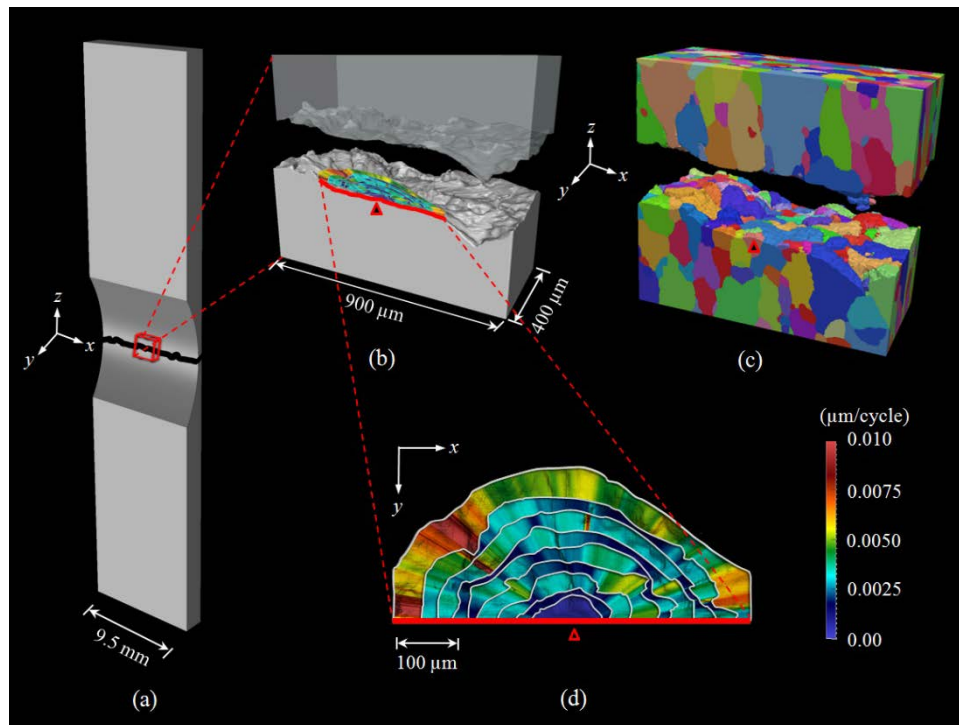


Figure 9.6-53. Snapshot of Results from 3D Study of Microstructurally Small Fatigue-Crack Evolution in Al 6061-T6. a) Schematic of Broken Fatigue Specimen Depicting Region of Interest (ROI) Containing the Dominant Fatigue Crack. b) X-Ray CT Reconstruction in ROI. c) HEDM Reconstruction in ROI with Color Map Corresponding to Grain Orientations. d) Local 3D Fatigue-Crack Propagation Rates Determined from Marker Banding and X-Ray CT Data. Red Triangle in b-d Indicates Approximate Location of Fatigue-Crack Nucleation

Results from this technical activity show that local fatigue-crack propagation rates varied by more than two orders of magnitude across the three-dimensional crack surface in an aluminum-alloy specimen. Additionally, both intergranular and transgranular crack growth were observed, with the latter occurring along a wide range of crystallographic planes. The results help to elucidate the complex behavior of early (i.e., microstructurally small) fatigue-crack evolution in three dimensions. Further understanding of this complex behavior will be necessary to improve methods by which structural life is predicted for aircraft.

9.6.18. Innovative Capability to Quantify Fatigue Damage and Assessment of Endurance Limit in Spectrum Load Histories

Nagaraja Iyyer, TDA, Inc.

Most fatigue life prediction models rely on experimental data sets representative of average material behavior derived from standard mechanical fatigue tests in specific damaging regimes. Using this limited dataset, fatigue life estimates of components experiencing a multitude of complex loading conditions can be highly affected, especially under long repeated service histories. For example, it has been known that load cycles with amplitudes below the traditional endurance limit do cause damage when they are a part of variable amplitude loadings that has a mix of high and low cycle fatigue load cycles. However, quantification of damage of these small amplitude load cycles has largely been empirical because of long testing times needed with conventional testing techniques limited to conventional LCF and HCF regimes. To improve this situation, we therefore need to develop (a) new testing techniques that utilize load histories reflective of actual component load history which may encompass V/HCF regimes and /or combined cyclic fatigue (CCF) regimes with load interaction effects and reproduce the same failure modes as observed in service, and (b) life prediction models and analysis toolkit that more explicitly reflect material damaging mechanisms in different fatigue regimes.

Innovative testing methodologies are used in this technical activity to perform fatigue tests of structural alloy metals subjected to complex loading histories. The testing apparatus combines servo-hydraulic and ultrasonic techniques to allow testing at a very large number of cycles and for complex representative spectrum sequences. Due to the nature of the ultrasonic testing apparatus, testing time is significantly reduced, and given the ability to construct superimposed representative spectrum loading (Figure 9.6-54), load interactions effects can be studied. Test results show failures well below the traditional endurance level and a high incidence of load interaction effects, including those occurring in very/high cycle fatigue, impacting total fatigue life.

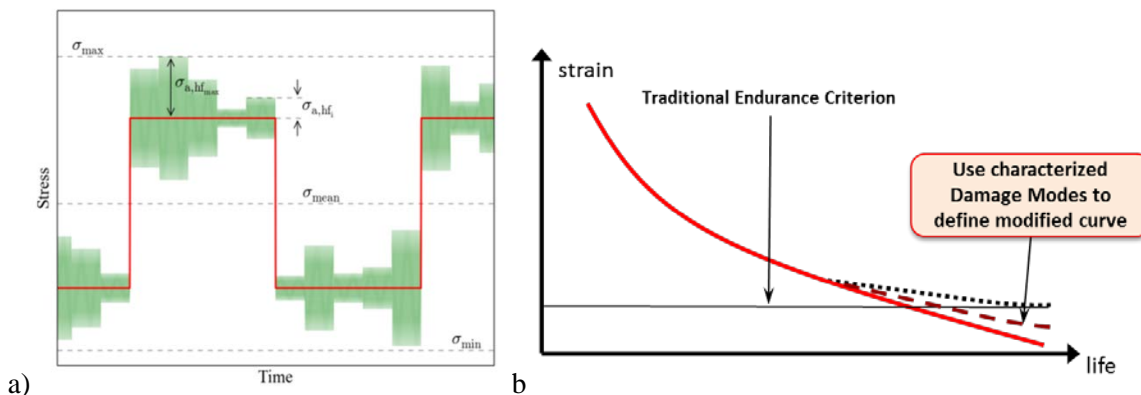


Figure 9.6-54. Fatigue Tests in the V/HCF with High Incidence of Load Interaction and Modified Local-Strain Approach

Analysis by using traditional criteria fails to capture the observed interaction effects and can highly over- or under-estimate the incidence of the large number of vibratory cycles in V/HCF regimes. An empirical-based modeling effort is currently focusing on the optimization of a strain-life or stress-life input for the development of useful guidelines in the analysis of complex loading histories (Figure 9.6-54). The approach justifies the strain-life or stress-strain input definition by experimentally observed and characterized failures in the critical regimes of interest.

To correctly capture damage accumulation mechanisms and interaction effects in a prognostics model, analytical formulations representing material energy dissipation mechanisms at different length-scales also need to be developed. Microstructural modeling of 7075-T6 material by using representative volume element techniques (Figure 9.6-55) to take into account material grain distribution and deformation mechanisms is being conducted. Validation of the developed model shows good correlation with constant amplitude loading data (Figure 9.6-55); extensions of the current model to variable amplitude loading data are sought. Continuum level energy dissipation mechanisms are also being postulated and implemented into continuum damage mechanics theories. Verification and validation work is being conducted for critical overload-underload tests and extended to the complex V/HCF spectrum sequences.

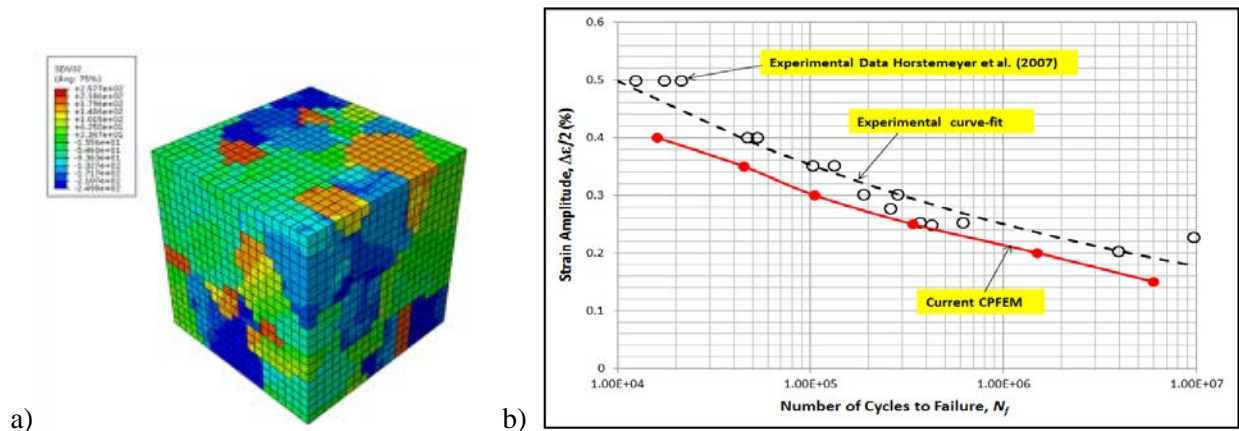


Figure 9.6-55. Developed Representative Volume Element for 7075-T6 Material and Constant Amplitude Loading Predictions

Additionally, a stochastic framework for the developed models needs to be developed to account for observed experimental scatter. The current focus is in the extension of the local strain-life approach: stochastic model parameters and uncertainty affecting spectrum sequence are being included in the model to allow the calculation of expected output variability.

The analysis tool being developed in this effort will implement the unique analytical formulations described, linking continuum scales and damage mechanics. Damage mechanics modules will be provided to perform life calculation at a component level for long spectrum histories in different fatigue regimes.

9.6.19. Integrated Structural Modeling and Simulation

Lawrence Stoker, USAF A-10 ASIP

The A-10 Analysis Group has developed capabilities to take large, globally modeled and loaded aircraft components with unique repair configurations and develop Stress Intensity Factors (SIFs) for fatigue crack growth for specific and unique geometries (References [1] and [2]). This method is completed using a combination of software packages, namely, Siemens NX, ESRD StressCheck, and LexTech AFGROW.

For the case that follows, a 10-foot section of B-1 wing was modeled for the purpose of estimating crack growth during the B-1's full scale fatigue test. Numerous cracks were discovered in the lower wing plank. Typically, a repair doubler would be fastened to the structure. However, underlying geometry and test apparatus would not allow this standard repair form. A bonded doubler repair concept was developed by the B-1 SPO. The A-10 Analysis Group modeled the doubler, performed the necessary research to accurately model the bond between layers, extracted surface stresses and loads, modeled and extracted geometry for SIF acquisition, and finally provided the SIFs to the B-1 SPO to determine the fatigue life using AFGROW.

The following brief list of capabilities are used for large-scale models to determine SIFs and other necessary analyses:

- 3D model creation using drawing reading, interpretation, and standard drafting practices
- Loads development and application from legacy reports and data
- Finite Element Analysis (FEA) data extraction including, but not limited to: loads, stresses, displacements, strains, load path determination, natural frequencies, and dynamic simulations
- Worst-case-scenario simulation
- Design optimization
- Visual representation of models to find regions of primary interest
- Repair configuration simulation and comparison
- SIF extraction for a virtually unlimited selection of crack sizes, materials, and shapes
- Embedding small detailed models into larger, lower fidelity models as a boundary condition

An accurate solid model is developed from complex drawings, Figure 9.6-56. Then, the local region of interest is separated from the model and the repair doubler installed, Figure 9.6-57. A crack was then introduced to the structure, the model meshed, and the loads applied. During this process, the most accurate way to model a bonded model using aerospace-grade epoxy was explored and vetted. Stresses were plotted using fringe plots. Load paths could be determined in addition to ensuring the model was behaving as expected. Grid point forces were extracted from Siemens NX and applied to ESRD StressCheck to obtain SIFs. A crack was embedded into the model in StressCheck, Figure 9.6-58, and a number of crack sizes and shapes were analyzed to determine the SIFs as a function of crack size. Finally, a plot of the SIFs (or betas, depending on the application) as a function of crack size can be generated and used in AFGROW for life simulation (Figure 9.6-59).

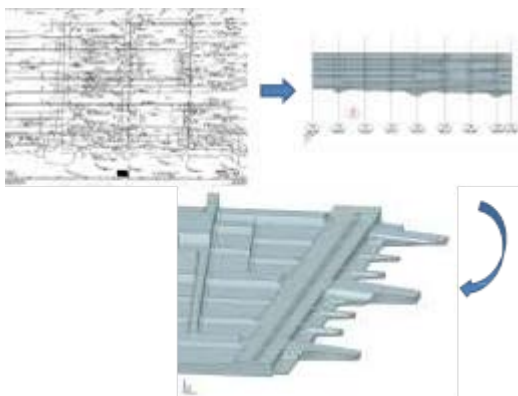


Figure 9.6-56. Building a 3D Model from Drawings

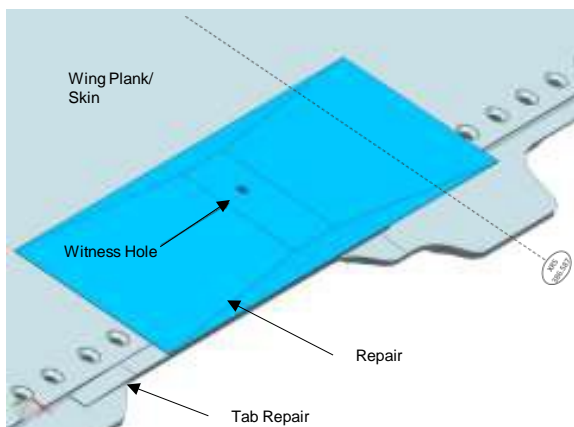


Figure 9.6-57. Local Geometry Applied

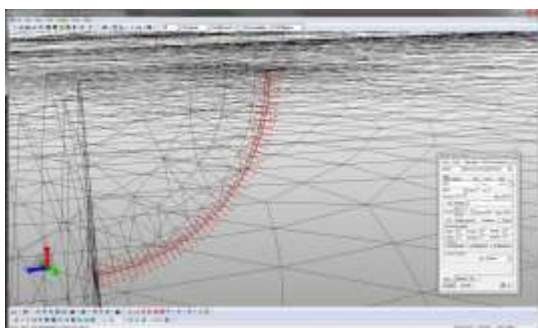


Figure 9.6-58. SIFs are Extracted from StressCheck

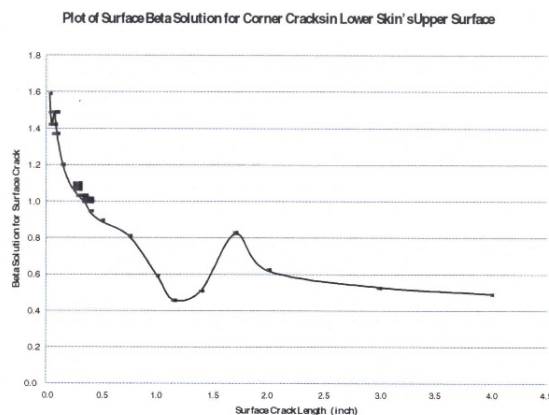


Figure 9.6-59. Betas as a Function of Crack Size

The tools available to the A-10 Analysis Group allow for an unlimited number of varying configurations: nominal and repaired, cracked and not cracked, different loading configurations, and other conditions as requested by the customer. Depending on the case desired, any imaginable set of simulations can be developed and evaluated. By having this ability organically within the United States Air Force, millions of dollars have already been saved. The time expediency and flexibility provide value beyond the monetary savings.

References

- [1] Pilarczyk, R, Carlson, S, Stowe, G, "Is ASIP Still Alive? The A-10 Lower Wing Skin Cracking Issue of 2008 – 2009", US Air Force Aircraft Structural Integrity Program Conference, Jacksonville, FL, 1 December – 3 December 2009.
- [2] Sedgwick, H, Clark, PN, Pilarczyk, R, Stowe, G, "FEA & DTA Development for A-10 Fuselage Longeron Cracking", US Air Force Aircraft Structural Integrity Program Conference, San Antonio, TX, 30 November – 2 December 2010.

9.6.20. The Evolution of BAMF

Joshua Lloyd Hodges, USAF T-38 ASIP

Over the past 4 years the T-38 and A-10 analysis groups have collaborated on a state-of-the-art fatigue crack growth capability. The group has been using a building block approach in refining and implementing a software plug-in that couples StressCheck™, a p-element Finite Element Analysis (FEA) software package, with AFGROW, a fatigue crack growth software program. In its current state the Broad Application for Modeling Failure (BAMF) is able to model multi-point planar crack growth as well as multiple elliptical cracks in complex models and geometries. Future efforts are geared towards creating capabilities to do multi-crack with multi-point (MCMP) as well as development to grow non-planar multi-point cracks (3-D crack turning).

BAMF development used a simplistic approach starting with elliptical crack growth in 3-D models where the a and c-directions were allowed to grow independently of each other based on their individual stress intensity factor (SIF) [1]. The basic structure of the plug-in has been maintained constant throughout this time with modifications being made to how the crack is being driven.

This basic approach of all BAMF iterations is that the user stress check model is loaded, meshed, solved, and stress intensities are extracted then sent to AFGROW to develop new crack lengths/lives. This simple loop (Figure 9.6-60) is repeated until the crack reaches a boundary.

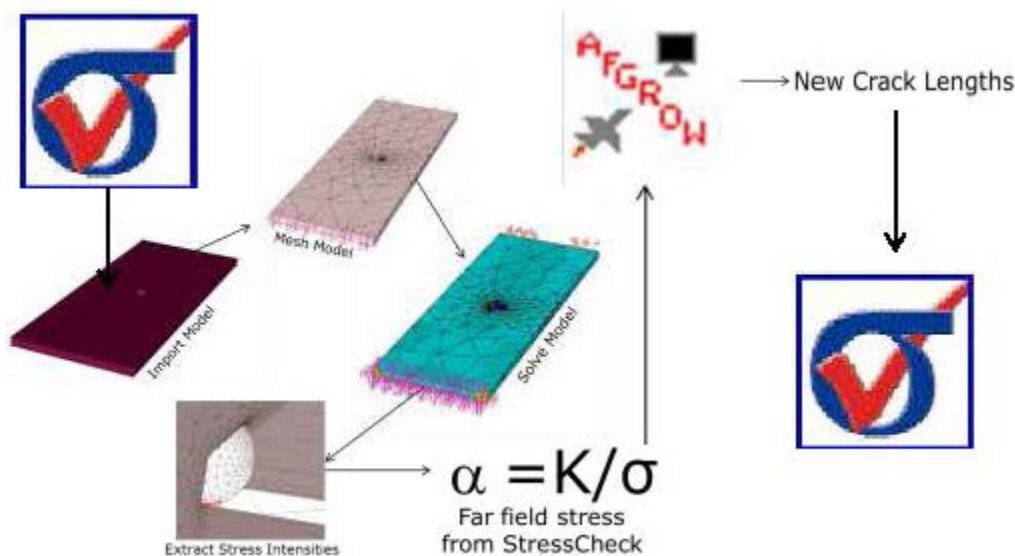


Figure 9.6-60. Standard Programming Loop for Crack Growth Evolution

The next step in development involved creating multipoint crack front evolution where each point along the crack front was driven by its SIF and grows normal to the crack front. This allowed for unique crack geometries paving the way for unique crack shapes driven by residual stresses (Figure 9.6-61).

9.6.21. Materials Characterization of High Strength Aluminum Alloys and Mixed-Mode Fatigue Crack Growth Test Development

Mark James, Jason Bely, and Robert Bucci, Alcoa Technical Center

Many innovative industries are looking for greater structural efficiencies and reduced manufacturing cost, for example, with single-piece aluminum structural components that are derived from thick plate. For thicker product forms, thru thickness (Short Transverse (ST) direction) property characterization becomes relevant, whereas typical design methods only utilize material property orientations that are typical for sheet and thin plate (Long (L) & Long Transverse (LT) orientations). Additionally, damage tolerant structural design methods do not typically account for fatigue cracks growing under mixed-mode loading conditions, and effects due to microstructure anisotropy are ignored. Properties such as those in the ST direction are known within the aluminum industry to sometimes differ significantly from those observed for the in-plane L and LT directions. Conventional fatigue crack growth rate characterization relies on test specimens fundamentally designed for Mode-I crack growth, where the crack path is assumed to be perpendicular to the applied load. The core objective of the described work was to develop and demonstrate the need for the experimental capability necessary to study fatigue crack growth (FCG) behavior under combined mode-I and mode-II loading, as they relate to crack propagation direction and life estimation. In addition, the current work strives to develop and move towards standardization for mixed-mode test capability and suggests the need to revisit many of the fundamental fracture mechanics tenets.

The compact tension-shear (CTS) specimen and loading fixture, based on the work of Richard [International Journal of Fracture, pp R55-R58, Vol. 22, 1983], were chosen for this work (Figure 9.6-63). In all cases the specimens were extracted from 7050-T7651 aluminum alloy thick plate, in S-L orientation, and subjected to constant amplitude loading at a stress ratio $R = 0.1$. An "equivalent" driving

force $\left[K_{eq} = \sqrt{(1 - \nu^2)K_I^2 + (1 - \nu^2)K_{II}^2} \right]$ approach was selected for simple comparison to mode I

analysis, with ΔK_{eq} tabulated against crack growth rate (da/dN), mode mixity (K_{II}/K_I) as well as initial kink angle when cracks were observed to begin out of plane. Initial kink angle analysis highlights a competition between mechanical driving force and planes of weakest microstructural resistance (Figure 9.6-64). At the lowest driving force, the crack growth direction approximately followed the well known maximum tangential stress criterion. As the driving force increased, particularly under elevated mode-mixity, results showed an increasing tendency for the crack path to align with the microstructure/rolling direction on the symmetry plane.

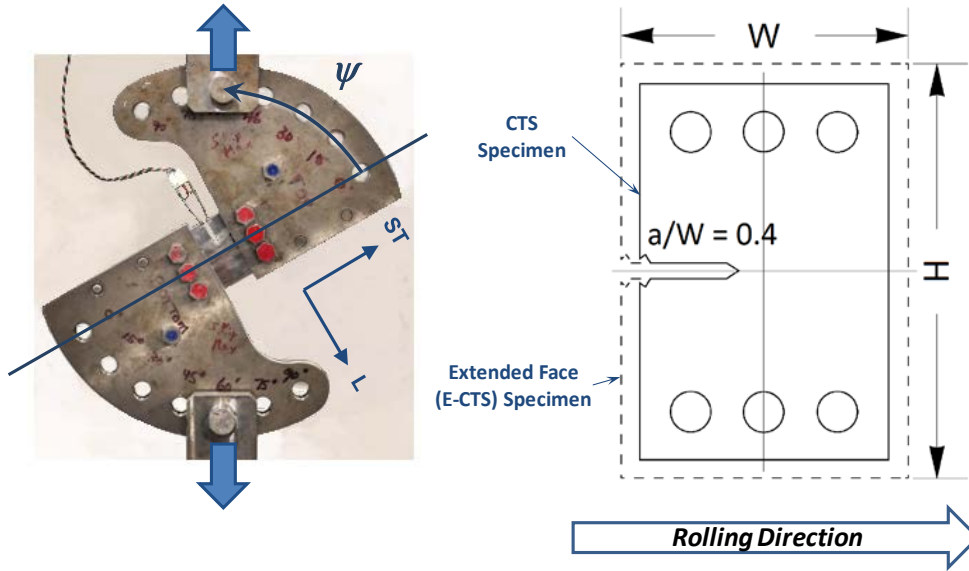


Figure 9.6-63. CTS Test Fixture & Specimen Dimensions that were Used for Mixed-Mode Tests

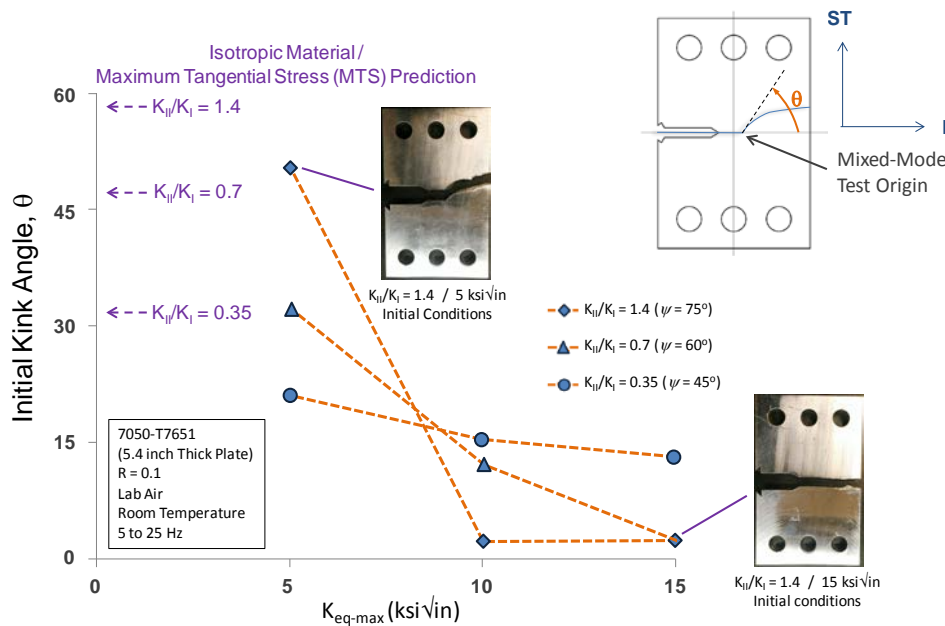


Figure 9.6-64. Crack Path Kink Angle Data Showing Crack Direction Dependence on Competition Between Maximum Mechanical Driving Force (K_{eq-max}) and Plane of Weakest Microstructural Resistance

Fatigue crack growth rate data analysis was performed for the test cases where the crack path followed the specimen microstructure on the symmetry plane (Figure 9.6-65). In this figure, a number of specimen results are pooled as one data set to compare the mixed-mode results with the traditional mode-I data. The results showed that some mixed-mode crack growth rates are significantly higher than those observed during mode-I tests of various material orientations. To produce the results in Figure 4, the mixed-mode results of Figure 9.6-65 were interpolated along lines of constant ΔK_{eq} to better understand the effect of mode-mixity (K_{II}/K_I) on FCG rate. The results in Figure 9.6-66 show that the FCG rate is a function of both applied ΔK_{eq} and mode-mixity. The FCG rate increases for constant values of ΔK_{eq}

under increased mode-mixity up to $K_{II}/K_I \cong 2$, where FCG rates are observed to have peaked, and then decrease for $K_{II}/K_I > 2$. These mixed-mode FCG results show that mode-I FCG could be un-conservative if applied to other configurations with complex (not purely mode-I) loading conditions.

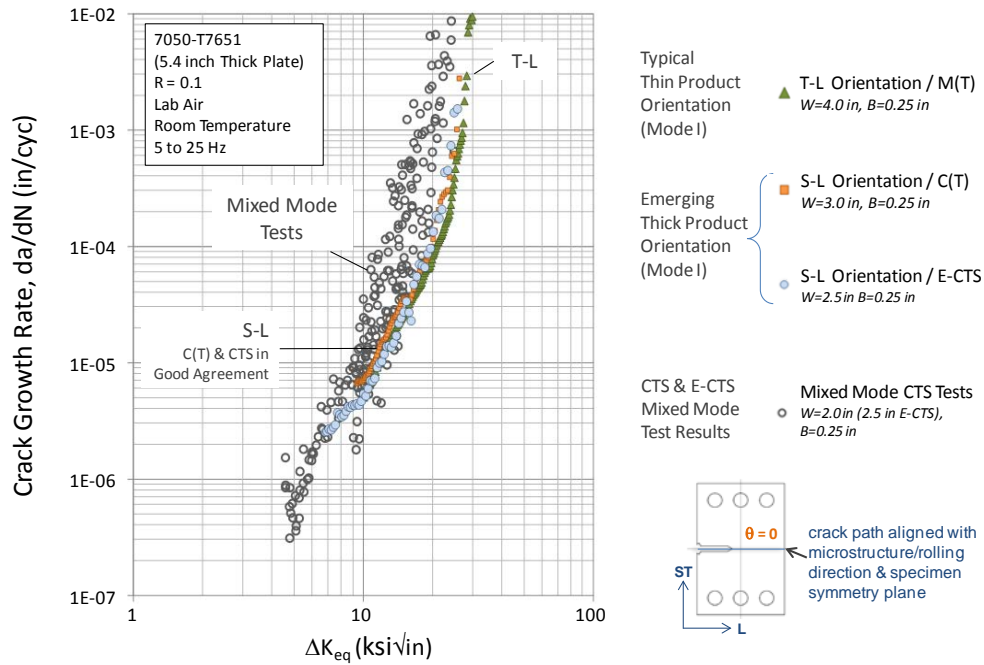


Figure 9.6-65. Mixed-Mode FCGR Tests from CTS & E-CTS Specimens have Generally Higher FCG Rates Compared to Mode-I Test Data

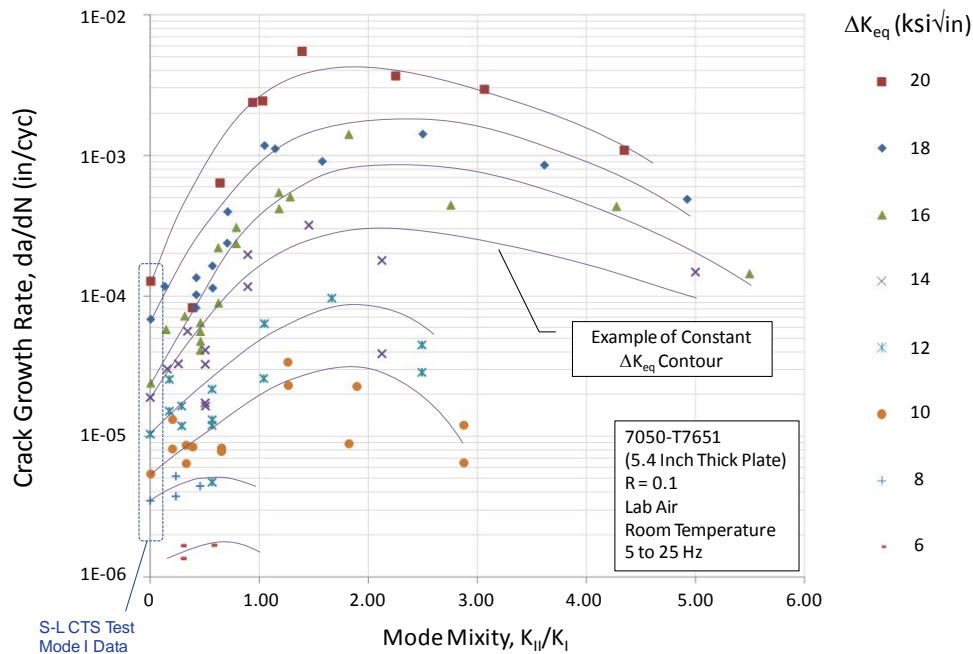


Figure 9.6-66. Crack Growth Rate vs. Mode-Mixity (da/dN vs. K_{II}/K_I) Shows “Worst Case” at About $K_{II}/K_I \cong 2$

The methodology and data developed here were intended to close gaps in mixed-mode fatigue crack growth rate data generation methodology and to understand the material response in emerging thick plate orientations. Beyond the capability development discussed here, one important observation is the apparent existence of a *worst case* mode-mixity and crack path that is sensitive to mixed-mode loading as well as microstructural anisotropy. Transferability from coupon to structure for the results in general, as well as the concept of worst case mode-mixity provides the drive for further study. Additionally, the lack of standardization in mixed-mode fatigue crack growth testing warrants additional efforts towards test standardization consensus.

For more information please refer to the ASTM Journal Entry that describes this test development in more detail at:

http://www.astm.org/DIGITAL_LIBRARY/JOURNALS/MPC/PAGES/MPC20140029.htm

9.6.22. Material Degradation Research Projects for OSD-CPO Corrosion Program

Gregory A. Shoales, USAF Academy - CASTLE

Corrosion technology and tools continue to be a national priority for the agencies of the United States Department of Defense. Similarly profession with the proper education and experience to be prepared to address material degradation due to environmental exposure are always in short supply. The Office of the Secretary of Defense Corrosion Policy and Oversight (OSD-CPO) office continues to execute a robust and diverse program to address these needs. Given the breadth of experience in education, corrosion, and other material degradation mechanisms of structures, CASTLE continues to serve the OSD-CPO goal in a number of arenas.

Technical Corrosion Collaboration (TCC)

CASTLE has performed research in the area of structural material degradation for the past 15 years. Since the last ICAF report CASTLE has used CPO support to contract with a number of university and private entities to conduct research programs aimed at both educating students and furthering the body of critical knowledge in the corrosion sciences. The university and private companies along with relevant government research labs form the Technical Corrosion Collaboration or TCC. One such TCC participant, SAFE, Inc., has conducted a number of projects in the CASTLE facility. Abstracts of these projects are included in this year's ICAF report and include;

- Development of a Fatigue Testing Method for Analysis of the Corrosion Pit to Small Crack Transition
- Development of Equipment and Methods for Stress Spectra Structural Testing
- Combined with Environmental Spectrum
- Stress Intensity Factors for Finite Width Plates

CASTLE helps OSD-CPO to evaluate the technical merit of new projects, determines the best means to fund selected efforts, monitors the technical performance and conducts on-site reviews of all TCC participants.

As indicated previously, government labs are also TCC participants. As a USAF research lab, one of the ways CASTLE participates is by using TCC inspired technology challenges to create projects for USAF Academy (USAFA) cadets that address the goals of both the TCC and OSD-CPO. Since the last ICAF report USAFA cadets have designed and successfully fabricated a chamber and integrated control system to interface with our fatigue test frames. During academic year (AY) 2013-2014 Cadets (now Lts) Sarah Collins, Ian Anthony, Andrew Fuerst, and Davis Gray designed the environmental control system to interface with the test chamber designed by cadets during AY 2012-2013 (reference 2013

ICAF report). This integrated system permits testing structural components under fatigue loading as well as a variety of environmental variables to include; relative humidity, temperature, gas type, ozone, and UV radiation. A schematic of the chamber with various sensors and environment introduction devices is depicted in Figure 9.6-67 — the UV system is highlighted in this figure. This chamber is designed to install in any of CASTLE’s 55 kip class MTS fatigue test frames.

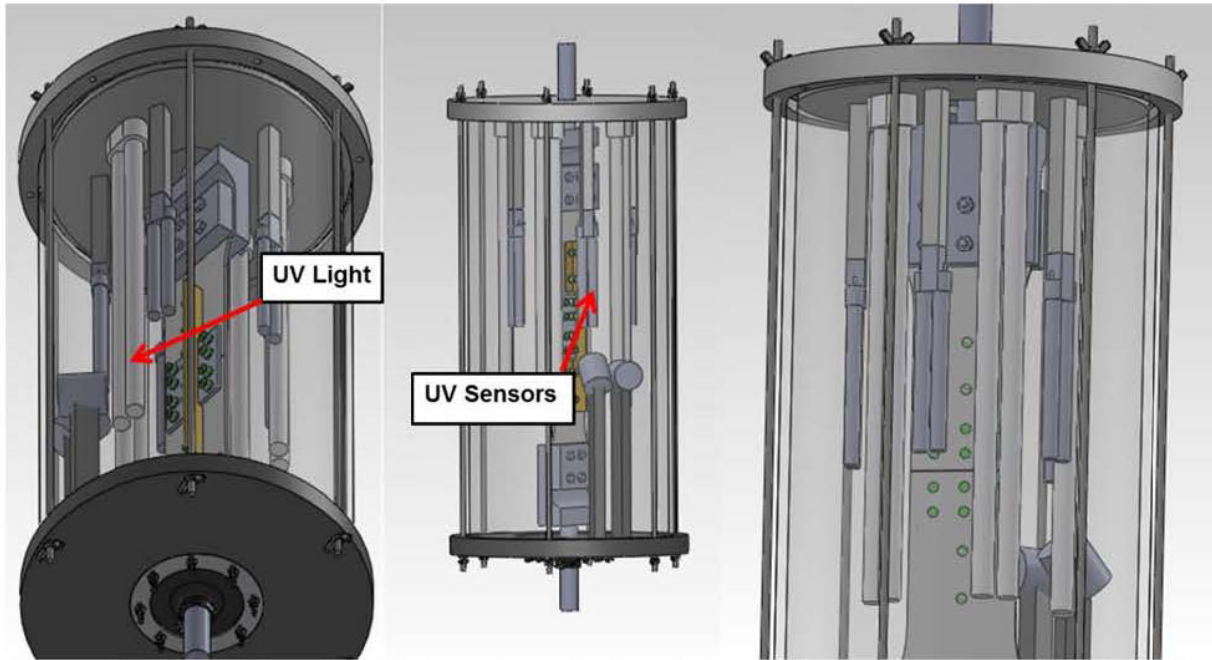


Figure 9.6-67. Depiction of Test Chamber Designed by Cadets to Test Structure Under Simultaneous and Programmable Stress Spectra and Environmental Spectra. The UV Sensor and Application System is Highlighted

The successful prototype designed and fabricated by the cadets was further developed into a more commercial form by the Air Force Research Laboratory and is reported elsewhere (reference *Development of Equipment and Methods for Stress Spectra Structural Testing Combined with Environmental Spectrum*). Since the CASTLE USAFA research facility also includes a 220 kips, four-post MTS load frame, the AY 2014-2015 cadet capstone team is endeavoring to design a chamber to tests specimens up to 12 times larger than the current chamber-nearly 12,500 cm². Experience has long proven the strong interaction of crack growth mechanisms (such as fatigue) and corrosion mechanisms on damage progression in structures. Therefore the “true” full environment required for accurate simulations of structural loading must include both stress and what is normally thought of as the environment. Both chambers permit such true full environmental testing of aircraft or other structural components.

Cadets also continued to research the influence of bacteria on fatigue growth since the last ICAF. Cadets Sarah Collins, Joseph Drake, and Alex Hooks researched the effect of *ralstonia pickettii* on corrosion fatigue. As reported to ICAF 2013, cadets in AY 2011-2012 discovered this bacteria, shown on a test specimen in the left side of Figure 9.6-68, can increase fatigue life by a factor of 5. The right side of Figure 9.6-68 is high magnification image of the subject bacteria. The goal of this continued research has been to understand the cause of the observed effect on fatigue crack growth and determine any potential to apply these factors in a controlled manner to beneficially impact structure damage progression. To date the cause of the effect on crack growth is better understood but a practical controlled application of these factors has yet to be identified.

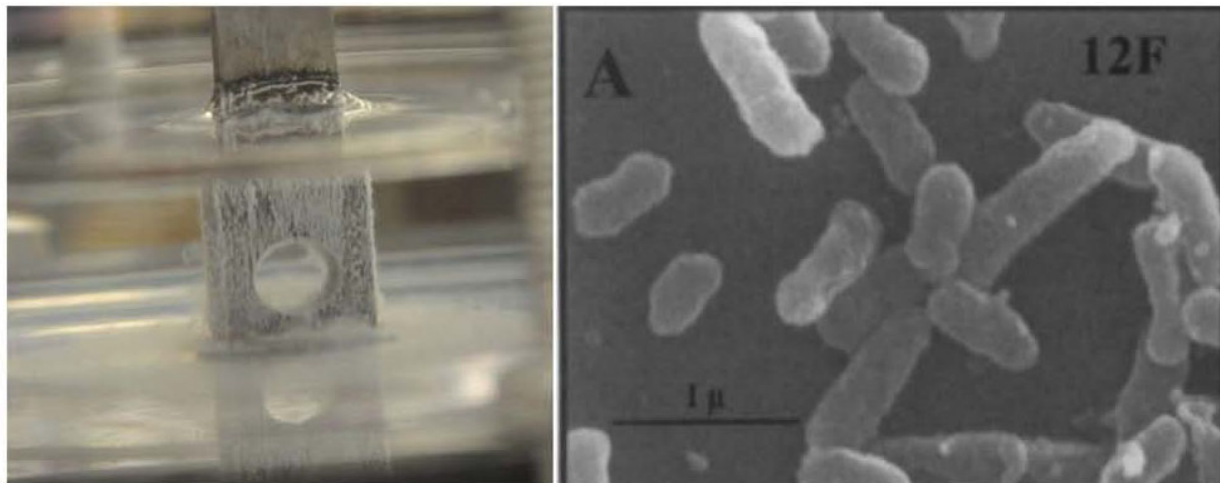


Figure 9.6-68. *Ralstonia Pickettii* (the White “Fuzz”) on a Fatigue Test Specimen After Several Days of Growth on the Left and High Magnification Image of the Bacteria on Right

Through the USAFA Cadet Summer Research Program CAStLE has sent cadets to research facilities to further their studies in material degradation related topics. In 2013 Cadet (now Lt) Sarah Collins examined *ralstonia pickettii* factors under Dr. Wendy Goodson at the Air Force Research Laboratory. This research exchange allowed Cadet Collins to explore factors not possible at USAFA due to specialized microbiologic examination equipment and protocols. During the summer of 2014 Cadets Alex Hooks and Dan Barbera investigated test protocols associated with material degradation in typical aerospace aluminum and steel alloys under Professor Tom Ladwein at Hochschule Aalen in Germany. This summer, 2015, Cadets Gill and Weinberg will work with Professor Ladwein at Hochschule Aalen to continue corrosion mechanism investigations. The cadets from the 2013 and 2014 CSRP are shown in Figure 9.6-69. This summer USAFA Department of Engineering Mechanics faculty, Capt. Ben Steffens, will begin a USAF sponsored corrosion research program for the next three years at BAM Federal Institute for Materials Research and Testing in Berlin.

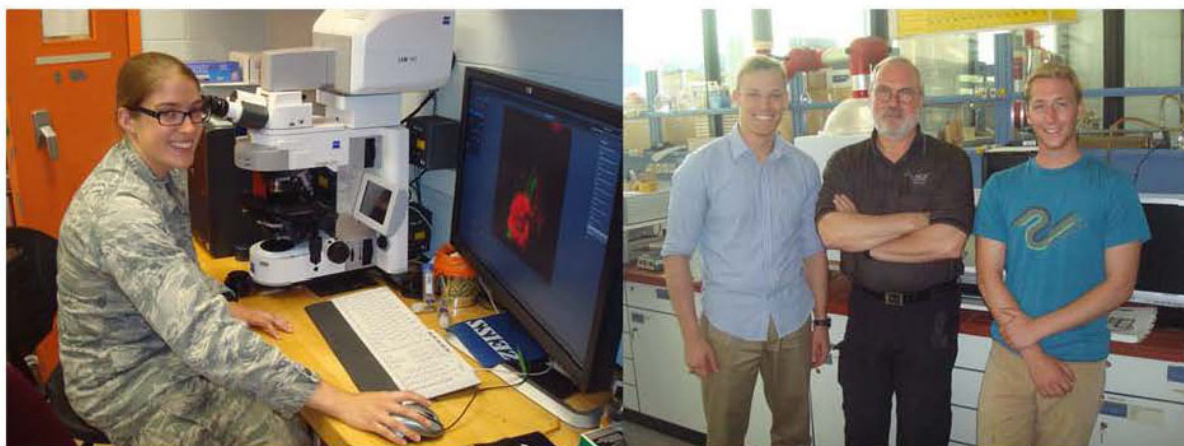


Figure 9.6-69. Cadet Collins Using Confocal Microscope at AFRL in 2012 (Left) and Cadet Dan Barbera, Professor Ladwein, and Cadet Hooks in the Corrosion Research Lab at Hochschule Aalen

Corrosion Education and Outreach

OSD-CPO has a large portfolio of education and outreach programs in corrosion topics. Since CASTLE is both experienced in corrosion topics and has designed and presented numerous short courses over the past 20 years on a number of topics that fall within our core competencies, CASTLE assists OSD-CPO with this aspect of their portfolio. Since the last ICAF these projects have included:

- Development of a corrosion material sustainment education program
- Development and prototyping of a university student corrosion design-applied solution competition to address DoD's corrosion related problems
- Corrosion focused web-tools development and consolidation
- Development of a corrosion science education exhibit with hands-on interaction for application to US public science centers
- Development of a material science long distance education course for advanced placement of high school and college students
- Development of booths education exhibits for conference displays and public outreach media articles
- Updates to the corrosion impact study
- Research into storage and dehumidification state-of-the-art and its impact on material degradation

CASTLE also cooperated with one of the TCC partners to develop a short course focused on corrosion mechanisms and their influence on the degradation of structures. Select lessons from this course were integrated into the cadet curriculum and are offered as requested to structural sustainment professionals.

9.6.23. Development of a Fatigue Testing Method for Analysis of the Corrosion Pit to Small Crack Transition

Justin Rausch and Scott Fawaz, SAFE, Inc.

This project is performed in support of the Office of the Secretary of Defense Corrosion Policy and Oversight (OSD-CPO) office sponsored Technical Corrosion Collaboration (TCC) by support contractors from SAFE, Inc. in the CASTLE facility. The goal of this work is to further the understanding of how fatigue cracks transition from corrosion pits to fully formed fatigue cracks by developing a standardized test method that incorporates specimen geometry and known high fidelity methods of crack length monitoring to provide researchers a standard methodology for conducting corrosion fatigue experiments. Standardizing corrosion fatigue tests would allow greater collaboration and data sharing between researchers investigating the effects of corrosion inhibitors and their interaction with crack nucleation and propagation. Corrosion fatigue is of great concern to the Department of Defense (DoD) as equipment and aircraft platforms are being used beyond their original design life. The cost of corrosion for DoD infrastructure and weapon systems is increasing every year due to the required continual use of these aging structures. Greater understanding of how corrosion damage affects fatigue crack formation will allow for better life prediction models and the ability to accurately test corrosion inhibitors that slow the transition from a corrosion pit to a fatigue crack. The resulting increase in time between pit formation and crack nucleation would cause an increase in the useful amount of structural life a component has before required inspection or replacement.

The pit-to-crack test protocol requires that four sub-tasks be completed. These tasks involve the development and implementation of a pitting protocol to generate consistent corrosion pits in the size range of 100 – 200 μm on both a center hole and surface fatigue specimen (Figure 9.6-70), a spot welding protocol to attach the voltage probes on either side of the corrosion pit for measurement of fatigue crack growth rates using the direct current potential drop method, fatigue crack growth testing in lab air with the introduction of marker band loading to establish fatigue crack progression (Figure 9.6-71) and flaw shape development (Figure 9.6-72), and the development of AFGROW simulations that can predict the pit-to-

crack transition from crack growth rate (da/dN) data. To develop the pit-to-crack test methodology a legacy aluminum alloy and temper, AA7075-T651, is being utilized. There is a large database of fatigue data for this alloy and it is a legacy alloy often used on US Navy aircraft so it is particularly relevant to the US Navy. The pitting protocol has been finalized with further work dedicated to reducing pit sizes. Figure 9.6-73 gives examples of pits produced by the protocol. The finalization of the spot welding protocol is underway along with the development of the fatigue protocol. Crack growth simulations using AFGROW are also in work.

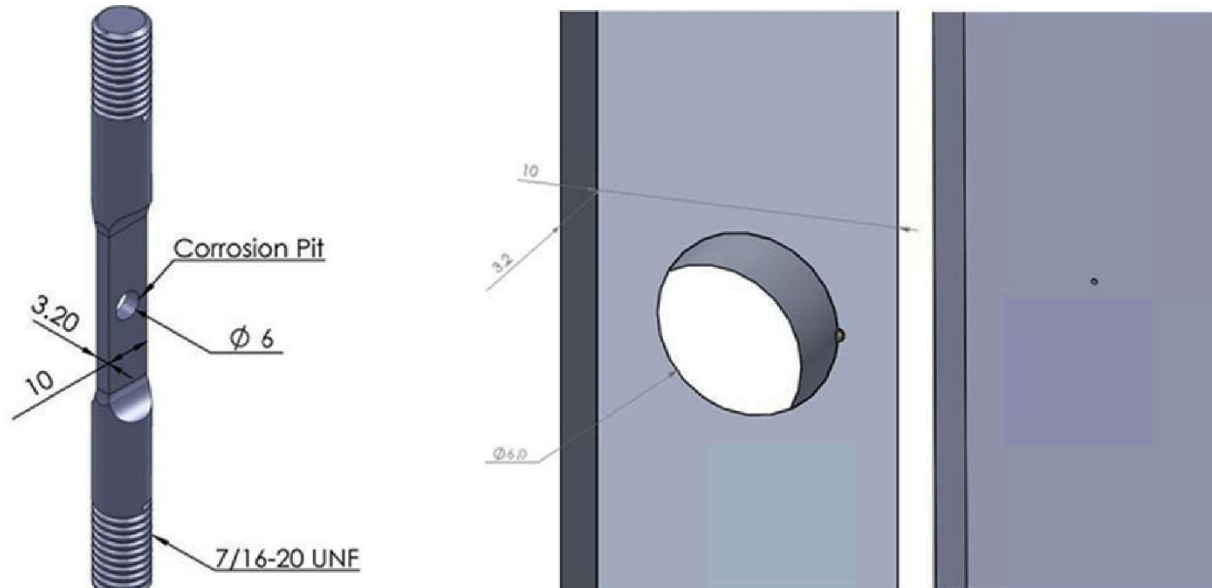


Figure 9.6-70. Corrosion Fatigue Sample with a Close Up of the Pit Location on Both the Corner of the Hole and on the Specimen Surface

Future work will apply the pit-to-crack transition protocol to determining how the corrosion damage to fatigue crack transition changes with the presence of corrosion inhibitor (chromate and chromate replacement coatings), material substitution alloys, environment and other aircraft relevant situations.

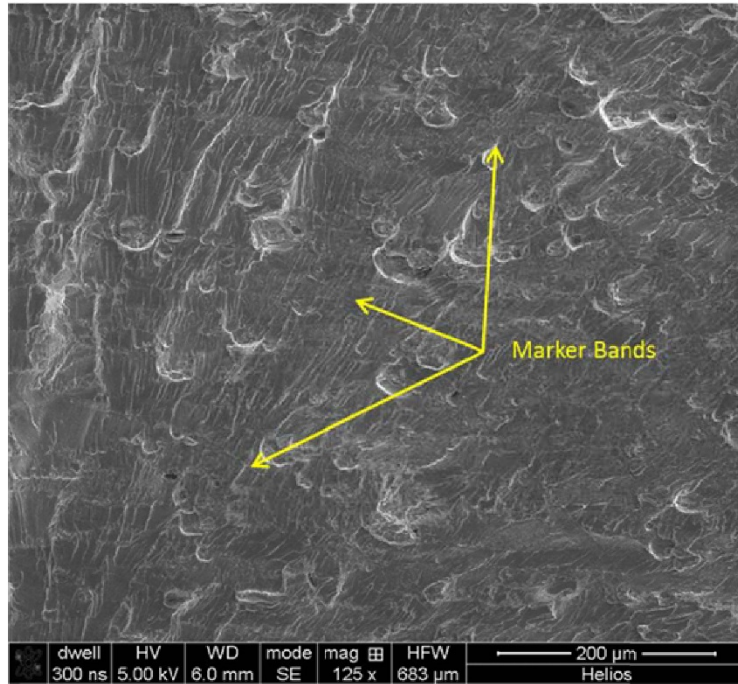


Figure 9.6-71. SEM Image of Fractured Surface of AA 7075 Sample Showing the Locations of the Applied Marker Bands

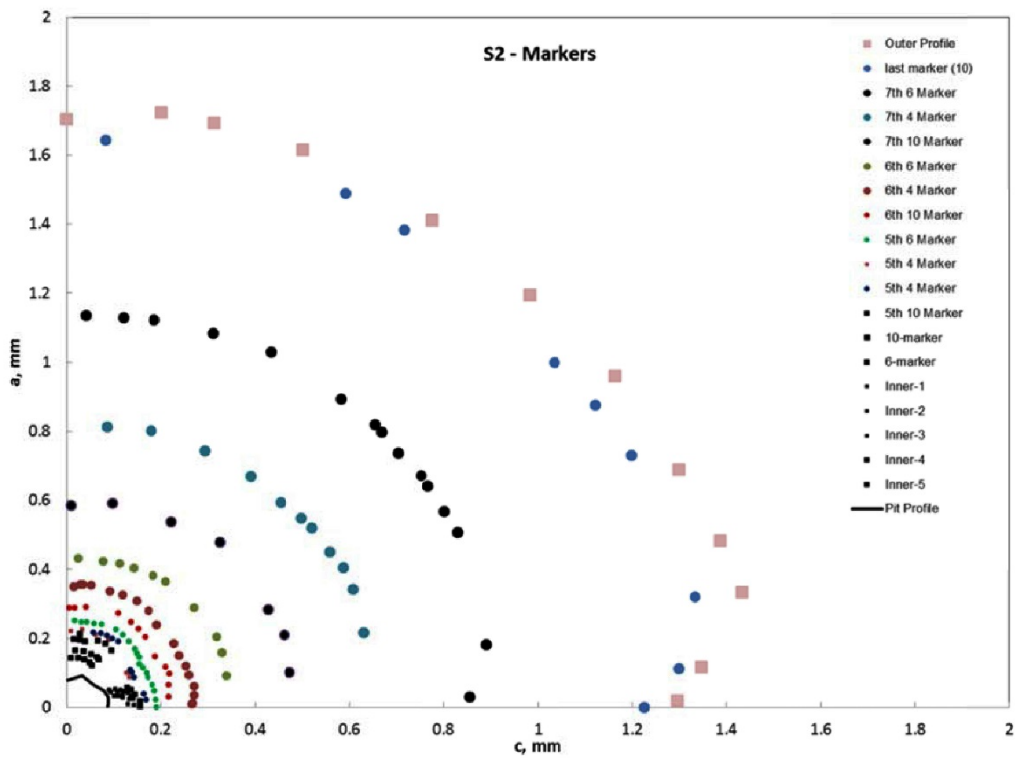


Figure 9.6-72. Marker Band Profiles of the Crack Growth in AA7075 Alloy Showing Flaw Shape Development

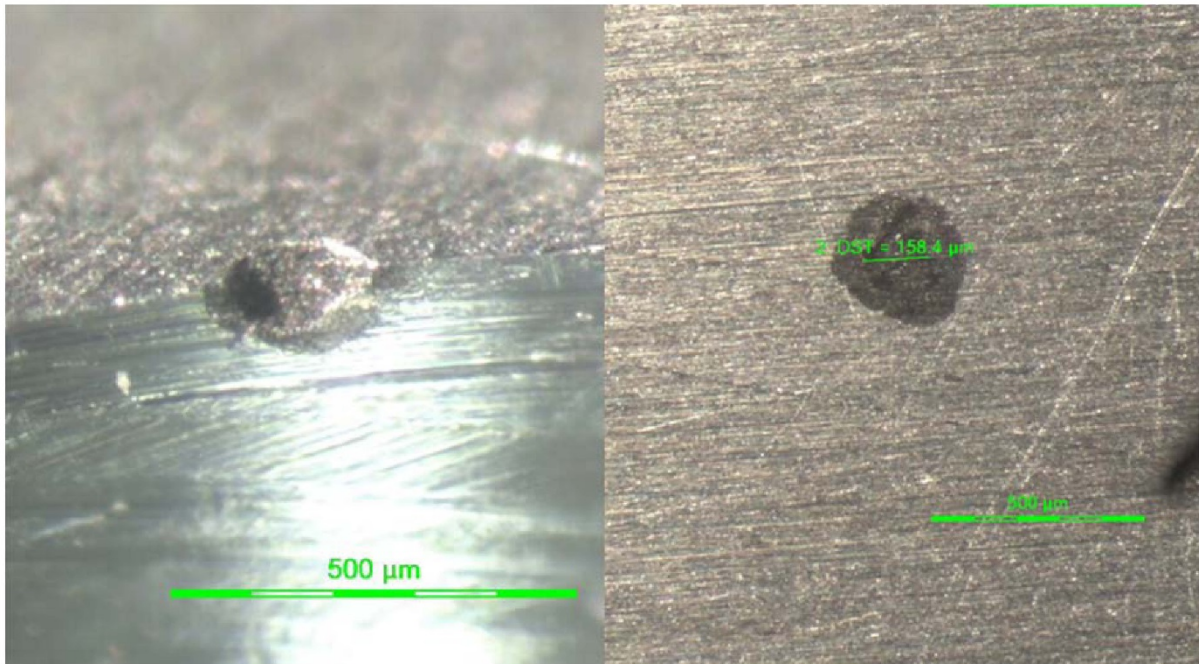


Figure 9.6-73. (Left) Corrosion Pit Produced with the Developed Pitting Protocol Along Center Hole. (Right) Corrosion Pit Created on the Surface of an AA 7075-T651 Specimen

9.6.24. Development of Equipment and Methods for Stress Spectra Structural Testing Combined with Environmental Spectrum

Sarah E. Galyon Dorman & Jason H. Niebuhr, SAFE, Inc.; Lt Sarah E. Collins, Lt Davis P. Gray, Cadet Ian A. Anthony, and Cadet Andrew S. Fuerst, USAF Academy - CASTLE

This project is performed in support of the Office of the Secretary of Defense Corrosion Policy and Oversight (OSD-CPO) office sponsored Technical Corrosion Collaboration (TCC) by support contractors from SAFE, Inc. in collaboration with USAFA cadets in the CASTLE facility. Corrosion fatigue research continues to be of great importance to the United States Air Force (USAF). Current efforts are underway to move towards more sophisticated methods of characterizing corrosion fatigue damage. Currently, most corrosion fatigue testing involve immersed samples or examine samples in humid environments. Corrosion in the atmosphere is more complex than these laboratory test environments and the corrosion morphology produced is often different. In the last several years, research has moved towards atmospheric testing in which a sample has salt deliquesced on the surface of the sample during to fatigue testing [1].

To produce better data for the examination of the role of corrosion on the reduction in fatigue life, it would be ideal to be able to test aircraft structure or aircraft representative structure under an environmental load spectrum. To this end, building off work completed under contract for the Office of the Secretary of Defense Corrosion Policy and Oversight Office by SAFE, Inc. at the United States Air Force Academy's Center for Aircraft Structural Life Extension (CASTLE), SAFE, Inc. improved upon the design of a test chamber for the environmentally assisted fatigue testing of aircraft representative structure. Based on the needed inputs for new testing methodologies, a control system has been designed to apply the following environments during a mechanical test using the chamber: salt spray of three separate salts (NaCl, CaCO₃, NaHCO₃), ozone (30 ppb-30 ppm), temperature (-65-250 F), relative

humidity (0-100%; $\pm 5\%$), interchangeable background gases related to pollution, and elevated UV-light application. Once complete this chamber will allow for the examination of an environmental spectrum in conjunction with a loading spectrum. This advance should allow for a much more comprehensive understanding of how environment degrades aerospace materials under real-world conditions. The control and monitoring system for each environmental parameter had to be designed and custom built to have the proper feedback. The complex environmental inputs of the chamber greatly limited the materials, sensors and control systems that could be selected for use with the chamber design.

Testing is underway to quantify and validate the applied environment inside of the chamber. Once complete the chamber will be used to test new and legacy aircraft alloys under relevant aircraft loading spectrum. Figure 9.6-74 shows a completely automated test of the relative humidity control system completed over 3.5 days. The starting ambient relative humidity was approximately 8%; the relative humidity was raised to 20% and then raised and held in steps of 10% to 60% over the course of the test. Testing was also completed to verify that the seal design for the chamber held the relative humidity constant during mechanical loading. Figure 9.6-75 shows the results of these tests. A sample was fatigue tested at a maximum load of 907 kg (2000 lbs.) with a stress ratio of 0.1 at four different frequencies; 0.02, 0.2, 2 and 20 Hz. Each environmental input system will be tested to ensure the best and most applicable control possible for future environmental fatigue testing.

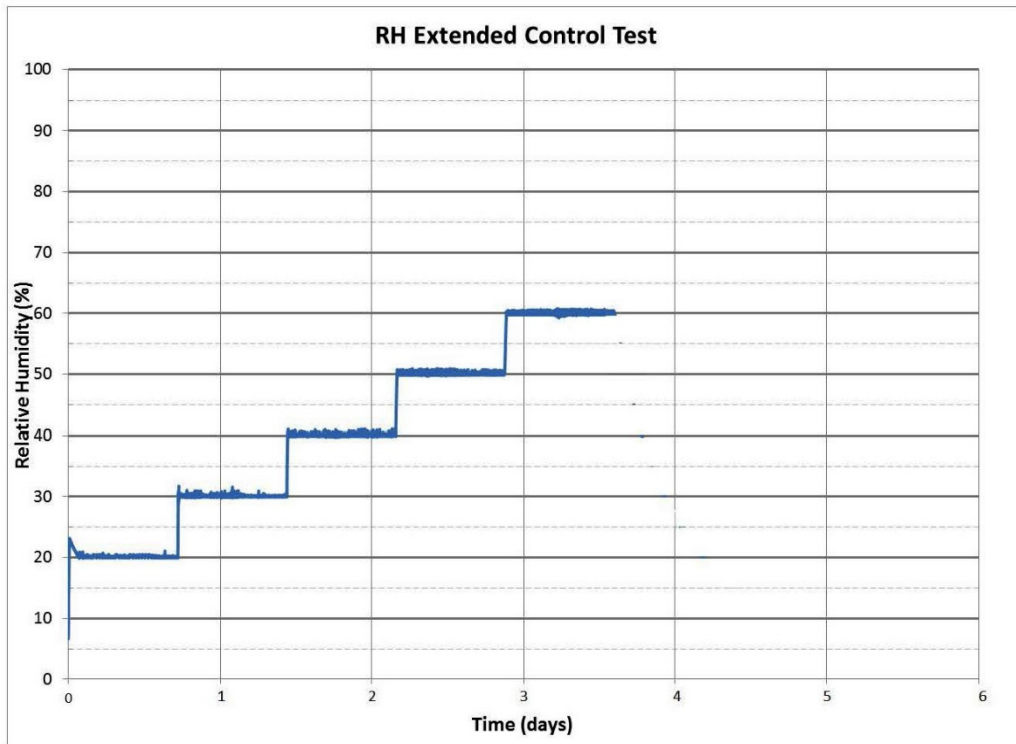


Figure 9.6-74. Automated Relative Humidity Test Completed Over 3.5 Days Using the Control System with the Chamber. The Relative Humidity was Increased and Held by the Control System Without Any User Interface Other Than the Initial Program Set-Up

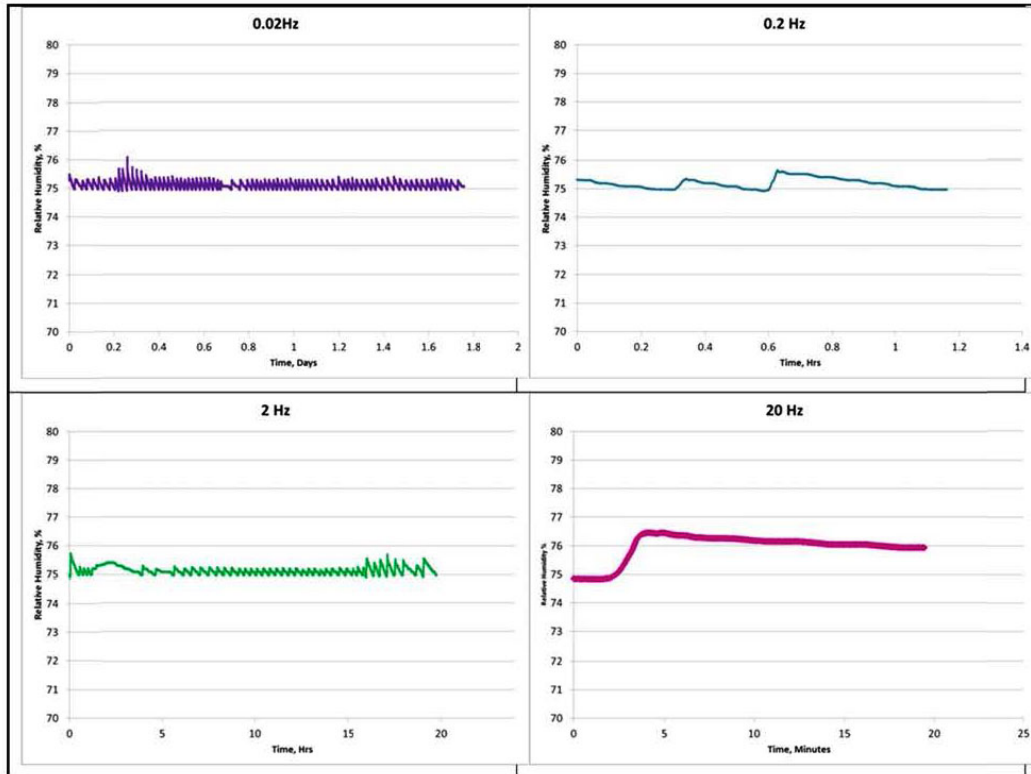


Figure 9.6-75. Results from the Relative Humidity Testing at 75% Under Fatigue Loading at a Maximum Load of 2000 Lbs. with an R=0.1 for the Frequencies of 0.02, 0.2, 2 and 20 Hz

References

- [1] Warner, JS. The inhibition of environmental fatigue crack propagation in age- hardenable aluminum alloys. PhD Dissertation, University of Virginia, Charlottesville, VA; 2010.

9.6.25. Stress Intensity Factors for Finite Width Plates

Matthew Hammond & Scott Fawaz, SAFE, Inc.

This project is performed in support of the Office of the Secretary of Defense Corrosion Policy and Oversight (OSD-CPO) office sponsored Technical Corrosion Collaboration (TCC) by support contractors from SAFE, Inc. Accurate damage tolerance analyses of aerospace structure will lead to a more cost effective and safe flying environment, especially as the average age of the United States Air Force's fleets continue to climb ever higher. This is only possible through a complete investigation of the material properties, crack Stress Intensity Factors (SIF), and Loads/Environment Spectra Survey (L/ESS), among others. As can be seen in Figure 9.6-76, there can be a significant impact on the crack growth life predictions with only a 10% increase in the SIF values.

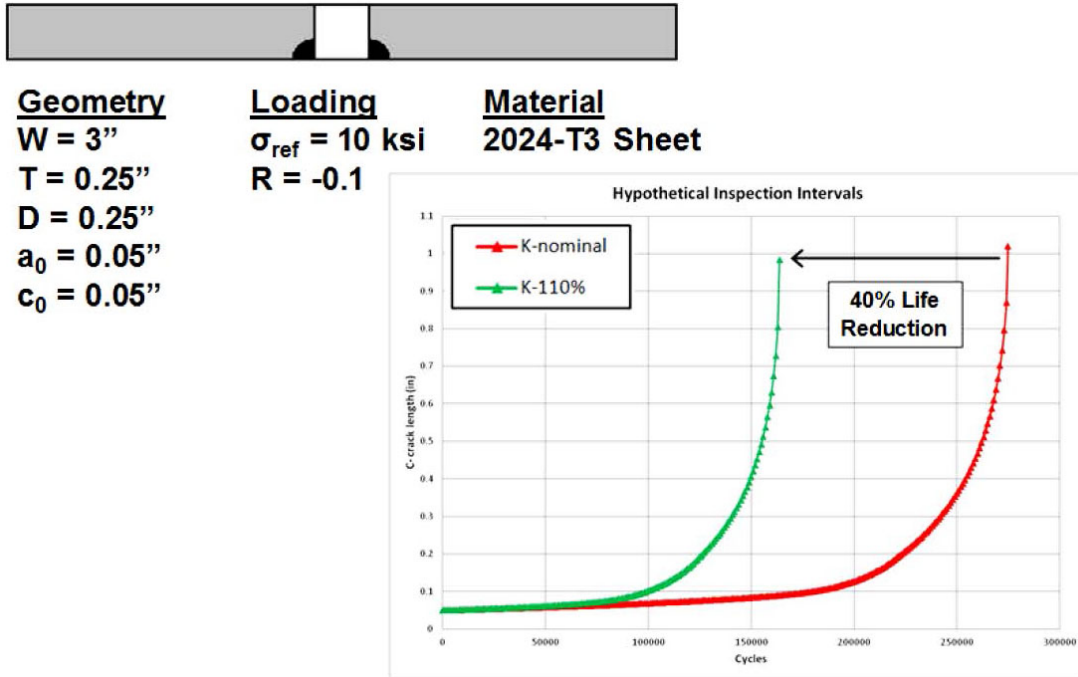


Figure 9.6-76. Impact of Inaccurate Crack Growth Analysis

The current investigation seeks to develop an extensive SIF database for elliptical corner cracks emanating from centrally located holes in finite width plates. The investigation includes uniaxial tension, out-of-plane bending, and bearing load cases. The range of crack and plate geometries is extensive. The large solution space covers the following geometries:

$$1.1 \leq W/D \leq 20$$

$$0.2 \leq D/t \leq 20$$

$$0.1 \leq a/t \leq 0.99$$

$$0.1 \leq a/c \leq 10$$

where W is the plate width, D is the hole diameter, t is the plate thickness, a is the through-thickness crack length, and c is the crack length in the transverse direction. These plate geometries cover many of the short edge distance to hole diameter ratios commonly found in aerospace structures, and encompass the following range:

$$0.55 \leq e/D \leq 10$$

where e is the distance from the centerline of the hole to the near edge.

Well-structured, fully hexahedral, finite element (FE) cracked plate models, like the one seen in Figure 9.6-77, are automatically generated and interrogated for mesh quality. Over 150,000 individual crack models are used to generate a sufficiently high-fidelity solution space as to minimize interpolation error in SIF extraction at intermediate crack/plate geometries in finite width plates.

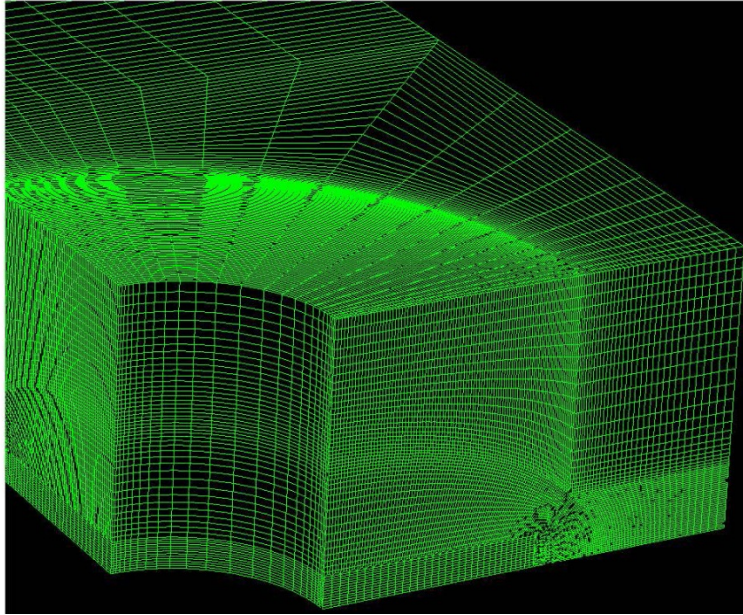


Figure 9.6-77. Well-Structured FE Mesh of Elliptical Crack in Finite Width Quarter-Plate (DSCC)

Early comparisons between double symmetrical corner cracks, DSCC, (Figure 9.6-78) and single corner crack, SCC, (Figure 9.6-79) geometries show potentially dramatic differences in the SIFs currently available in industry and the solutions developed within this effort for finite width plates, depending upon the specific crack scenario.

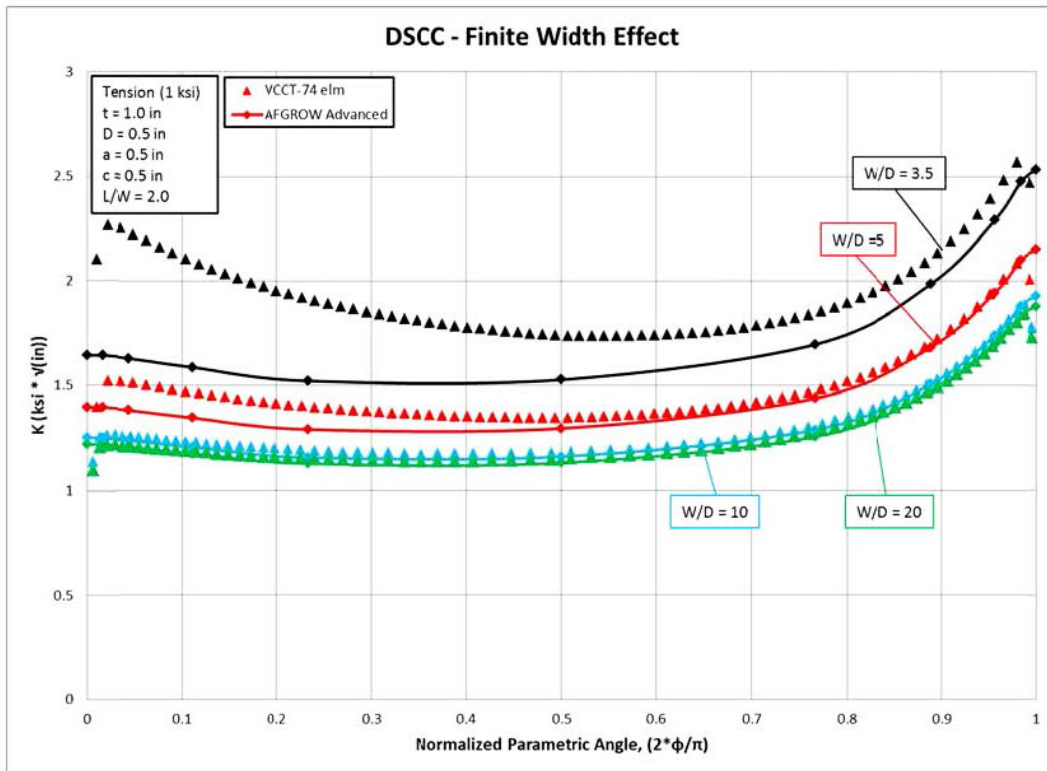


Figure 9.6-78. Variation in SIF with Various Width Plates

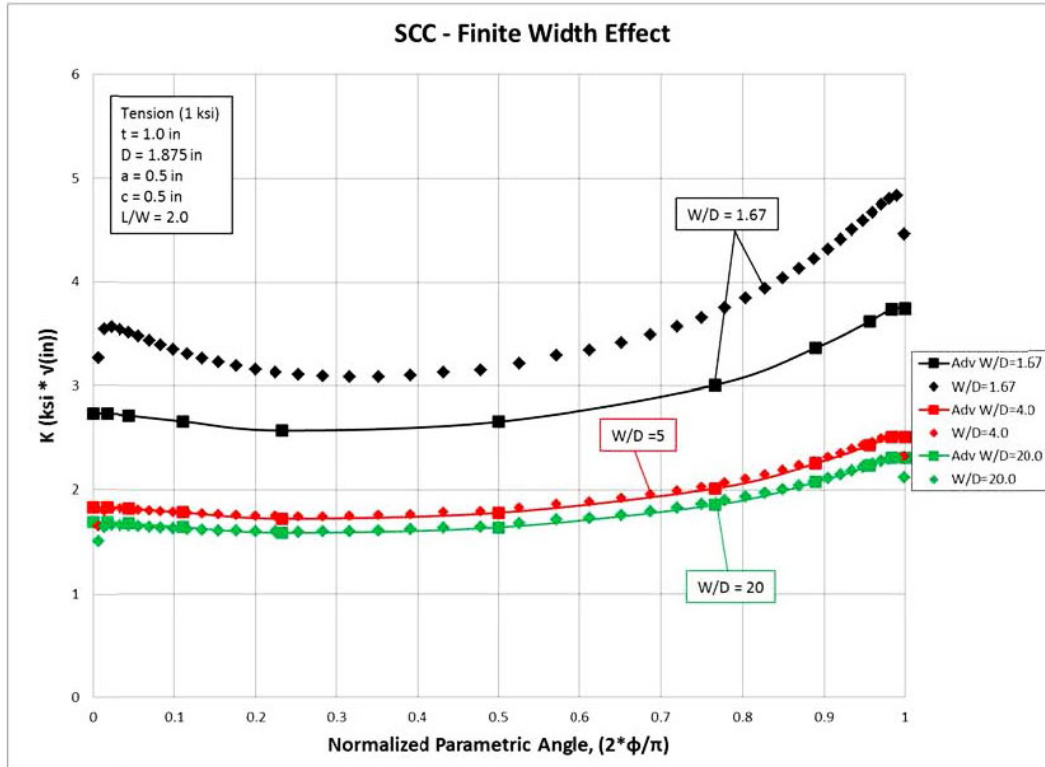


Figure 9.6-79. Variation in SIF with Various Width Plates

9.6.26. Test Methods to Partition Residual Stress From Fatigue Crack Growth Rate Data

Mark James, Alcoa Technical Center and Dale Ball, Lockheed Martin Corporation

The United States Air Force Research Laboratory sponsored Metals Affordability Initiative (MAI) consortium has conducted a detailed experimental and analytical study of bulk residual stresses, fatigue crack initiation, and fatigue crack growth in aluminum coupons extracted from material with intentionally induced residual stress. This ICAF contribution summarizes a portion of this work directed to improving the material fatigue crack growth rate (FCGR) characterization process to enable partitioning residual stress effects from the material “true” FCGR behavior, leading to FCGR design curves that are free of residual stress bias. In the program, material was processed intentionally to introduce significant residual stress, then various coupon types were extracted for residual stress measurement, constant amplitude and spectrum fatigue testing, as well as FCGR characterization. Figure 9.6-80 (a) contains FCGR characterization data from M(T) and C(T) specimen tests on a ΔK_{app} basis. Tensile residual stress effects on the M(T) specimen moved all of the low ΔK data left far enough that the data appear closure free. In contrast, compressive effects on the C(T) specimen moved the low ΔK $R = 0.1$ data far to the right. The various curves are crossing in ways not normally expected, and design curves cannot confidently be derived from the data as-is in Figure 9.6-80 (a).

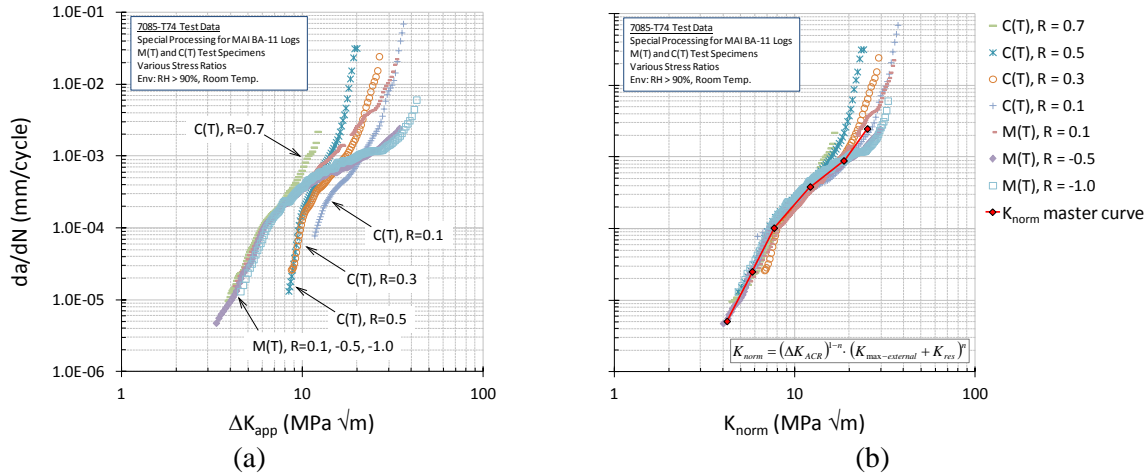


Figure 9.6-80. Fatigue Crack Growth Rate Data on (a) ΔK Applied and (b) K_{norm} Bases

Two key developments in recent years have enabled significant opportunity to understand such confounded data and to partition residual stress effects from FCGR data. The first of these was the development and standardization of the Adjusted Compliance Ratio (ACR) [1] approach to characterize the effects of crack closure remote from the crack tip [1]. The second of these was the development of the online crack compliance method to measure the stress-intensity factor due to residual stress in a specimen in real time during an FCGR test [2]. Donald and Lados [3] outlined a methodology to integrate the two developments into one post-test data analysis procedure to “collapse” the data into a single normalized stress-intensity factor (K_{norm}) based “master” FCGR curve that is free of residual stress bias and normalized for closure effects. The K_{norm} master curve is then used with a crack closure-based mechanics model to reintroduce the stress-ratio effect common to residual stress free data and necessary for fatigue life predictions [4].

Figure 9.6-80 (b) contains the FCGR data from the M(T) and C(T) tests on a K_{norm} basis. The equation used to calculate K_{norm} is taken from Reference 3 as $K_{norm} = (\Delta K_{ACR})^{1-n} * (K_{max-applied} + K_{res})^n$, where the exponent n is the K_{max} sensitivity and the equation is referred to as K_{max} normalization for the ΔK_{ACR} data (not shown due to space limitations). The value of $n = 0.25$ was selected for a visual best fit of the data in Figure 9.6-80 (b). Also included in Figure 9.6-80 (b) is the red diamond symbol labeled “ K_{norm} master curve.” This K_{norm} master curve was selected to approximate the average of the underlying data and will be used as the input of the design curve reconstruction process.

Figure 9.6-81 contains predicted “design” curves, where the K_{norm} master curve is first transformed into a typical closure free ΔK_{eff} curve for input to the plasticity crack closure model, and then the closure model is used to reintroduce typical stress ratio effects for a family of curves useful in industry standard FCG analysis software. Also included in Figure 9.6-81 are test data results for a second material similar to that in the MAI program, where special care was taken to generate data that are free of residual stress effects. The results show that residual stress effects can be partitioned from FCGR data that is strongly confounded by residual stress, and that stress ratio effects can be properly reintroduced for good agreement with the second material’s residual stress free FCGR behavior.

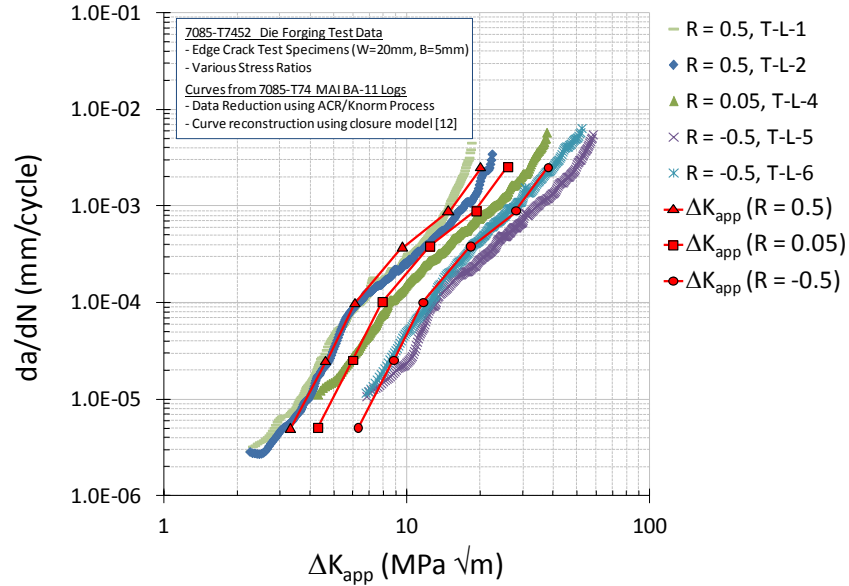


Figure 9.6-81. Fatigue Crack Growth Rate Curves Reconstructed Using the K_{norm} Master Curve and Crack Closure Mechanics, and Compared with a Second Residual Stress Free FCGR Data Set Derived From 7085-T7452 Die Forged Material

Additional validation testing and companion validation analyses were conducted for “design feature” (DF) coupons that contained simple features such as holes and pockets with structurally representative radii [4]. Again the specimens were machined from the material with intentionally induced residual stress. Fatigue tests were run on four different DF specimen configurations with both constant amplitude and spectrum loading. Figure 9.6-82 contains example residual stress measurement data for DF1 coupons (which contained a center hole in a simple panel). The color contours are measurement data using the contour residual stress measurement method and the figure also contains a line-plot comparison of measured and modeled results. The residual stress results were introduced into fatigue crack growth life predictions of the coupons using the weight function approach to calculate stress-intensity factors for the residual stress fields. Fatigue life predictions were run both with and without the residual stress field results to understand sensitivity in fatigue life to the presence of residual stress. Figure 9.6-83 is an aggregate comparison of analysis fatigue life versus tested fatigue life for the constant amplitude and spectrum cases across all four design feature specimen configurations. The results show that there is significant sensitivity to presence of residual stress and that when residual stress was included in the analysis, the fatigue life was predicted within the standard scatter factor of 2x (or the analyses were conservative).

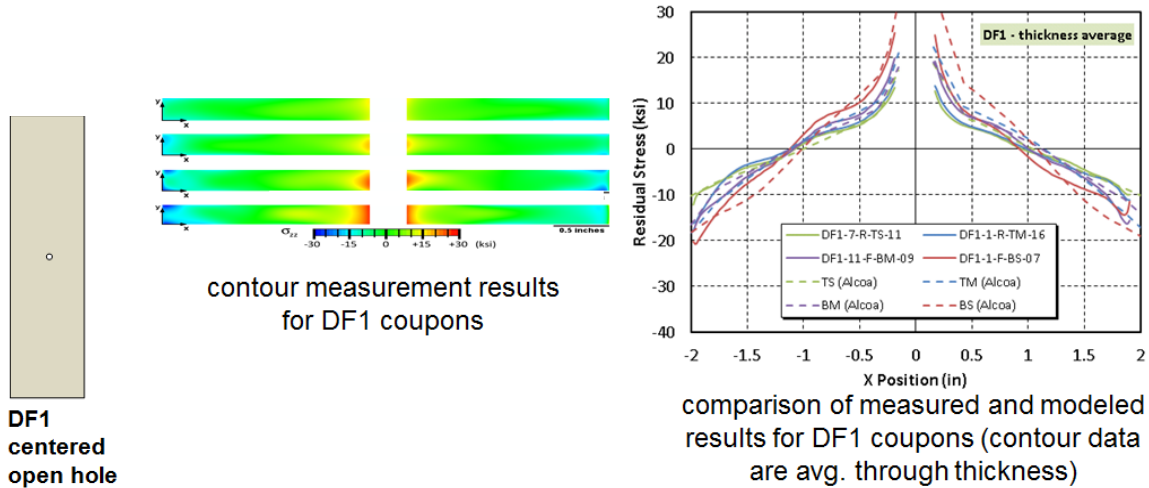


Figure 9.6-82. Contour Data for DF1 Coupons and Line-Plot Comparison of Measured and Modeled Results

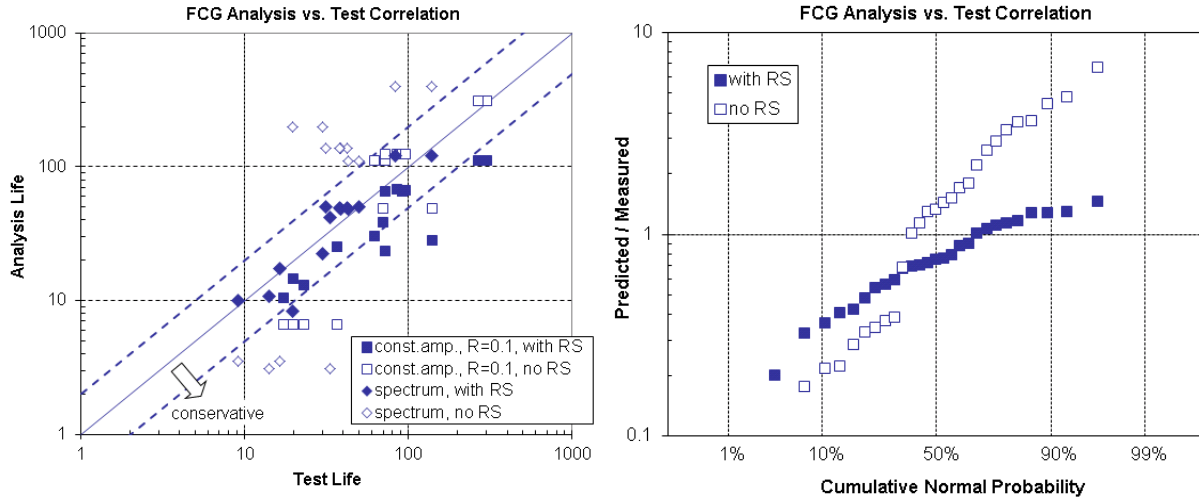


Figure 9.6-83. FCG Analysis vs. Test Correlation Summaries

The examples shown here provide compelling evidence that the ACR/K_{norm} approach to partitioning residual stress effects from fatigue crack growth rate data works well and is producing a set of intrinsic FCGR design curves that are residual stress free and that do represent the true material FCGR behavior. The results provide validation for the vision outlined in the past that when residual stress is known and correctly included in the fracture mechanics analysis, the residual stress effects can be accurately accounted for, enabling full benefit and broadened applicability of unitized structure solutions derived from a variety of thick and/or nearer net shape aluminum alloy product forms.

References

[1] G. H. Bray, J. K. Donald, "Separating the Influence of Kmax from Closure-Related Stress Ratio Effects Using the Adjusted Compliance Ratio Technique," *Advances in Fatigue Crack Closure Measurement and Analysis: Second Volume, ASTM STP 1343*, R. C. McClung, J. C. Newman, Jr., Eds., American Society for Testing and Materials, 1999, pp. 57-78.

- [2] Lados, D. A., Apelian, D. and Donald, J. K. (2006) “Fracture mechanics analysis for residual stress and crack closure corrections,” *International Journal of Fatigue*, 29, 687-694.
- [3] Donald, J. K. and Lados, D. A., “An integrated methodology for separating closure and residual stress effects from fatigue crack growth rate data,” *Fatigue Fract Engng Mater Struct* 30, 2006, 223–230.
- [4] Ball, D. L., James, M. A., Bucci, R. J., Watton, J. D., DeWald, A. T., Hill, M. R., Popelar, C. F., Bhamidipati, V., and McClung, R. C., “The Impact of Forging Residual Stress on Fatigue in Aluminum,” AIAA SciTech 2015, Kissimmee, FL, January 2015.

9.6.27. Dwell Fatigue Crack Growth in Alpha Titanium Alloy

Adam L. Pilchak, USAF Research Laboratory – Materials and Manufacturing Directorate

Cyclic and dwell fatigue crack growth rates were measured in single-phase Ti–7Al (wt. %) directly from fractured samples [1]. The quantitative tilt fractography technique was used to measure fatigue crack growth rates as a function of the crack growth mechanism (faceted versus striation growth) under cyclic and dwell fatigue loading conditions. Images showing typical examples of faceted and striation growth during dwell fatigue are presented in Figure 9.6-84. Classical fatigue striations, like those shown in Figure 9.6-84 (b), formed during normal cyclic fatigue are essentially indistinguishable from one another making the extensive faceted features near the origin of dwell fatigue cracks of particular interest. Indeed, the markings on the facet surfaces denoting the position of the crack front on successive cycles are quite distinct from striations and the spacing of these features can be used to quantitatively measure the local fatigue crack growth rates. Employing a quantitative technique to reduce errors associated with 2D projection images of complex, 3D features, the crack growth rates for each mechanism of growth were measured and are shown in Figure 9.6-85. These results indicate that the faceted growth mode during dwell fatigue was at least one and up to two orders of magnitude faster than striation crack growth under both cyclic and dwell fatigue loading at similar crack length, and therefore driving force. While the crack growth rate for faceted growth was invariably the fastest, the growth rates for striation crack advance were similar for both cyclic and dwell fatigue.

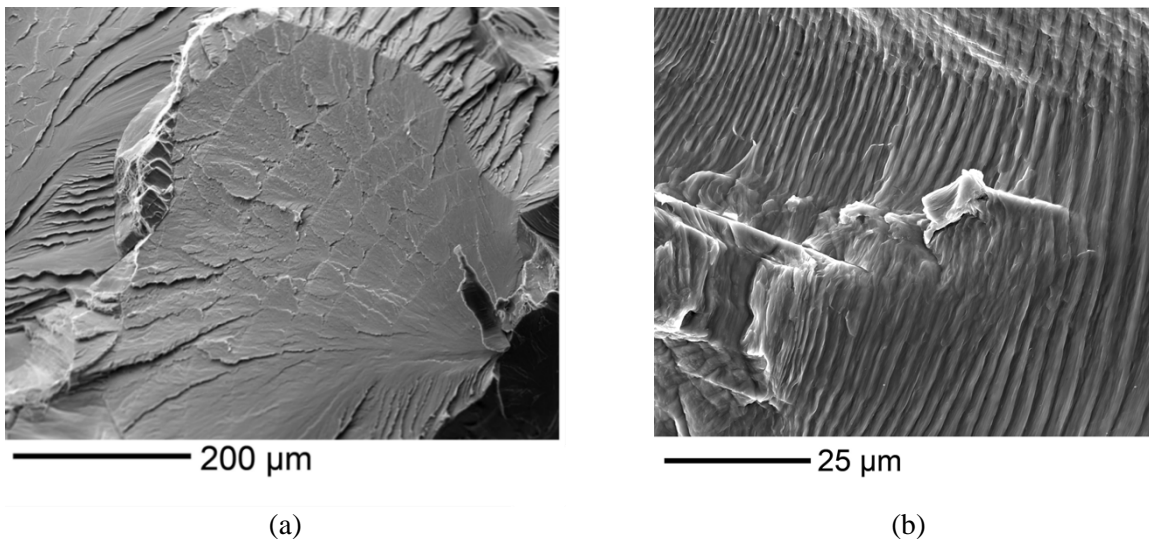


Figure 9.6-84. (a) Growth Markings on a Facet at the Crack Initiation Site of a Dwell Fatigue Sample at 0 Degree Tilt; Peak Stress=709 MPa. (b) Typical Example of Striations on a Dwell Fatigue Sample; 0 Degree Tilt; Peak Stress = 668 MPa, Crack Length ~0.95 mm

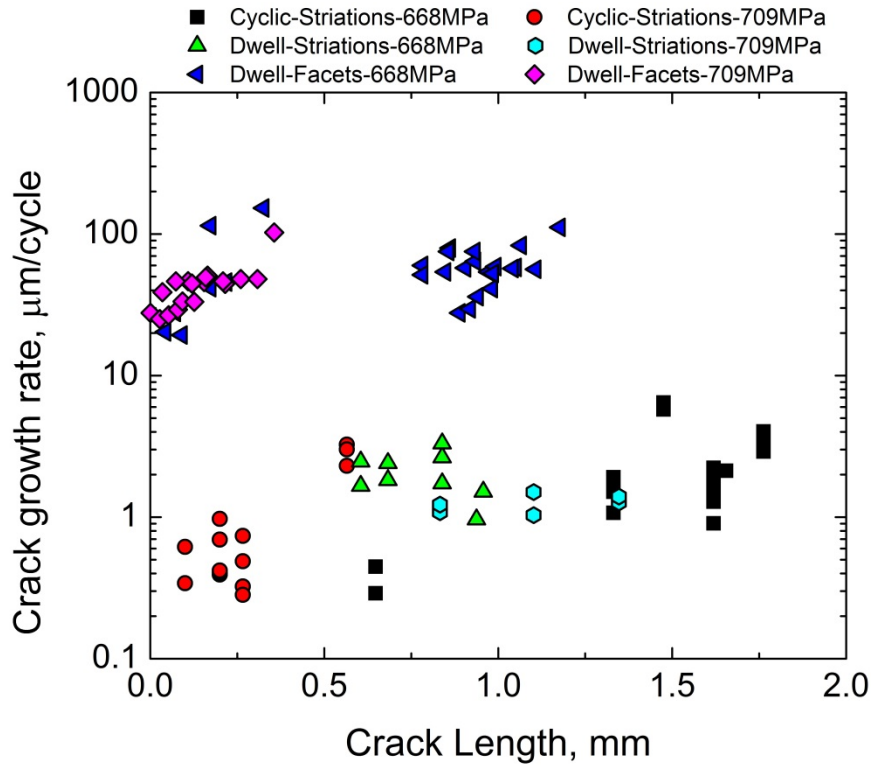


Figure 9.6-85. Fatigue Crack Growth Rates Under Cyclic and Dwell Fatigue Loading

A deterministic linear elastic fracture mechanics model to account for the effect of initial crack size, microtextured region size and aspect ratio on the mean cyclic and dwell fatigue lifetimes of titanium alloys was also developed [2]. The model was also used to quantify variability in lifetime within a particular group of tests due to differences in the position of the subsurface crack initiation site. The results indicated that dwell fatigue life and cyclic fatigue life depend most on microtexture region size and initial crack size, respectively.

References

- [1] Pilchak, A.L., "Fatigue crack growth rates in alpha titanium: Faceted vs. striation growth," *Scripta Materialia*, Vol. 68 pp. 277–280, 2013.
- [2] Pilchak, A.L., "A simple model to account for the role of microtexture on fatigue and dwell fatigue lifetimes of titanium alloys," *Scripta Materialia*, Vol. 74, pp. 68-71, 2014.

9.6.28. Effect of Stress Ratio on Small Crack Growth in a Titanium Alloy and Application in Probabilistic Life Prediction

Reji John, USAF Research Laboratory – Materials and Manufacturing Directorate

The effect of stress ratio on the statistical aspects of small fatigue crack growth behavior was studied in a duplex microstructure of Ti–6Al–2Sn–4Zr–6Mo at 260°C with particular emphasis on incorporating small-crack data into probabilistic life prediction and the influence of stress ratio on probabilistic lifetime limits [1].

A Focused Ion Beam was used to machine micro-notches in test specimens, which served as crack-initiation sites and enabled the acquisition of multiple small-crack growth data sets from a single

experiment. Stress ratios of 0.5, 0.05, and 0.5 were employed, and small-crack growth was monitored using the acetate replication method. A method of optimization of the small-crack growth model parameters that minimizes the error between the predicted and the measured crack length versus cycles data was demonstrated. This method was applied to the small-crack growth data obtained at various values of stress ratio. A power law model was used to represent the small-crack growth rate versus applied stress intensity factor range relationship, where the parameters (coefficient, C and exponent, n) were computed using the optimization method, Figure 9.6-86. By measuring multiple cracks at each stress ratio, distributions in the crack growth rate equation parameters were obtained for the probabilistic analysis, Figure 9.6-87.

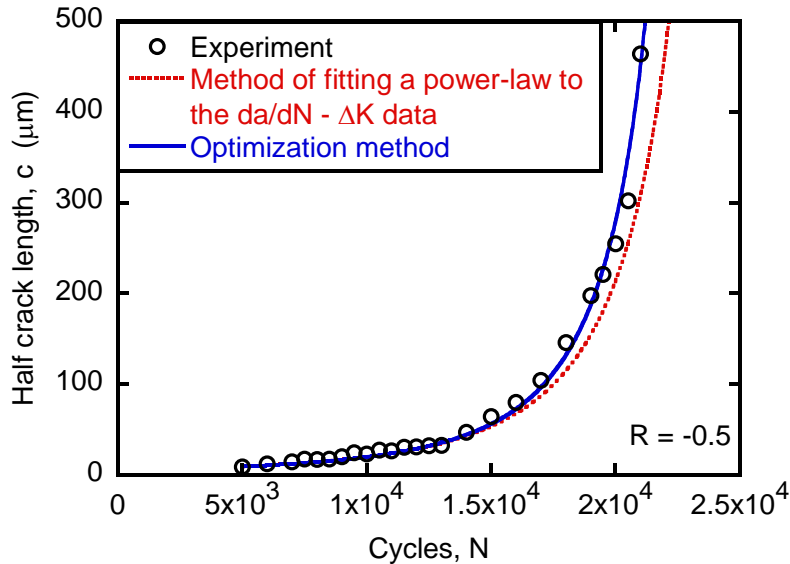


Figure 9.6-86. Comparison of Measured and Predicted Crack Length vs. Cycles Using the Crack-Length Increment Data Reduction Approach and the Optimization Method for a Crack at $R = -0.5$.

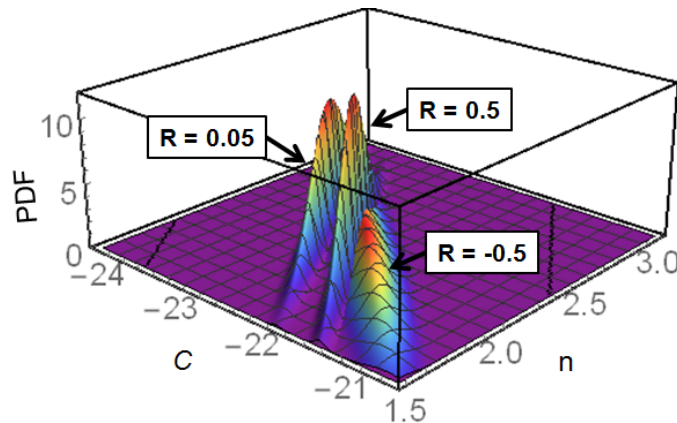


Figure 9.6-87. Joint Normal Distributions of Coefficient, C and Exponent, n at Stress Ratio = -0.5, 0.05, and 0.5 Used in Probabilistic Life Prediction

A probabilistic method, previously demonstrated by Jha et al. [2], was employed to represent the variability in the small-crack growth behavior and the statistical differences with respect to stress ratio. The probabilistic predictions revealed that, although the effect of stress ratio on the small-crack growth

behavior appeared qualitatively insignificant, the impact of the statistical differences with respect to stress ratio was significant on the probabilistic lifetime limit. The lifetime corresponding to the probability of failure of 0.1% (i.e., the B0.1 lifetime) varied in the range of -56% to +72% with respect to the baseline predictions when the effect of stress ratio on the small-crack growth was included, Figure 9.6-88.

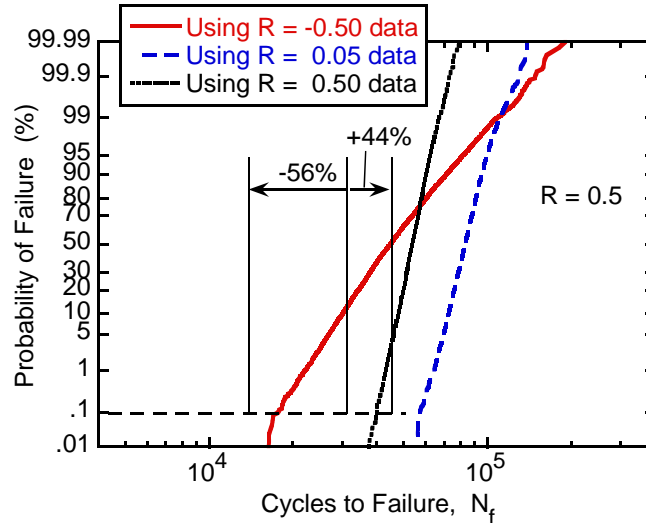


Figure 9.6-88. Influence of the Effect of Stress Ratio on the Small-Crack Growth Regime on the Prediction of Crack-Growth Lifetime Distributions and B0.1 Lifetimes at Stress Ratio = 0.5

References

- [1] Jha, S.K., John, R., and Larsen, J.M., “Incorporating small fatigue crack growth in probabilistic life prediction: Effect of stress ratio in Ti–6Al–2Sn–4Zr–6Mo,” *International Journal of Fatigue*, Vol. 51, pp. 83–95, 2013.
- [2] Jha, S.K., Caton, M.J., and Larsen, J.M., “A New Paradigm of Fatigue Variability Behavior and Implications for Life Prediction,” *Materials Science and Engineering A*, Vol. 468–470A, pp. 23–32, 2007.

9.6.29. Effect of Aging Treatment on Fatigue Behavior of an Al-Cu-Mg-Ag Alloy

Michael J. Caton, USAF Research Laboratory – Materials and Manufacturing Directorate

An investigation of the fatigue properties of an Al-Cu-Mg-Ag alloy with two different heat treatments—peak aged (T6), and peak aged interrupted (T6I4)—has been conducted [1]. While the strength levels resulting from the two heat treatments were similar, the main difference between the microstructures was that the peak aged interrupted material contained a higher volume fraction of the theta prime precipitates. This study specifically focused on the effects of these treatments on the fatigue lifetime distribution, and the role of crack initiation versus the small crack growth behavior. Several total fatigue lifetime tests were completed at room temperature and at a given stress level to characterize the distribution in fatigue lifetimes. The small crack growth behavior of the two aging treatments was studied both at room temperature and elevated temperature by means of a standard acetate replication method.

The conclusions drawn from this investigation include: (1) Mean fatigue lifetimes were ~10M cycles for both aging conditions. Minimum lifetimes on the order of 8000-21000 cycles were seen in the T6 aging treatment, whereas the lowest life-time observed in the T6I4 treatment was ~2M cycles, Figure 9.6-89; (2) Crack growth lifetime predictions showed that the minimum lifetimes seen in the T6 aging

treatment were dominated by fatigue crack growth, and the longer lifetimes were dominated by crack initiation; (3) Fractographic analysis revealed multiple crack initiation features including large grains, pores, non-metallic particles, and combinations of these features; (4) No apparent effect on small crack growth rates was seen due to the difference in aging conditions at room temperature. Furthermore, no difference was observed in small crack growth rates while comparing the room and elevated temperature (130C) dwell fatigue results, Figure 9.6-90; (5) Since the T6I4 aging treatment produces similar mean fatigue lifetimes and small crack growth rates as the T6 treatment condition and better minimum fatigue properties, the T6I4 treatment may be more desirable both from a minimum fatigue property consideration and manufacturing cost savings points of view due to reduced aging time (2 hours for T6I4 versus 10 hours for T6).

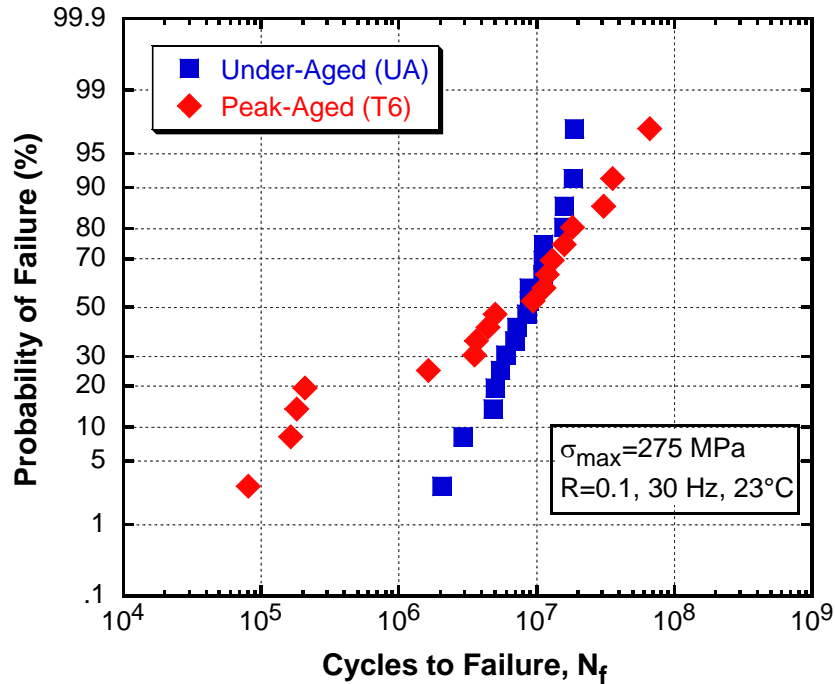


Figure 9.6-89. Cumulative Distribution Function (CDF) Plot of the 18 Fatigue Lifetime Tests for Each Aging Treatment. Mean Lifetimes are Similar for Both Treatments, But the Minimum Lifetimes are Only Seen in the T6 Aging Treatment Producing a Bimodal Distribution

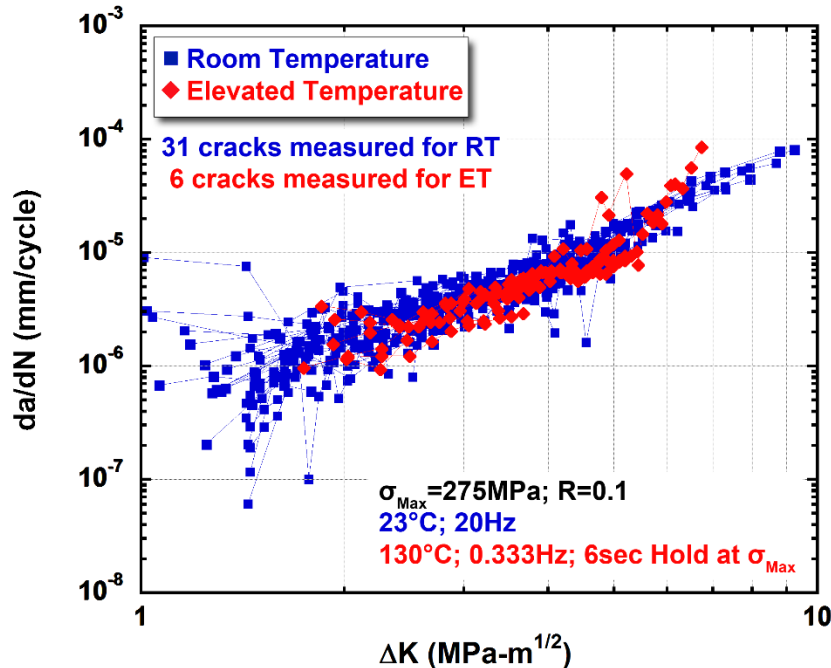


Figure 9.6-90. Small Fatigue Crack Growth Data for the Two Aging Treatments Compared at Room and Elevated Temperatures. On the Average, Both the Aging Treatments Show Similar Small Crack Growth Rates at the Two Temperatures

References

- [1] Burba, M.E., Caton, M.J., Jha, S.K., and Szczepanski, C.J., "Effect of Aging Treatment on Fatigue Behavior of an Al-Cu-Mg-Ag Alloy," Metallurgical and Materials Transactions A, Vol. 44A, pp. 4954-4967, November 2013

9.6.30. Thin Film Galvanic Modeling for Aircraft Structures

Robert Adey and Thomas Curtin, Computational Mechanics International, Inc.

Controlling corrosion is critical for maintaining structural integrity. The annual cost of Air Force aircraft and missile corrosion is estimated to be approximately \$5.4 billion with corrosion accounting for approximately 30% of the maintenance budget. In recent Navy studies, it was found that nearly 90% of cracks found in aviation systems are associated with galvanic corrosion attack.

The BEASY Corrosion Manager software (Figure 9.6-91) solves the galvanic corrosion problem of a complex three-dimensional assembly of different materials exposed to a thin film electrolyte using polarization curves experimentally determined under relevant conditions (Figures 9.6-92 and 9.6-93). The model requires structural geometry and polarization data as inputs and uses a thin film electrolyte solution to determine galvanic behavior. The BEASY Corrosion Manager software accepts typical CAD file formats to generate a design model. From this design, the model is divided into surface groups based on material type and discretized using automatic meshing routines. The computer model presently produces instantaneous (Time = 0) potential and current distribution across the active surface of a galvanic couple (Figure 9.6-94). The simulated current densities can be converted to corrosion rates and mass loss estimates. Research is ongoing to include time-based predictive capability so that service life analysis can be performed adding a forecasting capability that could be integrated with current ASIP procedures.

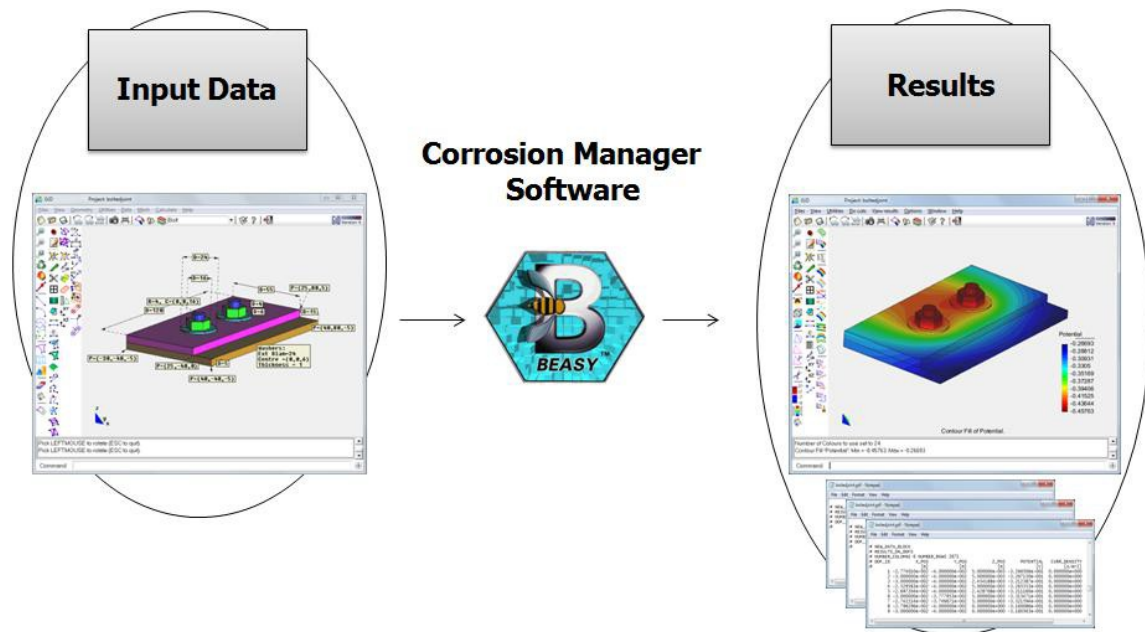


Figure 9.6-91. Thin Film Galvanic Modeling System (BEASY Corrosion Manager)

Corrosion modeling will enable aircraft engineers to quickly assess the corrosion risk of a structure and determine the effectiveness of surface protection systems. The geometry of the connections, the characteristics and extent of the electrolyte, and the type of mitigation methods employed affect the extent and rate of corrosion. Corrosion modeling software tools will enable engineers to replace the “find it and fix it” approach with a more fundamental approach based on the accurate simulation of the electrochemical process.

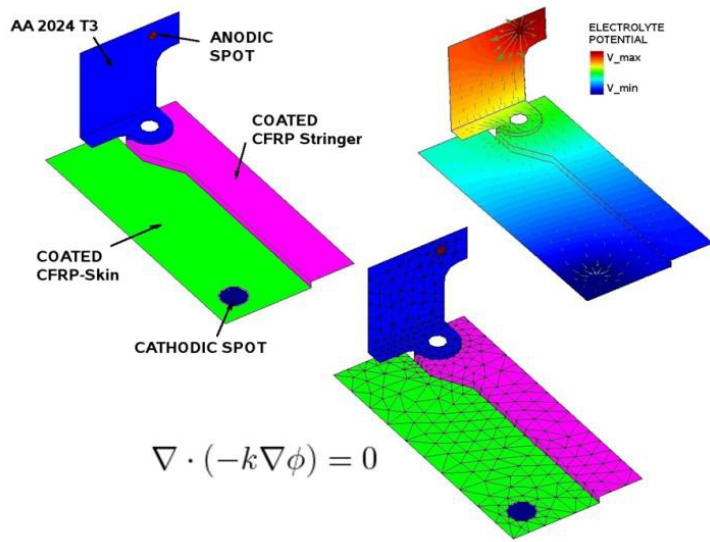
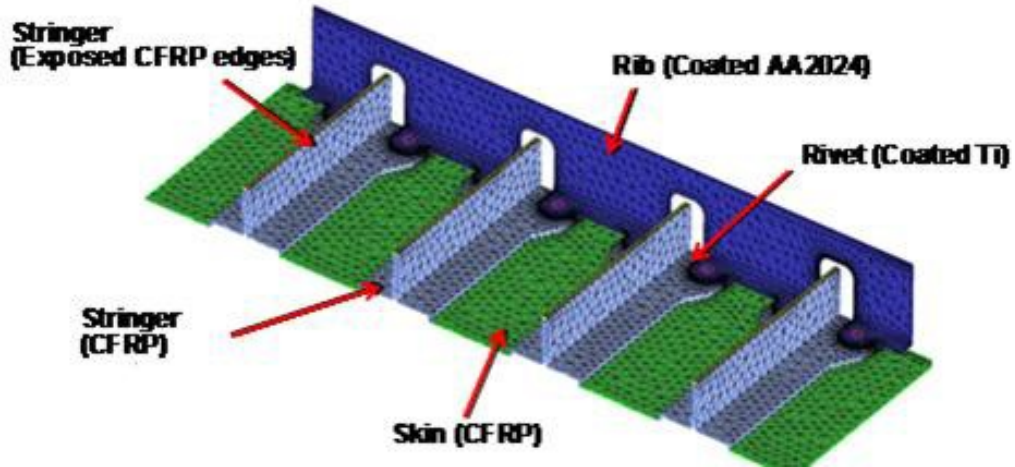


Figure 9.6-92. Typical Aircraft Structure with Galvanic Dissimilarity

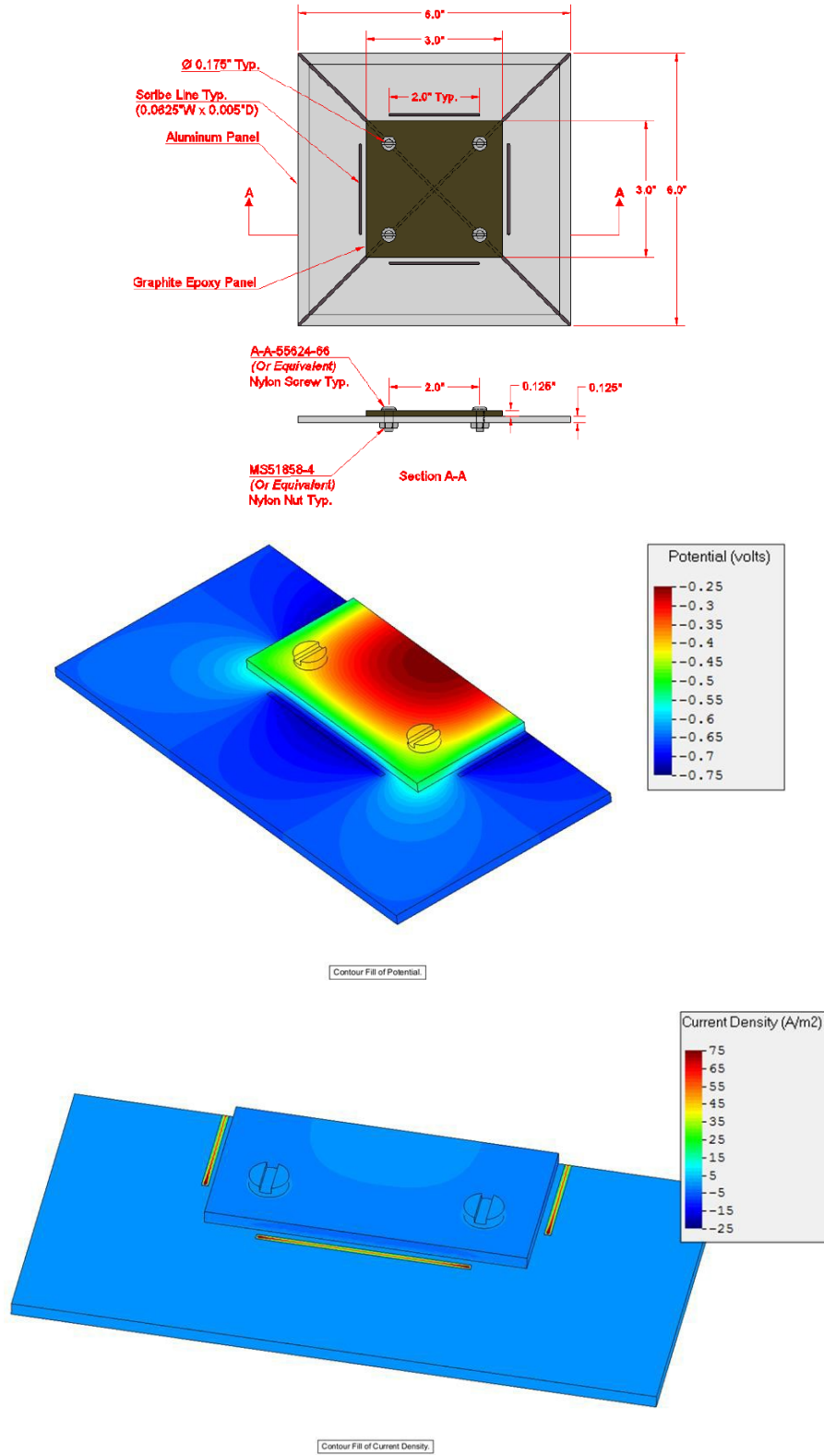


Figure 9.6-93. Validating Corrosion Models Using Long-Term-Exposure Testing (Galvanic Stack-Up)

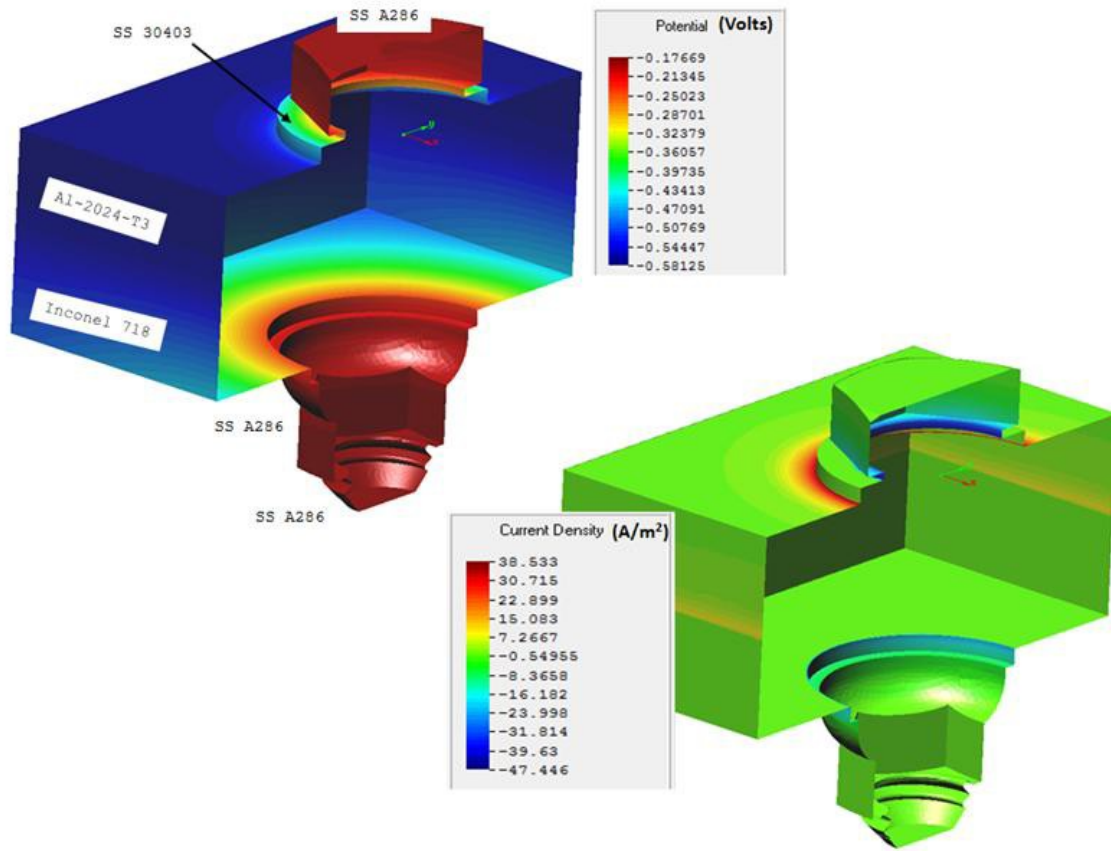


Figure 9.6-94. Galvanic Model of Fastener System Showing Contour Plots of Potential and Current Density

9.7. PROGNOSTICS & RISK ANALYSIS

9.7.1. Time-to-Failure Probability Distribution Estimate Using Monte Carlo Simulation

Eric Tuegel, USAF Research Laboratory – Aerospace Systems Directorate

Monte Carlo Simulation (MCS) is a sampling process that can be used to estimate the probability of failure (POF) for a structure or component. MCS is commonly used to estimate the reliability at an instant in time when the probability distributions for the strength and applied load are known for that time. A MCS is constructed to estimate the POF as a function of time for a structure with strength that degrades in service by randomly choosing an initial crack size and fracture toughness for the simulated component. Starting at the first flight, each flight that the component experiences is simulated by growing the initial crack with each flight and randomly selecting a maximum load during each flight. The component fails during a flight if the maximum stress intensity during a flight exceeds the fracture toughness. Once a component fails, the flight on which failure occurred is recorded and another component simulation started (Figure 9.7-1). Collecting the number of flights to failure for a large number of simulations enables the time to failure probability distribution to be estimated. From the time to failure probability distribution, the Single Flight Probability of Failure can be estimated. MCS takes too long to be of practical use in the design and support of an aircraft system; however, it can be used to develop benchmark examples to verify and validate the simplified probabilistic codes used. An example of such a benchmark problem will be presented (Figure 9.7-2). Code verification and validation with this benchmark will be demonstrated for the PROF software (Figures 9.7-3 and 9.7-4). In addition, MCS can be used to determine if important physics are being ignored in the problem formulation. For example, variation in crack growth rate is usually ignored in the formulation of the fracture reliability problem. It is argued that the variation in initial crack size is so dominant that the smaller variation in crack growth rate is lost in the noise. A MCS that includes variation in crack growth rate indicates that this may not be so and that the effect of crack growth rate variation needs to be explored further (Figure 9.7-5).

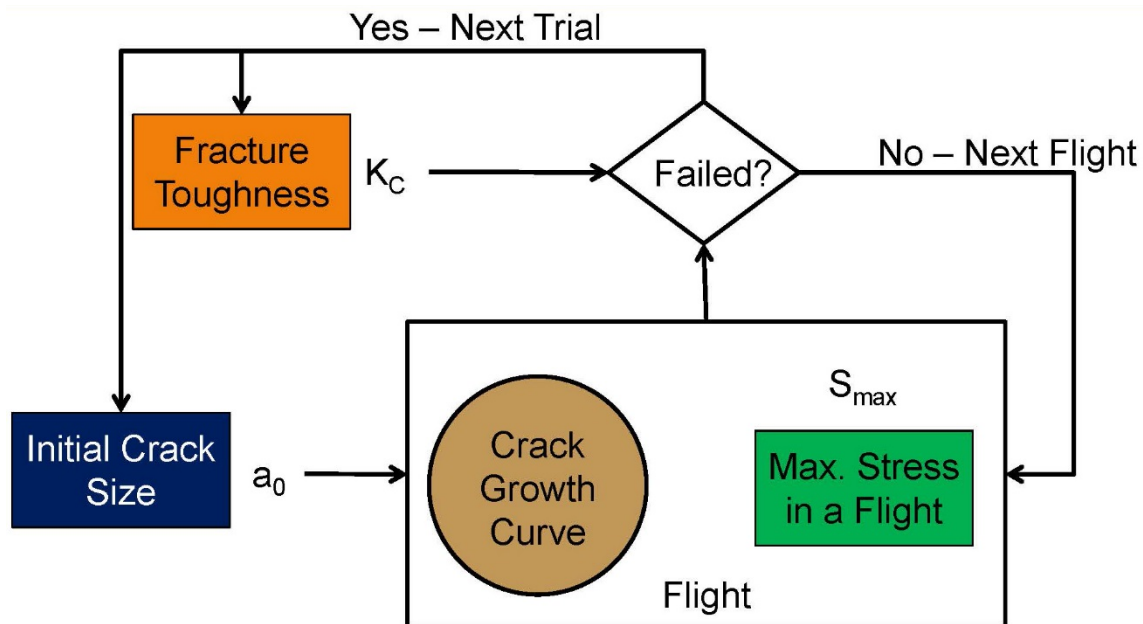


Figure 9.7-1. Monte Carlo Approach

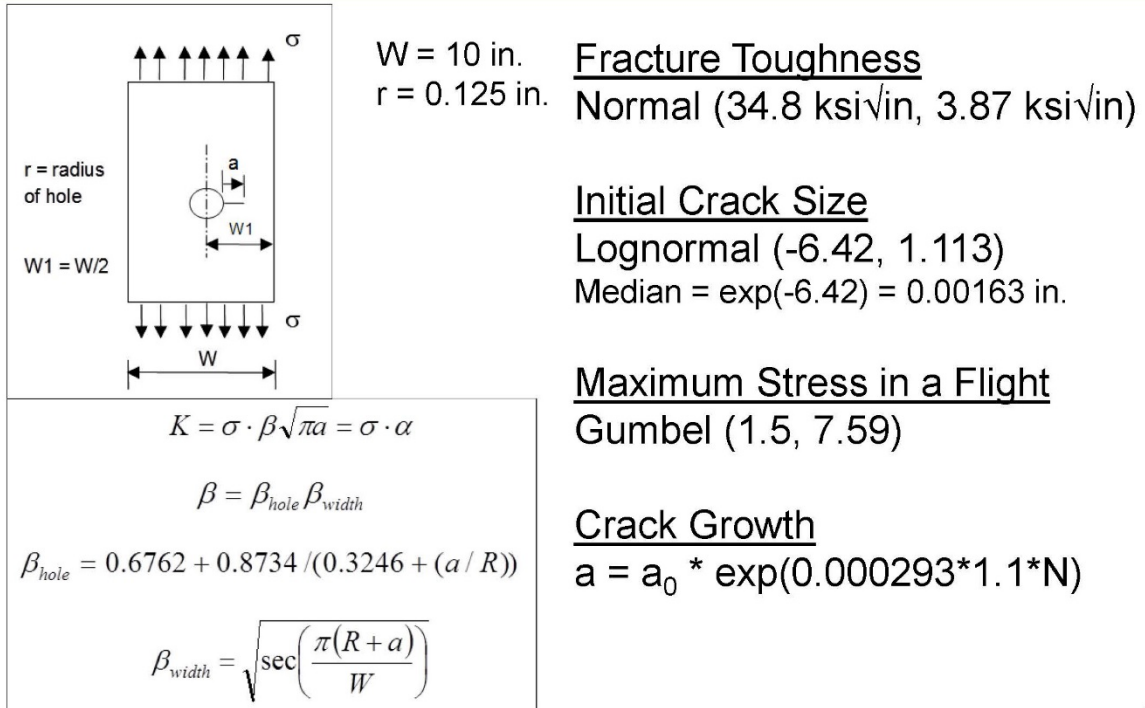


Figure 9.7-2. Test Case Inputs

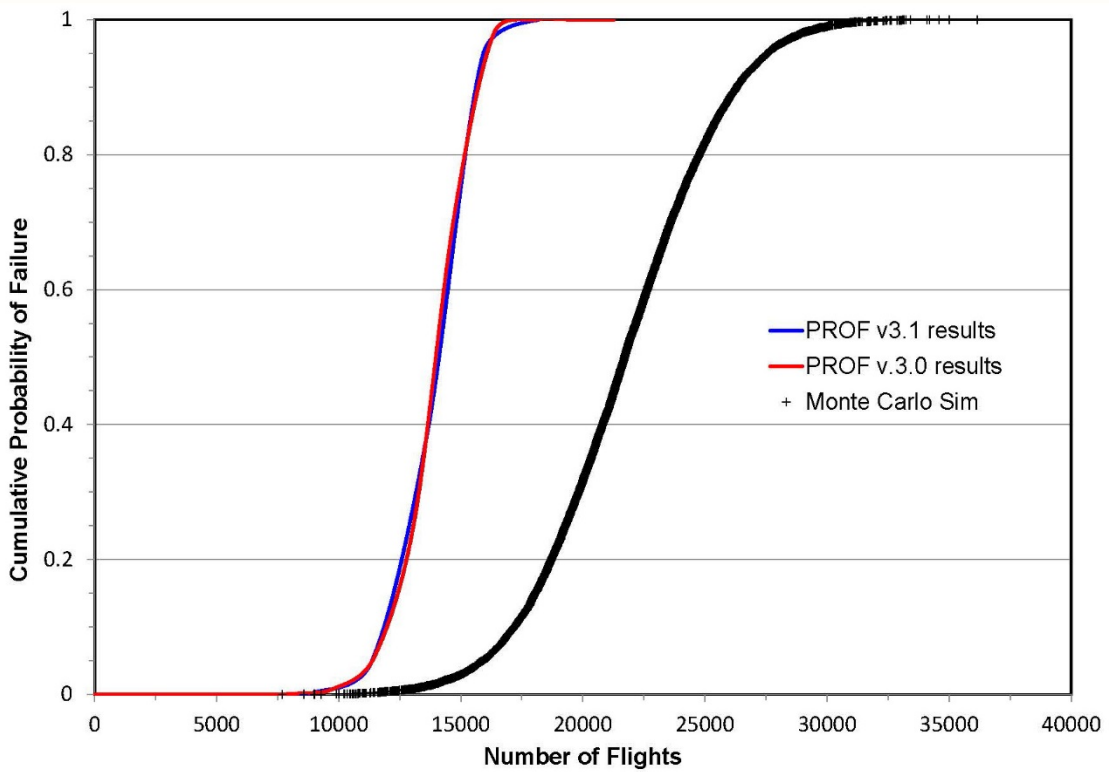


Figure 9.7-3. PROF Results vs. Monte Carlo

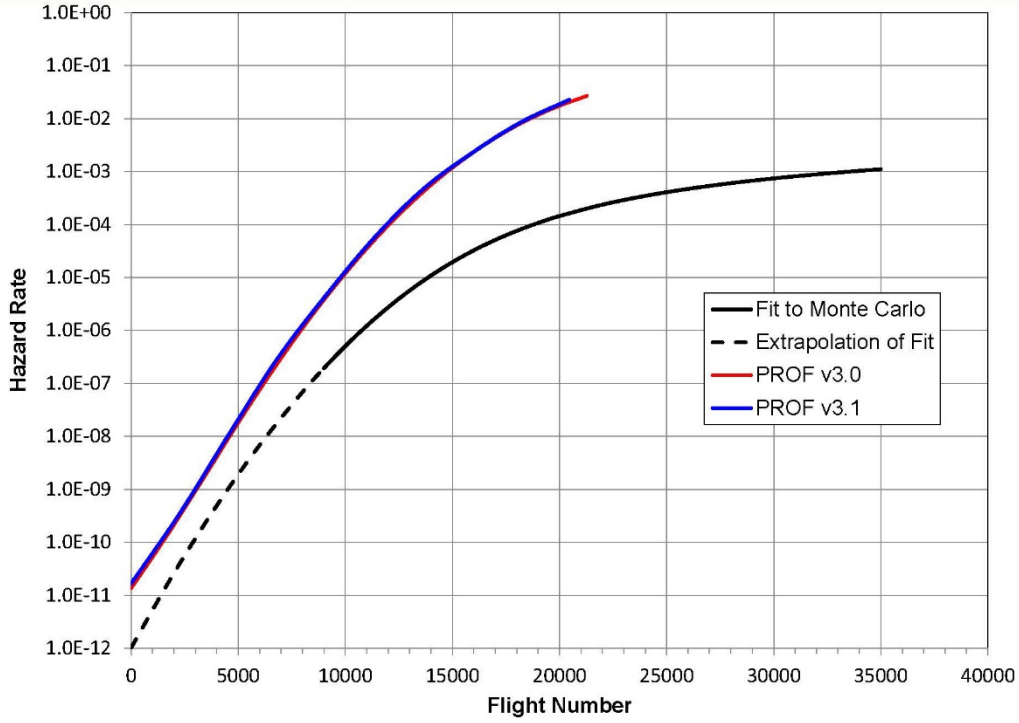


Figure 9.7-4. Hazard Rate Comparison

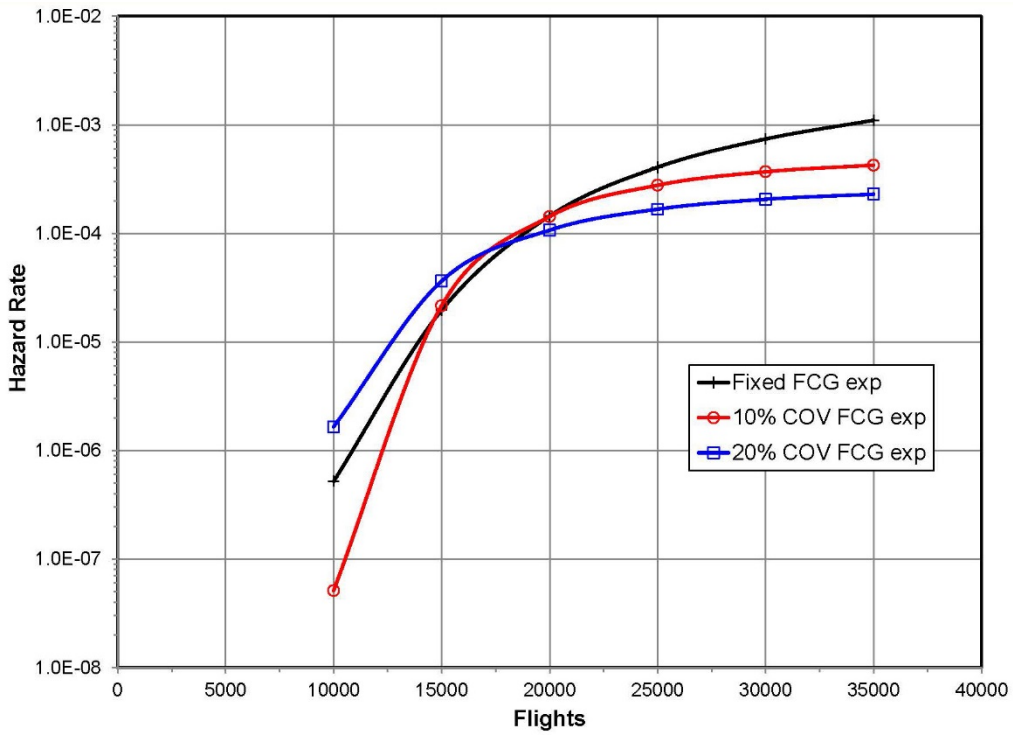


Figure 9.7-5. Effect of Crack Growth Variability on Hazard Rate

9.7.2. Modeling Repairs in Structural Risk and Reliability Assessments

Eric Tuegel, USAF Research Laboratory – Aerospace Systems Directorate

The current method of accounting for a structural repair in assessing the probability of failure is to only modify the probability distribution for crack size at the repair location. A survey of structural repair methods showed that small cracks are likely to be repaired by oversizing a hole or blending out the area for which a modification to the crack size distribution is an acceptable approximation. However, cracks have a small probability of being detected when they are small and so this situation may not be that common. More common will be the situation that a big crack is found. Repair methods for big cracks include drilling a large hole and installing an interference-fit bushing (Figure 9.7-6), stop drilling and installing a flush rivet, or installing a doubler/patch (Figure 9.7-7). With each of these repairs not only can the crack size distribution change, but also the distribution for the maximum stress during a flight, the stress intensity, and the crack growth curve can change. A proper structural reliability assessment must consider these changes to the inputs to the analysis. The complete reliability assessment must total up the products of the probability of failure for each of these repair options and the probability that the repair will be needed (Figure 9.7-8). In addition, every structural location has a unique set of repairs and limits for each repair. Thus, every location will have a unique series of analyses that are required to assess the probability of failure at the location. Thus, a distinct model for assessing the probability of failure must be constructed for each location for which the probability of failure is needed. A framework for a structural risk and reliability software package is proposed that accounts for the physics of the post-repair structure, accumulates the probabilities of failure for all repair options, and is flexible enough to accommodate the unique repairs at any location. The framework utilizes object-oriented programming. The proposed framework also enables easier updating of solution algorithms.

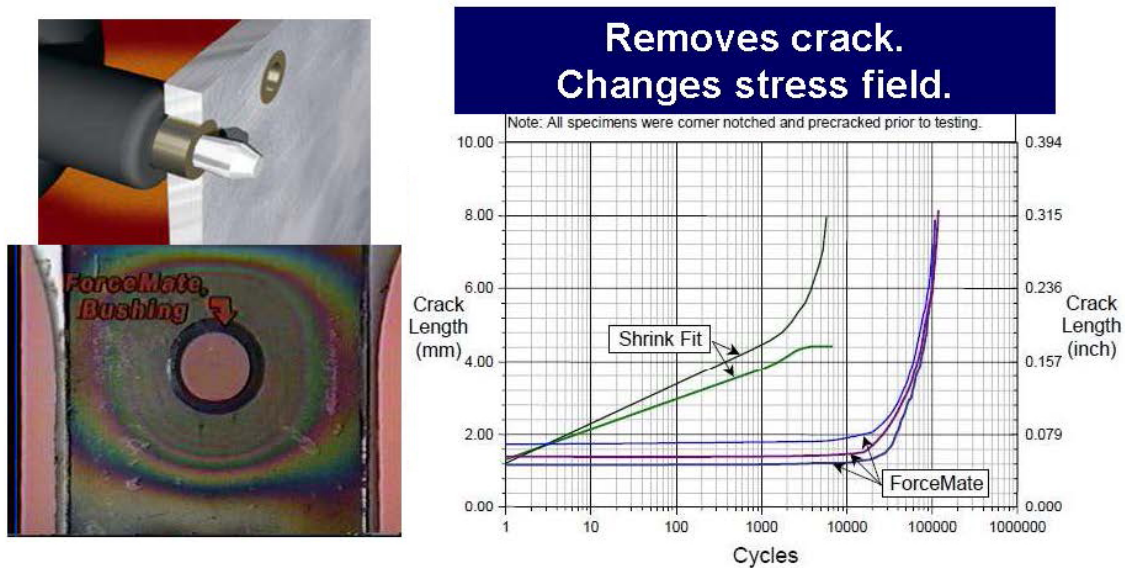
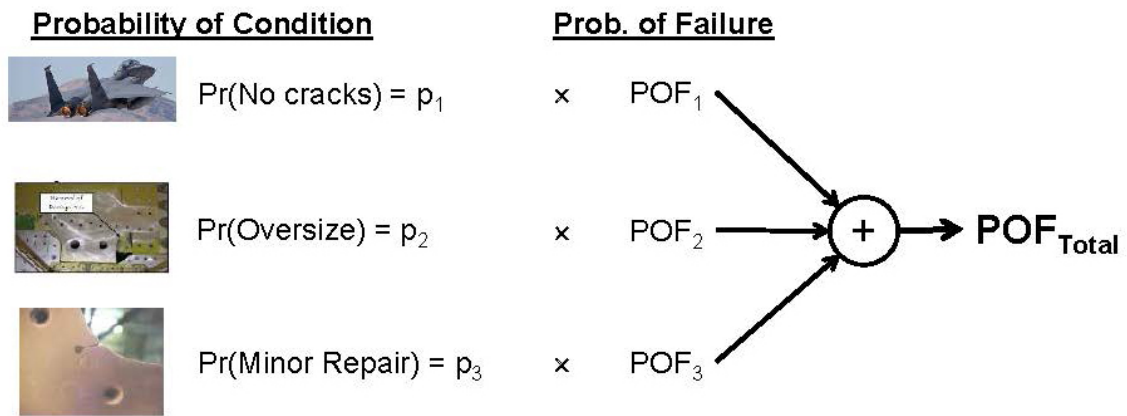


Figure 9.7-6. Example of Repair – Expanded Bushing



Figure 9.7-7. Examples of Repairs – Stop Drill and Patch



Build separate analysis for an aircraft with an engineering disposition.

Figure 9.7-8. Building Initial Reliability Model

9.7.3. Application of Structural Risk Analysis to Force Management and Force Structure Planning

Kevin Welch and Matthew Edghill, Lockheed Martin Corporation; Bryce Havris, USAF Life Cycle Management Center

Structural risk analysis is an additional tool to manage structural health of the force that provides insight that deterministic approaches cannot provide. USAF is implementing a culture of risk-based decision making and has included several risk analysis requirements in MIL-STD-1530C. Risk analysis is used to evaluate a potential hazard severity and probability of occurrence, determine how the risk varies with time and assess implications to the fleet. Risk analysis can determine which mitigating actions will maintain flight safety and provide a basis for cost benefit analysis of potential mitigation actions. Risk analysis can also quantify impacts to aircraft availability forecasts and support cost metrics. The F-16 CAS Risk Assessment Process was developed to address structural safety of operational aircraft. This process is a documented, standardized method that can be applied to any aircraft fleet with Individual Aircraft Tracking (IAT) data. A similar method can be used to address maintainability issues. This technical activity will discuss the concept of applied risk assessment for making force management and force structure decisions. While basic risk analysis focuses on safety and reliability (Figure 9.7-9), applied risk analysis focuses on cost and readiness (Figure 9.7-10). The objective of applied risk analysis is to provide useful forecasts and metrics to support force management and force structure decisions and to provide easily understandable metrics to support cost/benefit analysis for decision makers. Applied risk assessment is accomplished by applying the expected value function to forecast cumulative risk values of individual fleet aircraft (Figure 9.7-11). The value is chosen to be a quantity of significance to the maintainer, warfighter or force structure planner such as quantity of aircraft requiring unscheduled repairs, labor hours/cost for unscheduled repairs, downtime impacts of unscheduled repairs, etc. (Figure 9.7-12). The risk based forecast for these metrics can be compared to the actual data as it becomes available and the forecast updated as needed. An F-16 example analysis will be used to illustrate the applied risk analysis concept (Figure 9.7-13). This example will show relative metrics to compare two different approaches for managing a structural cracking issue (Figure 9.7-14).

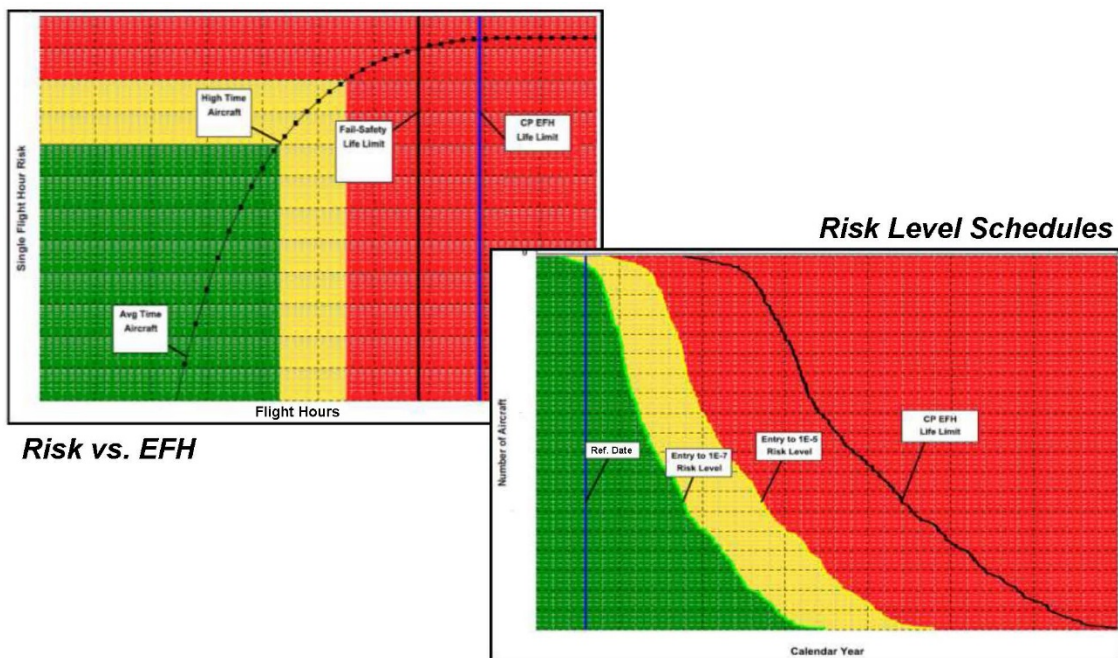


Figure 9.7-9. Example Products of Basic Risk Analysis

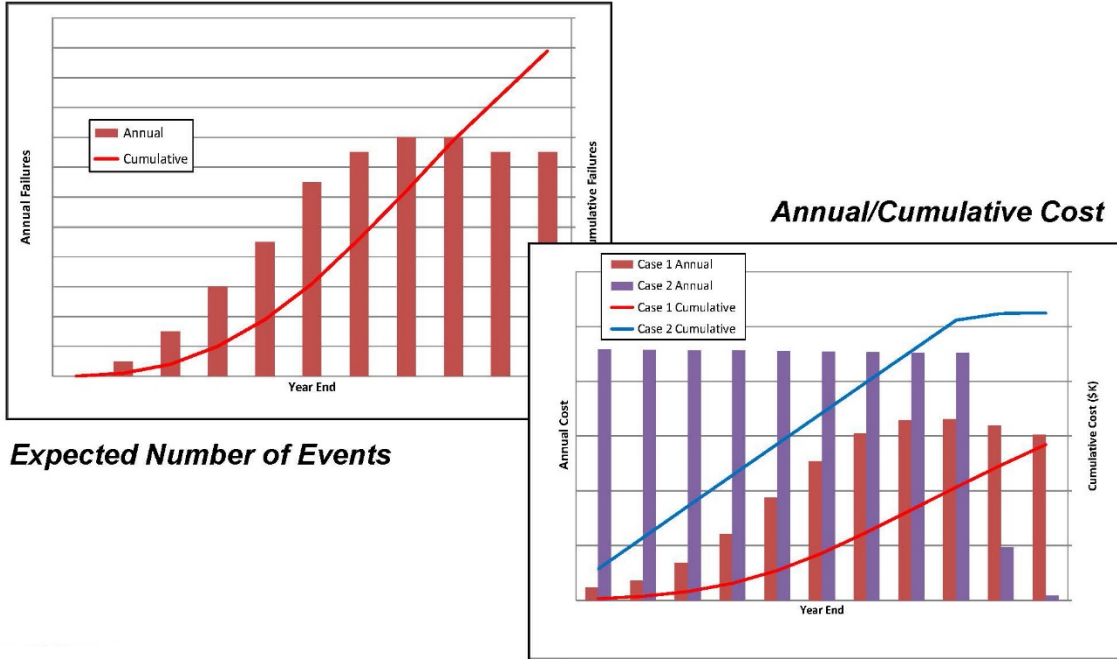


Figure 9.7-10. Example Products of Applied Risk Analysis

- **A Dice Game Costs \$5 per Throw**
 - If You Roll Even (2,4,6), You Receive Twice the Number on the Die (\$4, \$8, \$12)
 - If You Roll a 3, You Receive \$5
 - If You Roll a 1 or a 5 You Receive Nothing
- **What is the Expected Win/Loss per turn?**
 - Answer: \$0.17 Loss

Roll (x)	Prob [p(x)]	Value of x	Expected Payoff = p(x) * value of x
1	1/6	\$0	\$0/6
2	1/6	\$4	\$4/6
3	1/6	\$0	\$5/6
4	1/6	\$8	\$8/6
5	1/6	\$0	\$0/6
6	1/6	\$12	\$12/6
		Sum =	\$29/6 = \$4.83

Cost = \$5
 Expected Payoff = \$4.83
 Expected Value =
 \$4.83 - \$5 = - \$0.17

Figure 9.7-11. Expected Value Example #1

- A Fleet of 6 Aircraft is Inspected for Cracks at Location X
- If a Crack is found, a Repair Requires 100 Labor Hours (LH)
- The Risk Forecast for End of Years 1 & 2 is Shown in the Table below
- How much Repair Labor Should be Budgeted in each Year?

Aircraft	Year 1 Cum. Prob.	Year 2 Cum. Prob.	Repair Value	EV = prob (x) * value	
				Year 1	Year2
1	0.06	0.30	100 LH	6 LH	30 LH
2	0.10	0.34	100 LH	10 LH	34 LH
3	0.15	0.37	100 LH	15 LH	37 LH
4	0.21	0.43	100 LH	21 LH	43 LH
5	0.28	0.48	100 LH	28 LH	48 LH
6	0.36	0.54	100 LH	36 LH	54 LH
Cumulative Total =				116 LH	246 LH
Annual Total =				116 LH	130 LH

Repairs are in Units of 100 LH, therefore:

- Budget 300 LH total
- Budget 200 LH for Year 1 (to Ensure Budget if a Second Repair is needed)
- Budget for 100 LH for Year 2 (if Unused Budget Carries Over to Next Year)

Figure 9.7-12. Expected Value Example #2

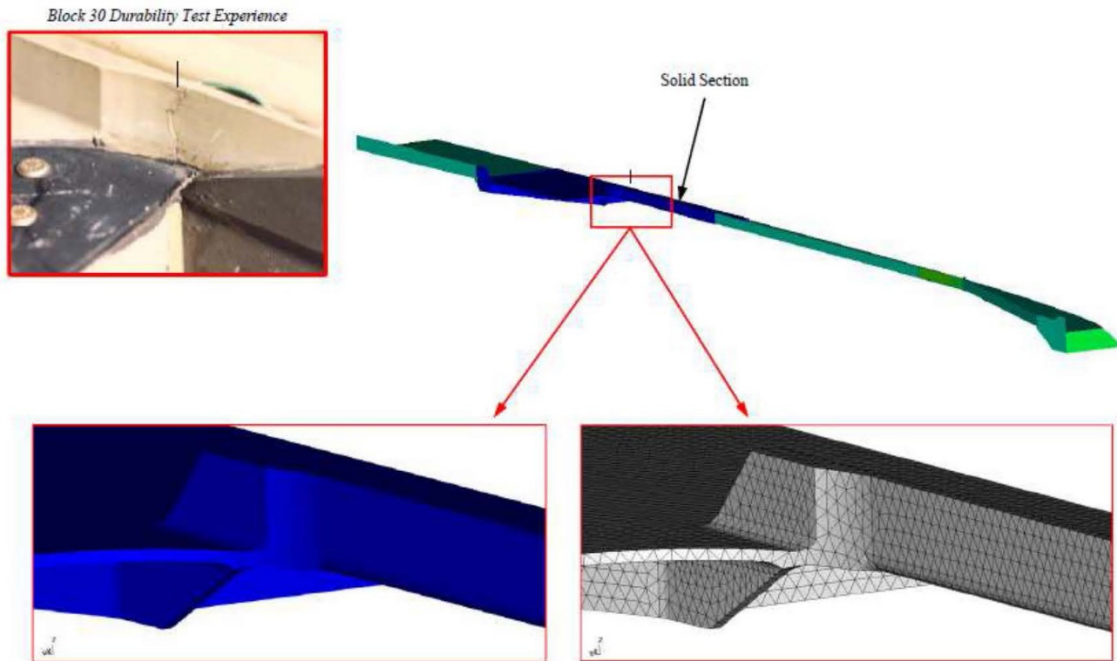


Figure 9.7-13. Canopy Sill Longeron

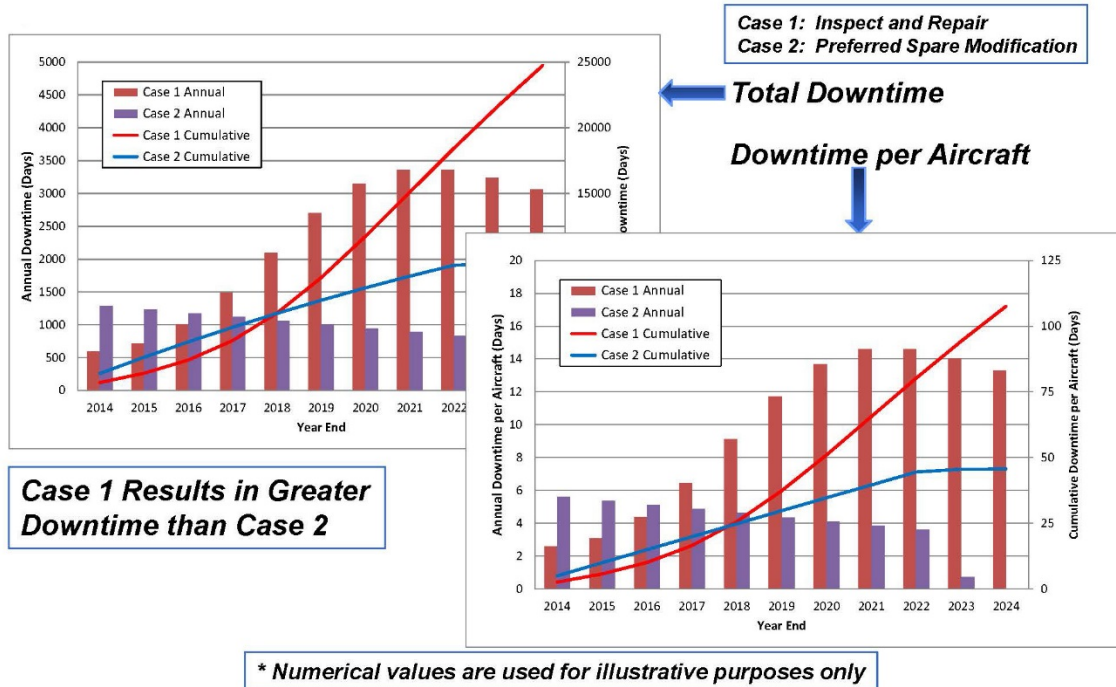


Figure 9.7-14. Aircraft Downtime Comparison

9.7.4. Weibull Analysis of Fatigue Data From Aircraft Paint Removal Techniques – Lessons Learned

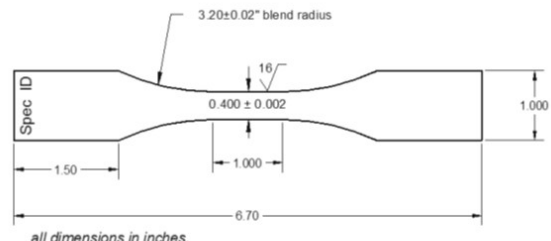
Paul Clark, Southwest Research Institute; Richard Crowther and Mark Thomsen, USAF-OO-ALC

The sustainment of aging aircraft presents numerous challenges. Among these challenges are understanding how to characterize the impact from and incorporation of emerging tools intended to streamline production or improve some other process performance metric. Removing paint, primer and other coatings is a necessary step in the maintenance of most aircraft. Mathematical analysis and computer simulations provide the sustainment team with the ability to make informed decisions regarding management and maintenance of aircraft. This technical activity will discuss the analysis of durability data generated from various techniques employed to remove paint (depaint) from aircraft. The techniques used to remove paint from prepared test coupons were: Chemical Stripping, Sand Stripping, Plastic Media Blasting (PMB), Laser Stripping using an automated robot (Fiber Laser Strip) and Hand-Held Laser Stripping (Figure 9.7-15). Baseline coupons were also characterized for each material of interest (Figure 9.7-16). Three materials were investigated; 2024-T3 Aluminum, 7075-T6 Aluminum and 4340 Steel (140 ksi Sty). Several decisions were made going into the program with schedule and cost in mind; lessons learned from early testing decisions will be presented and discussed as well as additional observations. While multiple techniques exist for the characterization of fatigue data, the Weibull Distribution is considered to be advantageous as it demonstrates the ability to provide reasonable projections of failure with relatively low sample sizes or minimal failures. Confidence of the data projected by the Weibull distribution was one of the focus points during the investigation and will be presented for all conditions (Figure 9.7-17). Several advantages and pitfalls of Weibull analyses were encountered on this program. These will be highlighted as well as suggestions improving test plans for future experimental endeavors related to qualifying processes for the sustainment of aging aircraft.



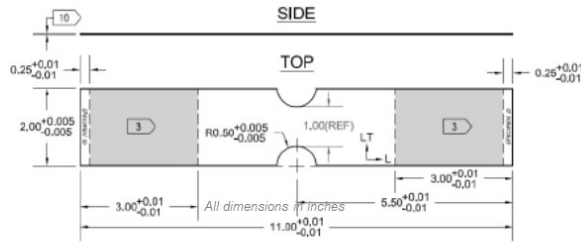
Figure 9.7-15. Hand-Held Laser Paint Removal Tool

- **All panels within each substrate type were fabricated from the same lot of material**
 - Details on Anodizing, Heat Treatment, Media Blasting and PreKote® Pretreatment are available in Reference 1
- **The panels were painted IAW Hill AFB paint procedures**
- **Each panel experienced 5 cycles of paint/cure/strip prior to tests**
- **Fatigue Testing IAW ASTM E466**



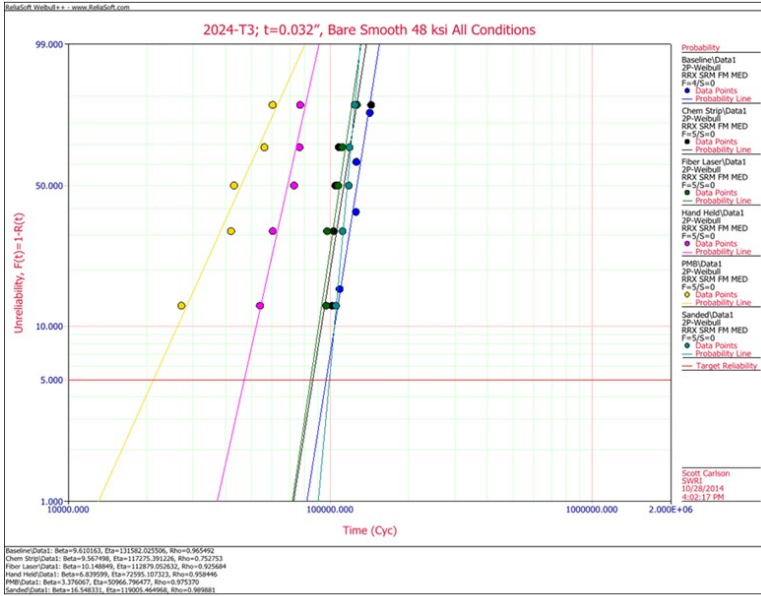
“Smooth” Coupon Configuration

Reference 1



“Notch” ($K_t \sim 1.6$) Coupon Configuration

Figure 9.7-16. Coupon Details



- **Compatible Betas (6.84-10.1) except...**
- **PMB lowest lives**
 - $\beta \sim 3.38$
 - Seen in FMF_{PMB}
- **Sanded slightly lower than BASELINE**
 - $\beta \sim 16.5$
 - Minimal confidence adjustment
 - Seen in FMF_{Sand}
- **All relatively comparable for $N_{95/95}$**

Fatigue Modification Factors (FMF)				
Automated Fiber Laser	Hand Held Laser	PMB	Sanded	Chemical
0.90	0.45	0.15	1.14	0.78

Figure 9.7-17. Comparison of 5-Depaint Techniques

9.7.5. Instantaneous Monte Carlo Calculation of Single Flight Probability of Failure

Thomas Brussat, Tom Brussat Engineering, LLC; Nathan Branch, Mercer Engineering Research Center (MERC)

Monte Carlo sampling is a straightforward probabilistic computation method with great versatility. However its application to aircraft structural risk analysis has been limited because the simplest of problems can require days of computer-run time. This technical activity describes a modified Monte Carlo approach, developed specifically for calculating Single Flight Probability of Failure (SFPOF) of aircraft structure (Figure 9.7-18), which eliminates the computer run time concerns. SFPOF results obtained instantaneously using an EXCEL spread sheet have actually proven to be accurate over a wider probability range than published Monte Carlo results that required 18 to 24 hours of computer time. This breakthrough in computational efficiency opens the door for application of Monte Carlo in risk analyses of more complex engineering problems not previously considered feasible. Such applications can include structural problems involving, for example, (1) Fail-Safe Structure, Crack-Arrest Structure, and Multi-Element Damage (MED); (2) Continuing Damage and Multi-Site Damage (MSD); (3) Random error in predicted usage spectrum severity and crack growth rate; or (4) Multiple inspection and repair cycles. Results are shown verifying accuracy and illustrating the versatility of the approach (Figure 9.7-19). The major concepts that save computation time and facilitate accuracy are described.

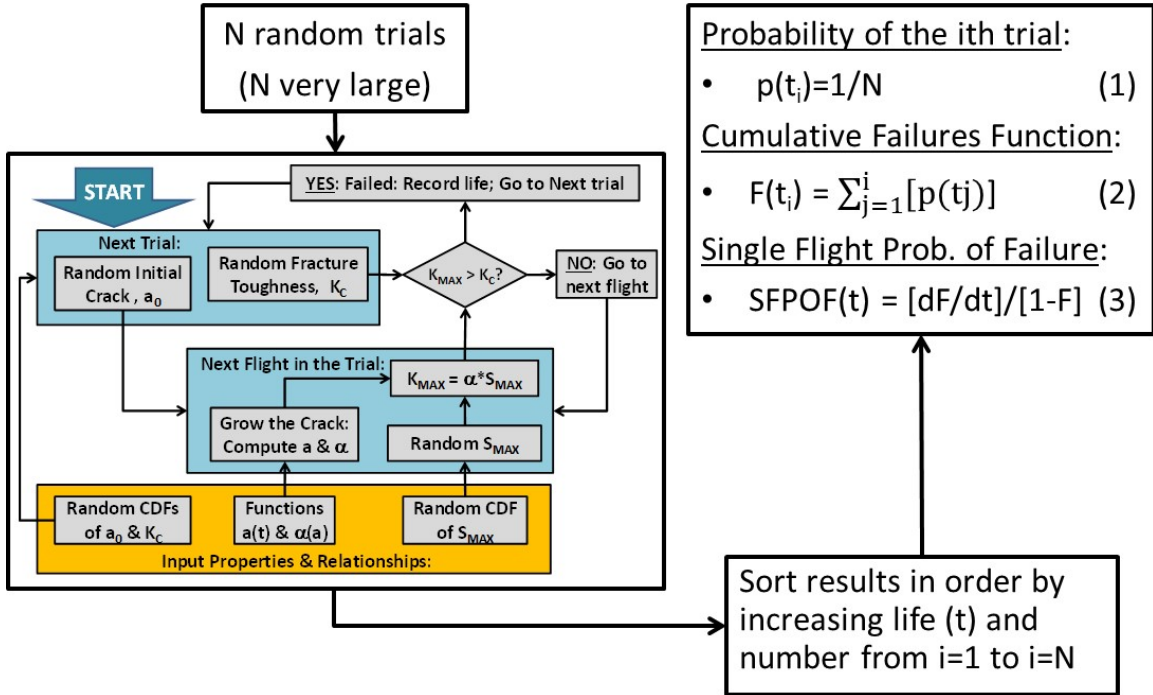


Figure 9.7-18. Monte Carlo Estimation of SFPOF(t)

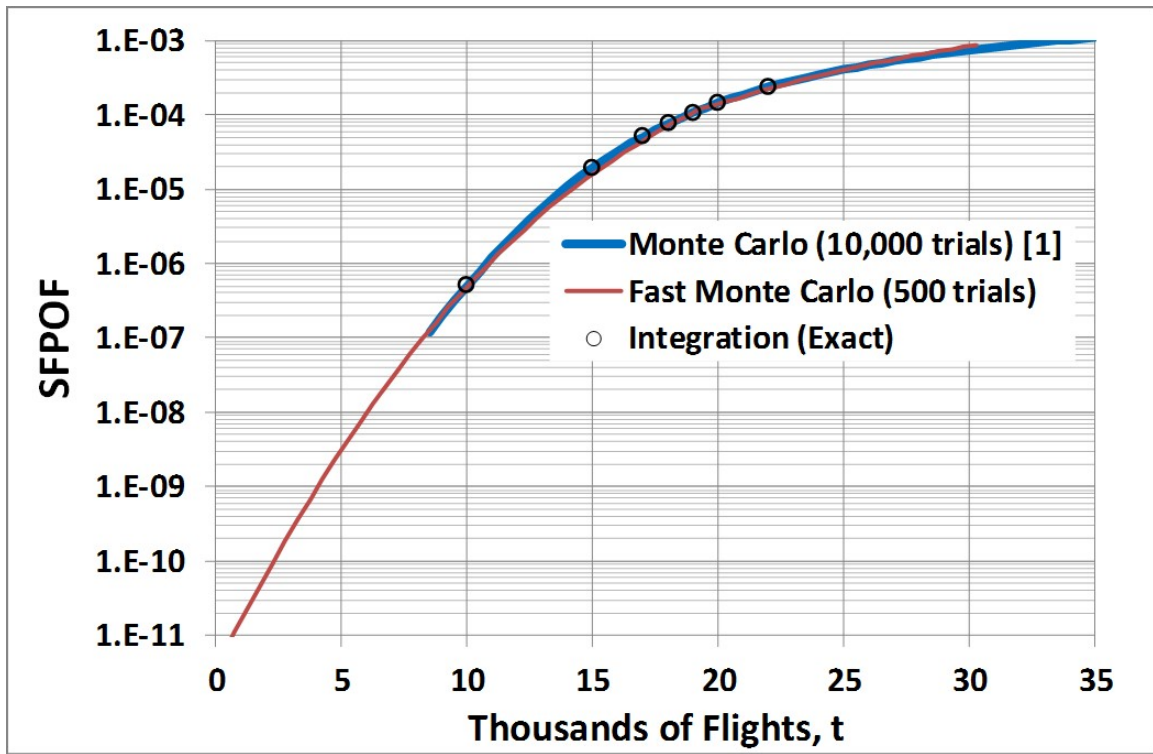


Figure 9.7-19. Conventional vs. Fast Monte Carlo

9.7.6. The F-16 Canopy Sill Longeron: Using Risk Analysis to Ensure Continued Structural Safety

Kevin Welch, Lynette Limer, and Daniel Lendzioszek, Lockheed Martin Corporation; Charles Babish, USAF Life Cycle Management Center; Bryce Harris, USAF F-16 SPO

After several F-16 aircraft were reported with cracking in the canopy sill longeron (Figures 9.7-20 and 9.7-21), structural analysis showed that the airframe does not have static residual strength with a complete failure of the longeron. Subsequent analyses and the resulting force management approach successfully protected flight safety; however, the field data which was obtained demonstrated more work was needed to fully control the issue. Also, an evaluation of different NDI approaches was needed in order to ensure recurring inspections protected fleet safety with the lowest impact to aircraft availability (Figure 9.7-22). Based on fleet findings, the crack growth models and the risk analyses were updated. Updates included use of a risk-based Design Limit Stress (DLS) value rather than a static-loads-based DLS value, time to failure established via censored Weibull method and the use of two different risk analysis programs (PROF and an F-16 specific program, PCSTRAP). As a result of this update, the inspection technique was modified and multiple TCTOs were issued based on calculated risk level (Figure 9.7-23). Continued fleet findings provided data to estimate equivalent initial flaw size distribution (EIFSD) parameters. Focus of the fleet management approach is shifting from initial inspections to managing recurring inspections until replacement longerons can be installed.

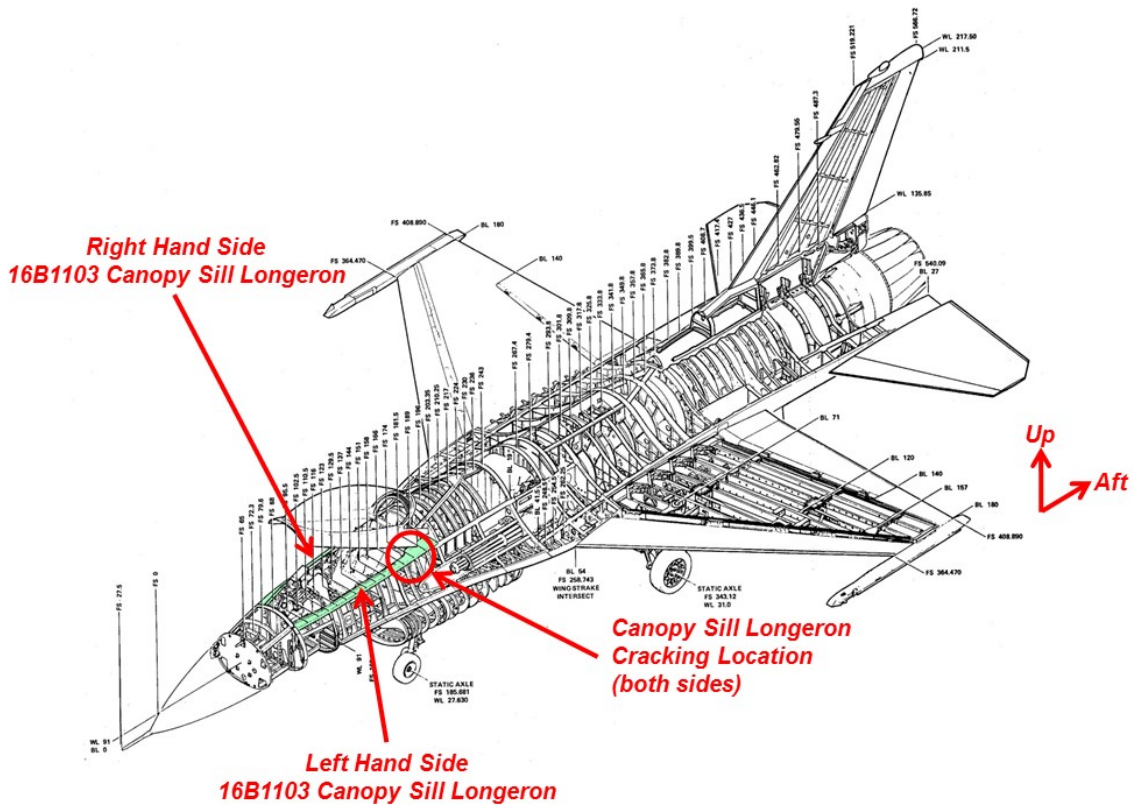


Figure 9.7-20. Canopy Sill Longeron Location

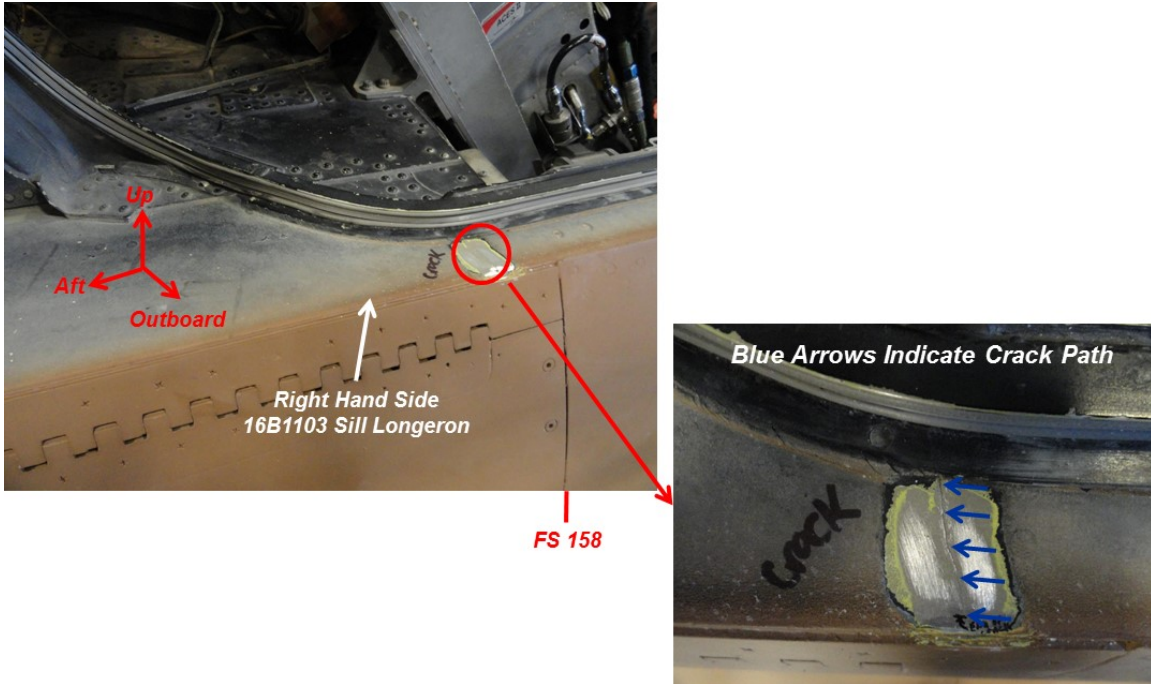


Figure 9.7-21. Photo of Cracked Area

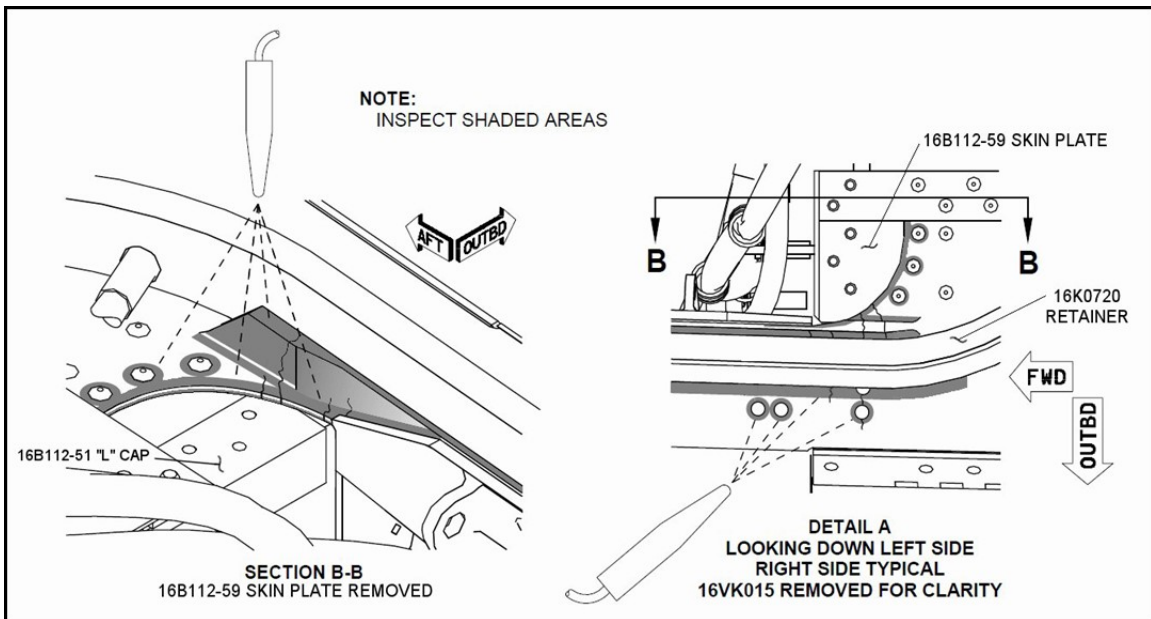


Figure 9.7-22. NDI Configuration

- **Based on the Risk Analysis, TCTO 2705 Findings and Additional PROF Analyses, USAF Initiated Fleetwide Inspections (Skin Panel Removed) in March 2014:**

TCTO	Affects	Compliance Period	Follow-On Inspection
2707	Aircraft > 10^{-5} risk	25 Hours	75 or 100, Based on Block
2708	Aircraft > 10^{-7} risk but < 10^{-5} risk	100 Hours	18 very High Risk Aircraft Required 3 x 10 Hour Inspections to Reduce Risk to Acceptable Levels
2706	Aircraft < 10^{-7} risk	Next Phase	

- **Supporting Tech Order Supplements were Issued:**
 - **-3 T.O. for Skin Panel Trim**
 - **-6 T.O. for Recurring Inspection Intervals**
 - **-36 T.O. for Improved NDI Procedure**

Figure 9.7-23. USAF Fleetwide Inspection

9.7.7. F-35A MLG Drag Brace Risk Analysis

John McClure and Ryan Vogel, USAF F-35 Joint Program Office

The F-35A is currently undergoing many ground tests required for structural certification. One of these ground tests that has been completed is the landing gear fatigue test. This technical activity details a particular part of the landing gear assembly (the drag brace) that failed and how this failure was used to analytically quantify the appropriate life limit of the drag brace (Figure 9.7-24). The landing gear drag brace is a safety critical part of the landing gear assembly. The toggle lug of the drag brace failed during fatigue testing short of the time required for full certification due to a shortfall in the analysis (Figure 9.7-25). The primary driver of the loads that caused this failure is simply the retract/extend (R/E) cycles of the landing gear, while the aerodynamic loads are practically negligible on this specific part. As the F-35A training fleet accrued sorties, the R/E rate at the F-35A base was found to be greater than design. Therefore, retrofits would not be able to be installed on the aircraft before the agreed upon life limit would be reached. The JPO and the contractor had to find an acceptable life limit without accepting too much risk. The JPO used a risk-based approach to determine the appropriate life limit for the drag brace. A Weibull distribution was assumed for the fatigue failure distribution of the aluminum drag brace. The shape parameter from previous USAF aluminum failure data was used. Then, the drag brace fatigue test failure time, along with the shape parameter, was used to calculate the scale parameter. A curve of the Single Flight Probability of Failure (SFPOF) vs. drag brace life limit was then generated using data from the Weibull Probability Density Function and Cumulative Distribution Function (Figure 9.7-26). This curve allowed the JPO to find the life limit that yielded an acceptable risk. Once the JPO calculated the life limit, we were able to work with the contractor to ensure all the retrofits were implemented on all aircraft before the life limit was reached (Figure 9.7-27).

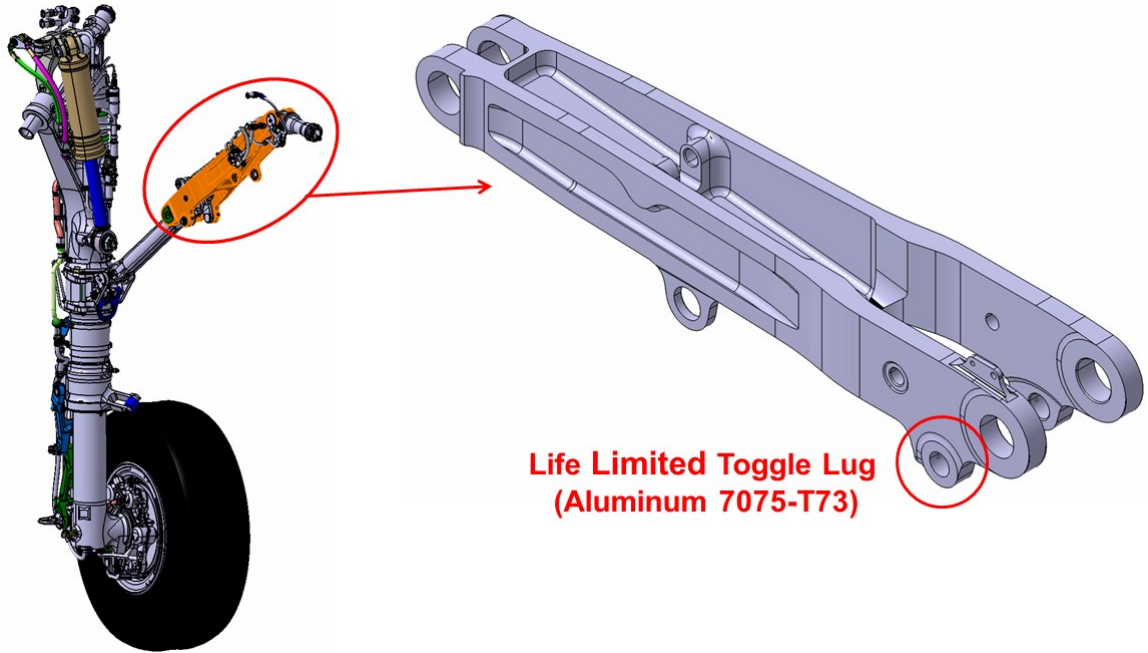


Figure 9.7-24. CTOL MLG Drag Brace

- **Safety Critical CTOL MLG Drag Brace toggle lug failed during full scale testing**
 - Effectivity: 81 aircraft

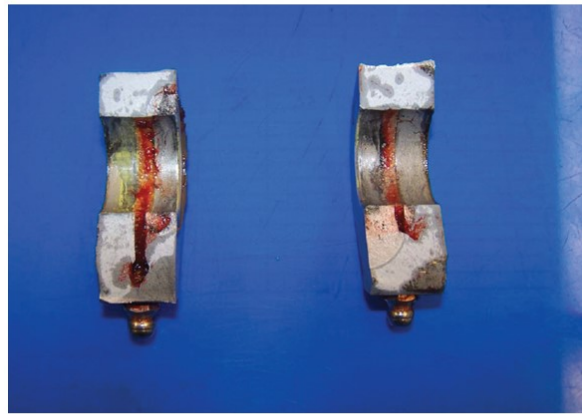


Figure 9.7-25. Drag Brace Failure

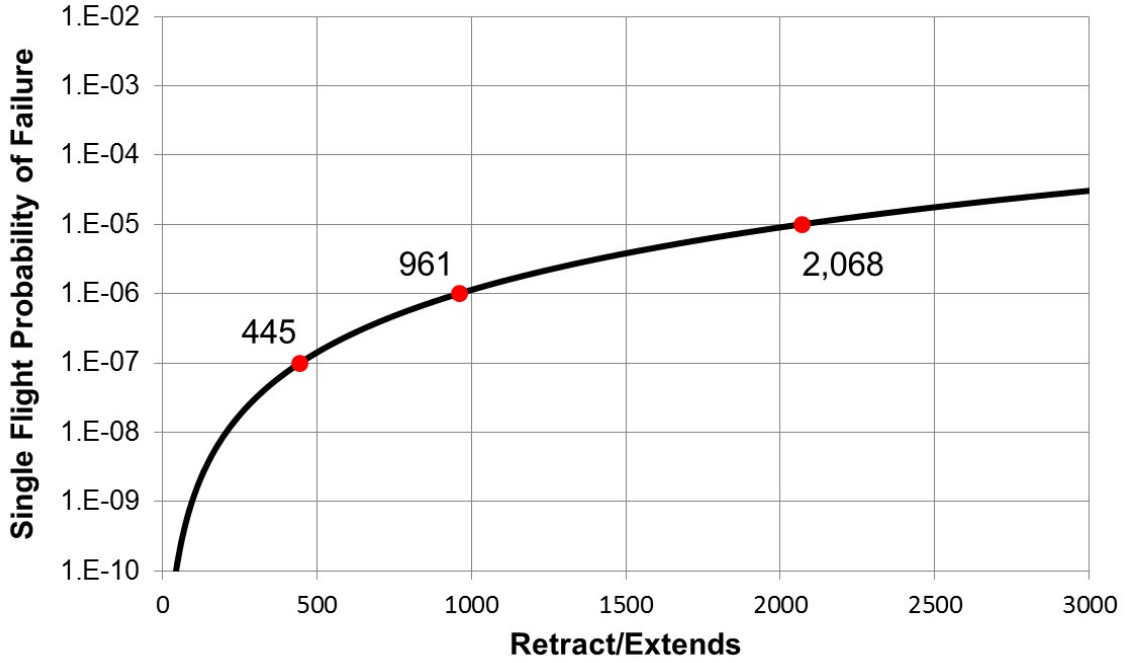


Figure 9.7-26. SFPOF vs. Retract/Extends

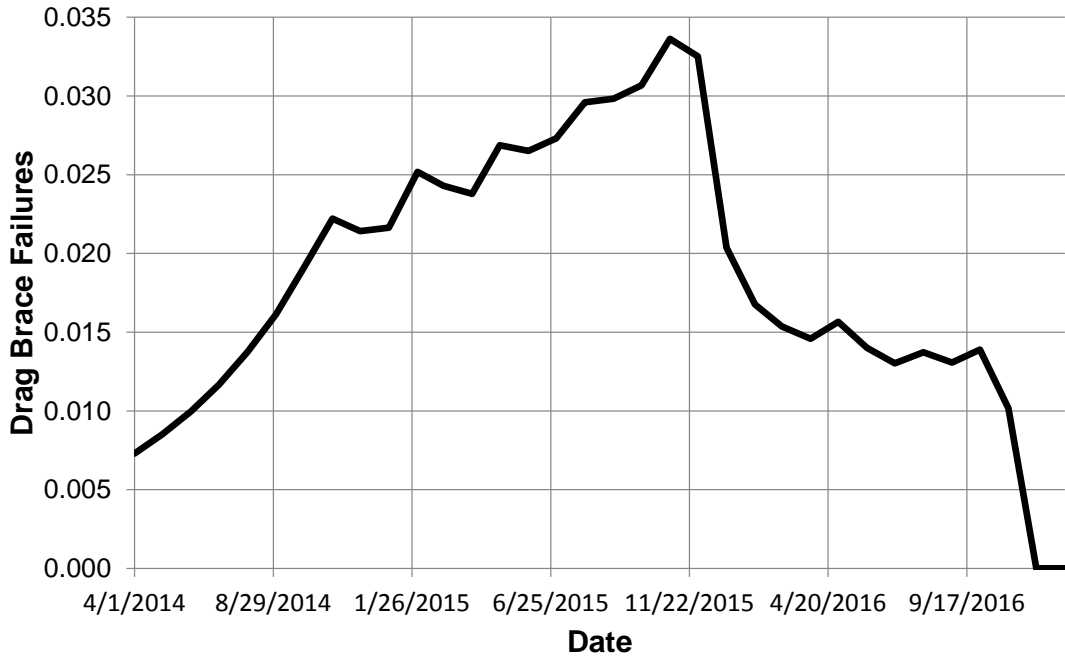


Figure 9.7-27. Drag Brace Failures vs. Time

9.7.8. Continued Development of the Darwin Software for Probabilistic Damage Tolerance Analysis and Risk Assessment

Craig McClung, Michael Enright, Yi-Der Lee, Jonathan Moody, James Sobotka, and Vikram Bhamidipati, Southwest Research Institute®; Simeon Fitch and Ben Guseman, Elder Research

High-energy rotating components in aircraft gas turbine engines may contain inherent or induced anomalies that can lead to rare but potentially catastrophic failures. Federal Aviation Administration (FAA) Advisory Circulars address specific types of inherent and induced anomalies (AC 33.14-1 and AC 33.70-2, respectively) and establish a general framework for all life-limited engine parts (AC 33.70-1). The associated risk of fracture can be predicted using DARWIN[®], an award-winning probabilistic fracture mechanics software code developed by Southwest Research Institute[®] under FAA R&D funding.

DARWIN (Design Assessment of Reliability With INspection) integrates 2D and 3D finite element (FE) models and stress/temperature results, advanced fracture mechanics models, material anomaly data, NDE probability of detection curves, and inspection schedules with advanced probabilistic methods and a powerful graphical user interface (GUI) to determine the probability of fracture of a component as a function of operating cycles, with and without inspections. Originally developed to address specific threats to the integrity of high energy rotating components in aircraft engines, DARWIN now includes general deterministic and probabilistic damage tolerance capabilities relevant to many applications, including airframes. DARWIN has been under continuous development since 1995, and recent advances have significantly enhanced its ease of use, efficiency, and accuracy.

DARWIN development activities during 2013-2014 focused on Versions 8.1 and 8.2.

One of the critical steps in the assessment process is the definition of fracture and risk models for inherent anomalies that may be present anywhere within a component. Over the past several years, new capabilities have been implemented in DARWIN to automate fracture model and risk zone creation processes. DARWIN 8.1 provides a new capability for automation of inspection assignments for autozoning (Figure 9.7-28 (left)). This enables the analyst to assign inspection regions directly to the finite element model geometry. Inspection definition has been consolidated to a single Inspection Events menu for specification of inspection methods (POD curves), timetables (schedules) and regions (geometry). Automation of the fracture model, zone creation, and inspection assignment processes reduces the human time and judgment that were previously required for risk assessment of materials with inherent anomalies.

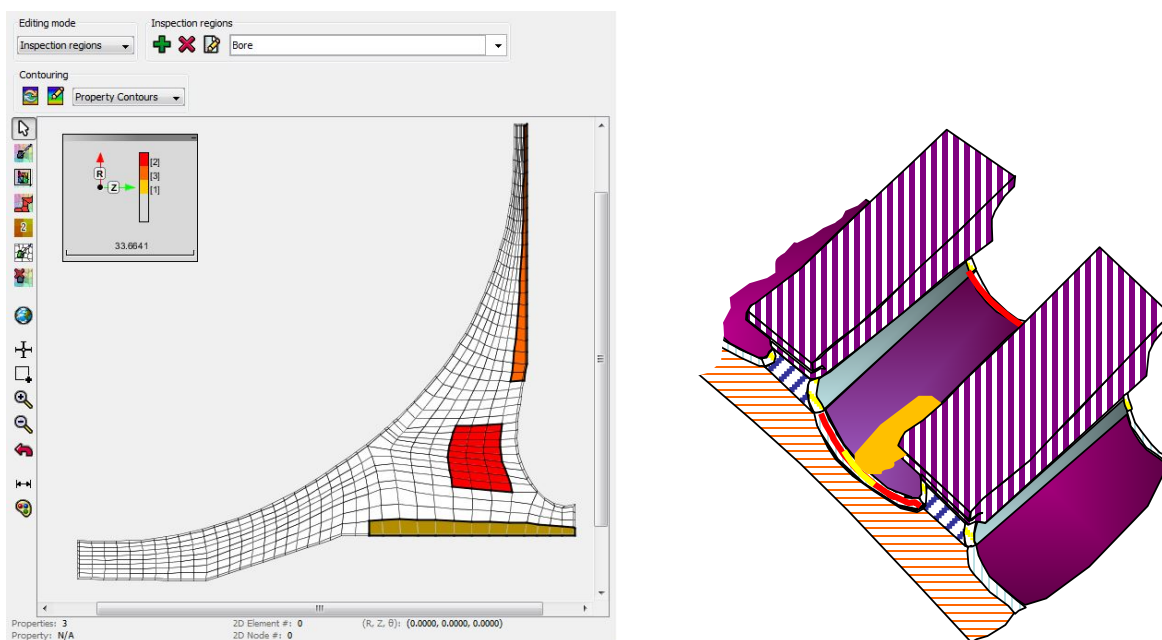


Figure 9.7-28. DARWIN 8.1 Includes (Left) a New Capability to Assign Inspections Directly to the Finite Element Model Geometry, Enabling Automated Assessment of Risk with Inspection for Materials with Inherent Anomalies; and (Right) a New Capability for Creating Zones on Surfaces and Edges of 3D Finite Element Model Geometries

In contrast with inherent material anomalies that can occur anywhere, significant surface damage typically occurs at key component features such as holes, blade slots, and turned surfaces. The FAA and the Aerospace Industries Association (AIA) Rotor Integrity Sub Committee (RISC) are developing an approach for risk assessment of blade slots that involves creation of zones along the leading edges and surfaces of a slot. To support this effort, DARWIN 8.1 includes a new capability for creating zones on surfaces and edges of 3D finite element (FE) model geometries (Figure 9.7-28 (right)). This capability enables the analyst to import and view complex 3D FE blade slot models and to select individual finite element faces or edges for inclusion in zones. It also supports surface damage anomaly distributions that are defined in terms of surface area or length (for application to FE surfaces and edges, respectively).

Previous versions of DARWIN included a capability for superposition of residual stresses associated with surface treatments with service stresses associated with 2D FE model geometries. In DARWIN 8.1, the surface residual stress capability has been extended for use with 3D FE models. It enables the analyst to manually define a univariant residual stress gradient and to superimpose it with service stresses that are extracted along the crack path in 3D FE models.

DARWIN also includes a Fleet Assessment module that can be used for Continued Airworthiness assessments associated with FAA Advisory Circular 39-8. This module enables the analyst to use results from multiple DARWIN runs to quantify risk factors and risk per flight values addressed in AC 39-8 for a fleet of aircraft. In previous versions of DARWIN, risk values were reported on a component basis in which components that failed an inspection were removed from the population. However, aircraft fleet assessments are based on a population of aircraft in which components are replaced following a failed inspection. DARWIN 8.1 provides a new option for replacement of components that fail inspections to support fleet assessments in compliance with AC 39-8. The initial version supports replacement of an identical component following a failed inspection. Future versions will provide the capability to introduce components with different geometries to support corrective action options.

DARWIN 8.1 also includes an expanded interface to manufacturing process simulation software for integrated computational materials engineering (ICME) and a new capability to introduce corrosion

pits with user-specified formation times and growth rates, and then determine when the pits will transition to become growing fatigue cracks.

In previous DARWIN versions, risk assessment for inherent material anomalies (for example, titanium hard alpha inclusions) was based on stress, temperature, and geometry information from 2D axisymmetric finite element models. However, advances in computational resources in recent years have enabled the design of complex engine components using 3D finite element models. DARWIN 8.2 provides new capabilities for life prediction and risk assessment of inherent material anomalies using 3D finite element models (Figure 9.7-29 (left)). It enables user definition of property region information (material response, anomaly distributions, inspection schedules, and mission regions) directly on the 3D FE model. DARWIN employs this information to determine the 3D zones in the model via an extension of the autozoning approach that was previously developed for 2D zones. Similar to 2D autozoning, 3D autozoning results include stress, life, and risk information. Zone-level information enables users to visualize 3D contours of the stress variations, life predictions, and risk assessments.

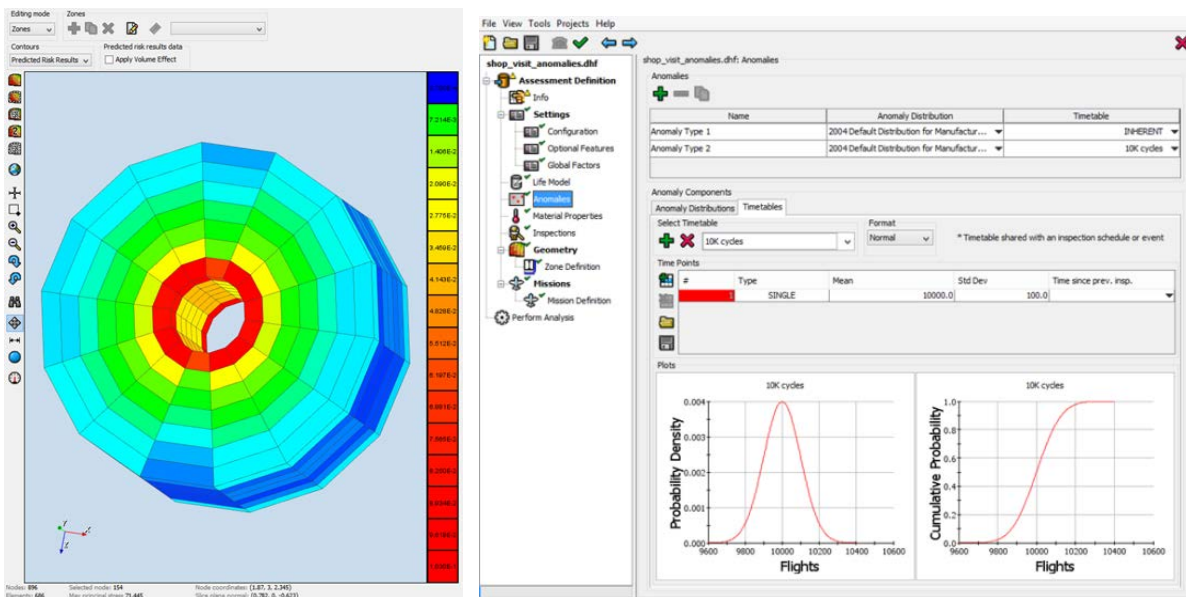


Figure 9.7-29. DARWIN 8.2 Provides (Left) a New Capability to Assess the Fracture Risk of Inherent Material Anomalies Using 3D Finite Element Models, and (Right) a New Capability for Risk Assessment of Anomalies that are Introduced During Shop Visits

Anomalies such as scratches or dents may sometimes be introduced inadvertently during routine inspection and maintenance operations (shop visits). Previous versions of DARWIN were limited to anomalies that were already present before a part had entered service. DARWIN 8.2 provides a new capability that enables the user to define shop visit anomalies (Figure 9.7-29 (right)) and to specify their associated timetables and size distributions. The timetable may be linked to the timetable of inspection schedules if desired. DARWIN tracks risk associated with shop visit anomalies and quantifies its influence on the overall probability of fracture.

DARWIN 8.2 includes a new bivariate stress intensity factor solution (CC12) for a quarter-elliptical surface crack at a chamfered corner. Cracks modeled using CC12 extend over the entire chamfered region. The next DARWIN version (9.0) will include a new stress intensity factor solution for cracks that originate at individual angled corners within chamfered regions.

DARWIN 8.2 also includes a number of additional new features such as improved mission mixing to characterize complex usage histories, a new interface to FRANC3D (advanced finite element

software for 3D fracture analysis), additional ICME features, and a new probabilistic method for more efficient fracture risk calculations.

More information about DARWIN is available at www.darwin.swri.org.

POC: Craig McClung, Southwest Research Institute, Craig.McClung@swri.org, 1-210-522-2422.

9.7.9. PRobability Of Failure (PROF) Risk Analysis Program

Francis Smith, University of Dayton Research Institute; Mark Thomsen, A-10 ASIP Program Office

The University of Dayton Research Institute (UDRI), under contract to the United States Air Force (USAF), has developed a structural risk analysis program, entitled PRobability Of Failure (PROF), that synthesizes the hazard rate and probability of fatigue failure as a function of flight hours based on data largely available from the USAF Aircraft Structural Integrity Program (ASIP). The current version of PROF, used today on a variety of AF systems, estimates the single flight probability of failure and probability of failure between inspections as a function of flight hours for a population of critical locations as defined by the unique damage tolerance analysis (DTA) for the location of interest. PROF comprises a comprehensive graphical user interface (GUI), a data management system, and computation modules.

The version of PROF which has been approved by the USAF as a valid tool for fleet management is currently being upgraded to incorporate additional features which include:

- a new analysis method which extends the legacy method of Jack Lincoln by including the survival factor (probability of surviving all prior flights) [1],
- the ability to implement multiple nondestructive inspection (NDI) probability of detection (POD) functions (e.g., field-level and depot-level inspections),
- the ability to enter tail numbers with individual aircraft inspection damage hours and perform a fleet risk assessment generating individual aircraft risk curves [2], and
- the ability to allow PROF to utilize the same loads/stress spectrum used for the aircraft DTA.

The basic PROF analysis calculates tables and plots of:

- the Single Flight Probability of Failure (SFPOF) as a function of flight hours for the combination of all similar control points (Figure 9.7-30),
- the probability of failure as a function of flight hours for the combination of all similar control points (Figure 9.7-31),
- the expected percentage of sites at which cracks will be found at each inspection,
- the predicted distribution of crack sizes before and after each inspection (Figure 9.7-32),
- the predicted distribution of crack sizes missed and found at each inspection, and
- the probability of failure as a function of crack size.

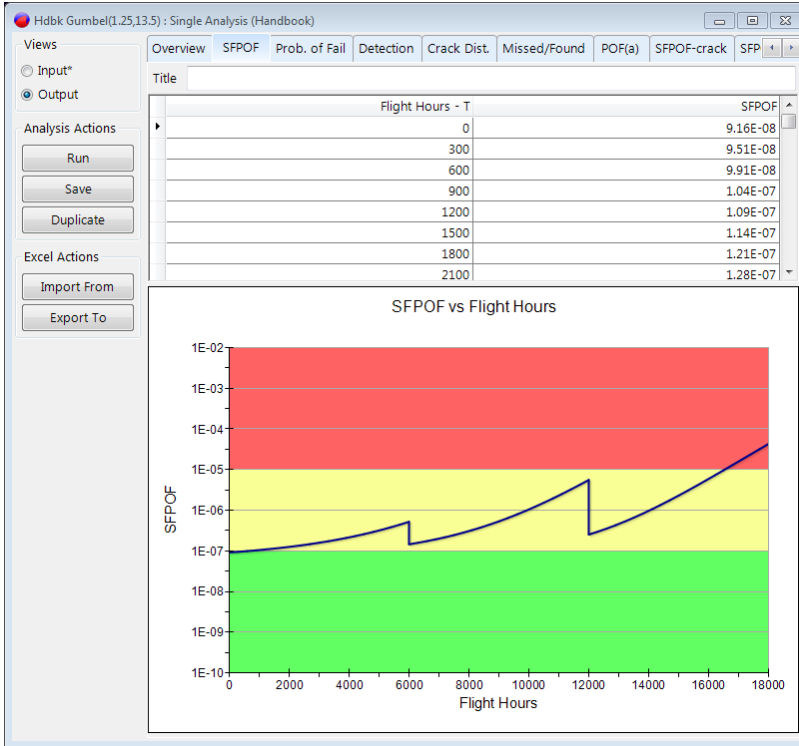


Figure 9.7-30. Single Flight Probability of Failure

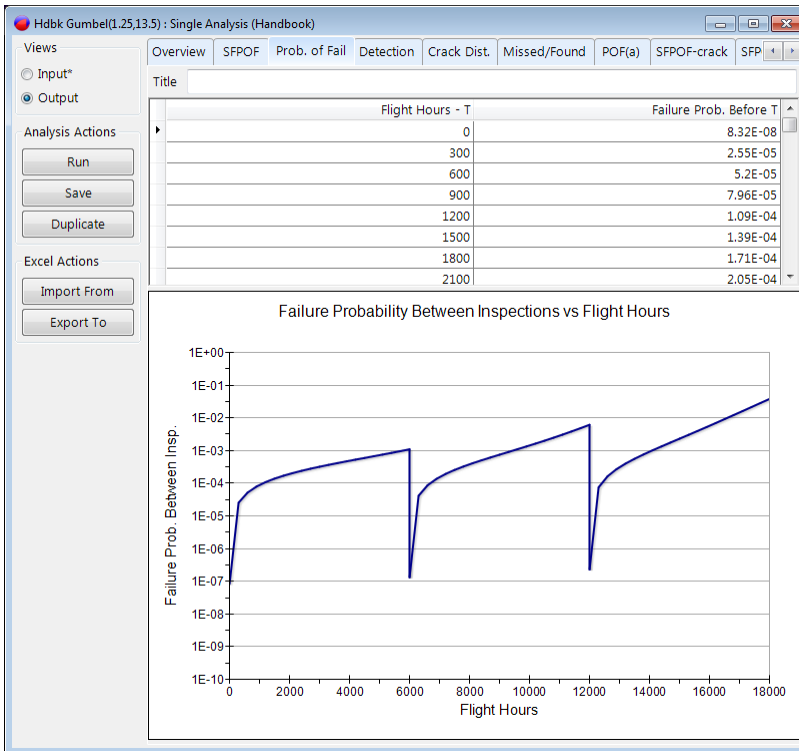


Figure 9.7-31. Failure Probability Between Inspections

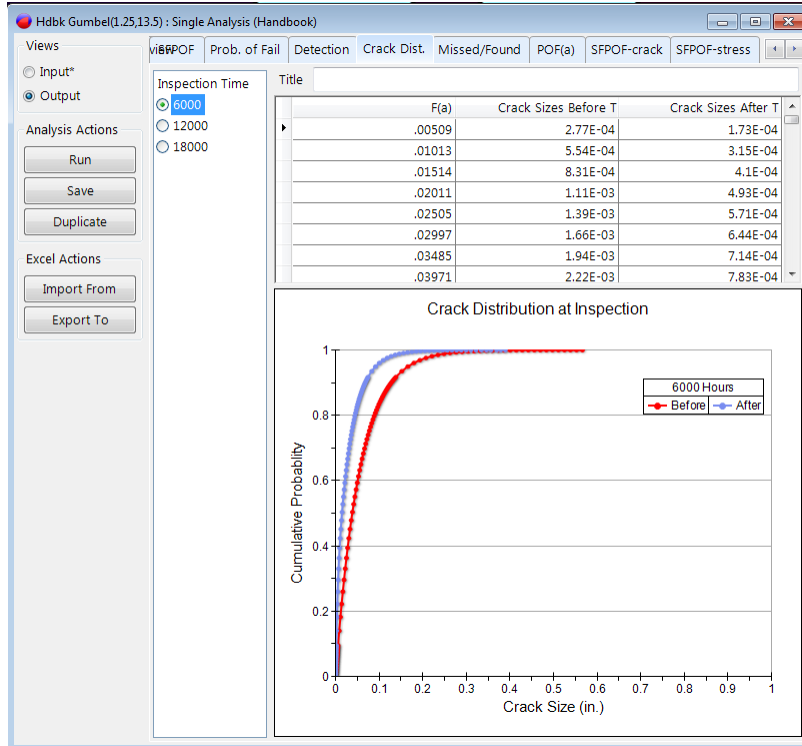


Figure 9.7-32. Crack Distribution at Inspection – Before/After

The SFPOF and probability of failure results from PROF can be combined in post-processing phases to describe failure risks for more-complex structural configurations and to calculate fleet summaries. In particular, PROF:

- facilitates such calculations by providing the ability to perform multiple analyses and export the results from the multiple analyses to an Excel file,
- combines SFPOFs from independent (non-interacting) control points to obtain failure probabilities for the combination, and
- calculates the expected number of fleet failures at selected combinations of control points as a function of calendar time from the projected number of flight hours for calendar periods of the individual aircraft in a fleet.

References

- [1] Freudenthal, Alfred, et al., “The Analysis of Structural Safety,” *Journal of the Structural Division, Proceedings of the American Society of Civil Engineers*, vol. 92, no. ST1, pp. 267-325, February 1966.
- [2] Thomsen, Mark L., et al. (2011, April 18-21) “*Development of a Quantitative Risk-Based Maintenance Prioritization Concept*,” Paper presented at 2011 Aircraft Airworthiness & Sustainment Conference, San Diego, CA

9.7.10. Risk Based Fleet Management Lessons Learned

Michelle K. Creps, USAF A-10 ASIP

The A-10 started using risk-based induction in 2010 to manage fleet inspections when depot delivery capabilities could not meet demand. The original implementation was based on a series of Excel worksheets integrating the output of fracture mechanics and risk analyses with maintenance and operational history that were linked together manually. This was done deliberately in order to ensure that the process could be implemented quickly and then updated during the initial implementation period and maintained in a sustainment environment. Now that the process has matured over the past five years, transition to a Product Lifecycle Management environment to incorporate and retain the data in a usable and updatable format into the future is ongoing.

Lessons learned through this process include the extensive cross-checking necessary to first understand the baseline, then to maintain a decision process based on product configuration and the changes associated with maintenance actions. The documents used to develop the intervals for scheduled maintenance are living and evolve with every risk run. There are four different excel documents ranging from one to 27 worksheets per document used to generate the risk run bi-annually. Data are gathered from at least three different sources and fed into the excel documents (Figure 9.7-33), which depend upon one another.

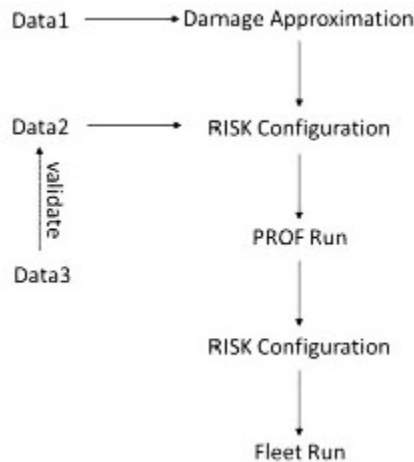


Figure 9.7-33. Interval Development Documents

Due to the living nature of the documents and the ever changing data integrated within, numerous updates to the original Excel code and methodology have been implemented. Tedious equation errors have been discovered and adjusted, which include misplaced symbols in formulas and using data from incorrect cells. Errors also arose as the configuration of the jet changed with wing swaps, wing condemnations, and new wings as well as the return of jets to the depot due to their higher than normal flight hours per year (Figure 9.7-34); this required additional logic to the code be incorporated.

As the methodology and code for risk-based induction matures, the resulting intervals and associated data are being applied to manage the fleet in a unique, economical way (Reference [1]). Waivers for hour extensions and decisions for retirements both focus on the risk results from each bi-annual interval run. Hour extensions are granted quickly using the associated aircraft risk and history while retirements are based on which aircraft have met economic exhaustion rather than where the jet was stationed. The Product Lifecycle Management environment will enhance the decision making

process further as data becomes condensed into one location within TeamCenter, and visualized with Nlign (Reference [2]) (Figure 9.7-35).

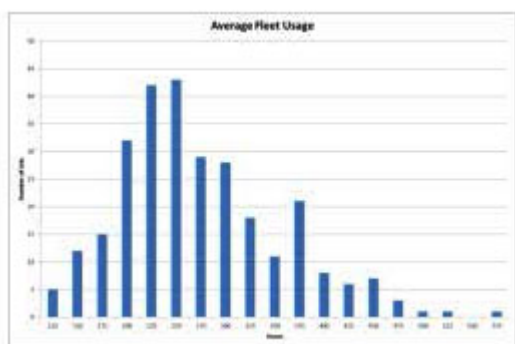


Figure 9.7-34. Average Hours Flown Per Year

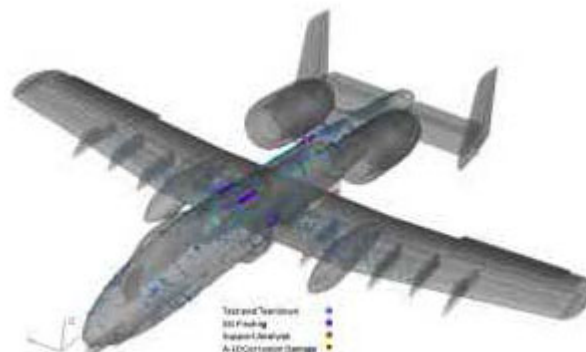


Figure 9.7-35. Damage Visualization Using Nlign

This type of database significantly reduces the time the engineer spends searching for information related to a specific aircraft and all the configurations it has undergone. The strategy for the future includes converting the multiple Excel workbooks into one automated database within the TeamCenter environment. The database will provide updated risk assessments for all operational aircraft and prioritize depot inductions based on the entire fleet metrics used in the existing spreadsheet.

The implementation of risk-based induction into the fleet management methodology has reduced the strain on depot maintenance and enhanced decision making in regards to waivers and retirements. As the process becomes more refined through continued use, further improvements to the code will be implemented in order to develop a high quality, low risk approach to fleet management.

References

- [1] Thomsen, ML, Clark, P.N, Pilarczyk, R, Whitman, Z, “Development of a Quantitative Risk-Based Maintenance Prioritization Concept”, NASA/FAA/DOD Aircraft Airworthiness and Sustainment Conference, San Diego, CA, 18-21 April 2011.
- [2] Sedgwick, H, Coyan, G, Hodges, J, Steffes, G, “Enabling High-Quality and Efficient Engineering Decisions with 3-D Visualization of Maintenance Data”, US Air Force Aircraft Structural Integrity Program Conference, San Antonio, TX, 2-4 December 2014.

9.7.11. Reducing Uncertainty in Fatigue Life Limits of Turbine Engine Alloys

James M. Larsen, USAF Research Laboratory – Materials and Manufacturing Directorate

For turbine-engine rotor materials, traditional design practice defines the safe-life fatigue limit as a statistical minimum life to form a small surface or corner crack. Alternatively, from a materials-microstructure perspective, one might define the minimum size of a small crack as the dimension of the microstructural features in which cracks initiate, which for the Ti-6246 alloy are primary alpha particles approximately 0.004 mm in diameter. Under the latter definition of cracking, our results on repeated tests indicated that the minimum number of fatigue cycles required to initiate such a microstructurally small crack, N_i , approached 0 cycles, which meant that the minimum total lifetime was spent almost entirely in the growth of a crack that begins on the microstructural scale. Although the probability of occurrence of $N_i \sim 0$ may be reduced by factors such as the imposition of surface residual stresses through shot peening,

in the stress range of rotor design, it appears difficult to preclude the rare occurrence of secondary damage, which also leads to $N_i \sim 0$.

This effort used electropolished specimens of the high-strength alpha+beta titanium alloy Ti-6Al-2Sn-4Zr-6Mo to explore fundamental variability and uncertainties in microstructurally based fatigue life limits under stresses and lifetimes representative of engine rotor design (nominally 8000 major cycles) [1]. In this life range, it is well known that the total fatigue lifetime (N_T) may be partitioned as $N_T = N_i + N_{SC} + N_{LC}$, where N_i , N_{SC} , and N_{LC} are, respectively, the numbers of cycles spent in crack initiation, small-crack growth, and large-crack growth to failure. N_i was often the dominant term contributing to the mean fatigue lifetime, but the mean fatigue behavior sometimes also encompassed a shorter-life fatigue response wherein N_i was small (approached zero). This minimum versus mean bimodal fatigue behavior appeared to respond differently to stress level, which may be expected depending on the relative contribution of N_i to the total fatigue lifetime, Figure 9.7-36. Assuming that $N_i \sim 0$, the expected lifetime can be calculated using small crack growth rate behavior and crack initiation depth from a microstructural feature. Figure 9.7-37 shows a probability plot of Monte Carlo model simulation of Type I (short life) fatigue lifetimes based only on microstructure (primary alpha particle size distribution) and small + large crack results plotted versus the short life data from the data obtained at 820 MPa.

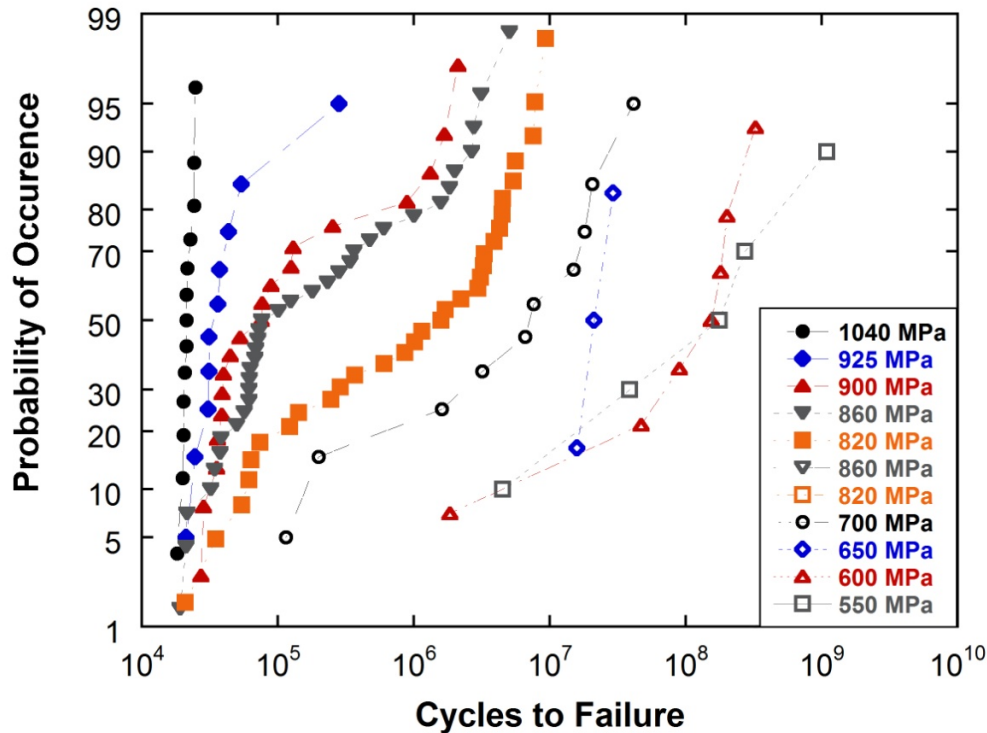


Figure 9.7- 36. Lognormal Probability Plot of Fatigue Lifetime Data for Individual Stress Levels. From Left to Right, Max Stress = 1040, 925, 900, 860, 820, 700, 650, 600, and 550 MPa

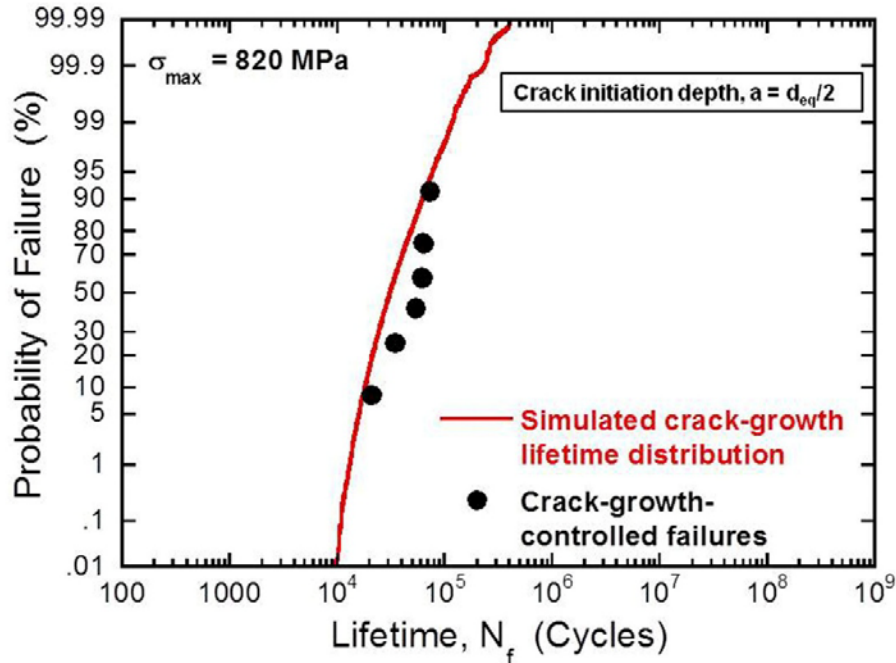


Figure 9.7-37. Probability Plot of Monte Carlo Model Simulation of Type I Fatigue Lifetimes Based Only on Microstructure (Primary Alpha Particle Size Distribution) and Small + Large Crack Results Plotted vs. the Short Life Data From the 820 MPa Data

Our research on Ti-6246 and other high performance materials suggests that the presumption of $N_i \sim 0$ for rotor design stresses may be of general applicability. If this is correct, it may be attractive to reinterpret conventional approaches and strategies for life-cycle design and management of turbine-engine rotor materials and components.

References

- [1] Larsen, J.M., Jha, S.K., Szczepanski, C.J., Caton, M.J., John, R., Rosenberger, A.H., Buchanan, D.J., Golden, P.J., and Jira, J.R., "Reducing Uncertainty in Fatigue Life Limits of Turbine Engine Alloys," *International Journal of Fatigue*, Vol. 57, pp. 103-112, 2013.

9.8. LIFE ENHANCEMENT CONCEPTS

9.8.1. Durability and Damage Evaluation of Tolerance Rivetless Nut Plates Installed in Short Edge Margin Conditions

Joy Ransom, Tim Johnson, and Matt Schultz, Fatigue Technology, Inc.

The Fatigue Technology, Inc. (FTI) ForceTec rivetless nut plate, used in both production and rework on several military aircraft, is retained in place by expanding a bushing-like nut retainer into the fastener hole (Figure 9.8-1). The expansion induces a residual compressive stress in the material surrounding the retainer that shields the hole from cyclic tensile stresses. In some applications the nut plates are installed in relatively short edge margin conditions (less than $e/D=2$). The reduced edge margin will influence the induced residual stress zone which may reduce the effectiveness of the ForceTec installation in preventing crack initiation or growth from the hole or may lead to accelerated crack initiation or crack growth from the adjacent structural edge (Figure 9.8-2). A test program was developed to evaluate an attachment hole in 7050 aluminum with a short edge margin. The goal of this program was to simulate a typical airframe location where a rivetless nut plate is required. This testing compared specimens with test hole configurations including: as-machined hole, a bonded-in neat fit nut plate and an expanded ForceTec nut plate. Because of the short edge margin (1.5 to 2) the crack initiation location of the specimens with expanded nut plates was not always at the hole. To fully understand the potential impact on damage tolerance, crack growth tests were performed on specimens with the expanded rivetless nut plates with initial flaws at both the hole and at the specimen edge. The test program encompassed both crack initiation and crack growth testing using 0% and 20% load transfer specimens tested at different stress levels. Crack initiation was defined as cycles to a 0.010 inch crack. Crack growth was defined as cycles from a 0.020 inch crack to short ligament failure. All testing was performed using a predominately compressive fighter aircraft spectrum. This technical effort will discuss the methodology used to perform the fatigue test and the results from the testing comparing the differences in cycles to crack initiation (Figure 9.8-3) and crack propagation (Figure 9.8-4) for fastener holes with short edge margins when rivetless nut plates are used.

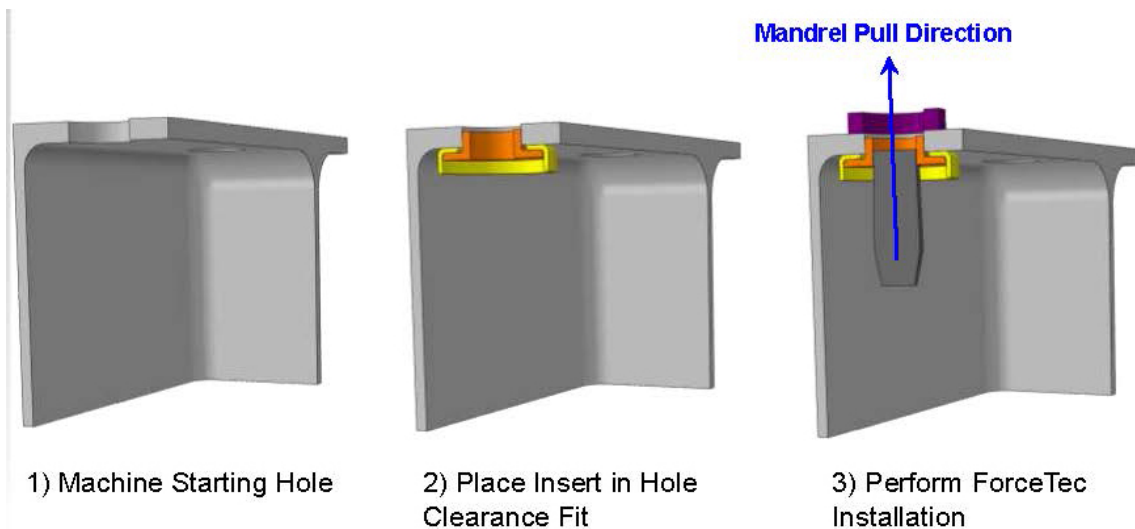


Figure 9.8-1. Modular ForceTec Process

- Short Edge Margins have shown they may reduce fatigue life improvement

- Effects of Short Edge Margin
 - Edge bulge
 - Can cause cracking away from hole

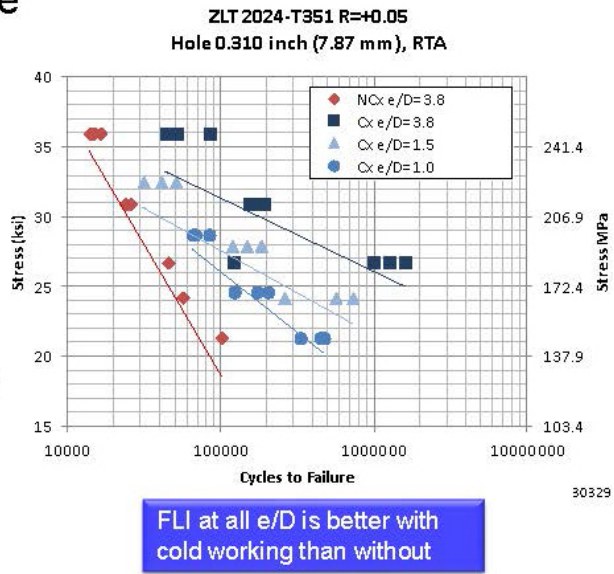


Figure 9.8-2. Edge Margin Effects on Cycle to Failure

- 0% Load Transfer Test
 - Cycles to 0.010 inch (0.25mm) crack

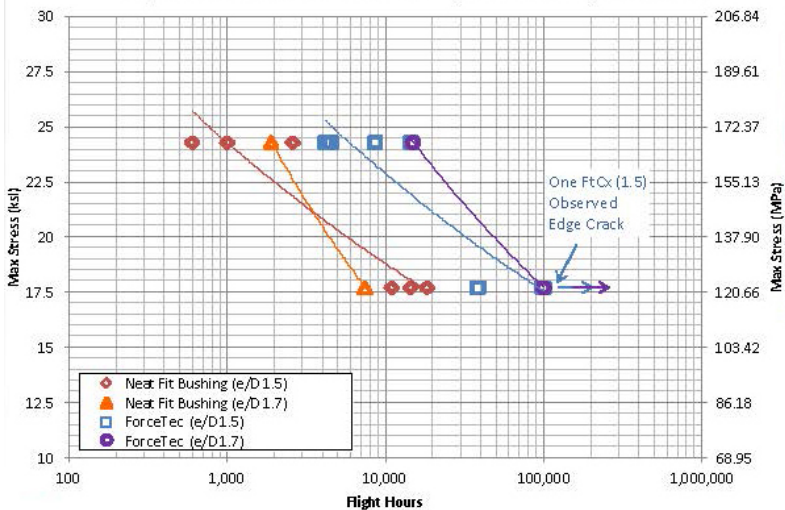


Figure 9.8-3. Crack Initiation Test Results

- 0% Load Transfer
 - Crack growth from 0.020 inch (0.51 mm) from edge of hole

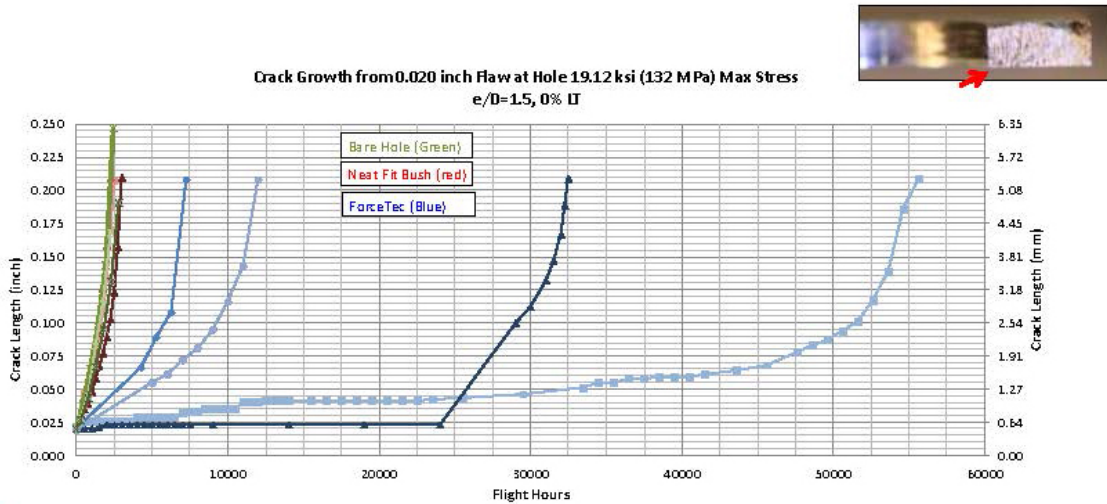


Figure 9.8-4. Crack Growth Test Results

9.8.2. Modeling Fatigue Failure From Cold-Worked Fastener Holes

Thomas Mills and Scott Prost-Domasky, APES, Inc.; Robert Pilarczk and Dallen Andrew, USAF A-10 ASIP; Josh Hodges, USAF T-38 ASIP

Residual stresses imparted through cold working of fastener holes have long been used in aircraft structure to improve the fatigue performance of material and joints at critical, high-stress locations. However, for reasons of risk mitigation, analysis guidelines established some 40 years ago do not allow for the inclusion of the residual stress fields in fatigue life prediction. This often results in a substantial inspection burden and thus a decrease in aircraft availability to the warfighter. The USAF-sponsored Rapid Innovation Program (RIF) discussed here will provide the USAF customer with an advanced analysis and inspection package that they can use to optimize fleet maintenance actions associated with cold-worked holes. The move towards a more holistic approach to model, analyze and inspect cold-worked holes has the capability to reduce maintenance costs and increase aircraft availability. This technical activity will focus on the analytical modeling and correlations with experimental data. In our technical approach, we first experimentally determine residual stress fields at cold-worked holes (using the Contour Method) and then use StressCheck to determine Stress Intensity Factors (SIF) using the Contour Integral Method for Loaded Cracks (CIMLC). We then extract the residual SIFs from StressCheck for use with the commercially-available crack growth code, AFGROW. APES is also working jointly with the USAF's A-10 and T-38 ASIP Analysis Group to incorporate BAMF (Broad Application for Modeling Failure) to automatically and progressively model irregular crack shapes associated with cold-worked holes. APES is using the analysis suite described above (Figure 9.8-5) to predict the performance of cold-worked holes under both constant amplitude and spectrum loading. Over 200 fatigue experiments (Figure 9.8-6) have been accomplished in this program and in previous efforts by APES and the USAF (Figure 9.8-7). This provides a large database for life prediction model development and validation. Our technical activity compares experimental fatigue crack shapes and growth data at cold-worked holes to analytically predicted crack growth lives and FEM crack shapes.

Model performance compared to experimental test data has shown excellent promise, with one recent set of 18-spectrum fatigue tests showing a ratio of the predicted to actual life of 0.91 +/- 0.30. These results, which use the new goal for life assessment guidelines (0.05 inch corner crack with residual stress), represent an analytical life improvement factor of up to five when compared with an existing ASIP practice for fatigue analysis at cold worked holes (0.005 inch corner crack, no residual stress) (Figure 9.8-8). Structural conditions where the current methodology is potentially unconservative relative to the proposed new guidelines, such as at low edge margin holes (as presented at ASIP 2012 by the A-10 Analysis Group), are also discussed.

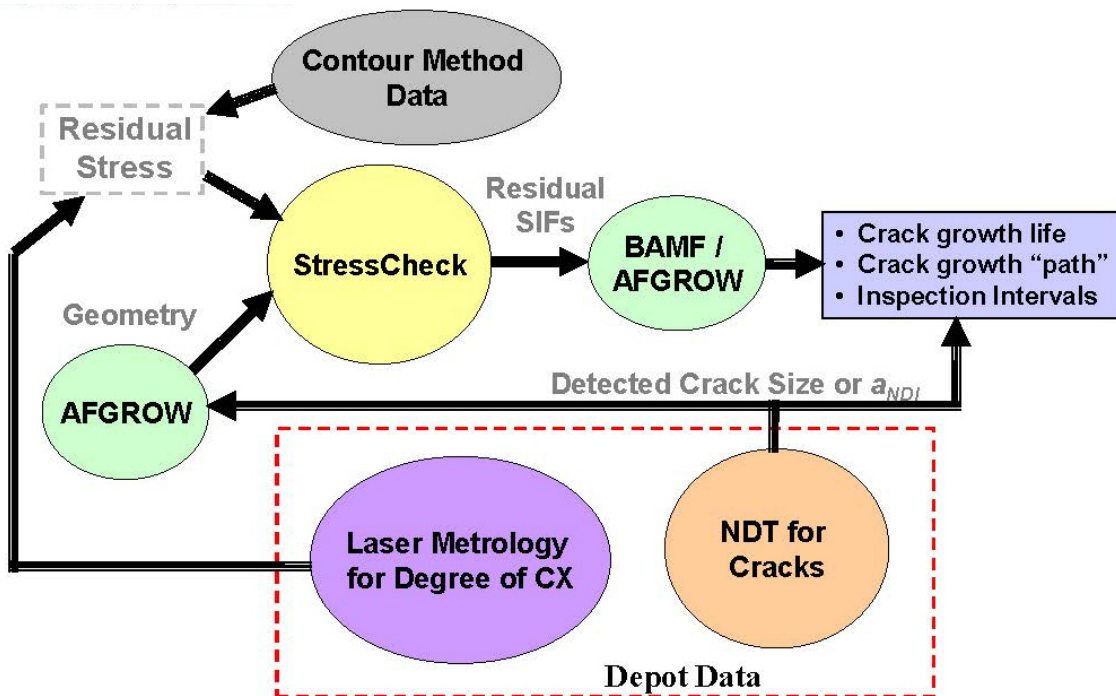
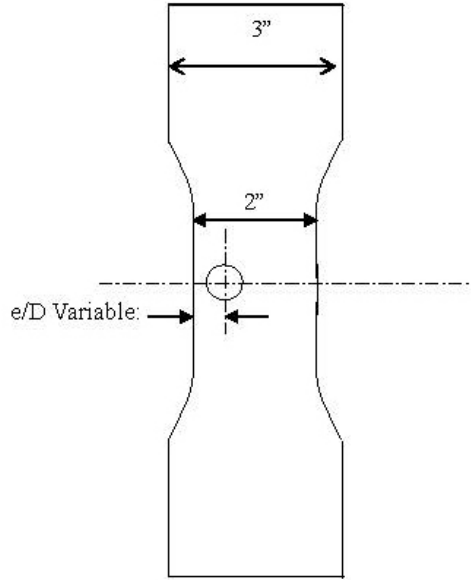


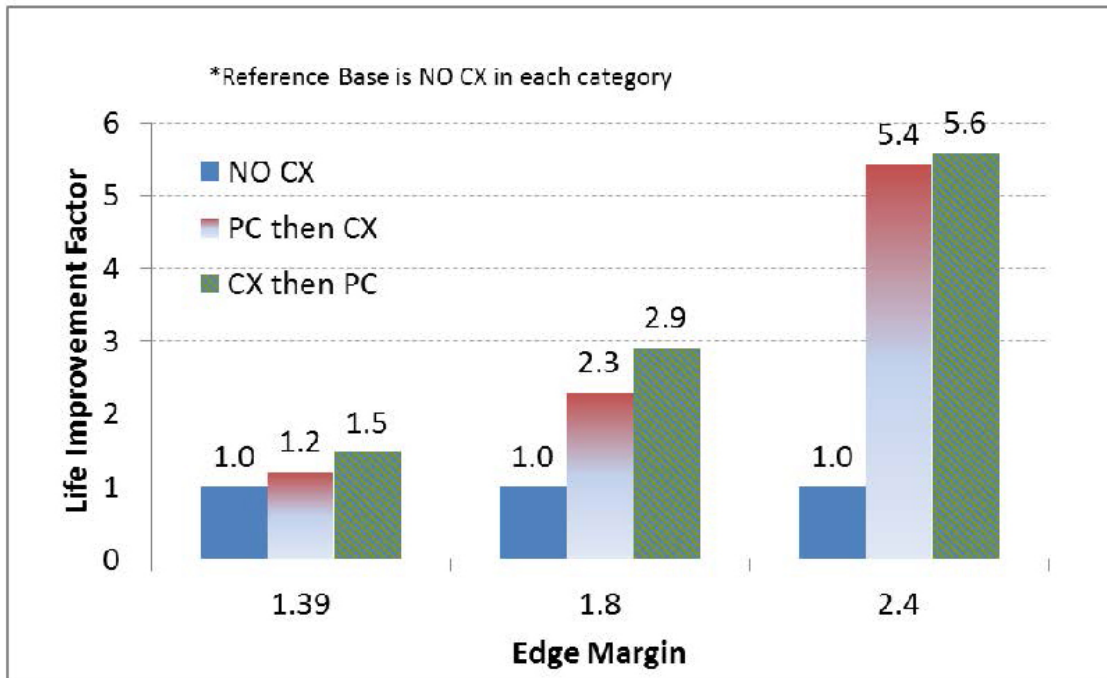
Figure 9.8-5. Integrated Package



2024-T351 Aluminum, 0.25" Thick, 0.25" Hole

CX Level 4.26% +/- 0.19% (FTI stock tooling)

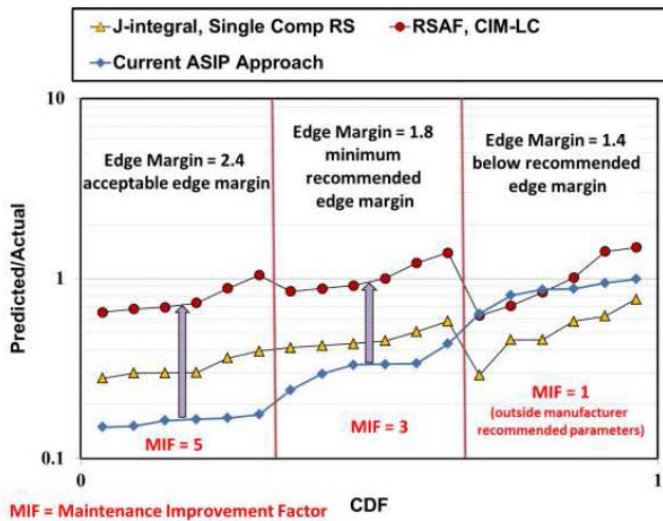
Figure 9.8-6. Specimen Schematic



LIF is based on the average for a given treatment.

Figure 9.8-7. Life Improvement Factors (LIFs) by Edge Margin

Results Segregated by Edge Margin



- ✓ Compares 0.05 initial crack in RS field with 0.005 inch crack with no RS
- ✓ Significant improvement relative to legacy method at higher edge margins
- ✓ As work by D. Andrew showed (see ASIP 2012), ineffective cold work at low e/D can drive new method to be unconservative relative to legacy method

Figure 9.8-8. Comparing Results to Current ASIP Approach

9.8.3. Computation of Stress Intensity Factors for Cracks in Cold-Worked Holes

Ricardo Actis and Matt Watkins, Engineering Software Research & Development, Inc.; Scott Prost-Domasky, APEX, Inc.; Josh Hodges, USAF T-38 ASIP

A fundamental question of computational engineering is whether it is possible to accurately predict the response of some physical system or process by numerical simulation to justify basing engineering decisions on the predictions. In life prediction of structural components containing an initial flaw it is particularly important to determine stress intensity factors (SIFs) to a high degree of accuracy. Since the exact solution for SIFs are generally not available for cracks in the presence of complex geometric features, Beta factors are often expressed as the superposition of the SIFs of several simpler cases (Figure 9.8-9). Beta curves are then compiled as a function of crack length to perform crack growth studies. An alternative to the superposition approach is the development of proper formulated models solved by the finite element method (FEM). The particular case of cracks emanating from cold-worked holes is of practical importance since cold-working is a commonly used approach to increase the fatigue life of structural components. To account for residual stresses in the computation of SIFs, two approaches were investigated to analyze cracks emanating from cold-worked holes: The J-integral and the Contour Integral Method (CIM). A modification of the Rice J-integral for cracks in a residual stress field was investigated in which the residual stresses are treated as initial strains. Aspects of implementation are discussed as well as how the residual stress field is introduced in the model and how the crack is introduced in the residual stress field. The J-integral works extremely well provided the complete residual stress field is available to perform the analysis. An alternative approach for computing SIFs was considered by applying the principle of superposition. The effect of residual stresses are accounted for by loading the faces of the crack with the traction distribution required to restore the traction-free boundary condition when the crack is introduced in the residual stress field. In the case of mode I SIF, the traction distribution can be obtained, for example, from experimentally measured residual stresses using the contour method. The use of the modified CIM to account for loaded crack faces was investigated and the results were compared with those obtained from the J-integral (Figures 9.8-10 and 9.8-11). Aspects of implementation in the commercial finite element analysis (FEA) software product StressCheck are

discussed and specific examples are presented. This work was performed in support of the project Integrating Residual Stress Analysis of Critical Fastener Holes into USAF Depot Maintenance (Rapid Innovation Fund - RIF - program AFRL-PK-11-0001).

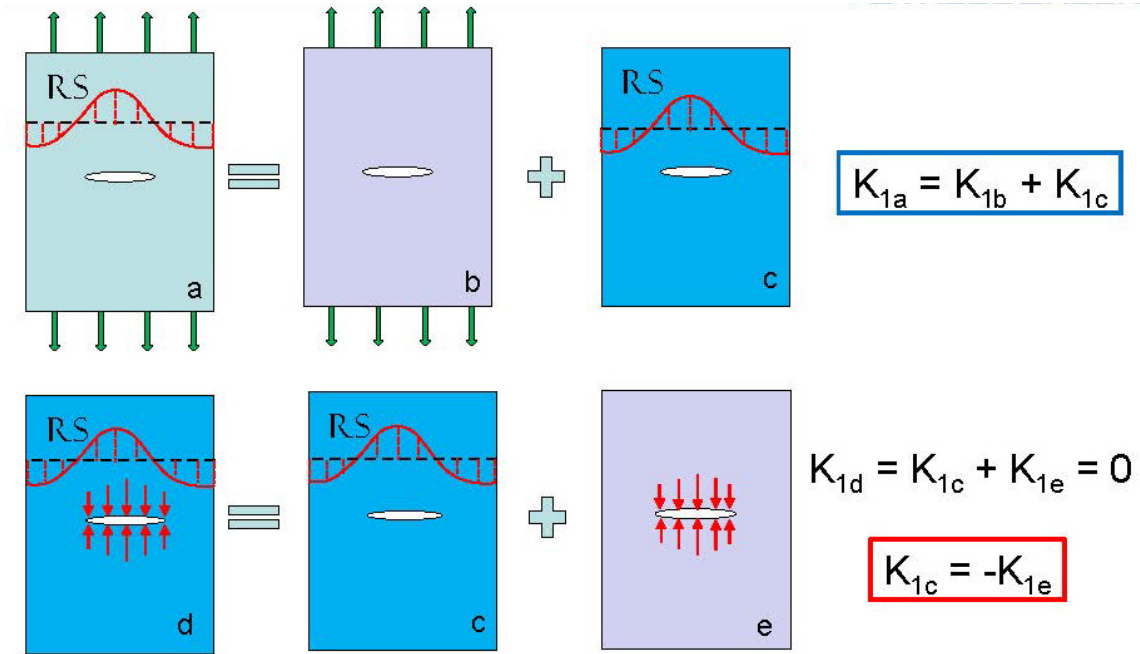


Figure 9.8-9. Stress Intensity Factors by Superposition

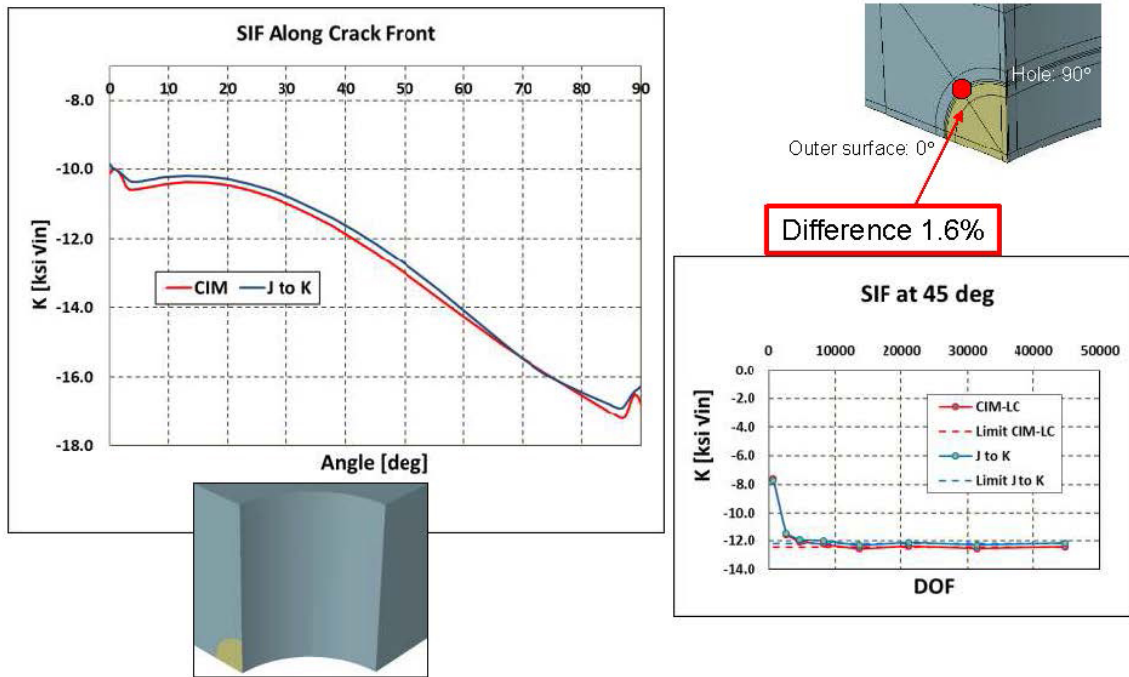


Figure 9.8-10. K_I From Residual Stress Only

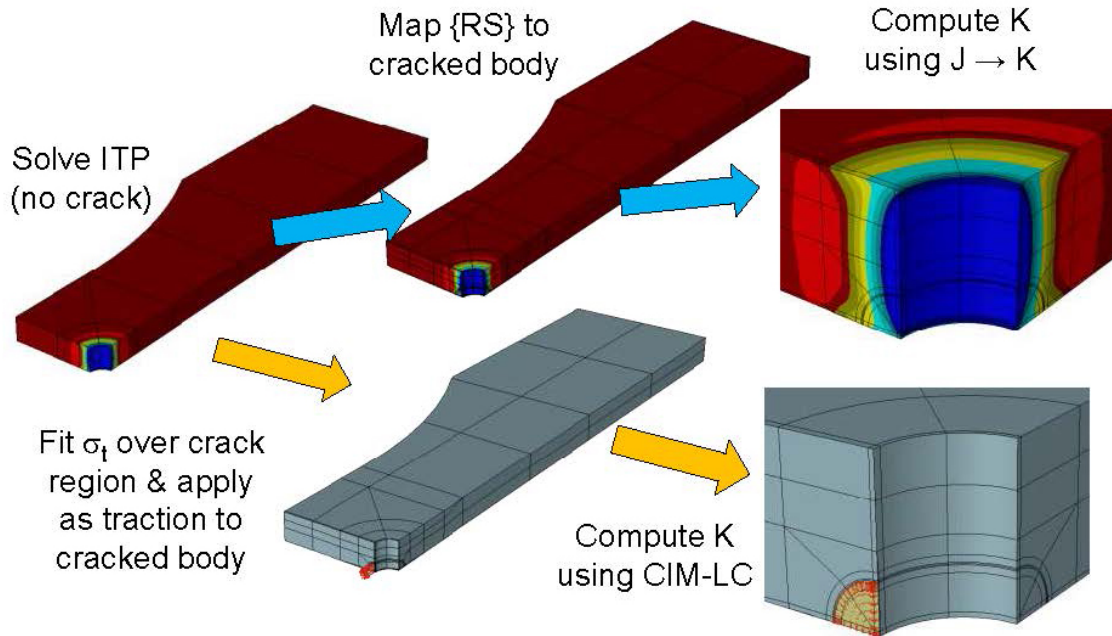


Figure 9.8-11. Plate with Cold-Worked Hole

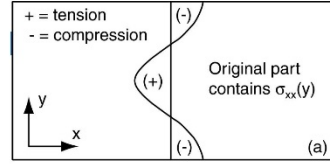
9.8.4. Residual Stresses From Cold-Working of Aircraft Fastener Holes

Adrian DeWald, Michael Hill, and John VanDalen, Hill Engineering, LLC; Bob Pilarczyk, Dallen Andrew and Mark Thomsen, USAF A-10 ASIP; Scott Carlson, Southwest Research Institute; David Marosok, Northrop Grumman Corporation

It is well established that compressive residual stresses provide improved fatigue performance and damage tolerance enhancement (Figure 9.8-12). Compressive residual stresses act to slow the growth of fatigue cracks (Figure 9.8-13), which can provide substantial benefits in terms of performance, safety, cost, and inspection intervals. To take advantage of this concept, cold-working processes are used to induce compressive residual stress near many critical aircraft fastener holes. A typical cold-working expansion process involves pulling a tapered mandrel through a hole. The material near the hole is plastically deformed resulting in a state of compressive stress near the hole. This technical activity provides a summary of recent experiments to quantify the effects of cold-working process variables on residual stress in aluminum test specimens. Residual stress measurements were performed on test coupons using the contour method (Figure 9.8-14), which provides a two-dimensional map of residual stress over the cross section. Process variables studied included cold-working percentage (Figure 9.8-15), hole diameter (Figure 9.8-16), and hole-to-edge distance (i.e., edge margin) (Figure 9.8-17). These variables had a measurable and consistent effect on the resulting residual stress. The data include some level of replication that allows mean and statistical trends to be determined. The new residual stress data can be used to investigate advanced damage tolerance assessments for cold-worked holes that are based on superposition of residual and applied stresses, in contrast with current assessments that are based on crack length adjustment (i.e., the 0.005 inch flaw).

❑ **Residual stresses are stress remaining within a body after outside forces removed**

- Must satisfy equilibrium
 - Forces & moments sum to zero on every plane



❑ **Common RS sources**

- Material processing (e.g., quench)
- Welding
- Surface treatments
- Cold working



❑ **Residual stresses play a significant role in many failure mechanisms**

- **Tensile RS** → **decrease** performance
- **Compressive RS** → **increase** performance

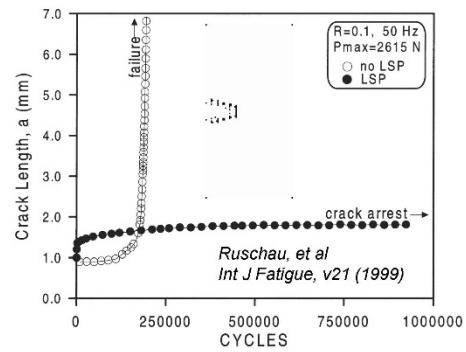


Figure 9.8-12. Background on Residual Stress

❑ **Residual stresses have a significant impact on observed fatigue behavior of materials**

- Affect the rate at which fatigue cracks grow
- Affect the shape evolution of fatigue cracks

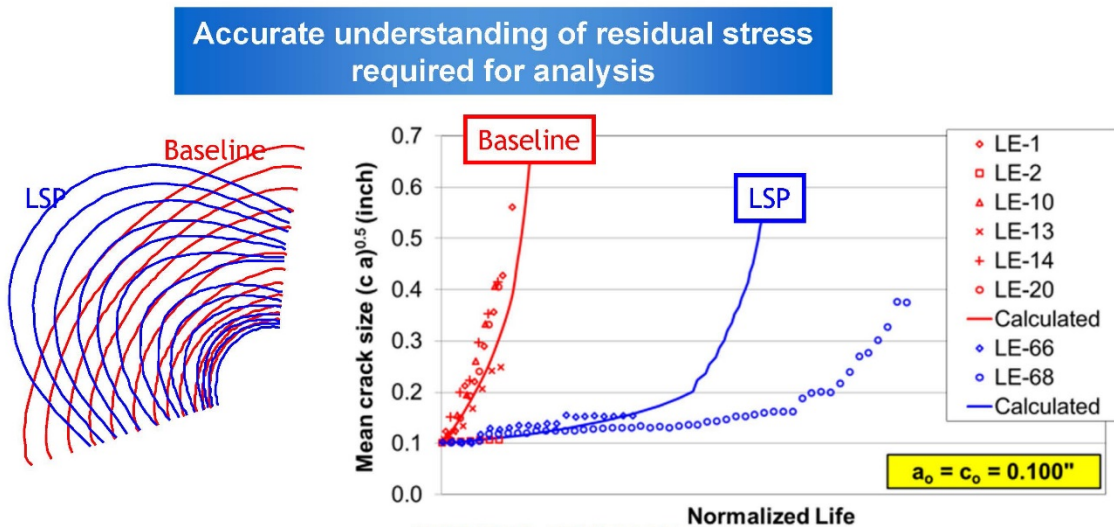
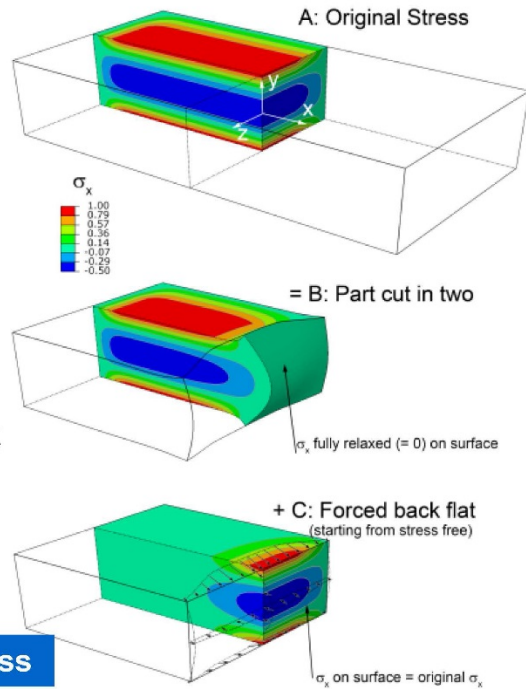


Figure 9.8-13. Effect of Residual Stresses on Fatigue Crack Growth

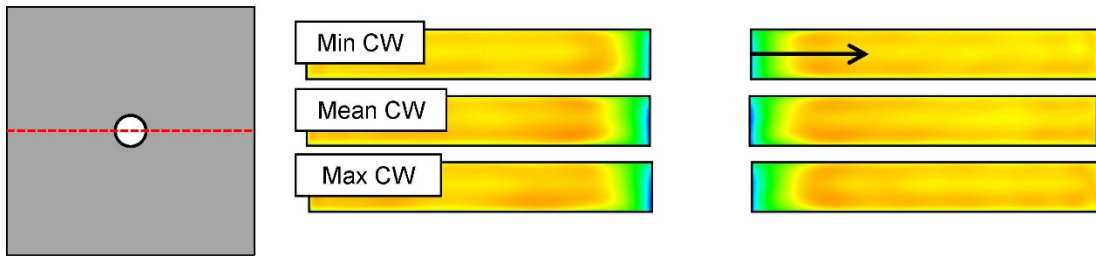
- ❑ 2D map of residual stress normal to a plane
- ❑ Part contains unknown RS (A)
- ❑ Step (B)
 - Cut part in two
 - Stress release \Rightarrow deformation
 - Stress normal to cut surface is fully released
- ❑ Step (C)
 - Force deformed surface back to flat
 - Apply reverse of deformation to surface
 - Stress on cut face in (C) equals original stress on cut face (A)



Cut \rightarrow measure \rightarrow FEM \rightarrow residual stress

Figure 9.8-14. Contour Method Principle

- ❑ Contour plots of measured residual stress



- ❑ Line plot illustrates variation with cold work
 - Peak compressive magnitude is similar
 - Larger applied expansion increases compressive region

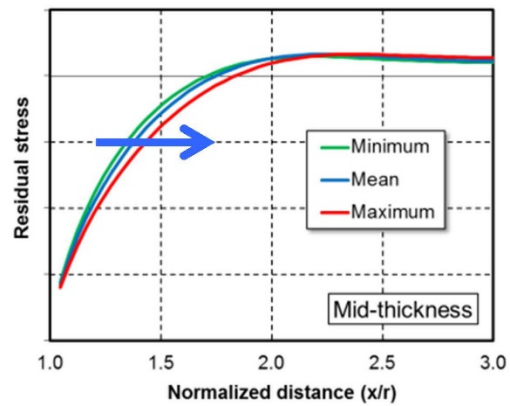
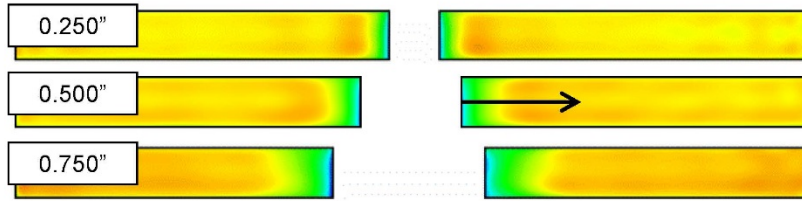


Figure 9.8-15. Effect of Amount of Applied Expansion

□ Line plot illustrates variation with hole size

- Significant difference in size of compressive region
- Peak compressive stress magnitude is similar



□ Normalizing by hole size collapses the data

- Size of affected region scales with hole size

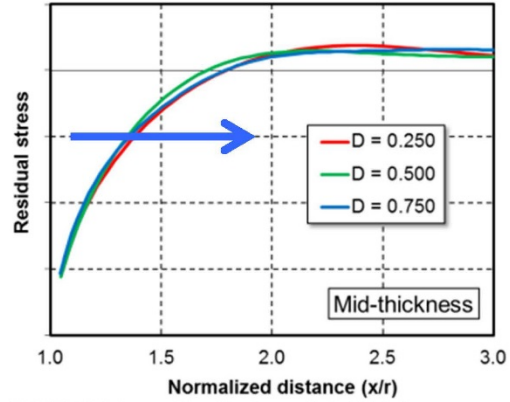


Figure 9.8-16. Effect of Hole Size

□ Plot stress on short ligament side

- Magnitude of compression at hole edge is similar
- Tensile residual stress higher for short edge margins
 - 1.5 highest of cases investigated
 - 1.2 exhibits “bulge”
- Near hole compression reduced for edge margin of 1.2
 - Due to “bulge”

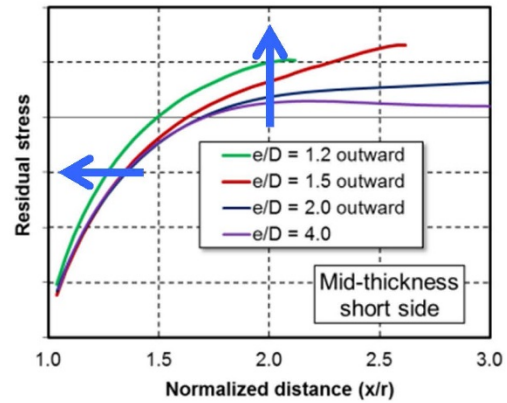
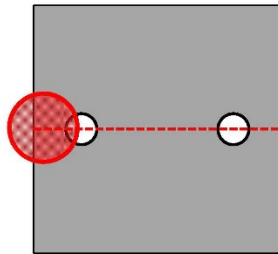
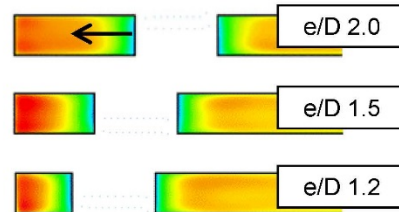


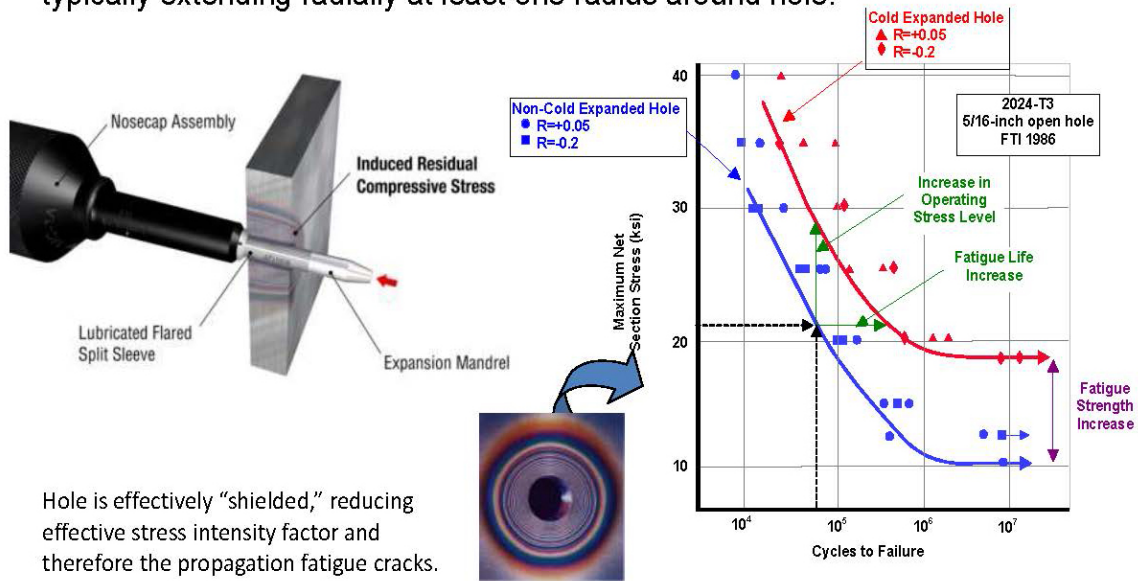
Figure 9.8-17. Effect of Edge Margin (Short Side)

9.8.5. Hole Cold Expansion in the Presence of Existing Cracks

Len Reid, Fatigue Technology, Inc.

Cracks and flaws of varying degrees are present in all aging aircraft. The objective of most life extension programs is to locate and remove the detectable cracks or flaws originating at holes in critical structure and joints. However, the effectiveness of current non-destructive inspection evaluation (NDE) methods and the probability of detection often impact the effectiveness of repairs. An integral part of the repair process often includes cold expansion (Figure 9.8-18) of the subject holes to prevent further crack growth or ultimately to expansion in the presence of an existing crack: What is the effect of the split-sleeve-cold-expansion process (Figure 9.8-19) in arresting or delaying crack growth should the hole have an existing non-detected crack prior to cold expansion? Will the expansion process cause fast fracture? Will the process be ineffective in inducing a residual compressive stress field around the hole due to the presence of the crack? Will the beneficial residual compressive stress be ineffective in slowing or arresting further growth of the crack? To answer these questions, many tests have been conducted that show that split-sleeve-cold-expansion is very effective in delaying, or even arresting the growth of a pre-existing crack/flaw in a hole. Cracks of up to 0.050" can be arrested in aluminum alloys subjected to typical aircraft stress levels. Even larger cracks, in the normal NDE threshold range, are significantly delayed in propagation if not arrested. This technical activity will review results from a number of tests that have been conducted over the years to examine the crack arrest capabilities of the process in different aerospace materials. The effect of flaw size on crack growth life in the presence of the induced residual compressive stress zone will be shown as well as the effect it has on the mode of crack propagation. From these test results it will be seen how hole cold expansion has been used to reduce the nominal 0.050-inch flaw size, typically used in damage tolerance analysis to establish inspection thresholds, to a generally accepted 0.005-inch flaw size for continuing airworthiness and inspection threshold determination (Figures 9.8-20 and 9.8-21). While not endorsing leaving detected flaws or cracks in holes, cold expansion can be an effective adjunct to NDE in providing assurance that small undetected cracks can be significantly retarded under typical aircraft stress levels and thereby lead to continued safe operation of the aircraft.

Cold Expansion (cold working) induces a controlled zone of residual compressive stress around and through a hole, typically extending radially at least one radius around hole.



Hole is effectively "shielded," reducing effective stress intensity factor and therefore the propagation fatigue cracks.

Figure 9.8-18. Cold Expansion Process

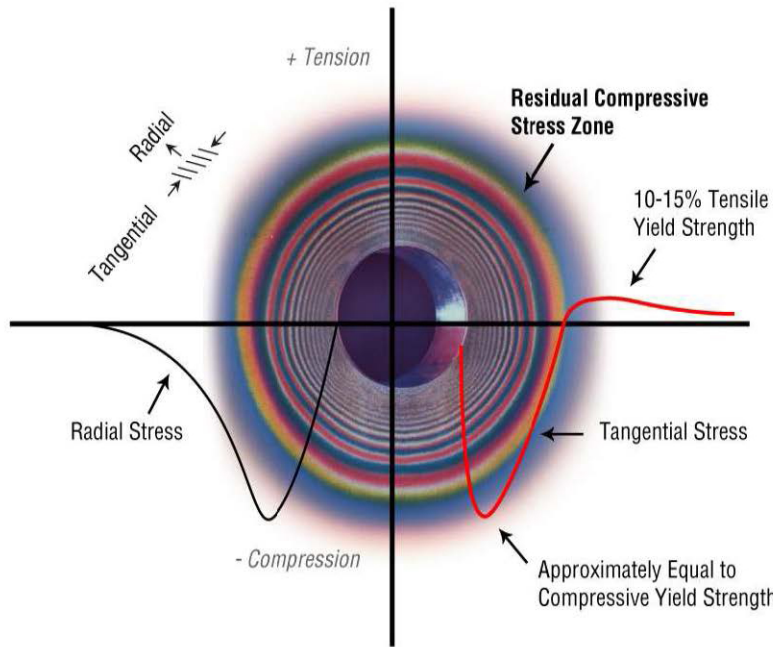


Figure 9.8-19. Typical Residual Stress Distribution for Split-Sleeve Cold Expansion (C_x)

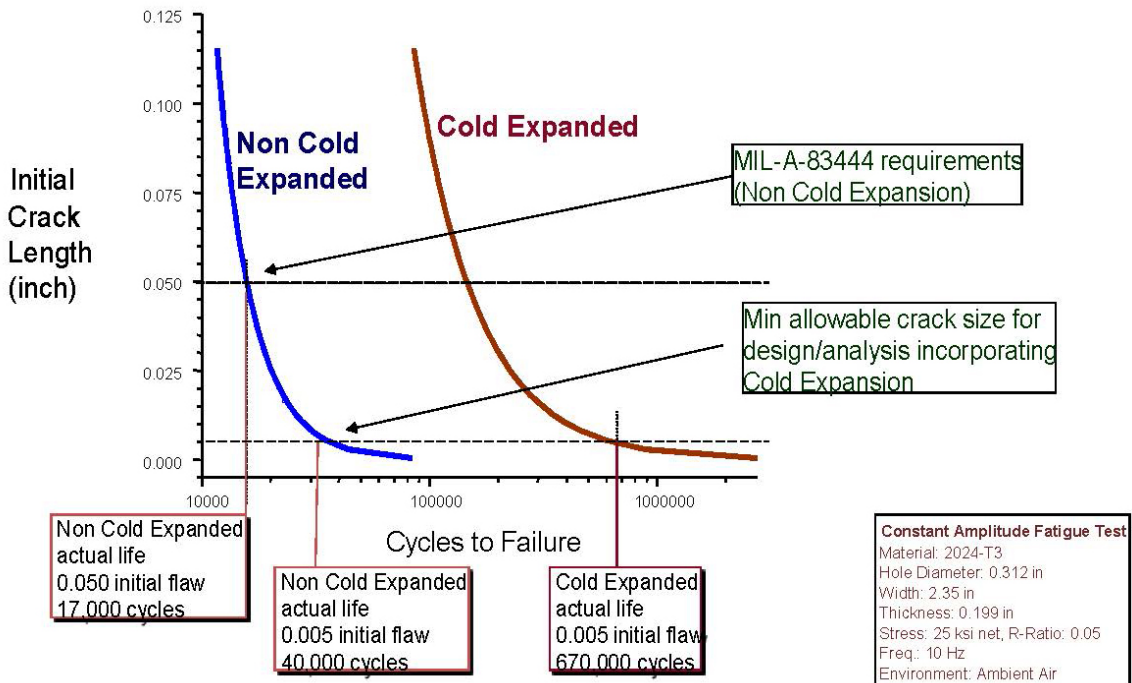


Figure 9.8-20. Conservatism of USAF DADTA Approach

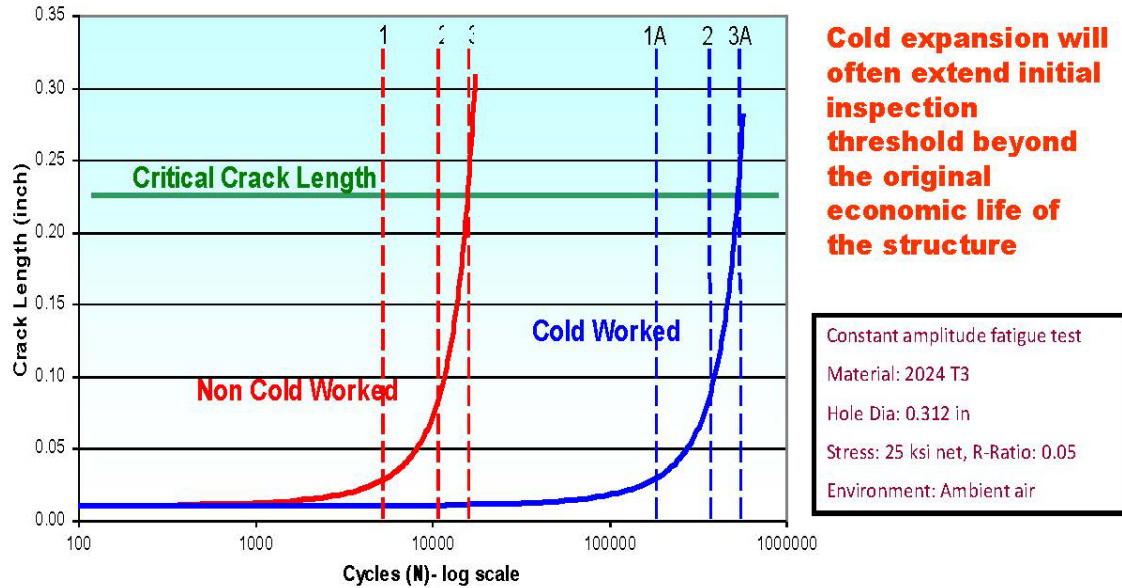


Figure 9.8-21. Extended Inspection Interval with Cold Expansion ($\alpha_i = 0.005''$)

9.8.6. Cold-Expansion Effects on Cracked Fastener Holes Under Constant Amplitude and Spectrum Loading in the 2024-T351 Aluminum Alloy

Jacob Warner, USAF F-22 SPO

This research compares the fatigue lives of clean (no detected discontinuities) cold-expanded holes (Figure 9.8-22) with the fatigue lives of holes that were cold-expanded after a fatigue crack had nucleated and grown to 0.050 inches. The experiments conducted herein investigated various stress levels under constant amplitude and wing spectrum loading conditions. The tested fatigue lives were then compared with analytical predictions using Lextech Inc. AFGROW software (Figure 9.8-23). The analytical approach used to account for the benefit of cold expansion assumed a 0.005 inch initial crack size, consistent with the United States Air Force damage tolerance analysis method. This research found that a 0.005 inch initial crack size analytical assumption to account for the fatigue life benefit of cold expansion does not yield conservative results at some stress levels (Figures 9.8-24 and 9.8-25).

- Tapered mandrel pulls through hole
- Creates a residual stress field
- Retards fatigue crack growth

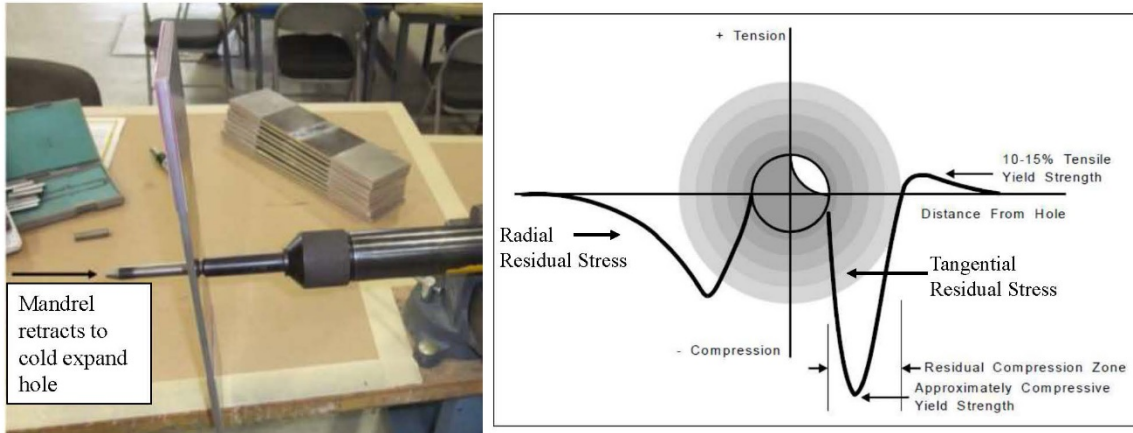


Figure 9.8-22. Cold Expansion Process

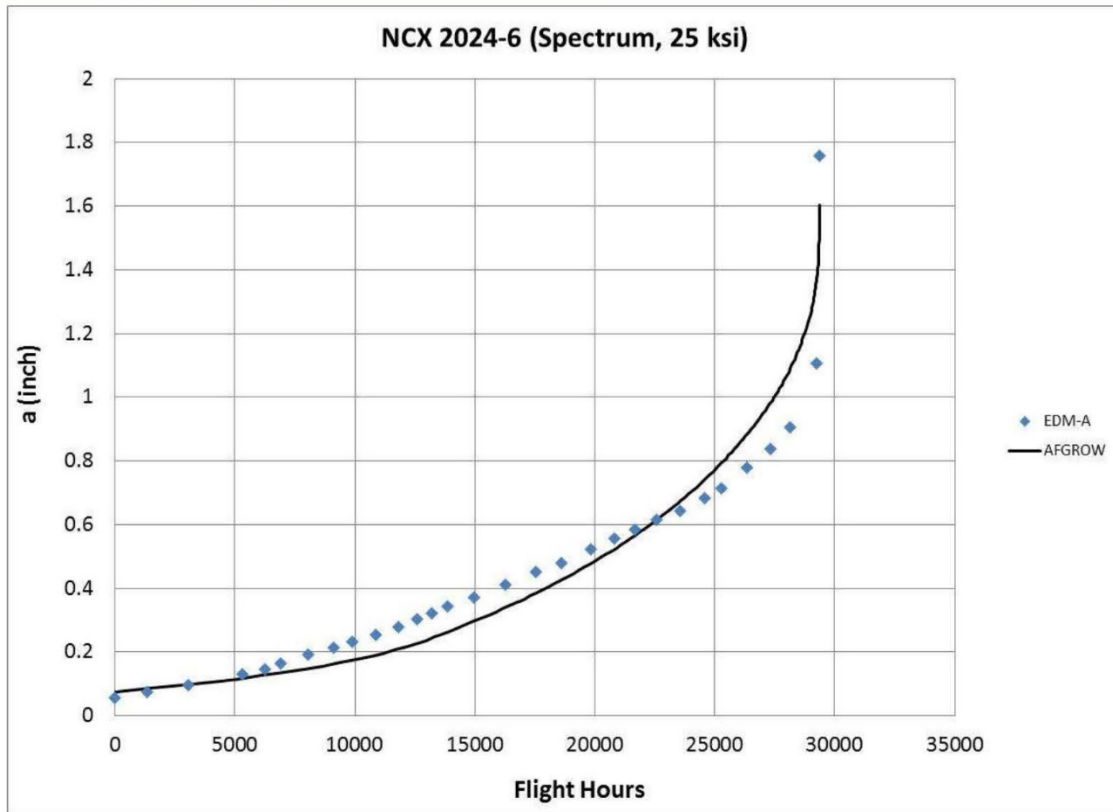
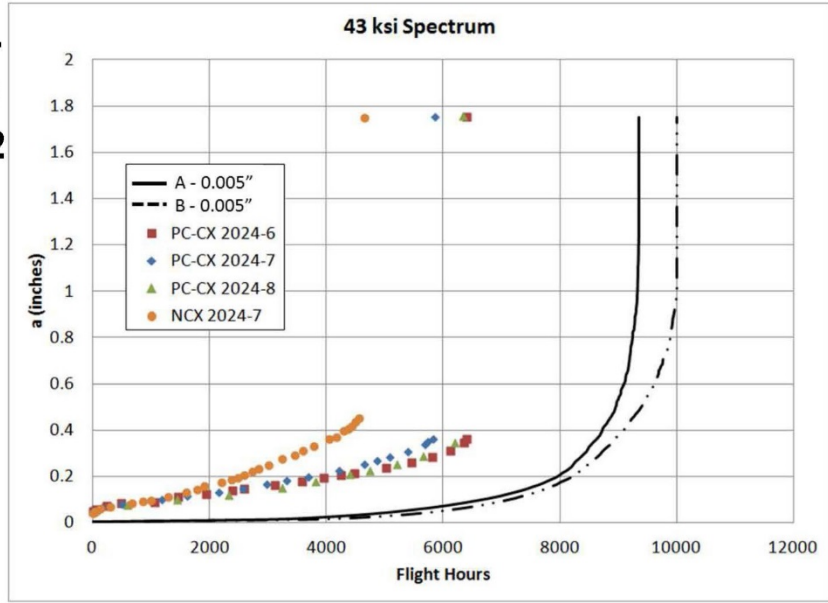


Figure 9.8-23. AFGROW Correlation to Test Results

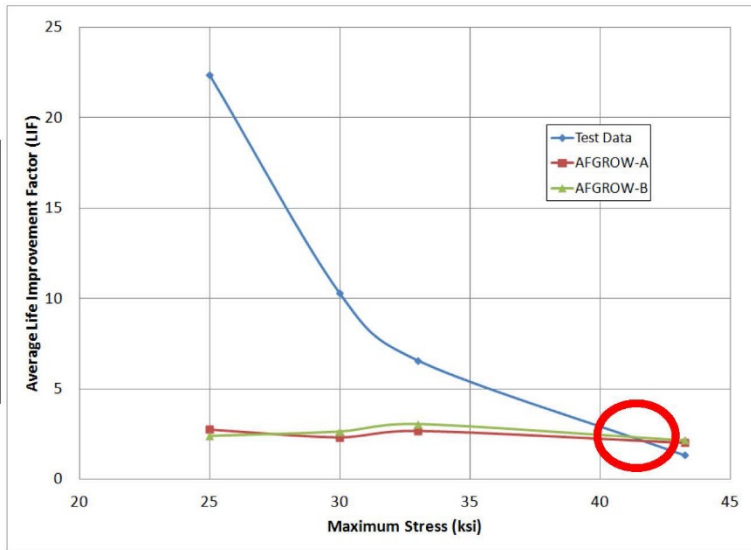
- Life: 6,201 hrs.
- Actual LIF: 1.3
- Analysis LIF: 2
- Weibull $\beta=19$
- 0.005" Model:
 - Lookup A: 9,357 hrs.
 - Lookup B: 10,031 hrs.



Test Data and AFGROW Results

Figure 9.8-24. Results for Pre-Cracked Cold-Expanded Holes

	Max Stress (ksi)	Non-CX Life (cycles)	PC-CX Life (cycles)	LIF NCX to PC-CX
Constant Amplitude	20	47443	4296067	90.6
	25	7443	452585	60.8
Spectrum	25	31521	704450	22.3
	30	N/A	194950	10.3
	33	12201	80220	6.6
	43	4658	6201	1.3



High Stress Decreases LIF

Figure 9.8-25. Life Improvement Factor Decreases with Increasing Stress

9.8.7. Laser Peening for Improved Fatigue Strength and Lifetime for a Wing Attachment Shear Tie

Jon Rankin, Tracy Racanelli, Jack Campbell and Lloyd Hackel, Metal Improvement Company; Thomas Mills, APES, Inc.

Laser peening is shown to improve fatigue strength and life in test parts simulating the Al-7050-T7451 wing attachment shear tie for an operational Navy aircraft (Figures 9.8-26 through 9.8-29). Fatigue tests were conducted on parts fabricated and treated in accordance with the process in current use (IVD coated and shot peened) and others with laser peening added. Additional parts were prepared with a 0.01 inch deep EDM notch to simulate damage or crack initiation. Without exception, laser peening outperformed all otherwise prepared specimens, including by as much as 10x for the case of the notched (simulated damage). Fatigue tests were completed on 40 parts using a 100kip MTS load frame and using a Navy specified load spectrum. Each spectrum block was sequentially repeated until failure or run-out. A marker-band sequence included in the load spectrum facilitated quantitative crack growth measurements (Figure 9.8-30). Test conditions, post-test part inspection, and crack growth analysis methods were developed and approved in collaboration with the Navy. Laser peening (LP) was applied with 300% coverage at 4GW/cm² in accordance to SAE AMS 2546 and shown to generate compressive residual stresses to 0.15 inch depth. This is in contrast to depths of only 0.016 inch achieved with the current IVD and shot peening (SP) process alone. This explains the fatigue life improvement provided by LP and agrees with the large database generated to support current commercial and defense LP applications for improving fatigue life in aircraft and aerospace components. Quantitative fractography was carried out on 22 primary cracks from 15 different coupons and used to evaluate the performance of the different surface treatment conditions. These analyses were done primarily through reconstruction of crack growth curves after coupon fracture. This was facilitated by use of a fatigue spectrum slightly modified to include a marker sequence that produced one band per test block. The marker band analyses reliably reconstructed crack growth to depths < 0.002 inch and occasionally < 0.001 inch and are found to correlate well with the measured residual stress field. For example, fractography reveals that crack growth behavior for SP and SP+LP treatments is similar for crack depths approaching 0.01 inch. Beyond this, however, the SP+LP treatment dominates, delivering crack growth rates 10 to 20 times slower than SP at a range of crack depths from 0.03 to 0.07 inch. These results indicate that the SP+LP treatment can produce life improvements over the SP treatment by at least a factor of two to four; moreover, >10x improvement is readily attainable relative to the as-machined baseline condition. Laser peening, an FAA qualified process, also has the advantage that it can be implemented on-aircraft as in the current application to mitigate fatigue cracking on F-22 fighters. Thus, it is ideally suited for many aging aircraft applications, such as the wing attachment shear tie reported here.

The problem: shear tie develops a “hot spot” during flight loading potentially leading to shortened lifetime

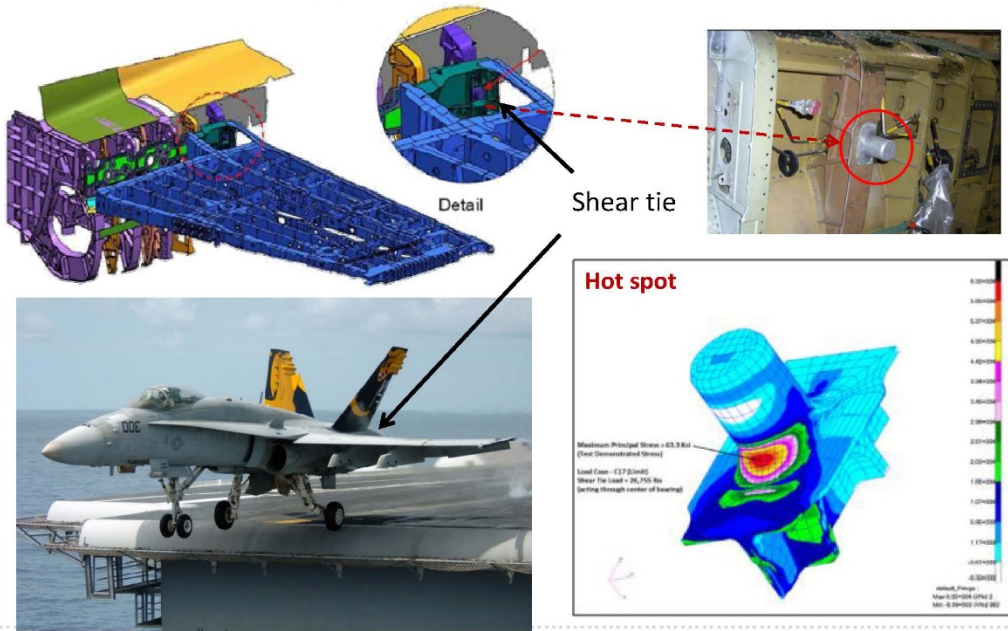


Figure 9.8-26. Shear-Tie Problem

Objective: Quantify “hot spot” fatigue improvement by laser peening

Contract deliverables:

- Quantify improvements in fatigue strength and life for laser peening vs. baseline process
- Quantify crack initiation and growth

Test articles:

- Aluminum 7050-T7451 coupons that simulate stress distribution at surface and below hot spot in shear tie.

Fatigue spectrum:

- Spectrum provided by NAVAIR

Laser peening process:

- Process parameters chosen using (a) extensive CWST laser-peening database on aluminum alloys (b) residual stress measurements on test coupons.

Ultimate Goal: Provide on-wing laser peening process for enhancing shear tie life

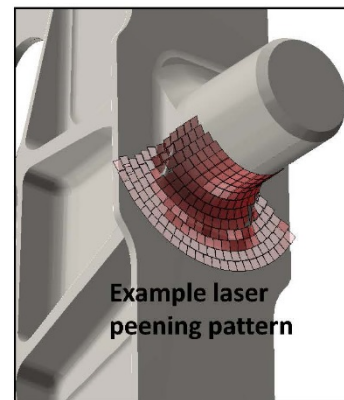
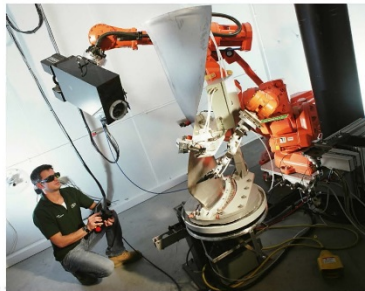
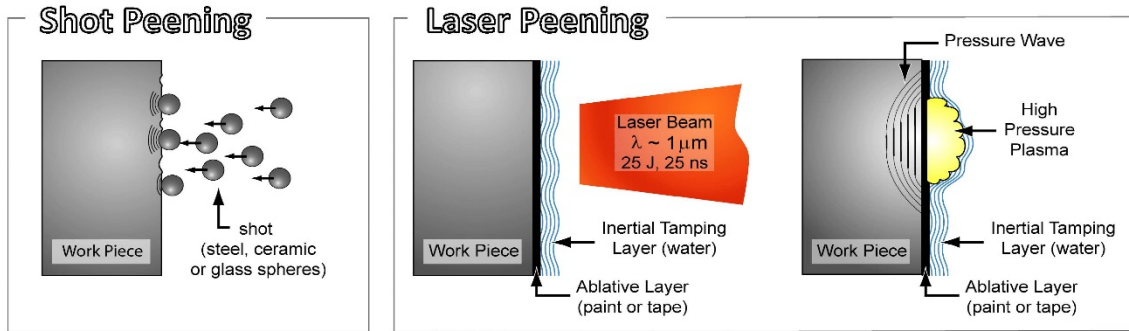


Figure 9.8-27. Goal of Laser Peening

Laser Peening employs advanced laser technology and shock physics



Process is robotically controlled thus precise and repeatable

Figure 9.8-28. Laser Peening Process

Laser peening compressive stress in aluminum is 10x deeper than shot peening

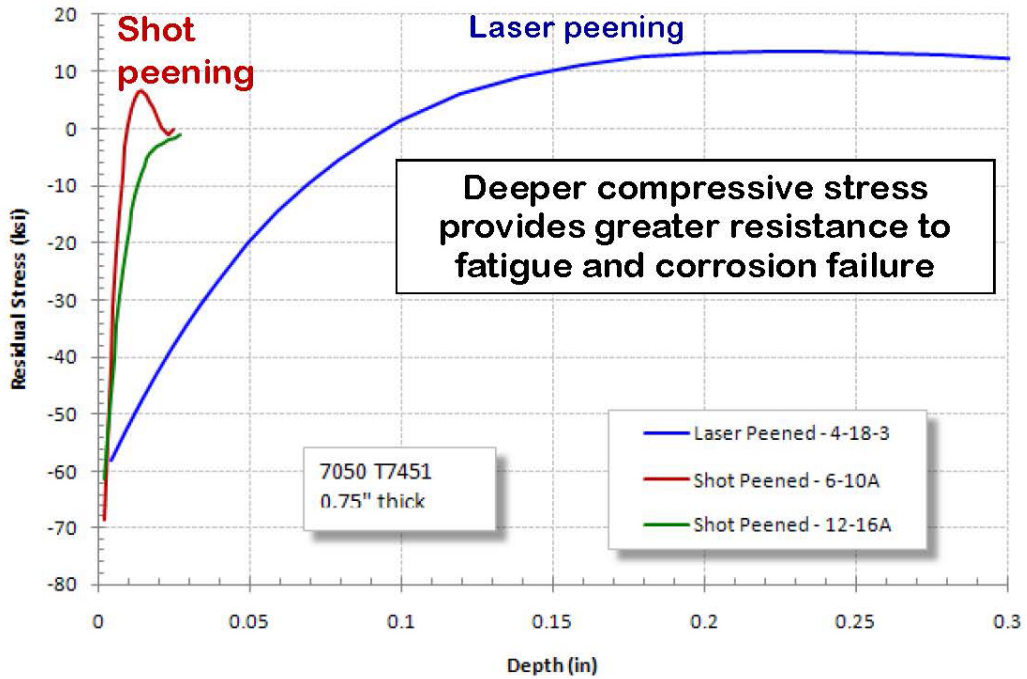
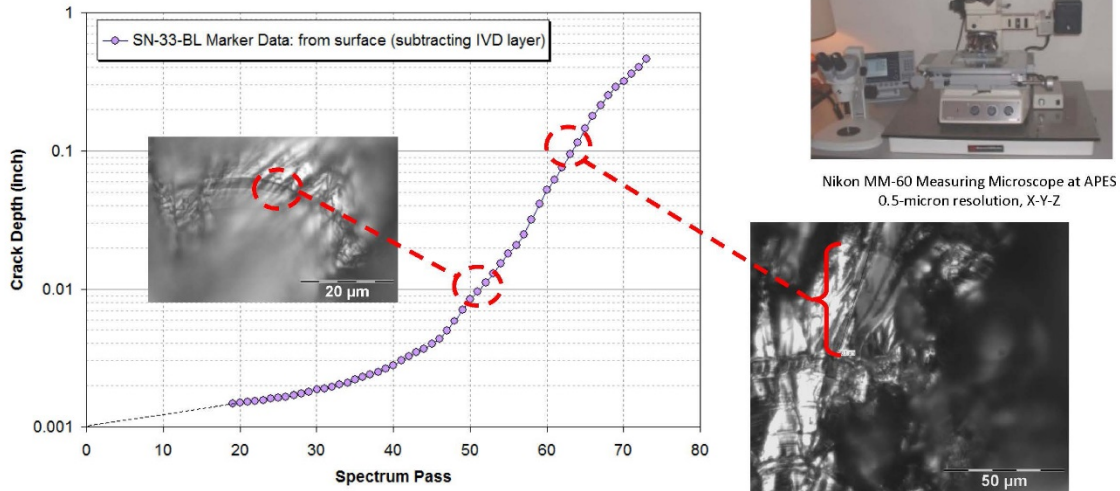


Figure 9.8-29. Effectiveness of Laser Peening

Determining crack growth from marker bands



Marker bands provide permanent record of crack growth on the fracture face

Figure 9.8-30. Determining Crack Growth From Marker Bands

9.8.8. Verification of Analytical Methodology to Minimize Inspection Burdens and to Utilize Full Benefits of Residual Stress Life Enhancement Technique

Hoegmei Cai, Jeffrey Bunch, LeAnn Palin and Mark Walker, The Boeing Company – Defense, Space & Security; Wirt Garcia, F-22 SPO

For fleet support, it is essential to have a reliable and accurate analytical crack growth prediction so that flight safety can be achieved with lower cost by minimizing the number of required inspections. In this technical activity, a new analytical methodology to predict crack growth for complex structure at baseline condition as well as with residual stress life enhancement is developed and verified by test data obtained from a major test program to validated life enhancement benefit of residual stresses. The verification is done progressively, first on a well-studied simple coupon (Figure 9.8-31), then on lug elements (Figure 9.8-32) representing a wing attach lug, and finally on full-scale components (Figure 9.8-33). The analytical predictions correlate well with the test data from the baseline condition as well as with Laser Shock Peening (LSP) induced residual stress field. Data will be presented that clearly shows that the current methods of using weight functions and stress intensity libraries is very conservative when assessing complex geometries. The effect of this conservatism is to add inspection burden and cost onto the aircraft operator. With this confidence, the method is used to predict the damage tolerance lives at the lug fillets of all the F-22 forward boom production frames, including the predicted benefit of LSP in these areas which is 5+ times in terms of damage tolerance lives (Figure 9.8-34). The new analysis methodology is used to update the F-22 Force Structure Maintenance Plan (FSMP) and the improved life predictions will provide significant relief on the inspection burden for the fleet.

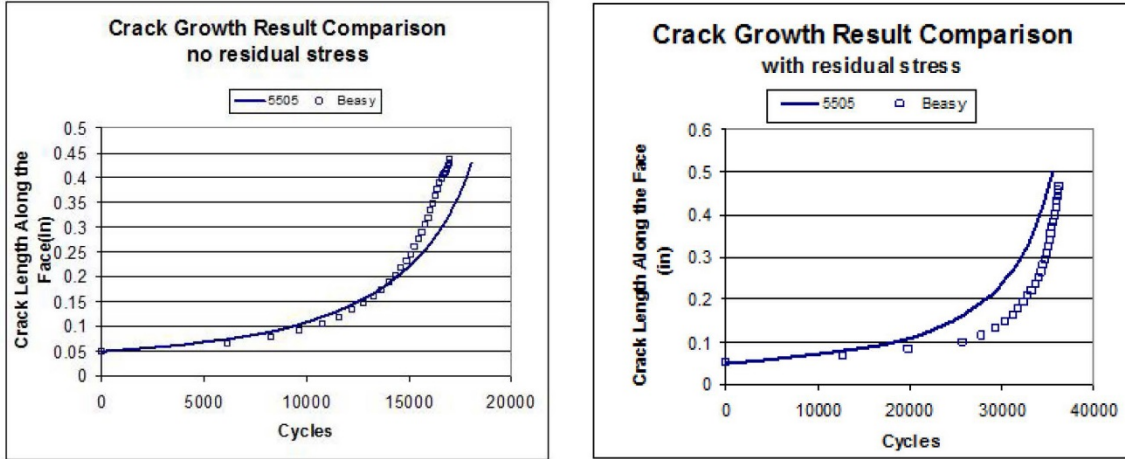


Figure 9.8-31. Verification of Methodology for Standard Tensile Coupon

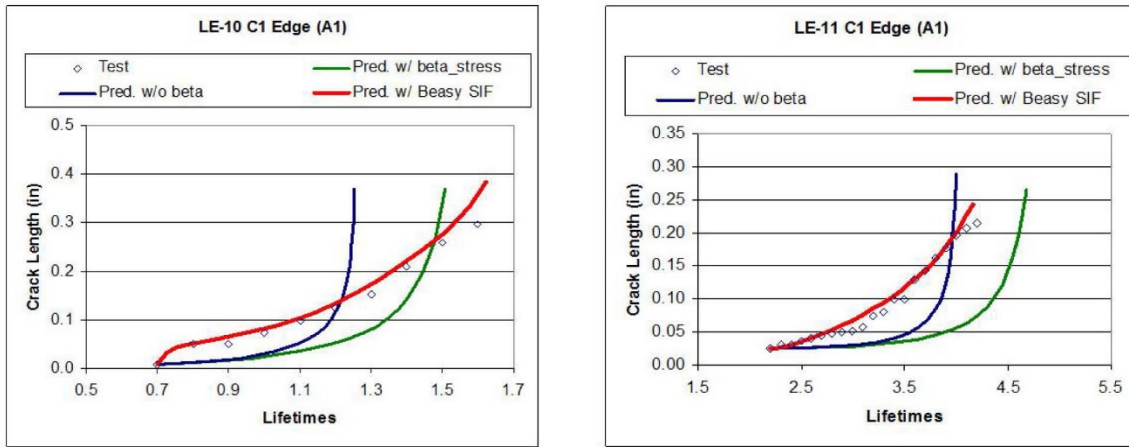


Figure 9.8-32. Verification of Methodology for Lug Element

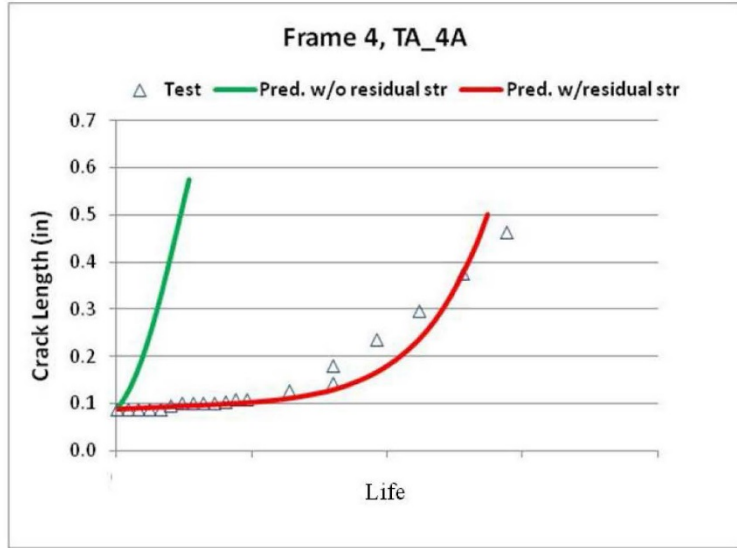
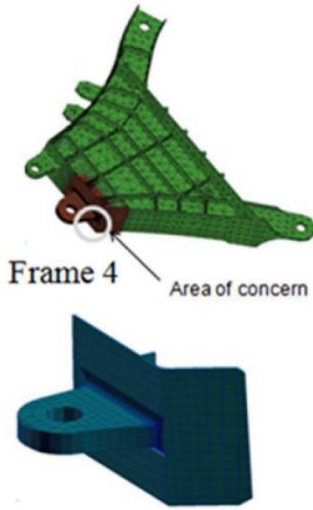


Figure 9.8-33. Verification of Methodology for Full-Scale Component

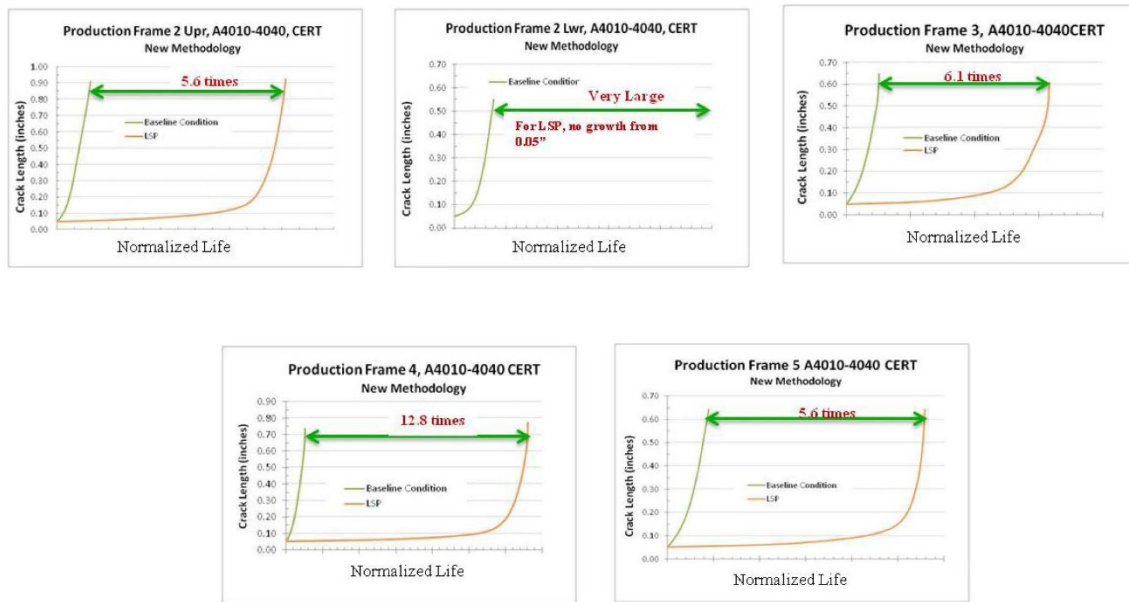


Figure 9.8-34. Benefits of LSP Induced Residual Stress

9.8.9. Simulation of Crack Growth at Cold-Worked Holes

Matthew Watkins and Ricardo Actis, Engineering Software Research & Development, Inc.; Scott Prost-Domasky, APES, Inc.; Robert Pilarczyk, USAF A10 ASIP

Cold working is a commonly used approach to increase the fatigue life of aircraft structural components. By inducing a circumferential compressive layer of residual stress around a cold-worked hole, crack growth is slowed. Experiments show that primary cracks tend to preferentially evolve at the mandrel entrance side of the hole as a result of the variation in the residual stress field, then grow more

quickly away from the hole, radially, than up the hole bore. Since the mandrel entrance face tends to be more difficult to inspect than the exit face, cracks may grow to become critical before they are detectable. To support the development of inspection intervals that are not overly conservative, a mathematical model for simulating crack growth at a cold-worked hole was developed and implemented based on input geometry, material properties, and residual stresses from cold working (Figures 9.8-35 and 9.8-36). The model assumes that the crack grows in a single plane radially away from the hole, but makes no other assumptions about the shape of the crack front to allow complex crack shapes to develop. Validation experiments were performed to assess the predictive capability of the model and simulation predictions compare favorably to experimental data (Figures 9.8-37 and 9.8-38). The procedures of verification, validation and uncertainty quantification (VVUQ) were followed during the development of the model and its usage in prediction. Additionally, the development of such a mathematical model allows for low-cost sensitivity simulations for assessing the influence of input parameters on the fatigue life prediction. It is well known that experimental fatigue lives can vary significantly between test specimens. The model could be used to simulate the effect of variation in each input parameter to quantify expected variation in fatigue life. For example, the model was used in this project to quantify how small variations in residual stress can cause substantial variations in predicted fatigue life, demonstrating how an accurate determination of residual stress and its uncertainty is critical for prediction (Figure 9.8-39). This work was performed in support of the project Integrating Residual Stress Analysis of Critical Fastener Holes into USAF Depot Maintenance (Rapid Innovation Fund - RIF - program AFRL-PK-11-0001).

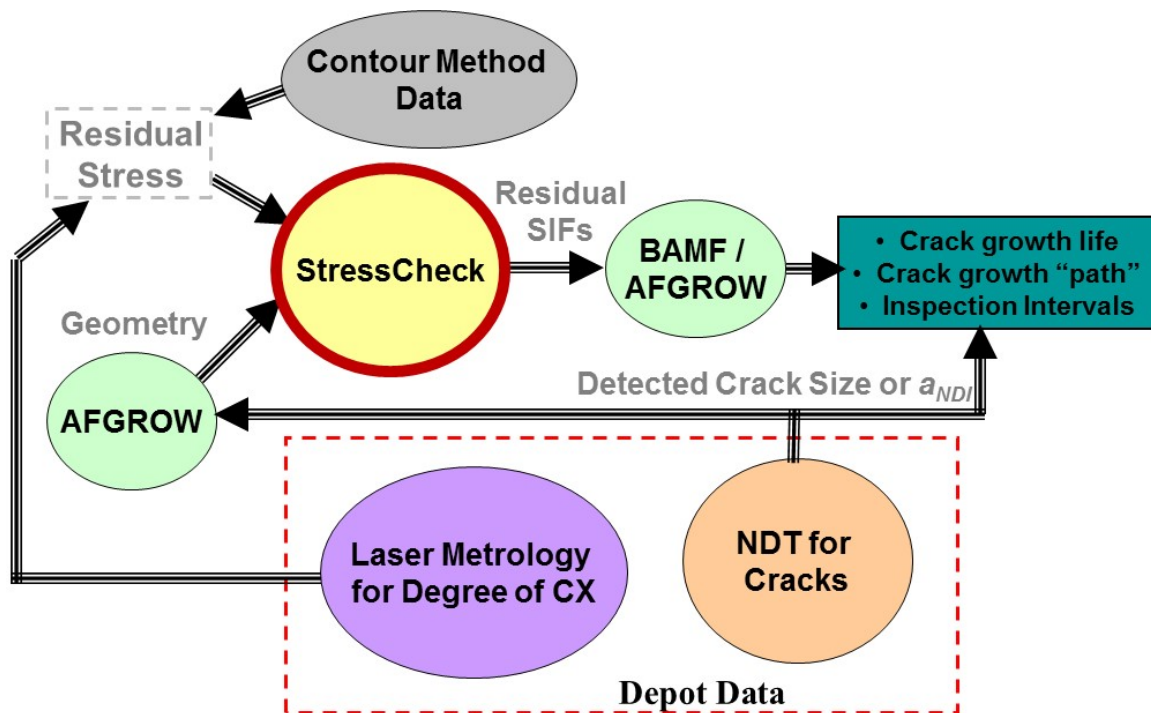


Figure 9.8-35. Integrated Package

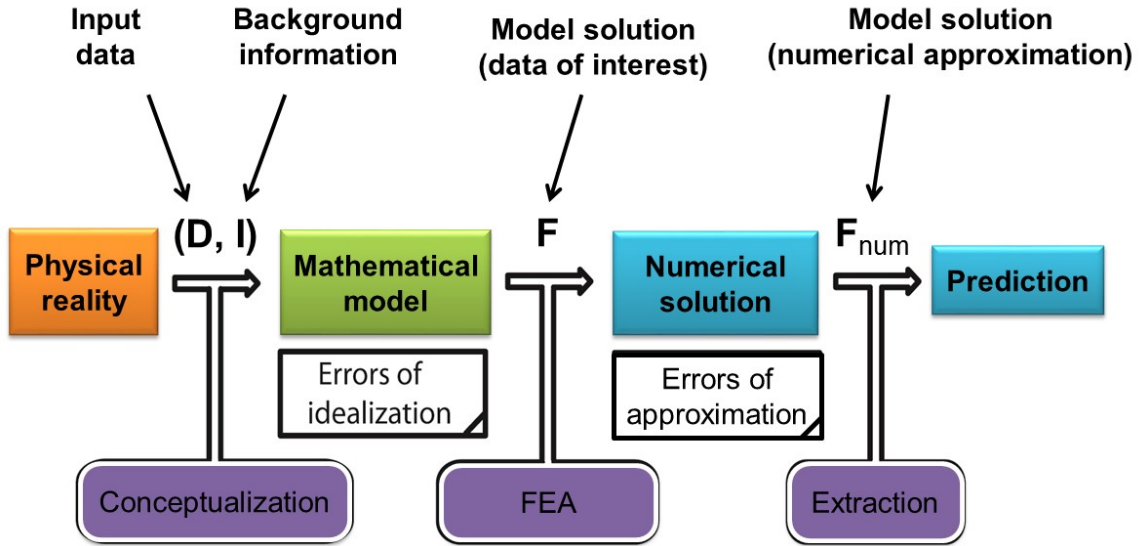


Figure 9.8-36. Simulation

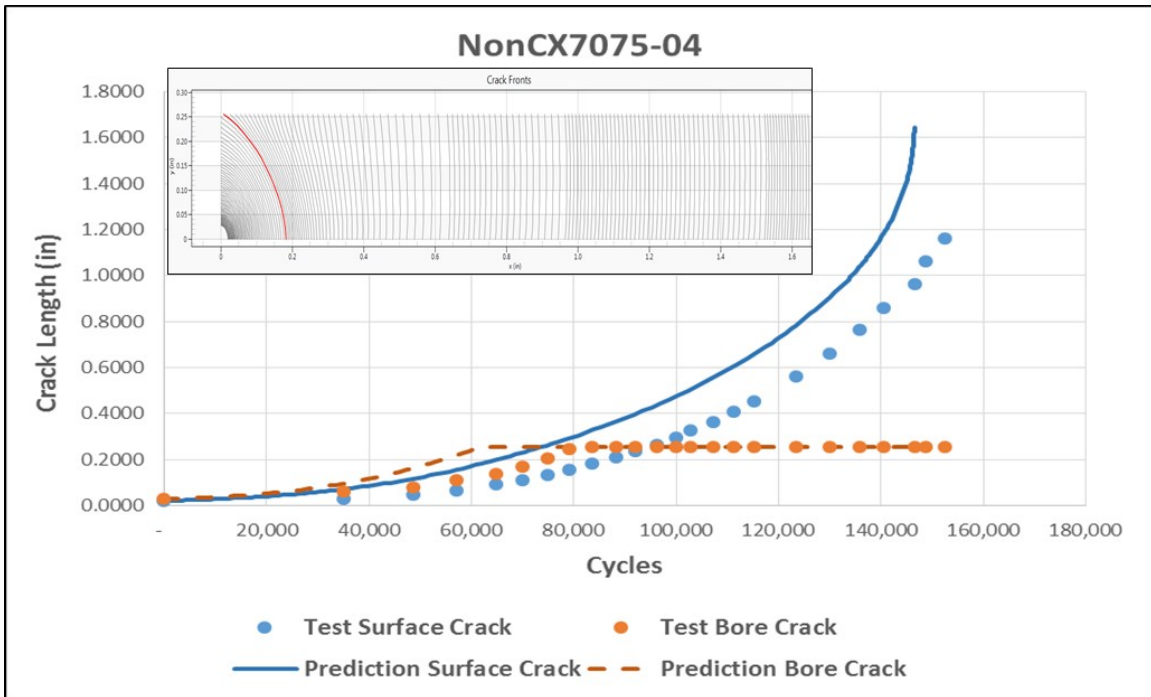


Figure 9.8-37. Experimental Comparisons: No RS (Not Cold Worked)

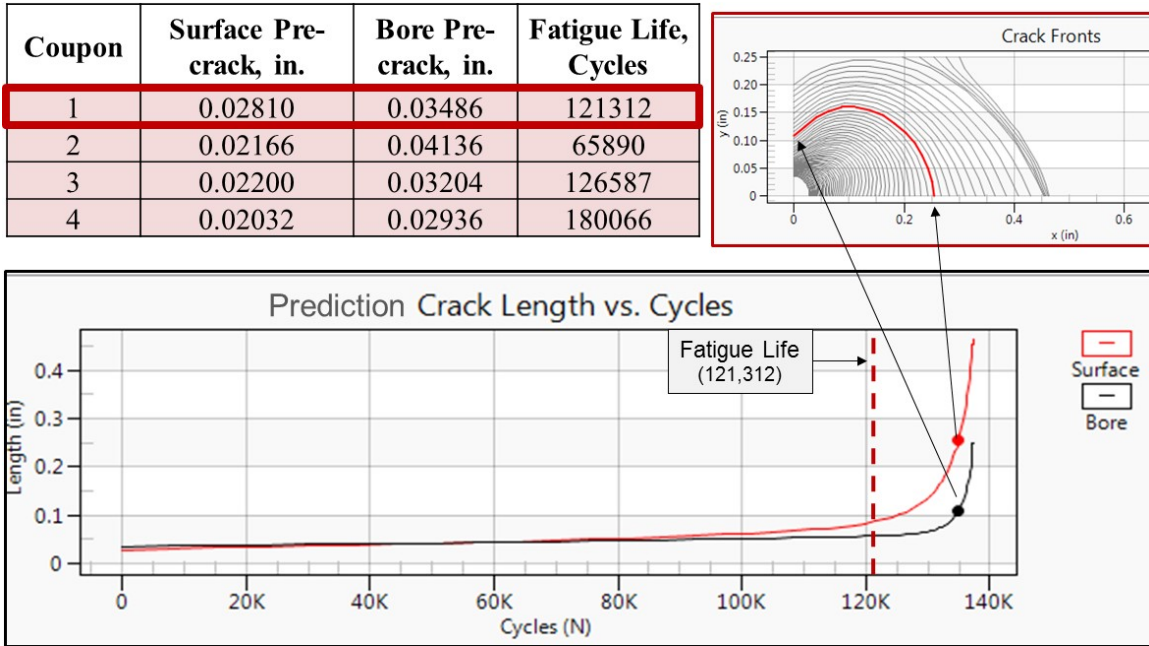


Figure 9.8-38. Experimental Comparisons: Cold-Worked & Pre-Cracked

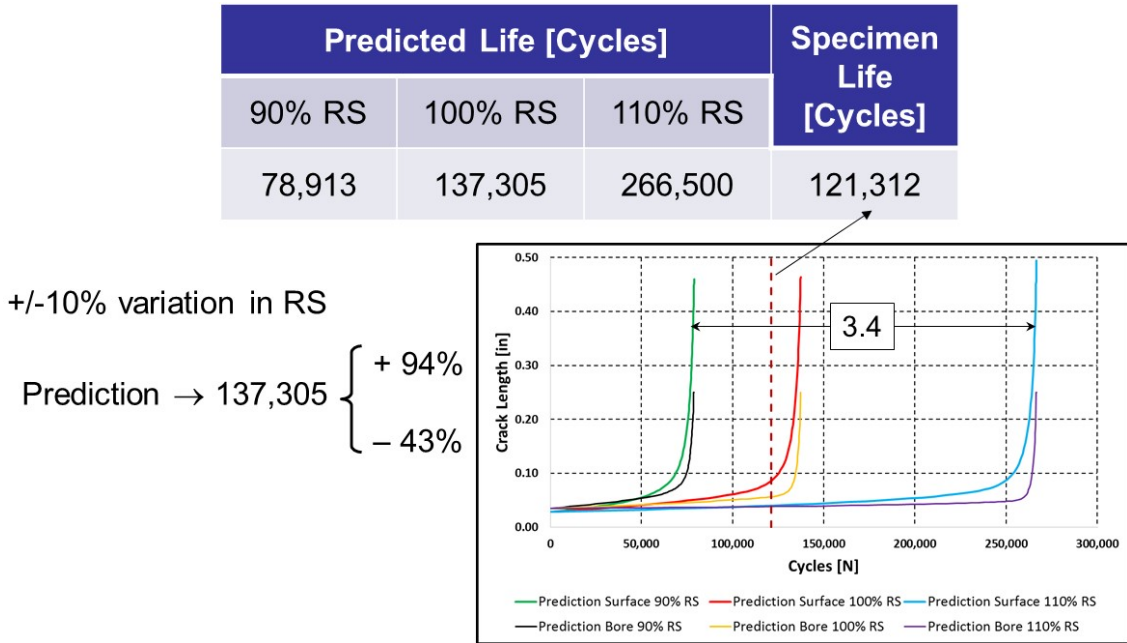


Figure 9.8-39. Experimental Comparisons: Sensitivity to RS

9.8.10. Integrating Residual Stress Analysis of Critical Fastener Holes into USAF Depot Maintenance

Matt Watkins and Ricardo Actis, ESRD, Inc.

Current damage tolerant analysis methods do not capture the beneficial effects of residual stress at cold worked holes, leading to overly conservative estimates of life and therefore unnecessarily short inspection intervals. The goal of this project was to incorporate residual stress into structural life assessments to decrease the burden of requirement maintenance, while mitigating risk with advanced quality control and inspection procedures. The United States Air Force (USAF) was expected to benefit by reduced inspection burden, increased asset availability, and reduced inspection cost for the A-10, F-16, and T-38 Aircraft Structural Integrity Programs, although the technology is applicable to any aircraft in any service with cold worked holes. Analytical Processes / Engineered Solutions (AP/ES), Inc. was the prime contractor for the program. Engineering Software Research & Development (ESRD), Inc. was a subcontractor.

ESRD's technical work on the project included three main contributions:

1. The industry-leading finite element analysis (FEA) software StressCheck was enhanced to provide efficient calculation of stress intensity factors with residual stress for arbitrarily-shaped cracks. Figure 9.8-40 shows a crack at a cold worked hole with the residual stress distribution before the crack was inserted, while Figure 9.8-41 shows examples of the arbitrarily-shaped crack fronts resulting from the load combination of residual stresses and service loads for which stress intensity factors are computed.

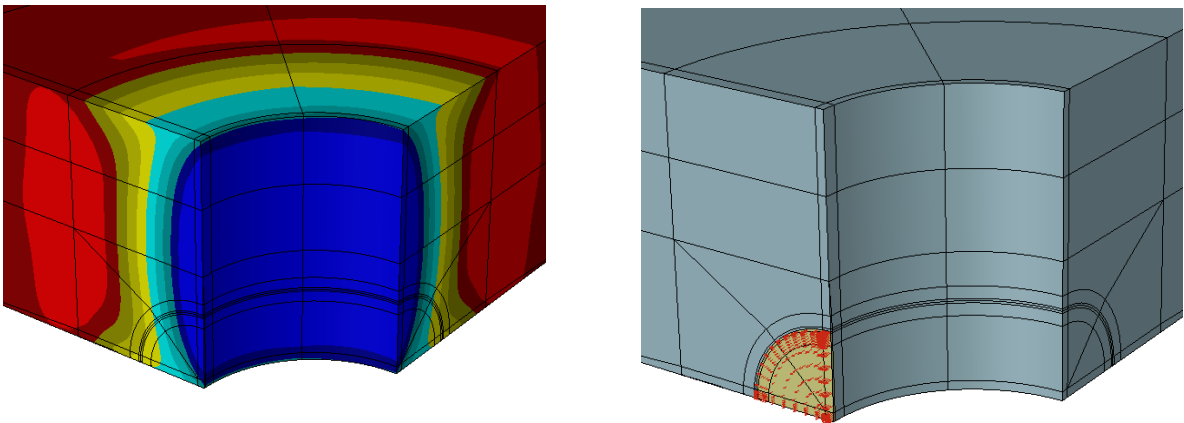


Figure 9.8-40. Residual Stress Distribution at a Cold Worked Hole (Left). Corner crack (Yellow Region) at the Same Cold Worked Hole for Computation of Stress Intensity Factors (Right)

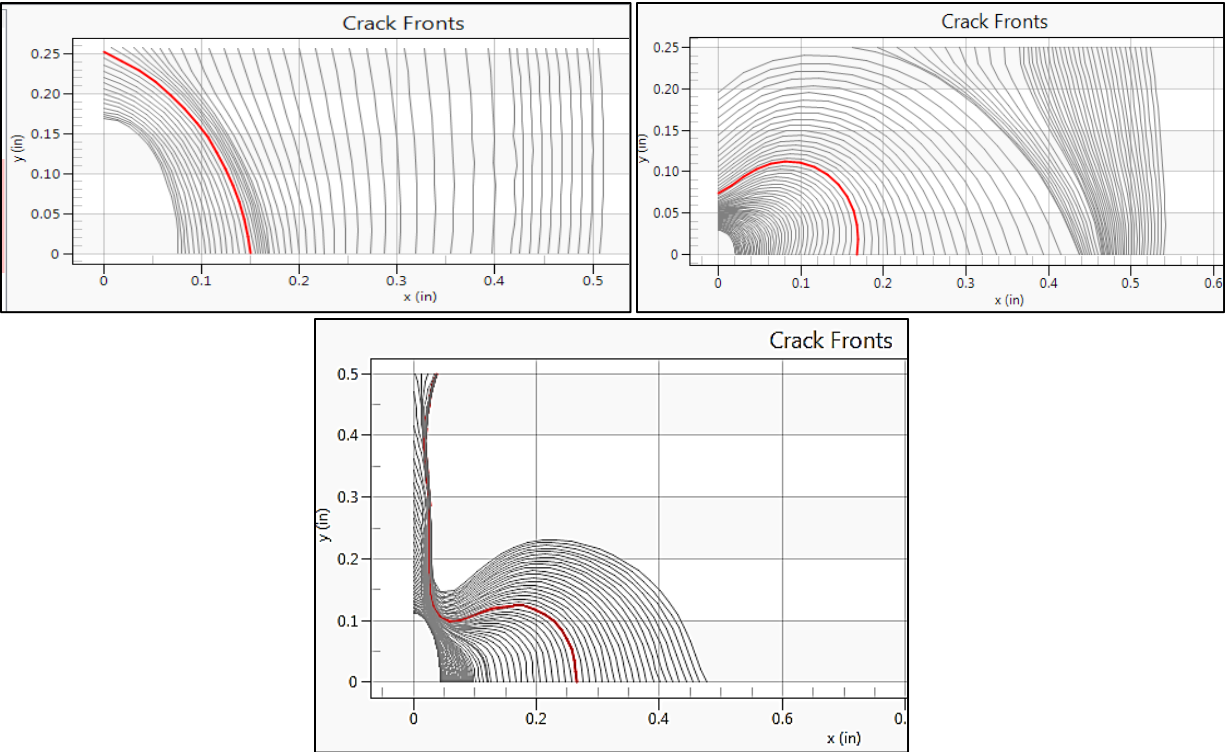


Figure 9.8-41. Example Plots of Simulated Cracks as They Grow Away from a Cold Expanded Hole. The Different Crack Shapes are Produced by Differences in the Residual Stress Distribution and the Applied Remote Mechanical Loading

2. A database was developed to store residual stress distributions at cold worked holes. Each residual stress distribution is tied to geometric and material parameters (hole diameter, edge distance, thickness, percent cold work, etc.) within the database, and a multi-dimensional interpolator was implemented to compute new residual stress distributions based on interpolations of existing data (Figure 9.8-42). The database design makes it possible to be populated by the end-user with public or proprietary data.

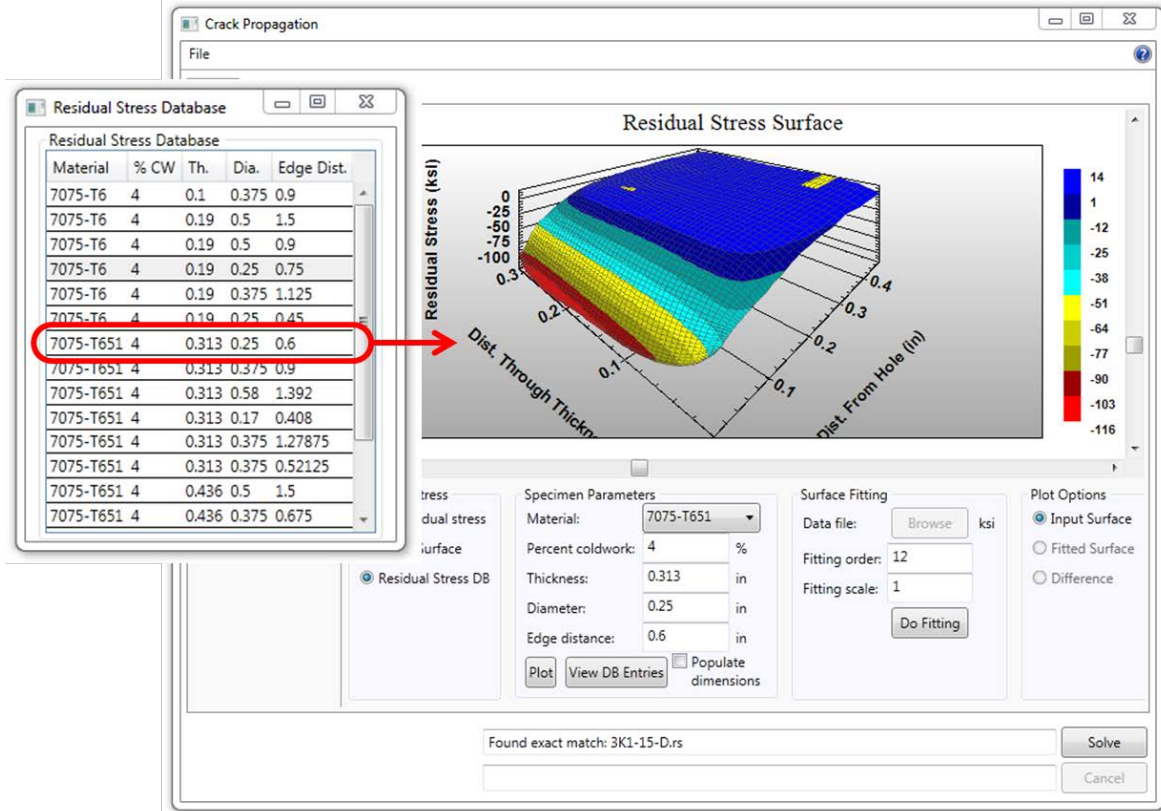


Figure 9.8-42. Residual Stress Distribution (Plotted, Center) Selected from Entries in the Residual Stress Database (Left)

- A crack propagation software tool was developed to simulate 3D crack growth through a residual stress field at a cold worked hole for a given spectrum loading. The cracks in such simulations begin as corner cracks and propagate to become through-cracks until final failure. The shape of the crack is determined by the software based on the values of the stress intensity factors and R ratio along the front as it grows. Good comparisons were observed between predicted crack shapes and experimentally determined crack shapes. Figure 9.8-41 shows examples of typical crack shapes predicted by the software tool.

References

- Actis, R., Watkins, M., Prost-Domasky, S., Hodges, J. "Computation of SIFs for Cracks in Cold-Worked Holes". ASIP 2013 Conference Presentation.
- Watkins, M., Actis, R., Prost-Domasky, S., Pilarczyk, R. "Prediction of Fatigue Crack Propagation from Cold-Expanded Holes". ASIP 2014 Conference Presentation.
- For information about the residual stress database, contact Hill Air Force base, A10-ASIP, Layton, Utah (robert.pilarczyk@us.af.mil)

9.8.11. Shot Peen Residual Stress Redistribution During Mechanical Loading

Raji John, USAF Research Laboratory – Materials and Manufacturing Directorate

Shot peening is a well-established surface treatment process that imparts large compressive residual stresses onto the surface and at shallow depths to retard initiation and growth of fatigue cracks. The plastic deformation developed during surface treatment sets up a constraint that retains compressive stresses on the surface balanced by tensile residual stresses in the interior. However, component service histories that produce subsequent plastic deformation may redistribute these residual stresses. In most engineering components, this additional plastic deformation is localized to stress concentration sites such as holes, notches, and fillets. In the case of gross plastic deformation where the entire cross section experiences material yielding, the residual stress profile may redistribute resulting in tensile stresses on the outside surface balanced by compression in the interior.

A series of experiments were combined with models to explain the redistribution in residual stress depth profiles subject to applied stresses producing gross plastic strains in shot peened laboratory specimens [1]. The predictions were made using a coupled creep-plasticity model that incorporates plastic strain and yield surface state variables [2]. Tensile load-unload and fatigue tests on shot peened IN100 were completed at room and elevated temperature. X-ray diffraction was used to measure the residual stress and cold work (plastic strain) profiles after mechanical loading. The modeling approach, which requires both the residual stress and plastic strain depth profiles were validated and shown to capture the residual stress profile after loading for room and elevated temperature mechanical tests. The experimental results and predictions reveal that for uniform gage sections with large applied stresses, or plastic strains, the residual stress profile can be redistributed leaving tensile stress on the surface after unloading in IN100, pure nickel, and pure copper, Figure 9.8-43. However, in the case of a notched geometry with similar applied stresses, compressive surface residual stresses remain at the notch after unloading, Figure 9.8-44. As a result, these retained compressive surface residual stresses will extend life by retarding initiation and growth of fatigue cracks.

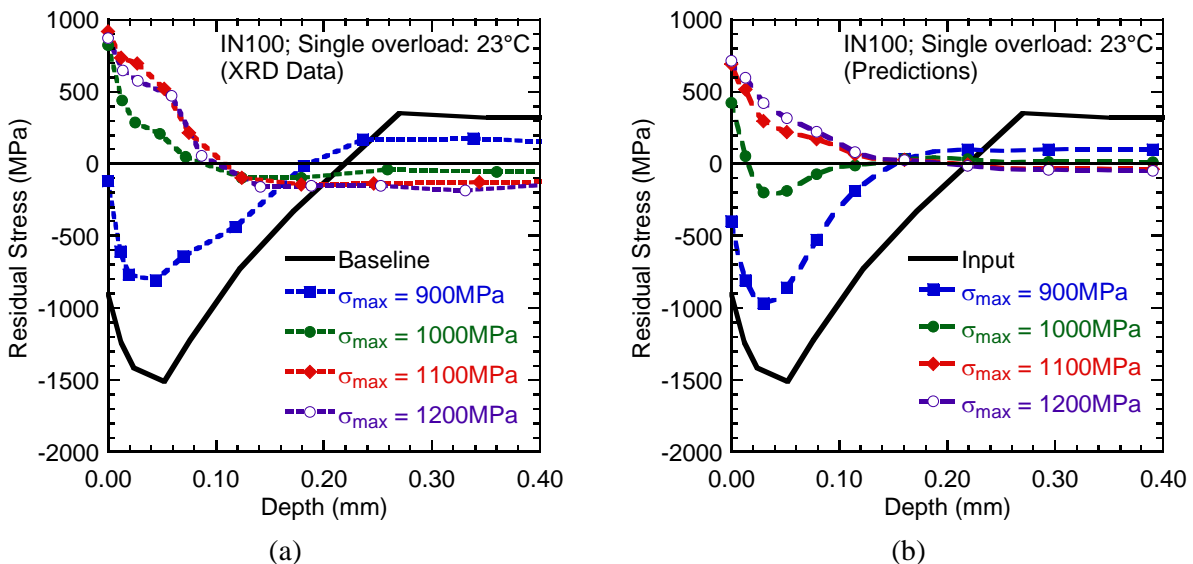


Figure 9.8-43. Effect of Monotonic Overload on Residual Stress Depth Profile in Shot Peened IN100 Flat Dogbone Specimens at 23°C: (a) Measured Depth Profiles From X-Ray Diffraction (b) Model Predictions

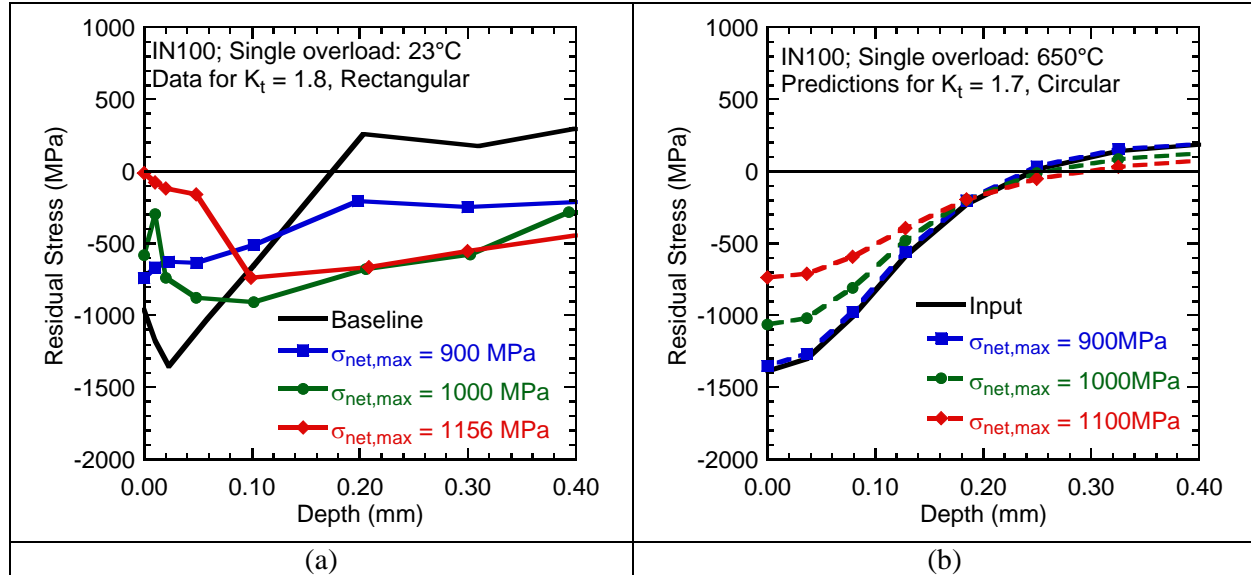


Figure 9.8-44. Residual Stress Profiles in Notched Specimen Geometry with Shot Peened Surface Treatment in IN100 650°C for Different Stress Levels Above the Yield Strength: (a) Data From a Rectangular Notched Specimen and (b) Predictions for a Circular Notched Specimen. Note: Depth=0 Corresponds to Base of the Notch

References

- [1] Buchanan, D.J. and John, R., "Residual Stress Redistribution in Shot Peened Samples Subject to Mechanical Loading," *Materials Science and Engineering A*, Vol. 615A, pp. 70-78, 2014.
- [2] Buchanan, D.J., John, R., and Brockman, R.A., "Relaxation of Shot-Peened Residual Stresses Under Creep Loading," *Journal of Engineering Materials and Technology*, ASME, Vol. 131, 031008-1-10, July 2009.

9.8.12. Modeling 3D Fatigue Crack Growth in Residual Stress Fields

Sharon Mellings, John Baynham, and Thomas Curtin, Computational Mechanics International, Inc.

Residual stresses commonly occur during surface treatment processes in aircraft structures (i.e., laser shot peening, cold working, etc.). These stresses alter mechanical properties and the intrinsic fatigue crack growth characteristics of the material. While many of these processes introduce beneficial compressive residual stresses, which impede the initiation and growth of cracks, they also may cause material and component variability when not well controlled. The BEASY Fatigue Crack Growth modeling system is routinely being used to investigate fracture behavior in residual stress fields.

In order to obtain accurate results it is also critically important that the residual stress field be precisely mapped onto the structural component. Recent work, by others, has shown that there has been good agreement between the mechanical residual stress distributions predicted by 3D elastic-plastic finite element analysis and the stresses measured using an experimental technique known as the contour method. The BEASY dual boundary element method (DBEM), used to simulate a crack in a solid body, has been enhanced to accept these residual stress fields as crack surface loading. As a result it is now possible to combine both the remote load and residual stress load in a single fatigue crack growth simulation (Figures 9.8-45 through 9.8-49).

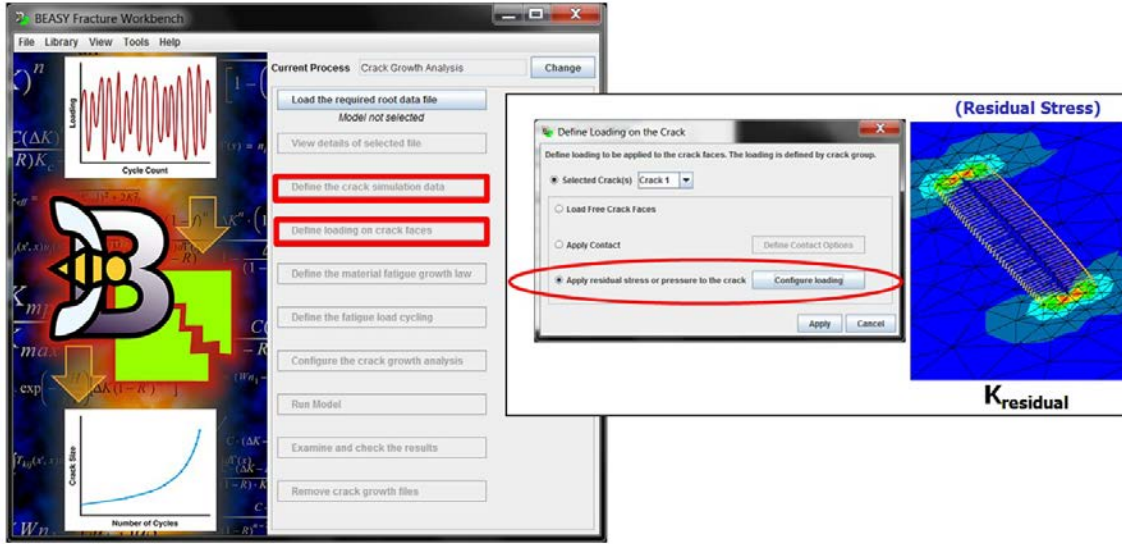


Figure 9.8-45. Applying Residual Stress Fields From Non-Linear FE Analysis to Cracks in 3D Structures Using BEASY's DBEM

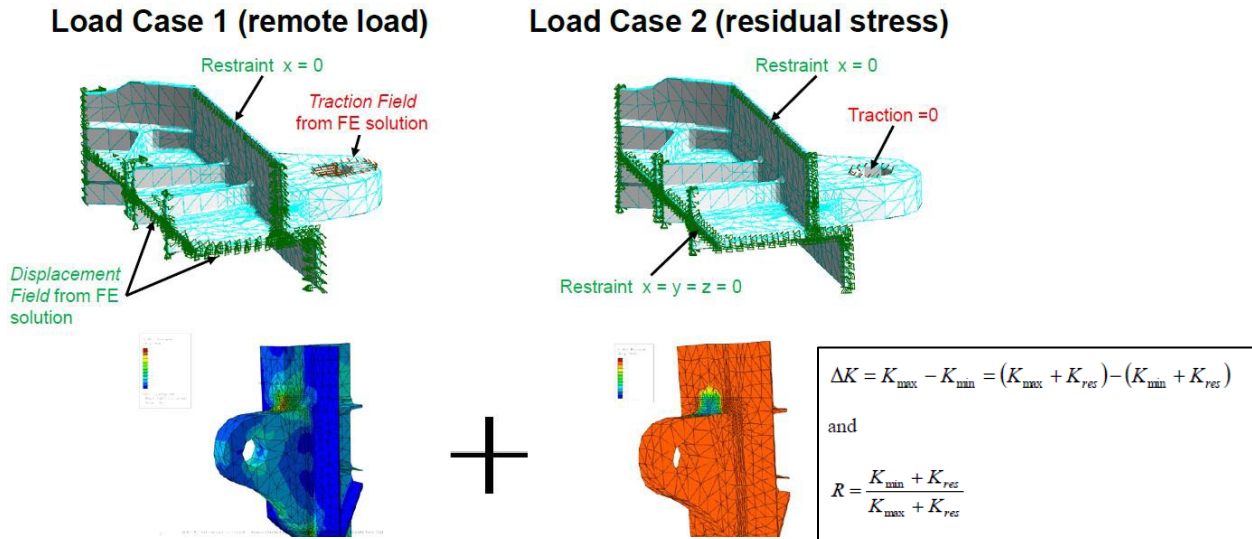


Figure 9.8-46. BEASY Model Showing Load Superposition Cases Used to Compute Stress Intensity Factors

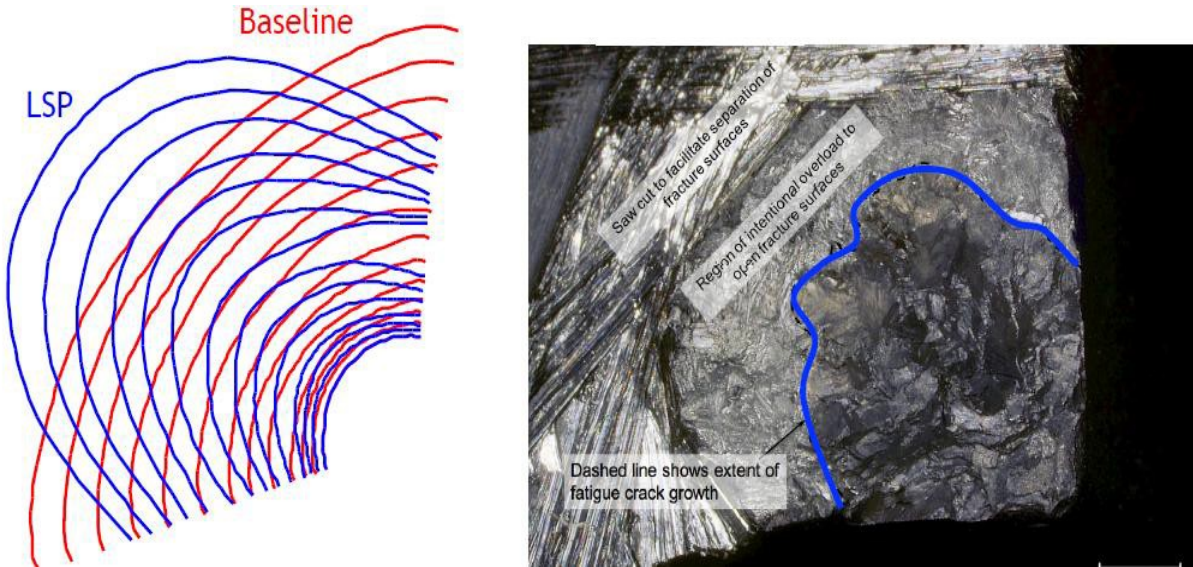


Figure 9.8-47. Comparison of BEASY Predicted Crack Front Evolution (Blue Line - Laser Shot Peening) with Flaw Shape in Structural Frame Specimen

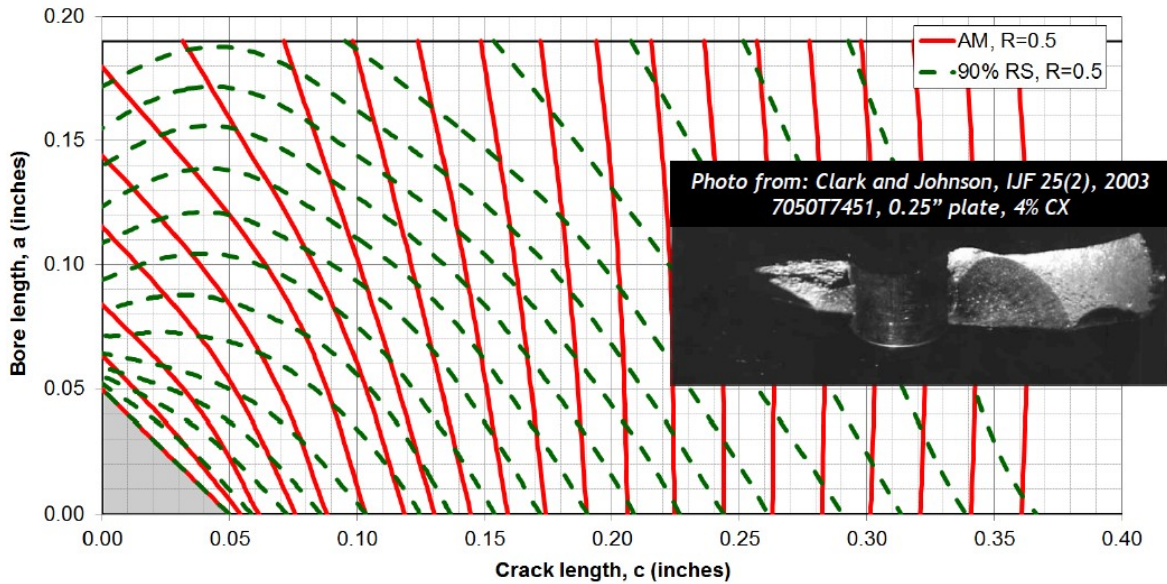


Figure 9.8-48. Predicted Crack Shape Evolution for Corner Crack in a Cold-Worked Hole Test Specimen (Red Line - Baseline, Dotted Green Line - Residual Stress)

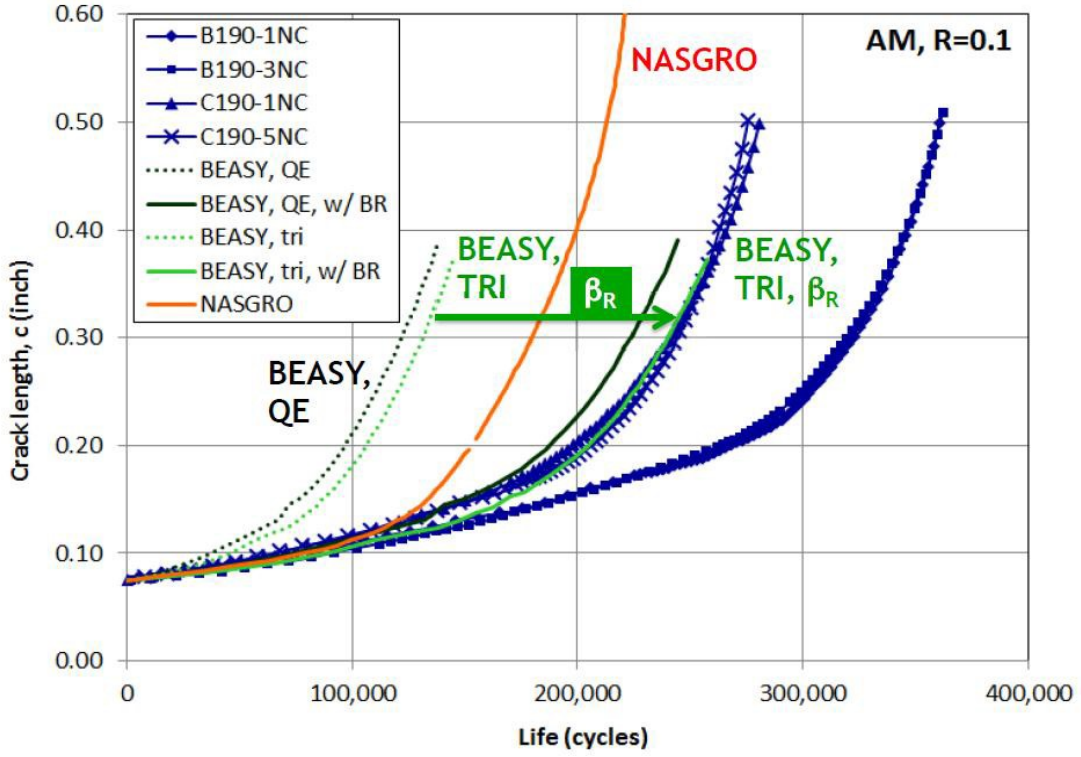


Figure 9.8-49. Comparison of Experimental and Predicted Crack Growth History for Cold-Worked Hole Test Specimen

9.9. REPAIR CONCEPTS

9.9.1. Quality Assurance and Bondline Strain Measurement of Patch Repairs Using Fiber Optic Strain Sensors and Digital Image Correlation

Waruna Seneviratne, Naman Garg, Upul Palliyaguru, and Alex Sang, Wichita State University - NIAR

Composite patch repairs provide several advantages over bolted repairs for composite structures. Some of the key advantages include introduction of minimal stress concentrations into the cracked/damaged structure, minimal effects on aerodynamics due to the absence of fasteners, ability to achieve targeted stiffness with thinner patch compared to metallic patches, and the ability to conform to complex contours. However, the quality assurance of composite repair patches is a key requirement to ensure safe operation of repaired structure. The goal of the current study is to evaluate the use of high resolution fiber optic strain/temperature sensing solution to monitor the cure process and the repair integrity as well as long-term performance of the repair patch over its life cycle. Embedded and surface mounted fiber optic temperature sensors (Figure 9.9-1) are used to monitor cure process and the temperature distribution of the composite repair patch in order to ensure optimal cure and as a means of quality assurance. Pulse thermography and through-transmission ultrasonic nondestructive inspection is conducted to evaluate the repair quality. Repair patches are then mechanically loaded in picture-frame shear loading configuration. A high resolution fiber optic strain sensing solution coupled with three dimensional Digital Image Correlation (DIC or photogrammetry) (Figure 9.9-2) are used to evaluate surface and embedded strain of a patch repair on a composite test article. Surface strains are monitored using standard, telecommunications grade optical fiber, DIC, and strain gages. Bondline and interfacial patch layer strains and temperature are exclusively monitored using optical fiber due to its minimally invasive footprint coupled with its high temperature capability, making it a viable candidate for embedding and surviving the adhesive curing process. DIC is a non-contact, optical, three-dimensional deformation measuring system that uses two high-definition cameras to track translation and rotation of the surface details (object characteristics) with sub-pixel accuracy. Surface measurements from the fiber, DIC and strain gage are compared (Figure 9.9-3) and the patch cross-sectional strain profile examined over various load conditions to investigate patch repair quality and integrity, and quantify optical fiber influence on the repair by examining impact on the test article life cycle.

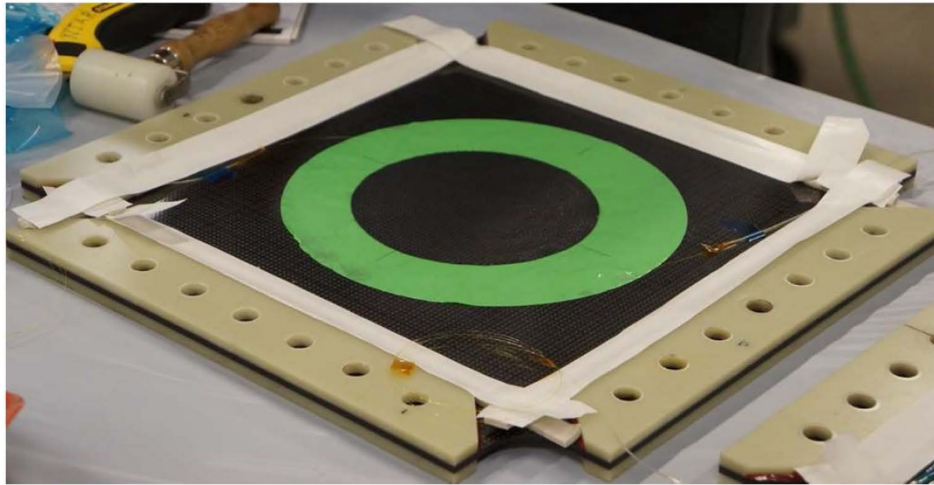
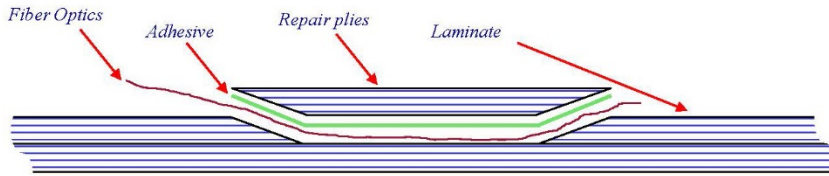


Figure 9.9-1. Embedded Fiber Optics

- Digital Image Correlation (DIC)** is a non-contact, optical, three-dimensional deformation measuring system that uses two high-definition cameras to track translation and rotation of the surface details (object characteristics) with sub-pixel accuracy.

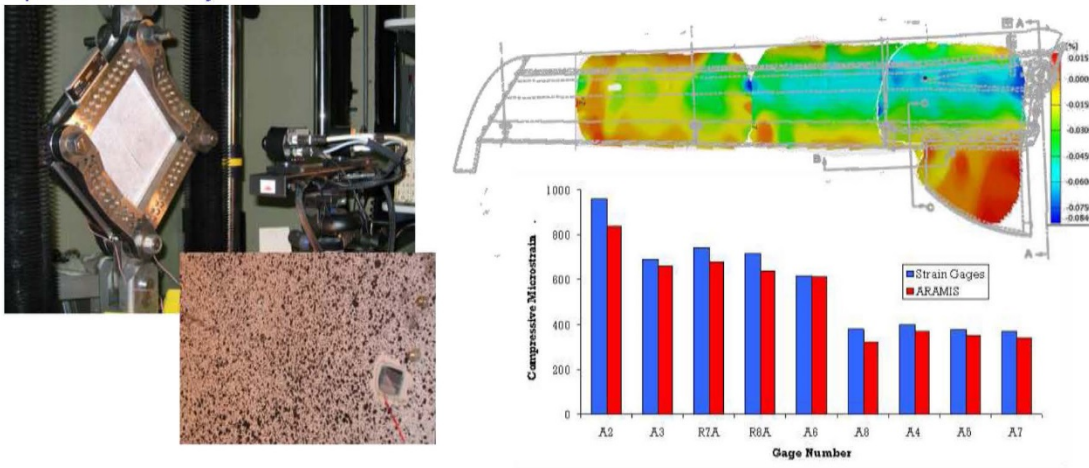


Figure 9.9-2. Digital Image Correlation

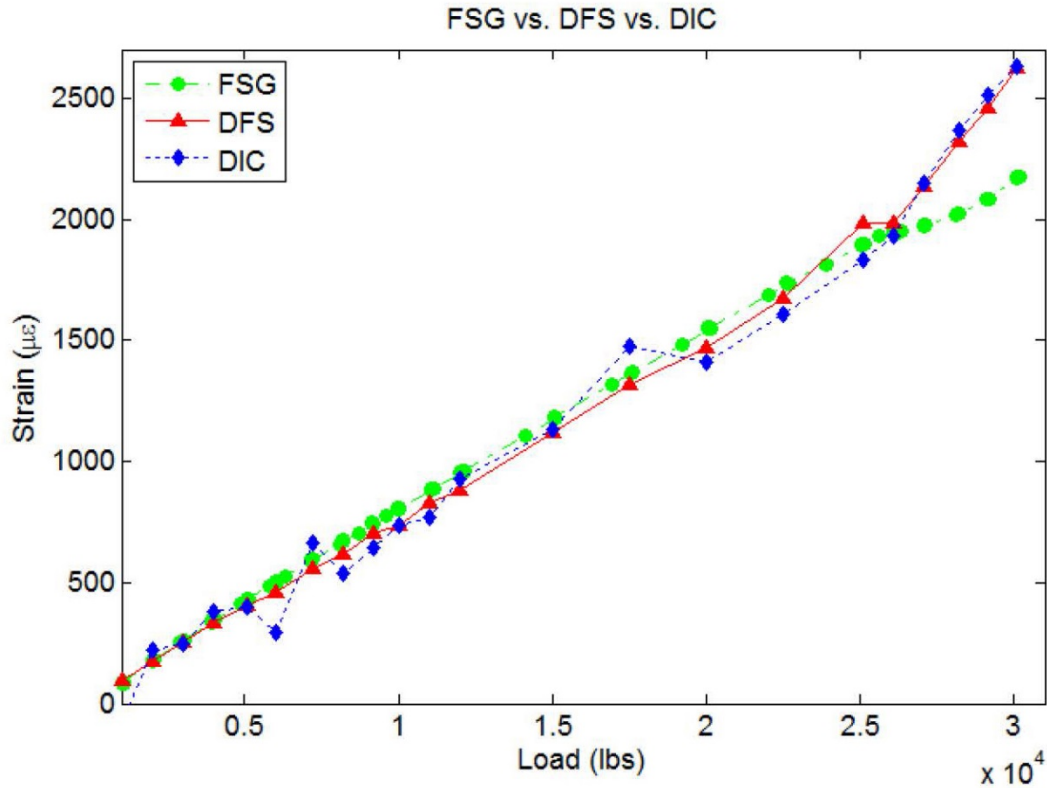


Figure 9.9-3. Strain Gage vs. Fiber vs. DIC

9.9.2. Friction Plug Welding of 2024-T3 Aluminum

Michael Lange, Mercer Engineering Research Center (MERC); Stephen Schwenker, USAF Research Laboratory – Materials and Manufacturing Directorate

A problem currently facing the USAF is the ability to economically repair damaged holes in structural components, such as elongated holes in access panels. Typically, damaged components are either scrapped or inadequately repaired with methods that cannot provide a sufficiently high strength result. Mercer Engineering Research Center was contracted by AFRL to develop a Friction Plug Weld (FPW) process applicable to the repair of aircraft panel assemblies (2024-T3 Aluminum, 0.125" thick) (Figures 9.9-4 and 9.9-5). Friction plug welding was developed by The Welding Institute and later used by NASA for a space shuttle fuel tank application. However, it is not widely used in industry for component repair despite its many benefits. During the FPW process, a plug constructed of material similar to the panel is rapidly spun and lowered into a hole which has been drilled at the damage location. A high axial force is applied to the plug, and held constant after it has stopped spinning, at which point the welding process is complete. Excess material from the plug and panel are then removed to provide a flush surface, equivalent to the original part. The process variables such as plug and hole geometry, spin rate, and axial force can be modified to customize this process to any application. The MERC-developed process makes use of an inertia driven friction push-plug welding machine (Figure 9.9-6), which provides a control loop algorithm to allow for consistent application of the weld procedure. MERC has developed an optimized process through iterative weld trials evaluated by specimen tensile testing (Figures 9.9-7 and 9.9-8) and cross-section microstructure inspections. The test and inspection results indicate that the FPW process results in a high quality weld joint at the plug perimeter, with little degradation of material

properties from the base material. The process resulted in specimens having an average value of 90% of the tensile strength of the baseline (non-welded) material, and highest performing specimens having equivalent tensile strength to the baseline material. The microstructure inspections of polished and etched cross-section samples reveal joints that are free of defects in the welded area. The use of friction plug welding for component repair can result in significant cost savings in the aviation industry, especially in cases of aging aircraft where original tooling for fabricated parts may no longer exist. A friction plug weld repair process has been optimized specifically for 0.125" thick 2024-T3 Aluminum, and is scalable for other combinations of material alloys, thicknesses, and damaged hole diameters.

FPW Process Steps:

- Hole preparation, fixturing
- The plug is spun at a predetermined speed and forced into the hole
- After the rotational motion has stopped, an axial force is applied for a short period of time
- Excess plug material is removed

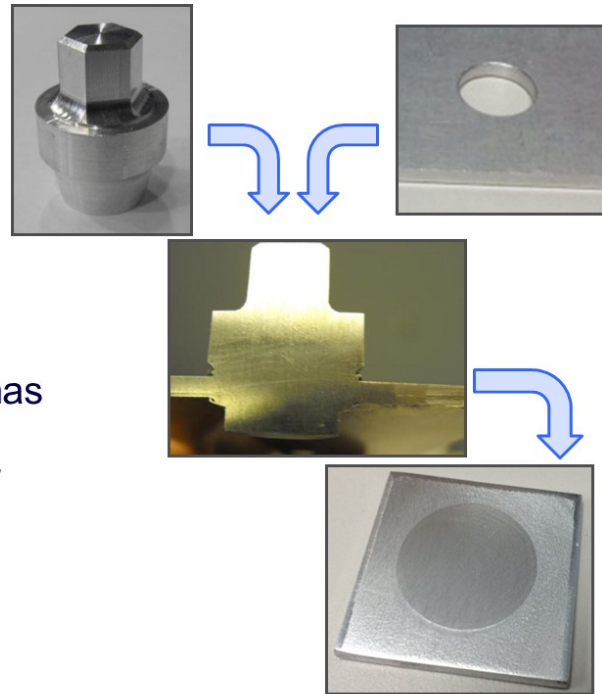
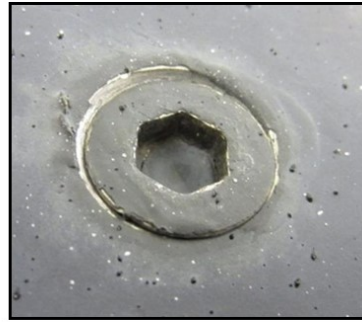


Figure 9.9-4. Friction Plug Welding

- MERC was funded by AFRL to develop a FPW repair process for 1/8" thick 2024-T3 aluminum, using friction plug welding



Damaged Hole

- 11/16" hole size
- Alternate to doubler plate repair methods



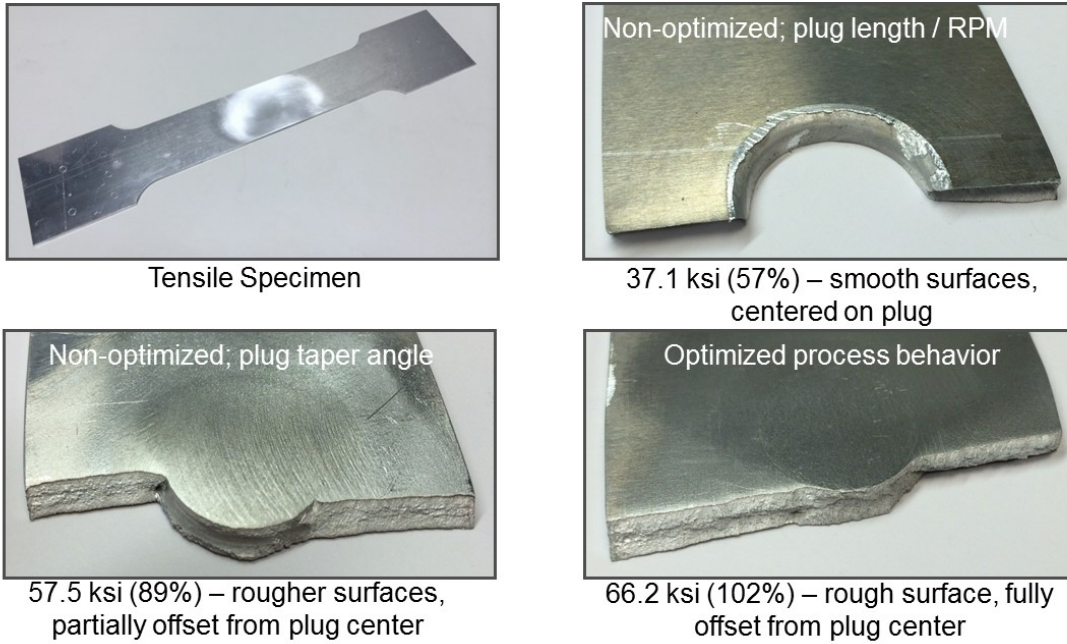
Doubler Plate Repair

Figure 9.9-5. Process Development

- Overhead lift mechanism supporting the weld head
- Hydraulically operated, inertia driven, push-weld machine
- Locks into fixture holding the item to be welded



Figure 9.9-6. Friction Plug Welding Machine



Evaluation of the weld specimens' fracture surface helped to guide the process development.

Figure 9.9-7. Tensile Test Specimens

- Example FPW force vs. deflection plot
 - Depicts a sample with an ultimate strength of 64,200 psi (99.2%)

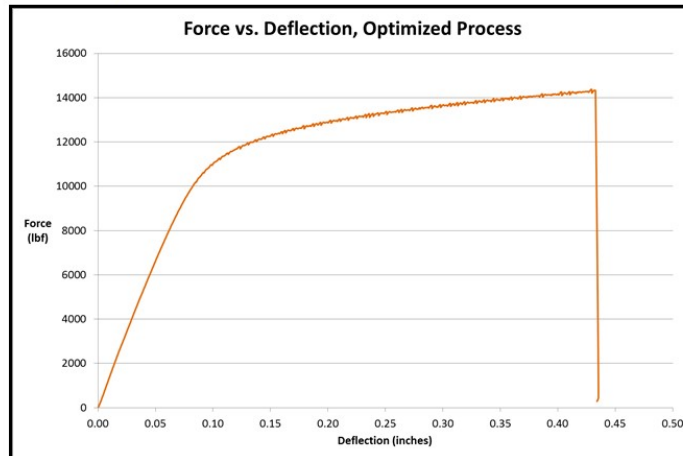


Figure 9.9-8. Tensile Test Results

9.9.3. Fighter Jet Wing Repair and Refurbishment

Christopher Garville, Merex Aircraft Company, Inc.

Life extension and sustainment solutions for aging military aircraft is a rapidly growing and dynamic field. The OEMs for these aircraft had no idea that they would be operating 25, 30 and more years past their intended service life. With advancements in avionics and weapons systems available at a fraction of their original costs, operators are modifying their existing fleets through modernization programs. Flat panel, multi-function displays coupled with solid state electronics provide the operators with systems that boast MTBF (Mean Time Between Failure) rates that are thousands-of-time longer than the vacuum tube systems and steam gauges they replace. Weapon systems available today are not only highly efficient and accurate, but relatively inexpensive considering their price performance. All this exciting equipment with no new cost effective aircraft to deploy it. What's an operator to do? Upgrade the aircraft; add more flight hours to the airframe through life extension solutions. That is what our international customer tasked us to do. Find a solution to the corrosion problem of the wings (Figure 9.9-9) on their F-5 fighter jets (Figure 9.9-10). So, we stepped up to the challenge and developed a cost effective solution to repairing the wing (Figure 9.9-11) and wing components on the aircraft. Using new technologies, we laser-scanned (Figure 9.9-12) the wing assembly, then studied the CAD models to figure out how best to fixture the wing so we could perform the work. We developed, and utility patented, a wing holding fixture (Figure 9.9-13) that secures the complete wing assembly in place so we can remove the wing skins, perform inspections of the wing components; spars, ribs, supports, electrical installations, fuel installations, and hydraulic installations. We remove the fasteners using EDM (Electronic Discharge Machining) technology (Figure 9.9-14). EDM is highly accurate. We are able to cut just the fastener heads off, then push the rest of the fastener through without any damage to the substructure of the wing. And it's fast; our EDM fastener removal takes 8-15 seconds per fastener as opposed to manual drilling time of 2-3 minutes. We incorporate additional advanced technologies using advanced-laser-tracker systems (Figure 9.9-15). The F-5 wing has about 3,000 fasteners. We can laser track every fastener hole in less than two days and locate each hole with incredible accuracy. We build a database that has fastener type and location. During re-assembly, we project the fastener types and locations onto the new replacement wing skins ensuring accurate reassembly of the wing. By incorporating new technologies, we are able to reduce the costs by over four (4) times the cost of a new wing and shorten delivery by factor of five to one. And we haven't stopped looking at other components of the aircraft that we can successfully repair and refurbish. Currently we are rebuilding leading edge flaps, horizontal stabilizers, canopies, and more. Without the aid of the technologies available to us, being able to find cost effective, short-lead-time solutions would not be possible. The key is identifying and matching new technology to life extension and sustainment of these aging platforms.



- ❖ Surface of Upper Skin – material loss at fasteners and on overall surface

- ❖ Material 7075-T651
- ❖ Deep pockets around several fasteners



Figure 9.9-9. Upper-Wing-Skin Corrosion



Figure 9.9-10. F-5 Fight Jet



- ❖ F-5 Wing removed from aircraft
- ❖ Entire fighter jet ready for transport

- ❖ Wing is one piece measuring 25 feet long
- ❖ Removes quickly, 6 attach points
- ❖ Easy to transport



Figure 9.9-11. F-15 One-Piece, Interchangeable Wing

- ❖ Using Laser scanning and tracking, a reference plane is created within the fixture
- ❖ The wing assembly is located precisely in the wing fixture ensuring tracking is performed with wing locked in reference
- ❖ The wing can be 're-located' in the event of accidental movement in the frame

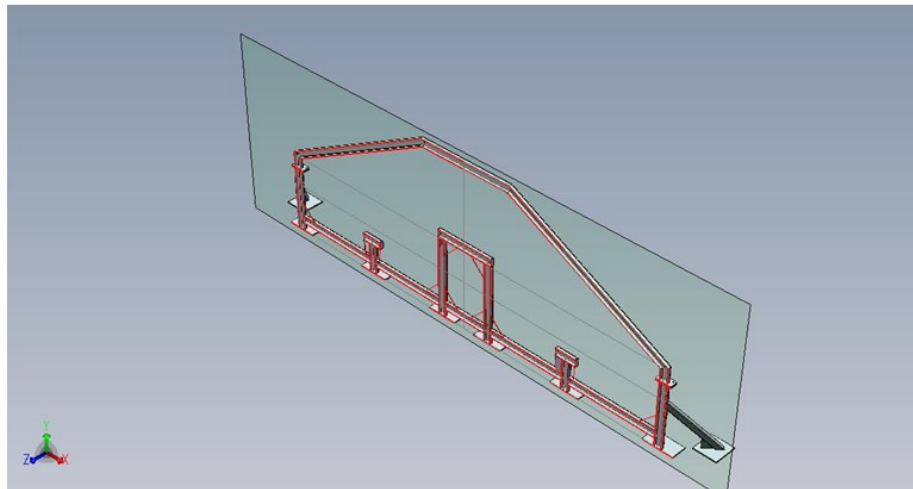


Figure 9.9-12. Laser-Scanned Fixture

❖ Wing Fixture:

- Fixture designed specifically for disassembly and re-assembly of wing assembly
- Provides unencumbered access by technicians
- Attach points secure each Wing Station section preventing any movement of wing frame.
- Dimensions of fixture are held to close tolerances ensuring precise location of wing

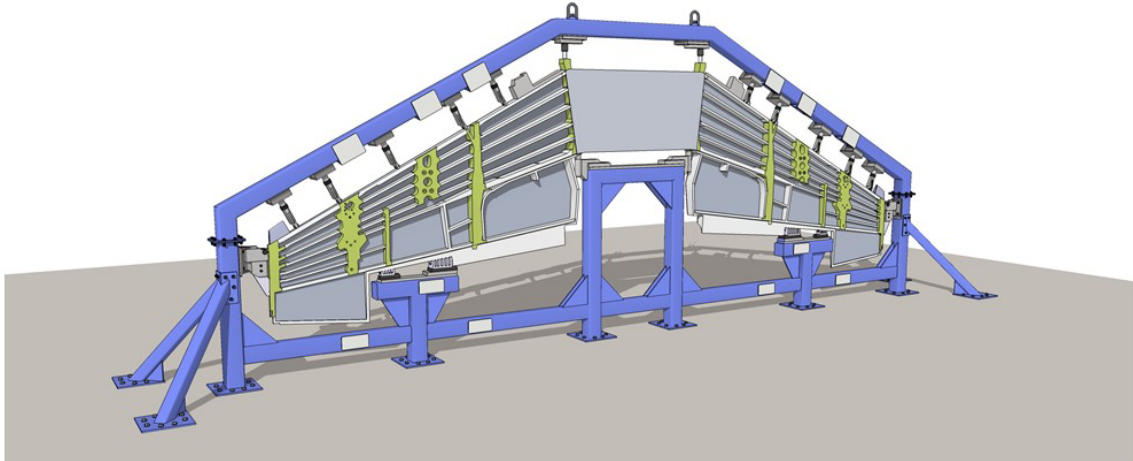


Figure 9.9-13. Wing Fixture

- ❖ Removes fasteners in 8-12 seconds rather than 10-15 minutes
- ❖ More efficient technology reduces technician fatigue
- ❖ No damage to ribs or spars from fastener removal
- ❖ Leaves no FOD or residue

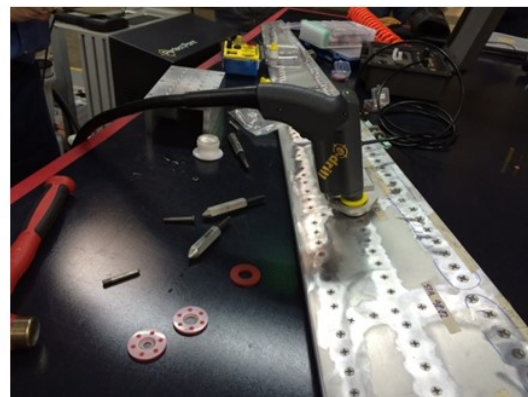


Figure 9.9-14. Edrill-EDM Technology

- ❖ Tracking the wing frame hole locations
- ❖ Captures X, Y, Z positions including fastener hole diameters
- ❖ Over 3,000 fastener laser scanned in 2 days with 2 technicians



Figure 9.9-15. Laser Tracking

9.10. REPLACEMENT CONCEPTS

9.10.1. Material Product Form and Process Substitution Guidelines for Metallic Components

Larry Butkus, USAF Research Laboratory – Materials and Manufacturing Directorate

The need to replace metallic components on USAF aircraft is increasing as the force continues to age, components experience failures, and aircraft reach the end of their service lives. The use or proposed use of different materials, product forms, and processes that were used when many of the USAF's current weapon systems were designed and/or manufactured is being driven by a number of factors including, but not limited to, advances in metallurgy and alloy development, the unavailability of legacy alloys and product forms, environmental concerns, and alternative processes (Figure 9.10-1). Many of the new materials, product forms, and processes present unique challenges when applied to legacy aircraft, and to properly exploit them, their advantages and disadvantages must be understood. Of paramount importance is to ensure that the proposed materials and processes are well characterized for the intended service environment, usage, and duration. In addition, careful consideration of all aspects of integrity and of requirements stated in the USAF integrity program specifications and guidelines related to selection of materials, product forms, and processes is required. To this end, the Air Force Life Cycle Management Center and the Air Force Research Laboratory's Materials & Manufacturing Directorate issued Structures Bulletin EZ-SB-13-001 (Figure 9.10-2), Material, Product Form, and Process Substitution Guidelines for Metallic Components in January 2013 to drive the need for better communications that are fundamental to the aforementioned requirements for proper choice and implementation of new materials and processes. This Structures Bulletin provides guidance to assist USAF and industry engineers in ensuring that proper considerations are made when selecting substitutions for metallic components and in minimizing the potential for unintended negative consequences when making material, product form, and/or process changes, and it applies across the entire life cycle of USAF systems (Figures 9.10-3 through 9.10-5). The technical activity will highlight the origin, development, and key aspects of the guidance provided in EZ-SB-13-001. Case studies will be used to provide realistic examples of the need for and use of this Structures Bulletin (Figure 9.10-6). Feedback is encouraged and will serve as a foundation upon which future improvements of the Structures Bulletin will be based.

- Laser cutting
- Laser stripping
- Titanium substitution
- Cold Spray
- RPA prop shafts
- “Re-manufactured” aileron hinges
- “Home Depot grade” threaded rod
- Non-chrome primer
- ...



Figure 9.10-1. Recent Examples

“Material, Product Form, and Process Substitution Guidelines for Metallic Components”

- Joint effort: AFRL/RX, AFLCMC/EZ, OO-ALC (reviewers)
- Issued in January 2013
 - <https://cs4.eis.afmc.af.mil/sites/1636/ASIP/ASIPDistroA/Forms/AllItems.aspx>
- Purpose
 - Ensure proper considerations are made for substitutions
 - Incorporate best technologies to meet requirements
 - Solicit independent review of proposed technologies
 - Ensure proper/prioritized testing is accomplished promptly
 - Minimize potential for unintended negative consequences
 - Capture and disseminate lessons learned
- Applies to all USAF integrity programs



Figure 9.10-2. Structures Bulletin EZ-SB-13-001

Substitution Type ▶	Same Alloy System, Same Heat Treatment (e.g., 7XXX-TXYZ A for 7ABC-TXYZ A)	Same Alloy System, Different Heat Treatment (e.g., 7XXX-TXYZ A for 7XXX-TABC A)	Different Alloy, Same Base (e.g., 2XXX A for 7XXX A)	Different Base (e.g., Al for Ti)	Different Class (e.g., Composite for Metal)	Hybrid Material (e.g., Metal-Composite Laminate for Metal)
▼Part Type▼						
Safety-of-Flight*	M	H	H	H	NR	NR
Durability Critical	L	M	M	H	H	NR
All Others	L	L	L	M	H	H
KEY	<i>Complexity / Risk</i>					
L	Low					
M	Moderate					
H	High					
NR	NOT RECOMMENDED without extensive testing and AFRL/RX support					

* Includes component types designated as Critical Safety Items (CSI), Safety Critical, and Mission Critical

- Specific Considerations – Material Properties
 - Maintain material properties used in original design & analysis
 - Use minimum set of data necessary to ensure that correct values are used in the design (e.g. A- and B-basis allowables)
 - Use materials that have applicable specifications
 - Use standardized test methods (e.g., ASTM)

Figure 9.10-3. Material Substitution Guidelines

Replacing ▶ ▼With▼	Forging	Extrusion	Machined Plate	Casting	Welded Structure	Built-Up Structure
Forging	L	L	L	L	L	M
Extrusion	M	L	L	M	L	M
Machined Plate	H	H	L	M	M	H
Casting	H	H	H	L	M	H
Welded Structure	H	H	H	H	L	H
Additive Mfg. ²	NR	NR	NR	NR	NR	NR
KEY	<i>Complexity / Risk</i>					
L	Low					
M	Moderate					
H	High					
NR	NOT RECOMMENDED without extensive testing and AFRURX support					

² Additive Manufacturing includes, but is not limited to, laser additive manufacturing, electron beam additive manufacturing, cold spray processes, etc.

• **Specific Considerations**

- Loading Direction & Type
- Residual Stress
- Defects & Inspectability
- Grain Flow
- Geometric Issues



http://www.asinternational.org/online/ASIM/3Dmodel/067886_3d.male.pdf



<http://www.a1-nill/News/Photos.asp?grno=200067504>

Figure 9.10-4. Product Form Substitution Guidelines

Replacing ▶ ▼With▼	Metal Cutting Processes	Metal Removal Processes	Paint Removal	Plating & Coating	Heat Treating	Engineered Residual Stresses	Joining Methods	Proprietary Processes
Alternative Methods ²	H	H	H	H	H	H	H	H
KEY	<i>Complexity / Risk</i>							
L	Low							
M	Moderate							
H	High							
NR	NOT RECOMMENDED without extensive testing and AFRURX support							

² Alternative Methods include processes such as laser cutting, water jet cutting, mechanical paint removal (e.g., abrasive media blast), thermal paint removal (e.g., laser, flashlamp), cold/thermal/plasma spray, alternative plating processes, and other processes not fully evaluated by AFRURX.

• **Specific Considerations**

- Laser Cutting
- Water Jet Cutting
- Cold Spray
- Paint Removal
- Alternative Plating/Coating

• **For Future Editions**

- Welding and Brazing
- Cryomachining

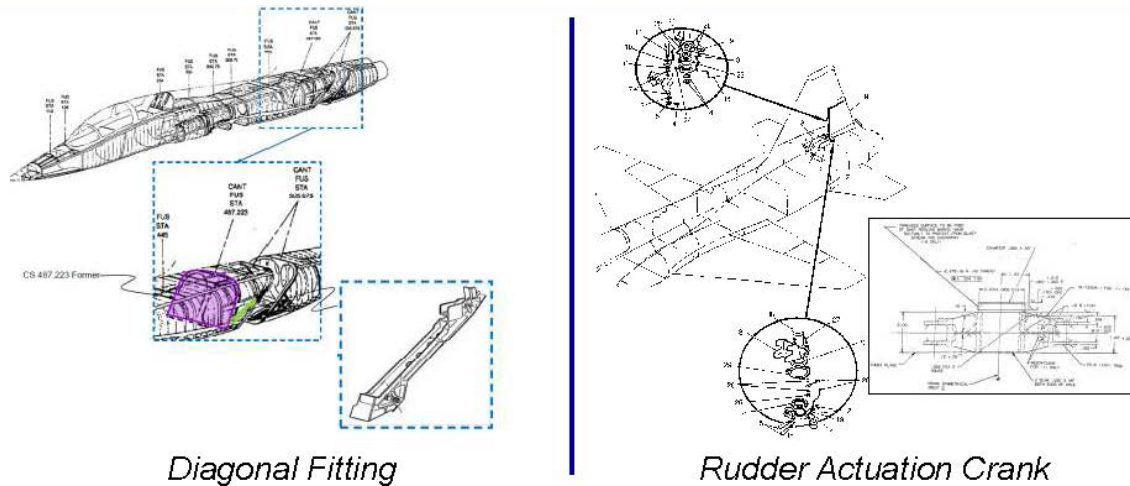


<http://www.gasnet.com/author/145/stock/waterjet-cutting.html>



<http://www.3d-machining.com/technology/cutting/waterjet-cutting-in-productivity-in-machining-technology>

Figure 9.10-5. Process Substitution Guidelines



- **Original Material & Product Form: 7075-T73 die forging**
- **Proposed Substitution: 7050-T7451 plate**
- **Reason for substitution: Procurement problems**

Figure 9.10-6. T-38 Case Study

9.10.2. Aluminum Alloy Substitution for Modernizing the Aging Fleet

Frank Shoup, Don Shrader, Frank Dicocco, and Milo Novak, Alcoa-Defense; Stephanie Flannigan and Christopher Jerome, USAF Research Laboratory – Aerospace Systems Directorate

Approximately three years ago, Alcoa Defense undertook a program entitled “Advanced Aerospace Material Technologies for Modernizing the Aging Fleet,” (also known as the Legacy Aircraft Structural Modernization Opportunity or LASMO) under the sponsorship of AFRL/RQVS (Structures Technology Branch, Aerospace Systems Directorate). The primary purpose of the program was to effectively transition modern high strength, fatigue and corrosion resistant aluminum alloys to legacy aircraft. The transition alloys were to be fully characterized and in commercial production such that they were readily available and affordable. These newer alloys generally exceeded the strength levels of the original T-6 (7075 & 7178) alloys while improving fatigue resistance and hugely improving corrosion resistance including Stress Corrosion Cracking (SCC) and Exfoliation. A major goal of the program was to document a successful process for transitioning newer materials for replacement of legacy aircraft structural components. Alcoa and AFRL, working with Boeing and Lockheed, formally invited each of the legacy weapons Systems Program Offices (SPOs) at the three primary Air Logistics Complexes to participate in the program. Positive responses were received from the KC-135, C-130, C-5, F-15, and later the B-52 SPOs. A number of structural components in critical need of replacement were transitioned to modern high strength corrosion resistant aluminum alloys; these included wing skins, structural extrusions, and forged structural components (Table 9.10-1). ROIs were computed, competing various process options from die forgings to machined plate to determine the most affordable option based upon part size, complexity, and projected replacement volumes. The program established a successful process to replace outdated aluminum components with modern high performance aluminums. In addition, projected acquisition and life cycle savings were computed for many of the identified components. Replacement processes and procedures, projected savings, and lessons learned from this program will be shared. Through the LASMO Program, a guide for aluminum alloy substitution was developed. The

substitution guide acknowledges and gives credence to the rules for alloy substitution provided by Structures Bulletin EZ-SB-13-001 developed by AFLCMC/EZ. The LASMO document, entitled “Aluminum Alloy Substitution for Legacy USAF Aircraft,” provides recommended drop-in replacement aluminum alloys from Alcoa, suitable for consideration when a structural engineer is working to resolve a wide array of issues found on aging aircraft. The guide also addresses factors to be considered for successful implementation such as commercial availability, business case development, and component qualification. The goal is to assist depot structural engineers in successfully inserting newer commercially available aluminum alloys onto legacy aircraft, thereby increasing aircraft readiness while reducing life-cycle costs. Also included is a recommended “Sheet and Plate Stocking Program” to provide recommended alloys and sizes to have on hand to meet the majority of the requirements for rapid fabrication of limited production parts.

Table 9.10-1. Property Comparisons of Typical Aluminum Forging and Replacement

ALLOYS EMPLOYED WITHIN THE AGING FLEET –
Normalized to OEM Baseline

Option	Mat'l & Product Form	F _{tu} - L	F _{ty} - L	K _{1C}	EXCO	SCC
OEM Baseline	7079-T6 & 7075-T6 4" Die Forging	1	1	1	D-	1
Current Material	7075-T73 6" T Hand Forging	.84	.82	?	A	3
Current Material	7050/7049-T7452 8" T Hand Forging	.92	.92	.88	B	3.5
Current Material	7050/7049/7249 - T7452 Die Forging	1	.97	1	B	3.5
Recommended Material	7085-T7452 8" T Hand Forging	.97	1.03	1	A	>3.5
Recommended Material	7085-T7452 Die Forging	1	1.06	1.12	A	>3.5
Recommended Material	7085-T7451 7" T Plate	1.04	1.18	1.12	A	>3.5

9.11. OVERVIEWS

9.11.1. When “What We Always Do” Won’t Solve the Problem

Thomas Brussat, Tom Brussat Engineering, LLC

Three aircraft structural integrity issues are discussed from the author’s experience that appeared to have major consequences and no acceptable solution. In the discussion of each case, the emotional and political concerns are interwoven with the technical in describing the improbable struggle to develop a resolution. The issues were as follows:

- 1) In 1996 the first F-22 aircraft was being fabricated and assembled in preparation for the critically important first flight milestone. Among the many F-22 innovations to save weight and cost was the first application of large “HIP’d” Titanium Casting in fracture critical primary structure, including wing-to-fuselage joints (Figure 9.11-1). But when 37 crack-like “shell inclusion flaws” were found in the first large cast part, there seemed no way to satisfy damage tolerance requirements, particularly the “rough flaw” requirement that large flaws must be extremely rare (Figure 9.11-2). (Resolution of this issue required an unprecedented probability of failure analysis to satisfy the intent of the rogue flaw requirement.)
- 2) In 2005 F-22 Production was nearing maximum rate. The full-scale airplane fatigue test has successfully completed 2.68 design lifetimes. However, during the post-test teardown inspection, a half-inch crack was found in the Titanium FS657 frame in the bore of the left-hand lower wing-attach lug (Figure 9.11-3). ForceMate™ bushings had been expected to provide very long fatigue life. According to the correlated damage tolerance analysis of this test crack, we now estimated 9 required inspections during the 8000 hour design lifetime. And it appeared that the inspections could not be accomplished without removing the wings! As engineers meticulously planned a damage tolerance test program to investigate this looming maintenance nightmare, the assembly line was cranking out 2 new airplanes a month with the current questionable design. (The testing would raise further drama before this issue was finally understood and nicely resolved.)
- 3) In October 2010 the author and 5 highly respected aircraft structural integrity experts were in the final stages of a USAF contract to draft and distribute an “Aircraft Structural Risk and Reliability Handbook” (Figure 9.11-4). In the 11th hour the author discovered what he believed to be a mathematical inaccuracy with the risk calculation method that was fundamental, not only to the handbook, but to how most calculations of Single Flight Probability of Failure had been calculated for over 2 decades. If his suspicions proved to be correct, it would mean cancelling distribution of the now-completed handbook, raising questions about excess conservatism of past risk analyses, and generating unwanted controversy. In short it seemed that no good outcome could result from raising this issue to the handbook co-authors and USAF sponsors, yet it was obviously necessary to do so. (The concern has proven to be valid, and it is anticipated that significant advances in structural risk analysis methodology will soon be implemented.)

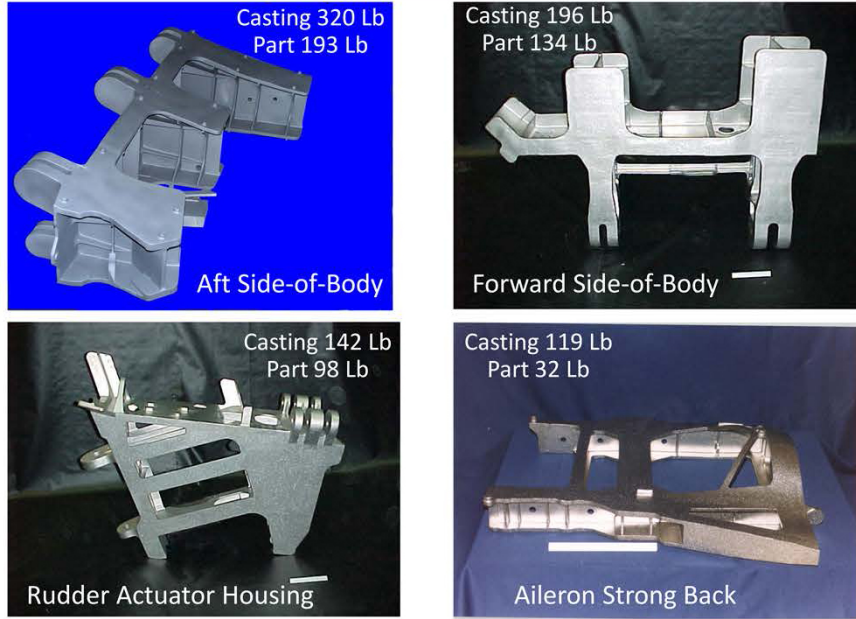
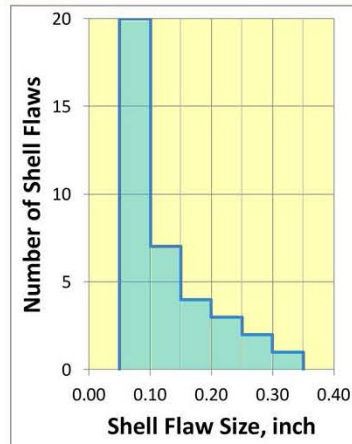


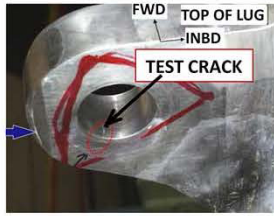
Figure 9.11-1. Largest F-22 Fracture Critical Cast Ti Parts

37 Linear Shell Flaws \geq .05 inch found in 1st Rudder Actuator Housing Casting, 4-4-96



Dozens of shell flaws found in several other large F-22 castings

Figure 9.11-2. Linear Shell Flaws in Rudder Actuator Housing Casting



Cracks found during teardown inspection of F-22 fatigue test A/C after 2.68 design lifetimes:

- 0.5x0.6 in. crack in fuselage lug bore at LHS lower wing-to-fuselage attachment at FS657
- Similar cracking in RHS lower lug
- Lugs are integral to Ti 6Al-4V carry-thru frame
- Bore Dia. = 2.2 in.; ForceMate™ bushing used
- No cracks in wing-attach lugs of other 5 frames

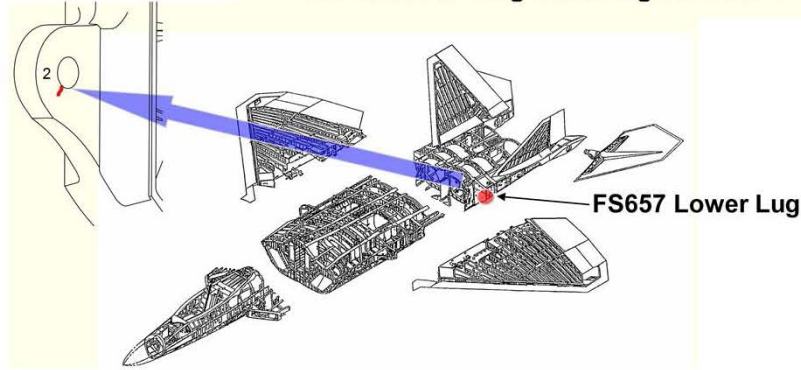


Figure 9.11-3. Fuselage Frame Cracks in Wing-Attach Lugs

Objectives:	Authors
<ul style="list-style-type: none"> • Provide Analytical Capability for Establishing Probabilities of Structural Failure <ul style="list-style-type: none"> • Tutorial on basic probability & statistics • Characterizations on available input data • Accepted analysis methods 	<ul style="list-style-type: none"> • Robert P. Bell • Alan P. Berens • Thomas R. Brussat • Joseph Cardinal • Joseph P. Gallagher • James L. Rudd (Editor-in-Chief)
18-Month Schedule:	AFRL Sponsor
	Eric Tuegel (AFRL/RQSS)
	Contractor
	Universal Technology Corporation

Figure 9.11-4. Aircraft Structural Risk & Reliability (ASRRA) Handbook

9.11.2. B-1 Full-Scale-Fatigue Test

Jerry Bohr, Bob Lee, and Richard Binder, The Boeing Company; Justin Evans and Rodney Harberson, USAF B-1 SPO

The fleet of B-1 aircraft (Figure 9.11-5) has been in operation since mid-1980 and is nearing its test-validated design life. The current certification is based on large component tests, which did not test all parts of the airframe structure. The Air Force has decided to continue the use of the B-1 aircraft into the decade of 2040 based on analytical life predictions. MIL-STD-1530C requires the analytical life be validated by a full-scale-fatigue test. To support this requirement, the Air Force SPO has decided to test one of its aircraft in storage to learn the true durability life of the aircraft. The fatigue test strategy will test the aircraft structure using a flight-load spectrum based on training missions obtained from the Loads/Environment Spectra Survey (L/ESS) program. These training missions are flown frequently and have proved to be the harshest usage of the aircraft relative to the other types of missions flown to date. The full-scale-fatigue-test program consists of two separate test rigs, a fuselage test rig (Figure 9.11-6) and a wing test rig (Figure 9.11-7). Several existing fleet repairs have been installed on the fuselage and wing structures (Figure 9.11-8). The aircraft structures (test articles) will be tested to two times the flight hours estimated for the fleet leader in year 2040. Each fatigue test will be followed up with a residual strength test and teardown inspection. The comprehensive test program has included test spectrum development, test loads verification, coupon truncation validation, test fixture assembly, instrumentation and inspection definition. The full-scale-fatigue-test program is based on the approach used for the initial certification of the aircraft for safe flight. The major objective of the test program is to identify potential structural problems before they occur in the fleet. Partial wing test results have provided valuable information for force structural maintenance and potential fleet implementation.



Figure 9.11-5. B-1 Aircraft



Figure 9.11-6. Fuselage Test Set-up



Figure 9.11-7. Wing Test Set-up

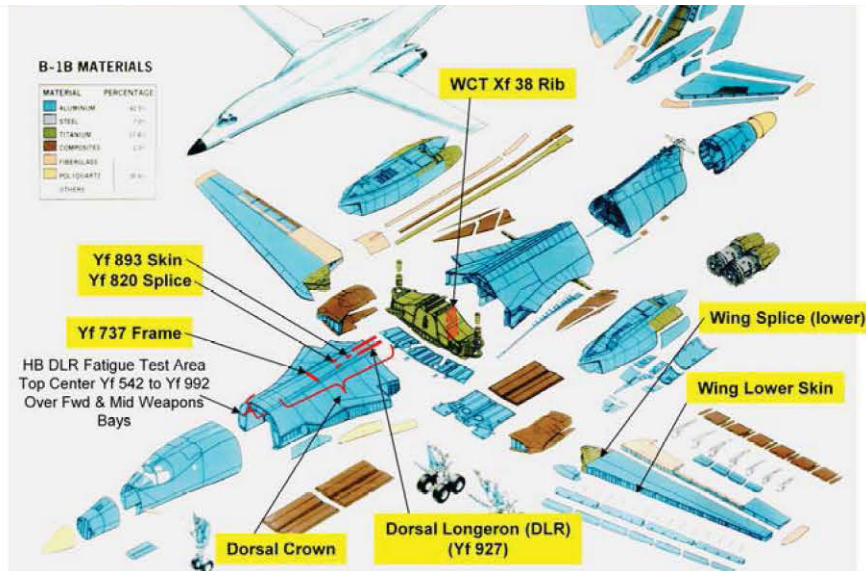


Figure 9.11-8. Major Structural Repairs

9.11.3. Equivalent Flight Hours Development for USAF HH-60G

Gregory Wood, Eric Winslette, and Brian Harper, Mercer Engineering Research Center (MERC); Steven Lamb, USAF-HH-60G ASIP

This technical activity details the development of equivalent flight hours (EFH) for the USAF HH-60G Pave Hawk helicopter. Difficulties in procurement of a replacement for the Pave Hawk have driven efforts to extend the service life of the aircraft. Structural cracking in airframe primary structure is responsible for a large amount of unscheduled maintenance and causes aircraft availability issues (Figure 9.11-9). Mercer Engineering Research Center (MERC) was tasked with EFH development for the HH-60G in order to establish component replacement and inspection intervals, as well as to better quantify the remaining useful life of the fleet. EFH development required the coordination of several efforts, including aircraft usage characterization with a Loads / Environment Spectra Survey (L/ESS), a flight strain survey (Figure 9.11-10), and the development and validation of a damage-tolerance based damage model for four locations on the airframe. A Loads / Environment Spectra Survey (L/ESS) has been ongoing for the HH-60G since 2008. Fourteen aircraft are currently instrumented across all HH-60G commands, collecting representative usage data for the fleet. These data were processed using regime recognition algorithms to establish an updated usage profile for the fleet. A flight strain survey was performed on an HH-60G in late 2012 using an augmented L/ESS system. The aircraft was instrumented with sixty-four strain gages and twenty-seven accelerometers. Prior to commencement of a flight strain survey, a crane lift was performed in order to apply a known static load to the helicopter. These data were used to validate a previously created finite element model (Figures 9.11-11 and 9.11-12). A set of prescribed maneuvers across the Pave Hawk's operational envelope was then flown for various gross weight / center of gravity configurations. Strain and accelerometer data were synchronized to the regimes calculated from L/ESS data. Instrumentation was left in place after the flight strain survey in order to perform an operational loads survey. A damage-tolerance-based approach was used to create a damage database from the flight strain survey data. This database consists of crack growth values at four locations on the aircraft for each regime flown during the flight strain survey. L/ESS data are then mapped to these regimes in order to calculate crack growth on a flight-by-flight basis. These data are then used to calculate equivalent flight hours at these structural locations for instrumented aircraft, and to

provide estimates of EFH for non-instrumented aircraft. Work is ongoing to recommend EFH-based component inspection intervals, component replacement intervals, and depot inductions. MERC and the USAF are working toward the implementation of an individual aircraft tracking program for the HH-60G based on parametric and regime data from the health and usage monitoring system (HUMS) being implemented on the fleet.

- USAF difficulties in procurement for HH-60G replacement aircraft have driven efforts to assess / extend aircraft service life
- Structural cracking is responsible for a large amount of unscheduled maintenance and causes aircraft availability issues
- Example: LBL 16.5 transmission beam crack

Figure 9.11-9. Structural Cracking in Airframe Primary Structure

- 60 Strain Gages ●
- 27 Accelerometers ●
- Sample rate 1000 Hz

Augmented L/ESS recorder used for test; HUMS (IVHMS) data also recorded

- 28 hours (5,513 regimes) captured for prescribed regimes across most of aircraft operational envelope
- Operational data also collected, bringing total to 121.3 hours (25,554 regimes)
- Regime recognition allowed use of all flight data, not only prescribed regimes

Sample of Flight Strain Data

Units are strain (in/in) on vertical axes and time (sec) on horizontal axes

Figure 9.11-10. Strain Survey

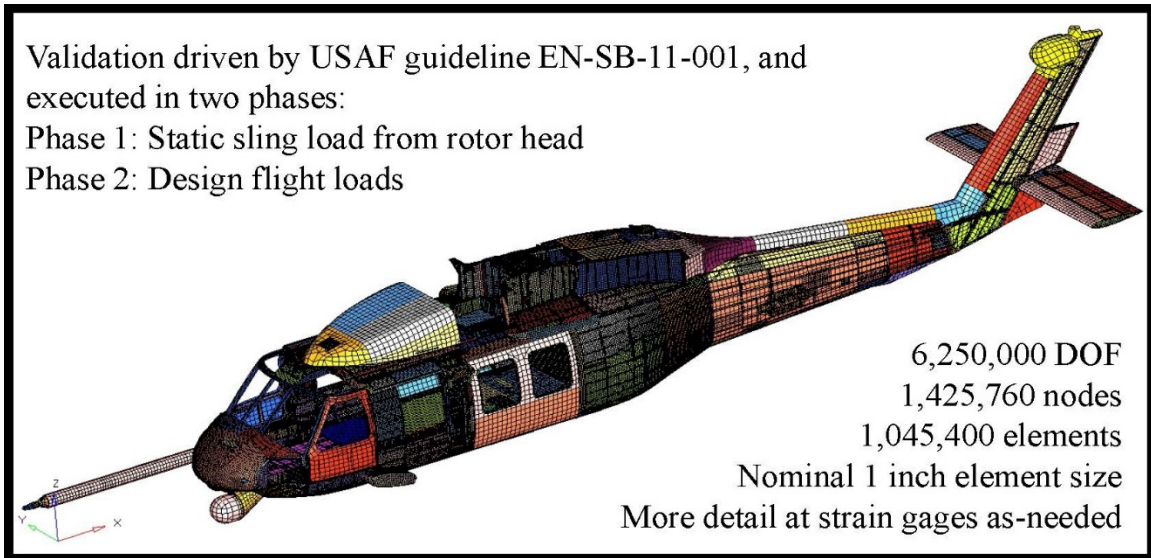


Figure 9.11-11. Global Finite Element Model

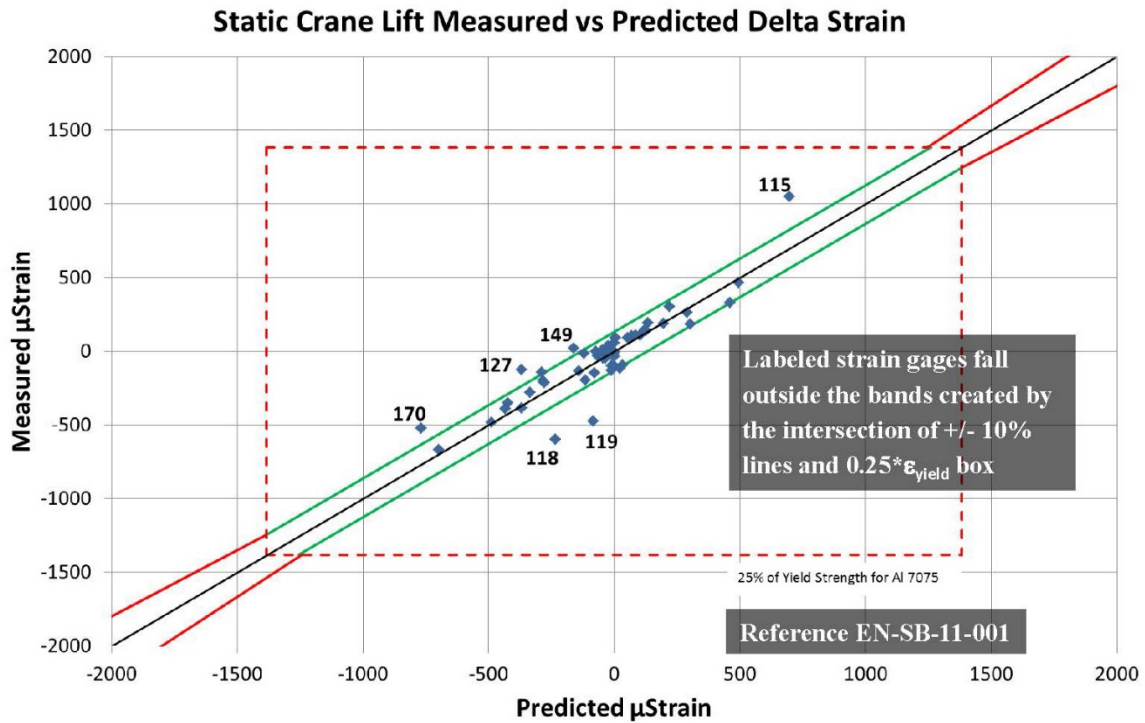


Figure 9.11-12. Global Finite Element Validation

9.11.4. E-6B SLEP Fatigue Analysis and Test Program

Richard Leist, The Boeing Company – Defense, Space & Security; Michael Bouchard, University of Dayton

This technical activity discusses the E-6B (Figure 9.11-13) Service Life Extension Program (SLEP) Fatigue Test Program. A review of the critical wing locations and analytical lives is presented. Coupon and wing panel design (Figure 9.11-14) approach is discussed, including decision-making for inclusion of both un-enhanced and enhanced fastener locations, manufacturing and finishing processes to ensure good structural representation, gripping, and load introduction and distribution into the gage section. Fatigue test fixturing (Figure 9.11-15), setups and protocol are described. Selected test results, including comparison of test and analytical fatigue lives, and static residual strengths, are presented. The E-6, a derivative of the Boeing 707, replaced the aging EC-130Q to perform the U.S. Navy's TACAMO ("Take Charge and Move Out") mission. Operations began in 1989. The E-6B aircraft, modified from the E-6A, was developed for additional mission functionality, specifically the Air Force Airborne Command Post mission. The first E-6B was accepted in December 1997. The E-6 fleet was completely modified to the E-6B configuration in 2003. In 2003, the U. S. Navy and Boeing undertook a Service Life Assessment Program (SLAP) to evaluate the repeated loads, fatigue life and damage tolerance characteristics of the E-6 fleet since it began operations in 1989. As a follow on to SLAP, the U.S. Navy requested that a Service Life Extension Program (SLEP) be performed for this aircraft. Based on the SLAP analysis, Boeing identified multiple wing fatigue critical locations that were approaching the end of their design life, and developed enhancements consisting of oversizing, cold working, and/or interference-fit fasteners or bushings. A SLEP Fatigue and Test Program was then required to validate analytical estimates of service life as well as to determine the life extension capability of the enhancements. Due to the limited fleet size, it was not possible to utilize an aircraft for enhancements and fatigue test validation. Boeing therefore designed structural coupons of the most critical wing features and a large representative section of the lower wing skin and stiffener structure that incorporated all of the critical wing features, most notably around the "C" and "D" access doors and the "WS-360" splice joint. Boeing competitively contracted manufacturing of the coupons to Advanced Welding Technologies LLC (AWT), fatigue testing to University of Dayton Research Institute (UDRI), and fractographic analysis to National Institute for Aviation Research (NIAR). The Fatigue Test Program successfully demonstrated efficacy of the enhancements to safely extend the fatigue life of the E-6B fleet, and revealed a limited number of additional fastener locations that require enhancements. The SLEP Fatigue Test Program also provided very useful guidance on the design of representative structural coupons for fatigue testing, which is discussed in the technical activity.



Figure 9.11-13. E-6B Aircraft

Wing Panel Specimen Final Design – Mid-wing Joint, S-4 to S-8

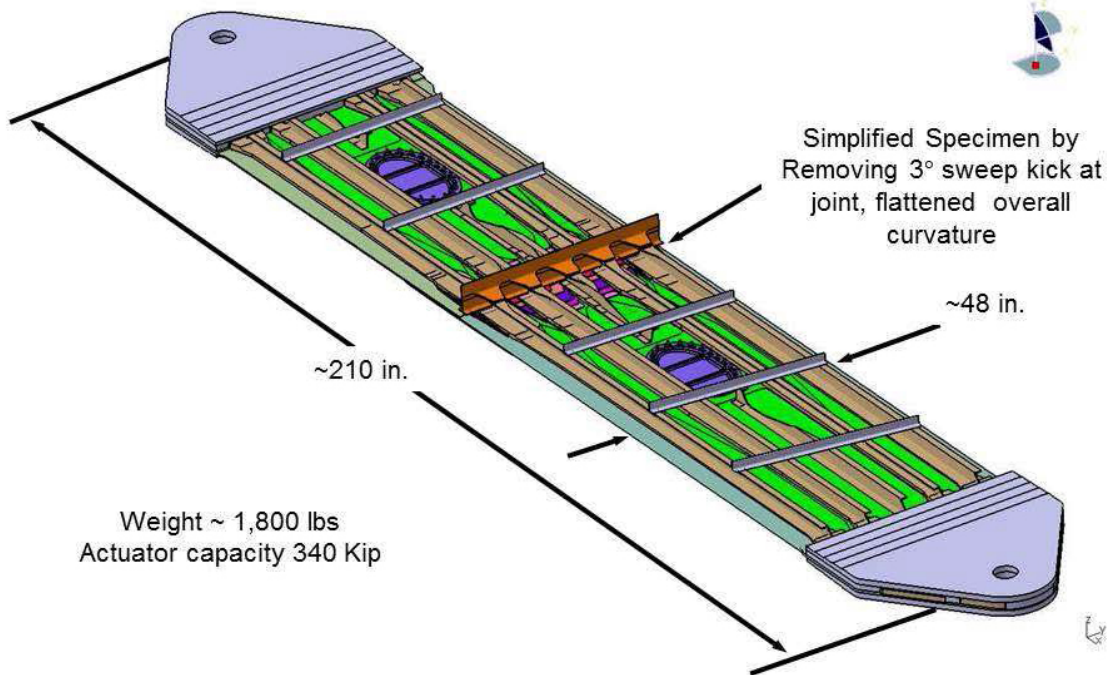


Figure 9.11-14. Wing Panel Design

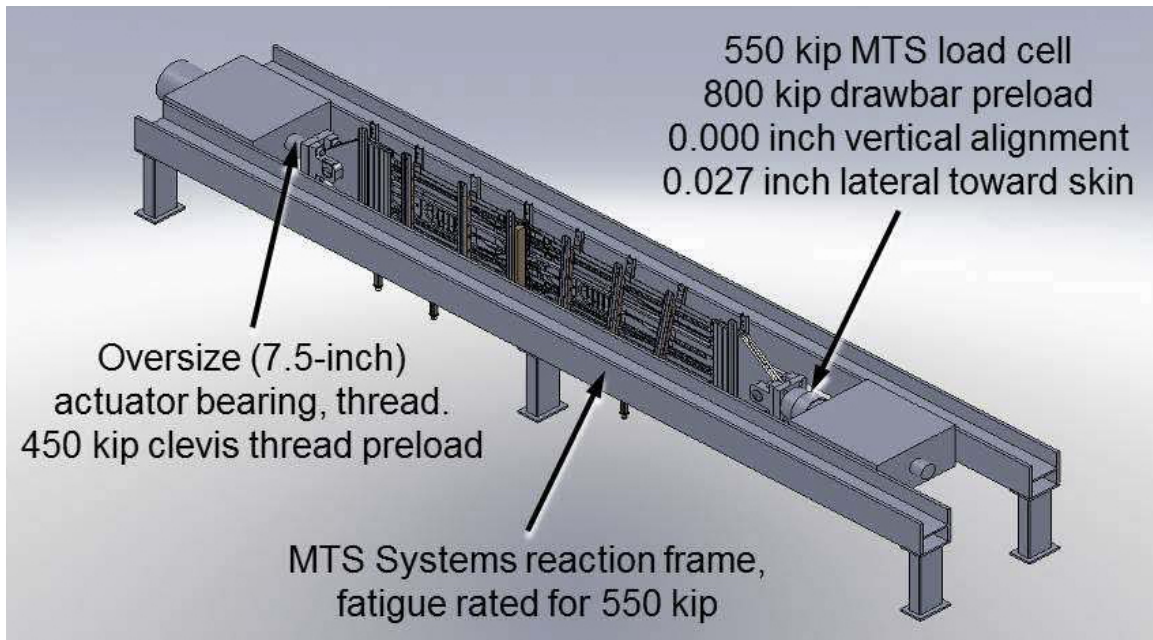


Figure 9.11-15. Wing Panel Test Fixturing

9.11.5. P-8A Poseidon Full-Scale-Fatigue Test

Jude Restis, Thomas Turner, and Hafizullah Wardak, The Boeing Company – Test & Evaluation; James Cantela, Michael Edwards, Nam Phan and Bradley Lloyd, USN - NAVAIR

The P-8A Poseidon (Figure 9.11-16) is a military derivative of the commercial Boeing 737 aircraft. The P-8A is currently undergoing a full-scale fatigue test (Figure 9.11-17) to demonstrate the ability to fulfill its intended NAVY usage. The P-8A airframe is being fatigue tested to a two-lifetime test to validate the Design Service Objective (DSO) for the airframe per NAVY defined usage and requirements. The full-scale-fatigue-test requirements, test loads, test event tape with flight sequencing, and test fixtures were developed by the Boeing engineering team in a close collaboration with NAVAIR. Test loads were applied to a finite element model to compare design and verification internal loads. The fuselage, wings (including all wing surfaces), vertical fin and rudder are being tested on the aircraft. The landing gears, both nose and main, and horizontal stabilizer are being tested off aircraft. The wing-leading-edge and trailing-edge surfaces, weapon bay doors, and UARRSI will be block load tested. Cyclic load application started with initial block-load (local) test of the UARSSI, weapon bay door, and engine strut, all on the aircraft. Testing then progressed to fully distributed testing of the entire airframe. Block-load testing of the wing control surfaces on aircraft will follow distributed testing. This will complete one lifetime testing cycle. A second lifetime test will follow the same process. Lessons learned from this full-scale-fatigue test, which is being tested with a severe loading environment, aggressive schedule, and budget constraints, will also provide data for future commercial airframe derivatives for military usage. The test program has taken extensive advantage of previous Boeing full-scale-test program experience at Boeing (Figure 9.11-18).



Figure 9.11-16. P-8A Poseidon Aircraft

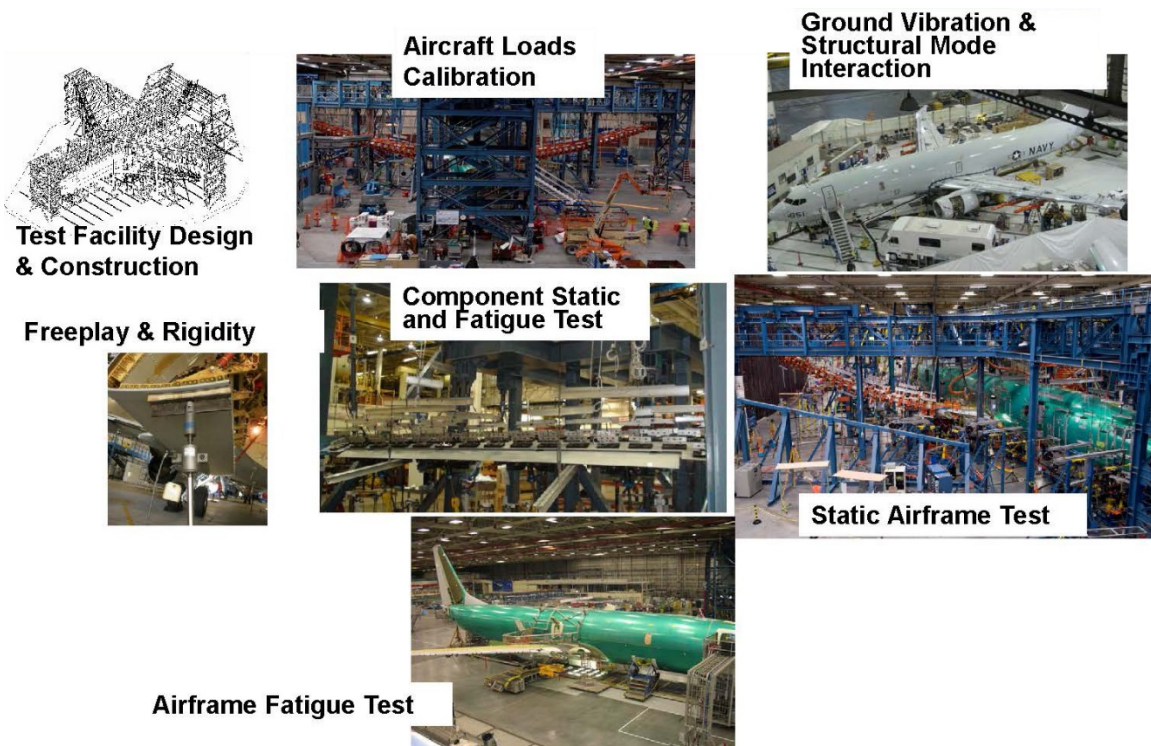


Figure 9.11-17. Elements of Structural Test Program



Figure 9.11-18. Fatigue Test Set-up

9.11.6. Full-Scale-Fatigue Test of FA-18 A/D Composite Structure for Aging Evaluation

Waruna Seneviratne and John Tomblin, Wichita State University – NIAR; Madan Kittur, USN - NAVAIR

At present, the first generation of composite primary structural components are entering the twilight of their certified service lives. Life extension efforts are underway for many of these aircraft, and these efforts are primarily geared to the continued safe operation of those metallic components of the airframe for which a fatigue life can be quantified. However, many of the composite components do not have a measurable fatigue life, so the extension of their lives cannot be accomplished via the same methodology. Scientists at the National Institute for Aviation Research (NIAR) at Wichita State University are investigating the aging effects of McDonnell Douglas (now Boeing) F/A-18 Hornet wing structure, which consist of AS4/3501-6 carbon/epoxy composite wing skins and composite-to-titanium stepped lap joints bonded with FM-300 film adhesive at wing root and pylon fittings. The research program is funded by the US Office of Naval Research and monitored by the Airframe Technology Branch of Naval Air System Command (NAVAIR)-Air Vehicle Department. This program provides a quantifiable, risk-based assessment methodology for determining the capability for life extension in composite structure, tying both original certification and operational usage methods. The full-scale test article consists of center fuselage, inner-wings, and trailing-edge flaps (Figures 9.11-19 and 9.11-20). Center barrel section of the fuselage is used as a part of the inner-wing test fixture to ensure proper load transfer at the wing root lugs. Simulated inboard leading-edge flap and the outboard wing are attached to each inner-wing box for fatigue load application. This structure provides an opportunity to look at the service life management and deliver useful insight into the sustainment of the active fleet. Current methods of certification for aircraft composite structure rely on the development of a safe usage life through fatigue testing. Since composite structure is designed to withstand environmentally compensated static loads with considerable analytic reductions in strength, it is rare that the full-scale-fatigue-testing of aircraft components exercises the capabilities of the composite structural members. In addition, the expense of fatigue testing rarely permits continued testing past the original design goals for the program.

These factors combine to prevent composite structures from being failed during the fatigue test. As a result, there is little capability over the course of the aircraft life to relate in-service events to known fatigue limitations of the original certification test and no mechanism to employ engineering principles for the extension of life. The ability to use end-of-life aircraft structural components has been shown to be beneficial in many instances for the support of the existing fleet and provides a pro-active approach to fleet maintenance.

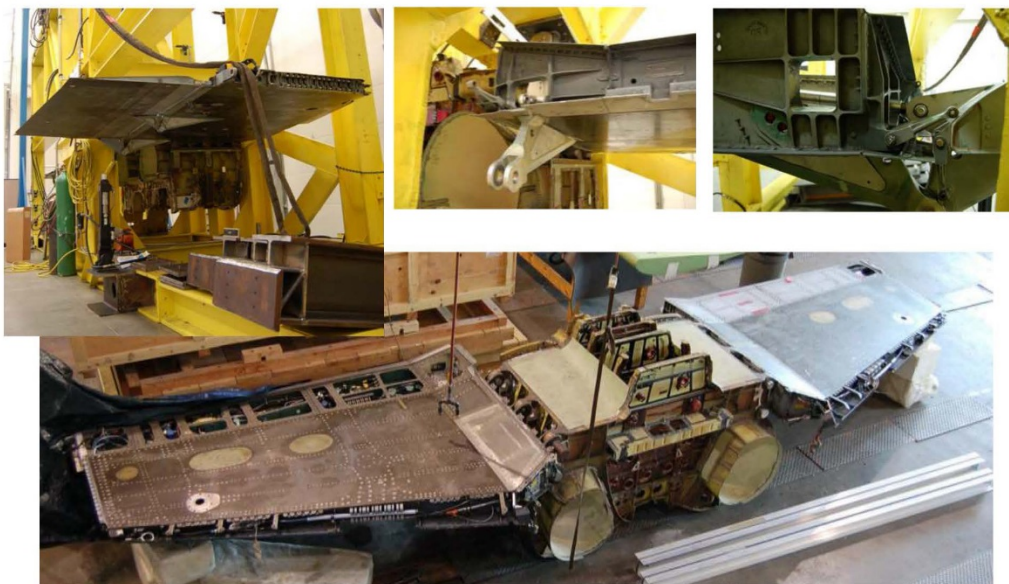


Figure 9.11-19. Full-Scale-Test Article



Figure 9.11-20. Full-Scale-Test Fixture

9.11.7 Enabling High-Quality and Efficient Engineering Decisions with 3-D Visualization of Maintenance Data

Hazen Sedgwick, USAF A-10 ASIP; Joshua Hodges, USAF T-38 ASIP; Gary Steffes, USAF Research Laboratory – Materials and Manufacturing Directorate; Gary Cohen, Etegent Technologies, LTD.

In a time where technologies have enabled the communication of vast amounts of information in mere seconds, a modern, common framework for tracking, communicating, and storing maintenance data within the USAF is missing. Although the current framework does get the job done and adequately maintains aircraft safety, there are improvements that can help communicate data from the maintainer to the engineer more efficiently. With the current budget constraints and the need to be more efficient, the A-10 (Figure 9.11-21) and T-38 ASIP groups have been proactively engaged in producing tools to improve engineering decisions based on real-time accurate data. Over the last two years these groups have been working with Etegent to develop a 3D visual tool for managing maintenance data. NLign is the tool that has been specifically designed for visually representing aircraft maintenance information on a 3D CAD model (Figures 9.11-22 and 9.11-23). It has also been designed to help facilitate data gathering and real-time visualization of new input data (Figure 9.11-24). Not only is this a tool to manage the fleet as a whole, but is capable of tracking the current configuration and maintenance history of each individual aircraft. These data would be useful to an engineer if he/she were tasked with analyzing a repair or modification that may interact with previous repairs. Without a tool like NLign, it is nearly impossible for the engineer to have visibility of work previously performed on an airframe, especially when those repairs have been performed in accordance with existing Tech Order (TO) limits when no records are kept of those repairs. Currently NLign has been tailored for the specific needs of the A-10 and T-38; however, other weapon systems in the USAF are adopting the tool as well. This technical activity will discuss: 1) A brief history and description of why a 3D visualization of maintenance data is needed, 2) The USAF's vision for developing this capability for multiple aircraft, 3) The A-10 & T-38's ASIP visions for utilizing the tool, 4) Current development of NLign and progress towards a fieldable system, 5) An example on how NLign will produce a more efficient maintenance program, and 6) Demo of the current A-10 NLign tool.

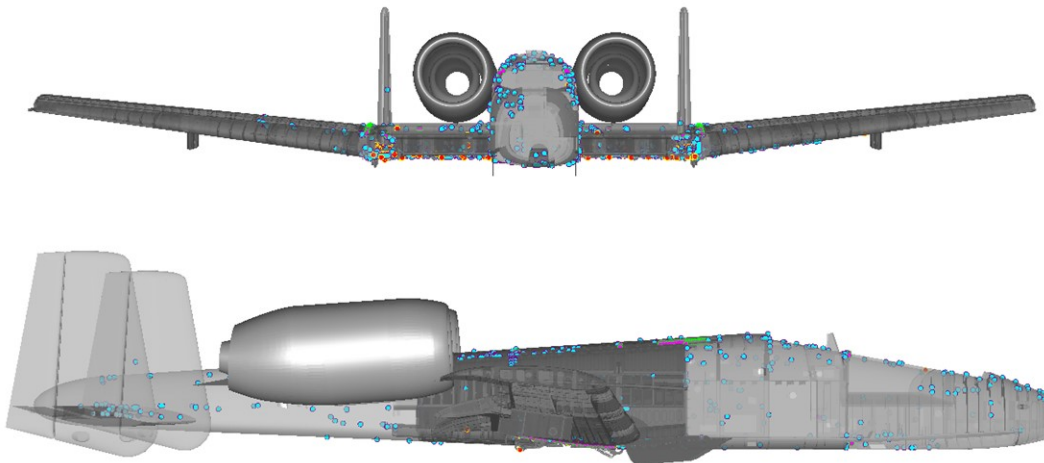


Figure 9.11-21. A-10 Aircraft

- **T-38 NLign current support for ASIP**

- Loft Model in 3D space
- Analysis data
- Maintenance data
- Current flight hour configuration
 - Fuselage
 - Wing

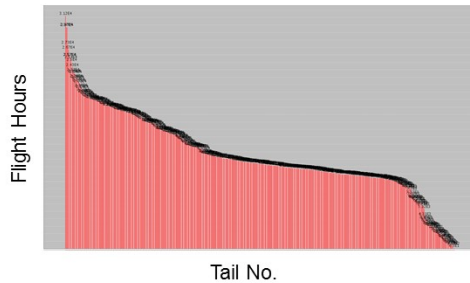
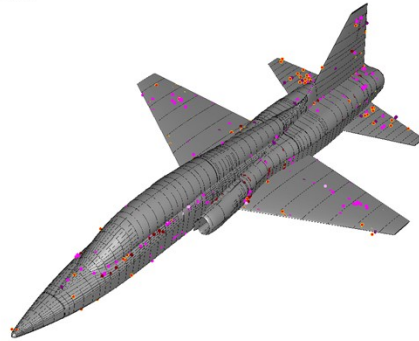


Figure 9.11-22. T-38 NLign Deployment

- **A-10 NLign current structure for ASIP support**

- Full 3D model with part tree
 - Basic 3D model functions
- Serialized component tracking
 - Component hour tracking for major assemblies
- Analysis support data
 - Analysis mapped visually onto 3D model
 - Clean metadata with AC (X,Y,Z)
 - Supporting documents 'one-click' away
- Maintenance inspection data
- Test and Teardown data
 - Each crack mapped onto 3D model
 - Supporting crack data 'one-click' away
- All data verified for quality

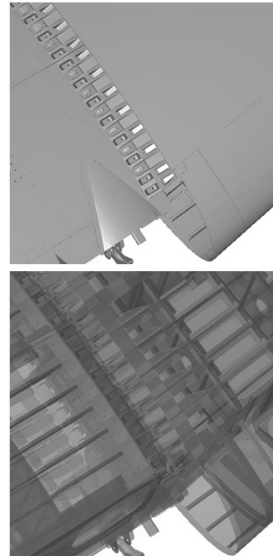


Figure 9.11-23. A-10 NLign Deployment

- Same 'clean' data but represented in a visual form

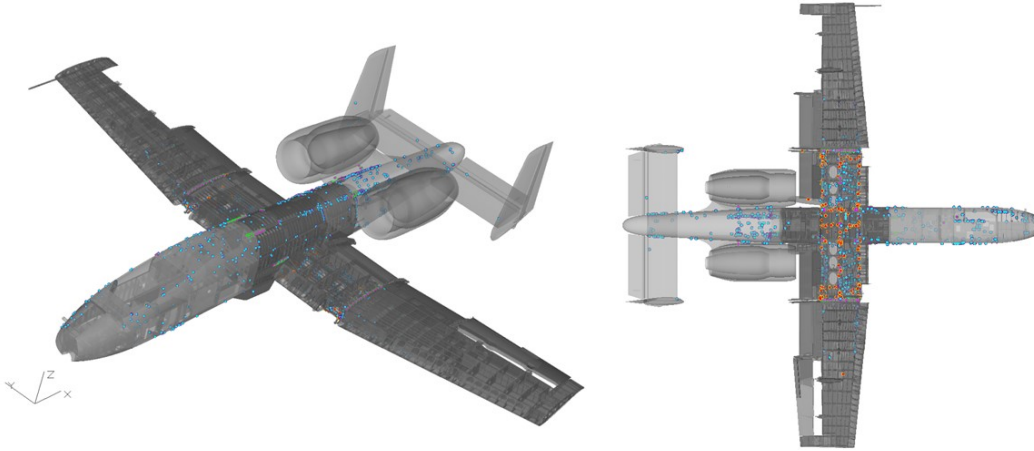


Figure 9.11-24. Visual Representation of Data

9.11.8. Strategies for and the Importance of DaDT Analysis Validation at the System Level

Dale Ball and Thomas Limer, Lockheed Martin Corporation

Durability and damage tolerance (DaDT) analyses are foundational to the ASIP process and are required during virtually every one of the five tasks: from the generation of DaDT-based design allowables during Task 2, to the development of representative full-scale test spectra in Task 3, to the planning of force structural maintenance in Task 4 and the execution thereof in Task 5. The criticality of these analyses cannot be overstated and demands that both validation of the methods and verification of their software implementation be conducted early and thoroughly in any ASIP guided structures development program. While the conduct of verification and validation (V&V) programs within ASIP is not new (Figures 9.11-25 and 9.11-26), the dramatic increase in both the number and complexity of DaDT analyses used to support the airworthiness certification process has raised new challenges to the efficacy of such programs. These challenges will undoubtedly continue as the industry moves toward virtual (digital) representation of products and even individual assets. In this technical activity we describe the validation of the individual components of an integrated software system used for the DaDT analysis of several major military aircraft programs (Figures 9.11-27 and 9.11-28). We then discuss several of the issues that can arise when system level V&V programs are either not performed or do not properly identify potential shortfalls (Figure 9.11-29). Several specific examples are cited, including the application of design factors that are applied at the system level and have not been addressed during validation testing, and the appropriate determination of local stress spectra when coarse-grid (internal loads) finite element models are used for spectrum generation. We conclude with suggested strategies both for system level V&V of an integrated design analysis tool, and for enhanced vetting of DaDT analyses.

- **Verification = demonstration that a mathematical model has been correctly implemented and that the algorithmic implementation executes properly**
- **Validation = demonstration that a mathematical model correctly represents the physical process / phenomenon which it is intended to represent**

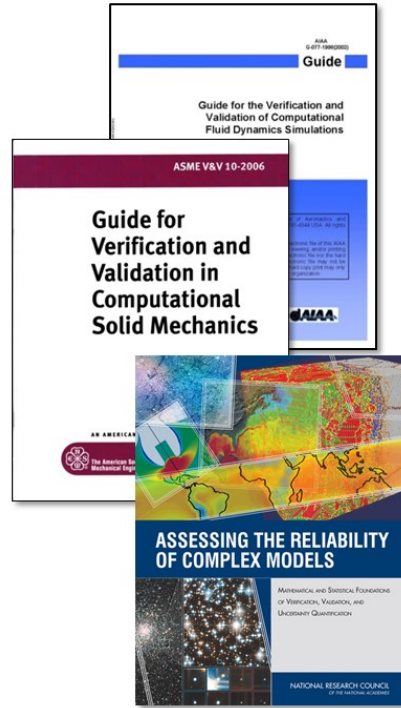


Figure 9.11-25. Definition of Verification and Validation

- **Model V&V typically conducted using ‘building block’ approach**
- **Parallels structures development test program**

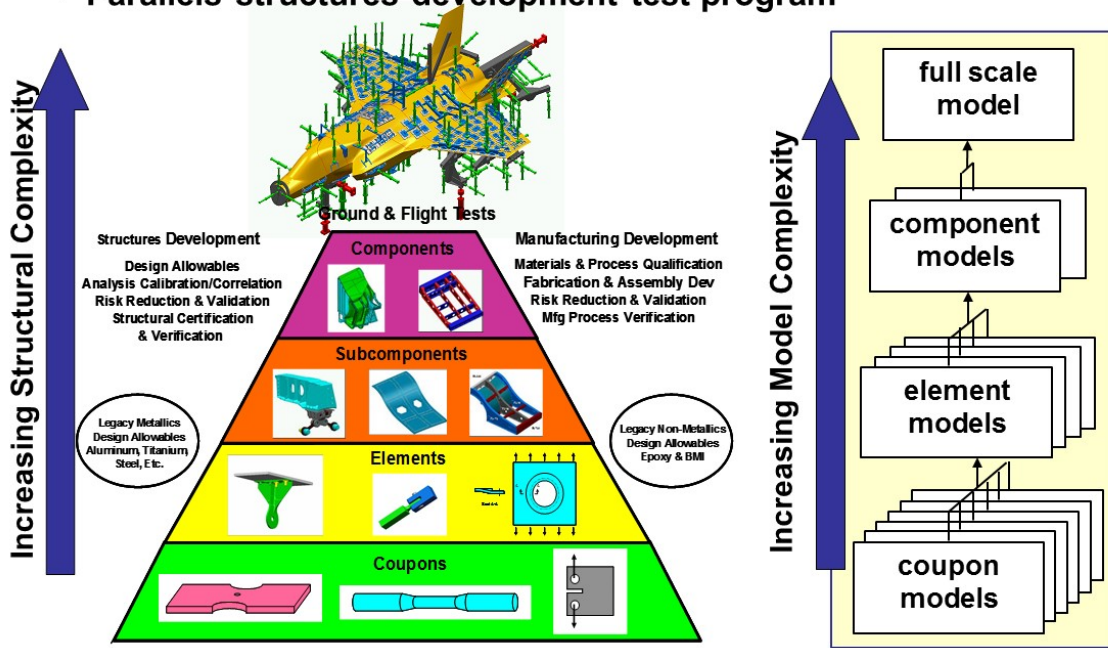


Figure 9.11-26. V & V Using ‘Building Block’ Approach

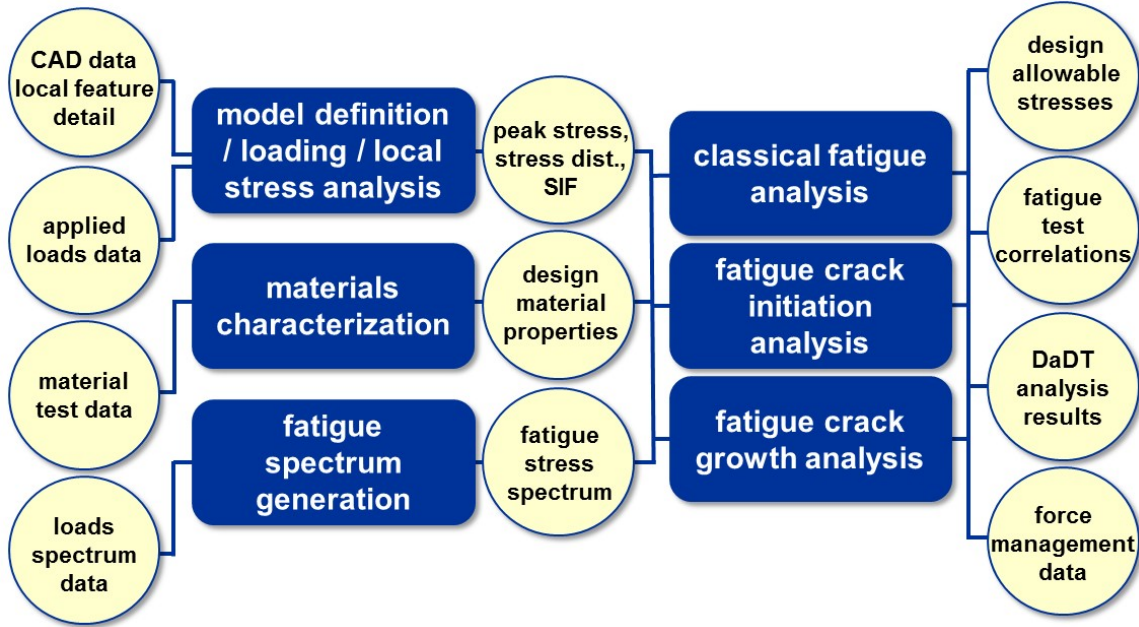


Figure 9.11-27. Six DaDT Analysis Components

- **FCG model fidelity can be improved with explicit inclusion of residual stresses where they are known to exist**

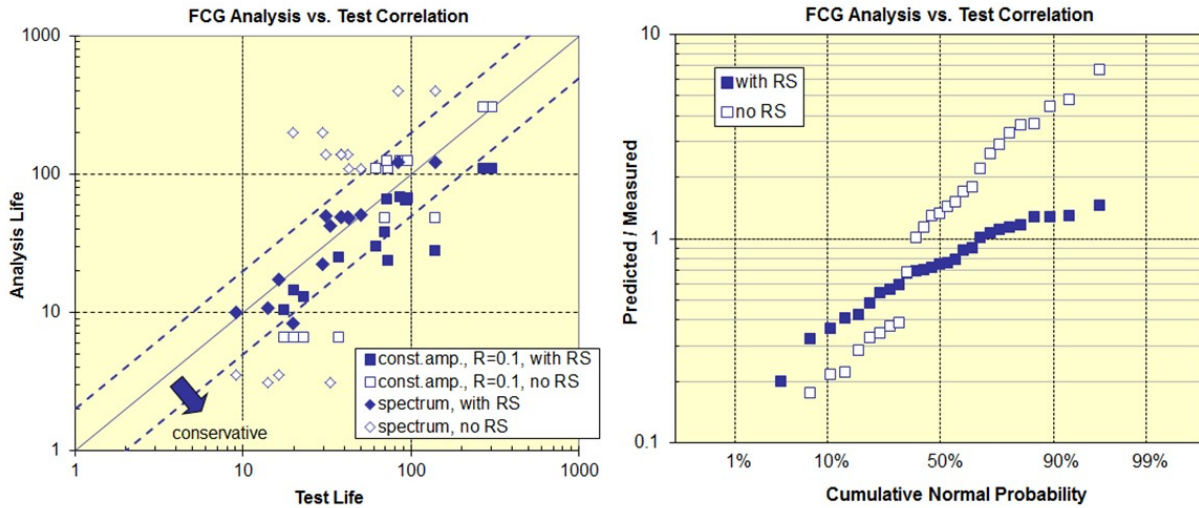


Figure 9.11-28. Validation of Fatigue Crack Growth Analysis

- The operation of the FCI and FCG analysis engines can be compared and the results of those comparisons evaluated over the full AV-FEM

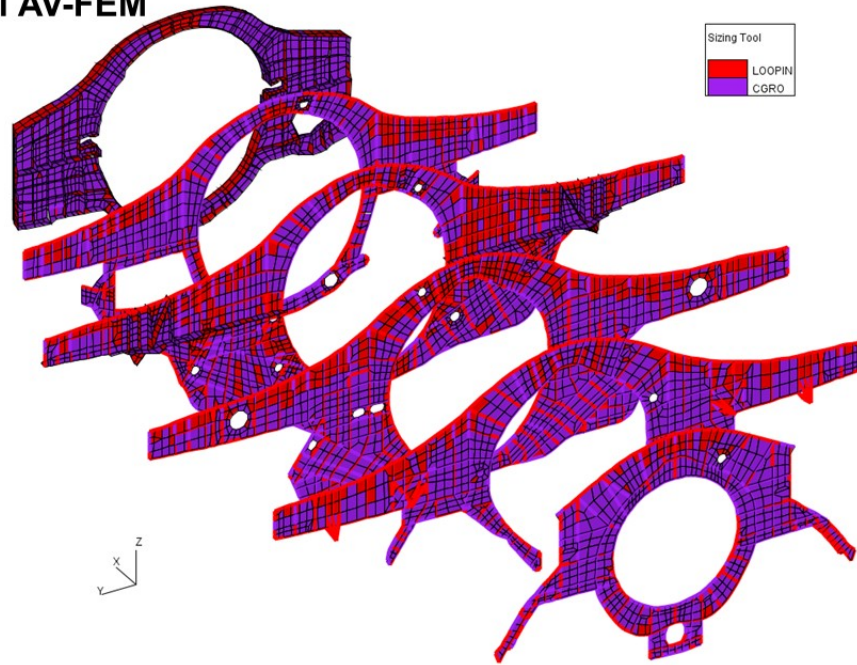


Figure 9.11-29. System Level Surveys

9.11.9. Integrated Technology Development Toward ASIP Corrosion Tools

Douglas Dudis, USAF Research Laboratory – Materials and Manufacturing Directorate

Corrosion represents the largest cost category associated with the maintenance of aircraft and is growing in terms of absolute cost (\$4.5 B per year) (Table 9.11-1) and proportion (24%) of aviation and missile maintenance costs. Corrosion-related maintenance also accounts for ~16% of system non-availability. While the aging fleet would naturally come to mind as a driver of corrosion issues, even the newest assets being deployed have presented corrosion problems. Consequences of not designing for corrosion resistance include higher life-cycle costs and reduced readiness. A key focus of the AFRL Corrosion IPT is the development of the scientific and engineering capabilities to enable ASIP-like tools for improved corrosion management. This technical activity will provide an overview of several key components under the AFRL Corrosion IPT that are intended to lead toward the ability to apply ASIP-like principles for fleet corrosion management as well as developing design tools to analyze corrosion sensitivities upfront. The overarching theme is the development of accelerated corrosion simulation capabilities (Figure 9.11-30) which has three key components: (1) the development of more realistic test specimens capturing complex material configurations, (2) the development of testing capabilities suitable for exploring combined environmental stresses on corrosion susceptibilities, and (3) the computational approaches required to model complex material specimens under the influence of combined stresses (Figure 9.11-31). Activities in each of these sub-thrusts will be discussed as well as the path toward eventual standards and specifications.

Table 9.11-1. Cost of Corrosion

- Annual Estimates on Corrosion Impact
 - DoD: \$20.9B (2010)
 - USAF: \$6.3B (\$4.5B for Aircraft & Missiles) (2009)
- Upward USAF Cost Trend, 2006-2009

	Corrosion Cost (in millions)	Total Maint. (in millions)	As a percent of maintenance
FY2006	\$3,105	\$14,659	21.2%
FY2007	\$3,537	\$15,925	22.2%
FY2008	\$3,908	\$16,403	23.8%
FY2009	\$4,485	\$18,657	24.0%

Preliminary Numbers for FY13: \$6.0 B, 25% of total Maintenance

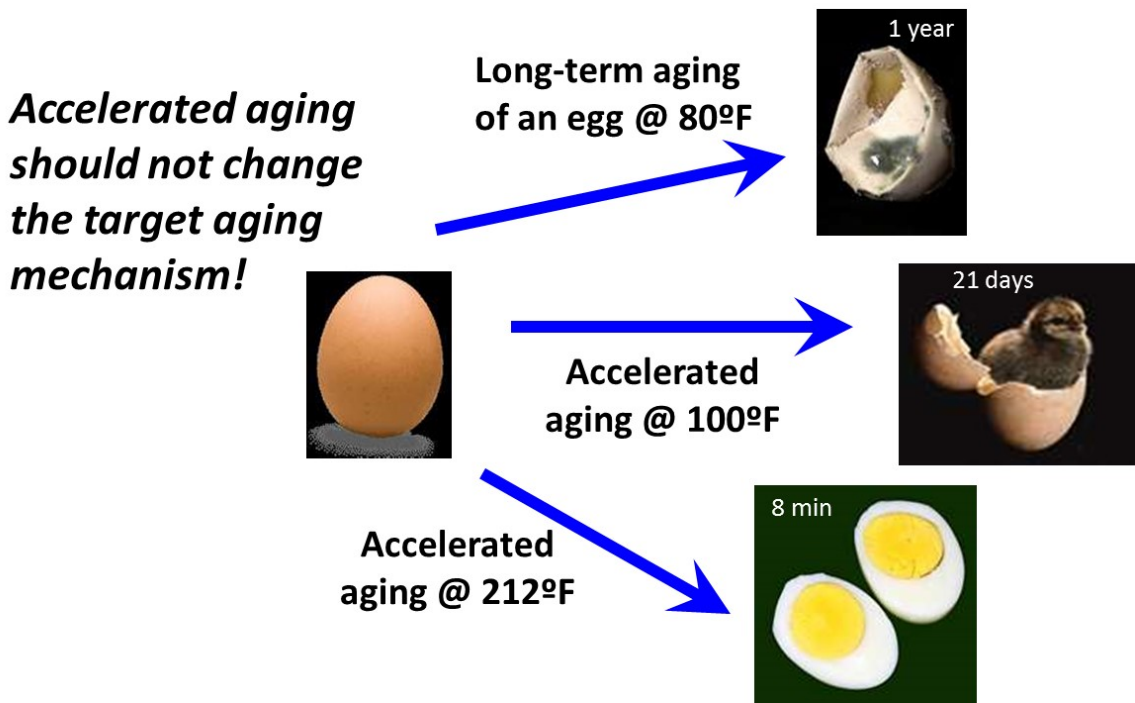
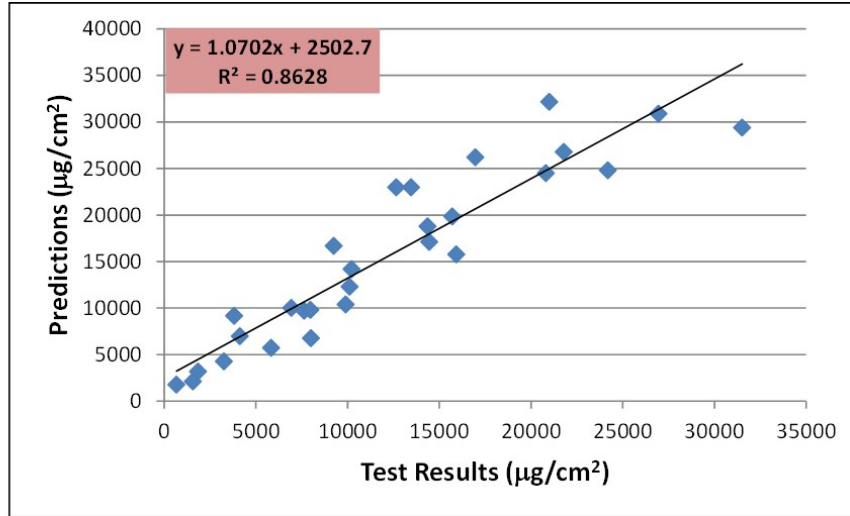


Figure 9.11-30. Accelerated Aging



R^2 value of 0.86 is higher than any published atmospheric corrosion rate prediction model intended for application at locations with diverse environmental conditions

Figure 9.11-31. Cumulative Damage Model Results

9.11.10. The F-16 Canopy Sill Longeron: Getting Control of a Multi-National Safety-of-Flight Issue

Kevin Welch and Tim Jeske, Lockheed Martin Corporation; Charles Babish, USAF Life Cycle Management Center; Bruce Harris, USAF F-16 SPO

After several F-16 aircraft were reported with cracking in the canopy sill longeron (Figures 9.11-32 and 9.11-33), a static residual strength analysis was performed to determine if the airframe could withstand a complete failure of the longeron. Prior to this investigation, this longeron was considered a non-safety-of-flight part. The results of this study showed that static residual strength was not maintained with a complete failure of the longeron; thus, the longeron must be managed with slow crack growth criteria and be treated as a safety-of-flight part. Since the fleet was well past the calculated damage tolerance inspection interval, more detailed finite element models (Figures 9.11-34 and 9.11-35) and updated crack growth models were developed. Also, short term repairs and a new longeron design were developed. A risk analysis was performed (Figure 9.11-36) to identify high risk aircraft and bases and to provide initial risk-based inspection requirements (Table 9.11-2). The resulting force management approach successfully protected flight safety while providing data that demonstrated more work was needed to fully control the issue. This technical activity will provide a chronology of how this issue was identified and describe the various structural analyses used to provide the information needed by the F-16 community to manage this issue.

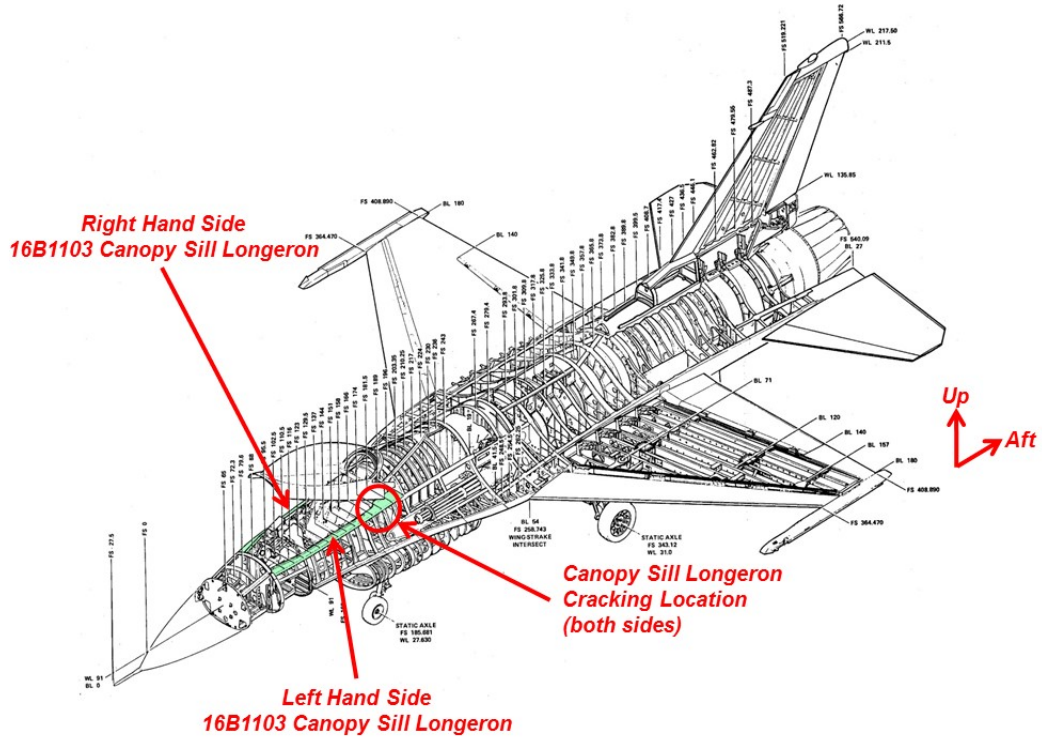


Figure 9.11-32. Canopy Sill Longeron Location

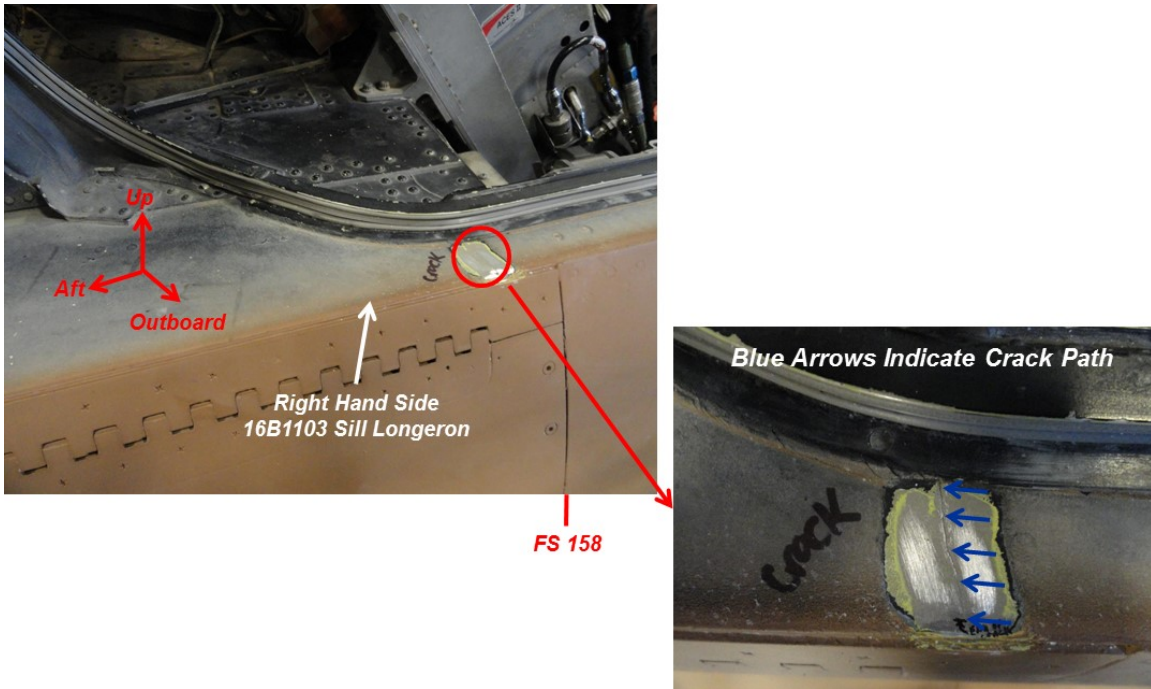


Figure 9.11-33. Photo of Cracked Area

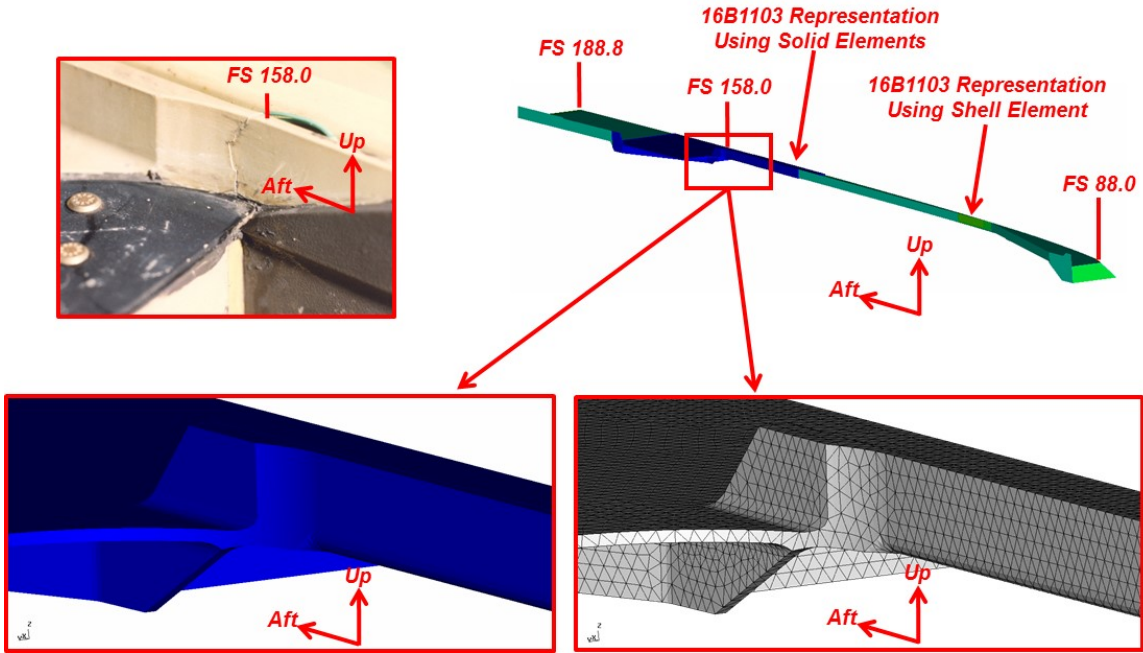


Figure 9.11-34. Finite Element Model Improvements

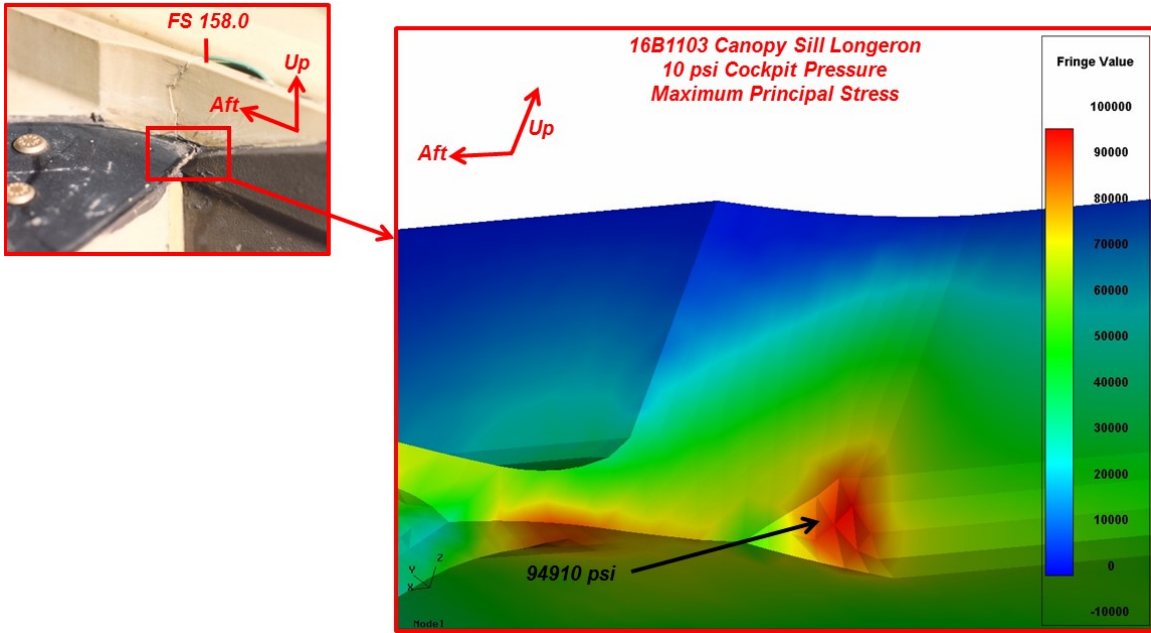


Figure 9.11-35. Improved Finite Element Model Analysis Results

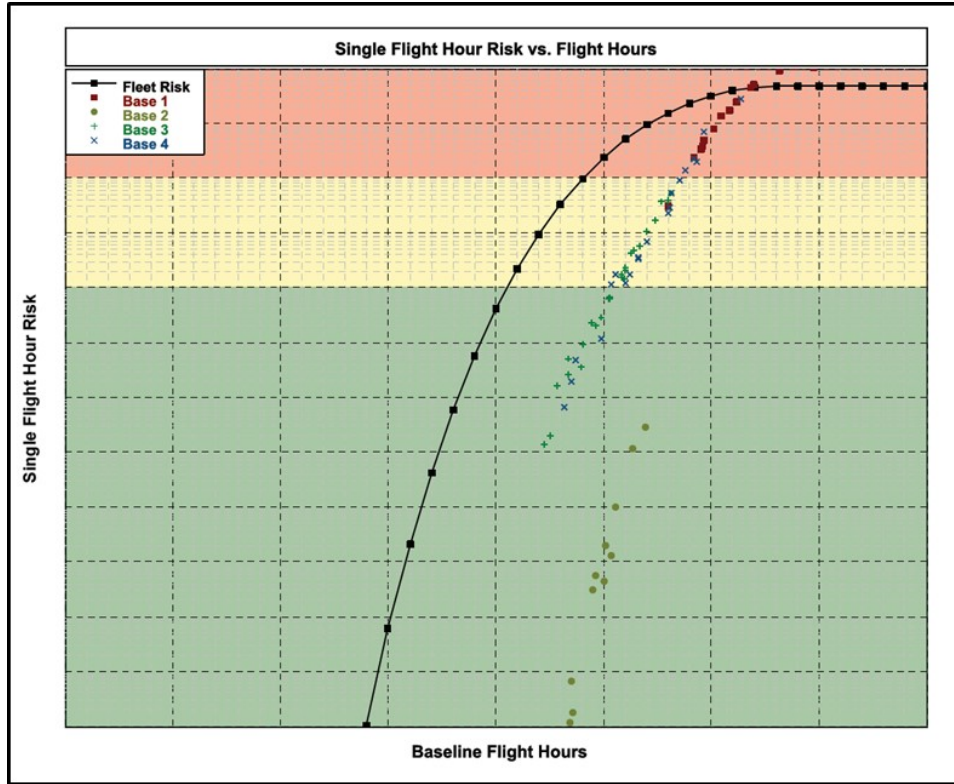


Figure 9.11-36. Initial Risk Analysis Results (Block 25/32)

Table 9.11-2. USAF Fleetwide Inspections

- Based on the Risk Analysis, TCTO 2705 Findings and Additional PROF Analyses, USAF Initiated Fleetwide Inspections (Skin Panel Removed) in March 2014:

TCTO	Affects	Compliance Period	Follow-On Inspection
2707	Aircraft > 10 ⁻⁵ risk	25 Hours	75 or 100, Based on Block 18 very High Risk Aircraft Required 3 x 10 Hour Inspections to Reduce Risk to Acceptable Levels
2708	Aircraft > 10 ⁻⁷ risk but <10 ⁻⁵ risk	100 Hours	
2706 (Included International Customers)	Aircraft < 10 ⁻⁷ risk	Next Phase	

- Supporting Tech Order Supplements were Issued:
 - -3 T.O. for Skin Panel Trim
 - -6 T.O. for Recurring Inspection Intervals
 - -36 T.O. for Improved NDI Procedure

9.11.11. Overview of the Full-Scale-Durability Tests on F-35 Lightning II Program

Robert Burt and Marguerite Christian, Lockheed Martin Corporation

The Aircraft Structural Integrity Program for the F-35 Lightning II is unique in that it includes dedicated full-scale static and durability test articles for each of the three variants included in the program: Conventional Take Off and Landing (CTOL), Short Take Off and Vertical Landing (STOVL), and Carrier Variant (CV) (Figure 9.11-37). These tests are a key component of the structural certification process. They provide the data required to validate the structural analyses and to demonstrate the strength and stability of the airframe. The static and durability tests enable efficiencies through test consolidation and also through economies of scale. Investments made in the test fixtures and data acquisition systems coupled with efficient test protocols enable testing to progress rapidly and efficiently. Durability testing of the airframe is conducted in dedicated fixtures at Lockheed Martin in Fort Worth, Texas and at BAE Systems in Brough, England (Figure 9.11-38). The Horizontal Tail (HT) and Vertical Tail (VT) tests are performed off aircraft and have completed the required two lifetimes of testing (16000 test hours) (Figure 9.11-39). Third lifetime testing is complete for HTs and is in progress for CV VT. All three full-airframe tests are in progress, having accomplished one lifetime of testing (8000 test hours). This technical activity provides an overview of the test methodologies, challenges faced, and the results to-date for F-35 durability test articles (Figures 9.11-40 through 9.11-45). The F-35 Static and Durability Test Programs, developed to satisfy the requirements of MIL-STD-1530C, continue to demonstrate the structural integrity of the F-35 airframe design.



Figure 9.11-37. Tri-Variant Joint Strike Fighter (JSF)

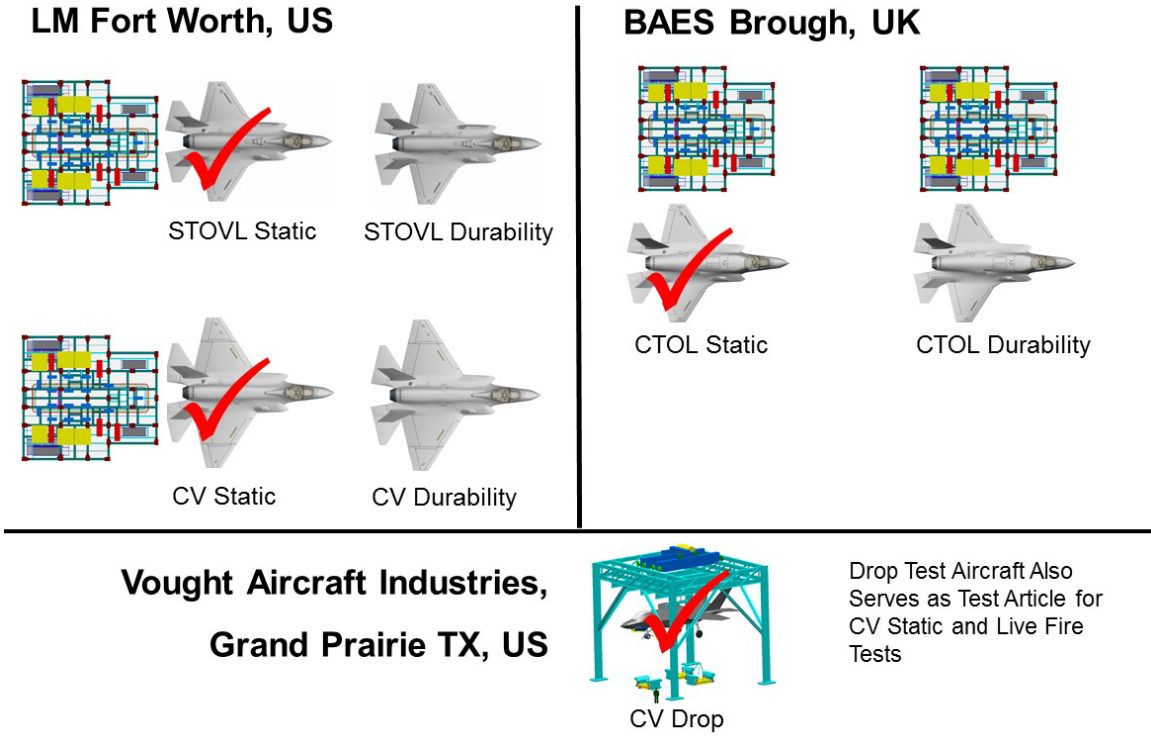


Figure 9.11-38. F-35 Full-Airframe Test Locations

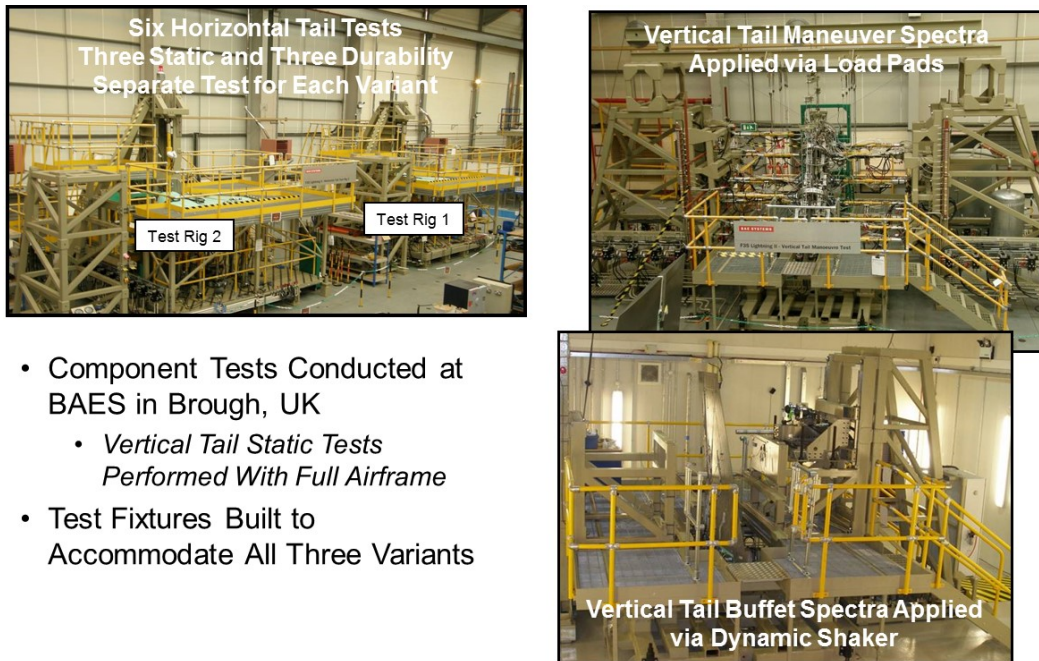


Figure 9.11-39. F-35 Off-Aircraft Component Tests

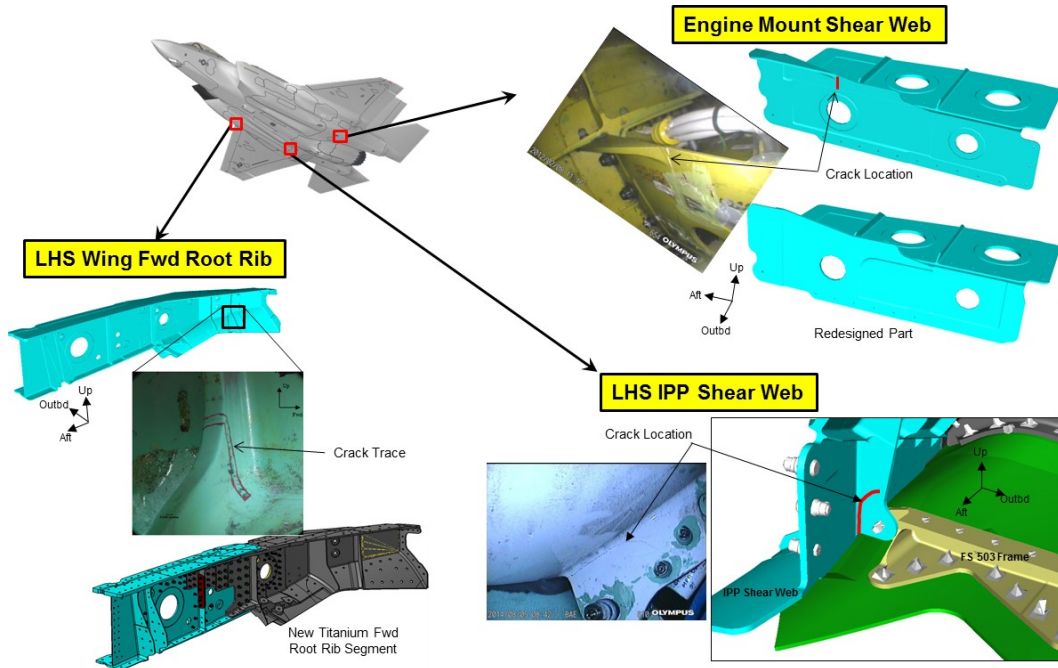
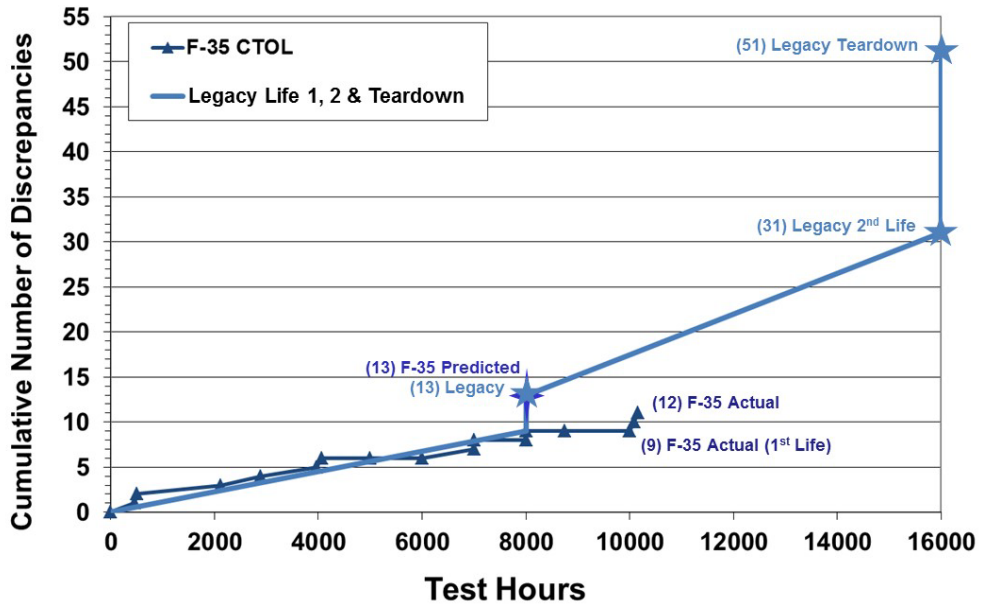


Figure 9.11-40. CTOL Test Findings



Note: Legacy Data coordinated through JSF Program Office to ensure accurate, consistent comparisons.

Figure 9.11-41. CTOL Discrepancies vs. Legacy

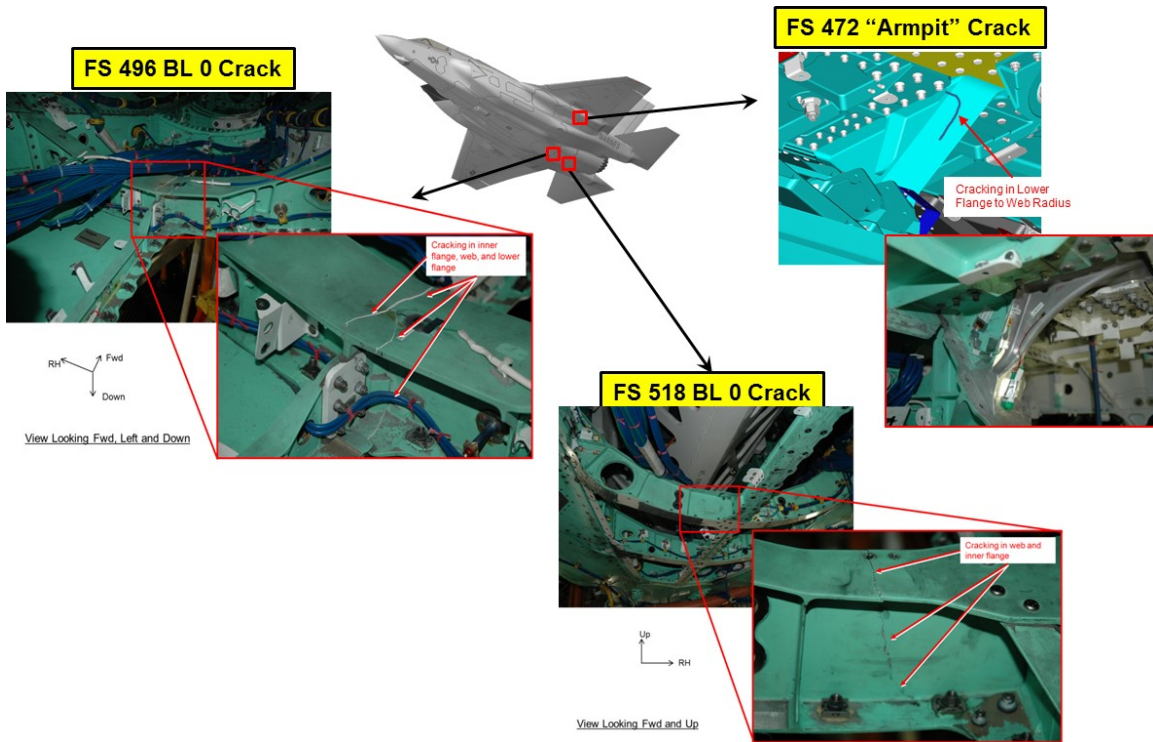
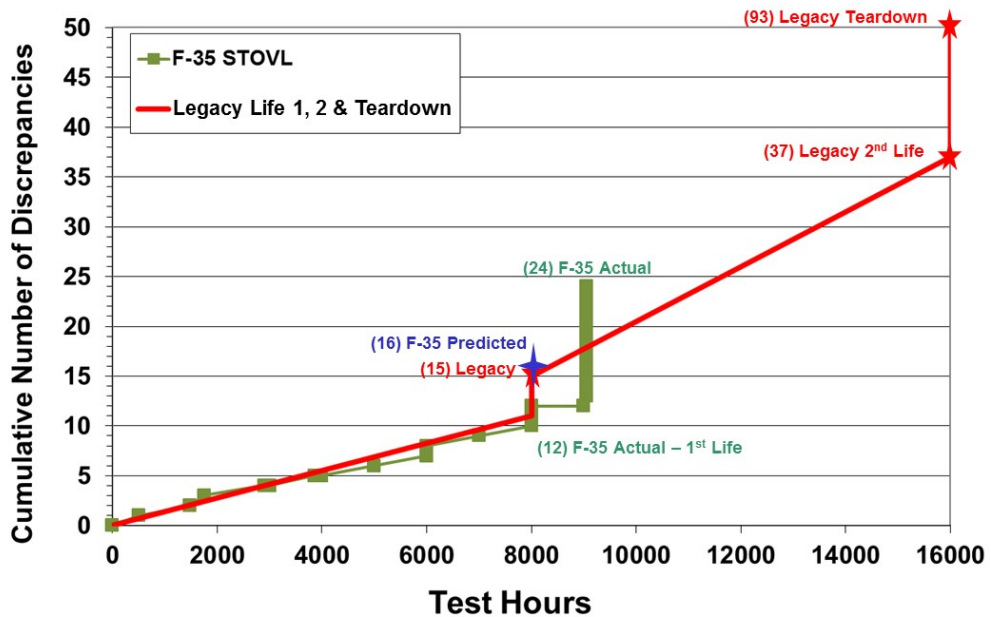


Figure 9.11-42. STOVL Test Findings



Note: Legacy Data coordinated through JSF Program Office to ensure accurate, consistent comparisons.

Figure 9.11-43. STOVL Discrepancies vs. Legacy

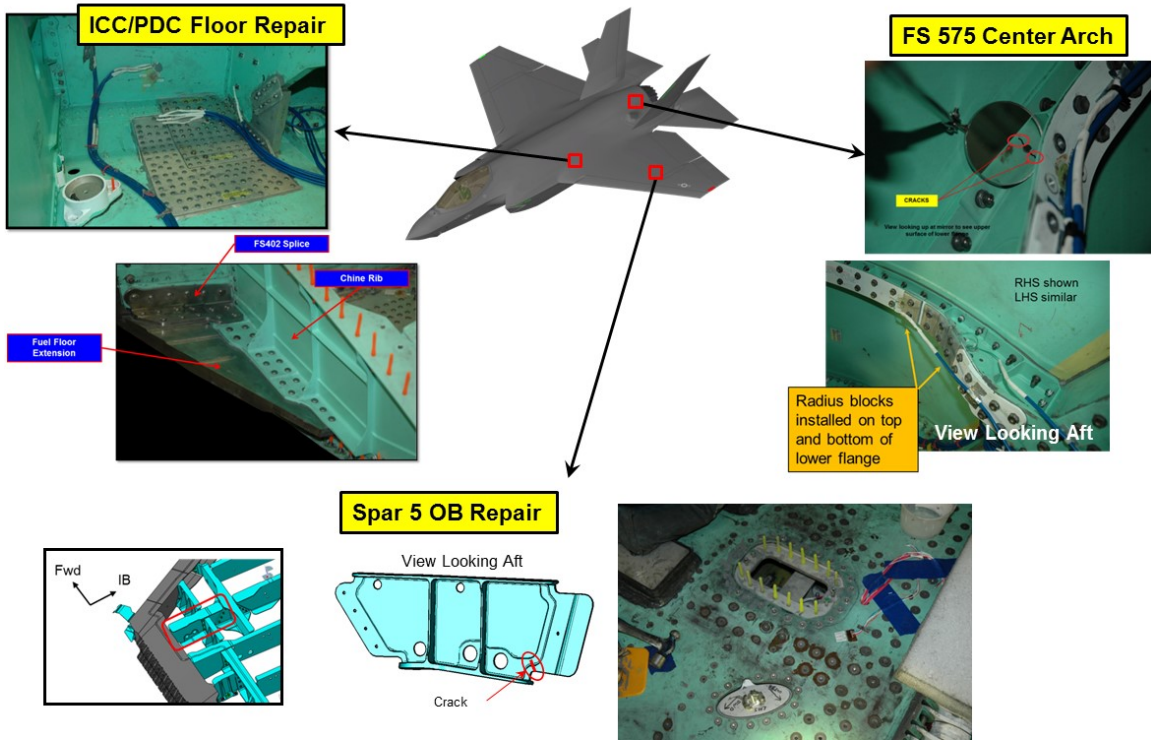
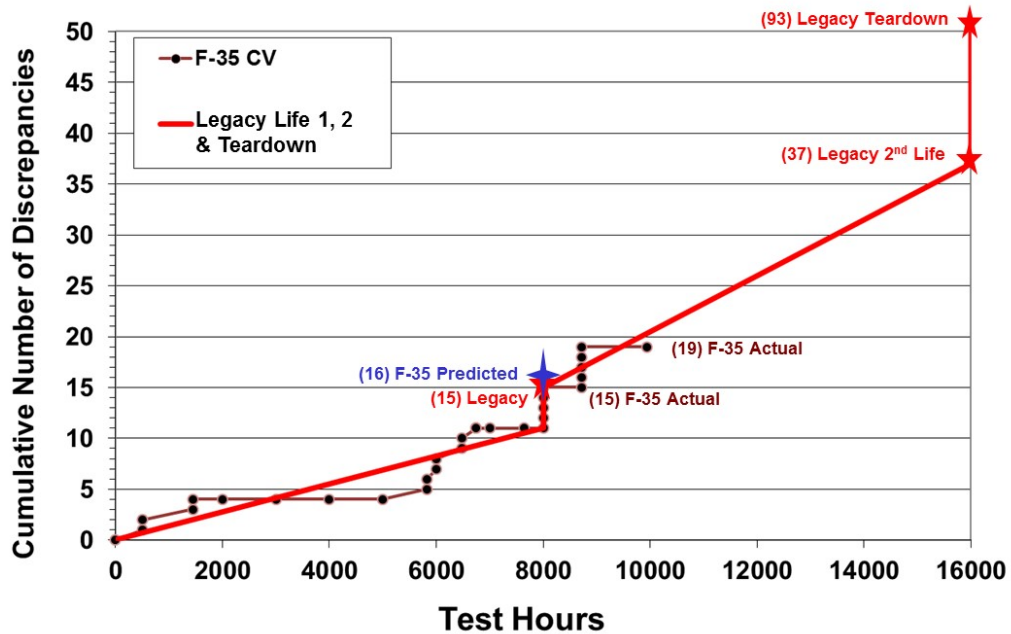


Figure 9.11-44. CV Test Findings



Note: Legacy Data coordinated through JSF Program Office to ensure accurate, consistent comparisons.

Figure 9.11-45. CV Discrepancies vs. Legacy

9.11.12. Importance of Corrosion Prevention Control Plans and Corrosion Prevention Advisory Boards

Terry Gabbert and Thomas Barfield, USAF Research Laboratory – Materials and Manufacturing Directorate

Corrosion prevention and control is defined as the rigorous application of engineering design and analysis, quality assurance, non-destructive inspection, manufacturing, operations, and support technologies to prevent the initiation of corrosion, avoid functional impairment due to corrosion, and define processes for the tracking and repair of corrosion problems. History indicates the effects of corrosion increase with system age, which only amplifies the need to consider corrosion prevention and mitigation strategies. The only way to ensure an effective, across-the-board response to prevention or a dramatic reduction of corrosion and its effects is to establish a standard corrosion control philosophy and methodology. With a clearly defined methodology, ASIP and corrosion engineers can initiate and execute plans and actions to employ acceptable materials, procedures and processes to mitigate the detrimental effects of corrosion. Corrosion prevention and control requires the coordinated efforts of numerous disciplines and organizations across the Air Force and Department of Defense. A detailed Corrosion Prevention and Control Plan along with a well-established and active Corrosion Prevention Advisory Board (Figures 9.11-46 and 9.11-47) can assist the ASIP manager in Structural Health Monitoring. MIL-STD-1530C, MIL-HDBK-1568, JSSG-2006 and Spiral IV of the DOD Corrosion Prevention and Control Planning Guidebook serve as references and venues for the Program Offices, structural and corrosion Program Managers and support staff responsible for tactical and strategic corrosion management planning. The basic approach for corrosion prevention and control has been modified a number of times during the life span of an aircraft. This becomes even more important as Aircraft Life Cycle Extension programs are put in place. Accurate and up-to-date information provided within a current Corrosion Prevention and Control Plan can assist the ASIP engineer in making operational and maintenance decisions. Corrosion Prevention Advisory Boards provide an avenue for direct feedback from the field/depot maintainer to the corrosion and ASIP communities, providing unique corrosion and structure related issues potentially affecting the airworthiness of the aircraft.

CPAB's are the Heart of a Corrosion Program



Figure 9.11-46. Corrosion Prevention Advisory Boards (CPABs)

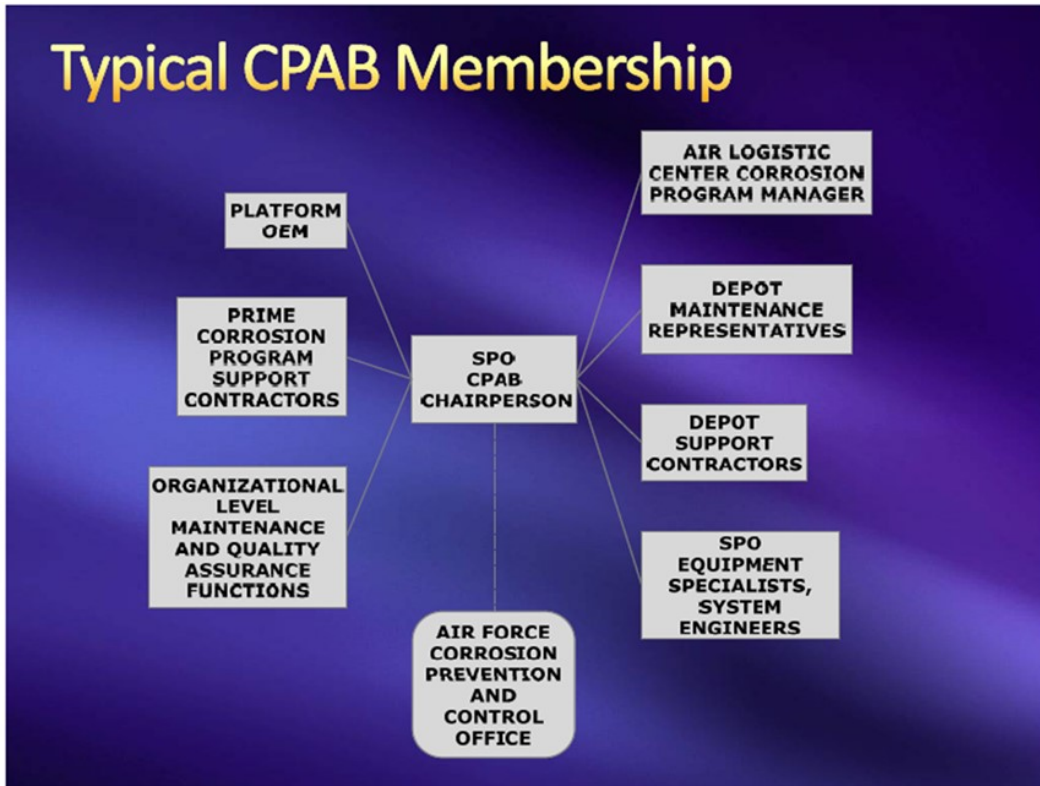


Figure 9.11-47. CPAB Membership

9.11.13. KC-135 Damage Tolerance Toolset Modernization Overview

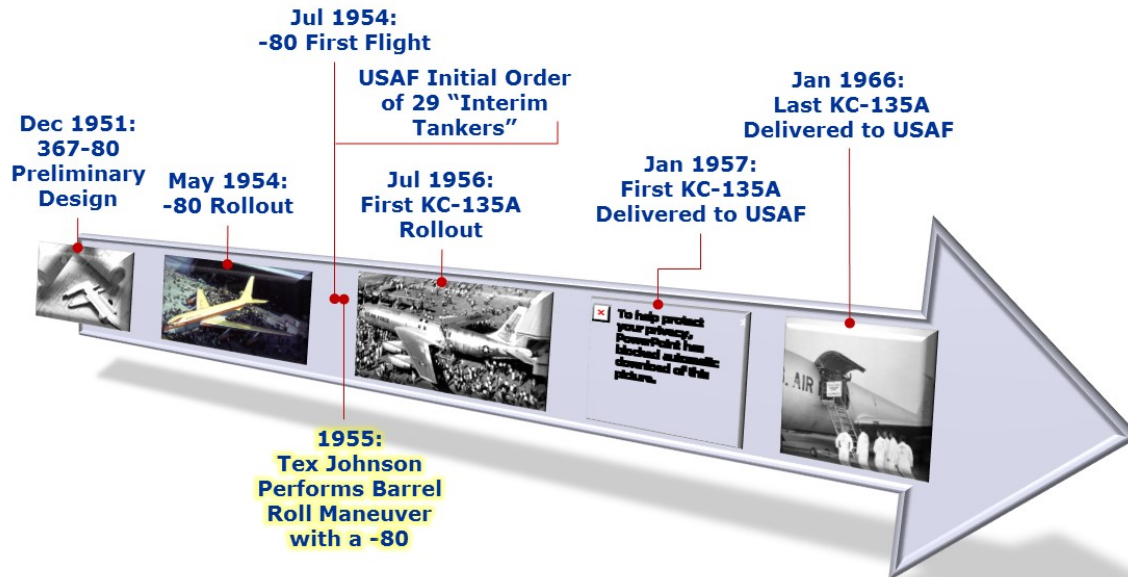
Lee Zambino, The Boeing Company

This technical activity summarizes a multi-year effort to modernize the 1970s-era KC-135 (Figure 9.11-48) Durability and Damage Tolerance (DaDT) toolset. The requirements, tasks, and decisions leading to the final modernized KC-135 toolset framework are discussed; an overview of the analysis flow is also provided. The KC-135 airframe is nearing 60 years of service and is anticipated to operate until 2040 (Figure 9.11-49). As the aircraft approaches its certified service life, it is apparent that modern, supportable, and more precise analysis software tools are needed to achieve the following objectives: - accurately predict current and/or anticipated damage findings - determine service life potential - define maintenance programs to safely achieve service life - evaluate potential onset of widespread fatigue damage. In 2011, a comprehensive finite element model (FEM) of the KC-135 airframe was developed and now provides the foundation for achieving the objectives stated above. To realize the full potential of the FEM, the legacy DaDT toolset (Figure 9.11-50) requires modernization. The modernization effort entails a complete overhaul of all existing tools (Figure 9.11-51). Legacy methodology, once implemented via FORTRAN source codes, is transitioned to modern software platforms and languages. Stress analysis, once reliant on gross-panel loads and unit-stress solutions, is now performed with detailed internal FEM loading in conjunction with advanced structural analysis tools. Stress spectra generation, once a black-box operation, now avails all computational steps to the user in a structured development environment. Crack growth analysis, once a command-line-driven action, may now be accessed through a full-featured Graphical User Interface (GUI). Improvements in the DaDT toolset also permitted improvement to the Individual Aircraft Tracking Program (IATP). Mission-by-

mission crack extension, once computed via a linear combination of factors, is now computed via cycle-by-cycle crack growth. In addition to toolset improvements, data management via modern data-basing constructs is also implemented. This provides the added benefit of facilitating full-cycle analysis automation, optimization, and rapid trade studies.



Figure 9.11-48. KC-135 Aircraft



- Boeing internally funded the development of the 367-80.
- Tooling and production infrastructure also internally funded prior to a single Air Force order.
- Of the 820 -135 aircraft, ~400 still remain in service; most are designated as USAF R/T model tankers.

Figure 9.11-49. Brief Production History

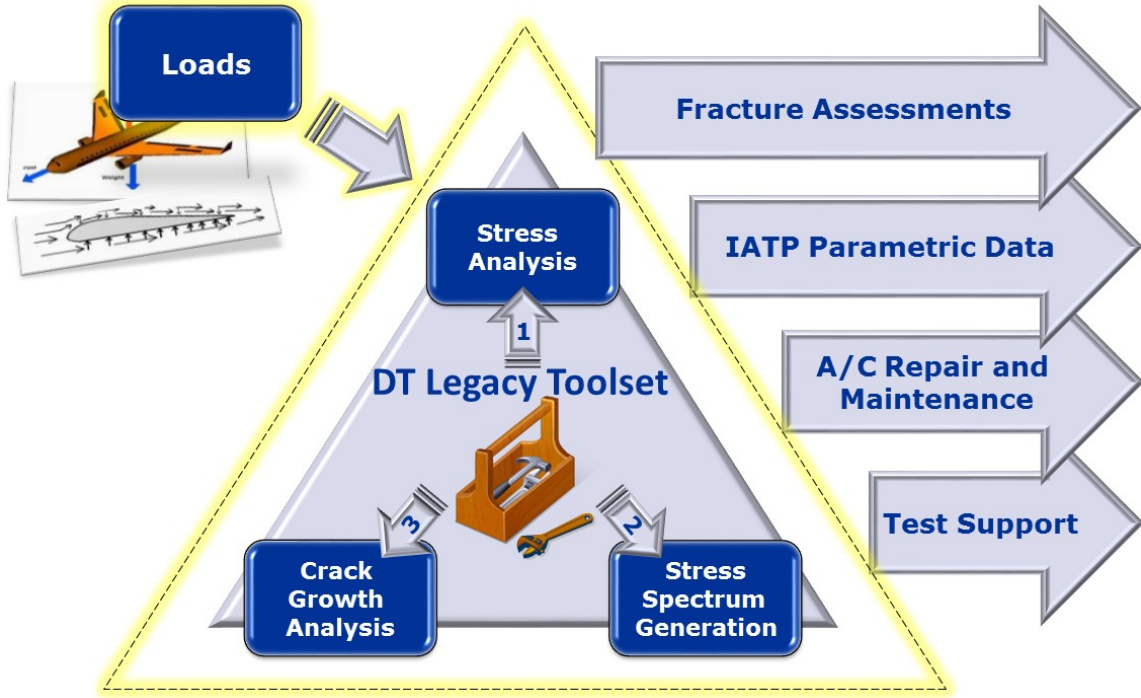


Figure 9.11-50. Damage Tolerance Legacy Toolset

– **Stress Analysis**

- » MS Office (Legacy)
- » CSW*, IAS*
- » PTC® Mathcad



```

@CCCCC 99999999 AAAA  @CCCCC KK KK 11111111 777777
@CCCCC 99999999 AAAA  @CCCCC KK KK 11111111 777777
CC CC 99 99 AA AA CC CC KK KK 11 11 77
CC 99 99 AA AA CC CC KK KK 11 11 77
@CCCCC 99999999 AAAA  @CCCCC KK KK 11111111 777777
CC CC 99 99 AA AA CC CC KK KK 11 11 77
@CCCCC 99 99 AA AA @CCCCC KK KK 11111111 77
@CCCCC 99 99 AA AA @CCCCC KK KK 11111111 77
A FLIGHT-BY-FLIGHT CYCLE-BY-CYCLE CRACK GROWTH PROGRAM (94)
    
```



– **Crack Growth**

- » CRACKIT (Legacy)
- » DTANAL*, LifeWorks*
- » AFGROW, NASGRO,



– **Stress Spectrum Generation**

- » FORTRAN (Legacy)
- » CSW*, IDTAS*
- » Custom code written in a modern programming language



* Boeing developed Tool

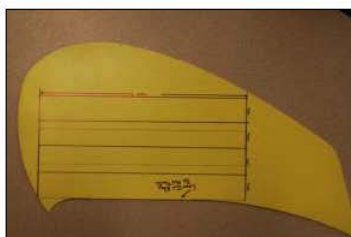
Figure 9.11-51. Tools Considered for Toolset Modernization

9.11.14. Durability Assessment for Non-Legacy Manufacturing Methods

Scott Carlson, Southwest Research Institute

This technical activity will present a method for assessing durability equivalence or variations for parts that were manufactured using Non-Legacy manufacturing techniques. Non-Legacy methods include processes such as laser cutting, water-jet cutting and wire Electro Discharge Machining (EDM). The legacy weapon systems operating in the USAF were certified for airworthiness under design and manufacturing techniques that are rapidly being replaced by advanced cutting and or melting techniques that allow for more rapid manufacturing and processing. The current airworthiness methodology assumes that parts and sub-assemblies used during maintenance conform to the original drawing requirements and specifications. This technical activity outlines a method for assessing durability related to new manufacturing methods that may not be qualified for use in airframe applications. The importance of performing these evaluations has been heightened by the diversity of the supplier base and the widespread use of alternative manufacturing methods supporting multiple aircraft types. The methodology presented will allow other weapon systems to review part suppliers' manufacturing techniques and determine process equivalency and ultimately consistency with maintaining airworthiness. In 2011, the A-10 ASIP Analysis Group was informed that over 100 part numbers were manufactured by a company that was known to produce parts using a Non-Legacy cutting method. The criticality of these parts ranged from non-structural hinges to fatigue and fracture critical items. A detailed review was conducted of each part number and its criticality to continued safe operation of the aircraft. Four parts were determined to be most critical and durability testing was necessary to assess the impact of the use of the Non-Legacy procedure. Three of the parts were manufactured from 7057-T6 Al and one was made from 4340 Steel, heat-treated to 180ksi (Figures 9.11-52 through 9.11-55). This technical activity will provide insight into the development of a durability test plan, coupon development, fatigue testing, microstructural evaluation, fractographic examination of fractured specimens (Figure 9.11-56), and Weibull data analysis (Figure 9.11-57) to support fleet management decisions. All coupons were manufactured from parts received from supply with as-manufactured edge conditions and heat treatments. This presented unique design requirements and constraints that were overcome with the lessons learned. In addition to durability testing, an extensive microstructural evaluation was performed to characterize the effect of the cutting process on the surface integrity. Recommendations and lessons learned will be provided to the ASIP community to help reduce the impact of Non-Legacy parts and processes on airworthiness and structural integrity of other weapon systems.

- Slat Fence (P/N 160D611501-105)
- Trunnion Shear Tie (P/N 160D611109-11)
- Lwr. Wing SLEP Strap (P/N 160D611653)



Incoming Condition of Provided Slat Fence – P/N 160D611501)



Incoming Condition of Provided Trunnion Shear Tie (P/N 160D611109)



Outboard Section of Lwr. Wing Skin SLEP Strap (P/N 160D611653)

Figure 9.11-52. Evaluation of 3 Critical Parts

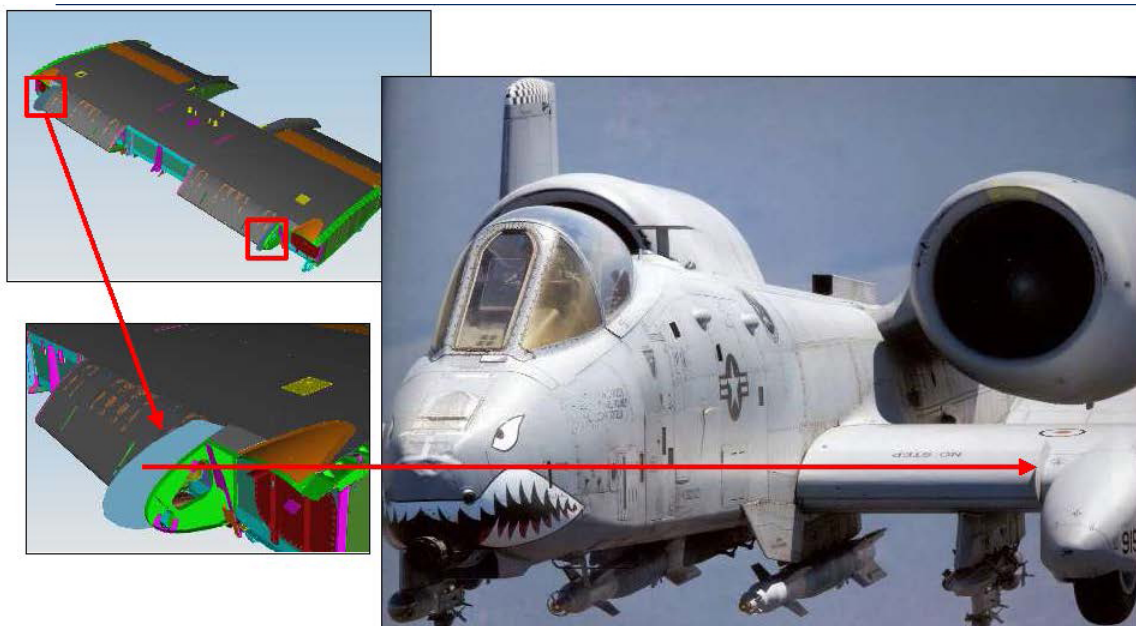


Figure 9.11-53. Location of Slat Fence

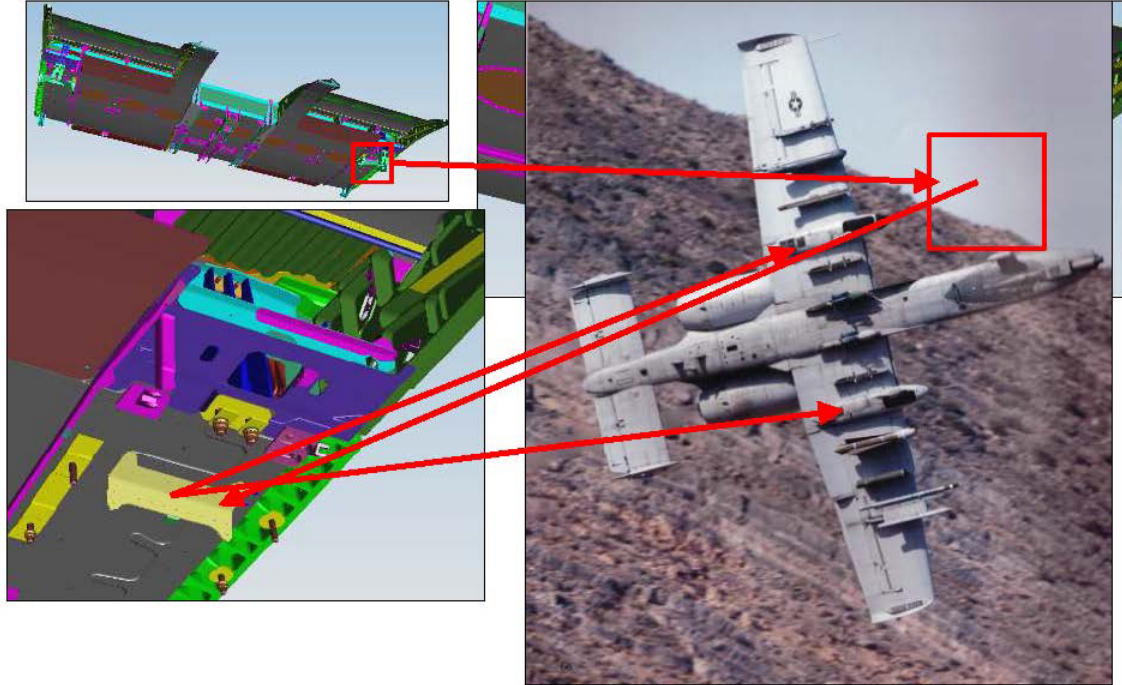


Figure 9.11-54. Location of Trunnion Shear Tie

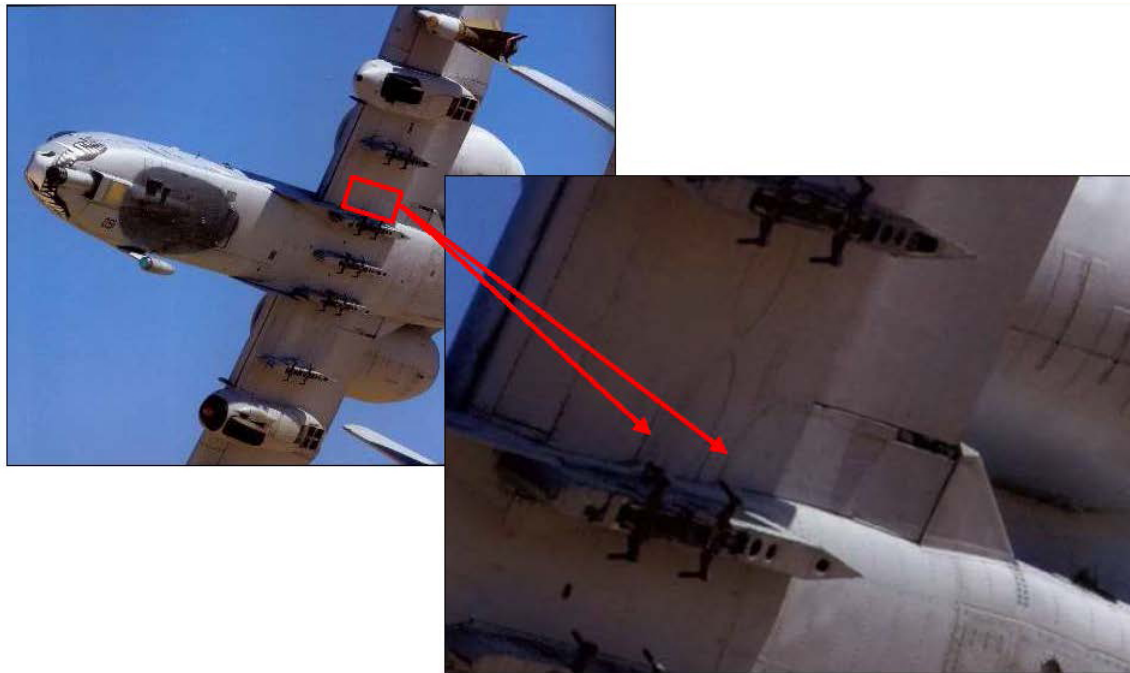


Figure 9.11-55. Location of SLEP Straps

- View Looking Down on Laser Cut Edge

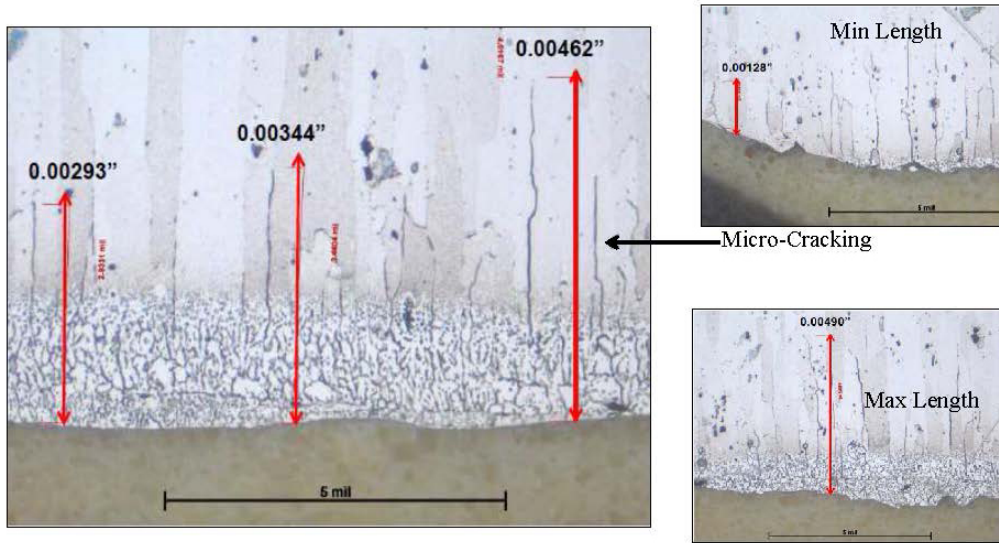


Figure 9.11-56. Metallurgical Evaluation of 7075-T6 Al

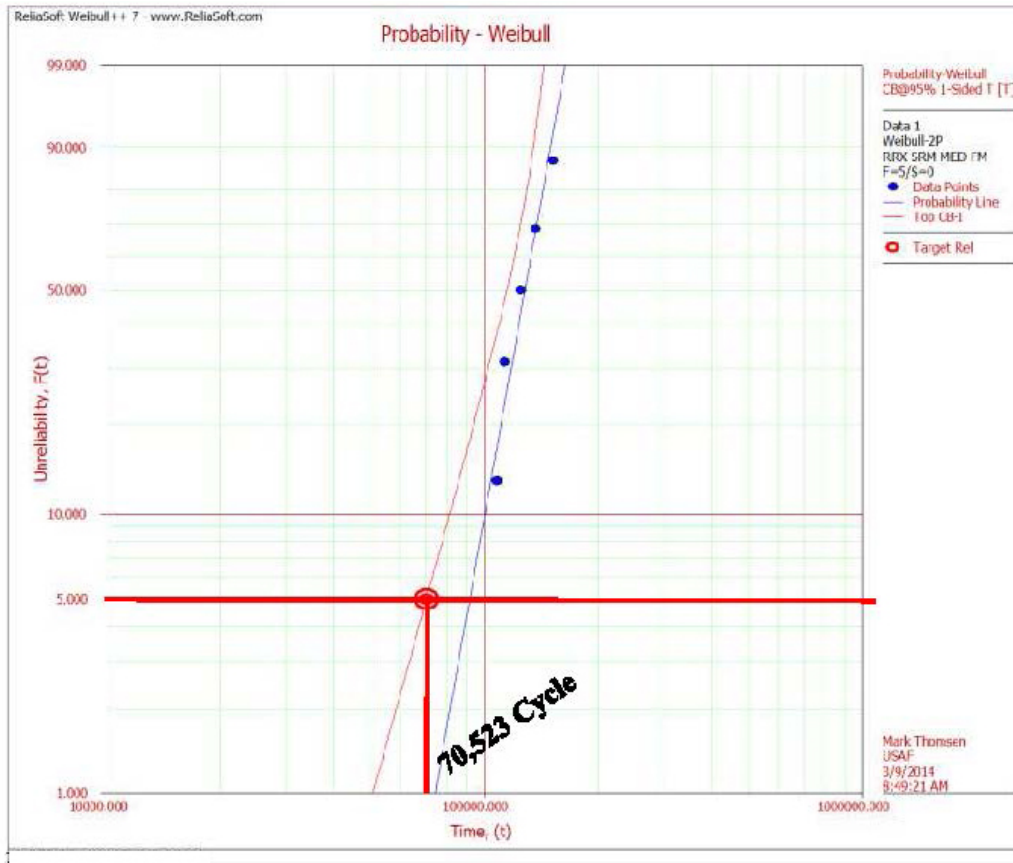


Figure 9.11-57. 2-Parameter Weibull Distribution for Baseline Material

9.11.15. Structural Component Corrosion Simulation – Test Program Update

Steven Thompson and Michael Spicer, USAF Research Laboratory – Materials and Manufacturing Directorate; Nicolas Jacobs, University of Dayton Research Institute

In response to calls from the ASIP and structural design communities regarding the aging fleet and serious environmental concerns about the continued use of corrosion protection schemes, the Air Force Research Laboratory's Materials and Manufacturing Directorate (AFRL/RX) is performing a novel multi-year building-block-testing program aimed at providing qualitative structural corrosion data for use in airframe risk assessments. Currently, much of the data used for qualifying materials or corrosion protection schemes are collected using coupon-level testing under tightly controlled conditions (Figure 9.11-58). However, operational airframes are not manufactured or operated in the same tightly controlled conditions nor are coupon tests always able to capture synergistic effects among the variables. The gap between coupon-level testing and an airframe's operational experience has limited the value and utility of much of the corrosion-related test data generated to date. ASIP managers do not currently have sufficient corrosion information required to translate operational and sustainment requirements into usable risk analyses. A new paradigm for corrosion testing was required that eliminates any materials bias and provides information on corrosion protection systems as they perform in the actual (or very close to actual) environment (stress, as well as environment). The objective of this building-block approach is to bridge the S&T gap by developing a test specimen (or series of test specimens) that simulate airframe structural elements and simultaneously subject the specimens to conditions similar to that of an operational airframe (Figure 9.11-59). This testing effort is intended to lead to a protocol for a well-defined and accepted methodology to provide corrosion susceptibility for a range of aerospace materials, structural designs, environments (Figure 9.11-60), and corrosion protection schemes that may be used in future USAF and industry risk assessment efforts. To date, a feasibility study has been performed that has laid the groundwork for the effort, including the initial test specimen design, testing protocols, and inspection processes (non-destructive and tear-down) (Figure 9.11-61). This technical activity will focus on the results from this initial effort as well as discuss the design of experiments that is being used for a scaled-up program using beach exposure.

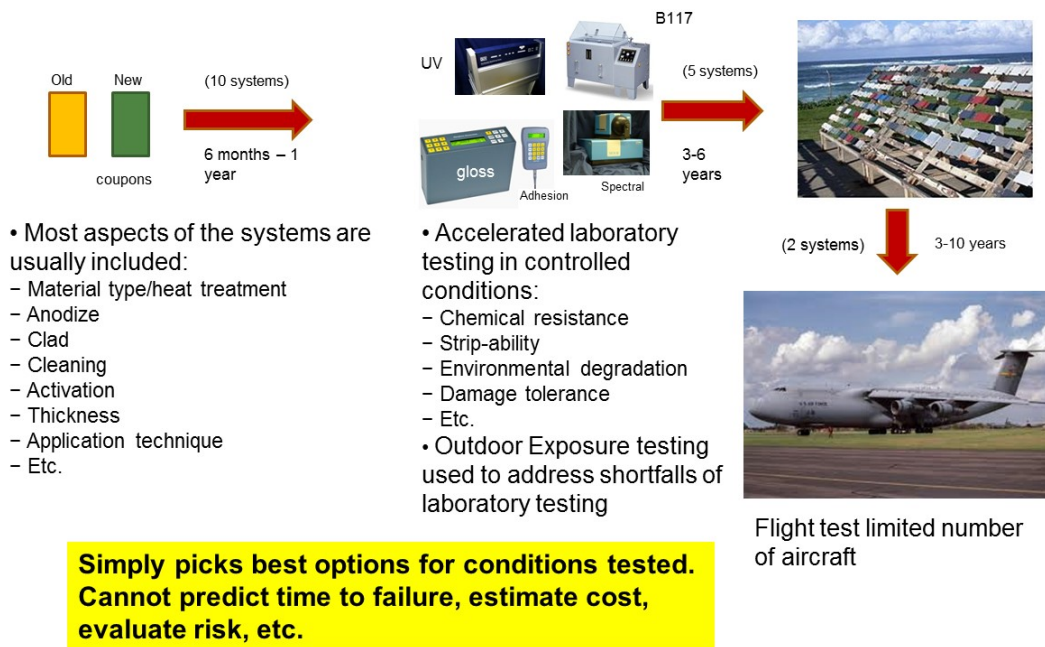


Figure 9.11-58. Current Design and Material Qualification

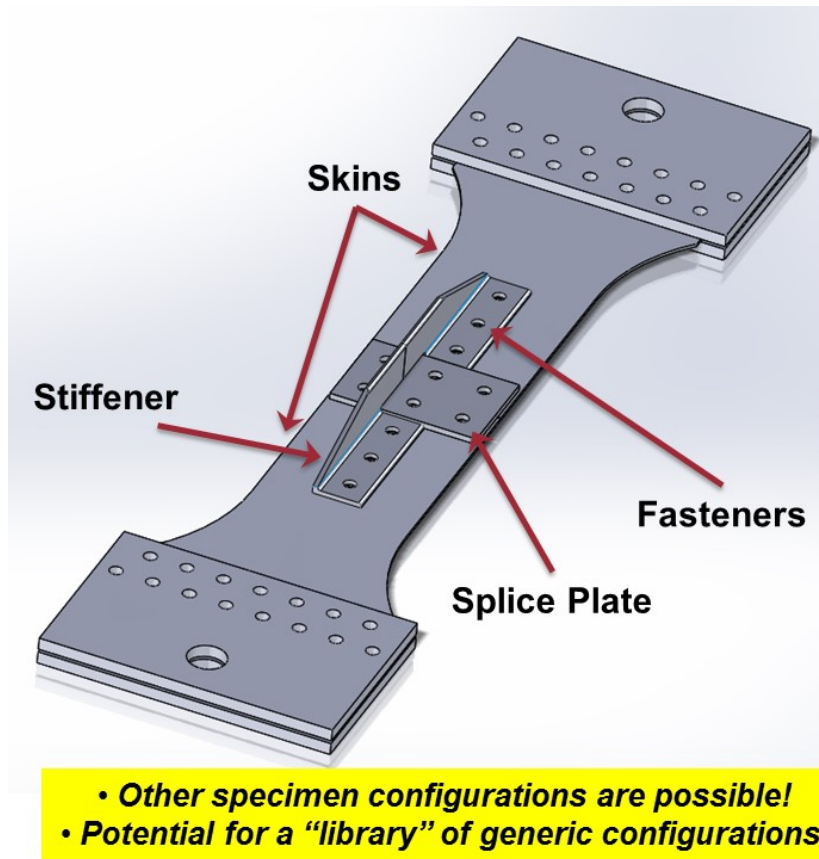


Figure 9.11-59. Test Specimen Design for Cargo Fuselage



Figure 9.11-60. Fatigue Test Chamber

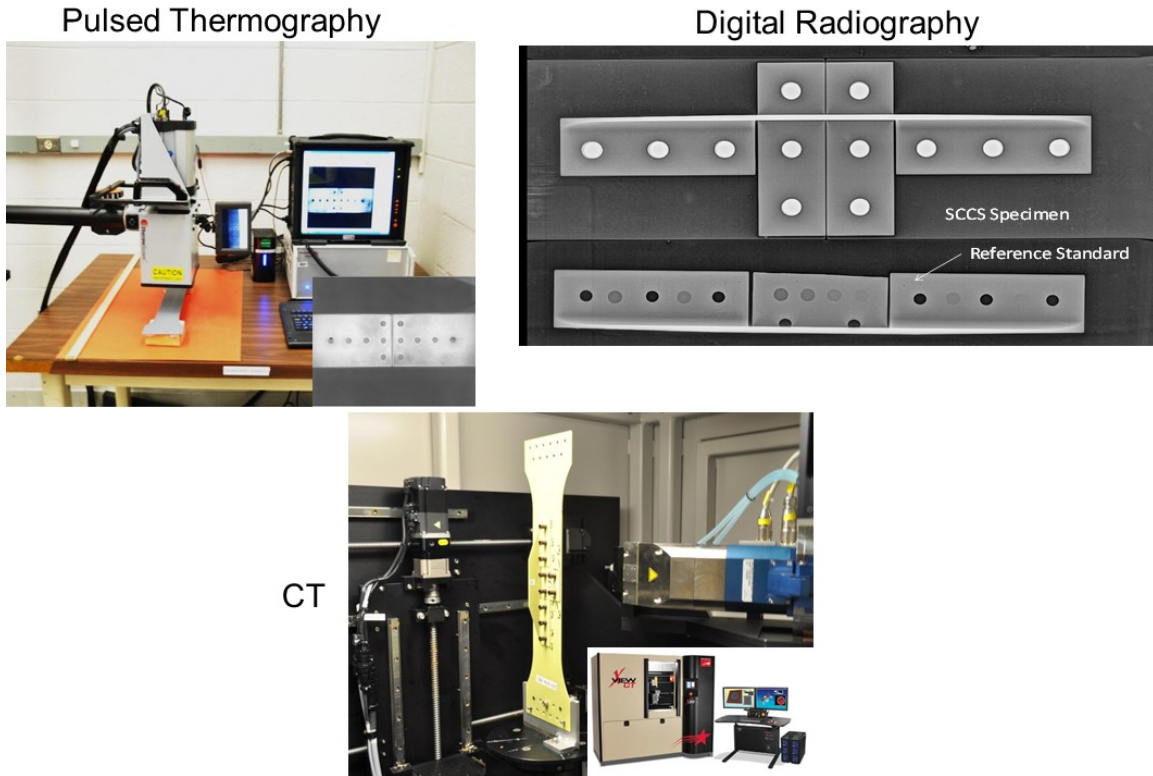


Figure 9.11-61. NDE Protocol

9.11.16. Investigation of C-5 Honeycomb Floor Panel Dent Limits

Chad deMontfort and Gregory Wood, Mercer Engineering & Research Center; David Wilkinson and Kevin Reid, USAF C-5 ASIP

C-5 honeycomb floor panels (Figure 9.11-62) undergo a high number of costly repairs and replacements in the field and at depot under current 1C-5A-3 technical order (TO) guidelines. This prompted the United States Air Force's (USAF) C-5 system program office (SPO) to initiate research into increasing the allowable dent limits in order to reduce maintenance downtime and costs. The C-5 SPO tasked Mercer Engineering Research Center (MERC) to evaluate existing C-5 dent limits and to investigate the extent to which they may be safely relaxed. MERC's investigation included laboratory strength testing as well as finite element analysis of several floor panel configurations. MERC designed and built fixtures for controlled denting and testing of floor panel coupons to the point of failure in bending, tension, compression, and shear. Of these four failure modes, bending was found to be the mode most affected by the presence of dents located on the compression side of panels (Figures 9.11-63 and 9.11-64). The resulting failure is highly localized buckling across the facesheet experiencing compression. This was followed by tests involving multiple dents of different sizes and spacing. The conclusion from this testing is that dent spacing is also a significant factor in reducing floor panel bending strength. The experimental work was complemented by finite element analysis (FEA) to characterize the parametric relationships between panel bending strength and dent diameter, depth, and the center-to-center spacing between dents. LS-Dyna was used for the FEA, which required nonlinear simulations due to the large deformations and nonlinear material behavior of the aluminum honeycomb core and facesheet when subjected to denting (Figures 9.11-65 and 9.11-66). FEA permitted rapid simulations of many combinations of dent geometries, enabling MERC to characterize the relationships among the primary

variables: dent diameter, depth, and center-to-center spacing. The study produced updated TO dent limits that safely permit panels with larger dents to remain in the aircraft. In addition, the new limits represent center-to-center dent spacing as a multiple of the largest dent diameter. Finally, the update allows dents to be closer to panel edges than previous TO limits allowed.

- Project focused exclusively on the floor panels of the relief crew compartment and troop compartment (primary structure)
- Panel construction:
 - Core: 3.1-1/8-7N 5056 aluminum, .625" thick
 - Facesheets: .030"-0.032" thick 7075-T6 aluminum

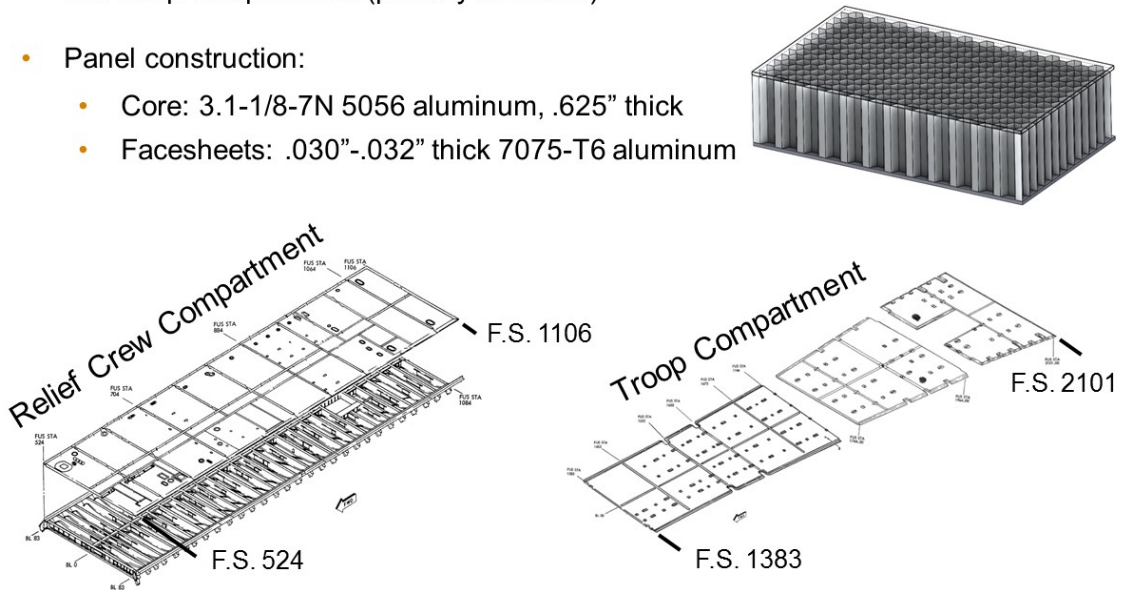


Figure 9.11-62. Areas of Focus

- Typical 4-point bend test. Constant moment/stress between upper load arms.
- Failure mode is instantaneous buckling.
- Undented baseline tests all failed under load arms.
- Noticeable decrease in dented panel residual strength

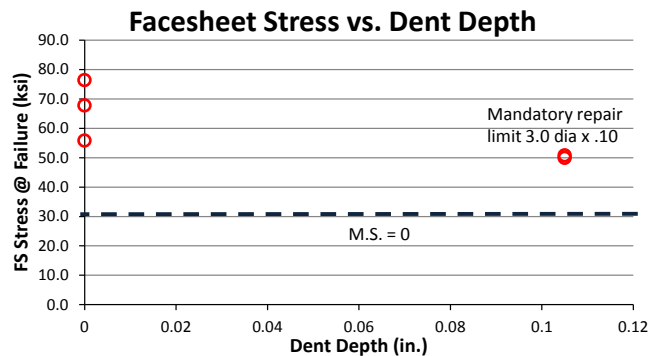
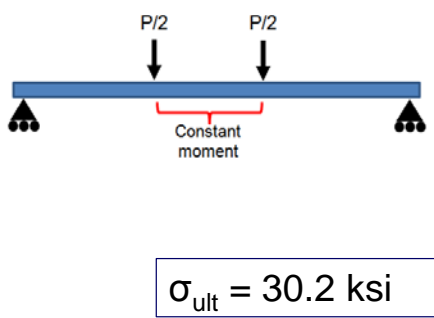


Figure 9.11-63. Bending Sensitivity Testing

- MERC concluded from the baseline testing that the bending scenario was most “sensitive” to the presence of a dent
- Single dent failure M.S. = 0.68.
- Validate dent separation requirement.

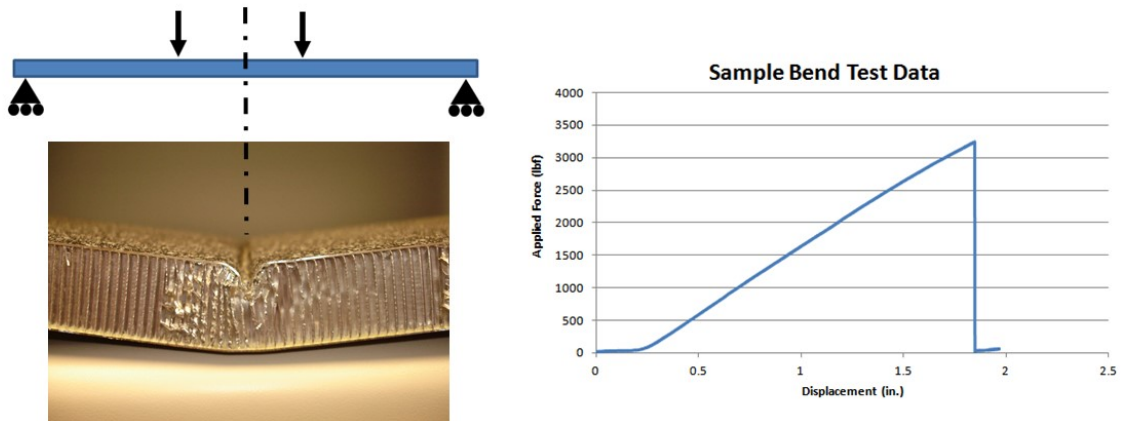


Figure 9.11-64. Bending Sensitivity Test Results

- Compare FEA failures with matching physical test failures
- Good correlation for smaller dents
- Under predicting failure stress for large dents
→ Conservative

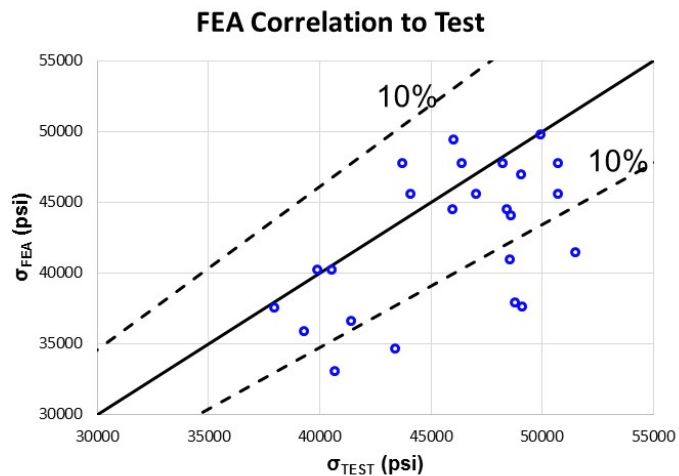


Figure 9.11-65. FEA Validation

- Predictions based on characteristic equation shown for all test points
- Trends similar
- Conservative failure predictions

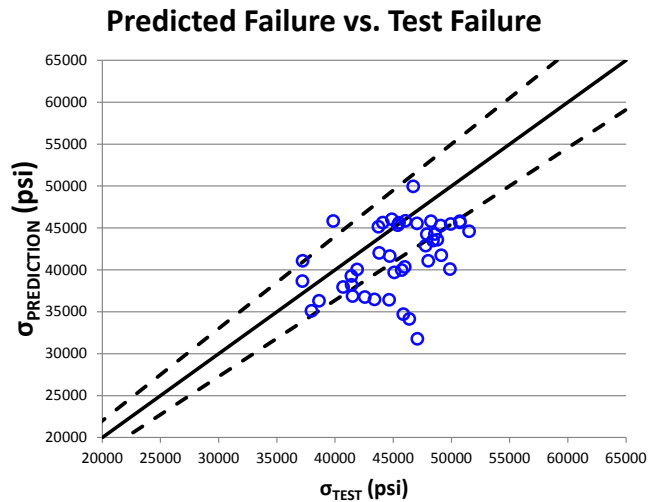


Figure 9.11-66. Analytical/Experimental Correlations

9.11.17. Integrity of F/A-18 A-D Wing Root Stepped-Lap Joint

Waruna Seneviratne, Wichita State University (NIAR) and Madan Kittur, “USN-NAVAIR

The United States Navy undertook extensive effort in the original certification [1], [2] of the F/A-18 A-D wing-root structure which consists of an AS4/3501-6 carbon/epoxy composite stepped-lap joint bonded (Figures 9.11-67 and 9.11-68) with FM-300 film adhesive to a 6Al-4V titanium splice fitting. This joint is complex and is considered one of the most critical in aircraft; therefore, its static and fatigue strengths were thoroughly evaluated [3].

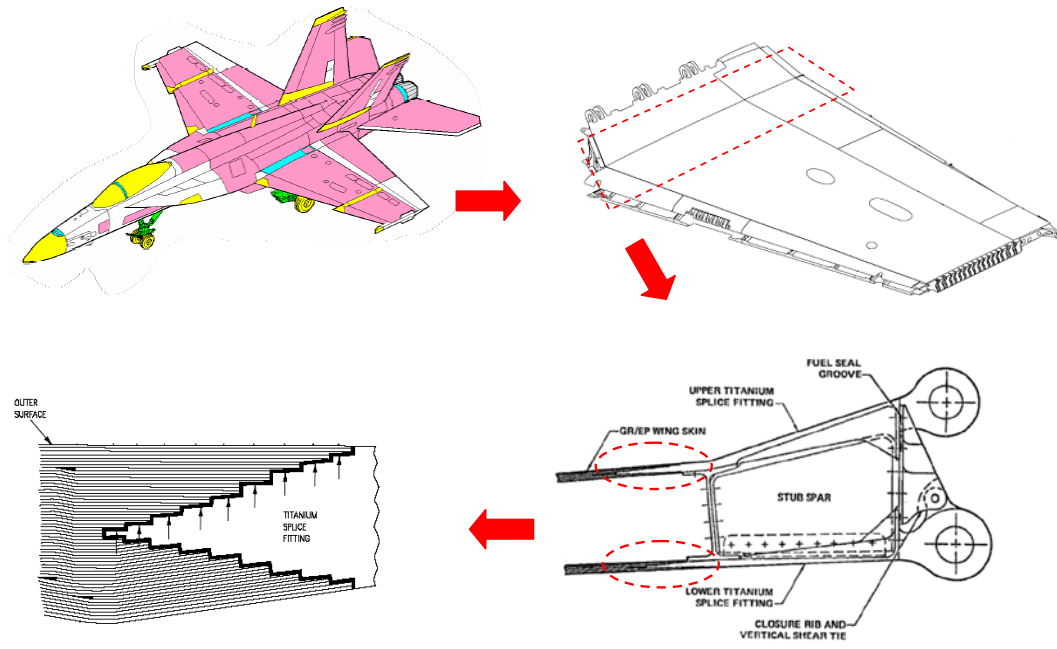


Figure 9.11-67. F/A-18 A-D Inner-Wing Composite-to-Titanium Stepped-Lap Bonded Joint

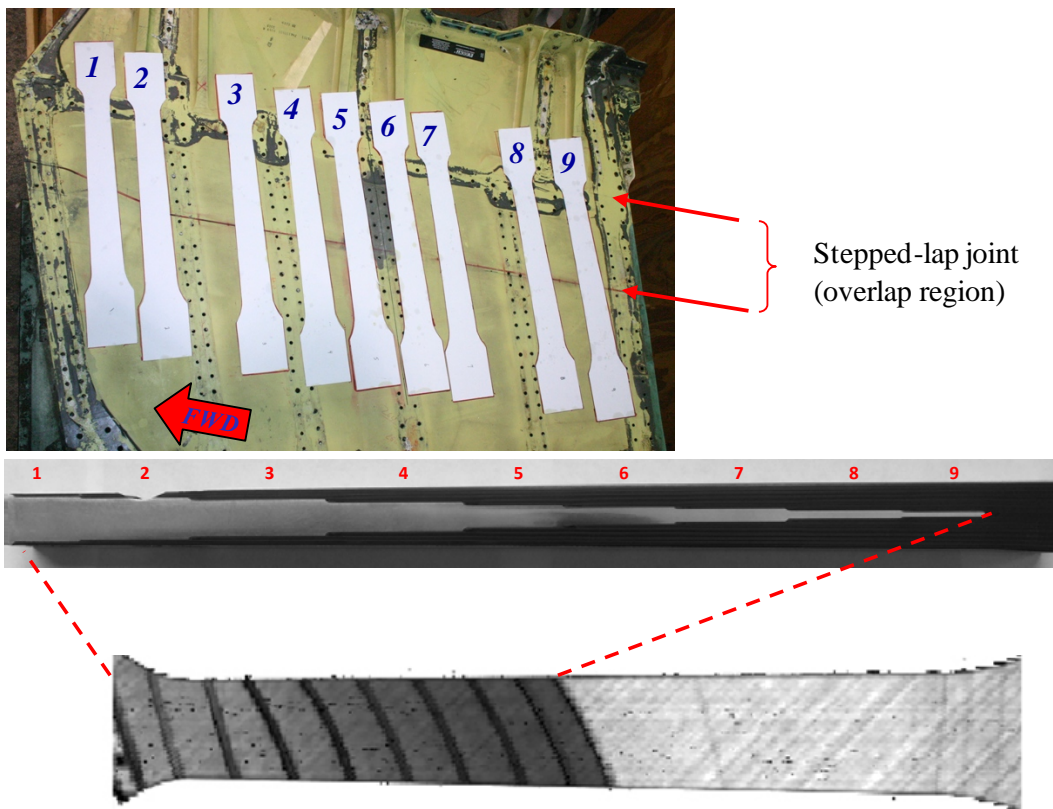


Figure 9.11-68. Specimens Extracted for Retired Wings

Now that the F/A-18s are nearing their sun set, the Navy undertook a study at the National Institute for Aviation Research (NIAR) in Wichita State University (WSU) to evaluate the residual static strength and remaining life of this joint after fleet service. Specimens were extracted from both upper and lower skins from decommissioned F/A-18 wings with expended wing-root fatigue lives ranging from a half lifetime to one lifetime. These specimens were subjected to static [4] and fatigue tests exactly as the specimens were tested on scrapped wings and test articles during original certification [5]. Static tests results showed no loss of strength (Figure 9.11-69). Fatigue test results show a minimum of 5 lifetimes of life remaining (Figure 9.11-70). The residual strength tests on those specimens that were stopped after 10 or more lifetimes of testing showed very little loss in strength as well. Fatigue failures in the joint typically initiated in the titanium step root radii (Figure 9.11-71). As the crack progressed a distinct drop in the joint stiffness was observed. The crack then progressed as delaminations after the crack had severed the titanium step [6], [7].

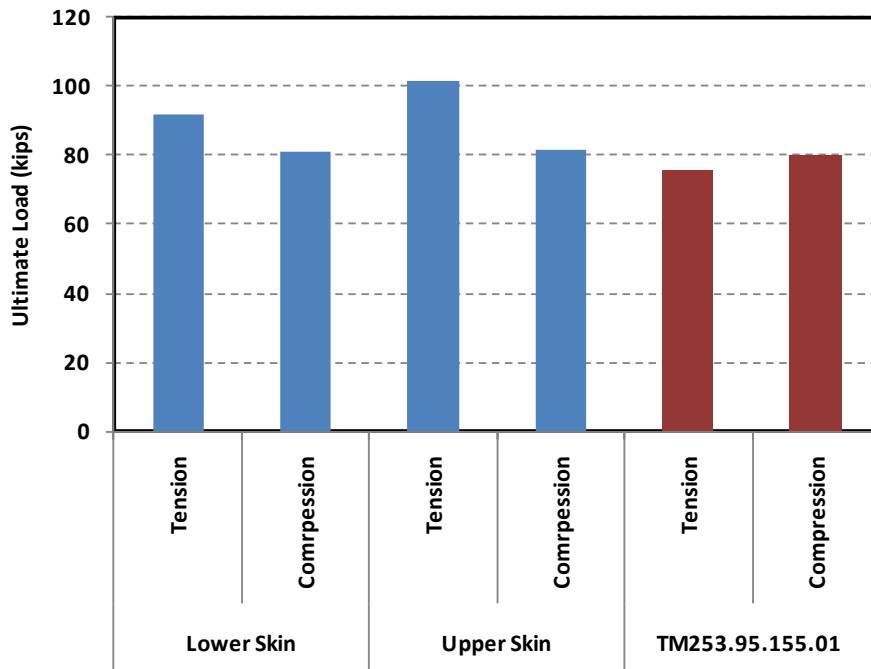


Figure 9.11- 69. Averages of Static Test Results (Blue) Compared with Original Tests (Red)

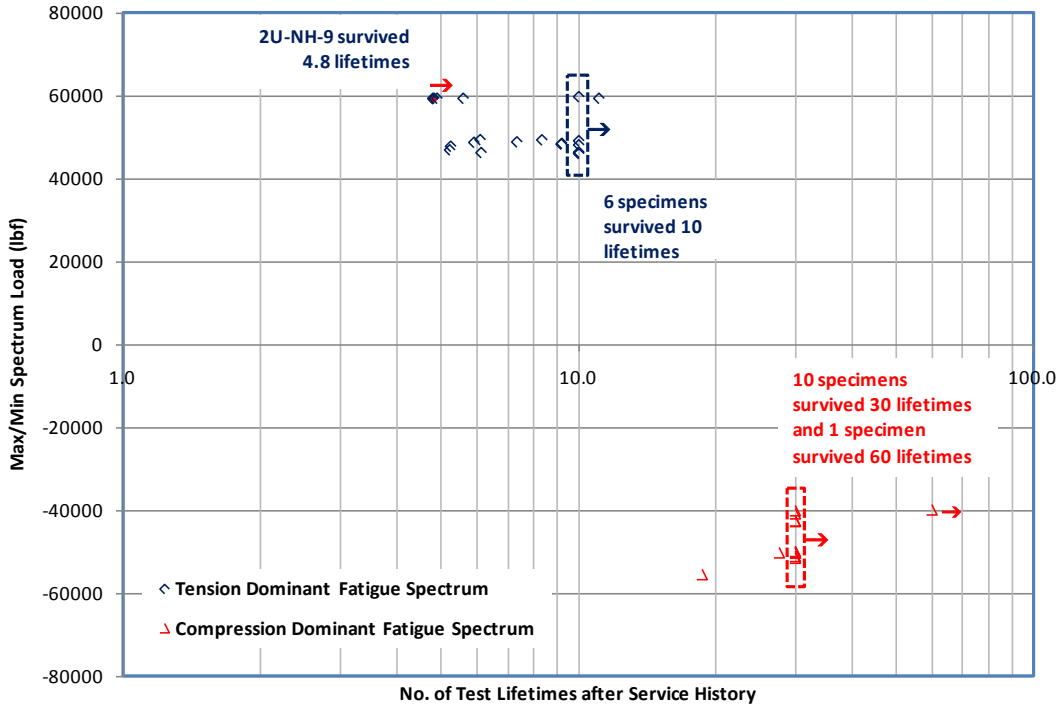


Figure 9.11-70. Results of Fatigue Tests Showing a Minimum of 5 Lifetimes of Fatigue Life Remaining After Fleet Service

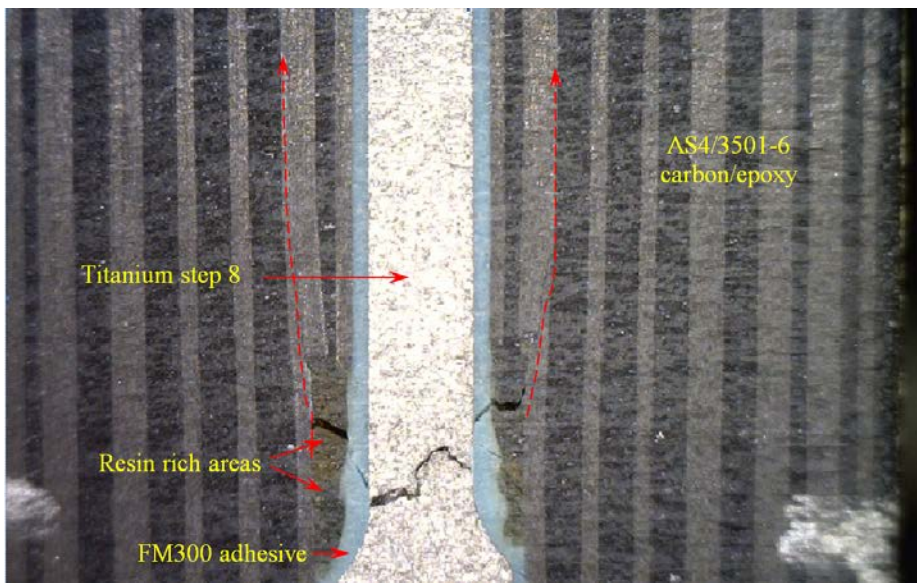


Figure 9.11-71. Failure Typically Initiated in the Titanium and Progressed as Shown in Red Dotted Lines

Next, a full-scale test was carried out at NIAR. The test article consisted of a center fuselage, left and right inner wings with their trailing-edge flaps (Figure 9.11-72). Both wings were obtained after aircraft retired after one full lifetime of service. They were exposed to various operational environmental conditions during the course of aircraft deployments. Fatigue test [8], [9] was carried out for 1.38 of a

lifetime using the original test spectrum before the test was stopped. No significant damage was noted in the composite structure or bonded stepped-lap joint areas.

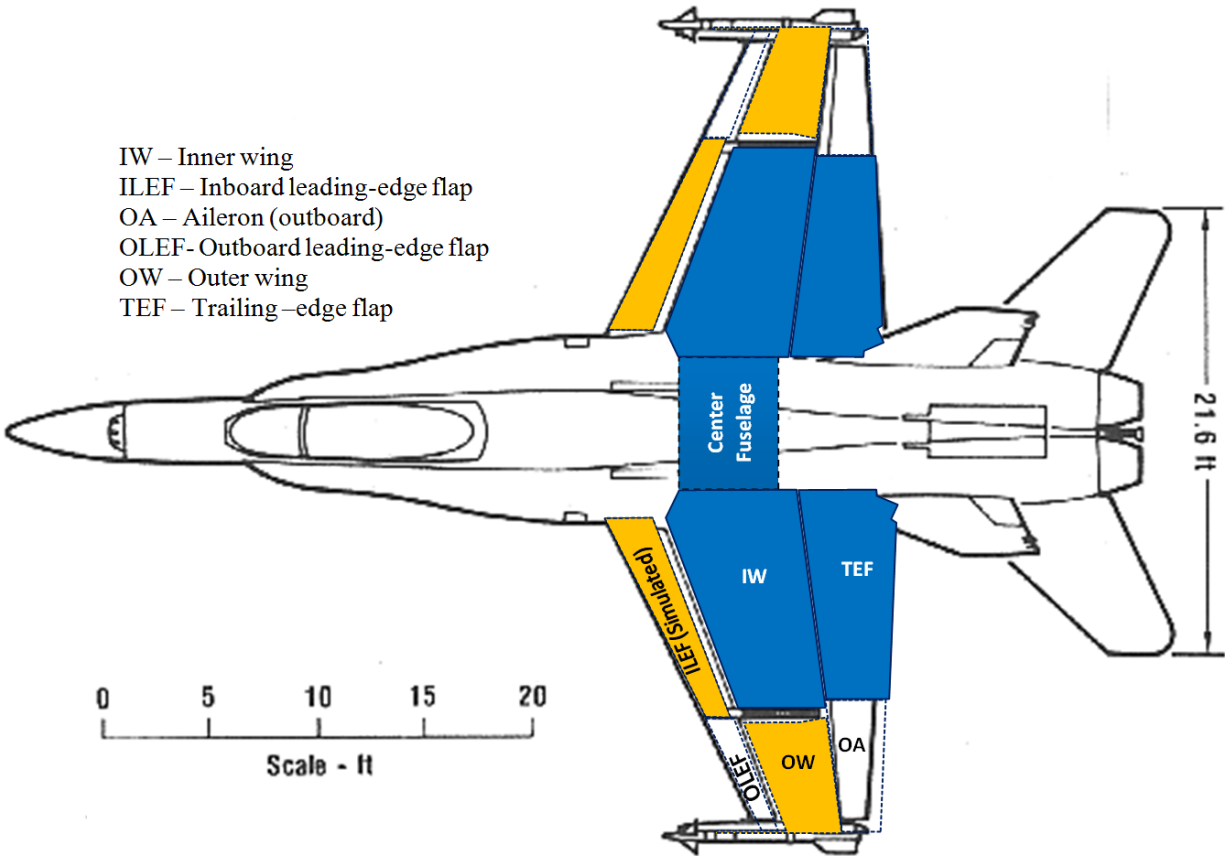


Figure 9.11-72. Full-Scale Test Article (Shown in Blue, Loads from Components Shown in Yellow were Simulated)

The results of both tests – coupon and full-scale - have provide adequate assurance on the integrity of the joint. Additional discussions are available in the references below.

References

- [1] Whitehead, R. S., Kan, H. P., Cordero, R., and Saether, E. S., "Certification Testing Methodology for Composite Structures," Report No. NADC-87042-60, Vol I and II, October, 1986.
- [2] Sanger, K. B., "Certification Testing Methodology for Composite Structures," Report No. NADC-86132-60, January, 1986.
- [3] Chrissos, P., and Coffey, F., "Process Verification Testing for the F/A-18C/D Net Resin Inner Wing Root Steplap Joint," TWD LMA03.12-006 Supp. 532, March 18, 1996.
- [4] Tillman, M. S., Tsai H. C., and Peek, M., "An Investigation of the End-of-Life Residual Strength of the F/A-18A-D Inner Wing Step Lap Joint," NAWCADPAX/TR-2009/139, August 26, 2009.
- [5] Hurd, M., and Coffey, F. J., "F/A-18 C/D Steplap Joint Overlap Evaluation—Axial Pull Specimens," Technical Memorandum 253.95.0155.01, The Boeing Company, St. Louis, MO, October 26, 1995.

- [6] Seneviratne, W., et. Al., “Aging Evaluation of Advanced Materials Used for Military Aircraft,” Aircraft Airworthiness & Sustainment Conference, San Diego, April, 2011.
- [7] Seneviratne, W., et. Al., “Durability and Residual Strength Assessment of F/A-18 A-D Wing-Root Stepped-Lap Joint,” 11th AIAA ATIO Conference, AIAA Centennial of Naval Aviation Forum, September 2011.
- [8] Seneviratne, W., “Composite Fatigue Testing,” Aerospace International Testing Magazine, June 2013, pp 56-58.
- [9] Seneviratne, W., Tomblin, J., and Kittur, M., “Durability and residual strength of adhesively bonded composite joints: the case of F/A-18 A-D wing-root stepped-Lap joint,” Chapter 10 of Book Titled “Fatigue and Fracture of Adhesively Bonded Joints”, Woodhead Publishing, 2015.

9.11.18. NDI and Maintenance Data Collection in a Digital Environment

Hazen Sedgwich, USAF A-10 ASIP

In a time where technologies have enabled the communication of vast amounts of information in mere seconds, a modern, common framework for tracking, communicating, and storing maintenance data within the USAF is missing. Although the current process works adequately to maintain aircraft safety, there are significant improvements that can help communicate the state of the aircraft across all stakeholders more efficiently and cost effectively. With the current budget constraints and the need to be more efficient, the A-10 and T-38 ASIP groups have proactively engaged in producing tools to improve engineering decisions based on real time, accurate, data.

Over the last two years these groups have been working with Etegent Technologies to develop a 3D visualization tool for managing maintenance data (References [1] and [2]). NLign has been specifically designed for collecting, organizing and visually representing aircraft maintenance information on 3D CAD models (See Figure 9.11-73). It has also been designed to help facilitate data gathering and real time visualization of other repair and process data. Not only is this tool able to manage the fleet as a whole, but it is capable of tracking the current configuration and maintenance history of each aircraft.

The tool is useful in many ways. It can provide maintenance planners a visualization of the incoming aircraft so parts and processes can be pre-planned. It is also useful to the program engineer when tasked with analyzing a repair or modification that may interact with previous repairs. Without a tool like NLign, it is nearly impossible for the engineer to have the proper visibility of work previously performed on an airframe; especially when those repairs have been performed in accordance with existing Tech Order (TO) limits with no record retention requirement for those repairs.

Currently NLign is configured to meet the specific needs of the A-10 and T-38; however, other weapon systems in the USAF such as the F-15, F-22, F-35, B-1 and Global Hawk are currently adopting or evaluating the tool as well. The Navy is also using it on the F-18.

NLign has been developed to visualize and produce trending data in the following areas for the A-10:

- Test and teardown (NDI)
 - Visualize cracking sizes, direction and develop trends for full scale aircraft fatigue test specimens (see Figure 9.11-74)
- Aircraft critical inspection findings (NDI)
 - Visualize cracking sizes, direction and develop trends for current fleet flight time
 - Data input GUI
 - Pre-populated x, y, z coordinates for common inspection locations
- Serialized component tracking
 - Track major serialized component movement in the fleet, e.g., wings, horizontal, etc.
 - User-friendly GUI for data input
- Request for engineering (107/202)

- Support analysis
 - All in-house analysis developed in response to 107/202 requests
- Corrosion damage mapping (see Figure 9.11-75)
 - Photographic based corrosion mapping directly into NLign
 - NLign automatically determines corrosion boundaries and creates trends
- Live charting (see Figure 9.11-76)
 - Global or user specific live charting
 - Real-time charts readily available for briefings

Other areas which are not currently developed within the A-10 NLign environment, yet under development are:

- Non-conformance data for each new wing
- All maintenance actions found on the AFTO 95, TCTO and TO
- Database communication (Interaction with other databases)

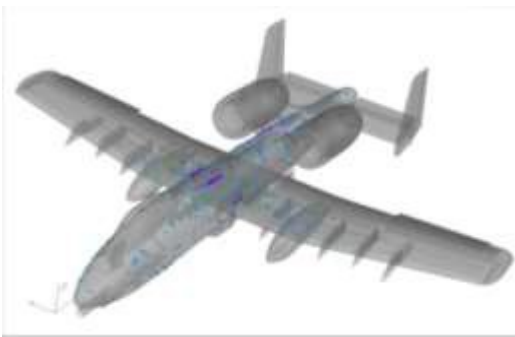


Figure 9.11-73. Visual Representation of Maintenance Data



Figure 9.11-74. Test and Teardown Visual Cracking Direction Data



Figure 9.11-75. Corrosion Mapping from a Photo to the 3D Model

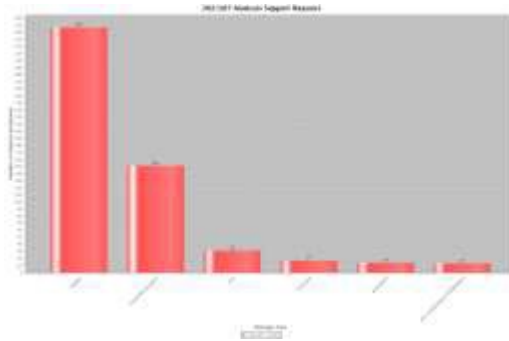


Figure 9.11-76. Live Charting

NLign is designed to effectively communicate high quality information to the people who need to make time-critical decisions for the airframe from planning through delivery of the end product. Several metrics can be realized by using NLign in its current state, such as; quality, time savings, and cost. However, the main metric that should result from this effort is reliable data to be used within the ASIP process ensuring and improving fleet health and state awareness.

References

- [1] Steffes, G, Paredes, S, “Improving ASIP Analysis Using Structural Data Visualization Organization and Archival Techniques”, US Air Force Aircraft Structural Integrity Program Conference, San Antonio, TX, 3-5 December 2013.
- [2] Sedgwick, H, Coyan, G, Hodges, J, Steffes, G, “Enabling High-Quality and Efficient Engineering Decisions with 3-D Visualization of Maintenance Data”, ”, US Air Force Aircraft Structural Integrity Program Conference, San Antonio, TX, 2-4 December 2014.

9.11.19. Full-Scale-Fatigue Test Truncation Spectrum Verification

Saravanan R. Arunachalam, Independent Consultant to USAF Academy - CASTLE

The USAF Aircraft Structural Integrity Program requires that cyclic load tests be performed on critical structural parts to demonstrate that durability and damage tolerance design requirements are met. Typically, this is done with a full-scale test of the entire airframe. On the subject aircraft of this work several large structural airframe components were tested during the original production; however, per agreement between the manufacturer and the USAF, a full-scale test was never performed. The manufacturer identity and type of the aircraft is withheld due to proprietary, confidentiality and export control of the nature of the program. Due to current life goals full-scale testing of the aircraft structure is now needed to reestablish the airframe’s durability life and assure it meets these current life goals. As is the case for many large aircraft, the full-scale test is being accomplished in two separate tests—one for the wing and one for the fuselage.

Military Specification MIL-A-008867B [1] states that truncation through elimination or substitution of load cycles is allowed to reduce the time and cost of full-scale testing. A series of material coupon tests were required to verify the spectrum truncation. The goal of this program was to verify the damage caused by the truncated spectra was equivalent to the damage caused by the full spectra. Additionally, the test quantified any differences between the full and truncated spectra.

The planned coupon test program would validate the planned method of truncating the aircraft analytic spectra to an acceptable number of cycles for test expediency. The difference in damage between coupons tested with the full analytic spectra versus coupons tested with the truncated spectra was measured. The truncated load cycles were developed by eliminating the more frequent low amplitude cycles, which were determined by analysis to be less damaging, without disturbing the basic ordering of the spectrum. The basic spectrum order was maintained in order to preserve the spectra’s load interaction influences such as damage retardation and acceleration. Some damage restoration was also included in the truncated spectra to account for the impact on damage growth lost by eliminating cycles. The aircraft manufacturer adjusted several of the minimum load end points to alter the stress range while maintaining the peak load end points.

Tests were carried out by applying three types of spectra to six different sets of specimens representing various structural materials and locations used on the airframe. The three spectra included full un-truncated spectra, truncated spectra, and marker spectra. The full spectra contained approximately 86,500 cycles for a 100 flight block. The truncated fuselage spectra contained approximately 40,000 cycles for a 100 flight block. The marked spectra were a variation of the truncated spectra. Damage was determined by crack growth measured in repeats of the 100 flight block.

The six material/location combinations included 2024 Al which was typical for the forward intermediate fuselage (FIF) skin, 7075 Al which was typical for the FIF shoulder longeron, Ph13-8Mo steel which was typical for the FIF dorsal longeron, 7075 Al which was typical for the aft intermediate fuselage (AIF) longeron, Ti-6AL-4V which was typical for the wing carry through (WCT) structure, and 9Ni-4Co-0.2C from typical steel spindle fittings. The test coupons representing these structural regions were received pre-machined and first tested to evaluate the effectiveness of the marker spectrum to produce its signature on the fracture surface.

Experimental Procedures

The six different material/locations tested in this program are given in Table 9.11-3. As stated, all coupons were received in an as-machined condition. The test coupons were 30 inches long, 4.0” wide and 0.405” thick with three 0.5” diameter holes spaced 5 inches apart on the center line. Each hole had a 0.02” electrical discharge machined (EDM) notch through the thickness on one side of the specimen. A schematic of the coupon geometry for the test is shown in Figure 9.11-77.

Table 9.11-3. Six Different Materials and Locations Tested

Structural analysis area	Material	Test Specimen ID
Wing Carry Through (WCT-12-004)	Ti-6Al-4V	WCT-004-UnTrunc_1, 2, 3
Wing Carry Through (WCT-12-004)	Ti-6Al-4V	WCT-004-Trunc_1, 2, 3
Wing Carry Through (WCT-12-004)	Ti-6Al-4V	WCT-004-Mark_1
Forward Intermediate Fuselage (FIF-04S-005) skin	2024 Al	FIF-005-UnTrunc_1, 2, 3
Forward Intermediate Fuselage (FIF-04S-005) skin	2024 Al	FIF-005-Trunc_1, 2, 3
Forward Intermediate Fuselage (FIF-04S-005) skin	2024 Al	FIF-005-Mark_1
FIF shoulder longerons (FIF-12L-006)	7075 Al	FIF-006-UnTrunc_1, 2, 3
FIF shoulder longerons (FIF-12L-006)	7075 Al	FIF-006-Trunc_1, 2, 3
FIF shoulder longerons (FIF-12L-006)	7075 Al	FIF-006-Mark_1
FIF dorsal Longerons (FIF-36L-007)	PH13-8Mo-Steel	FIF-007-UnTrunc_1, 2, 3
FIF dorsal Longerons (FIF-36L-007)	PH13-8Mo-Steel	FIF-007-Trunc_1, 2, 3
FIF dorsal Longerons (FIF-36L-007)	PH13-8Mo-Steel	FIF-007-Mark_1
Aft Intermediate Forward Longerons (AIF-01-008)	7075 AL	AIF-008-UnTrunc_1, 2, 3
Aft Intermediate Forward Longerons (AIF-01-008)	7075 AL	AIF-008-Trunc_1, 2, 3
Aft Intermediate Forward Longerons (AIF-01-008)	7075 AL	AIF-008-Mark_1
Aft fuselage Spindle fitting (AF-02-009)	9Ni-4Co-0.2C Steel	AF-009-UnTrunc_1, 2, 3
Aft fuselage Spindle fitting (AF-02-009)	9Ni-4Co-0.2C Steel	AF-009-Trunc_1, 2, 3
Aft fuselage Spindle fitting (AF-02-009)	9Ni-4Co-0.2C Steel	AF-009-Mark_1

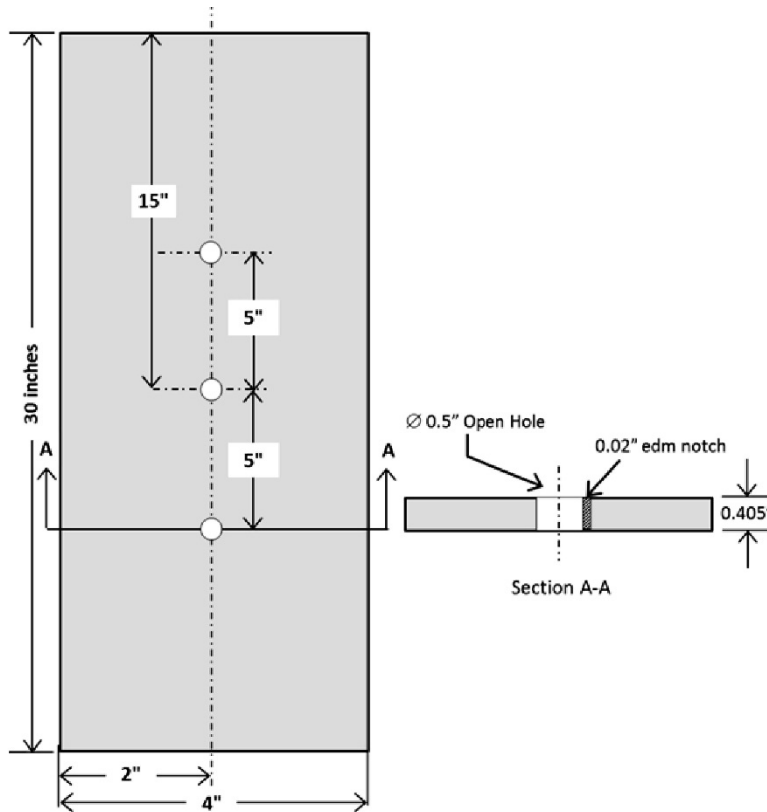


Figure 9.11-77. Schematic of the Test Coupon Geometry

Test Procedures

Three tests were conducted for each material corresponding to a specific location using full un-truncated, and truncated spectrum versions. In addition, one test was conducted using marker spectra to identify the location of markers from fractographic studies that were introduced at specific crack lengths. Tests were carried out using either the MTS 110 kip or MTS 55 kip computer controlled servo-hydraulic test frame depending on the load requirements. All tests were done at laboratory conditions where the temperature was maintained at $72^{\circ} \pm 3^{\circ}$ F ($22^{\circ} \pm 1.5^{\circ}$ C) with an average relative humidity of 30% ($\pm 5\%$) and cycled at constant frequency of 4 Hz. Visible crack length was measured with the aid of a travelling microscope at a magnification of 10X mounted on a liner encoder, and the crack length was measured digitally to an accuracy of 0.0001 inch (0.00254 mm). Three separate microscopes were used to measure crack lengths from the three individual holes for convenience. Further crack length was measured at the completion of full or truncated spectrum, for example, in the case of truncated fuselage spectra at the end of ~ 40000 cycles. Pre-cracking was carried out for all tests prior to application of spectrum loading. The 0.02 inch (0.5 mm) EDM notch was pre-cracked to 0.04 ± 0.005 inch (1.0 ± 0.127 mm) using constant amplitude loading with R of 0.1 at 20 Hz frequency.

In the case of the marker spectrum test, the main objective was to see whether markers were visible on the fracture surface when introduced during full-scale-fatigue testing. At the same time, it would not be possible to know whether any crack existed during the full-scale-fatigue test or the crack length at which the marker was introduced. To address this issue, markers were introduced at three different crack lengths based on the slope of the crack length vs. number of cycles curve during the truncated spectrum test. Once the pre-cracking was completed, a truncated spectrum was run up to the first crack length where the marker spectrum was introduced. Marker spectrum was a modified version of truncated spectrum with 10 stripes of 10 markers load cycles so that the markers can be easily identified on

the fracture surface. Once the marker spectrum cycles were completed, the crack length was measured and truncated spectrum was continued until the next designated crack length, and so on. Table 9.11-4 shows the marker spectrum insertion location for all the materials and the order in which the tests were conducted.

Table 9.11-4. Marker Spectrum Insertion Location for Difference Materials

Order	Specimen ID	Marker spectrum insertion length, in		
		First	Second	Third
1	FIF-006	0.05	0.55	1.1
2	FIF-007	0.05	0.25	0.6
3	AIF-008	0.05	0.75	0.9
4	WCT-004	0.05	0.15	0.5
5	FIF-005	0.05	0.45	1
6	AF-009	0.05	0.25	0.6

Macro photographs of all coupons were taken prior to testing as well as after the completion of each test (i.e. failure). Further, coupons were hand polished using 600 grit emery paper with final polishing using 9 micron diamond paste near the EDM side before testing to enhance the visibility of tiny cracks and to maintain control of the pre-cracking stage.

The fracture surface of all the coupons was studied under an optical microscope to measure the pre-crack length and compare the lengths measured using the travelling microscope. Also, an optical or scanning electron microscope was used to locate the markers on the fracture surface.

Results

A summary of all the test results is provided in Table 9.11-5. The results included spectrum location, number of cycles for each spectrum (un-truncated, truncated, and marker), total number of cycles to failure, crack length at failure, and test frame used. The raw data were plotted in Microsoft® Excel as crack growth (damage accumulation) curves as well as a comparison between the marker spectrum and truncated spectrum for each material tested. The data were not normalized to a constant pre-crack length or averaged pre-crack length measured from the post failure analysis. In general, for all the aircraft locations except for the AF-009 spindle fitting location, the un-truncated, truncated and marker spectra damage cycles for each locations were within the acceptable range. A representative plot of measured crack length as a function of number of cycles for each hole is given for AIF-008 in Figure 9.11-78. Measured crack growth rates between the truncated and un-truncated spectrum remained within 10%, indicating the damage accumulation using truncated spectra was equivalent to un-truncated spectra. In the case of the AF-009 spindle fitting, the data shows high scatter even for the same spectra, i.e., un-truncated or truncated sets (Figure 9.11-79) and conclusions about the effectiveness of the truncated spectrum could not be drawn. The observed problem with this spindle fitting was communicated to the customer. The customer indicated that this particular material had difficulty with finding suppliers and the coupons were derived from two batches which originated from two different vendors. The customer further indicated that one of the batches did not meet the material specification.

Table 9.11-5. Summary of the Test Results

Spectrum location	Specimen ID	No. of cycles for one complete spectrum	Total No. of cycles to failure	No. of passes to failure	Crack length at failure, in	Test Frame used
6Al-4V-Ti Wing Carry Through	WCT-004-UnTrunc_1	85985	632850	7.36	1.328	110 kip
	WCT-004-UnTrunc_2		645429	7.42	1.289	
	WCT-004-UnTrunc_3		670683	7.80	1.038	
	WCT-004-Trunc_1	33401	290589	8.70	1.293	
	WCT-004-Trunc_2		272886	8.17	1.230	
	WCT-004-Trunc_3		257188	7.70	1.296	
	WCT-004-Mark_1	25974	262963	8.54	1.230	
2024-Al Forward Intermediate Fuselage skin	FIF-005-UnTrunc_1	82180	2656879	32.33	1.515	55 kip
	FIF-005-UnTrunc_2		2768644	33.69	1.480	
	FIF-005-UnTrunc_3		2660988	32.38	1.530	
	FIF-005-Trunc_1	32939	1023415	31.07	1.515	
	FIF-005-Trunc_2		997064	30.27	1.317	
	FIF-005-Trunc_3		1014851	30.81	1.416	
	FIF-005-Marker_1	25744	1004605	31.24	1.498	
7075-Al Forward Intermediate Fuselage shoulder Longeron	FIF-006-UnTrunc_1	85632	3087034	36.05	1.551	55 kip
	FIF-006-UnTrunc_2		3124712	36.49	1.494	
	FIF-006-UnTrunc_3		3244596	37.89	1.571	
	FIF-006-Trunc_1	33038	1159964	35.11	1.510	
	FIF-006-Trunc_2		1110077	33.36	1.470	
	FIF-006-Trunc_3		1204565	36.46	1.515	
	FIF-006-Marker_1	25775	969351	30.00	1.454	
PH13-8Mo Steel Forward Intermediate Fuselage Dorsal Longeron	FIF-007-UnTrunc_1	85431	1170405	13.70	1.208	110 kip
	FIF-007-UnTrunc_2		953410	11.16	1.057	
	FIF-007-UnTrunc_3		1049093	12.28	0.812	
	FIF-007-Trunc_1	32825	340067	10.36	0.781	
	FIF-007-Trunc_2		435916	13.28	0.973	
	FIF-007-Trunc_3		403091	12.28	1.120	
	FIF-007-Mark_1	25701	424392	13.58	1.192	
7075-Al Aft Intermediate Forward Longeron	AIF-008-UnTrunc_1	85322	1470951	17.24	1.492	55 kip
	AIF-008-UnTrunc_2		1581017	18.53	1.471	
	AIF-008-UnTrunc_3		1689376	19.80	1.506	
	AIF-008-Trunc_1	32543	558763	17.17	1.368	
	AIF-008-Trunc_2		555509	17.07	1.487	
	AIF-008-Trunc_3		621246	19.09	1.467	
	AIF-008-Mark_1	25512	600153	19.09	1.480	
9Ni-4Co-0.2C Steel Aft Fuselage Spindle Fitting	AF-009-UnTrunc_1	86279	5496835	63.71	1.121	110 kip
	AF-009-UnTrunc_2		6055060	70.18	1.312	
	AF-009-UnTrunc_3		3350214	38.83	1.350	
	AF-009-Trunc_1	33208	1606935	48.39	1.435	
	AF-009-Trunc_2		2181766	65.70	1.325	
	AF-009-Trunc_3		743859	22.40	1.488	
	AF-009-Mark_1	24643	2015601	61.47	1.318	

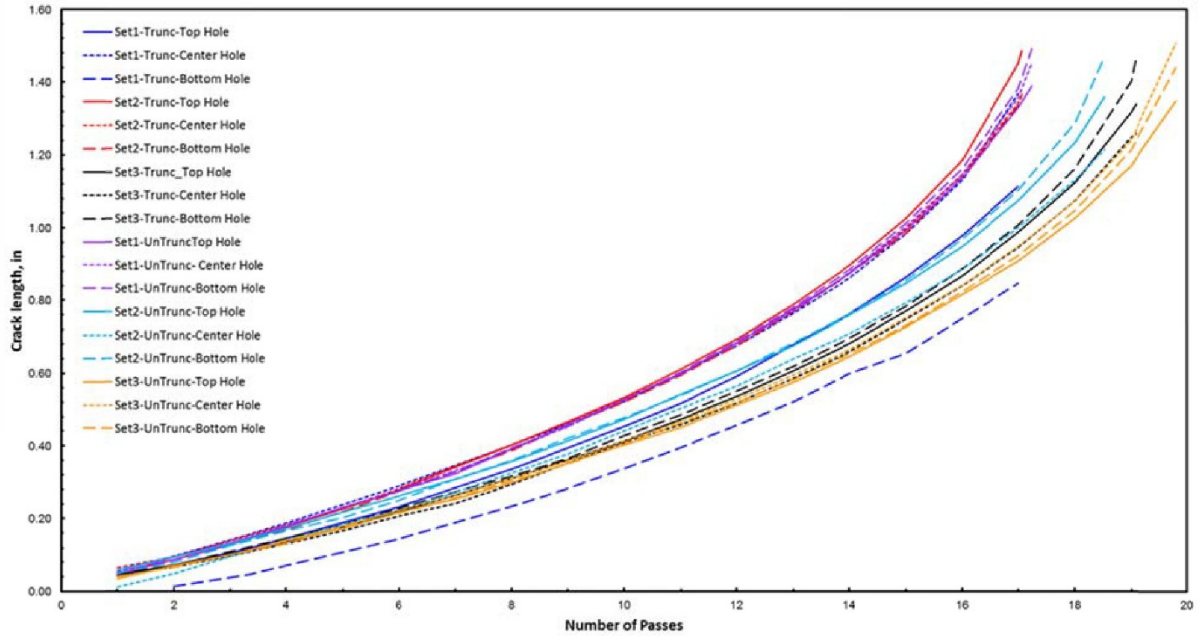


Figure 9.11-78. Crack Growth Curves for AIF-008-7075-Al Un-Truncated and Truncated Spectrum for All Holes

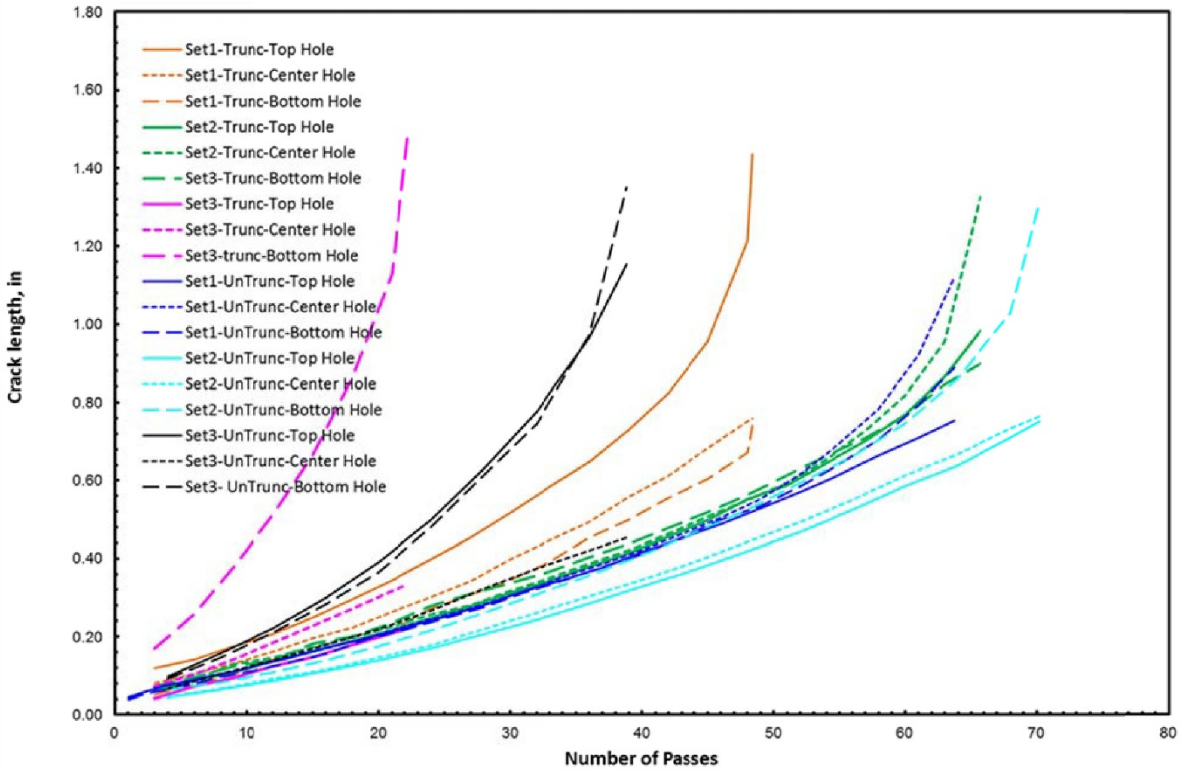


Figure 9.11-79. Crack Growth Curves for AF-009-9Ni-4Co-0.2C Steel Un-Truncated and Truncated Spectrum for All Holes

Figure 9.11-80 shows a representative crack growth curves for AF-008 where the marker spectrum was introduced. For each of the sets of un-truncated and truncated coupons, the crack growth curves for the hole corresponding to the failure is shown in the plot of this figure. Even with maker spectrum, the damage accumulation for the modified truncated spectrum (with 10 stripes of 10 markers) is within the acceptable range of damage accumulation of truncated and un-truncated spectrum.

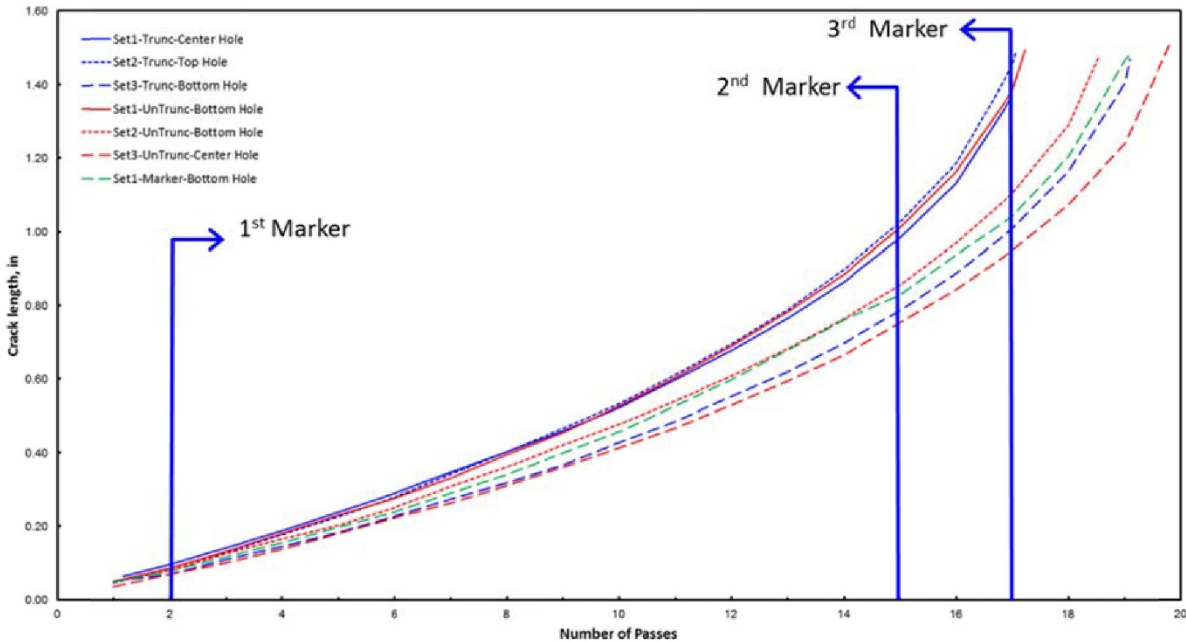


Figure 9.11-80. Crack Growth Curves for AIF-008-7075-Al Un-Truncated, Truncated and Marker Spectrum

The effectiveness of the marker spectrum was also verified by post failure analysis. Marker spectrum was effective in showing 10 stripe markers on all fracture surfaces for all locations, again, except for AF-009 locations. AF-009 corresponds to spindle fitting made of tempered marten site and it is also difficult to see any striations on the fracture surface. No further action was required to develop new marker spectrum specifically for this AF-009 location. Figure 9.11-81 shows optical micrographs of 10 stripes markers on the fracture surface of FIF-005 (2024 Al) location at the failed hole.

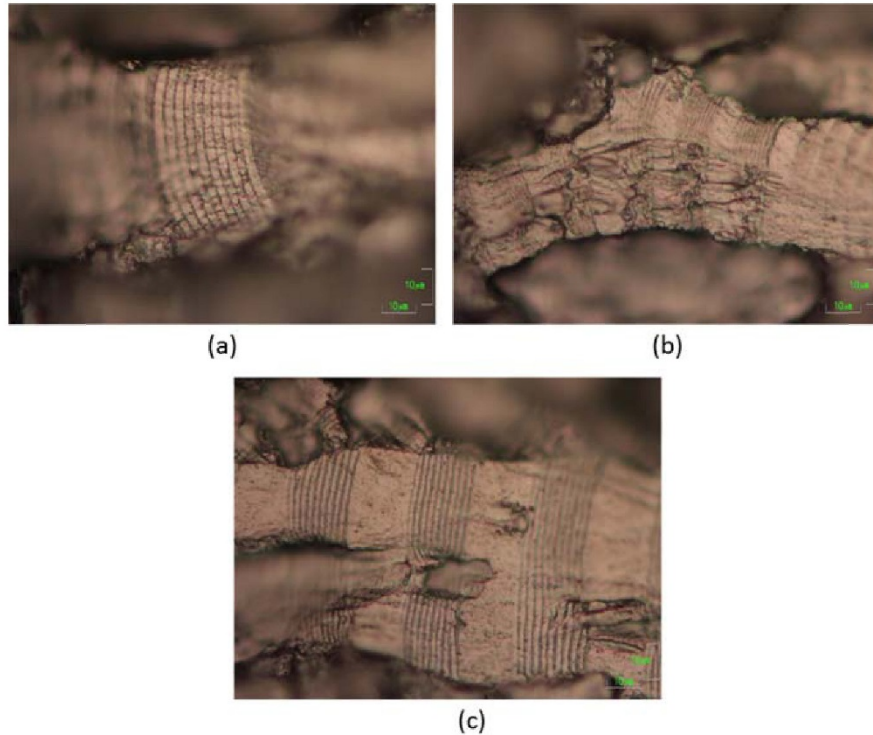


Figure 9.11-81. Optical Micrographs Show 10 Stripe Markers on the Fracture Surface of FIF-005 Specimen at Failed Hole: (a) 1st Marker Location (0.0789\"), (b) 2nd Marker Location (0.493\"), and 3rd Marker Location (1.0711\")

Conclusions

Tests were successfully performed to verify the full-scale-fatigue testing truncated spectrum validation for six different materials from different aircraft structural locations. The six material/locations included 2024 Al (FIF skin), 7075 Al (FIF shoulder longerons), Ph13-8Mo steel (FIF dorsal longeron), 7075 Al (AIF longeron), Ti-6AL-4V (WCT), and 9Ni-4Co-0.2C steel (spindle fitting). For five of the six materials, the coupon crack growth rate using the truncated spectrum was compared to that of the un-truncated crack growth rate. The crack growth rates between truncated and un-truncated spectrum remained within 10%, indicating that the damage accumulated using truncated spectra was equivalent to un-truncated spectra.

For the 9Ni-4Co-0.2C steel (spindle fitting), the material showed too much scatter in the crack growth rates and was identified as a problem related to different vendors and material not meeting specification. In addition, the effectiveness of the marker spectrums was also successfully studied. Marker band spectrum was affective in showing 10 stripe markers on the fracture surface, except for the AF-009 spindle fitting. Because AF-009 steel was tempered marten site, it was also difficult to see striations on the fracture surface.

References

[1] MIL-A-008867B, Airplane Strength and Rigidity Ground Tests.

9.11.20. General Aircraft Structural Integrity Program (ASIP) Support

James. M. Greer, Jr., USAF Academy - CASTLE

Stress Intensity Factor Solutions

Work at CASTLE continues on developing stress intensity factors for accurate crack growth simulations. Using Department of Defense High-Performance Computing assets, CASTLE contractors are using state-of-the-art finite element codes to generate solutions for more complex crack geometries, including multiple cracks at countersunk fastener holes (Figure 9.11-82). The overarching goals of the work are to improve the accuracy of available solutions and to expand the parameter space to encompass more geometries. Achieving these goals will lead to more accurate crack growth predictions, which will in turn lead to safer, more economical aircraft operations.

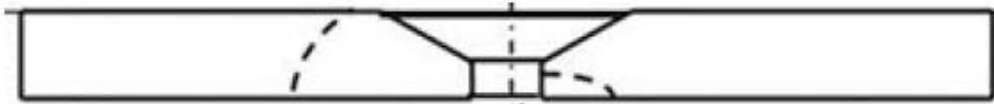


Figure 9.11-82. Two Cracks at a Hole having a Deep Countersink

Root Cause Failure Analysis

CASTLE routinely performs failure analyses for various fleet managers. Typically, the failure analyses (Figure 9.11-83) reveal the damage nucleation site(s), the mechanism(s) of crack growth (fatigue, SCC, intergranular attack, corrosion-fatigue, etc.) or corrosion types/progression (general, pitting, exfoliation, filiform, etc.), exact dimensions of damage and information on loading history. Parts examined by CASTLE have been of various sizes and product forms (extrusions, castings, forgings, plate/sheet, etc.).

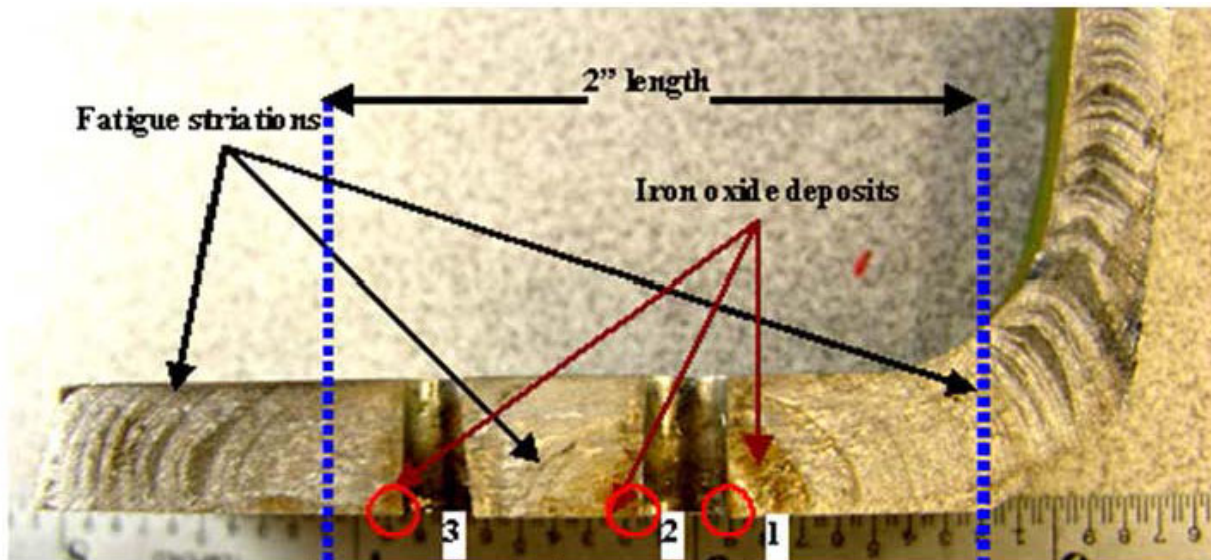


Figure 9.11-83. Some Typical Macroscopic Failure Analysis Features

Probabilistic Lap Joint Crack Predictions

CAStLE has performed multiple residual life and residual strength tests on retired fuselage lap joints. These data are being put to good use to develop a Monte Carlo simulation tool to predict the health of a lap joint with a known geometry and service history. This work will be presented at ICAF 2015.

Support to T-53 Vent Window Evaluation

In order to alleviate high cockpit temperatures on hot days, the idea of installing vent windows in the T-53A (Figure 9.11-84) was explored with help from CAStLE.



Figure 9.11-84. The USAFA T-53A Aircraft

CAStLE developed an installation template for the pilot and co-pilot windows to speed installation of the vent windows for testing. A novel method was developed to capture the complex curvature of the window, which was then fed into a solid modeling program (Figure 9.11-85) for refinement. The final model was ported to a CNC mill to fabricate the steel templates. Other support to T-53 included root cause failure analysis and recommendations for a part experiencing repeated issues.

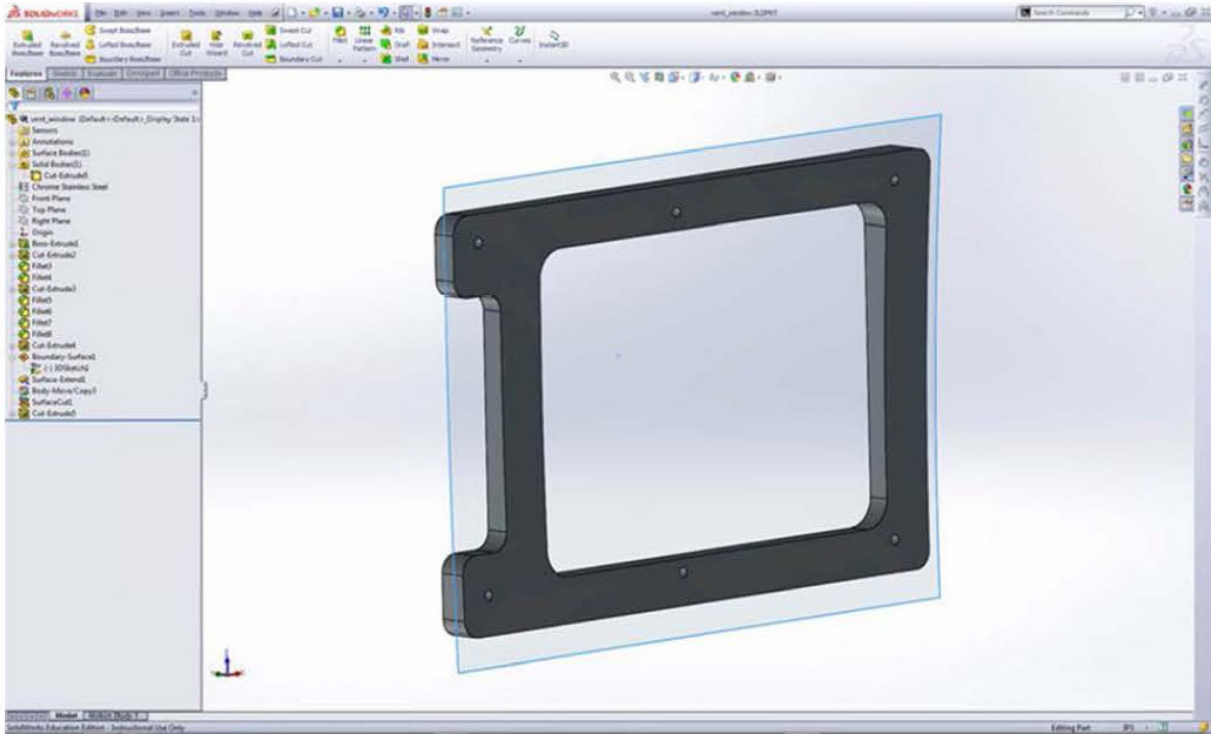


Figure 9.11-85. CASTLE Template Model for Vent Window Installation

In-Plane Stress Corrosion Cracking Study

CASTLE has been leading the way in trying to understand an unusual form of cracking in this sheet: in-plane cracking. Using very low frequency four-point bend specimens (Figure 9.11-86), CASTLE has succeeded in growing the cracks in a laboratory environment. In the field, these cracks have been seen in fuselage and wing skins. Engineers and cadets have performed multiple projects to determine when these cracks transition between fatigue and SCC modes of propagation.

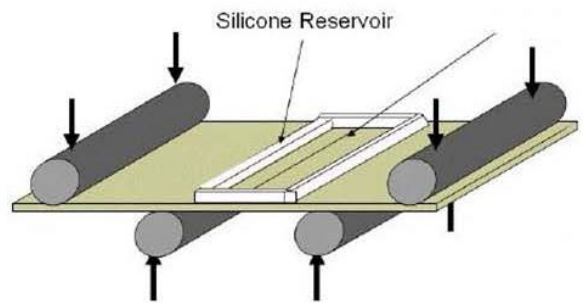
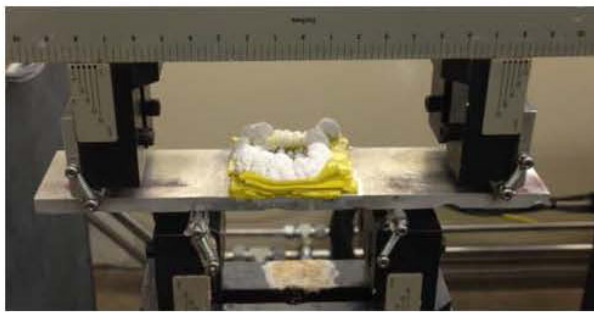


Figure 9.11-86. A Four-Point Bend Specimen with a Silicone Reservoir for Holding a NaCl Solution

Support to U.S. Navy P-3

At the request of the Navy, CASTLE performed research involving an assessment and refurbishment of a P-3 (Figure 9.11-87) horizontal stabilizer and material substitution for a nose landing gear truss rib. As a sidelight to the horizontal stabilizer work, a cadet team instrumented and tested a trim tab actuator push rod, verifying the margin of safety from 50-year old OEM stress analysis.



Figure 9.11-87. The U.S. Navy P-3 Orion

T-38 Shut-Off Overload Ratio Testing

Cadets at the U.S. Air Force Academy, under the guidance and direction of CASTLE engineers, have performed multiple tests to verify the Shut-Off Overload Ratio (SOLR) for T-38 (Figure 9.11-88). The SOLR is a modeling parameter used to capture crack growth retardation effects due to plastic zones created by overloads near the crack. The results of these tests feed Durability and Damage Tolerance Analyses (DADTA) used to set inspection intervals for aircraft fleets.

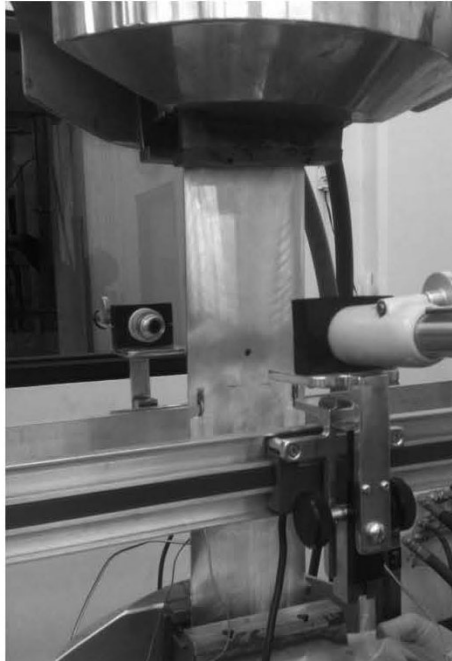


Figure 9.11-88. Aluminum Plate with Hole as a Subject for SOLR Testing

T-38 Full-Scale Wing Testing

As part of the T-38 ASIP manager's ongoing efforts to safely extend the life of the supersonic trainer, CASTLE, Sabreliner and the Southwest Research Institute partnered to do a full-scale test of two T-38 wings (Figure 9.11-89). One wing was tested to the Specialized Undergraduate Pilot Training (SUPT) load spectrum, and one was tested to the more severe Introduction to Fighter Fundamentals (IFF) spectrum. Following testing, both wings will be subjected to a destructive teardown analysis in order to fully understand the effects of fatigue on the T-38 wings.



Figure 9.11-89. T-38 Full-Scale-Fatigue Test

9.11.21. Detecting Crack Nucleation/Damage Mechanisms in Sea-Based Aviation Environments

Bill Nickerson, USN-Office of Naval Research

Ensuring the safety and future condition of aircraft requires the analysis of damage accumulation at critical locations due to both applied stresses and local environmental conditions. To address this need, this project effort focuses on developing sensing technologies able to reliably inform about the progressive damage state of corroding structural material, and prognostics models that can take into account variation of loading and environmental conditions for calculation of components' remaining life. A coupling of reliable measurements of severity of the environment and corrosion damage progression, and analytical tools capable of forecasting material degradation is targeted in this research effort. The near term objectives are to develop a corrosivity and corrosion activity measurements device for structural aluminum alloy in representative aggressive environments, and develop an analysis tool that implements unique analytical formulations linking environmental damage to perform life calculation at a given component level.

Current efforts are directed towards the testing of combined sensing technologies, able to provide both continuum time-varying information and discrete (go/no go) signal information on the status of the material exposed to the environment. The techniques being integrated are direct current potential drop (DCPD), foil perforation, and multi-electrode-array (MMA). A sensor head has been designed to include sensing elements of different thicknesses, subjected to different stress levels, and monitored by using a combination of DCPD and foil perforation. Sensing elements are designed to maximize the sensitivity of the DCPD measurement and to allow application of stress. Each sensing element is equipped with a perforation detection circuit, able to signal when degradation resulted in perforation of the element. Additionally a zero resistance ammeter is used to monitor corrosion currents among sensing elements (Figure 9.11-90).

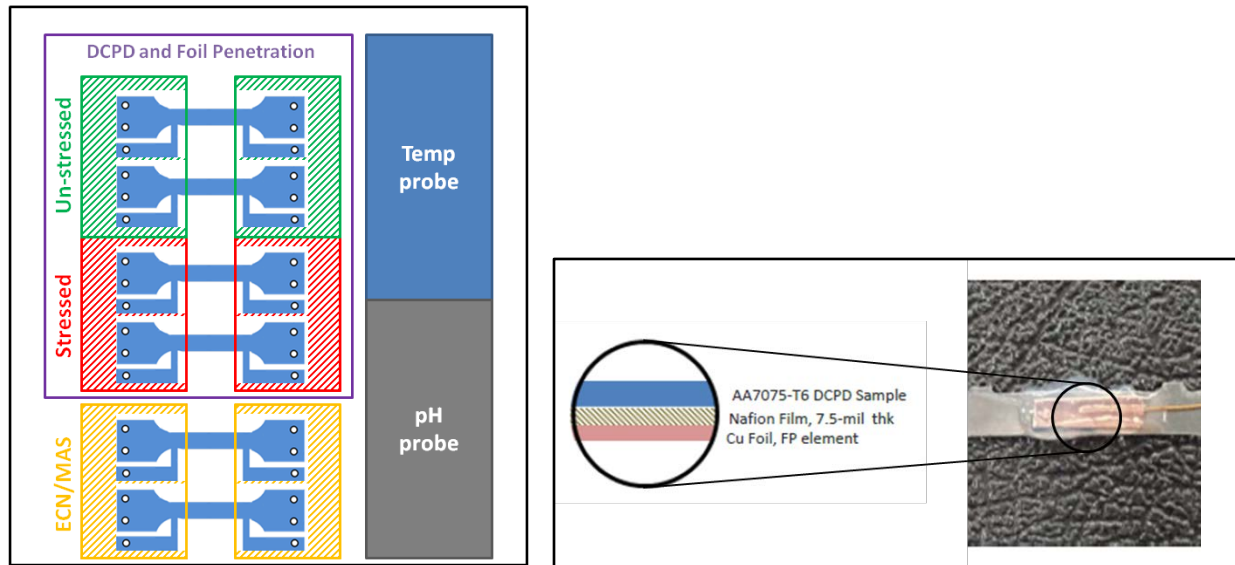


Figure 9.11-90. Sensor Head Concept and Foil Perforation Element Structure

Critical tests are being performed by stressing the sensing elements in bending at different stress levels and immersing them in an aggressive environment known to promote intergranular corrosion (IGC); a correlation of progressive degradation, monitored through DCPD, and stress level has been successfully shown. Further improvements in DCPD sensitivity are being investigated to refine the sensing element design and to improve methods of DCPD electrode positioning. Different environments and degradation through potentiostatic polarization to promote different types of corrosion attack are being investigated. Critical tests are also being performed to verify the current setup for foil perforation in unstressed and stressed conditions. Successful results were carried out in both conditions, although challenges exist to ensure isolation of sensing element from electrolyte for the portion of the specimen containing the perforation sensing electrode. Future tests will combine the DCPD and foil perforation techniques for sensing elements of different thicknesses, subjected to different stresses, simulating a sensor head setup. Sensor head design in terms of needed electronic components and power supply needs are also being investigated. Partnership with prototype manufacturers is being sought for future sensor head construction.

A damage prediction model within the framework of continuum damage mechanics (CDM) for 2024-T3 aluminum that accounts for pit to crack transition life in corrosion fatigue has been developed. Damage is defined as degradation of mechanical properties of the material due to environment and cyclic stress. An evolution law for damage accumulation is adopted that accounts for high-cycle fatigue at constant load amplitude and for the influence of the stress on pit growing from constituent particles. Model predictions compare well with experimental results in corrosion fatigue (Figure 9.11.91).

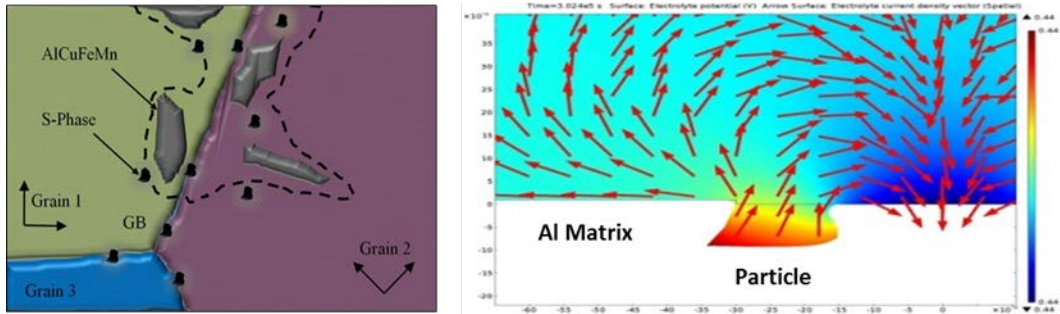


Figure 9.11-91. CDM Model for Corrosion Fatigue Crack Initiation at Constituent Particles

The work is progressing towards the accomplishment of the stated objectives both in sensor development and modeling efforts; testing times and results are critical for the successful evaluation of the testing technology being developed.